GEOLOGY, GEOCHEMISTRY AND ECONOMIC SIGNIFICANCE OF THE CELESTITE DEPOSITS OF AVON

by

Christopher John Brown

DECEMBER 1982

A thesis submitted for the degree of
Doctor of Philosophy of the University of London

Geology Department,
Imperial College,
London SW7 2BP

Frontispiece. View across the Bristol Coalfield from the Tortworth Ridge at Yate Rocks (ST 719846) showing the re-exhumed desert landscape of Carboniferous rocks on which the celestites were deposited.

In the beginning was the Word, and the Word was with God, and the Word was God. He was in the beginning with God; all things were made through him, and without him was not anything made that was made. (John 1;1-3)

.....and they lead him out to crucify him. (Mark 15;20)

GEOLOGY, GEOCHEMISTRY AND ECONOMIC SIGNIFICANCE OF THE CELESTITE DEPOSITS OF AVON

by Christopher John Brown

ABSTRACT

The project investigated the celestite deposits of the County of Avon and assisted the mining industry to locate and evaluate them.

These deposits contain seams of nodules in cyclothems of the Mercia Mudstone Group that were deposited as a sabkha facies on a desert landmass. Epigenetic celestite also veins the Millstone Grit bedrock of the pediment. As the landscape was re-exhumed during Quaternary times the deposits were broken up into 'mumblers', Head deposits, and in some cases, reworked as celestite sands and gravels.

Thin sections of the celestites showed fabrics indicating Primary growth and replacement of anhydrite and, more rarely, gypsum. A paragenesis was determined with the accessory minerals calcite, dolomite, megaquartz and chert. The calcite, the principal impurity present in the ore, is a recrystallization produce of the cement of the marl. By contrast, the epigenetic celestites are mostly mono-mineralic replacements of the Millstone Grit.

Statistical analysis of the Sr, Ba, Cu, Zn, Na, K analyses of the celestites together with the calcite and dolomite contents (determined by quantitative XRD analysis) indicated that most of the celestites conformed to a 'normal' composition from which barian celestites, containing 0.96% Ba, and calcitic celestites were recognized. The geological, petrographic and geochemical evidence were combined to assess the origin of the celestites.

Size distribution studies examined the breakdown of celestite in the celestite sands and the Clay Head. Because of the erratic distribution and dispersion of the celestite, geochemical prospecting using soil sampling or stream sediment sampling techniques could only be

successfully applied regionally, to detect the subsurface celestite. A resistivity survey was also undertaken, with only limited success. The use of other exploration, assessment and exploitation techniques was also critically reviewed. Finally, the spatial extent of the celestites was discussed.

ACKNOWLEDGEMENTS

Principal thanks are due to my mother for financial assistance during writing-up of the project and the fellowship of Holy Trinity Brompton for spiritual support and encouragement in what turned out to be a morally demanding task. I would also like to thank my supervisors; Dr. R.J. Howarth for constructive criticism help and Dr. H.F. Shaw for patiently reading and correcting the final drafts. The interest of many other lecturers, students and research workers is also noted.

The friendly assistance of many technicians is acknowledged, in particular Ray Curtis (XRD Lab.), Jim Dare (Geophysics) and Alan Jones (rock-cutting). Mr. M Ramsey helped with the geochemical analyses. The staff of the Cartography and Photography Departments were always cheerful and obliging.

Fieldwork was carried out on land owned by the Bristol Mineral Company Ltd.. I am indebted to Mr. E. Young for easy access to the sites and for many detailed consultations. First class accomodation during fieldwork was provided by the Collimore family.

Financial assistance was provided for by a NERC CASE Studentship in collaboration with the Bristol Mineral Company. I am most grateful for this funding and the opportunity to pursue research. The Sedimentology Department contributed towards photographic costs.

Finally I would like to thank Robert, Izzy, Valerie and Sally for typing the manuscript, free of charge.

TABLE OF CONTENTS

Page

ABSTRACT iv

ACKNOWLEDGEMENTS vi

CHAPTER ONE - INTRODUCTION TO THE CELESTITE DEPOSITS 1

1.1 THE CELESTITE INDUSTRY.....2
1.1.1. History of Exploitation and Useage.....2
1.1.2. The extent of the resource.....4
1.1.3 Mining and Processing.....4
1.2 HISTORY OF RESEARCH.....8
1.3 OBJECTIVES OF THE PRESENT STUDY.....10
1.4 GEOLOGICAL BACKGROUND.....12

CHAPTER TWO - THE NATURE AND OCCURRENCE OF THE CELESTITE DEPOSITS OF THE STUDY AREA 24

2.1 INTRODUCTION.....25
2 2 STRATIGRAPHY OF THE CELESTITES.....25
2.2.1. Introduction.....25
2.2.2. The stratigraphy of the study area.....31
2.2.3. Regional correlation.....32
2.3 DEFINITION OF TERMINOLOGY.....38
2.3.1. Colour.....38
2.3.2. Grain size.....39
2.3.3. Crystal habit.....39
2.3.4. Morphology of nodular celestites.....42
2.4 TYPE A CELESTITE DEPOSITS.....42
2.4.1 Sedimentary setting of the Triassic rocks...42
2.4.1.1. Introduction.....42
2.4.1.2. The Yate Formation.....44
a. Mudrocks.....47
b. Carbonate rocks.....51
c. Evaporites.....52
2.4.2. Form of celestite horizons.....56
2.4.3. Varieties of Type A celestite.....60

2.4.3.1. Massive celestite.....60
2.4.3.2. Macrocellular celestite.....62
2.4.3.3. Impregnations of celestite.....65;
2.4.3.4. Quartz-rich celestites.....65
2.4.3.5. Other megascopic textures.....72
2.4.4. Carbonate minerals.....74
2.4.5. Gypsum.....76

2.5 EPIGENETIC CELESTITE DEPOSITS.....77
2.5.1. Description of the host lithologies.....78
2.5.1.1. Paleozoic rocks.....78
2.5.1.2. Triassic marginal deposits.....80
2.5.1.3. ? Triassic rocks at Summer Bridge, Tytherington.....85
2.5.1.4. Possible Quaternary terrace gravels of the Yate Bypass exposure.....85
2.5.2. Description of the Epigenetic Celestites....93
2.5.2.1. Celestites replacing Carboniferous mudrocks.....93
a. Celestite veins.....93
b. Thin celestite veins.....97
c. Spheroidal celestites.....97
d. Celestite nodules.....98
2.5.2.2. Celestites replacing Carboniferous sandstones.....102
2.5.2.3. Celestites replacing Permo-Triassic ironstones.....103
2.5.2.4. Celestite replacing Triassic marginal deposits.....103
2.5.2.5. Celestites replacing ? Triassic rocks at Summer Bridge, Tytherington.....105
2.5.2.6. Celestite replacing terrace gravels of possible Quaternary age.....108
2.5.3. Other epigenetic minerals of the Carboniferous mudstones.....109
2.5.3.1. Baryte.....109
2.5.3.2. Gypsum.....109

2.6 MUMBLER DEPOSITS, CELESTITE SANDS AND CELESTITE GRAVELS.....111
2.6.1. Introduction.....111
2.6.2. Periglacial weathering of the celestites...114

2.6.2.1 Mumbler deposits.....116
2.6.2.2. Type A celestite gravels.....117
2.6.3. Other celestite sands and gravels.....118
2.6.3.1. The Rectory.....118
2.6.3.2. Winter's Field.....121
2.6.3.3. Interpretation of the sands and gravels..121

CHAPTER THREE - PETROGRAPHY OF THE CELESTITES 126

3.1 PETROGRAPHY OF THE TYPE A CELESTITES..... 127
3.1.1. Introduction.....127
3.1.2. Celestite.....127
3.1.2.1. Classification.....127
3.1.2.2. Description and interpretation of celest-
-ite subtypes.....130
a. Celestite-with-anhydrite.....130
b. Anhydrite-free celestite.....136
c. Granular celestite.....142
3.1.2.3. Barian celestites.....145
a. Introduction.....145
b. Distribution of Ba in specimen SB07.146
c. Distribution of Ba in Poundhouse
Farm celestite.....146
d. Interpretation.....149
3.1.2.4. Conclusions.....149
3.1.3. Calcite.....150
3.1.3.1. Aphanitic calcite.....150
3.1.3.2. Sparry calcite.....150
a. Description.....150
b. General discussion.....154
c. Epigenetic calcite rock.....155
d. Grey Pseudocubic calcite.....155
3.1.3.3. Conclusions.....156
3.1.4. Dolomite.....156
3.1.4.1. Introduction.....156
3.1.4.2. Description.....156
3.1.4.3. Interpretation.....157
3.1.4.4. Conclusions.....159
3.1.5. Authigenic silica.....159
3.1.5.1. Lozenge quartz and lenticular aggregates.160

a. Description.....160
b. Interpretation.....160
3.1.5.2. Pervasive Megaquartz.....161
a. Description.....161
b. Interpretation.....162
3.1.5.3. Chert.....162
a. Description.....162
b. Interpretation.....163
3.1.5.4. Origin of the geopetal fabric.....165
3.1.5.5. Conclusions.....165
3.1.6. Other minerals present in Type A celestite...166
3.1.6.1. Gypsum.....166
3.1.6.2. Anhydrite.....168
3.1.6.3. High-Sr carbonate.....169
3.1.6.4. Non-ferrous sulphides.....170
3.1.6.5. Amorphous goethite.....170

3.2. PETROGRAPHY OF THE EPIGENETIC CELESTITES.....171
3.2.1. Introduction.....171
3.2.2. Description and interpretation.....171
3.2.3. Conclusions.....177

3.3. PETROGRAPHY OF THE GYPSUM ROCKS.....177
3.3.1. Description of gypsum types.....177
3.3.1.1 Granular macrocellular gypsum.....177
3.3.1.2. Alabastrine gypsum.....178
3.3.1.3. Selenite.....178
3.3.2. Interpretation.....178
3.3.2.1. Granular macrocellular gypsum.....179
a. Anhedral porphyroblasts.....179
b. Granoblastic fabric.....179
3.3.2.2. Alabastrine gypsum: platey porphyroblasts and granoblastic fabric.....179
3.3.2.3. Selenite.....179
3.3.3. Conclusions.....180

CHAPTER FOUR - GEOCHEMISTRY OF THE CELESTITES 181

4.1. INTRODUCTION.....182

4.2. THE ANALYTICAL METHODS.....186
4.2.1. Selection of samples 182
4.2.2. Description of analyses.....185
4.2.3. Comparison of the analytical methods.....186

4.2.4. Conclusions on the applicability of the techniques....198

4.3. STATISTICAL INTERPRETATION OF THE ANALYTICAL DATA....199

4.3.1. Introduction....199

4.3.2. Results....201

4.3.2.1. Population types and significance test...201

4.3.2.2. R-Mode Analysis....201

a. Similarity matrices (assay data)....208

b. Dendrograms (assay data)....212

c. Similarity matrices and dendrograms (presence/ absence data)....212

4.3.2.3. Q-Mode Analysis....217

a. Dendrograms (assay data and presence / absence data)....217

b. Interpretation....221

4.3.2.4. Simultaneous RQ-Mode Analysis of presence / absence data....221

4.3.2.5. Simultaneous RQ-Mode Analysis of presence / absence data and assays/mineral content223

4.3.2.6. Non-linear Mapping....227

a. Method....227

b. Comparison of Non-linear Mapping with Cluster Analysis....229

4.4. INTERPRETATION OF OTHER DATA....229

4.4.1. Comparison of the MAS analyses with those of other celestites....229

4.4.2. Celestite sands and gravels....230

4.4.3. Gypsum....230

4.5. DISCUSSION - THE DISTRIBUTION OF Sr, Ba, Ca, Zn, Na AND K....232

4.5.1. Introduction....232

4.5.2. Strontium....232

4.5.3. Barium and Ba/Sr....234

4.5.4. Calcium, calcite and dolomite contents....237

4.5.5. Zinc....240

4.5.6. Sodium, Potassium and Na/K....243

4.5.7. Other elements....244

4.6. SUMMARY....244

CHAPTER FIVE - THE ORIGIN OF THE CELESTITES 246

5.1. INTRODUCTION....247

5.2. DIAGENETIC HISTORY OF THE CELESTITES AND THE GYPSUM ROCK....247

5.2.1. Diagenetic framework....247

5.2.1.1. Stratigraphic analysis....247

5.2.1.2. Early diagenesis....253

5.2.1.3. Origin of the red celestite....253

a. Light red macrocellular celestite...254

b. Reddish brown impregnations....254

c. Cause of the pigmentation....255

5.2.1.4. Late diagenesis....256

5.2.2. Problems in the diagenetic framework and 'Quaternary' celestites....256

5.2.3. Conclusions....257

5.3. DEPOSITIONAL ENVIRONMENT OF THE CELESTITES...257

5.3.1. Introduction....257

5.3.2. Facies Analysis....259

5.3.3. Sedimentary history of the Yate Bypass celestites....262

5.3.4. Sedimentary history of the Wapley Common celestites....265

5.3.4.1. Source of the silica....268

5.3.4.2. The Wapley Common celestites....268

5.3.5. Sedimentary history of the celestites of the study area and Wapley-Bitton area....270

5.4. SOURCE OF THE STRONTIUM....270

5.4.1. Triassic origin....270

5.4.2. Carboniferous Limestone source....273

5.4.3. Magmatic or hydrothermal source....274

5.4.4. Discussion....275

5.4.5. Conclusions....278

CHAPTER SIX - MINING AND EXPLORATION GEOLOGY 279

6.1. THE GRAIN SIZE DISTRIBUTION OF CELESTITE....280

6.1.1. Introduction....280

6.1.2. Method....280

6.1.3. Distribution of celestite within the Clay Head....287

6.1.4. Distribution of celestite within the Type A celestite gravel....288
6.1.5. Distribution of celestite within the other celestite sands and gravels....289
6.1.6. General conclusions....290

6.2. GEOCHEMICAL EXPLORATION....291
6.2.1. Introduction....291
6.2.2. Sampling technique....291
6.2.3. Analysis....298
6.2.4. Interpretation of the soil assays....299
6.2.4.1. Goose Green West....300
6.2.4.2. Goose Green East....300
6.2.4.3. Winter's Field....301
6.2.5. Dispersion of Sr and Ba....302
6.2.5.1. Strontium....304
a. Yate Formation....304
b. Millstone Grit....305
c. Soils....305
6.2.5.2. Barium....306
a. Rocks....306
b. Soils....306
6.2.5.3. Summary....307
6.2.6. Geostatistical Analysis of the soil data....307
6.2.6.1. Introduction - basic principles....307
6.2.6.2. Application....308
6.2.6.3. Discussion....308
6.2.6.4. Summary....312
6.2.7. The applicability of a stream sediment survey....313
6.2.8. Summary and Discussion....318

6.3. GEOPHYSICAL EXPLORATION....319
6.3.1. Resistivity Survey....319
6.3.1.1. Method....320
6.3.1.2. Results and interpretation....320
a. Goose Green and Tyler's Farm....323
b. The Rectory....323
c. Winter's Field....324
6.3.1.3. General discussion....324
6.3.2. Other Methods....325
6.3.3. Summary....325

6.4. A REVIEW OF CURRENT METHODS OF EXPLORATION AND ASSESSMENT....326
6.4.1. Current Exploration practice....326
6.4.2. Current Assessment practice....326
6.4.3. Critical appraisal of the Exploration and Assessment methods....328
6.4.4. Geostatistical Assessment of the test hole data....330
6.4.5. Conclusions....334

CHAPTER SEVEN - CONCLUSIONS AND RECOMMENDATIONS 336

7.1. ECONOMIC SIGNIFICANCE OF THE CELESTITE DEPOSITS....337

7.2. EXPLORATION FOR AND ASSESSMENT OF CELESTITE DEPOSITS....343

REFERENCES CITED 346

APPENDIX I - GRID REFERENCES OF LOCALITIES AND LOCATION INDEX FOR SPECIMENS REFERRED TO IN THE TEXT 357

APPENDIX II - DETAILS OF ANALYTICAL METHODS: WET CHEMICAL ANALYSIS, BETAPROBE ANALYSIS, QUANTITATIVE XRD ANALYSIS, ANALYSIS OF SOILS 357

II.1 WET CHEMICAL ANALYSIS....358
II.1.1. Sampling Error....358
II.1.2. Sample Preparation....358
II.1.3. Analytical Errors....358
II.1.4. Sodium Carbonate Fusion....359
II.1.5. Hydrofluoric Acid Leach....360
II.1.6. Mixed Carbonate Fusion....360
II.1.7. Lithium Metaborate - Lithium borate fusion...360
II.1.8. Assessment of the wet chemical methods....361

II.2. BETAPROBE ANALYSIS....361

II.3. QUANTITATIVE XRD ANALYSIS....364
II.3.1. Introduction....364
II.3.2. Method....365
II.3.3. Determination of calcite and dolomite content....366

II.3.4. Errors.....366
II.3.5. Effect of Absorption.....368

II.4 CHEMICAL ANALYSIS OF SOILS.....368
II.4.1. Sample Preparation.....368
II.4.2. Nitric Acid Leach.....369
II.4.3. Sodium Carbonate Fusion.....369
II.4.4. Precision.....369

APPENDIX III - EXPLANATION OF BINARY CODED VARIABLES USED TO DESCRIBE CELESTITES OF THE MAIN ANALYTICAL SERIES 370-371

CORRIGENDA

LIST OF PLATES

F. View across the Bristol Coalfield from the Tortworth Ridge at Yate Rocks.....9

2 Exploitation of the celestite..... 9

3. Prismatic crystals of Type B celestite impregnating reddish brown mudstone with dolomite.....41

4. Druse of granular celestite in epigenetic vein celestite.....41

5. Light red macrocellular celestite.....43

6. Section of the face at Tyler's Farm South showing the rhythmic alternations of red and green marl, and celestite seams F, G and H.....50

7. Section through a massive tabular celestite nodule, showing pink colour centres, druses and rim of calcite-cemented marl.....57

8. Typical massive celestite nodule showing celestite of coarse tabular, fine tabular and fine granular habit.....57

9. Section through compact celestite showing colour zoning which transects an earlier 'macrocellular' texture.....61

10. a. Impregnations of white celestite separated by an erosion surface. b. Celestite with ovate drusey macrocells.....63

11. Sections through macrocellular and 'stratified celestites.....64

12. Upper surface of massive pancake celestite showing druses, grooves and flute-like structures and chert/ white celestite crust.....64

13. Sections showing a sparrudite rim surrounding a macrocell of fine white tabular celestite.....66

14. Textures in red and blue celestite: 66

15. Upper surface of celestite showing giant flat lying blue crystal dusted with ochreous dolomite.67

16. Section through dolomitized spararenite and nodule of calcite rock.....67

17. White celestite pervading red marl.....68

18. a. Section of funnel-shaped evaporite block.....68
b. Section of evaporite block showing schistose fabric.....68

19. Section of funnel-shaped evaporite block showing slump structures.....70

20. Section through an evaporite block showing foliation in celestite overgrowths on pink celestite granules with massive quartz.....70

21. Quartz-rich celestites.....71

22. Granular macrocellular celestite.....71

23. Grey pseudocubic calcite in celestite.....75

24. Granular macrocellular gypsum.....75

25. Rocks of the cut-and-fill channel deposit at Goose Green, arranged stratigraphically.....84

26. East face of the celestite working at Winter's Field, showing a vein of celestite in Millstone Grit mudstones breaking up into a 'mumbler deposit' in the overlying Clay Head.....84

27. A typical vein celestite.....94

28. Celestite vein with thick microcrystalline selvedge.....94

29. Section of typical compound vein celestite, showing densely-packed lenticular zones separated by mudstone impregnated with tabular celestite.....96

30. Spheroidal celestite.....96

31. A large spheroidal celestite, with drusey cavity.99

32. A mineralized quartzite from the Yate area, clearly displaying the cross-cutting relationship of the celestite to the earlier iron metasomatism.99

33. Celestite replacing ironstone concretion with selective replacement of hematized mudstone.....104

34. Re-exhumed desert reg with quartzitic sandstone and ironstone debris mineralized with epigenetic nodular celestite.....104

35. The Type B celestite orebody at Goose Green East, looking north.....104

36. Epigenetic celestite vein at the contact of Units 12 and 14, on the north bank of the Yate Bypass cutting, north of Yate.....107

37. A typical alabastrine gypsum nodule from the gypsum zone of the Type C celestite belt at the Yate Bypass site.....110

38. Selenite from near Hall End.....110

39. Detail of south face, Winter's Field, showing celestite sand in Clay Head, overlain by terrace gravels deposits.....103

40. Photomicrograph of Carboniferous Clay Head, showing celestite fragments and mudstone clasts in a hematite, white mica and quartz silt matrix. 113

41. Western pit face at Goose Green West, showing the effects of cryogenic weathering.....119

42. Photomicrograph of celestite sand from Winter's Field.....119

43 Photomicrograph of evaporite block showing lozenge quartz crystals, P3 celestite and overgrowth of S1 celestite.....133

44. Photomicrograph of bent S1 celestite of 'spindle' habit and sparry calcite.....133

45. Photomicrograph of drusey macrocellular celestite showing herringbone texture of S3 celesite in sparry calcite.....134

46. Photomicrograph of fine tabular celestite macrocell, showing mosaic of S3 celestite.....134

47. Photomicrograph of celestite of 'flattened rhombohedron' habit.....135

48. Photomicrograph of microcrystalline macrocellular celestite showing inequigranular mosaic of S5 celestite.....135

49. Photomicrograph of massive tabular celestite showing S6 celestite with belts of anhydrite and gypsum inclusions.....137

50. Photomicrograph of massive tabular celestite showing stacking of P1 celestite in 'pile-of-brick' texture.....137

51. Photomicrograph of light red macrocellular celestite; subtype P2.....139

52. Photomicrograph of compact microcrystalline celestite showing celestite of subtype G1 enclosing smaller crystals of subtype G4 and S3 celestite..139

53. Photomicrograph of medium-grained red and white granular celestite, showing G3 fabric.....140

54. Photomicrograph of fine-grained granular celestite, showing G3 and G4 subtypes.....140

55. Photomicrograph of granular celestite showing mosaic G2 celestite with many inclusions of anhydrite, calcium carbonate and ?gypsum.....141

56. Photomicrograph of barian P1 celestite showing deformed nature of individual celestite laths....141

57. Barian celestite with sparrudite.....148

58. Photomicrograph of indurated marl rim of massive celestite nodule showing syntaxial replacement of micrite clots by sparry calcite.....151

59. Photomicrograph of the erosion surface depicted in Plate 10a.....151

60. Photomicrograph of geopetal fabric in quartz-rich celestite showing veneer of chert and calcite scalenohedra on upper surface of S1 celestite lath in megaquartz mosaic.....153

61. Photomicrograph showing detail of veneer in geopetal fabric.....153

62. Photomicrograph of evaporite block showing 1, microquartz, with fine sparry calcite in marl trails in P3 celestite and 2, spherulites of chalcedony surrounding earlier lozenge quartz.164

63. Photomicrograph of quartz-rich celestite showing pervasive chalcedony in S2 and S3 celestite.....164

64. Photomicrograph of 'wasp-waisted' thick tabular celestite, subtype E4.....173

65. Photomicrograph of microcrystalline vein selvedge , subtype E3 showing characteristic badly-formed laths in hematitic mudstone and quartz silt matrix.....173

66. Photomicrograph of vein celestite replacing colloform, banded hematite-goethite ironstone (subtype E5).....174

67. Photomicrograph of E6 celestite replacing quartz-itic sandstone, showing corroded quartz relics...174

68. Photomicrograph of granular epigenetic celestite, subtype E7, in mudstone host.....176

69. Photomicrograph of granular macrocellular gypsum showing anhedral porphyroblasts poikilotopically enclosing earlier prismatic gypsum.....176

LIST OF FIGURES

1.1 Celestite in Avon and Somerset (from Thomas,1973)..3

1.2 Communications, and general outline of celestite-bearing land in the study area (after Nickless et al., 1976).....5

1.3 The area north-east of Bristol (after Nickless et al., 1976).....6

1.4 The resource categories of the study area (after Nickless et al., 1976).....7

1.5 The geology of the northern part of the county of Avon (based on published one-inch sheets).....12a

1.6 Sketch-map of the area to the north-east of Bristol (after Kellaway and Welch, 1948; Audley-Charles, 1970; Cave, 1977).....16

1.7 Norian paleography of England and Wales (after Audley-Charles, 1970).....17

1.8 Correlation diagram of selected English Norian sequences.....20-21

1.9 Geomorphology of the study area (after Smith, 1963 ; Findlay, 1975).....23

2.1 Celestite occurrences in the study area (after Nickless et al., 1976).....27

2.2 The geology of the Goose-Green - Yate Bypass area to the north of Yate, Avon.....28

2.3 Measured sections through celestite-bearing Triassic strata.....29

2.4 Geological section along A-B in Fig 1.5 (after Cave , 1977).....30

2.5 Geological sketch-map of the Wapley Common site....33

2.6 Geological sketch-map of the West End site.....34

2.7 Geology of the Little Avon Platform (based on published one-inch sheets).....35

2.8 Geological cross-section of the Little Avon Valley near the Post Bridge, Wickwar.....36

2.9 Geological sketch-map of the Poundhouse Farm site..37

2.10 Principal habits of celestite (after Berry and Mason, 1959).....40

2.11 Norian morphological and sedimentological elements of part of the study area.....46

2.12 Semi-quantitative estimates of the gypsum, celestite, sparry calcite and megaquartz content of the evaporites of the study area (compiled from data in Curtis,1974; Nickless et al., 1976; Wood and Shaw, 1976 and current investigation).....53

2.13 The relationship between the three previously recognized celestite types (after Nickless et al., 1976).....55

2.14 Geological cross section of the Goose Green site (X-Y in Fig 2.2).....59

2.15 Massive drusey celestite (sketch of hand specimen GG47).....61

2.16 The Hercynian basement of the Yate Platform.....79

2.17 Sections of the north and south banks of the Bypass cutting at Broad Lane, Yate.....81

2.18 Isometric drawing illustrating the field geology of the Type B celestite orebody at Goose Green, Yate.....83

2.19 Geology of part of the Marle Hills Basin (based on published one-inch sheets).....86

2.20 Geological sketch-map of the Summer Bridge site...87

2.21 Structural interpretation of the Summer Bridge site along section X-Y-Z (Fig 2.20).....88

2.22 Cryoturbation features at the Winter's Field site.89-90

2.23 Geological sections at The Rectory.....100-101

2.24 A 'celestite' of mineralized sandy mudstone.....106

2.25 The effects of cryogenesis on Type C and Type A celestites.....115

2.26 Geological sketch-map of The Rectory site.....120

2.27 Geological sketch-map of the Winter's Field and Yate Court sites.....122

2.28 Geological sketch-map of the Yate Lower Common site.....124

3.1 Temporal relationships between the authigenic minerals of the celestites of the study area.....144

3.2 Sections of celestite specimens PF32 and SB07 showing location of microprobe analyses.....147

3.3 Microprobe point traverse across specimen PF35...148

3.4 Graph showing the compositional range of the microprobe carbonate data.....158

3.5 Formation of the geopetal fabric in Wapley Common celestites (schematic).....167

4.1 Location of celestite specimens along the Yate Bypass cutting.....183

4.2 The study area, showing location of analysed celestites referred to in text.....184

4.3 Comparison of wet chemical and spectrometric methods.....197

4.4 Histograms of assay and mineral content data.....203-207

4.5 Interpretation of the distance coefficent,d (Fig. 4.5b after Davis,1973).....211

4.6 Dendrograms of variables (Pearson coefficent).....213

4.7 Dendrograms of variables (distance coefficent).....214

4.8 Dendrogram of variables of the presence/ absence data.....216

4.9 Q-mode analysis dendrograms for the celestites of the main analytical series.....218-220

4.10 Interpretation of the Yate Bypass celestites by Q-mode Cluster Analysis of assay and mineral content data.....222

4.11 Interpretation of the Yate Bypass celestites by simultaneous RQ-mode analysis of presence/ absence data.....225

4.12 Classification of 95 celestites by non-linear mapping.....228

4.13 Distribution of Sr in the celestites of the study area.....233

4.14 Distribution of barian celestites along the Yate Bypass cutting.....236

4.15 Distribution of Ba in the celestites of the study area.....238

4.16 Variation of the ratio: 100Ba/Sr in the celestites of the study area.....239

4.17 Distribution of calcite and dolomite along the Yate Bypass cutting.....241

4.18 Distribution of Ca in the celestites of the study area.....242

5.1 The Wapley-Bitton area, as defined by Nickless et al., (1976).....248

5.2 Flow diagram showing relationship of gypsum and celestite parageneses.....249

5.3 Regional extent of the celestite (C) and gypsum rock (G) (after Nickless et al., 1976).....250

5.4 Semi-quantitative estimates of the gypsum, celestite, sparry calcite and megaquartz content of the evaporites of the Wapley-Bitton area (compiled from data in Curtis,1974; Nickless et al., 1976; Wood and Shaw,1976 and current investigation).....251

5.5 Borehole logs of the Wapley-Bitton area (from descriptions of borehole cores recorded by Nickless et. al., 1976).....252

5.6 Sedimentary environments of the Norian celestites.260

5.7 Facies of the Yate Formation at Goose Green.....261

5.8 Map showing contours drawn on the sub-Triassic surface (from Cave,1977).....264

5.9 Reconstruction of the sedimentary history of the Yate Bypass area.....266-267

5.10 Reconstruction of the early diagenetic history of the Wapley Common quartz-rich celestites.....269

5.11 The study area and Wapley-Bitton area in Severnside Evaporite Bed times.....271

6.1 The Goose Green area, showing distribution of the soil series (modified from Soil Survey sheet 251) and sample locations.....281

6.2 Cumulate frequency curves of celestite populations283

6.3 Histograms of grain size distribution data.....284-286

6.4 Geochemical plots for the elements at Goose Green West.....292-293

6.5 Geochemical plots for the elements at Goose Green East.....294-295

6.6 Geochemical plots for the elements at Winter's Field.....296-297

6.7 Chemical dispersion of Sr and Ba in the host rocks of the celestites and their soils.....303

6.8 Semi-variograms of the Sr and Ba data of Goose Green West.....309-311

6.9 Sr and Ba in the stream sediments of the study area.(after Webb et al., 1978).....314

6.10 Sr and Ba in some stream sediments of the Wapley-Bitton area.(after Nickless et al., 1976; Webb et al., 1978).....316

6.11 Sr anomalies in the stream sediments of the south Bristol-Mendip district (after Nickless et al., 1976; Webb et al., 1978).....317

6.12 The resistivity traverses at the Rectory, Winter's Field and Goose Green/ Tyler's Farm sites.....321

6.13 Apparent resistivities at the field sites.....322

6.14 The Leechpool area; location of test holes and semi-variograms of yields.....327

6.15 Semi-variograms of the test hole yields of the Poundhouse Farm site.....331

6.16 Semi-variogram of the test hole yields of the Wapley Common site.....332

7.1 Extent of celestite-bearing land in the study area (after Nickless et al., 1976).....338

7.2 Extent of celestite-bearing land in the Wapley-Bitton area (after Nickless et al., 1976).....339

II.1 Interpretation of the uncalibrated data.....363

II.2 Calibration curves for standards (after Cuff,1973)367

LIST OF TABLES

1.1 List of formations in the area north-east of Bristol (after Nickless et al., 1976).....13

1.2 Stratigraphic nomenclature of the Triassic rocks of south Gloucestershire and Avon.....14

2.1 A complete cyclothem of the cyclic facies.....82

3.1a Quantitative electron microprobe analysis of carbonate minerals.....128

3.1b Quantitative electron microprobe analysis of anhydrite.....128

3.2 Quantitative electron microprobe analysis of barian celestite.....129

3.3 Summary of the main features of the 13 Type A celestite subtypes.....131

3.4 Summary of the main features of the 10 Type B and Type C celestite subtypes.....172

4.1 Sodium carbonate fusions and HF acid leach analyses of twenty celestites and concentrates....187

4.2 Sodium carbonate-potassium carbonate fusion analyses of nine quartz-rich celestites from Wapley Common.....188

4.3 Lithium metaborate fusion analyses of four quartz-rich celestites from Wapley Common.....188

4.4 Lithium metaborate fusion analyses of the main analytical series.....189-191

4.5 Composition of twenty-one celestites and celestite concentrates.....192-193

4.6 Composition of nine celestite sands and gravels...194

4.7 Lithium metaborate fusion analyses of seven gypsum specimens.....194

4.8 Calcite and dolomite content of the evaporite mineral fraction of selected celestites as determined by X-Ray Diffraction analysis.....195-196

4.9 Frequency distributions of assays and mineral contents.....202

4.10 Pearson Coefficient correlation matrices.....209

4.11 Distance Coefficient correlation matrices.....210

4.12 The principal R-mode clusters of the presence/ absence data.....215

4.13 Relationship of the R-mode clustering structure to the Q-mode clustering structure for the presence/ absence data.....224

4.14 Relationship of the R-mode clustering structure of the presence/ absence data to the Q-mode clustering structure for the assay data.....226

5.1 Correlation of the calcitic celestites of the study area and Wapley-Bitton area with contemporary shore-line events.....263

6.1 Grain-size parameters of the celestite component of the Clay Head, celestite sands and celestite gravels (from Inman, in Blatt, Middleton and Murray, 1980).....282

6.2 Comparison of Sr estimates.....282

6.3 Details of background soils.....298

6.4 Means of the soil assay distributions.....299

6.5 Variation in test hole yields as shown by replic--ate test holes at the Poundhouse Farm site.....329

6.6 Comparison of expected and actual yields for the West End and Yate Lower Common sites.....329

II.1 Values of the relative standard deviation for four elements.....358

II.2 Precision of the LMF/AAS method.....359

II.3 Relative standard deviation values for seven oxides as determined by Betaprobe analysis.....362

II.4 Mass absorption coefficients of 10 minerals and oxides, calculated from the data of Klug and Alexander (1954).....368

CHAPTER ONE - INTRODUCTION TO THE CELESTITE DEPOSITS

1.1. THE CELESTITE INDUSTRY

1.1.1 History of exploitation and useage

Celestite, the mineral form of $SrSO_4$ also known as celestine or less correctly "spar" or "strontian" is the principal raw source of strontium in the U.K. and has been extracted from localities in Avon and Somerset, in particular the belt of land between Yate and Charfield, for over a century (Fig. 1.1) (Anon, 1960). The mineral was first used in 1890 in desaccharising sugar beet molasses in Germany. At that time many small operators hand-dug the mineral as required, exploiting the richer, purer, superficial deposits. The trade increased and in 1912 the Bristol Mineral and Land Company (B.M.C.) Ltd was founded by a merger of the three principal local celestite merchants, headed by the Pauli family (Threlfall, 1951). Later on the property of strontium to impart a red colour to a flame was realised and the pyrotechnics industry in the U.S.A. became an important market for the mineral. Other applications were in the ceramic, electronics, paint and rubber industries and in the production of caustic soda (Anon, 1960).

In 1969 English China Clays (E.C.C.) Ltd. acquired the company, possibly in anticipation of the increase in demand expected by the growth of new markets in a restructuring of the celestite industry. The company was sold back to a consortium of investors in 1974 and at present produces about 10,000 tonnes of celestite per annum, almost all of which is exported, mainly in the production of colour TV sets and also for the electrolytic purification of zinc. Other applications are in pyrotechnics, and the manufacture of ferrite magnets, ceramics, fertilisers and toothpaste.

There is no shortage of demand for celestite, but the mineral is only of medium value so that not all of the known English celestite occurrences in Avon and Somerset can be profitably mined. Only the deposits of the Yate-Cromhall area have been systematically exploited to date (Fig. 1.1). Other economic deposits of celestite occur in Mexico and Spain.

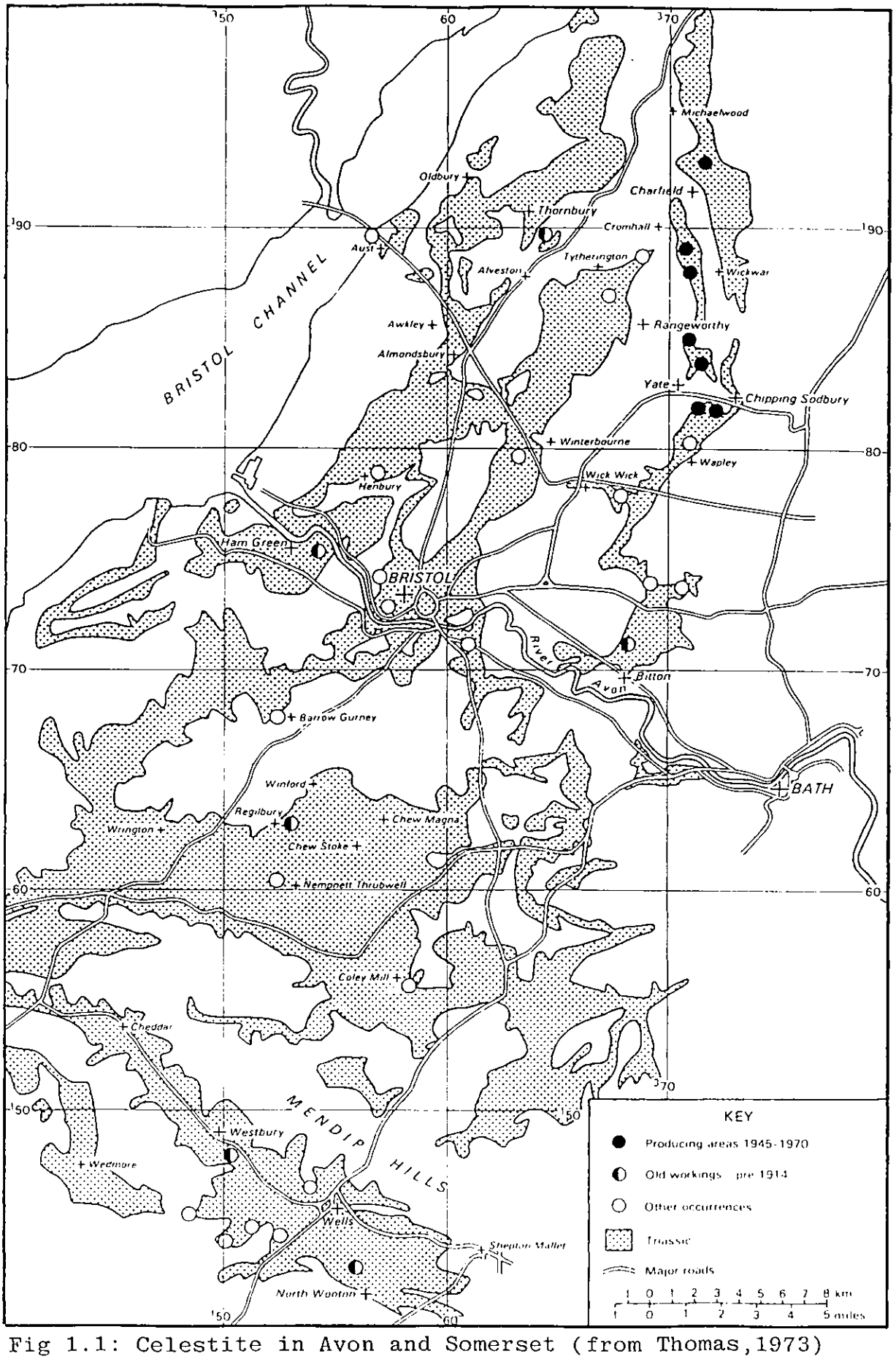

Fig 1.1: Celestite in Avon and Somerset (from Thomas,1973)

1.1.2 The extent of the resource

Little was known about the extent of celestite reserves in what was then southern Gloucestershire until a Celestine Conference, held in 1951, recognised areas of proven, probable and possible reserves (Fig. 1.2). Prior to this the industry itself had undertaken little exploratory work being content to work the celestite, as encountered, in the narrow belt of land between Yate and Cromhall. Later in 1970, the Department of the Environment, concerned about the sterilization of celestite-bearing land by urbanization, commissioned an Institute of Geological Sciences survey which was subsequently published by Nickless et al. (1976). These workers prepared a 1:25,000 resource sheet showing the extent of the celestite resource, in the area to the north-east of Bristol (Fig. 1.3) as well as order-of-magnitudes estimates of the tonnage of celestite expected. Part of the resource sheet showing the hypotheoretical, inferred and indicated resource categories is redrawn in Fig. 1.4. The aim of this survey was to provide a guide for the planning of local authorities and not to prove celestite reserves for the industry, and its findings at a field level have not always corresponded with the observations (or expectations) of the mineral extractors.

1.1.3 Mining and Processing

The means of exploiting and treating the recovered celestite remain basically the same as those described by Anon (1960). A full account of the quarrying and processing operations is given in that work, but are summarised below.

After the presence of an economically viable celestite deposit has been established, mainly by the excavation of test holes during the exploration stage, the top-soil to a depth of 30cm is first removed by bulldozer from the entire site, usually a field of surface area 1-4 Ha.

The mineral is usually found near the ground surface as nodules or blocks in weathered clay and mudstone so that separation from the host rock is easily accomplished, greatly simplifying the extraction of the ore. At present

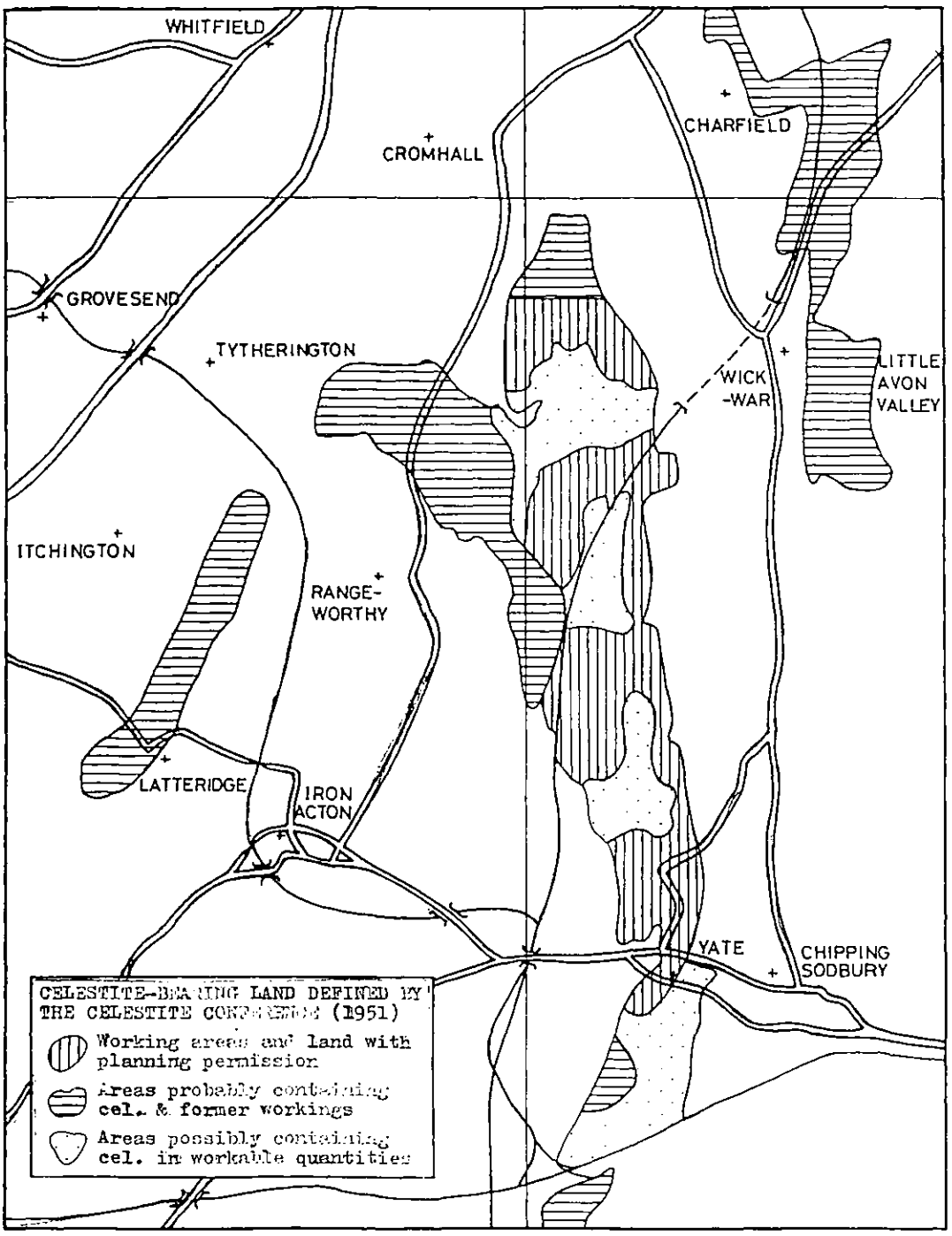

Fig 1.2: Communications, and general outline of celestite -bearing land in the study area (after Nickless et al., 1976)

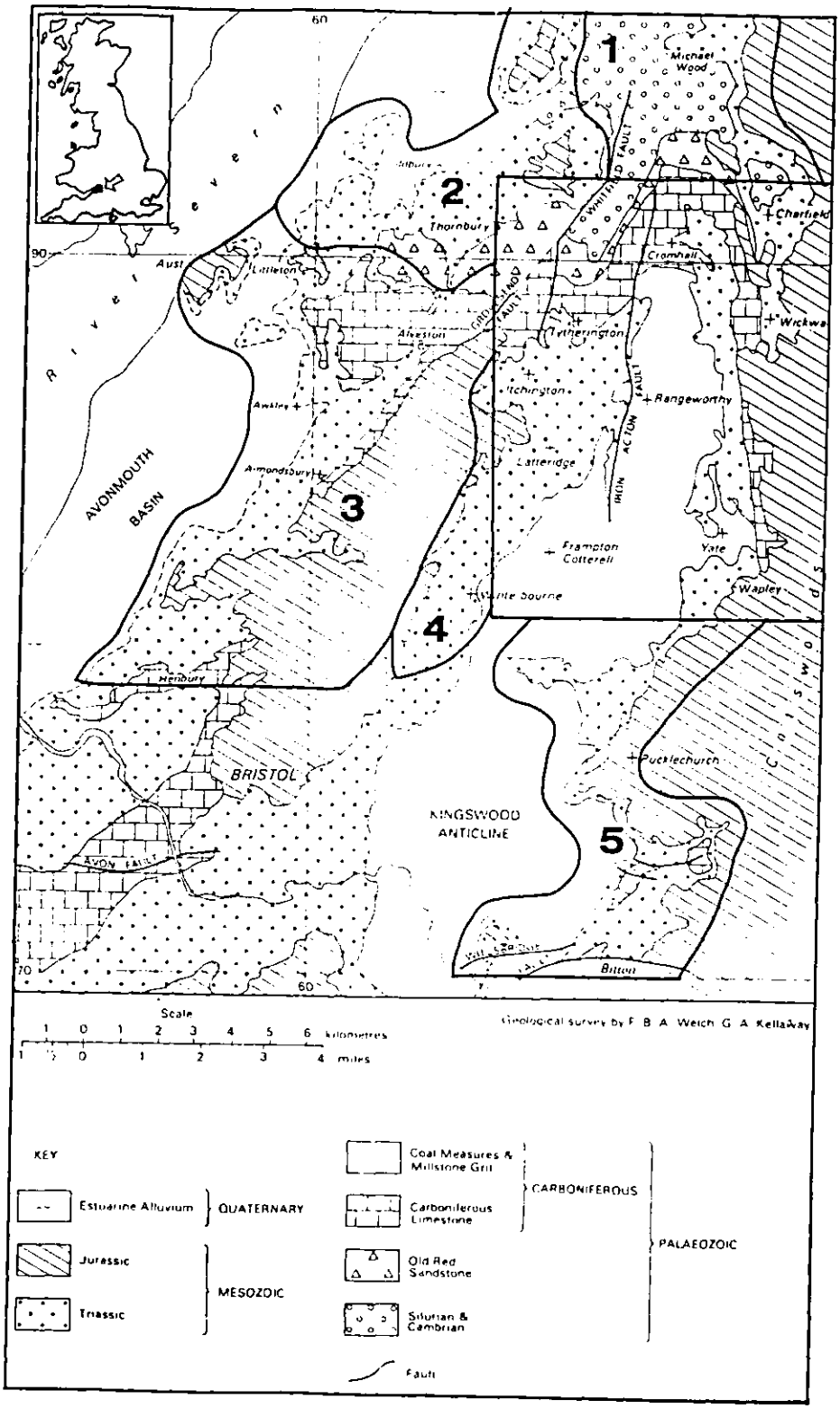

Fig 1.3: The area north-east of Bristol, showing celestite -bearing areas 1-5 (Nickless et al., 1976) and location of the study area (after Nickless et al., 1976)

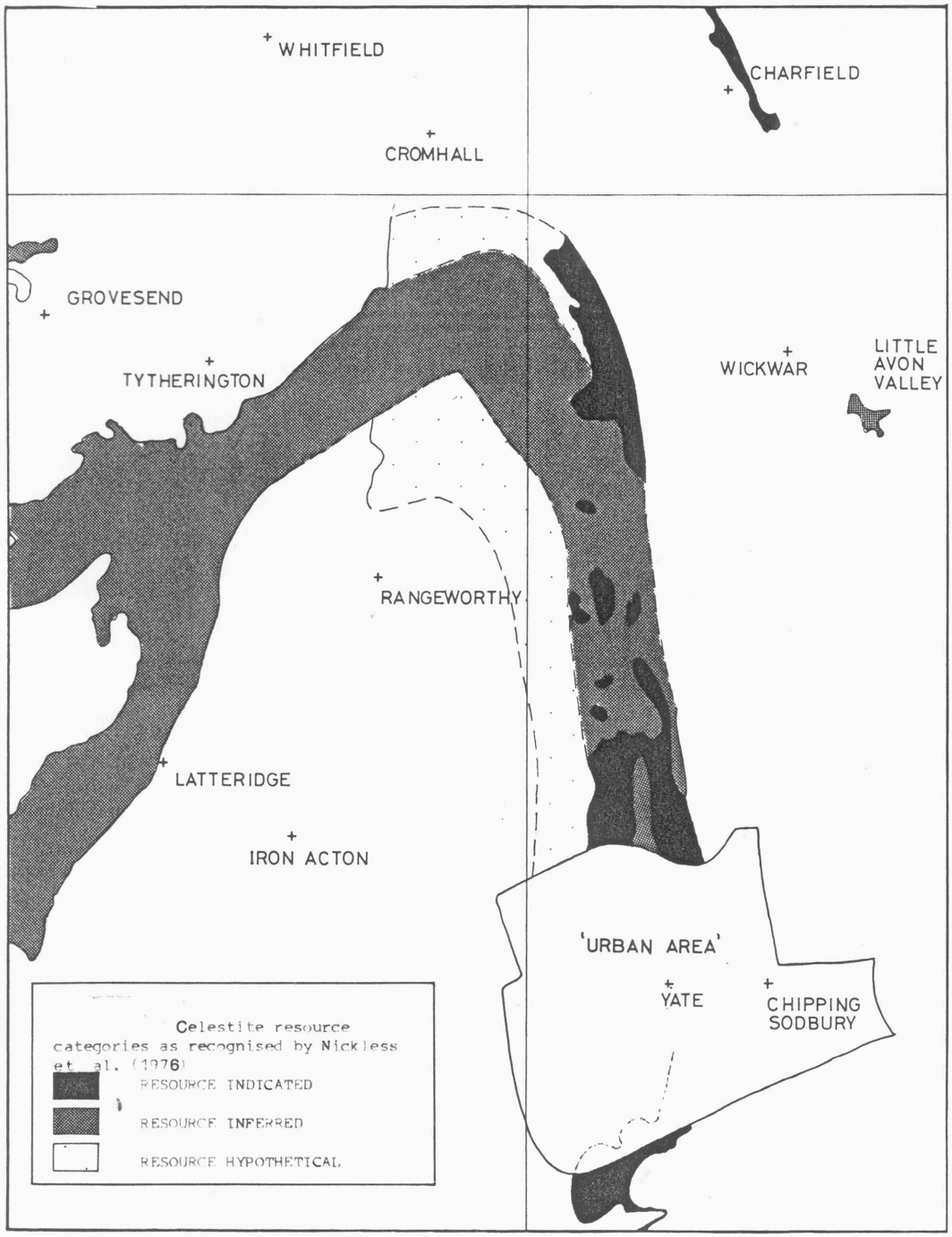

Fig 1.4: The resource categories of the study area (after Nickless et al., 1976)

there are two different methods of mining the celestite. The first traditional method is to quarry pits in the bedrock by the successive excavation of slices by tracked mechanical shovels (Traxcavators). The celestite dug during this process is carried away from the face and tipped on a sloping track on a spoil heap at the opposite end of the pit where it is hand sorted and collected in the centre of the track as a "row". As handpicking proceeds the Traxcavator removes any overburden in preparation for the next shovelload of ore (Plate 2). When about 50-60 tonnes of celestite has been collected in this manner the ore is transferred by the Traxcavator to a haulage truck and ferried to the washing plant at the Hall End site.

An alternative more recent innovation is to employ a Himac front-hoe bucket excavator to dig smaller trench-like excavations. The celestite and clay or mudstone is quarried from the face, tipped and hand sorted on the stripped ground surface by the side of the machine and collected on a circular stock-pile to be removed at intervals, as before. This technique is particularly applicable where the celestite occurs as large nodular masses and a minimum of hand sorting is needed.

In both methods backfilling is concomittant with excavation so that at the end of the life of the site a minimum of restoration work is required other than the reinstatement of the top-soil.

At the Hall End plant the run-of-mine ore is crushed, washed, sized, de-watered and stock-piled as a -3/4 in. gravel. Quality control is effected at the hand-sorting stage, and by periodic analysis of the concentrate. The product is marketed as a +95% $SrSO_4$ gravel and also as a -240 mesh powder, milled and bagged as required. Finally the celestite product is transported to Sharpness docks for shipment overseas.

1.2 HISTORY OF RESEARCH

The earliest reference to celestite in either Somerset or southern Gloucestershire (now known as Avon) can be found in Nicholson's Journal for 1799. In 1822, Sutcliffe

Plate 2: Exploitation of the celestite. The 'row' of celestite nodules is hand-sorted (foreground) while the Traxcavator removes overburden from the face (R.H. side). Note alignment of flame structures in green marl down-slope under lighter coloured layer of comminuted marl.

reported "strontian earth" at Bedminster Bridge, Bristol (Sutcliffe, 1822). Slowly many occurrences of the mineral came to be known, and celestite was recorded by Buckland and Conybeare(1824), Weaver(1824), Collie(1879) and Smithe(1892) In 1902 Baker (1902) suggested that the Yate-Cromhall celestites and the occurrences north of Wickwar had formed from precipitation in two lakes.

Sherlock and Smith (1918) gave the first full account of the properties, uses, geology and distribution of celestite. At this time many small pits had been opened up in the Yate-Cromhall district. In a later edition (Sherlock and Hollingworth, 1938), Sherlock proposed that the celestite had formed from the influx of strontium salts in a river flowing into the Newark Gypsum sea at Yate. Post-war quarrying of the celestite was described by Anon (1960).

The 1970s saw a renewal of interest in the geology of the celestites. Thomas (1973) published a major review of the celestite deposits and also suggested that the celestite mineralisation may be genetically related to the base metal mineralisation of the Mendip area. Wood and Shaw (1976) studied the geochemistry of the celestites of Avon and concluded that the celestites had formed in an arid inland basin from Sr released during the dolomitization of Carboniferous Limestone. Finally Nickless, Booth and Moseley, having previously published an abstract of their findings (Nickless et al. 1975) produced the report referred to in 1.1.2 (Nickless et al., 1976). These workers suggested that the celestite had formed in a sabkha environment; in some cases by the replacement of nodular calcium sulphate minerals.

1.3 OBJECTIVES OF THE PRESENT STUDY

The project commenced in 1978 as a response to the Bristol Mineral Company Ltd.'s request for professional assistance on the locating of economic celestite deposits, quality control of the extracted celestite and the estimation of recoverable reserves. Thus at the commencement of the study the following objectives were defined: -

1) To follow up the geochemical soil survey of Nickless et al. (1976) to see if this can be applied at a larger

(field)scale and to investigate the feasibility of applying geophysical prospecting techniques to the exploration of celestite.

2) To make an economic assessment of known celestite deposits. As the processing of the ore involved rather specialized aspects of mineral technology it was decided to relinquish this aspect of the assessment to other investigators, consequently work on the processing of celestites appeared by Alanby (1979), Altounyan (1979) and Page (1980).

3) To investigate the geology and mineralogy of the celestite deposits with an aim to improving quality control.

An interim report identified seven further topics in which more work was required: -

1) A study of the Quaternary Geology of the region and the distribution of the periglacially reworked deposits.

2) More detailed petrographic work on the different mineral associations and lithofacies.

3) Further study on the breakdown of the celestite in the soil.

4) Further assessment of the soil data.

5) The dispersion of the celestite in the stream sediments of the region, and the use of stream-sediment sampling to indicate celestite deposits.

6) The use of the Portable Isotope Fluorescence Spectrometer (P.I.F.) as an assay tool in celestite analyses.

7) The application of test hole yields in assessing tonnage estimates.

The work is chiefly concerned with more recent exposures than those recorded by Nickless et al. (1976) and is based upon an investigation of the celestite deposits of the Goose Green, Cooper's Field, Winter's Field and Yate Court sites of the B.M.C. Ltd.; an assessment of the exploratory work at the Wapley Common, Poundhouse Farm, Summer Bridge, Yate Lower Common and West End sites; mapping of the strata exposed during the excavation of the

Yate Bypass and of house foundations at The Rectory, Yate and further fieldwork in the Little Avon valley and at Yate.

The area of interest was selected to include the most northerly and southerly of these new deposits, the Poundhouse Farm and Wapley Common sites respectively. Its western and eastern limits are of necessity fixed by areas of Jurassic rocks where the overburden increases to subeconomic depths (> 9m). The study area, as defined, includes the Yate-Cromhall area, most of the Tytherington-Winterbourne area, and smaller fragments of the Thornbury-Oldbury, Michaelwood-Wickwar and Wapley-Bitton areas as recognised by Nickless et al. (1976) (Figs 1.3, 1.4 and 1.5).

Six-figure grid references of all the main localities are listed in Appendix I, together with the key of the prefix nomenclature used to describe specimens illustrated throughout the account.

1.4 Geological background

The geological history of the area to the north-east of Bristol is now briefly described. It may be divided into four main episodes (E1-E4) (Fig. 1.3, Table 1.1).

E1 The deposition of the Paleozoic sediments

The Paleozoic deposits consist essentially of a sequence of Cambrian, Silurian and Devonian shelf sea sediments whose deposition was interrupted in Llandoverian and Upper Old Red Sandstone times by a period of uplift, largely due to Caledonian movements along the Lower Severn and Bath axes (Kellaway and Welch, 1948). The sequence from the Upper Old Red Sandstone to the Supra-Pennant is considered to be the result of the gradual infilling of a former terrestial basin by a continuing marine incursion (Cave, 1977).

E2 The Hercynian orogeny and deposition of the Triassic Formations (Table 1.2)

In early Permian times the area was affected by Hercynian tectonism. Although the trend of the deformation

Fig 1.5 : The Geology of the northern part of the County of Avon (based on published one-inch sheets 250,251,264 and 265)

0 1 2 3

SCALE IN KM

KEY

- QUATERNARY (First Terrace only)
- JURASSIC
- TRIASSIC: RHAETIC
- TRIASSIC: TEA GREEN MARL
- TRIASSIC: KEUPER MARL (S.E.B.= Severnside Evaporite Bed)
- TRIASSIC: KEUPER SANDSTONE
- TRIASSIC: DOLOMITIC CONGLOMERATE
- SANDSTONES IN BELOW
- SP SUPRA-PENNANT MEASURES
- SANDSTONES IN BELOW
- P PENNANT MEASURES
- SANDSTONES IN BELOW
- LM LOWER AND MIDDLE COAL MEASURES
- MG MILLSTONE GRIT
- CARBONIFEROUS LIMESTONE
- D DEVONIAN
- LP LOWER PALEOZOIC
- PRINCIPAL FAULTS

LOCALITY KEY

CF: Cooper's Field; CH: Poundhouse Farm,Charfield;GG: Goose Green; LA: Little Avon Valley; LC: Lower Common; LP: Leechpool; NC: New Courthouse; RI: The Ridgeway; SB: Summer Bridge; SI: Swan Inn; TF: Tyler's Field; WE: West End; WF: Winter's Field; WN: Wellstead Farm/Nursery; WP: Wapley; YB: Yate Bypass; YC: Yate Court

		DRIFT	
Quaternary	Recent & Pleistocene		Alluvium Terrace Gravels Estuarine Alluvium Head Deposits
		SOLID	
	Jurassic	Lias	White and Blue Lias
Mesozoic		Rhaetic	Cotham Beds Westbury Beds
	Triassic		Tea Green Marl Keuper Marl
		Keuper	Dolomitic Conglomerate Butcombe Sandstone
		Major unconformity	
		Upper Coal Measures	Supra-Pennant Measures Pennant Measures
	Carboniferous	Lower & Middle Coal Measures	
		Millstone Grit Carboniferous Limestone	Quartzitic Sandstone Group
Paleozoic		Upper Old Red Sandstone	Tintern Sandstone Group Quartz Conglomerate
	Devonian	Major unconformity	
		Lower Old Red Sandstone	Thornbury Beds
	Silurian	?Ludlow Series Wenlock Series Llandovery Series	
		Major unconformity	
	Cambrian	Tremadoc Series, including	Micklewood Beds

Table 1.1: List of formations in the area north-east of Bristol (after Nickless et al., 1976)

*- Note classical nomenclature for Triassic.

EUROPEAN STAGE NAME		CLASSICAL NOMENCLATURE		LITHOSTRATIGRAPHIC CLASSIFICATION PROPOSED BY WARRINGTON ET. AL. (1980)	
TRIASSIC	RHAETIAN	LIAS	APPROXIMATELY 5m OF LOWER LIAS	PENARTH GROUP	LISTOCK FORMATION
		RHAETIC	COTHAM BEDS		
			WESTBURY BEDS		WESTBURY FORMATION
	NORIAN	KEUPER	TEA GREEN MARL	MERCIA MUDSTONE GROUP	BLUE ANCHOR FORMATION
			KEUPER MARL		UNDEFINED IN S.W. GLOUCESTERSHIRE, AVON, GWENT, DYFED AND GLAMORGAN
			CELESTINE BED		
			DOLOMITIC CONGLOMERATE		MARGINAL DEPOSITS
	PART OF CARNIAN		BUTCOMBE (KEUPER) SANDSTONE		BUTCOMBE SANDSTONE MEMBER

Table 1.2: Stratigraphic Nomenclature of the Triassic rocks of South Gloucestershire and Avon.

was regionally east-west, in the north of the area the deformation was locally influenced by the lower Severn and Bath axes producing the northerly trending Avonmouth Basin and Bristol Coalfield Syncline. The latter forms the principal structure of the study area and plunges south, away from the intersection of the two axes.

Faulting accompanied the Hercynian earth movements, producing east-west trending faults in the south of the area and also rejuvenating earlier north-south faults of Caledonide origin in the north.

Erosion of the Hercynian Mountain range occurred throughout the Permian up to late Carnian times to produce a landscape roughly similar to that illustrated in Fig. 1.6. The area shown in Fig. 1.6 between the Mendip Hills in the south, the Caledonian massif of the Welsh Uplands to the north-west and the line of the Bath Axis to the east formed an area of positive relief in marked contrast to the slowly subsiding Permo-Triassic basins to the south and east in which thick deposits of sediment were accumulating (Kent 1949, Wills 1976, Audley-Charles 1970).

Fig. 1.6 shows that the structurally positive area described above consisted of an arcuate belt of hills composed mainly of beds of the Carboniferous Limestone series flanked by pediments of gradually sloping land labelled as 'Platforms' in Fig. 1.6, underlain by, on the outer edge of the parabola, older Devonian, Silurian and Cambrian strata and inside the limestone range, Millstone Grit and Coal Measures rocks, mainly mudstones from which the interbedded quartzite sandstones stood out as ridges. The destruction of the sandstone and mudstone core of the Bristol Coalfield Syncline leaving the outer 'shell' of limestone hills could only have occurred under conditions of desert weathering (Kellaway and Welch, 1948), further evidence of which is supplied by the reddening of the Paleozoic rocks by iron metasomation (Kellaway, 1967).

Subsidence over the Michaelwood and Little Avon platforms was at a slower rate than inside the parabola (Cave, 1977). These two areas may have been separated by a narrow strip of high ground (Fig. 1.7). By way of

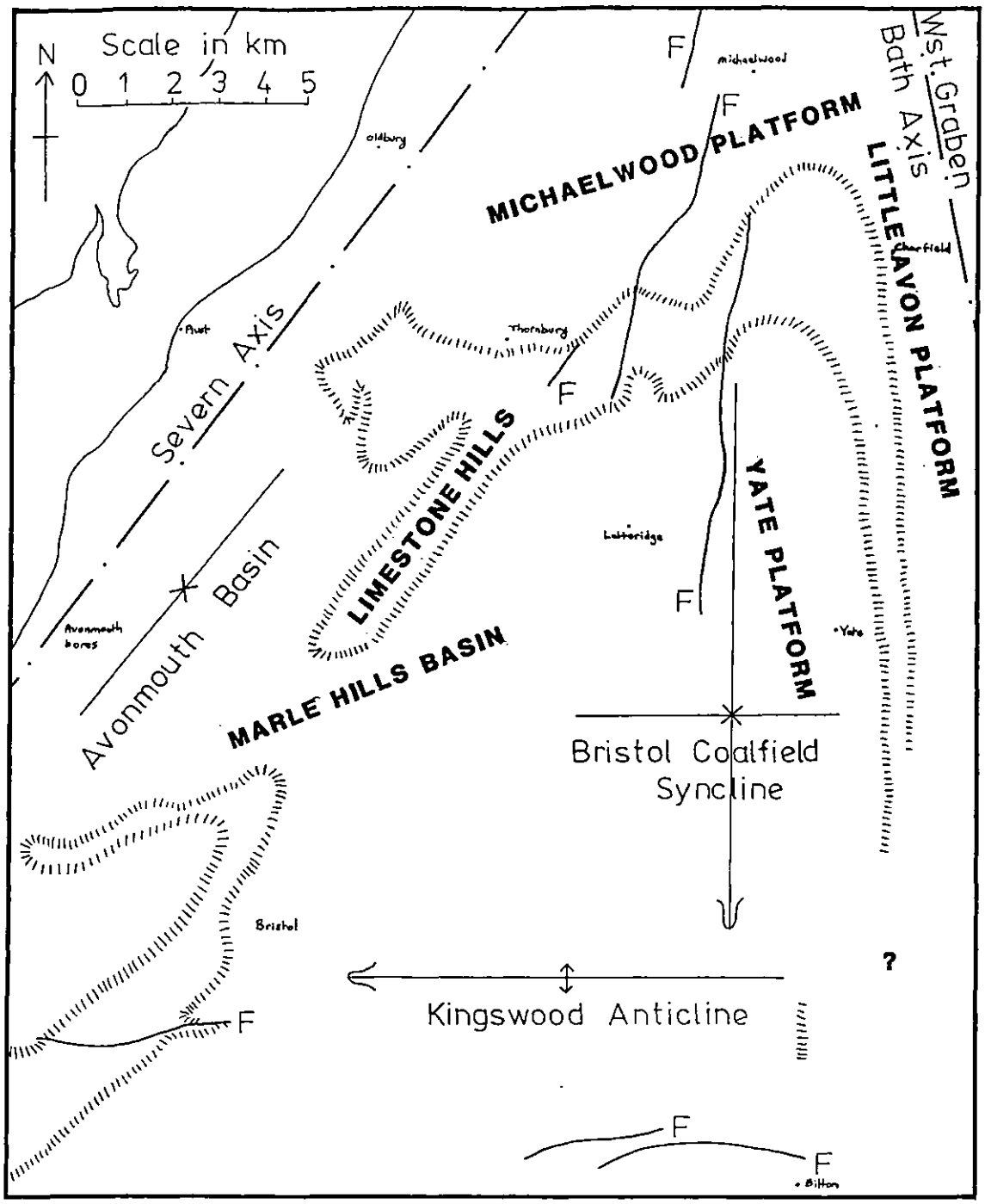

Fig 1.6: Sketch map of the area to the north-east of Bristol, showing the structural fabric of the Hercynian basement (faint) and major features of Norian geomorphology (heavy) (after **Kellaway and Welch, 1948;** Audley-Charles, 1970 and Cave, 1977)

Key: F= fault, ?= structure unknown

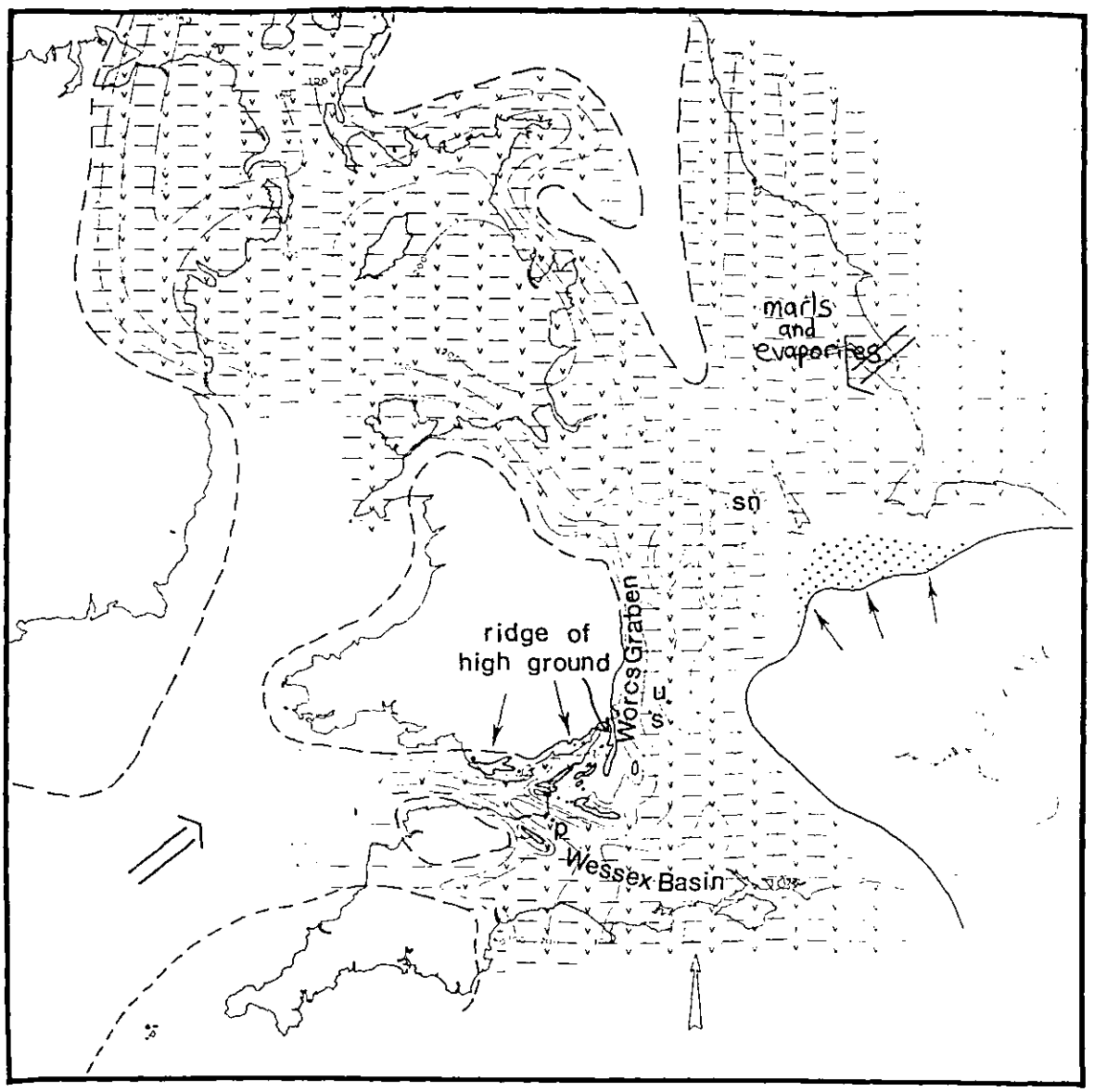

Fig 1.7: Norian paleogeography of England and Wales (after Audley-Charles, 1970).
Key to boreholes: p- Puriton, s- Stowell Park, u- Upton.
sn- South Nottinghamshire district

contrast, 130m of Triassic sediments accumulated where the Marle Hills Basin breaches the limestone ridge (Fig. 1.6).

In the area under review the Permo-Triassic weathering did not produce peneplanation. At the end of the Carnian, before a base-level plain was established, an inland sea or lake started to encroach over the topography burying successively higher morphological features until in Rhaetian times only small isolated pinnacles of the Carboniferous Limestone hills projected through the sedimentary cover. According to Cave (1977) the transgression took place from the south-west, north-west and east. The reconstruction by Audley-Charles (1970) of the geomorphology at this time shows a narrow cuvette extending from the Bristol Channel area through the gap occupied by the Marle Hills Basin, suggesting that the south-west transgression took advantage of this feature. The basal sandstones of the Butcombe Sandstone Member, the stratigraphic equivalent of the Arden Sandstone of the West Midlands (Warrington et al., 1980) are found at this locality; their environmental interpretation is uncertain.

During this time three main sediment types were deposited in the area.

Alluvial fans of coarse-grained limestone and sandstone detritus began to accumulate at the foot of the Carboniferous Limestone hills forming the 'marginal deposits'. Fine-grained siliclastic and carbonate sediments, washed down from the hills by ephemeral streams and winnowed from the alluvial fans by strong desert winds were reworked by the incoming water body and deposited as 'marls'.

During periods of high aridity the transgression was momentarily halted and evaporites formed along the shore line in small depressions cut off from the main body of water and also in the sediment itself. It was during such intervals that the celestites were deposited at various levels, including the horizon known as the Stoke Park Rock Bed (Kellaway, 1961), Celestine Bed (Welch and Kellaway, 1961) or Severnside Evaporite Bed (Nickless

et al., 1975). One form of celestite replaced a bed of calcium sulphate minerals (Nickless et al., 1975) which persist at some localities as alabastrine gypsum and can be traced, as the Newark Gypsum horizon (Sherlock and Hollingworth, 1938) some 170km north-east into Nottinghamshire (Fig. 1.8). Other types of celestite directly crystallized on the surface of the Paleozoic rocks, uppediment of the bedded deposits and thus provide additional evidence for the nature of the late-Carnian transgression.

The 'continental' Triassic deposits are capped by the green marls of the Blue Anchor Formation. It is generally accepted that these sediments indicate reducing conditions as precursors of a later shelf sea in episode E3 (Kellaway and Welch, 1948 ; Cave, 1977).

E3 The Mesozoic marine transgression

From the Rhaetian to Oxford Clay times the area became once again submerged and a thick cover of sandstones, clays and limestones was deposited, interrupted by periodic uplift along the Bath Axis (Kellaway and Welch, 1948).

E4 Tertiary Erosion and Quaternary disturbances

From about middle Tertiary times renewed uplift and easterly tilting caused the Mesozoic cover to be eroded back to the Cotswolds scarp, exposing successively lower formations on a remarkable series of erosion levels (Trueman, 1938, Smith, 1963): marine or subaerial erosion surfaces formed when the sea stood at relatively higher levels than the present day (Trueman, 1938). Smith (1963) has shown that a 60-85m surface levels most of the strata of the study area at the level of the Triassic unconformity, subsequently re-exhuming the celestite deposits (Fig. 1.9). Smith (1963) dated the surface as of Lowestoft Glaciation age but could not decide whether marine denudation or subaerial base levelling was the agency responsible.

Up to now, no evidence for glacial till has been reported from the area and it is generally accepted that during the Quaternary glaciations the South Wales ice sheets did not cross the Bristol Channel. However the

Fig 1.8: Correlation diagram of selected English Norian sequences.

STUDY AREA

a. Aust G.R. ST572810 (from Curtis,personal communication)

b. Poundhouse Farm ST720916 (simplified from Fig 2.3)

c. Tortworth Copse ST716926 (simplified from Fig 2.3, from Nickless et al., 1976)

OTHER AREAS

d. Stowell Park, Wiltshire SP084118 (from Green and Melville , 1956)

e.Upton, Oxfordshire SP232131 (from Worssam, 1963)

f.Southern Nottinghamshire, generalized succession (after Elliot, 1961)

KEY

Evaporite minerals: a- alabastrine gypsum, c- calcite, s- celestite, d- dolomite

Lithologies: dark banding- green beds, dark vertical streaking- variegation, dark spotting- mottles

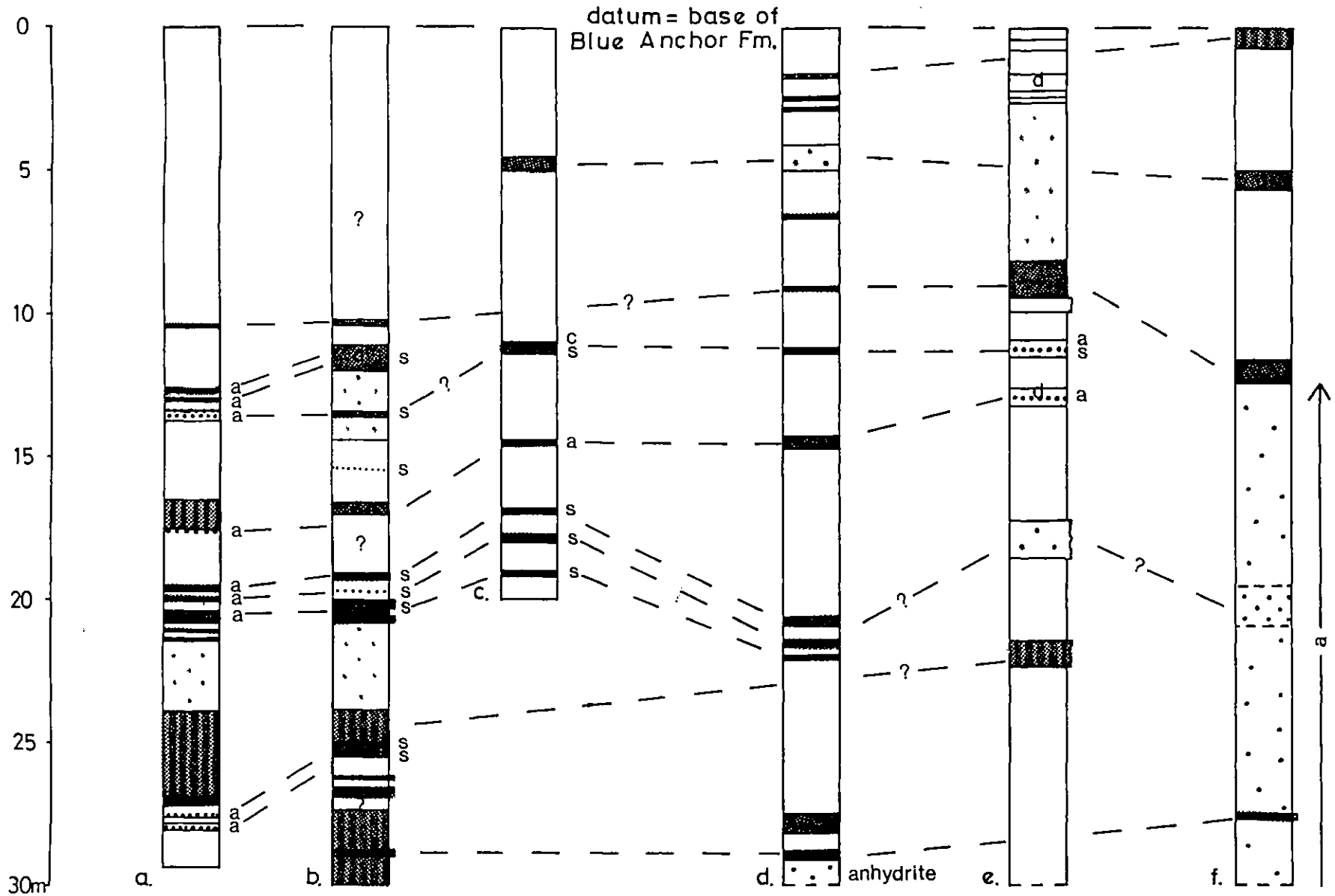
datum = base of
Blue Anchor Fm.
0
5
10
15
20
25
30m
a.
b.
c.
d.
e.
f.
anhydrite
a
s
c
d
?

area was still affected by surface deformation produced by periglacial weathering. Sections in celestite quarries and clay pits usually show frost shattering and cryoturbation, associated with the formation of in-situ head deposits. Finally Drift deposits of terrace gravels, taele gravels and alluvium were laid down in the area. The main morphological elements of the study area as recognised by Findlay (1975) are shown in Fig. 1.9.

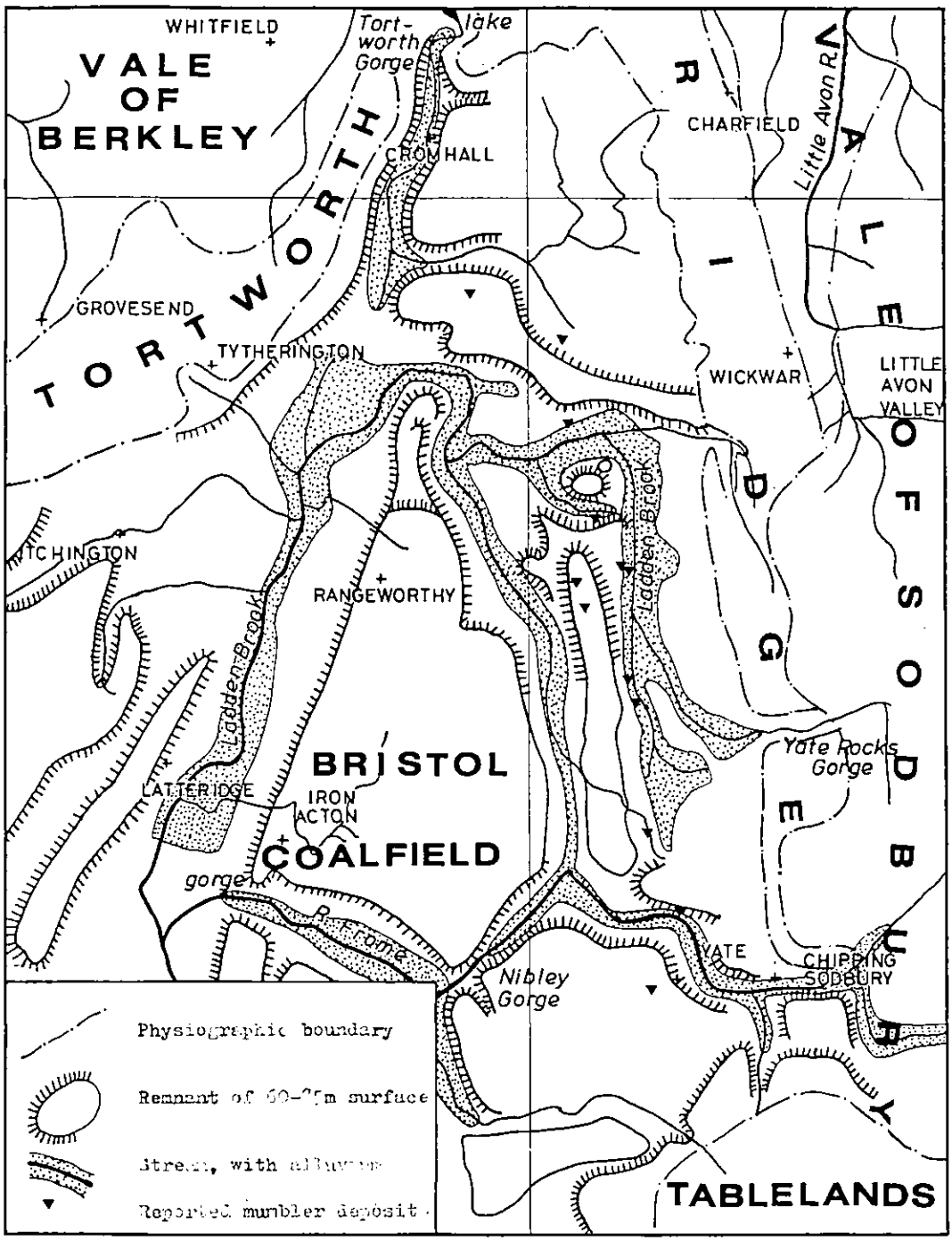

Fig 1.9: Geomorphology of the study area (after Smith, 1963; Findlay,1975)

CHAPTER TWO - THE NATURE AND OCCURRENCE OF THE CELESTITE DEPOSITS OF THE STUDY AREA

2.1 INTRODUCTION

Celestite is found in Triassic 'Keuper Marl' sediments which outcrop over much of the Somerset-Avon area (Fig. 1.1) and in the Yate-Cromhall area in sediments of the Millstone Grit series. Thomas (1973) proposed a classification of the deposits which was later modified by Nickless et al. (1976) to include three main types:-

1) Type A celestites are nodular and disseminated celestites typically 10 to 15m below the 'Tea Green Marl' at the top of the Keuper.

2) Type B celestites are nodular and disseminated celestites at the unconformity of the 'Keuper Marl' and underlying Paleozoic rocks (mainly Millstone Grit).

3) Type C celestites occur as veins, sheets and vuggy infillings in Millstone Grit series rocks beneath the present or former cover of Keuper Marl. In some instances celestite may form the matrix in a breccia of Paleozoic material. (Nickless et al. (1976) also included some Keuper Marl celestite in this category.)

The Type B and Type C celestites are known collectively as 'epigenetic celestites' for unlike the Type A celestites they are younger than their host.

In addition two further types of celestite have been identified in this study, both resulting from the reworking of the epigenetic celestites. Type D celestites, or mumbler deposits, are frost-shattered blocks ('mumblers') of periglacially disturbed Type C celestites in reconstituted Millstone Grit mudstone or 'Clay Head'. Celestite sands and gravels are locally developed over the epigenetic celestites and, in some cases, over the Type A celestites.

2.2 STRATIGRAPHY OF THE CELESTITES

2.2.1 Introduction

During the survey of the country south of the study area, the Geological Survey mapped a single horizon of bedded celestite (the Celestine Bed) in a prominent green calcareous sandy Triassic mudstone at a height of 10-15m below the base of the Blue Anchor Formation, as far north as Wapley (Fig. 1.3). Kellaway (1961) mapped

the equivalent Stoke Park Rock Bed in the Triassic strata north-east of Bristol to approximately 1.5km north of Winterbourne (Fig. 1.3). Later, Nickless et al. (1975, 1976) included these two beds into a unit which they named the Severnside Evaporite Bed and were able to correlate with equivalent beds in the study area (Fig. 2.1) and beyond, to include the evaporites at Aust Cliff and Michaelwood (Fig. 1.3). The Severnside Evaporite Bed was not formally defined, being referred to as an evaporite-bearing sequence of marl up to 2m thick. It was not mapped south of Yate to the Summer Bridge district as in this region Nickless et al. (1976) considered that only Type B and Type C deposits occurred (Fig. 1.5). However, at Goose Green, Yate Bypass (Fig. 2.2, 2.3) eight celestite seams occur at up to 7m above the Triassic unconformity which are clearly of Type A celestite.

The epigenetic celestites of the Yate-Summer Bridge region lie in Triassic marginal deposits, Millstone Grit and Lower Coal Measures sediments along an arcuate belt, 1-2km in diameter (Fig. 2.1) (Anon, 1960; Nickless et al., 1976). Although Nickless et al. (op. cit.) were able to distinguish a regional control producing larger deposits of Type C celestite in the heavily fractured rocks on the hinge of the Bristol Coalfield Syncline the distribution of celestite within this belt is still complex. At a smaller scale, celestite preferentially occurs in mud-stones adjacent to quartzitic sandstone beds.

Fig. 2.4 shows the relationship of the Type A celestites to the epigenetic celestites along a N-S section of the study area. The interpretation of this figure is critical to the understanding of the origin of the deposits for it shows that <u>the distribution of both forms of celestite is stratigraphically controlled</u>, for if the celestites were a shore-line deposit of a marginal facies then all of the Paleozoic rocks would be mineralized and this is clearly not the case. Instead <u>the Type C celestites are restricted to the area of land underlain by Paleozoic rocks that were exposed and overstepped by the Severnside Evaporite Bed at the time of Type A celestite formation</u>.

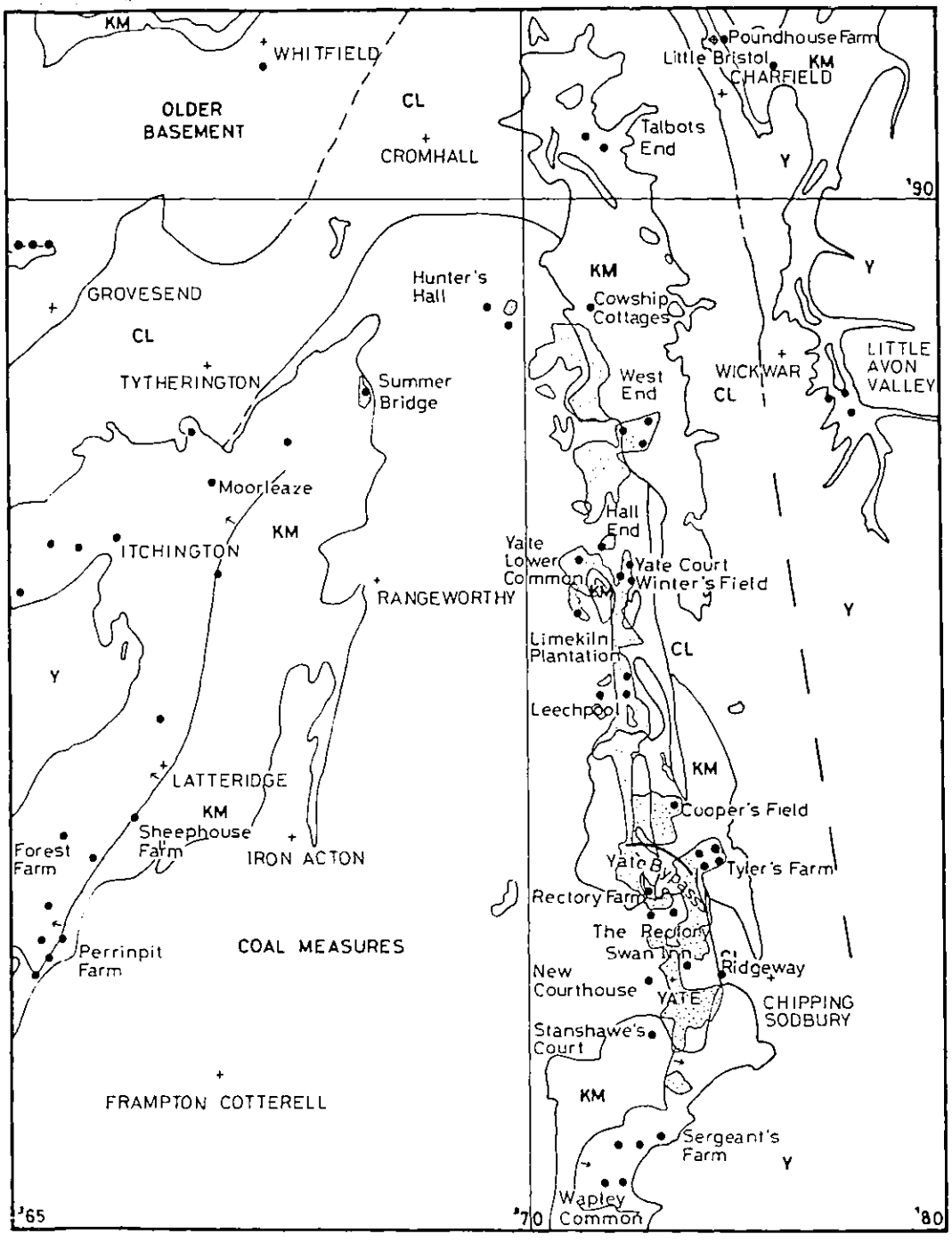

Fig 2.1: Celestite occurrences in the study area
Geological legend: CL- Carboniferous Limestone; KM- Keuper Marl or Yate Formation; Y- mainly younger strata. Severnside Evaporite Bed outcrop shown by unbroken line, with dip. Stippled- extracted areas up to 1.12.80 (after Nickless et al., 1976)

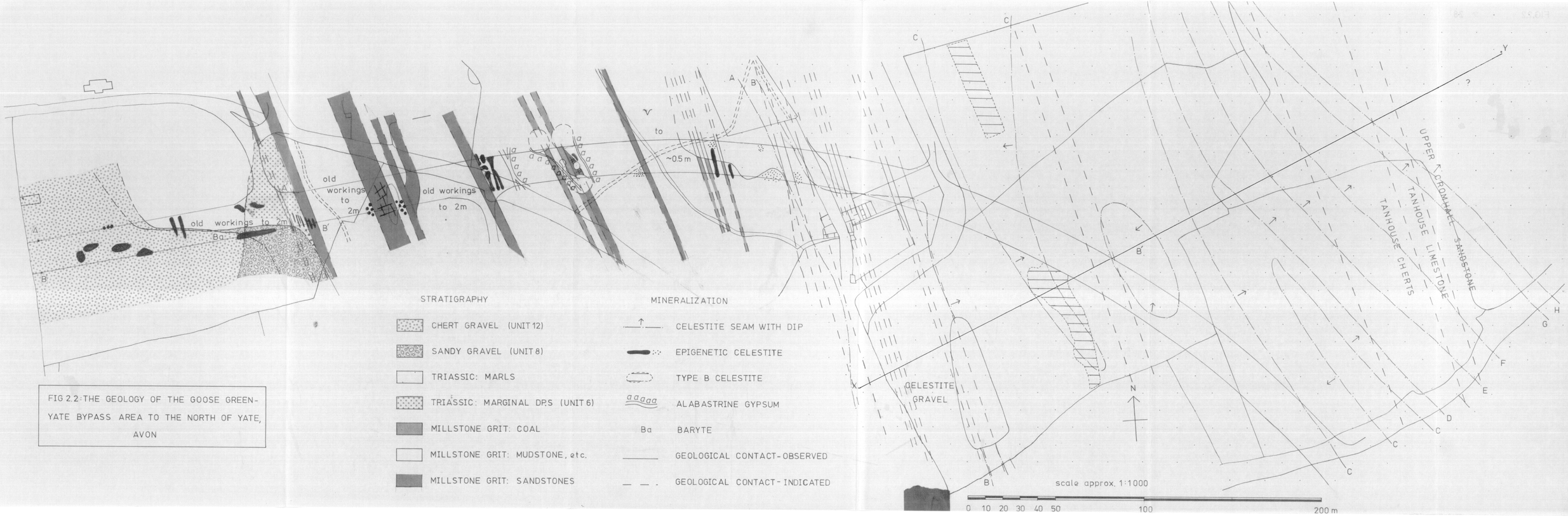

FIG 2.2: THE GEOLOGY OF THE GOOSE GREEN-YATE BYPASS AREA TO THE NORTH OF YATE, AVON

FIG 2.3 MEASURED SECTIONS THROUGH CELESTITE-BEARING TRIASSIC STRATA

1 Goose Green and Wellstead Nursery, near Yate. Composite section, centred near ST716837, 77-92mOD

2 Poundhouse Farm, Charfield. Composite section, centred near ST720916, 44-68m OD.

3 Tortworth Copse, Charfield (from Nickless et. al. ,1976). ST716926, 45-50m OD.

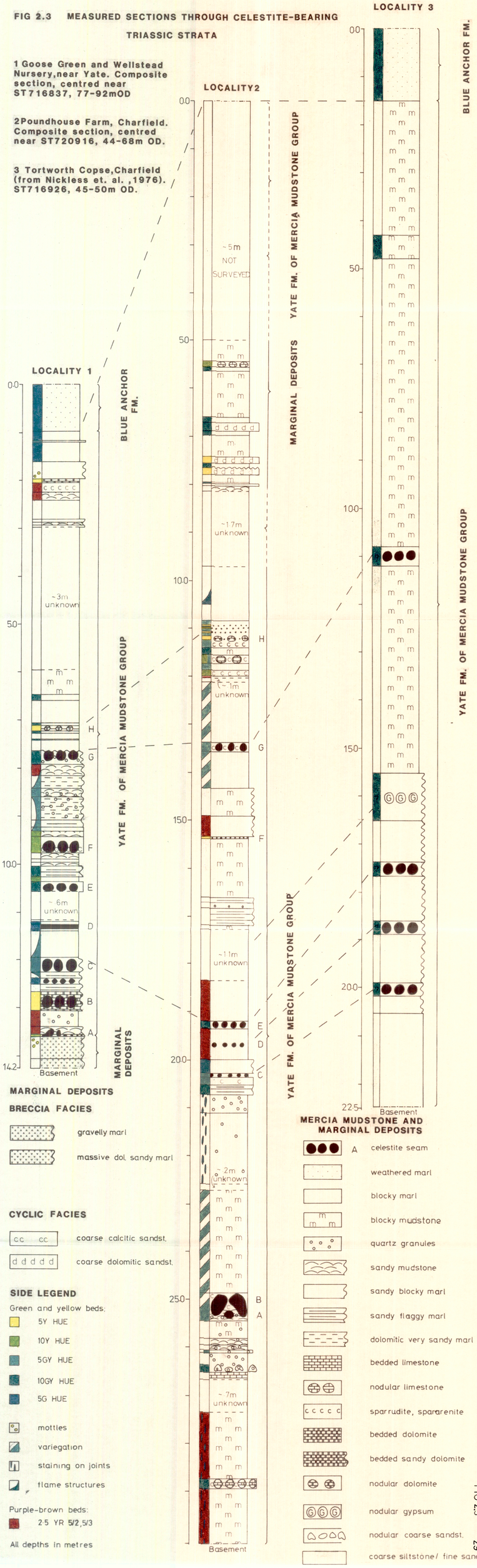

FIG 2.3

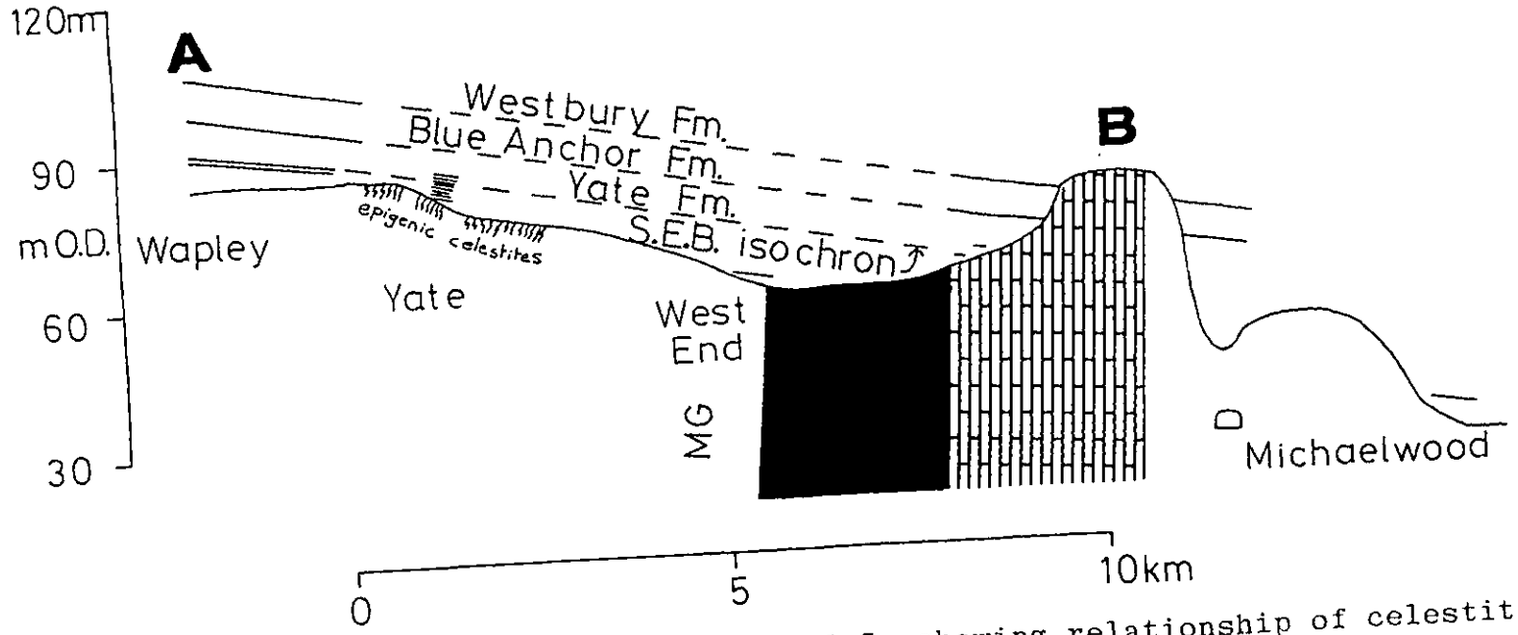

Fig 2.4: Geological section along A-B in Fig 1.5, showing relationship of celestite horizons to Paleozoic topography. Vertical scale greatly exaggerated (after Cave,1977)

Epigenetic celestites also occur in sedimentary deposits of possible Quaternary age along the Yate Bypass, north of Yate.

2.2.2 The Stratigraphy of the Study Area

Fig. 2.3 shows that, provided the logs do not include a faulted sequence, bedded Type A celestite must occur at other horizons apart from the 2m interval recognised by Nickless et al. (1976), at least at the Goose Green and Poundhouse Farm sites. Note that although the Goose Green profile was compiled from sections through superficial disturbed,strata eight celestite horizons also occur at Poundhouse Farm where there was no evidence of deformation. The repetition of the celestite beds is therefore held to be of primary origin. Of the eight Goose Green celestite horizons at least two are associated with green sandy units and may be equivalent to the Severnside Evaporite Bed. Due to partial erosion of the sequence, or the presence of stratigraphically higher or lower beds, only part of the Goose Green sequence may be present at other localities along the Yate Platform (Fig. 2.4). However, most of the indicated Type A resource mapped by Nickless et al. (1976) (Fig. 1.4) should contain at least one celestite bed.

Nickless et al. (1976) mapped the Severnside Evaporite Bed along the Marle Hills Basin as a surface bench feature on the scarp face of the Marle Hills from Perrinpit Farm to Latteridge and thence traced it by augering to the east of Moorleaze (Fig. 2.1). Stratigraphic control over the basin is provided by the deep boring at Frogland Cross (64478383) near Frampton Cotterell, 1.4km north-west of Perrinpit Farm (Fig. 1.3). Here the basinal facies of the Yate Formation is present as a 50m sequence with three separate occurrences of celestite at 9-18m, 26.5-30m and 45-46m below the base of the Blue Anchor Formation. On the resource sheet Nickless et al. (1976) correlated the middle horizon with the Severnside Evaporite Bed. However, a correlation with the upper bed, which these workers illustrated in one instance (ibid., Fig. 2.5.b) fitted their geochemical data equally well. The character of the Severnside Evaporite Bed varies along the strike,

with four celestite horizons in up to 1.8m of red and green marls and sandstone at Perrinpit Farm, two celestite horizons in 0.6m of red mudstone and green sandstone near Latteridge, and three beds in 1.0m of mudstone south of Moorleaze (Nickless et al., op. cit.). At Itchington and Moorleaze a single seam of celestite has been correlated with the Severnside Evaporite Bed by Nickless et al. (op. cit.). The floor of the basin is at shallow depths in this vicinity and the depositional dip has apparently become shallower.

From Wapley Common to the south of Yate, the Severnside Evaporite Bed consists of two beds of celestite in green mottled mudstone (Fig. 2.5) which may be correlated with any Goose Green major celestite horizon in Fig. 2.3. North of Yate celestite occurs at Coopers Field and at West End (Fig. 2.6) in two green marl or sandstone horizons. At the most northerly exposure, Cowship Cottages, only one seam is present (Nickless et al., 1976).

On the Michaelwood Platform, Type A celestite outcropping at Grovesend (Fig. 2.1) has been tentatively correlated with the Severnside Evaporite Bed (Nickless et al., 1976). The Triassic stratigraphy of the Little Avon Platform (Figs. 2.1, 2.7) is better understood and at Tortworth Copse (Fig. 2.3) and in the Little Avon Valley (Fig. 2.8) the Severnside Evaporite Bed consists of three celestite horizons in green mudstone. Trenching at Poundhouse Farm, however, proved a further five celestite horizons mostly in green mudstone (Figs. 2.3, 2.9).

2.2.3 Regional Correlation

There is excellent stratigraphic agreement between the Poundhouse Farm and Tortworth Copse successions and other well documented examples of Norian 'platform' environments (positive areas, (Wills, 1976)) elsewhere in England (Figs. 1.3, 1.8). In particular, the Newark Gypsum horizon at 20m in the South Nottinghamshire succession is well correlated with the tripartite Severnside Evaporite Bed horizon and the equivalent beds at Aust.

Celestite is present in Oxfordshire at four horizons

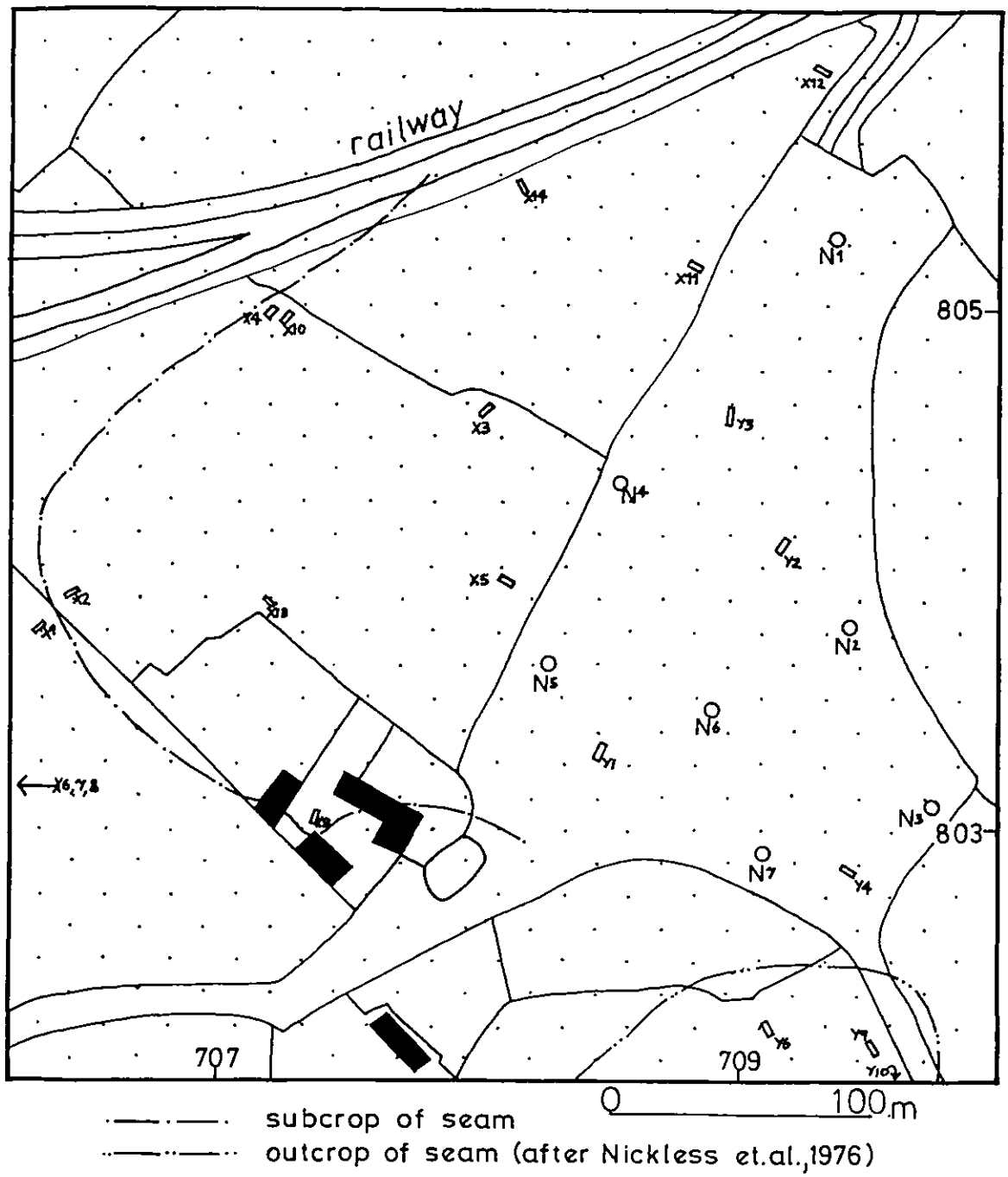

Fig 2.5: Geological sketch-map of the Wapley Common site, showing location of I.G.S. test holes (circles) and B.M.C. test holes (rectangles)

Geological legend as in Fig 1.5

Fig 2.6: Geological sketch-map of the West End site, showing location of I.G.S. test holes (circles) and B.H.C. test holes (rectangles)
Legend as in Fig 1.5
NB. Terrace gravels ommitted

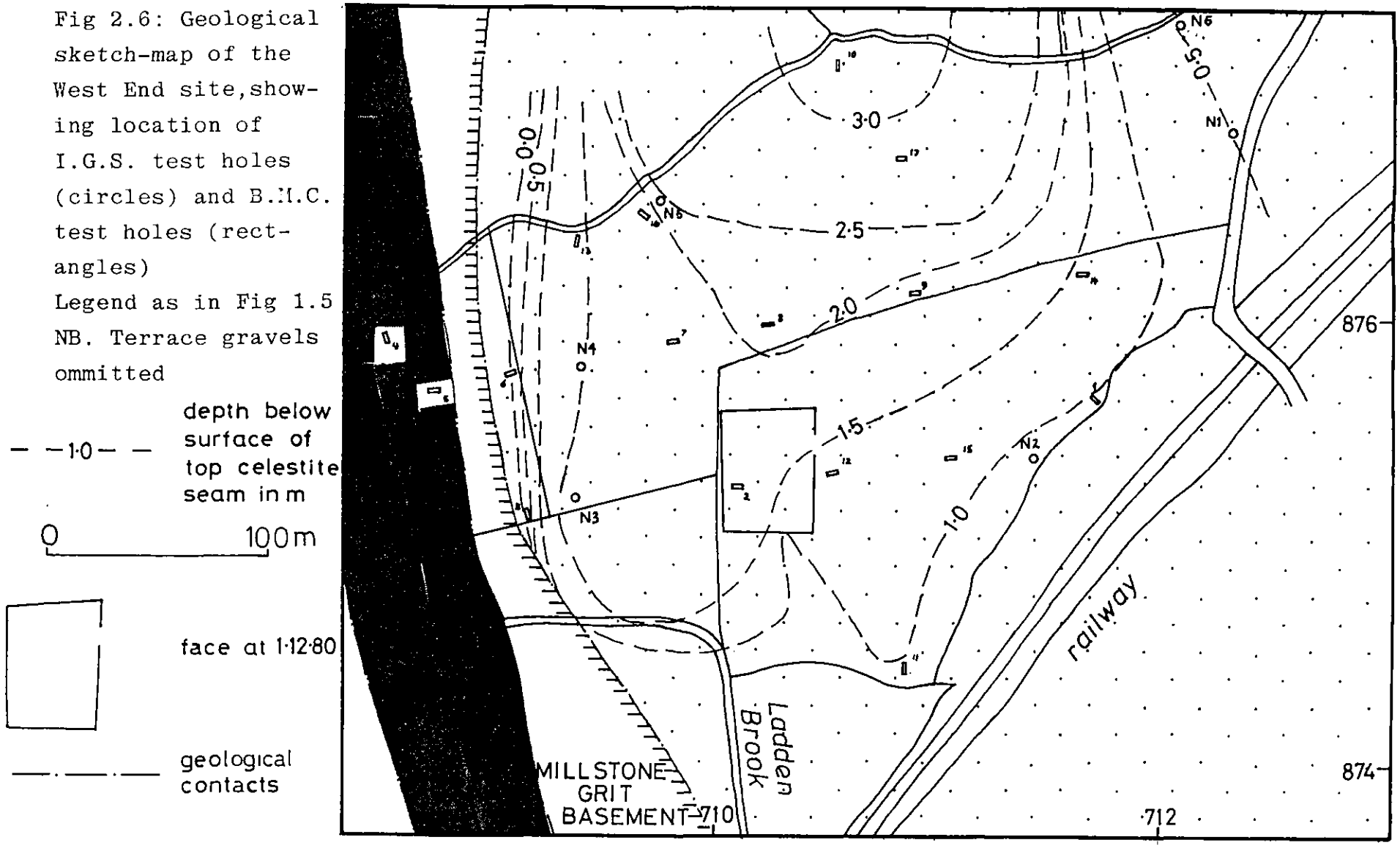

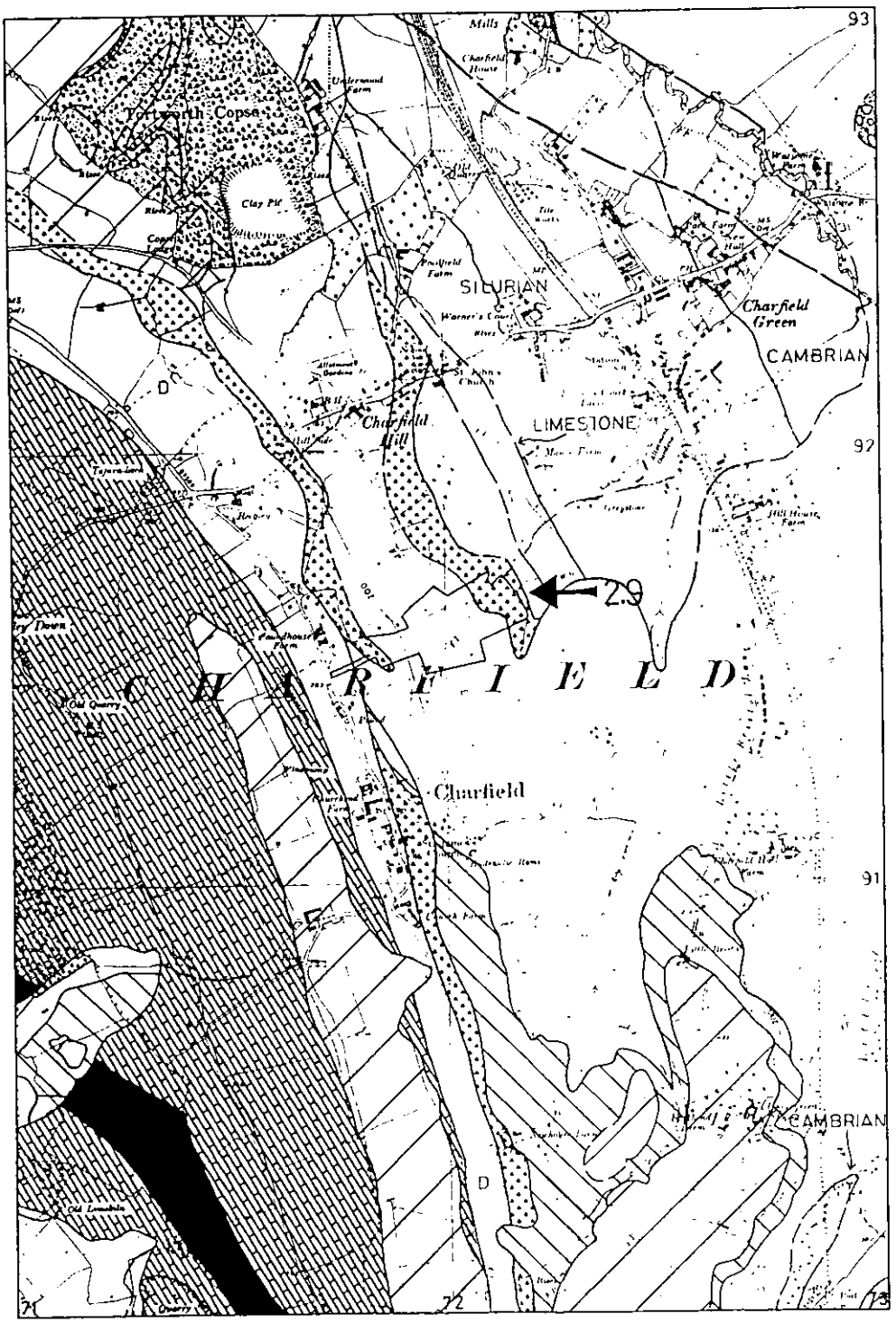

Fig 2.7: Geology of the Little Avon Platform (based on published one-inch sheets).
For explanation of geology see Fig 1.5

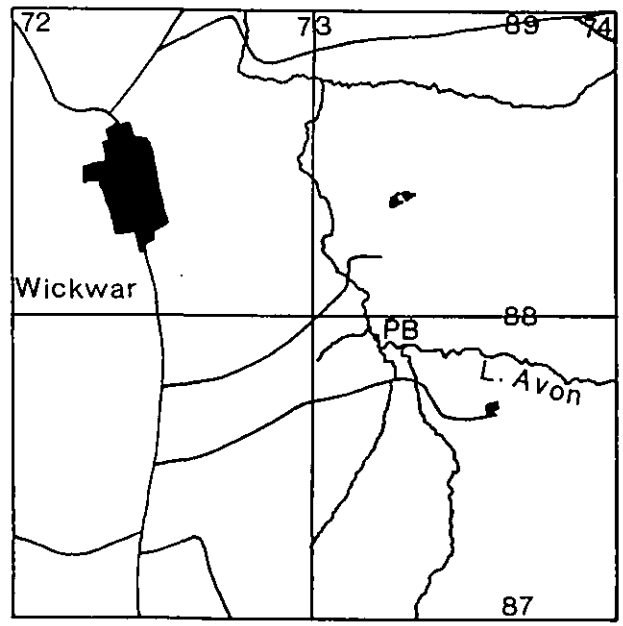

Fig 2.8: Geological cross-section of the Little Avon valley near the Post Bridge, Wickwar. (PB in inset)

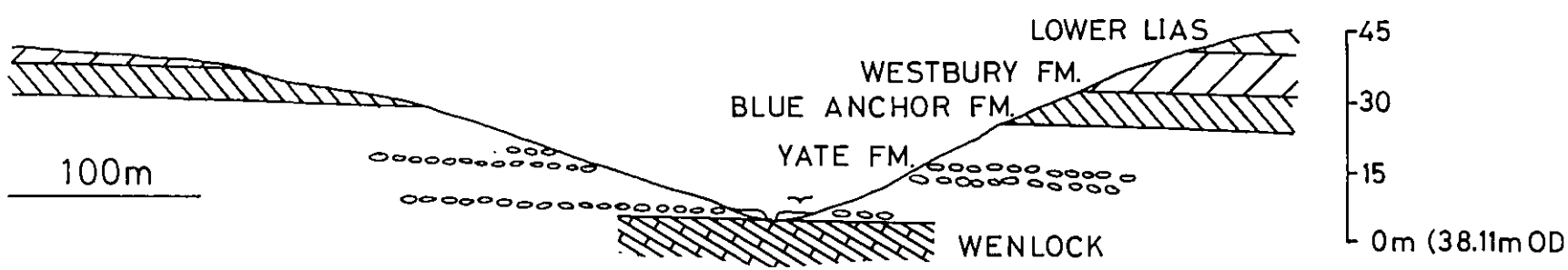

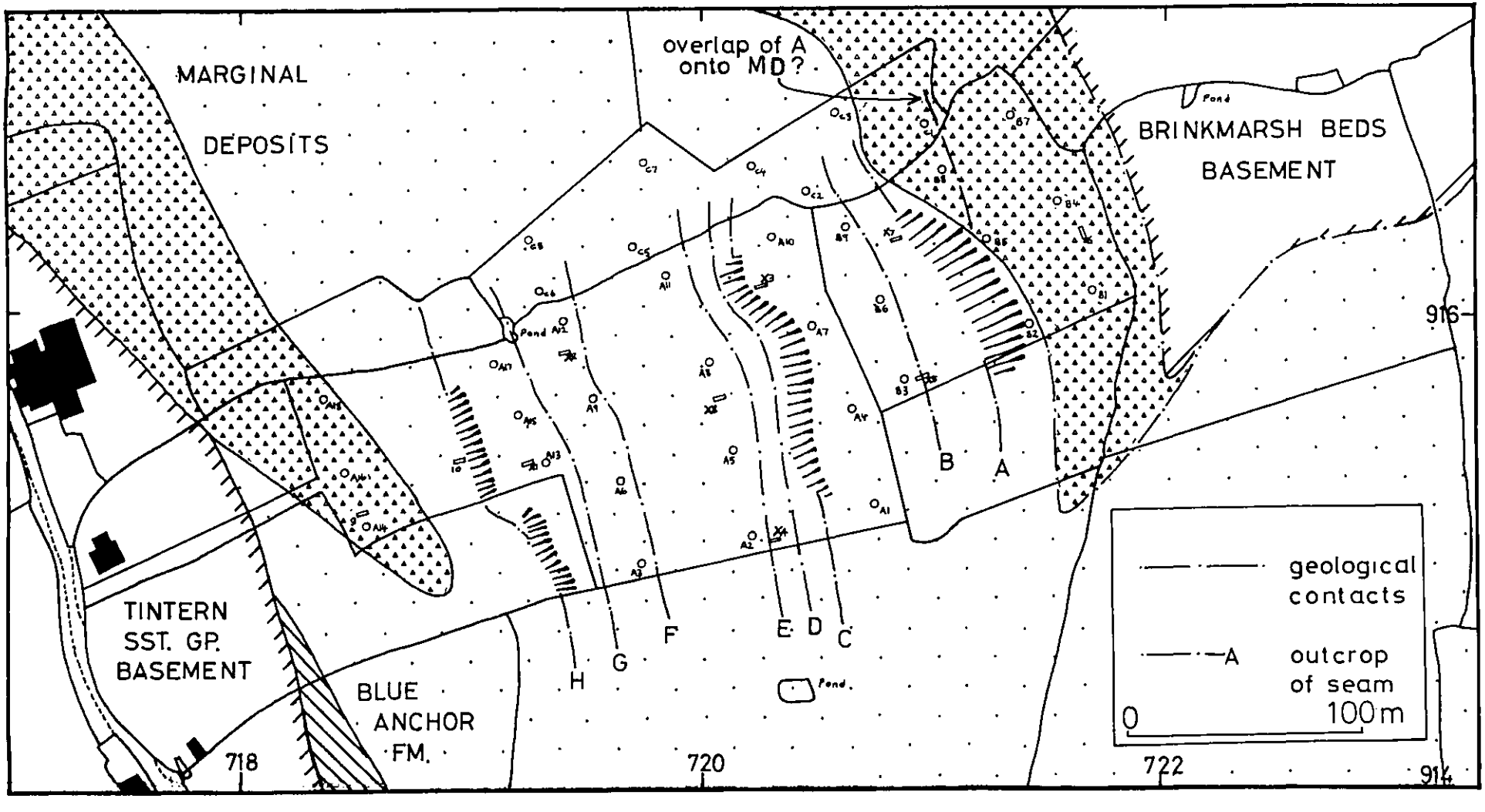

Fig 2.9: Geological sketch-map of the Poundhouse Farm site, showing location of E.E.C test holes (circles) and B.M.C. test holes (rectangles). Geological legend as in Fig 1.5

in the Upton borehole sequence (Worssam, 1963):-

1) With gypsum nodules, probably of the secondary porphyroblastic variety (see 3.3) in red mudstone approximately 11.5m below the base of the Blue Anchor Formation (Fig. 1.8), at the Newark Gypsum horizon.

2) With calcite in grey sandstones of the 'Passage Beds', 116-122m beneath the Blue Anchor Formation.

3) With calcite at one horizon in the Triassic Sherwood Sandstone Group.

4) With ankerite and gypsum, veining Upper Coal Measures Sandstones.

2.3 Definition of Terminology

A field classification of the celestites was established using the four main characteristics of colour, grain size, crystal habit and morphology. This was later expanded into a larger more comprehensive classification for the purposes of computer analysis (see Appendix I, Chapter 4). Before describing the varieties of celestite the characteristics are briefly explained:-

2.3.1 Colour

Celestite crystals may be coloured blue, grey, white, orange, pink, two shades of red, or purple.

The famous translucent blue colour is responsible for the mineral name (Latin Coelestia = celestial). The grey colour, and purple colour in epigenetic celestites, is produced by back-reflection of impurities on the faces of transparent crystals. Other crystals are a porcellaneous white.

The colour of orange, and some pink and red celestite, particularly in druses of celestite, is produced by the staining of crystal faces by goethite or hematite. However, the pink or red pigmentation of most Type A celestite is pervasive and in some cases suggests a relict texture. Reddish browns (10R 5/6)* can be distinguished from 'redder' light red hues (5R 4/4 - 6/4)*; both colours may be present on the same specimen. Pink shades are produced by less intensive colouration. Purple Type A celestite is uncommon and is only found in certain massive schistose celestites (see below). Its interpreta- is uncertain. Other minor colours are described in the text.

* Munsell colour chart

2.3.2 Grain size

The terms used in describing the size of the celestite crystals are based upon those in common usage in igneous and metamorphic petrology. Fine grained celestite consists of crystals less than 1mm in diameter, medium grained celestite contains crystals in the size range 1-2mm and coarse grained celestite is composed of crystals of size greater than 2mm. Where tabular or prismatic celestite is described the figures represent distance along the greatest crystallographic axis.

2.3.3 Crystal habit

Celestite belongs to the orthorhombic crystal system, class 2/m 2/m 2/m (see Fig. 2.10). The pinacoid c {001} and rhombic prism 0 {011} and 1 {102} forms are almost always present as faces in celestite crystals; these are usually elongated along the a axis so that the commonest habit of celestite produced is tabular on {001} . Celestite has perfect {001} cleavage and a good {210} cleavage which is only occasionally seen as a crystal face in the Type A celestites. One specimen of Type C celestite shows parallel growth along the vertices of the prism faces resulting in tabular crystals that appear to be 'toothed'.

Celestite aggregates are described as granular where equant grains are present. These usually contain celestite of a true granular habit, but truncated grains of tabular or prismatic celestite may also be present. In some crystals of thin celestite veins (see below) more rapid growth at right angles to c {001} has produced equidimensional crystals showing the faces characteristic of tabular celestite.

The rare 'rhombohedral' habit is restricted to certain Type A drusey celestites (see below) and geodic Type C celestites. In this variant the m {210} form dominates.

Prismatic crystals are elongated along the a axis and are principally a combination of the m {210} and 0 {011} forms. These are restricted to Type B and Type C celestites (Plate 3). Some examples of drusey Type C

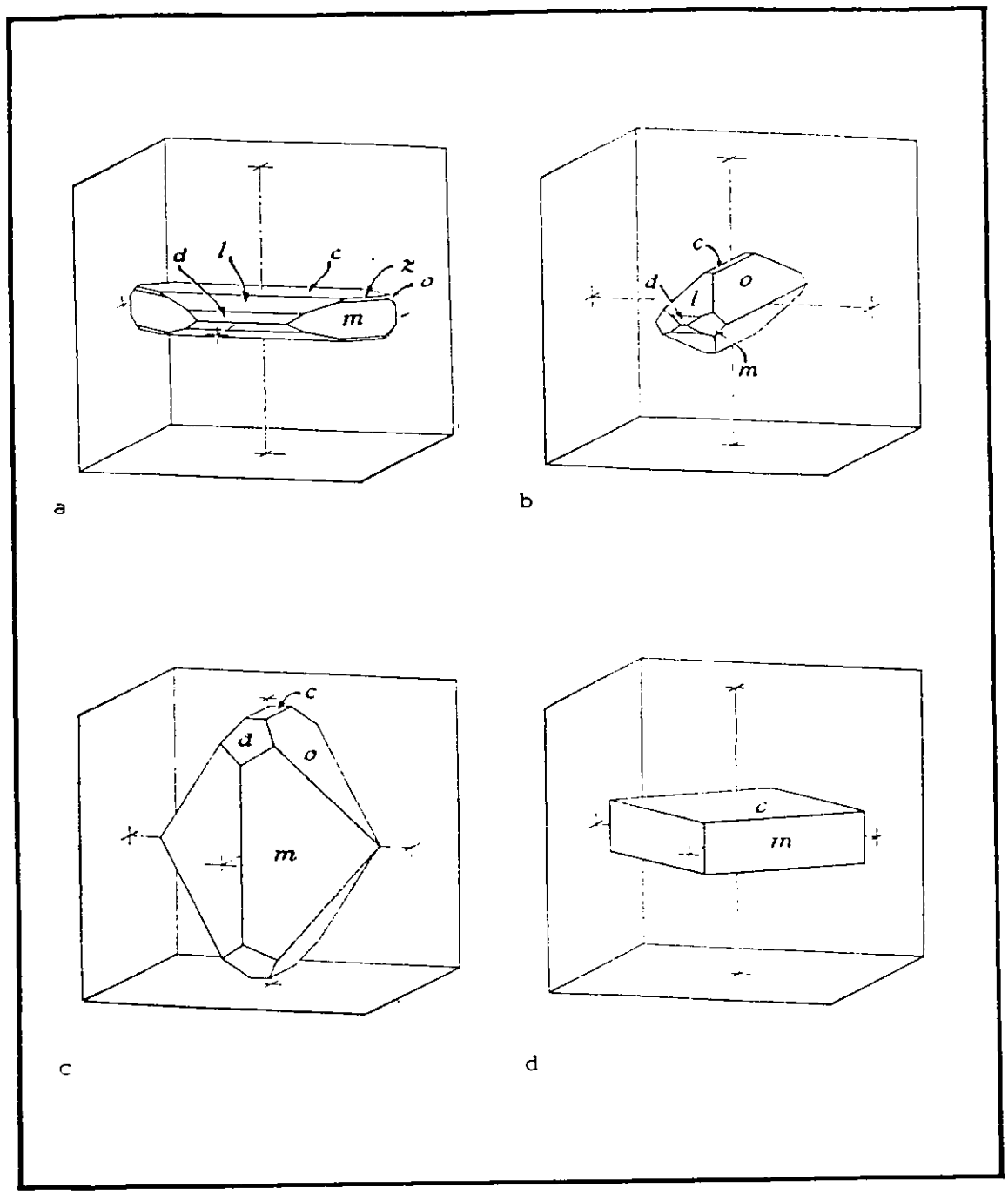

Fig 2.10: Principal habits of celestite (after Berry and Mason, 1959)
a: tabular habit; b: prismatic habit; c: granular habit; d: 'rhombohedral' habit.

Forms: pinacoid c {001}
rhombic prisms m {210}, o {011}, l {102}, d {101}
rhombic dipyramid z {211}

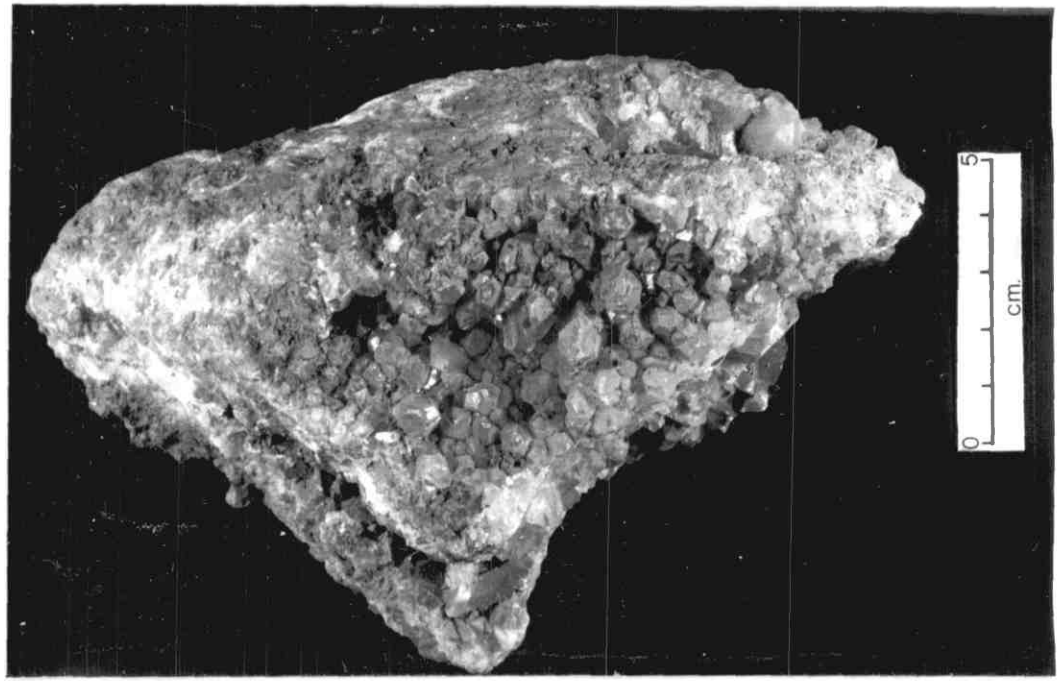

Plate 4: Druse of granular celestite in epigenetic vein celestite. Specimen WF38

Plate 3: Prismatic crystals of Type B celestite impregnating reddish brown mudstone with dolomite in both fragmentary (bottom L.H.S.) and spherical concretionary (bottom R.H.S.) forms.
Specimen GG48

celestite show crystals of an unusual 'prismatic' habit, elongated along b, in which m {210} , d {101} and l {102} combine to produce forms in which c {001} is absent.

Granular celestite crystals show more or less equal development of the 0 {011} , m {210} and d {101} forms (Plate 4). These tend to occur with the epigenetic celestites.

2.3.4 Morphology of nodular celestites

The celestites may be classified as consisting of massive, macrocellular or impregnations of celestite crystals, depending upon the degree of packing and the textures produced by the individual crystals.

The term massive celestite is applied where a dense homogeneous crystalline fabric extends up to the rim of the nodule, or where the nodule contains irregularly defined zones of such celestite in marl. Massive as used here refers to medium and coarse celestite as well as in its more usual sense, to a fine and microcrystalline aggregate.

Macrocellular celestite is used in this account to refer to ovate areas of celestite, typically 3-10cm across coalescing into a mosaic fabric. The macrocells (terminology after West (1965)) are usually defined by light red celestite, or by ovate celestite druses (Plate 5). The term has no genetic implications and macrocellular texture can only be interpreted in accompaniment with petrographic studies (see Chapter 3).

2.4 TYPE A CELESTITE DEPOSITS

2.4.1 Sedimentary setting of the Triassic rocks

2.4.1.1 Introduction

Although all six principal Triassic units outcrop in the study area (Fig. 1.5, Table 1.2) almost all of the Type A celestite occurrences are in the stratigraphic equivalent of the Keuper Marl, undefined in the revised nomenclature of Warrington et al. (1980). For this reason it is proposed that the Keuper Marl of the study area

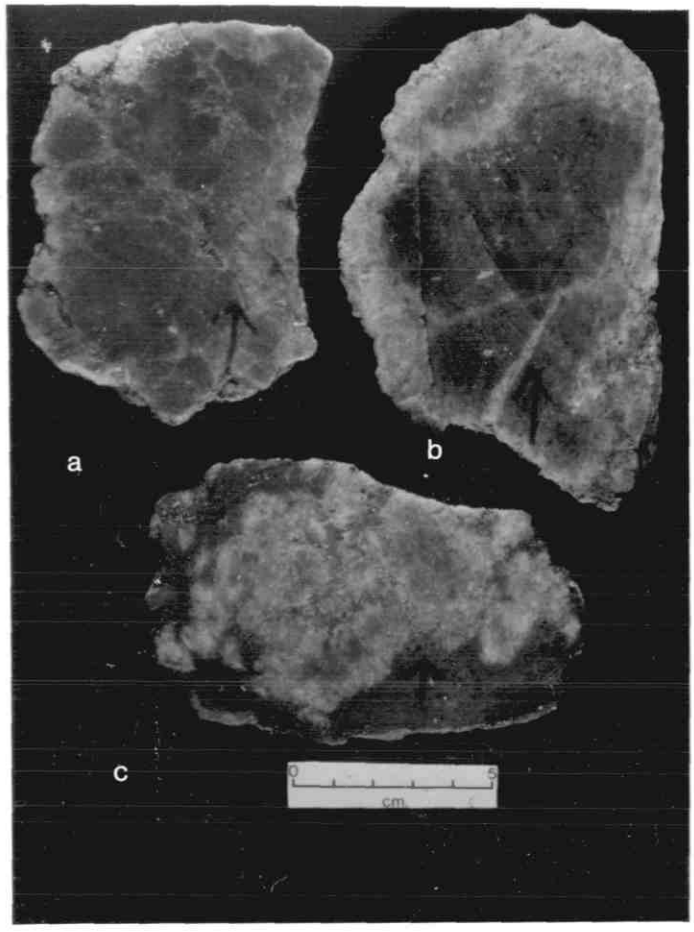

Plate 5: Light red macrocellular celestite, showing

a individual macrocells, in 'chickenwire structure' (specimen PF14)

b macrocell cross-cut by white veinlike celestite (specimen PF21)

c macrocells surrounded by white tabular celestite (specimen PF11)

be referred to as the Yate Formation, after the type sections in the celestite workings at that site.

The Butcombe Sandstone Member is effectively over - lapped by the Yate Formation north of Frampton Cotterell (Fig. 1.5) although accumulations of local sandstone have been recorded by Ollier (1955) and Findlay (1975) near Tytherington (667877) and 'north of Yate' by Findlay (1975). Ollier (1955) described 'Triassic Sandstones' as well sorted fine to medium grade quartz sandstones containing detrital goethite but unfortunately did not mention the localities or the stratigraphic position of his specimens.

As the Butcombe Sandstone Member was deposited before the celestite beds it is not mineralised. Trace amounts of celestite, barite and'barito-celestine' were however recorded by Ollier (1955) "at several localities" in the Bristol region.

The green marls and limestones of the Blue Anchor Formation and marine mudstones of the Penarth Group contain traces of celestite at some horizons as elsewhere in England (Thomas, 1973), but these are not considered to be related to the main celestite beds and are of no economic significance.

2.4.1.2 The Yate Formation

The Yate Formation is volumetrically the most important rock-type of the Mercia Mudstone Group (Fig. 1.5), and also contains the main celestite horizons. Except for the pinnacles on the limestone ridge where it was overlapped by the Blue Anchor Formation, the Yate Formation formerly covered most of the Paleozoic rocks in the study area. The maximum thickness of the Yate Formation within the limestone parabola varies from about21m in the south near Wapley Common to less than 9m in the north, to the west of Wickwar (Cave, 1977), (Fig. 2.1), clearly illustrating the transgressive nature of the sequence.

The main sequence of the Yate Formation consists of a succession of mudrocks, carbonate and evaporites (Fig. 2.3). The closest modern analogue of the Mercia Mudstone

Group in England as a whole, according to Wills (1976) and Arthurton (1980), is the Rann of Kutch. This is a large arid supratidal flat composed mainly of siliclastic debris and authigenic gypsum on the east of the Indus delta (Glennie and Evans, 1976). There is, however, no detailed published account of the sediments of the Mercia Mudstone Group in the area to the north-east of Bristol and this has led to conflicting ideas on the Triassic sedimentary environment. For example Wood and Shaw (1976) postulated that deposition took place in arid desert basins of inland drainage whereas Nickless et al. (1975) favoured a coastal sabkha environment. Klein (1962) interpreted sedimentary structures at Aust Cliff and Thornbury (Fig. 1.6) as evidence for lacustrine sediments which steadily buried a previously exposed terrain. On the whole, however, in the study area as elsewhere in the British Carnian-Norian beds (Audley-Charles, 1970), sedimentary structures are rather rare.

The main difficulty appears to be to reconcile the Norian transgression, for which there is clear evidence in the area to the north-east of Bristol, and southern England as a whole (Audley-Charles, 1970) with the subaerial, sabkha origin of the evaporites as agreed by both Wood and Shaw (1976) and Nickless et al. (1976) on the one hand and the absence of intertidal and subtidal indicators such as stromatolites (Shearman, 1966) and dolomite flats (Illing, Wells and Taylor, 1965) on the other. This aspect was considered in depth by Tucker (1977, 1978), who investigated the Triassic sediments of Glamorgan, South Wales which were laid down in a similar structural setting to those of the area north-east of Bristol (Fig. 1.6). Without being more specific, Tucker (1977) considered that a 'rising base level' was responsible for the spread of the lacustrine Keuper Marl facies although he did not totally discount a marine connection.

A reconstruction of the sedimentary setting at the time of deposition of the Yate Formation, based on the accepted 'dissected Hercynian landmass' model, and modified by observations made during the course of this study, is shown in Fig. 2.11. This model attempts to

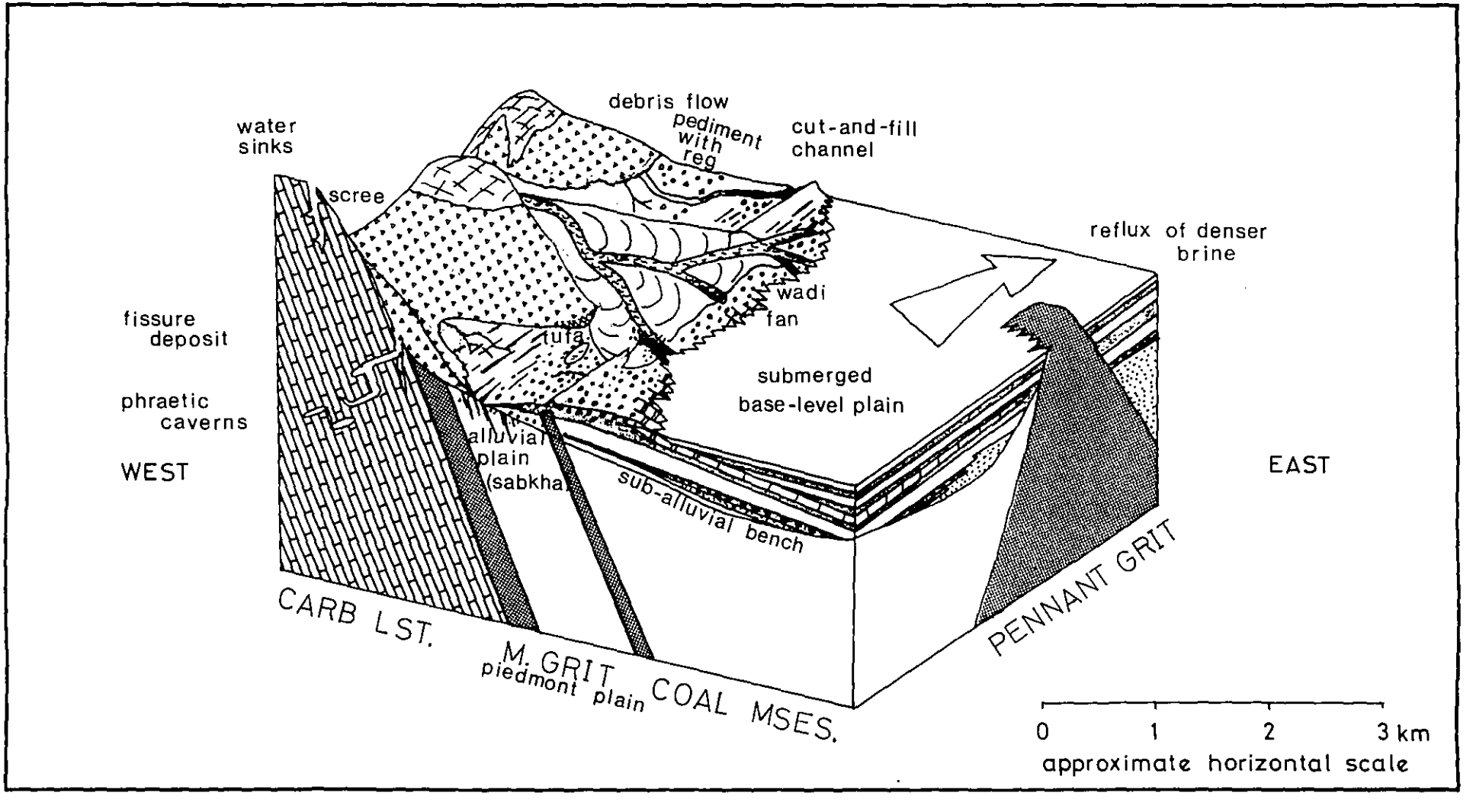

Fig 2.11: Norian morphological and sedimentological elements of part of the study area

include contemporary dynamic sedimentary processes and thereby explain the apparent contradiction of nodular evaporite formation and preservation in what is essentially a transgressive sequence. Most nodular evaporite models involve regression, and accretion of a sedimentary wedge (e.g. Kendall, 1978). The general situation is of a desert basin containing the fine-grained erosion debris of the Hercynian landmass reworked by gradual submergence beneath the Norian (?)inland 'sea'.

a Mudrocks

The dominant mudrock type is a marl, or calcareous mudstone, consisting of aphanitic illite, hematite and calcite with a coarse quartz silt and a medium quartz sand component. The calcite may be present as a cement and as fine-grained limestone clasts. Three main varieties of marl have been recognised (Fig. 2.3): massive blocky marls (or mudstones), flaggy sandy marl, and very sandy dolomitic marl, in addition to which sandy mudstones with a prominent conchoidal fracture may also occur.

Many previous workers (e.g. Wills 1976, Arthurton 1980) have divided the 'Keuper Marl' into two facies: a blocky mudstone facies, coloured reddish brown or chocolate brown, breaking with a conchoidal fracture and a laminated mudstone facies containing red, grey or green mudstones and siltstones. The blocky mudstone facies, which includes the blocky marls, blocky mudstones and sandy mudstones of the Yate Formation, is interpreted as a loess deposit by Wills (1976) sedimented onto the sabkha surface by a rising water table, forming a seal to an evaporite sequence beneath. On the other hand, Arthurton (1980) suggested that some of the blocky mudstone facies, particularly where hosting evaporite, may be reworked by the growth of these minerals within the sediment.

The laminated facies include the flaggy sandy marls that form the host rocks to many of the celestites. These sediments are moderately well indurated well bedded units that show in thin section fissures due to the weathering out of carbonate laminae. The laminations indicate

water-laid rather than aeolian sediment and are thought to represent material deposited during an influx of fresh continental water, reworked aeolian detritus or aeolian detritus that settled out in the water body. The laminations may be destroyed by processes such as the discharge of groundwaters, formation of ephemeral evaporite crusts (e.g. Kendall, 1978) or by the effects of more recent weathering; all of which may explain the relative lack of laminated facies rocks in the Yate Formation. The absence of desiccation cracks implies a more or less continual submergence of the sequence.

Very sandy dolomitic marls are a relatively minor form of the laminated facies and have only been recognised at Goose Green, coupled with sandy mudstone intercalations (Fig. 2.3) and reminiscent of the blocky marl-laminite pairings recognised by Arthurton (1980). Here the intercalations may also be taken to represent couplets of calcite-poor and calcite-rich sediment. Further evidence of an early diagenetic calcite cement is provided by nodular marls of the above type, similar to other examples of calcareous nodules described in the literature (e.g. Pettijohn, 1975).

The coarse siltstones are massive bedded units usually less than 50cm thick consisting mainly of a 0.05-0.10mm grade quartz detritus. They are familiar features of the Mercia Mudstone Group in England and are described elsewhere as siltstones (Wills, 1976) and skerries (e.g. Elliott, 1961). Particles of this grade are always contained in the suspended load of the stream (Allen, 1970). The absence of cross-lamination and of intraclasts (e.g. Tunbridge, 1981) in these rocks suggests that they were deposited from sheet flooding of the sabkha surface rather than channelled streams. A similar origin, under conditions of greater surface run-off is also suggested here for the rarer lenticular sandstones and isolated quartz grains of the Yate Formation (Fig. 2.3).

The mudrocks are coloured red, green or yellow (Fig. 2.3). In the first case, reddish browns and browns of hue 2.5YR* and 5YR, value 4-5 and chroma 4 have been

* Munsell colour charts are used throughout this account.

distinguished from more neutral 'purple-browns' of chroma 2 and 3. Approximately 30% of the sequence consists of green-bedded, mottled, variegated, stained or 'flame-structured' mudrock (Plate 6); streaks and wisps of green marl extending upwards for up to 100cm from green beds into overlying red marl (Plates 2 and 6).

Because most of the celestite seams occur in green beds the cause of the red/green pigmentation was investigated. As both red and green mudrocks contain hematite and illite is the principal component of both types of marl it is suggested that the pigmentation is caused by differences in the REDOX state of the adsorbed iron in the illite. Similar conclusions were reached by Tomlinson (1916) and Potter et al. (1980). Furthermore, an increase in the proportion of chlorite is responsible for the richer greens of the 10GY and 5G hued rocks.

It is suggested that the oxidation/reduction of the iron in the bedded or mottled strata reflects periodic incursions of the sea, the red sediments indicating an oxidising subaerial environment and the green sediments reflecting the more saline waters of the incoming sea. Most of the siltstones and sandstones are green, indicating that the initial impetus to flood was still produced by eustatic effects. Arthurton (1980) investigated the Mercia Mudstone Group of the Cheshire-Shropshire Basin and argued similarly that the grey colour of these rocks was a secondary effect due to submergence.

It may also be argued that the red/green colour division may be due to fluctuations in the position of the water table giving oxidised and reduced sediment as observed in present-day sabkhas (Illing, Wells and Taylor 1965, Glennie and Evans 1976). Were this to be the case however it is difficult to envisage how red beds would be preserved, as they would all pass through the reducing zone as sedimentation commenced. Variegated beds, however, may have been formed in this manner. These have been logged separately from mottles in Fig. 2.3. McPherson (1979) interpreted variegation in the Aztec Siltstone redbeds of Antarctica as evidence for periodic, possibly seasonal waterlogging produced by a

Plate 6: Section of the face at Tyler's Farm South site showing the rhythmic alternations of red and green marl, and celestite seams F (at base of face) G and H (near the top of the face). Note clearly defined contacts between coloured beds and flame structures showing passage from seam F to G.

fluctuating watertable during periods of submergence. The distinction between mottling and variegation reported in this account is thought to have a similar significance.

Green stainings along joints are commonly of 10GY or 5GY hue (Fig. 2.3) and probably represent present-day gleying.

The flame structures are rather enigmatic large-scale mottles. Their formation cannot be attributed to cryogenesis for they are observed in the deepest excavations. Their restriction to the thicker evaporite horizons suggests that they were formed by the percolation of saline groundwaters along structural surfaces perhaps in response to earth movements during early diagenesis.

The yellow colouration of the marls is produced by a limonite pigment derived from the weathering of dolomite (see below).

b Carbonate Rocks

Carbonate rocks of the Yate Formation include bedded and nodular limestones, dolomites, spararenites and sparrudites (terminology after Folk, 1959), calcite-lined vugs, grey 'pseudocubic' calcite and 'epigenetic' calcite rock. The last five mentioned varieties occur as a sparry calcite accessory of the celestite and are described separately below.

In hand specimen the limestones usually appears as white to grey calcarenites pervading the marl host so as to produce nodules of limestone intermixed with marl, usually in the order of 10cm across. A bedded limestone unit, 16cm thick appears at Poundhouse Farm (Fig. 2.3). Nickless et al. (1976) regarded similar 'argillaceous limestone nodules' as a pedogenically-formed calcrete produced by the precipitation of calcite during seasonal evaporation although they do not contain typical calcrete fabrics such as vertically-elongated glaebules, crystal tubes, rootlets, internal fragmentation, marmorization or 'pseudo-anticlines' (Allen, 1974, Freytet et al 1976, McPherson, 1979).

Sections through these rocks show no diagnostic fabrics of any particular sedimentary environment. However, Smoot (1978) proposed 4 hypotheses to account

for carbonates forming below wave-base which may be relevant here; 1 precipitation of micrite from lake waters; 2 intrasediment growth from pore waters; 3 detrital origin and 4 erosion of syndepositional crustose precipitates (e.g. travertine tufas, calcite crusts and cements, dolomite crusts) by flash flooding. Although a subaqueous environment cannot be demonstrated with certainty it is thought that similar mechanisms may have produced the limestones of the Yate Formation (Fig. 2.11).

Although many of the Yate Formation sediments contain dolomite in minor amounts, true dolomites are relatively rare (Fig. 2.3). These occur at certain horizons only as thin beds or spherical concretions, up to 5cm thick greyish yellow (5Y 8/3, 8/4) in colour, in some cases with fine red tabular celestite (see below). In places the dolomite is fragmentary (Plate 3).

Mottling on a centimetre-scale of red and green marl by yellow (2.5Y 8/6) dolomite occurs at one horizon at Goose Green. Dolomitization of limestones and the dusting of the surfaces of celestite with fine dolomite ochre (see below) are common phenomena of the evaporite beds.

Wills (1976) and Arthurton (1980), among others, have assigned both dolomitic mudstone and dolomite rock to the flood or laminated facies. In this context it is interesting to note that the bedded dolomites are associated with green lithologies (Fig. 2.3), suggesting a marine derivation (see above) and that dolomite as a component is present in red very sandy dolomitic marl and also in fanglomerates and breccias or'Dolomitic Conglomerate' of the marginal deposits (Kellaway and Welch, 1948) indicating a continental source. The notion of two separate dolomite types is further discussed in Chapter 3; it is sufficient to state here that the dolomite probably crystallized out following the evaporation of any kind of floodwater.

c Evaporites

Fig. 2.12 summarises the available information on the mineralogy of the Type A celestites based upon this investigation, and the work of Curtis (1974), Nickless et al. (1976) and Wood and Shaw (1976). It shows that

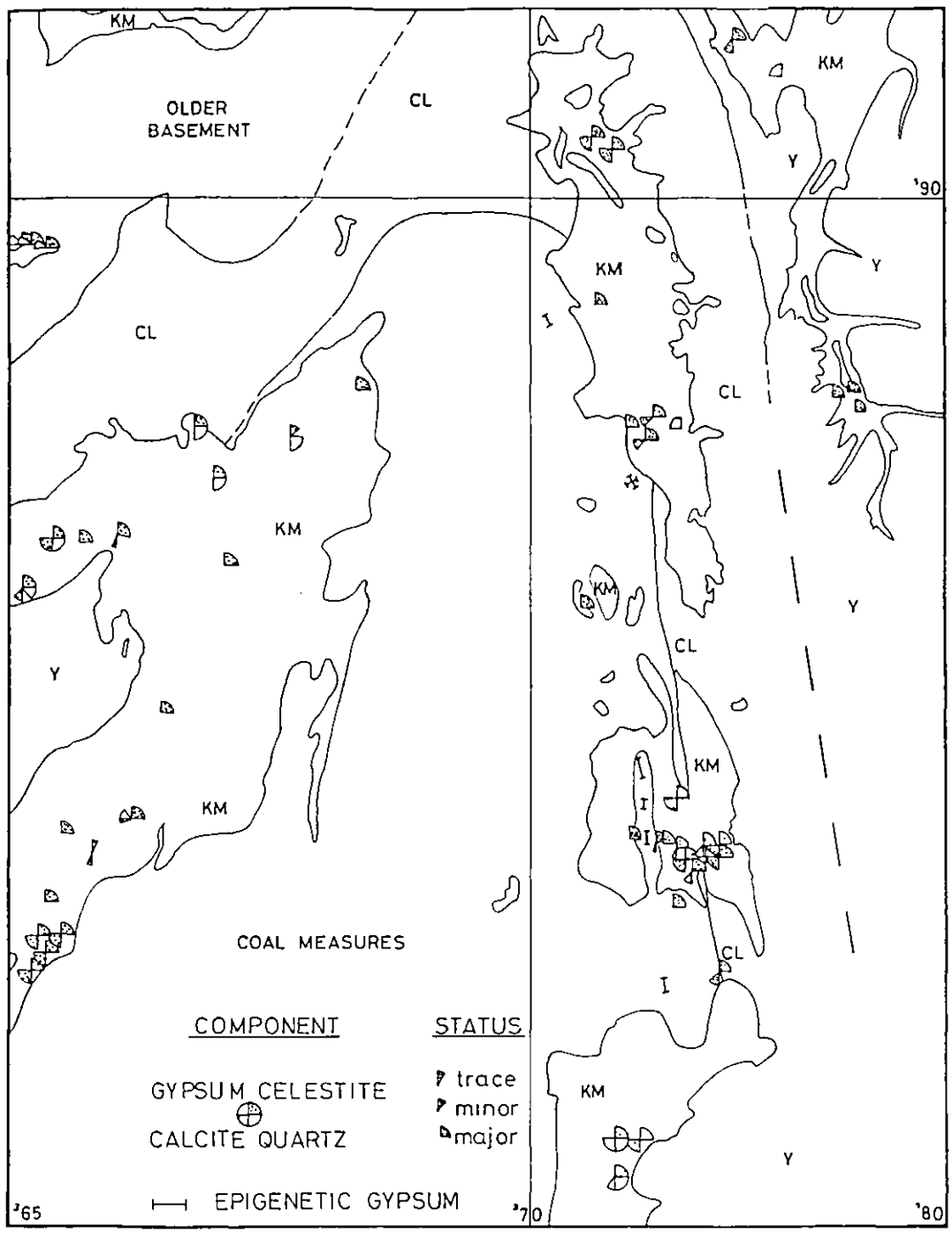

Fig 2.12: Semi-quantitative estimates of the gypsum, celestite, sparry calcite and megaquartz content of the evaporites of the study area. (Compiled from data in Curtis,1974; Nickless et al.,1976; Wood and Shaw,1976 and current investigation)
For explanation of geology see Fig 2.1

celestite occurs at almost every locality within the study area whereas stratiform gypsum is generally restricted to the Little Avon and Michaelwood Platforms. Authigenic quartz is associated with the evaporites in the Wapley Common and Itchington-Moorleaze districts, in some cases as the principle component in 'quartz-rich celestites'. Sparry calcite occurs at most of the evaporite locations. The evaporites are discussed in detail in 2.4.2 and 2.4.3 below. However, sufficient is known about the Triassic evaporites for the depositional environment to be briefly outlined here.

The syngenetic-early diagenetic sabkha model for nodular sulphate deposits proposed by Shearman (1966) for the evaporites of the Abu Dhabi coast is both well established globally (e.g. Kendall, 1978) and also, more specifically for the celestites of the area to the north-east of Bristol (Thomas, 1973, Nickless et al., 1975, Wood and Shaw, 1976) and will be accepted here. Sabkhas are defined by Kinsman (1969a) as "deflation-sedimentation equilibrium surfaces governed by the outcrop of the capillary fringe". The evaporites crystallized by the method known as explosive growth (Shearman, 1966) as a result of the cementation of the salt in the vadose sabkha sediment, probably by the evaporitic pumping mechanism proposed by Hsu and Schneider (1973). The establishment of a vertical hydraulic gradient arises from the reduction in pore pressure caused by the evaporation of interstitial vapour.

A sabkha is shown fringing the sea in Fig. 2.11. The sabkha contains the Type A occurrence (Nickless et al., 1976). Up-platform of the alluvial plain epigenetic Type B or Type C celestites (Nickless et al., op. cit.) are found where the pediment cover is thin or absent (see below). The relationship between the three modes of occurrence according to Nickless et al. (op. cit.) is shown in Fig. 2.13.

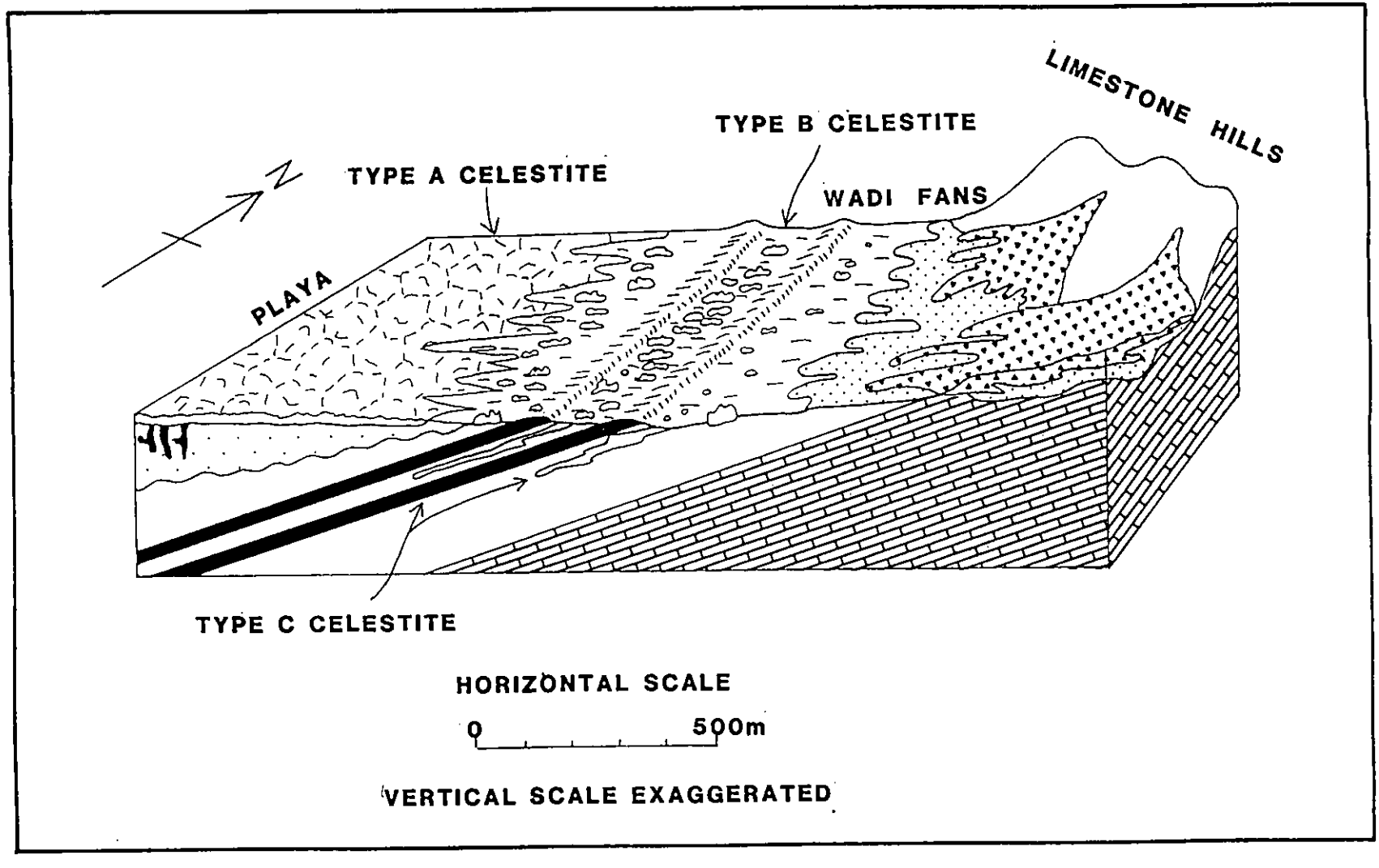

Fig 2.13: The relationship between the three previously recognised celestite types (schematic) (after Nickless et al (1976))

2.4.2 Form of celestite horizons

The Type A celestites occur at specific horizons in the formation as beds of evaporite rock, conveniently referred to as seams. (Plate 6) The commonest occurrence is of stratiform layers of nodule trains of celestite. The distribution of the nodules along the seam is extremely irregular; in some parts of the seam celestite may be absent whereas in others the nodules may coalesce to form sheetlike masses. The vertical dimensions of the celestite bed also vary and may change along the seam from less than 5cm thick to over 40cm. The seam is not always plane bedded and attenuation and bifurcation of the seam occurs. Other features of celestite seams are sudden reversals in the direction of dip, producing qua quaversal dips in some cases and "feathering out" of the seams, that is, the replacement of one seam for another at progressively lower depths.

In general celestite seams occur in green rather than red strata, and are also present in most of the coarser units (Fig. 2.3). Celestite specimens show that celestite crystallized after the completion of the reduction/variegation process (Plate 7) .

At Goose Green isolated nodules in near-surface seams are characteristically surrounded with an aureole of green clay often with fine granular crystals of celestite, weathering out to a celestite "sand". These nodules are in the order of 15-40cm in diameter, contain massive microcrystalline, or granular celestite or geodic macrocells and in distribution and morphology are similar to epigenetic gypsum nodules in nearby Clay Head (see 2.5.3.2)

The sporadic occurrence of the celestite seams is probably a reflection of irregularities in the topographic or piezometric surface such as blistered desert crusts (Arthurton, 1980), deflation hollows and small lagoons as well as the distribution of the original evaporite if the celestite is secondary.

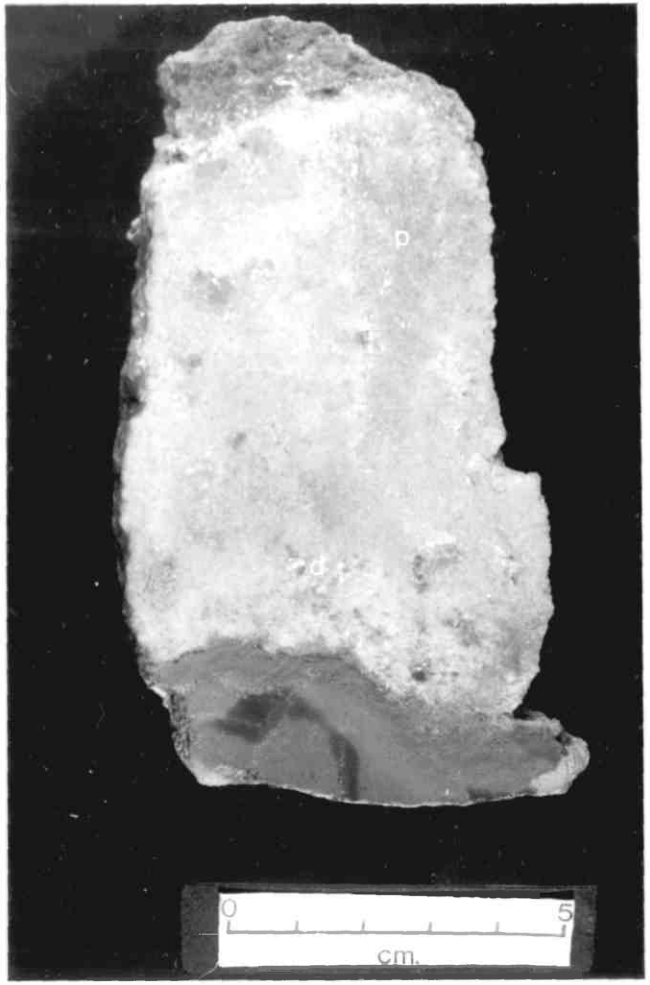

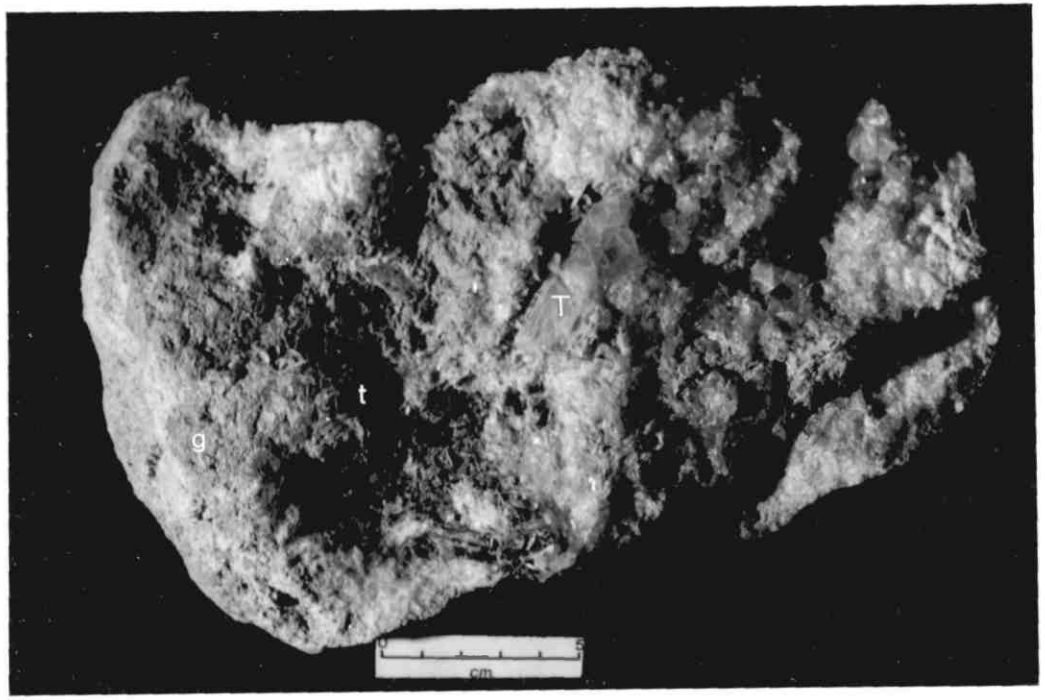

Plate 8: Typical massive celestite nodule showing celestite of coarse tabular (T), fine tabular (t) and fine granular (g) habit. Specimen GG05.

Plate 7: Section through a massive tabular celestite nodule, showing pink colour centres (p), druses (d) and rim of calcite-cemented marl on base of specimen containing mottles traversed by celestite veins. Specimen GG22.

In places along the celestite seam, the celestite nodules do not occur as a stratum but are found scattered throughout a larger interval of marl. These accumulations of celestites are well demonstrated at Poundhouse Farm (Fig. 2.9). Here, two test holes 110m apart at the same stratigraphic level show, in one (test hole 8) three nodule trains in red and green layered marl and in the other (test hole 4) an accumulation of celestite nodules in variegated mudstone. A similar phenomenon also occurs at a lower celestite horizon where a gradation in rock type was observed between a celestite accumulation over a bedded nodule train in green marl (test hole 3) through two seams in variegated marl (test hole 7) to a lower seam beneath barren variegated mudstone (test hole 5) over an area of less than 10^4 m^2. The nodule trains appear to pass through intervals of variegation which are unrelated to surface topography; there is no evidence for landslip or other forms of mass movement at the Poundhouse Farm site. The origin of the accumulations is discussed in Chapter 5, where evidence from outside the study area is also considered.

Some excavations at the Goose Green site also show that the celestite seams are buckled to form drape folds, or upright folds of small amplitude (Fig. 2.14). No examples of growth faulting were recognized at this locality and it is thought that the folding is primarily a product of syn-depositional effects such as differential subsidence and compaction of the sediment on the alluvial plain, reinforced in some cases by later slumping following superficial disturbances.

The overall effect of the stratigraphic irregularities is to extend the area of outcrop or subcrop, complicating mapping and the prediction of outcrop pattern. The positions of the celestite seams in the sketch maps are only approximations for the centres of the seams.

As well as external variations in the aspect of the seam, the variety of celestite shown in the nodules may also change rapidly. Seams rarely consist only of one celestite fabric; it is common for several petrological types to occur at one horizon. The petrographic variation of celestite is well shown at the Goose Green site and is

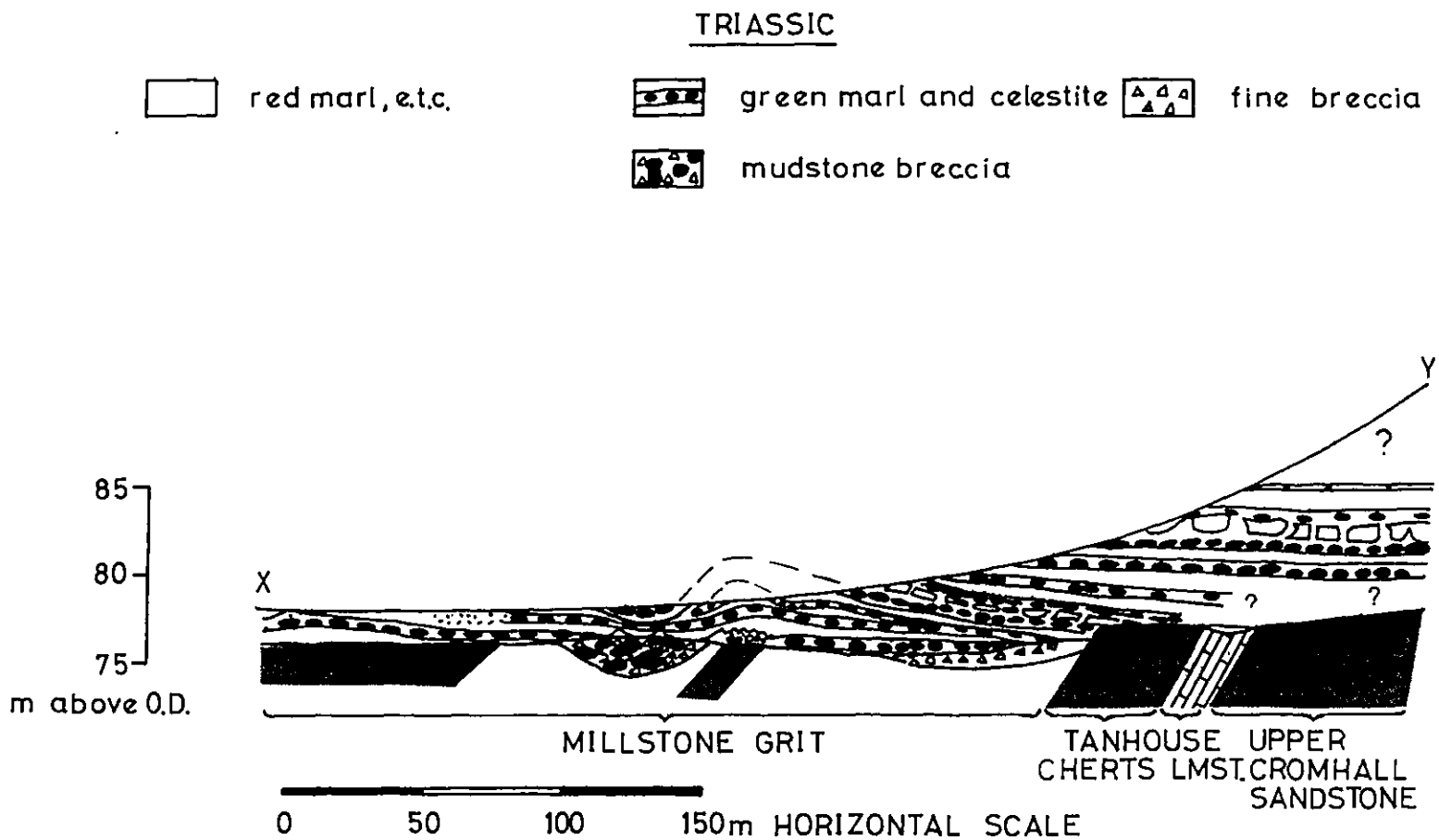

Fig 2.14: Geological cross-section of the Goose Green site (X-Y in Fig 2.2)

fully discussed in Chapters 4 and 5.

2.4.3 Varieties of Type A celestite

The commonest varieties of Type A celestite as observed in celestites from the study area are as follows. Note that one variety may be a gradation of another, and that two or more may coexist together.

2.4.3.1 Massive celestite

The most abundant form of massive celestite consists of blue and white tabular, or less commonly granular celestite and forms nodules 6-35cm in diameter (Plates 7 and 8). Such celestite is especially common in the Itchington-Moorleaze district, and towards the north of the Yate Platform. The fine white massive celestite nodules may be bedded as slabs of celestite ~ 5cm thick, or form discontinuous nodules with plane sides; these usually occur in minor seams (e.g. Goose Green C and D) away from the main mineralized horizon. Pastel colours of pale orange, pink and purple may also colour the tabular celestite; this may also show foliation, in extreme cases producing almost a schistose texture. Four possible causes of the foliated fabric are: -

1) pseudomorphing of an earlier foliated anhydrite texture
2) explosive or displacive growth of the celestite (c.f. Shearman, 1966)
3) compaction during early diagenesis (Shearman and Fuller, 1969)
4) compaction adjustment in response to recrystallization (Holliday and Shephard-Thorn, 1974)

The foliated, pastel celestite is a common associate of the light red macrocellular celestite of the Little Avon Platform (see below).

In many cases the celestite includes druses, of a lenticular, triangular or pear-shaped cross-section, up to 5cm across, lined with tabular celestite and scalenohedral calcite (Plate 7, Fig. 2.15). These are thought to be hollows left from the dissolution of an earlier calcium sulphate mineral. Evidence of a former macrocellular calcium sulphate is also found in an uncommon variant of compact celestite, showing a pronounced vitreous lustre, in which coloured zones of transparent, blue, light red or light yellowish grey (10 YR 7/2) celestite transect an earlier macrocellular texture (Plate 9).

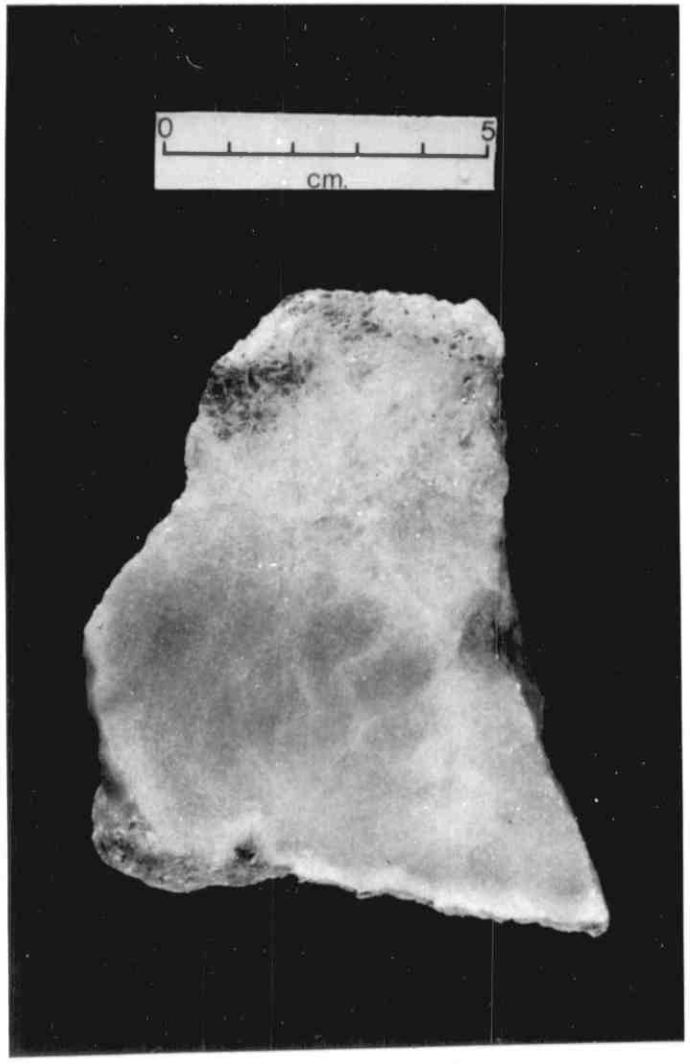

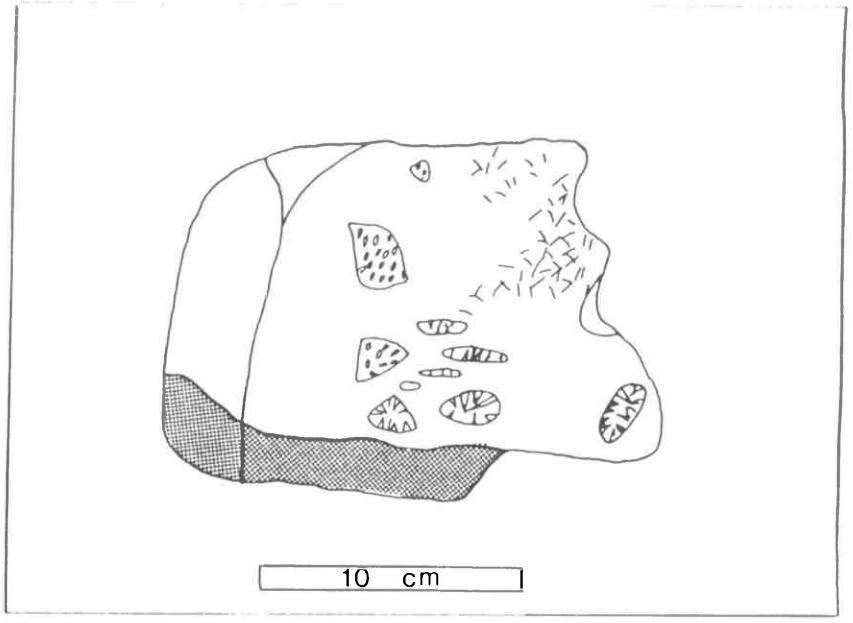

Fig. 2.15: Massive drusey celestite (sketch of hand specimen GG47)

Plate 9 : Section through compact celestite showing colour zoning which transects an earlier ' macrocellular' texture. Top of specimen shows pervasive calcite stained with Alizarin Red S. Specimen GGO6.

2.4.3.2 Macrocellular celestite

This term is applied in two ways: first, in referring to drusey cavities and secondly, to rounded zones of celestite in many cases of a characteristic light red colour.

Included in the drusey macrocells are the druses in massive celestite (see above), stratified celestites, 'pancake' celestite and geodic celestite. The compact examples observed have elliptical cross-sections and are lined with fine tabular celestite (Plate 10), and also in many cases, calcite. Other tabular celestites show voids that have been completely filled.

Colour banding of fine and medium grained drusey tabular celestite is responsible for the texture of 'stratified' celestites (Plate 11). The bands, in the order of 1cm thick, probably represent flattened macrocells for the banding ends at the nodule edge and does not extend into the marl. An allied fabric is the 'pancake' celestite reported from one horizon only at Goose Green and at Wapley Common. This consists of oblate druses of white or orange celestite, in most cases of the flattened rhombohedron habit separated by wisps of fine celestite. Some of the druses are arcuate, concave-upwards indicating negligible overburden pressure. In these cases massive celestite where present may show alignment of the tabular crystals within the macrocells. The druses may in some cases pervade the rock so as to produce a delicate lace-like fabric of partially-infilled voids. Alternatively massive pancake celestite may occur, showing grooves and flute-like structures on the surfaces of the macrocells, aligned parallel to the principal axis of the specimen (Plate 12). These structures indicate movement of the upper macrocell over the lower.

The geodic celestite appears as spherical nodules containing a core of coarse blue or white laths surrounded by medium grained red or white granular celestite or vice versa.

Celestite of the second macrocellular structure forms the most abundant variety of Type A celestite along the Little Avon Platform and in the south of the study area. The zones consist of spherical or ovate masses of fine to medium grained usually tabular celestite,

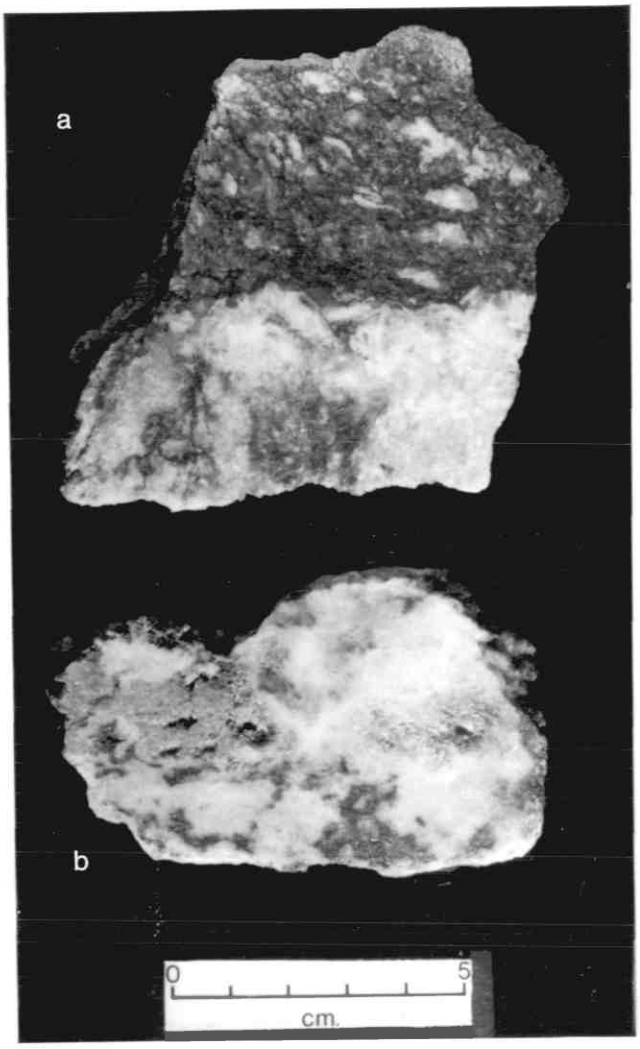

Plate 10: a. Impregnations of white celestite ('net-texture') separated by an erosion surface.

The relationship of the crystallization to the sedimentation is uncertain. Thin sections show that the scattered celetite crystals in the upper unit replace gypsum; and anhydrite, gypsum and calcium carbonate in the lower unit. Some of the individual celestite grains are embayed or corroded suggesting a reworking of the original gypsum, with a later crystallization of celestite concommitant with sedimentation. See also Plates 55, 59. Specimen WP25.

b. Celestite with ovate drusey macrocells infilled with grey pseudocubic calcite (left) and fine red and white lathlike celestite (right). Specimen WP16a.

Plate 12: Upper surface of massive pancake celestite showing oblate druses, grooves and flute-like structures and chert/ white celestite crust. Specimen WP20.

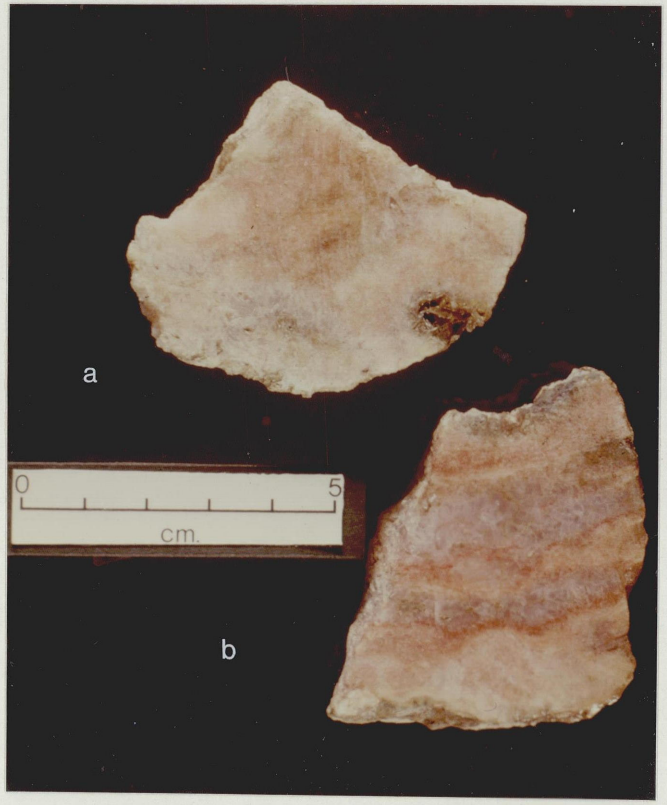

Plate 11: Sections through macrocellular and 'stratified' celestites.

a. pink macrocell fringed with blue laths. Specimen BY71.

b. Flattened macrocells of celestite separated by druses. Note the resemblance of the blue mineral to that in a., however the mineral here is megaquartz. Specimen WP06.

in blue celestite of similar habit (Plate 5b and Plate 13), surrounded by marl (Plates 5a and 5b) or fringed with a rim of medium to coarse grained white or blue tabular celestite. These globular macrocells may coalesce, producing nodules reminiscent of cauliflower anhydrite and cauliflower chert (Chowns and Elkins 1974) with a surface of cerebral protuberances;where the tabular celestite covering is extensive these rocks are known as 'desert roses' (Nickless et al 1976). Sections through such celestites (Plate 5a) show chickenwire texture (Shearman 1966) indicating displacive growth in soft unconsolidated sediment, or compaction adjustment in response to recrystallization (Holliday and Shephard-Thorn 1974). Sparry calcite is common in many examples of light red macrocellular celestite either as yellow scalenohedra infilling interstices or as sparrudite, forming the edge of the evaporite specimen (Plates 5 and 13).

2.4.3.3 Impregnations of celestite

Celestite impregnations occur where the celestite grew at random in the sediment. The 'celestites' or evaporite blocks are defined by the extent of the celestite or associated calcite cement. This variety includes the very common medium to coarse grained white/blue and light red/reddish brown celestite (Plate 14b) in which giant crystals are found (Plate 15). Yellow scalenohedral calcite is a common accessory, especially in the thicker evaporite seams (Plate 14b).

Celestite impregnations also occur as scattered medium-grained laths of white, grey or orange celestite in nodular limestone or spararenite (Plate 16), or coalesced into layers of hummocky relief as 'evaporite crusts'. Impregnations of granular and tabular celestite of a distinctly different appearance ('net-texture' of West (1964, 1965)), occurring in red marl only, are illustrated in Plates 10 and 17 .

2.4.3.4 Quartz-rich celestites

The so-called 'quartz-rich celestites' include approximately 30% of the celestites from the Severnside Evaporite Bed proven in the Wapley Common test holes (Fig. 2.5) which contain authigenic quartz and chert giving a characteristic duller appearance and a waxy lustre. These

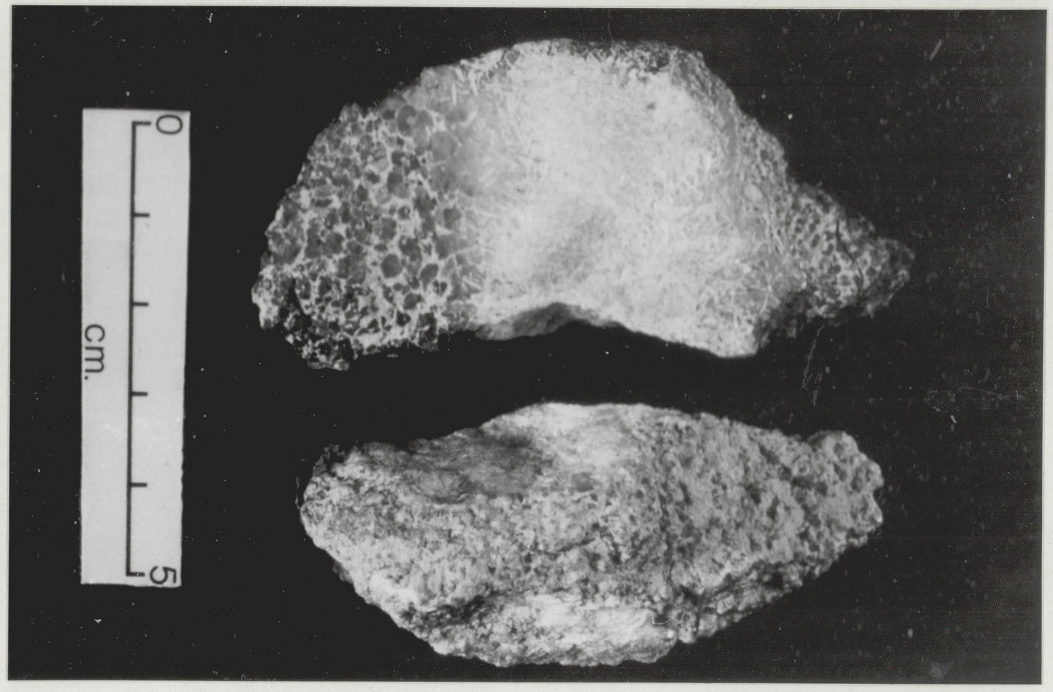

Plate 13: Sections showing a sparrudite rim surrounding a macrocell of fine white tabular celestite, pink at the centre, calcite stained with Alizarin Red S. Specimen GG25.

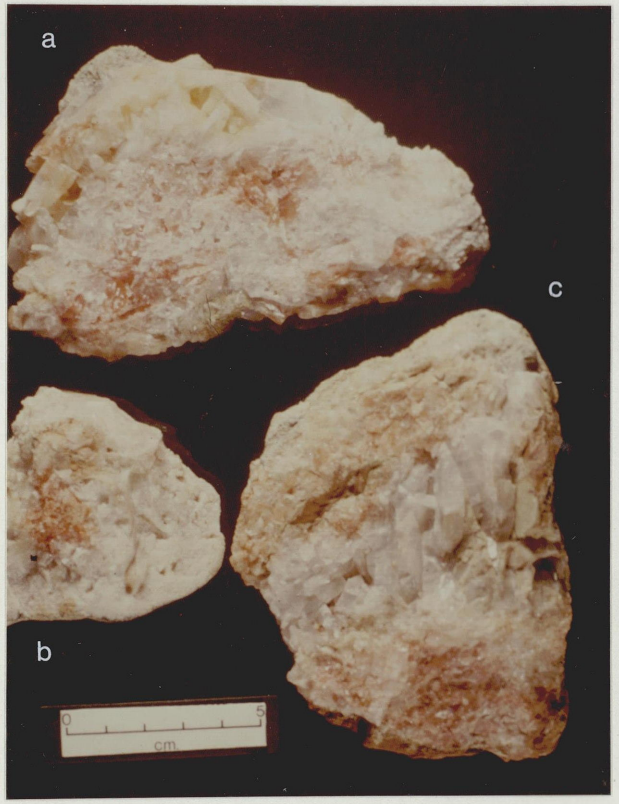

Plate 14: Textures in red and blue celestite; impregnations.
a Reddish brown coloured centres in blue with yellow, scalenohedral calcite. Specimen GG07.
b Coloured centre in mauve calcite rock; note sulphides on rim. Specimen TF14.
c Composite specimen (GG8b) showing reddish brown and light red granular celestite separated by blue lath intercalation.

Plate 15: Upper surface of celestite showing giant flat lying blue crystal dusted with ochreous dolomite.

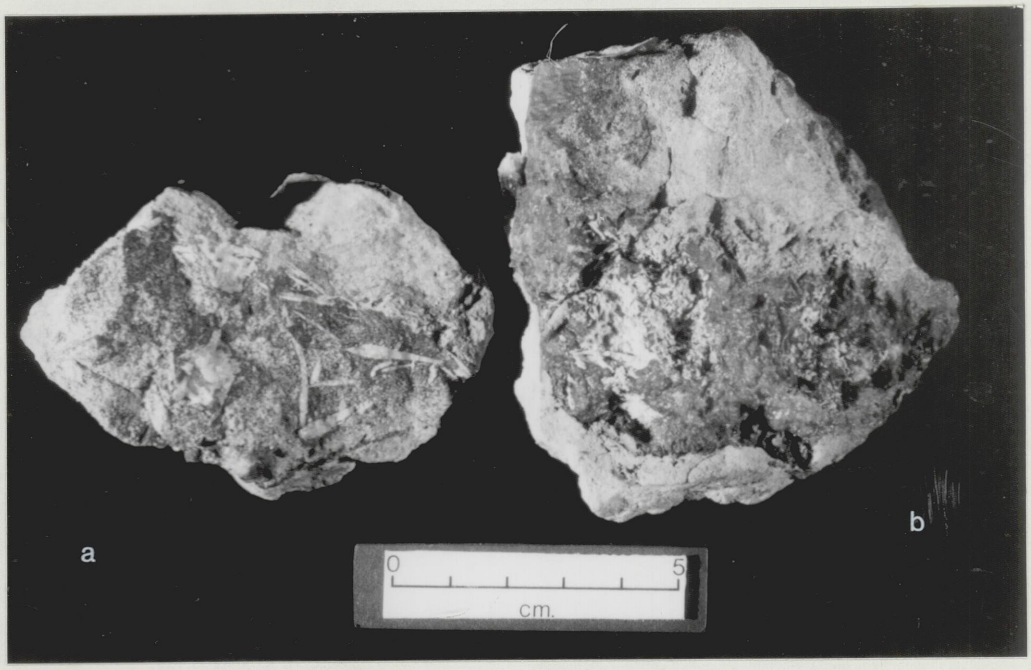

Plate 16: Section througha dolomitized spararenite (a) and nodule of calcite rock (b). In each specimen dark grey areas are calcite stained with Alizarian Red S. Note the patchy distribution of the calcite, and the bent celestite laths in the spararenite; and the lath-shaped moulds (centre right), celestite (shown in white mineral) and thin layer of opaques at the base of the calcite rock. Specimens GG24(a) and CF02 (b).

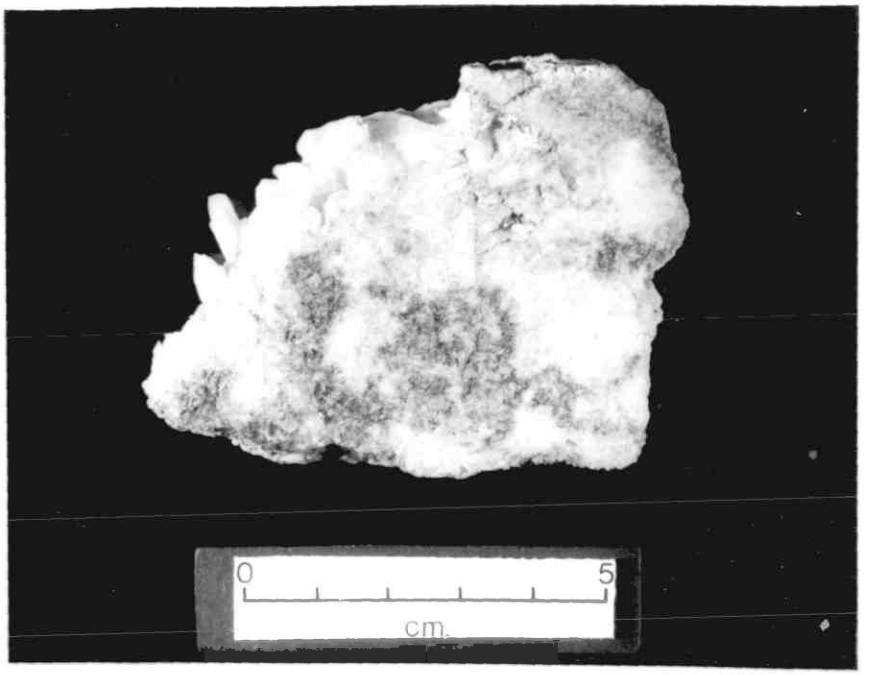

Plate 17: White celestite pervading red marl. Note the tendency for the crystals to coalesce into macrocell-type units ('net-texture'). Specimen GG20.

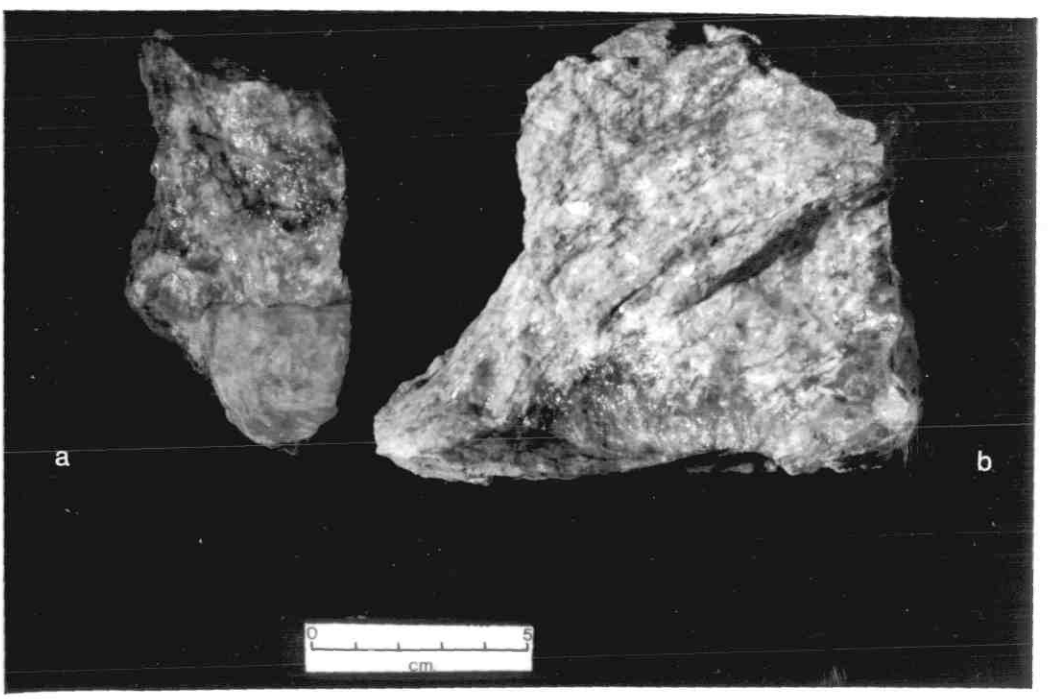

Plate 18:
a Section of funnel-shaped evaporite block. Specimen WP08.
b Section of evaporite block showing schistose fabric produced by alignment of overgrowths in celestite granules. Specimen WP22.
Note characteristic dull waxy lustre of both specimens.

usually appear as blocks of evaporite, up to 15cm across, with smooth, well defined outer surfaces. The edge of the blocks corresponds to the extent of the sparry calcite cement. Many of the blocks are funnel-shaped and in section reveal slump structures showing deformation and foliation of the internal fabric parallel to the walls of the block (Plates 18 and 19). Individual celestite laths are bent, perhaps implying that the slumping occurred after celestite emplacement. The shape of the celestite blocks suggests that the minerals formed in trough-shaped depressions in the soft marl, which were later preserved by selective cementation in these areas. The significance of these structures is not fully known, but a subaqueous origin seems most likely.

Small lensoid crystals or aggregates of quartz 0.5-10.0mm in diameter are present in most of the evaporite blocks; in some cases as the only visible mineral in hand specimen (Plates 18 and 19). These also occur in limestones at Poundhouse Farm. Small 'granules' up to 5mm across of pink (7.5YR 7/4) celestite also occur scattered throughout evaporite, in many cases with overgrowths of blue tabular celestite (Plates 18 and 20).

The pink celestite 'granules', or granules with overgrowths may pass upwards into coarse white tabular celestite with coarse megaquartz (Plate 20); nodules with quartz cores were also recorded by Nickless et al (1976) and nodules, in the order of 10cm across, consisting entirely of celestite and megaquartz (Plate 21) are also occasionally found. The celestite laths form a framework for, and may be corroded by the megaquartz which can be colourless, light brown or purple (var. amethyst). The megaquartz forms prismatic crystals up to 2cm in diameter, with rhombohedral terminations prominent where there are druses. A geopetal fabric occurs where a dust veneer is trapped on the laths. The fabric is described more fully in Chapter 3; this together with an offset of the quartz cores (Plate 20) indicates that silicification took place on the upper surface of the celestite.

Megaquartz also occurs in the massive and drusey macrocellular celestites from Wapley Common. Pink, doubly terminated elongate quartz crystals are present in some

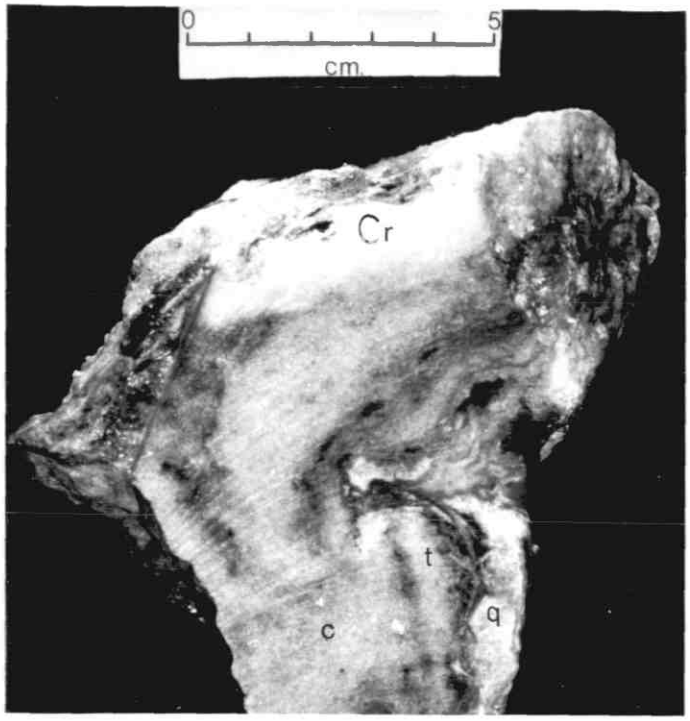

Plate 19: Section of funnel-shaped evaporite block showing slump structures. Specimen consists of microcrystalline celestite and chert (c) bordered by fine white tabular celestite (t) and lozenges of quartz (q); encrusted by chert and white celestite (Cr). Specimen WP10

Plate 20: Section through an evaporite block showing foliation in celestite overgrowths on pink celestite granules with massive quartz. Upper part of specimen shows a core of megaquartz in coarse white tabular celestite with geopetal fabric (arrows). Specimen WP09.

Plate 21: Quartz-rich celestites.

a. Geodic quartz-celestite nodule, with reddish brown tabular celestite on the outer surface of amethystine megaquartz, with central, ovate voids. Specimen WP33.

b. Quartz-celestite nodule, showing amethystine megaquartz in framework of coarse white celestite laths. Specimen WP23.

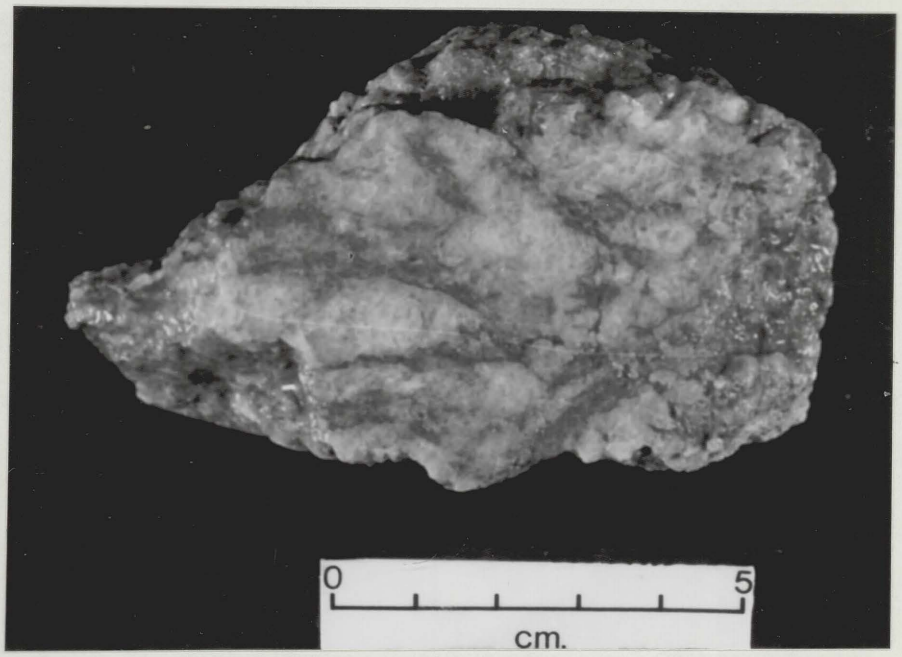

Plate 22: Granular macrocellular celestite. The celestite is apparently pseudomorphing on earlier lozenge quartz fabric. Compare also with granular macrocellular gypsum in Plate 28. Specimen WP15.

specimens scattered throughout the massive celestite and also lining druses. Some are geodic with fine crystals of amethyst outlining ovate voids at the centre of a spherical nodule of reddish brown tabular celestite. The voids indicate that the celestite only partially replaced the calcium sulphate mineral before silicification (Plate 21).

In addition bands of blue quartz approximately 1cm thick are observed in some examples of stratified macrocellular celestites (Plate 11). Because of the blue colour and the granular habit, this quartz has previously been confused with the granular celestite.

Other specimens of massive or macrocellular celestite show a thin fine celestite-chert encrustation (Plate 19). These may be analogues of 'ploughed ground' described by Arthurton (1980) from supratidal salt-lake flats in Iran which consist of blistered, convoluted superficial sediment. Similar 'puffy ground surfaces' were attributed by Kendall (1978) to groundwater discharge, crystallization of ephemeral salts and drying. These processes are only recorded where preserved in subsurface evaporites and suggest that the silicification of the Wapley Common celestites was penecontemporaneous with deposition. Other specimens (Plate 22) show granular macrocellular celestite in which the celestite apparently replaces earlier quartz.

2.4.3.5 Other megascopic textures

Bent crystals may be observed in hand specimen, aligned parallel to the edge of massive celestite nodules and also as individuals, with sparry calcite in spararenites (Plate 16). Nickless et al (1976) used the presence of bent celestite crystals as a criterion for near-surface growth in a soft sediment, the crystals being deformed during the burial of the sediment. The bent laths in the massive celestite nodules can also be used as evidence for expansive growth from a centre of crystallization, the laths along the edge of the nodule being deformed by pressure of crystallization.

Celestites from Goose Green and Wapley Common, in particular, show structures reminiscent of erosion surfaces. Care must be taken, however, not to refer to the upper surfaces of all celestite nodules as erosion surfaces unless

they include indicators of exposure such as hummocky relief, truncated surfaces (Plate 10) or evaporite crusts (Plate 12). Some sectioned celestites show cycles of evaporite deposition, from isolated crystals in marl coalescing into massive celestite, truncated by an erosion surface (Plate 10); see also Plate 1A in Nickless et. al. (1976). In some of these cases it appears that the celestite crystallized contemporaneously with the deposition of the marl. These cumulate layers are not as abundant in the study area as Nickless et. al. suggested; although it is recognised that these may represent an ideal sequence only, most of the celestites sectioned showed a clear isotropic morphology.

Only one clear example of a dissection crack was recorded in the celestites examined. In this specimen celestite was selectively formed in the draped layer. The most striking texture in hand specimen of Type A celestite is, without doubt, produced by the distribution of the red celestite in the white or blue celestite. The origin of this fabric is of special importance and is discussed in the light of other petrographic and geochemical evidence in 5.2.1.3 . A summary of the megascopic information is now briefly given:

The reddish brown celestite occurs:

1) As coloured centres throughout an impregnating fabric, ranging in magnitude from small flecks to ovate zones about 3cm across; the borders of the colour centres crossing grain boundaries (Plates 14a, 14b).

2) As sharply defined ?growth zones at the centres of individual blue celestite laths.

3) As discrete crystals sandwiched between blue tabular crystals.

4) In close association with blue celestite of a different habit (Plate 14c).

5) As colour centres in fine white massive celestite (Plate 7).

The light red celestite is apparently more abundant than the reddish brown and occurs as whole macrocells, or nodules of massive celestite. In association with white or blue celestite the following features may be observed:

1) The light red/blue colour contact transects a homogeneous celestite fabric and individual crystal boundaries so that, for example, laths of celestite may be half light red and half blue (Plate 5b).
2) Light red celestite forms the centres of efflorescences of blue tabular celestite (Plate 13).
3) Celestite crystals of both colours may occur in contact, impregnating marl.

2.4.4 Carbonate minerals

As the preceding section has shown, sparry calcite and to a lesser extent dolomite are common accessory minerals of the celestites. The main varieties of the carbonate minerals are now briefly described as follows.

Spararenites and sparrudites (Plates 13,16) are the commonest variety of sparry calcite. Despite a superficial resemblance to 'calcite sandstones' they are believed to share a common origin with the limestones and nodular limestones (see 2.4.1.2b).

Vugs and druses containing yellow scalenohedral calcite ('dog's tooth spar') are also a common feature of many Type A celestites particularly the main horizons (Plate 9a). The scalenohedra which are generally of coarse grade are considered to be the free-space form of the spararenites and sparrudites. Although replacement of celestite is not as extensive as in other well-known calcitized evaporite sequences, for example the Basal Purbeck (Holliday and Shephard Thorn, 1974), there is a clear implicit genetic relationship between this calcite and the celestite (see petrographic descriptions in 3.1.3).

The variety described as grey pseudocubic calcite consists of fine granular and coarser drusey calcite, usually associated with a black sooty mineral (?manganese dioxide) and has only been recorded in the Wapley Common celestites (Plate 23). The term 'pseudocubic' refers to certain crystals that appear at first glance to be cubic (Curtis, 1974), but are found on closer inspection to be combinations of the rhombohedra $\{10\bar{1}1\}$ and $\{20\bar{2}1\}$. It is not known why this variety should form

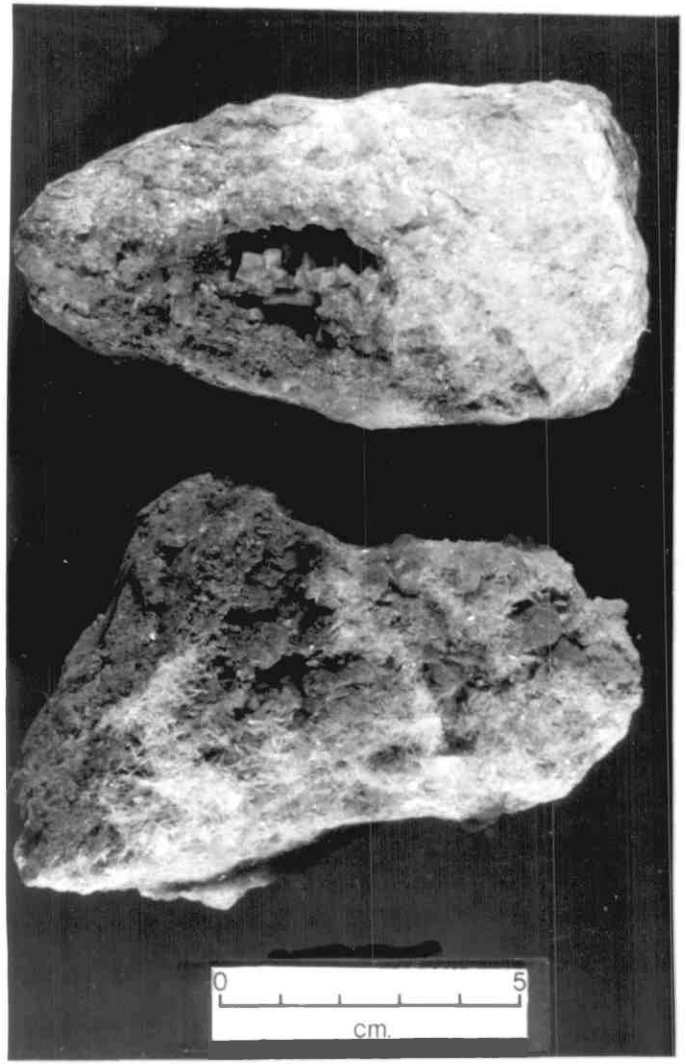

Plate 24: Granular macrocellular gypsum. Most of the gypsum from the area to the north-east of Bristol appears to be of this variety.
Compare with Plate 22. Specimen MI03

Plate 23: Grey pseudocubic calcite in celestite. Note 'cubic' outline of forms in upper specimen, black coatings of ?manganese oxide in lower example. Specimens WP35, WP36

instead of yellow scalenohedral calcite.

Epigenetic calcite rock is used to refer to massive, macrocellular calcite, of a characteristic pale lilac hue which is usually found associated with small amounts of galena and sphalerite, and in one case, malachite; for which an epigenetic origin is implied (Plates 14 and 16). The calcite rock at Goose Green and Cooper's Field occurs in nodular masses with the celestite or forms a rim, with an outer layer of fine sulphides on the base of the celestites, separated from the main nodule by a streak of marl.

Dolomite occurs as a powdery yellowish-orange (10YR 7/8) ochre on the surfaces of celestites from the larger seams (Plates 14 and 15). This dolomite may have crystallized by desiccation after flooding of the evaporite horizons.

Structures referred to as lath-shaped moulds (Plate 16) occur adjacent to apparently unaltered crystals of celestite in limestone, dolomitized limestone and calcite rock at one horizon at Goose Green and Cooper's Field. The moulds, which are presumably of celestite, imply that alkaline fluids dissolved the celestite, leaving the carbonate host. It is interesting to note that similar fabrics have been reported from other localities (e.g. Mukherji, 1969) of supratidal carbonates.

2.4.5 Gypsum

Triassic gypsum is only rarely found in the Triassic rocks of the study area (Fig. 2.12) and was not recorded at any of the sites visited during this investigation. A reconnaisance survey was made of the gypsum deposits of the Newark Gypsum or Severnside Evaporite Bed horizon to the north of the study area, at Michaelwood (704954), Tortworth Copse (716926) near Charfield and at the classic Aust Cliff section (572810) (Fig. 1.6).

The Michaelwood exposure contains two areas of interest (Nickless et al., 1976). In the first (70399550) three thin beds of gypsum occur in about 1m of red and green marl. The basal bed is of oblate nodules containing

white and clear granular gypsum crystals coalescing into lenticular macrocells, approximately 8cm inlength (Plate 24). Above a thin layer of satin spar an upper gypsum horizon, similar to the lowest, contains spherical nodules of white crystalline gypsum, up to 10cm in length with relic lath texture and small tabular celestite crystals on the outer surfaces. At 70449537 pink alabastrine gypsum containing fine red acicular porphyroblasts occurs in beds up to 3m thick.

Pink alabastrine gypsum nodules at Tortworth Copse (Fig. 2.3) are in some cases rimmed with 2cm layers of red satin spar.

The Aust Cliff section (described by Reynolds, 1947) contains two principle varieties of gypsum. The first, similar in appearance to the granular macrocellular gypsum from Michaelwood, consists of spherical masses of microcrystalline white or clear gypsum, typically 1-4cm in diameter, locally producing macrocellular structure. This gypsum is extensively veined by thin (less than 2cm diameter) sheetlike masses of satin spar gypsum arranged sub-parallel to bedding. Nickless et al. (1976) also recorded alabastrine gypsum hereabouts. A 5cm vein of blue tabular celestite occurs near to one of the bridge ramparts.

The above exposures are thought to be typical of the gypsum in the Severnside Evaporite Bed in the area to the north-east of Bristol. At this stage a common macrocellular fabric can be noted in both celestite and gypsum, implying a possible genetic link between the two minerals. Further comment however must be reserved until the petrography and distribution of the gypsum are discussed in Chapters 3 and 5.

2.5 EPIGENETIC CELESTITE DEPOSITS

Epigenetic celestites, or those that are younger than their hosts mainly occur in Paleozoic rocks (Type C celestites) or Triassic marginal deposits (Type B celestites). In addition, minor types of more uncertain origin also occur in possible Triassic sediments at Tytherington

(Type T celestites) and at the Yate Bypass site where the host sediments are believed to be river terrace deposits of Quaternary age (Type Q celestites).

Apart from the Type C celestite, the Millstone Grit and Lower Coal Measures also contain epigenetic baryte and gypsum. Before these minerals or any of the celestites are described the main features and field geology of the host rocks of each of the celestite Types are briefly outlined.

2.5.1 Description of the host lithologies

2.5.1.1 Paleozoic rocks

Apart from the isolated occurrences in Wenlock rocks near Whitfield (Reed and Reynolds, 1908) and at Charfield (Weaver, 1824) Type C celestite is restricted to the Carboniferous rocks of the Yate Platform (Fig. 2.17). The principal formations of the Yate Platform are summarised in Fig. 2.16. Although the strata range from the Carboniferous Limestone to the Supra-Pennant Measures only those of the Millstone Grit and Lower Coal Measures host celestite deposits. These consist mainly of mudrocks and quartzitic sandstones, with subordinate quartz pebble conglomerates, cherts, coals and siderite ironstones and quartzites.

The mudrocks comprise rather more than half of the above sequence and are typically well bedded, extensively fractured elite-quartz-feldspar-hematite mudstones of a characteristic purple (5R 5/2) hue. Contemporaneous 'Red-Bed' claystones (Kellaway, 1967) comprised principally of hematite and illite and carbonaceous shales also occur in the sequence.

The quartzitic sandstones are massive to fine bedded very well indurated recrystallized rocks, most of which are texturally coarse siltstones although fine and medium-grained sediments are also locally present.

Both mudrocks and quartzitic sandstones are locally mineralized by hematite-goethite ironstones of Permo-Triassic age (Kellaway, 1967). Apart from small quantities of celestite in some conglomerate horizons, no other

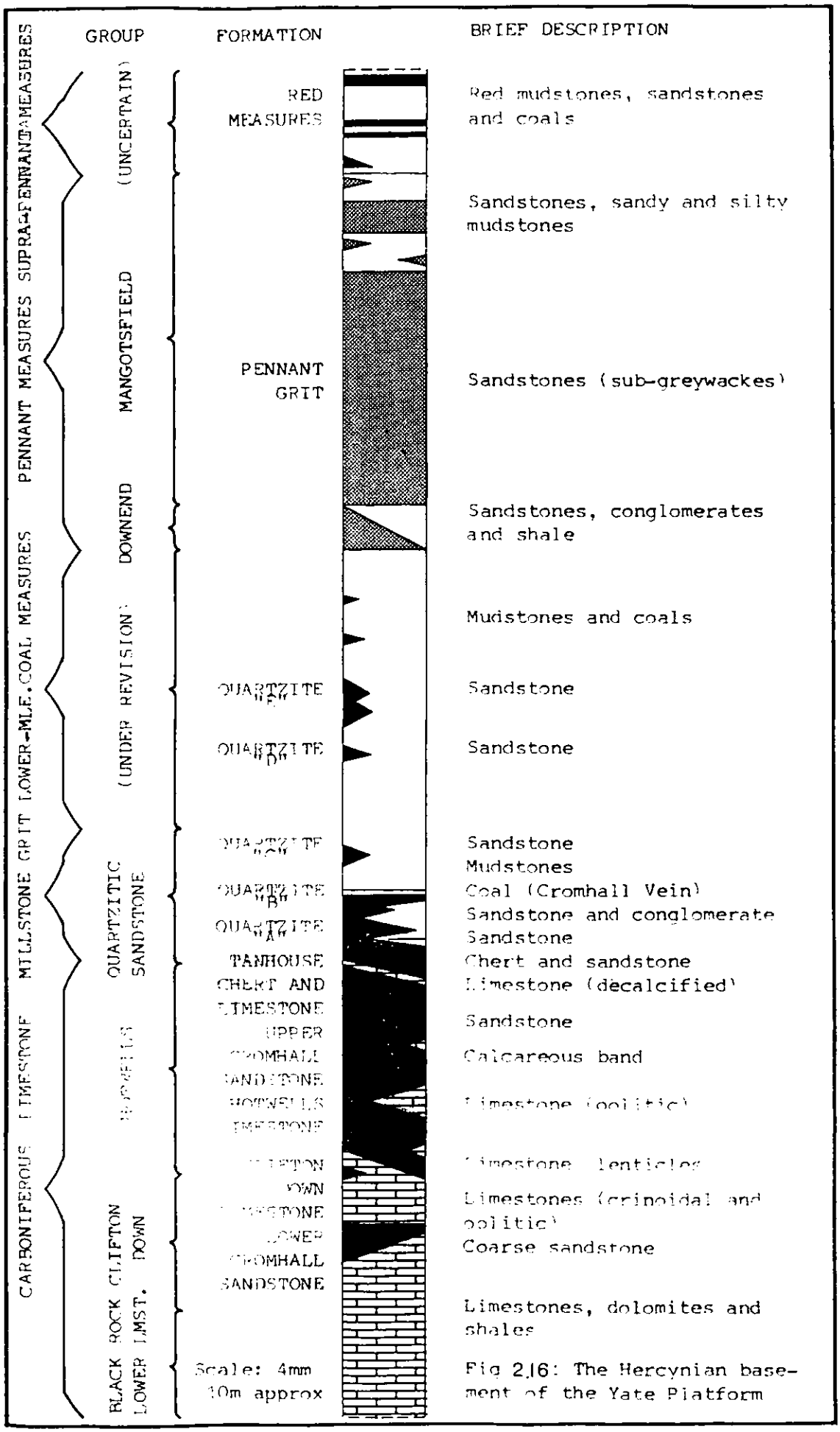

Fig 2.16: The Hercynian basement of the Yate Platform

lithologies are of economic importance.

2.5.1.2 Triassic marginal deposits

The marginal deposits are mainly the product of continental weathering on the sediment 'up-slope' of the alluvial plain sediments (Fig. 2.11) They include representatives of all the main sedimentological features of modern arid-zone drainage basins such as alluvial fans, cut-and-fill channels and desert regs (e.g. Cooke and Warren, 1963).

The alluvial fans consist mainly of fanglomerates, containing ill-sorted coarse fragments of Carboniferous Limestone set in a dolomitic marly matrix. These represent screes or talus fans banked up against the Carboniferous Limestone slopes (Kellaway and Welch, 1948; Cave, 1977). Fine-grained breccias on the borders of those fans (Kellaway and Welch, 1948) have been mapped as marker horizons at Goose Green (Fig. 2.3). Other wadi fans consist of cones of alluvium built up by streams (Cooke and Warren, 1963) with channel and inter-channel sub-environments. These have been mapped in the study area as the sandy mudstone facies and cyclic facies of the marginal deposits respectively. A microcosm of the alluvial fan environment is exposed in the Yate Bypass cutting (Fig. 2.17), where a lobate asymetric tongue of cross-bedded channel sands containing mudstone clasts ('sandy mudstone facies'), banked up against a ridge of quartzitic sandstone is overlain by a scree deposit ('breccia facies'). A small intercalation of well-bedded sandy mudstones ('cyclic facies'), dipping north, forms the inter-channel deposits of the western bank of the channel.

Marginal deposits mapped by the Geological Survey along the Little Avon Platform are well exposed at the Poundhouse Farm site (Fig. 2.9). These sediments resemble the main sequence and are cyclic. The most complete cyclothem is shown in Table 2.1.

FIG 2.17

SECTIONS OF THE NORTH (TOP) AND SOUTH (LOWER) BANKS OF THE BYPASS CUTTING AT BROAD LANE YATE.

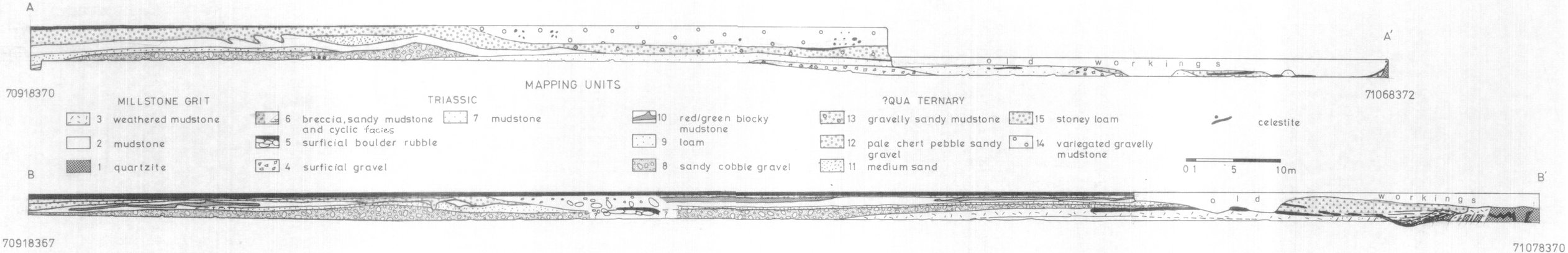

Table 2.1: A complete cyclothem of the cyclic facies

red blocky mudstone	
green blocky marl	
coarse dolomitic sandstone	1 metre
green blocky marl	
red blocky mudstone	

An unusual sinuous deposit of brecciated Millstone Grit mudstones, mapped at the Goose Green site as the mudstone breccia facies and containing a large deposit of Type B celestite is interpreted as a cut-and-fill channel deposit (Cooke and Warren, 1963) (Fig. 2.18). In modern deserts the drainage network is not restricted to the wadi fans and the pediments are cut by many channels, 1-3m deep, filled with alluvium up to the pediment surface (Cooke and Warren, op. cit.). Detailed examination of hand specimens (Plate 25) indicates that the mudstones were first dolomitized and then brecciated, the brecciation was both pervasive and also involved movement and rounding of some of the clasts. Fabrics indicitative of a paludine origin (e.g. Freytet, 1973) are absent and the mudstone breccias resemble pene-contemporaneous vein-type breccias described by Elliot (1961), in Triassic rocks of south Nottinghamshire, as morphologically distinct from simple desication cracks. It is suggested that the brecciation was a result of hardening and shrinking of the mudstone subsequent to dolomitization (Van Houten, 1962) and subaqueous reworking of the mudstone bedrock along a stream channel. The fine mudstone debris produced was deposited as an overbank deposit of soft clay (Fig. 2.18).

The reg or deflation debris of the Triassic land-surface is exposed at the Yate Bypass site and mapped as Units 4 and 5 (Fig. 2.17). Unit 4 consists of angular hematised sandstone fragments in a typical residual deposit of sand, iron oxide with some mud (e.g. Gardner, 1974, p317). Unit 5 is similar to Unit 4 but also contains many different exogenic blocks up to 40cm across and is cemented by sparry calcite. It probably represents the

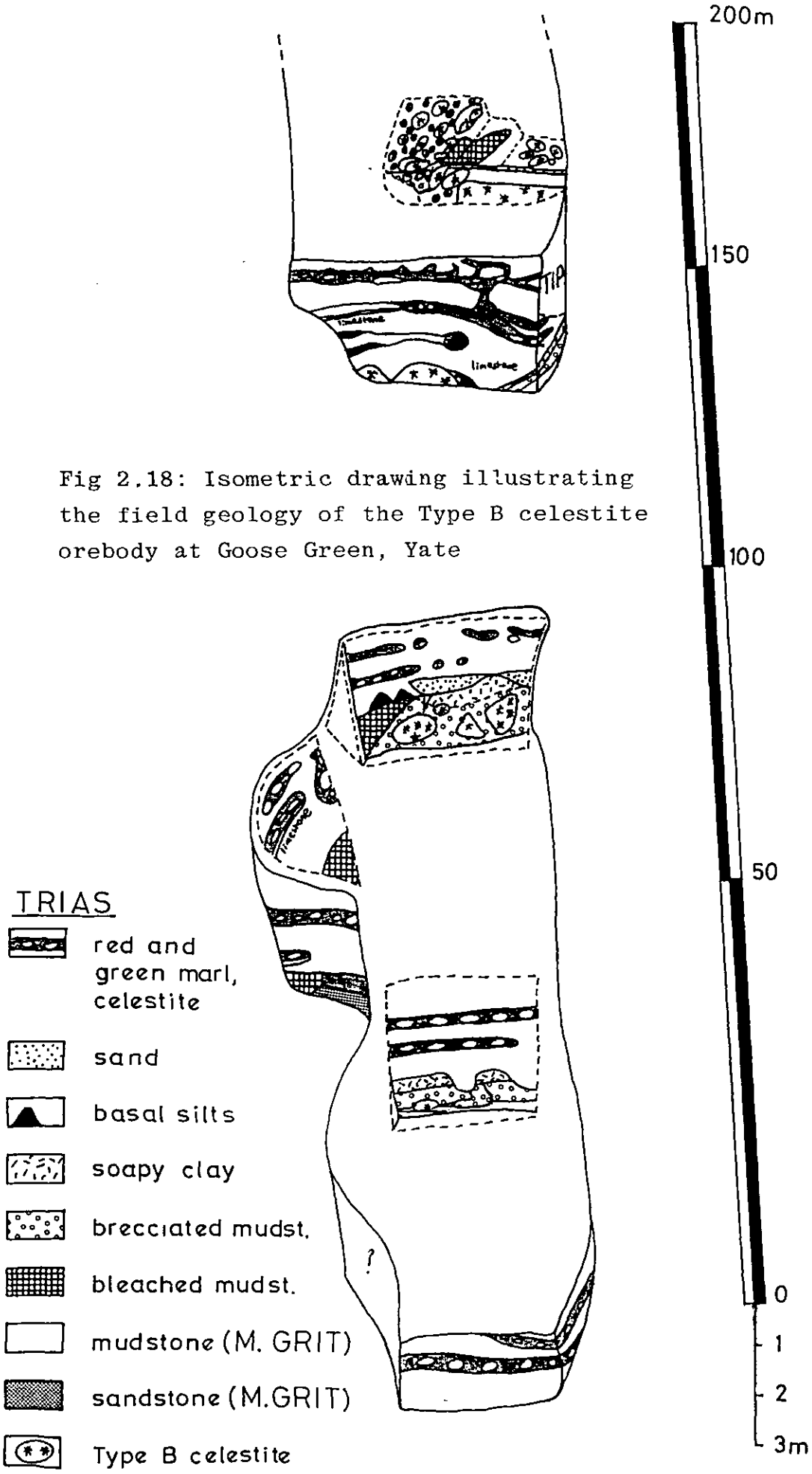

Fig 2.18: Isometric drawing illustrating the field geology of the Type B celestite orebody at Goose Green, Yate

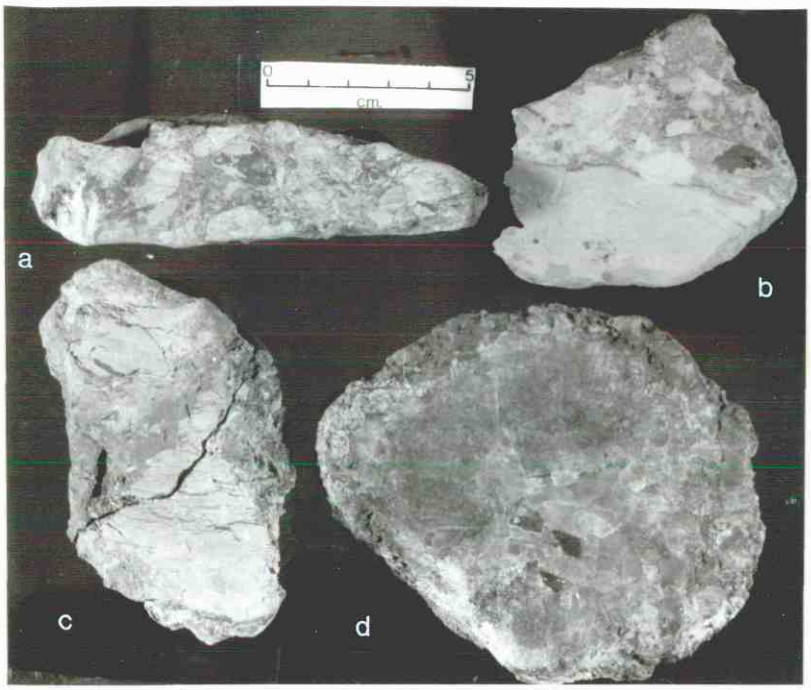

Plate 25: Rocks of the cut-and-fill channel deposit at Goose Green, arranged stratigraphically and showing
a) rounded outline and juxtaposition of clasts,
b) diffuse contact of clast with parent material,
c) pervading stringers of marl brecciating mudstone,
d) spherical impregnation of grey prismatic Type B celestite.

Plate 26: East face of the celestite working at Winter's Field, showing a vein of celestite (in shadow) in Millstone Grit mudstones, breaking up into a 'mumbler deposit' in the overlying Clay Head.

lag of a powerful ephemeral stream that produced upon evaporation a cluricrust of calcite cement.

2.5.1.3 ?Triassic rocks at Summer Bridge, Tytherington

The celestites at this locality occur in sediments that have been mapped as 'Keuper Marl' by the Geological Survey (Fig. 2.19, 2.20) but are of a deep 10R hue and contain a mineralogy of quartz, dolomite, illite and hematite with a large sanidine component (XRD analysis). Cross sections of the site show drape folding associated with penecontemporaneous movement along Iron Acton Fault, and the sediments are thought to be mostly reconstituted Carboniferous rocks, deposited along the fault scarp (Fig. 2.21).

2.5.1.4 Possible Quaternary terrace gravels of the Yate Bypass exposure

River Terrace gravels have been recorded by the Geological Survey at (708890) and (711876) near West End (Fig. 1.5). The second occurrence, as exposed at the West End site, consists of up to 150mm of light brown pebbly sandy clays. Very similar rocks are also present at the Winter'sField and Yate Lower Common sites, as a cover of reddish yellow (7.5YR 6/6) clayey sands and sands with occasional quartz or quartzite pebbles. The lower contact of these sediments is clearly defined and has also been cryoturbated (Fig. 2.22) showing that they are not pedogenically derived from the clay Head beneath. The gravels are younger than the dissected 60-85m surface and may possibly represent aggraded terrace deposits of the north-flowing river, before headwater capture by the Ladden Brook, described by Smith (1963). The gravels contain only isolated cleavage fragments of celestite and are of no direct economic importance but can interfere with exploration work where not previously recorded.

A quite different type of deposit however has been mapped as River Terrace gravel by the Geological Survey near the River Frome at Yate (Fig. 1.5). Exposures along the Yate Bypass cutting show a reddish brown cobble gravel

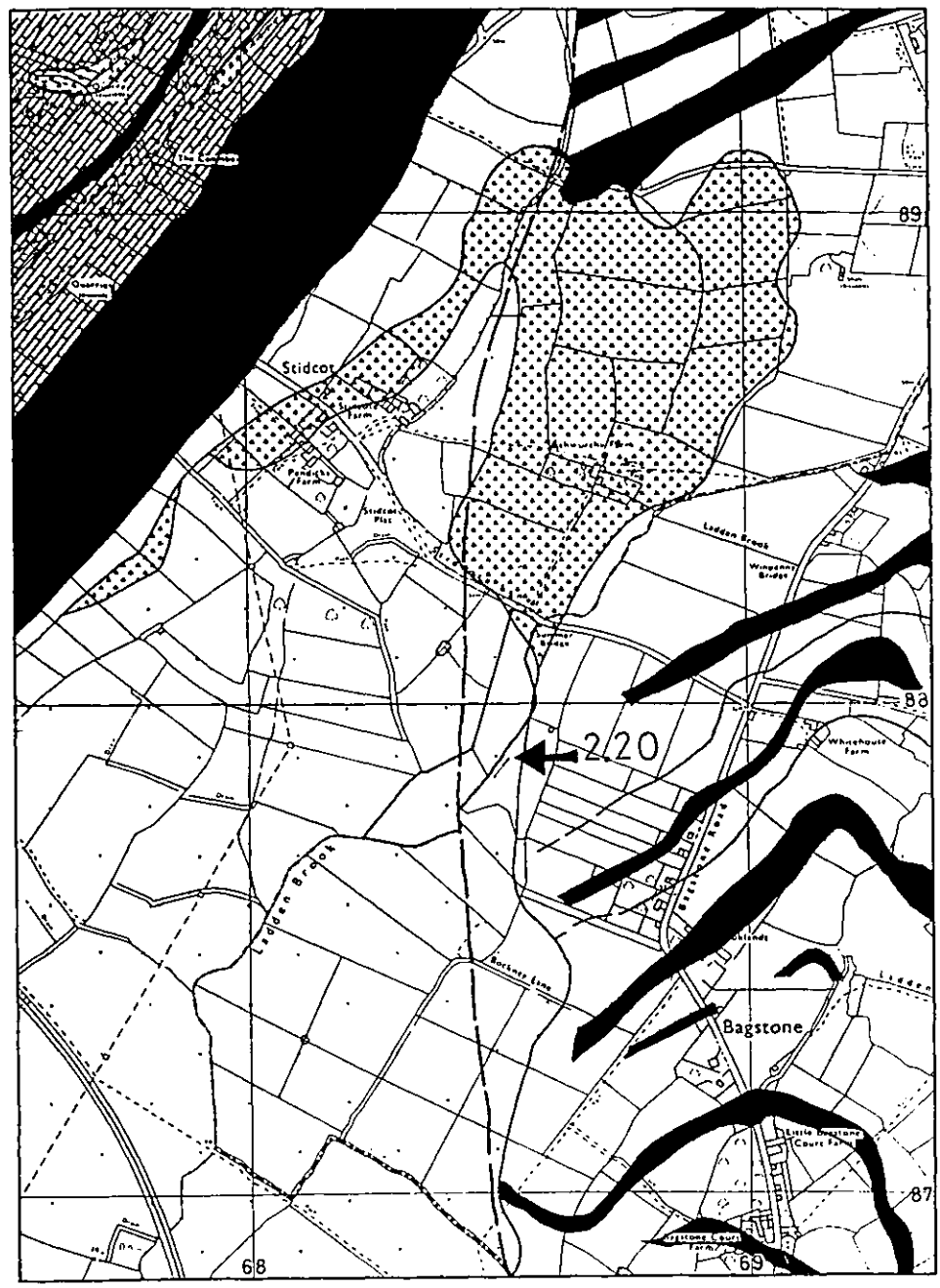

Fig 2.19: Geology of part of the Marle Hills Basin (based on published one-inch sheets).
For explanation og geology see Fig 1.5

Fig 2.20: Geological sketch-map of the Summer Bridge (Tytherington) site, showing location of B.M.C. test holes
Geological legend as in Fig 1.5

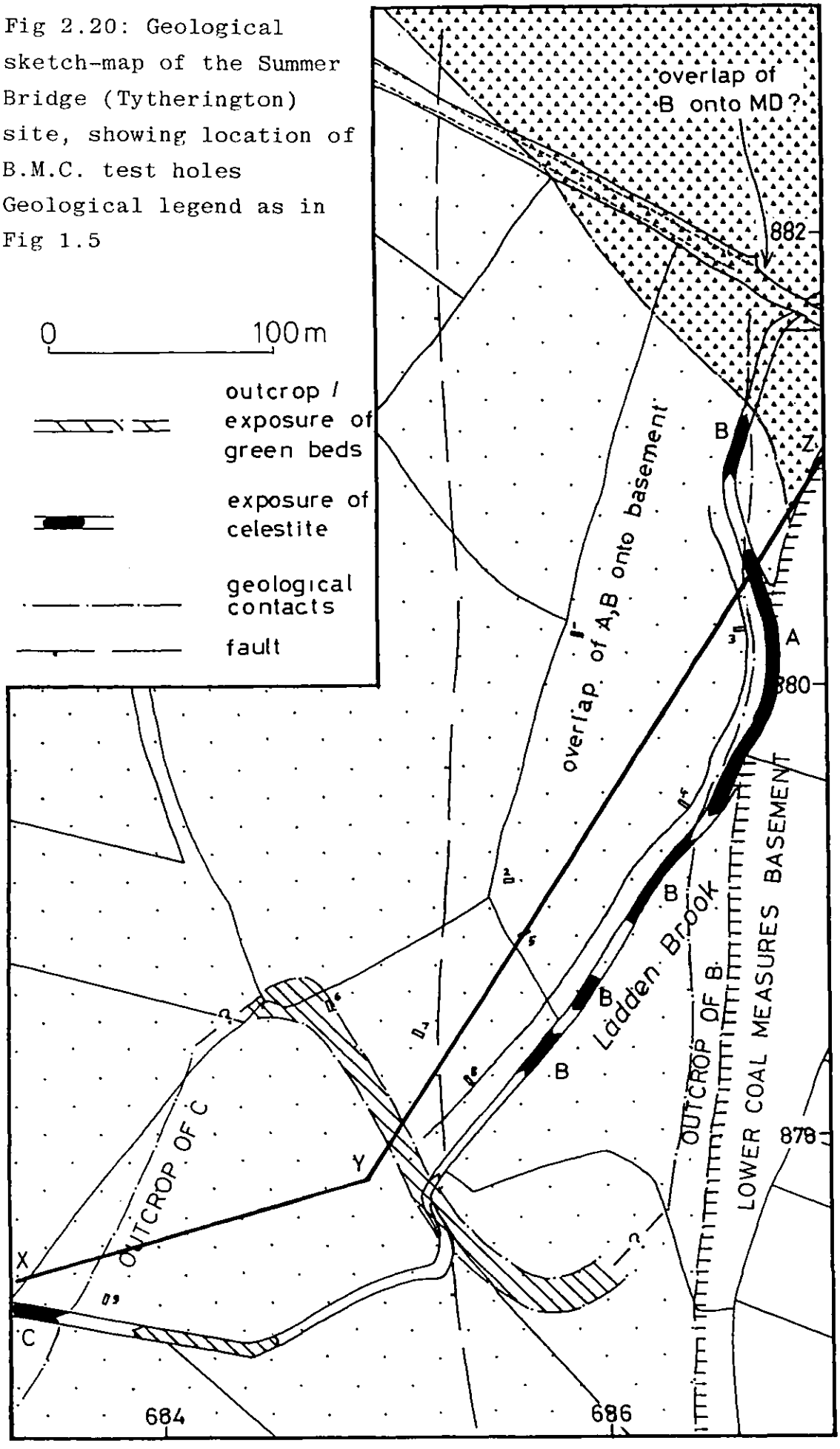

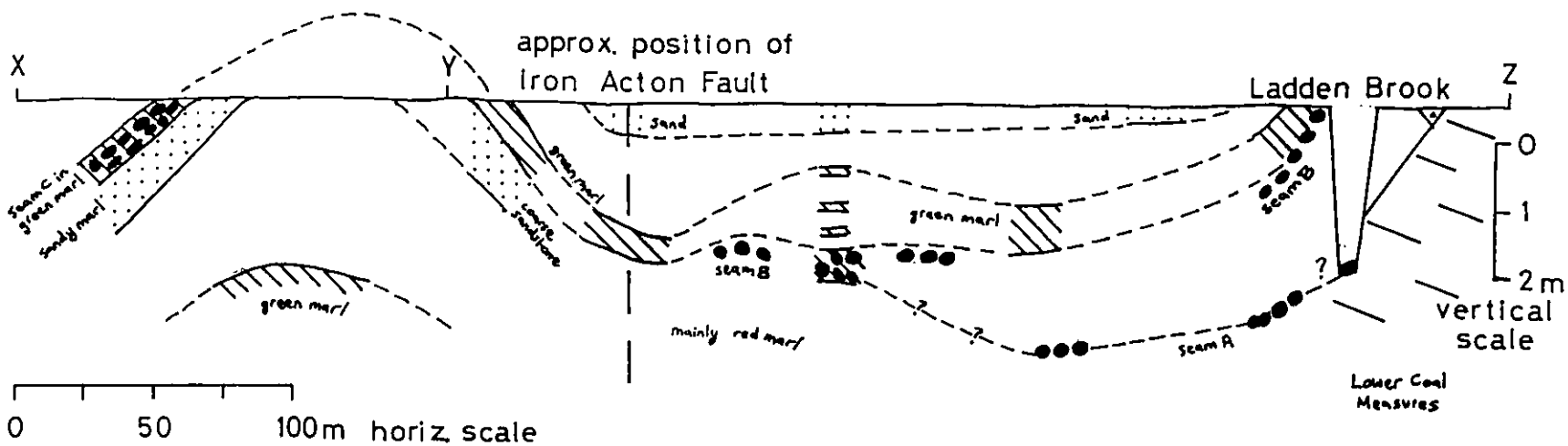

Fig 2.21: Structural interpretation of the Summer Bridge site along section X-Y-Z (Fig 2.20)

Fig 2.22: Cryoturbation features at the Winter's Field site, showing plug and pocket structures.

1) South face, 29.4.80, showing cryoturbation both before and after deposition of Terrace Gravel sands (c,d). Note segregation of detrital celestite into gravel and sand (a,c) and stratification (b). Field relationships in (d) indicate the the mumblers were formed before a cryoturbation phase.

2) South face, 16.5.80.

(a) Detail of sand/Head contact showing mumbler truncated by the sand, which includes fragmented Type C celestite.

(b) Sand pocket, mineralized in upper horizon with giant celestite crystals. Note 'in-situ' mumblers of celestite in positions of growth on the L.H. side.

(c) Detail of carbonaceous shale showing reworking and inclusion in stratified celestite sand.

3)South face, 10.6.80. (a) shows carbonaceous shale overlain by upper Head horizon, indicating two stages of Head formation.

4) Detail of south face, 1.9.80, showing flow textures in carbonaceous shale, rafts of stratified celestite sand and injection plug of Clay Head.

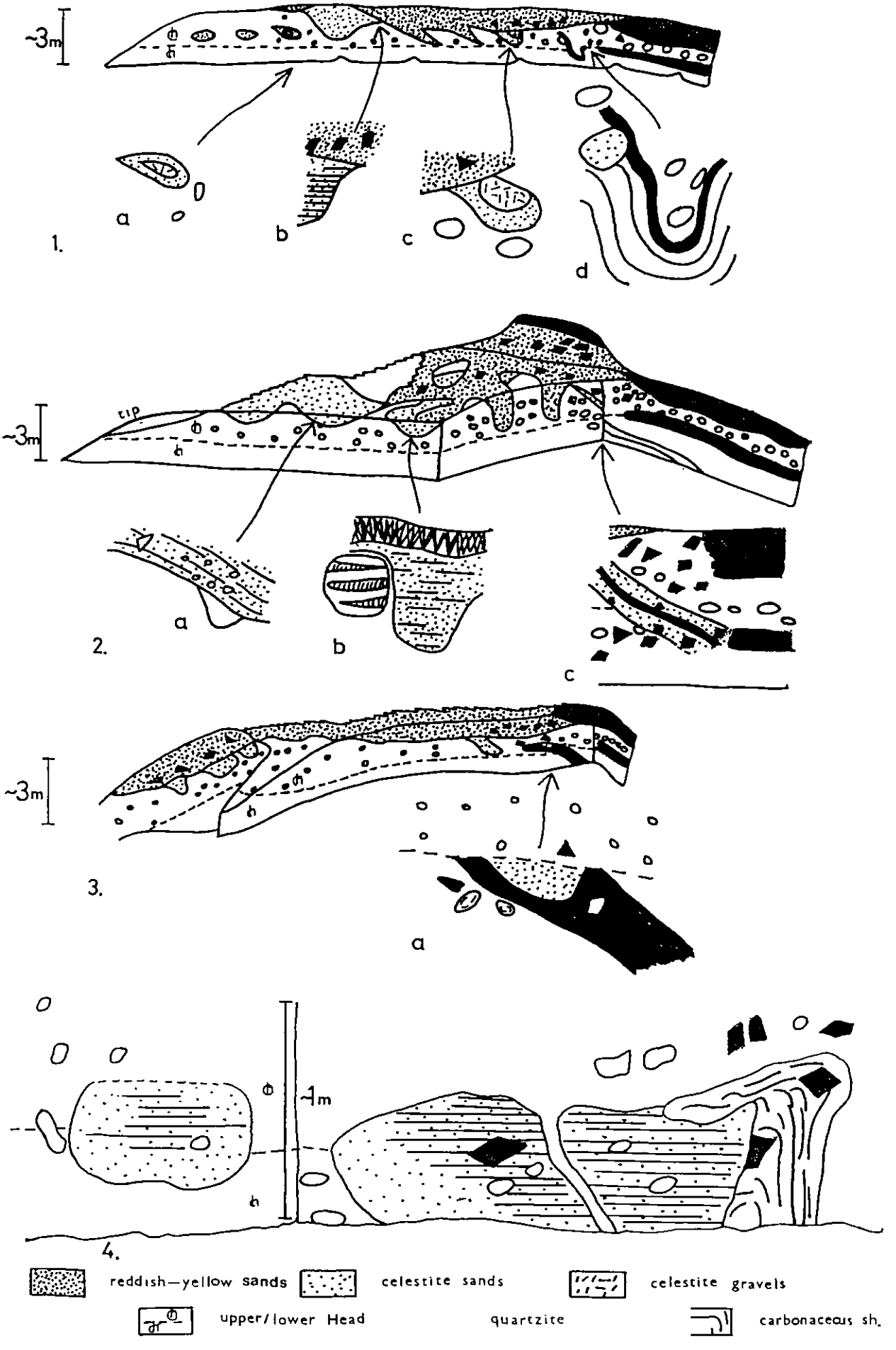
~3m
1.
a
b
c
d
~3m
tip
2.
a
b
c
~3m
3.
a
1m
4.
reddish—yellow sands
celestite sands
celestite gravels
upper/lower Head
quartzite
carbonaceous sh.

adjacent to marginal Yate Formation deposits overlying a celestite seam (Fig. 2.2, Unit 8 in Fig. 2.17). The gravel is a well bedded moderately well sorted sandy very coarse gravel with rounded quartzite, chert, ironstone, sandstone, crystalline limestone and corroded celestite with scalenohedral calcite clasts fining upwards through a sandy very silty mudstone 'loam' (Unit 9) to a reddish brown blocky mudstone with greyish yellow festoons (Unit 10). Whereas textures clearly indicate a fluvial origin the age of the deposit is uncertain. It may be that the three units are Quaternary alluvial or fluvio-glacial deposits laid down following the unroofing of the Triassic rocks during that time (see 1.4) for Unit 8 occurs at a constant height of 8m above present day alluvium; that is at a similar level as the second Terrace of the River Avon. However Units 8 and 10 could also be interpreted as Triassic marginal deposits of post-celestite age; they resemble microcyclothems (Wills, 1976) of low angle alluvial cone or torrent delta gravels overlain by sheetflood sands, which dried out producing the mudflats above. Supplementary evidence is provided by the localized occurrence of the deposit and their existence so close to the Frome.

The Yate Bypass section also exposes a higher, pebble gravel, mapped as Unit 12 that rests with unconformity on the beds beneath (Figs 2.2, 2.17). This is a paler (10YR-2.5Y) gravel of white chert with lesser quantities of sandstone and subrounded quartzite clasts in a sand and white mica matrix with sandy partings. It is possible to interpret this bed as a river gravel, deposited in response to the exhumation or re-exhumation of the Tanhouse Cherts outcropping ~1km to the east and therefore either of Triassic marginal deposits or Quaternary age; the upper surface of the unit is also veined by celestite. The situation is complicated further still by the nature of the succeeding strata. On the north bank of the cutting Unit 12 passes through a hybrid rock, Unit 13, into a variegated mud or clay, Unit 14, containing chert pebbles of a similar (bimodal) size distribution as those

recorded for Unit 12. Unit 14 also contains heavily weathered celestite nodules which appear to be concentrated near to beds of celestite beneath, and also cleavage fragments of celestite, suggesting a derivation from the bed beneath. Texturally, Unit 14 may be equally well interpreted as a boulder clay (e.g. Pettijohn, 1975 p171) or a Triassic mudflow conglomerate (e.g. Tucker 1977). To date glacial till, though suspected (Hawkins and Kellaway, 1971) has not been reported in the study area. However supplementary evidence may be provided by the thrust-like disturbance on the south wall of the cutting (Fig. 2.17); dipping at a low angle to the chert gravel and brecciating the formation beneath, which may have been produced by an overriding ice sheet.

In the absence of dates or paleontological evidence Units 8 to 15 cannot be proven to be either Triassic marginal deposits or Quaternary strata. Thus the possibility of Post-Triassic or'Quaternary celestites' must always be borne in mind specifically for the Yate Bypass area and more generally in all of the discussions which follow.

2.5.2 Description of the Epigenetic celestites

The lithology and textures shown by the epigenetic celestites are most conveniently described with reference to the different varieties of host rock within which they occur. In the account below most consideration is given to the Type C celestites in Carboniferous mudrocks and the Type B celestites in the mudstone breccias of the marginal deposits for it is in these occurrences that the bulk of the epigenetic celestite occurs. In all situations the celestite displays textures indicating fracture filling or replacement.

2.5.2.1 Celestites replacing Carboniferous mudrocks

The celestite occurs as veins, spherical masses and scattered nodules in the Carboniferous mudrocks, especially near to quartzitic sandstone beds.

a Celestite veins

These are tabular masses, of usual thickness 5-10cm that extend downwards from the unconformity dipping with the bedding, along leading planes or fractures or discordantly, for up to 200m along the strike (Plate 26). The depth to which the veins are worked varies from about 5-6m at Leechpool, Winter's Field and Yate Court to 10m at Cromhall (Nickless et al., 1976). Three principal fabrics may be present, each one gradational to the others. The tabular veins may consist of a central zone of coarse celestite, usually surrounded by a selvedge of wallrock impregnated with celestite; of compound veins, consisting of alternating layers of celestite crystals and impregnated wallrock or of massive celestite in which textural distinctions are not present.

The central zone contains white or blue tabular, or granular, celestite crystals set perpendicular to the wall rock and coalescing in the centre or lining druses, typically 3cm wide (Plate 27). The area of impregnation, known as 'rab', may be of greater diameter than the central zone, up to 20cm in diameter. Two varieties of such impregnated wallrock are recognised. The first forms a clear contact to the coarse celestite and consists

Plate 27: A typical vein celestite, showing from bottom upwards, s: foot-wall selvedge of microcrystalline celestite, c: central zone of coarse tabular celestite, i: impregnated zone of medium tabular celestite in mudstone hanging-wall. Specimen YC02.

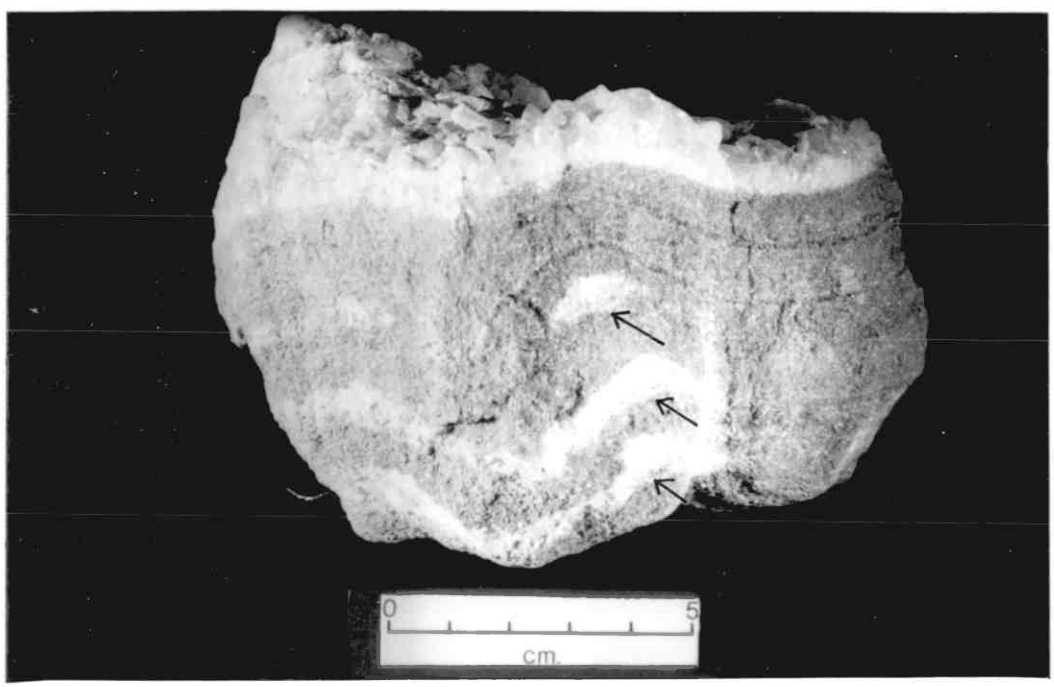

Plate 28: Celestite vein with thick microcrystalline selvedge. Note 'saddle-reef' texture of medium-grained tabular celestite in arcuate flexures over thin yellow laminae (arrowed). For explanations, see text. Specimen WF35.

of fine celestite laths barely visible to the unaided eye which cement an area 0.5-5.0cm across. The second variety is transitional to the central zone and, where present, contains fine-to-medium grained tabular or granular purple, blue or white celestite crystals set in a mudstone matrix.

Certain specimens of vein celestite that show a sharply defined lower surface of microcrystalline celestite cement, sharply contrasted with comb-textured central zone celestite that grades into an upper area of coarse celestite crystals pervading wallrock provide clues for the origin of the fabric (Plate 27). Also, elsewhere, thin veins of coarse blue celestite are also observed traversing the microcrystalline cement and passing into the mudstone host. It is suggested that, after an initial phase of mineralisation of the wallrock by microcrystalline celestite, a fracture fill of coarse celestite crystals grew inward, after which mineralisation was directed upward, first brecciating and then replacing the host rock on the upper surface of the vein.

"Saddle-reef" textures occur in wallrock cemented with microcrystalline celestite where there are small arcuate flexures of fine-to-medium grained tabular or granular celestite interbedded in the selvedge (Plate 28). These structures are always associated with yellow coloured bands in which fine single crystals of celestite may be scattered. The anticlinal arching over the flexures may be of sufficient amplitude to disturb the central zone of the vein. The flexures range in magnitude from 0.5cm in height to, in one specimen, lenticular pockets of drusey celestite 4cm across.

Sections through compound veins show lenticular areas of fine or medium grained white, blue or purple tabular or granular celestite separated by less densely packed zones impregnated with tabular celestite; or druses (Plate 29). The areas of lower concentrations of celestite are probably bedding planes along which the coarse celestite crystals were able to freely grow.

The third form of vein celestite is extremely common and consists of tabular, massive celestite, typically 5-7cm thick with smooth, regular contacts to the wallrock.

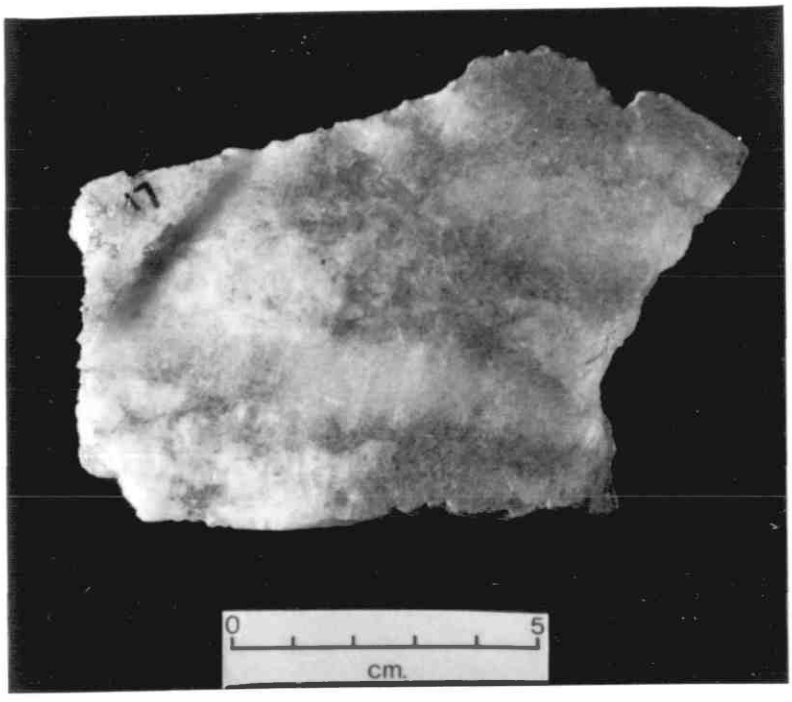

Plate 29: Section of typical compound vein celestite, showing densely-packed lenticular zones separated by mudstone impregnated with tabular celestite. Specimen WF31.

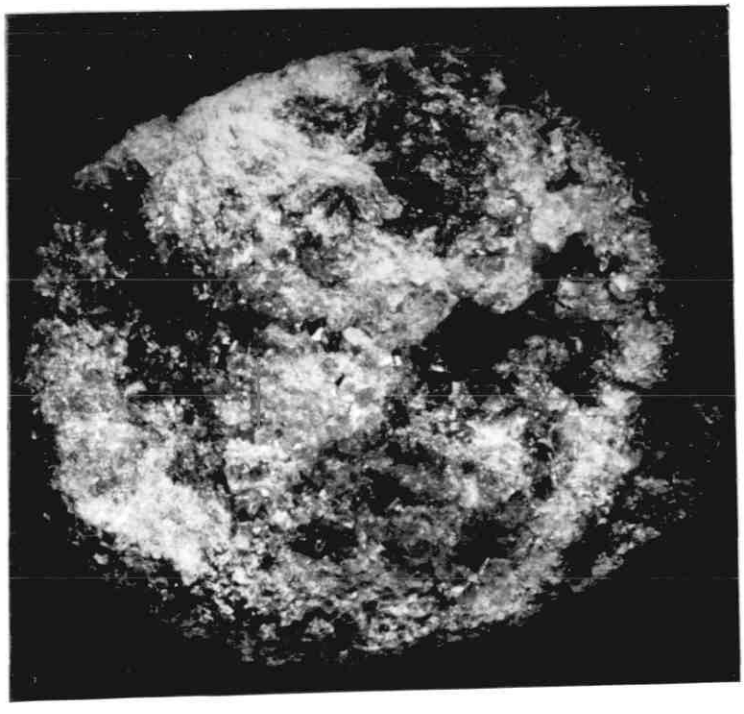

Plate 30: Spheroidal celestite. Specimen WF37.

This celestite may form veins or occur as nodular masses, and consists of fine-to-medium grained tabular or granular celestite and is coloured blue, white or purple. Presumably this form of celestite crystallized in blocky mudstone, without well defined bedding planes, along which coarser tabular celestite would have developed.

Some of the specimens of compound vein celestite bear a fancied resemblance to the "macrocellular" varieties of Type A celestite (compare Plate 29 with Plates 11a and 22) and it is possible that these too may be relic fabrics of an earlier calcium sulphate.

A two-stage origin may be applicable here:-

1. Celestite first replaced the macrocells of calcium sulphate, preserving the morphology so that the outer surfaces of the macrocells on the edge of the nodule, where separated from the mudstone, appear smooth.
2. Later coarser celestite crystals grew in the mudstone along small fractures or bedding planes. Small druses were produced by solution of the clays in the mudstone.

b. Thin celestite veins

As well as the large veins described above thin tabular bodies, less than 5cm in diameter also occur, particularly in the mudstones on the peripheries of the orebody, in which a central zone is irregularly defined and convoluted bands of medium and coarse grained blue or white tabular celestite occur in wallrock with coarse blue impregnated celestite or a microcrystalline celestite cement. In this situation the coarse impregnating celestite may show crystals of the thick tabular habit (see 2.3.3). This form of celestite, common in shaley mudstones probably resulted from growth in a heterogenous fabric in which the fracture-wallrock division is not differentiated.

c. Spheroidal celestites

The Type C celestite orebodies may locally contain spheroidal bodies of granular celestite usually in the order of about 10cm across which differ from the nodular celestites described below in the colour of the crystals

(always purple, blue or white) and nature of the outer surface of the spheroids, which are covered with granular or prismatic crystals facing radially outward (Plate 30). Some of the spheroids are geodic and consist of thick tabular, granular or rarely rhombohedral crystals projecting into a void (Plate 31).

It is difficult to account for the origin of the spherical celestites. They cannot be concretionary, for some contain voids. It is unlikely that they are replacements of an earlier authigenic mineral because of their shape (gypsum and anhydrite nodules are ovoid). It is suggested that they are the infillings of cavities present in the basement mudstones at the time of celestite mineralisation.

d. Celestite nodules

In some localities, Type C celestite does not form sheetlike vein deposits but occurs as beds of oblate nodules, typically 10cm in length, with noticeably angular, rugged outer surfaces. These nodules of celestite resemble those of Type A celestite apart from differences in the nature of the host rock and consist of fine white, pink or purple celestite laths, in some cases showing alignment parallel to the edge of the nodule.

Mudstone inclusions in the nodules are usually a green hue, (e.g. 5GY8/1) in contrast to the reds in the vein celestite. In some cases where coarser crystals are present the nodules may be drusey.

Such nodules of epigenetic celestite usually occur in association with quartzitic sandstone beds either near the unconformity at the contact with thin mudstone layers or scattered in the surface head over the quartzites and mudstones. Specimens of nodular celestite from Winter's Field show massive medium-grained pink tabular celestite cementing blocks of quartzite, indicating that brecciation of the quartzite took place before the celestites were formed. Pink, white, orange or yellow epigenetic celestite nodules, of granular habit occur in the Millstone Grit mudstones and celestite sands at The Rectory (Fig. 2.23).

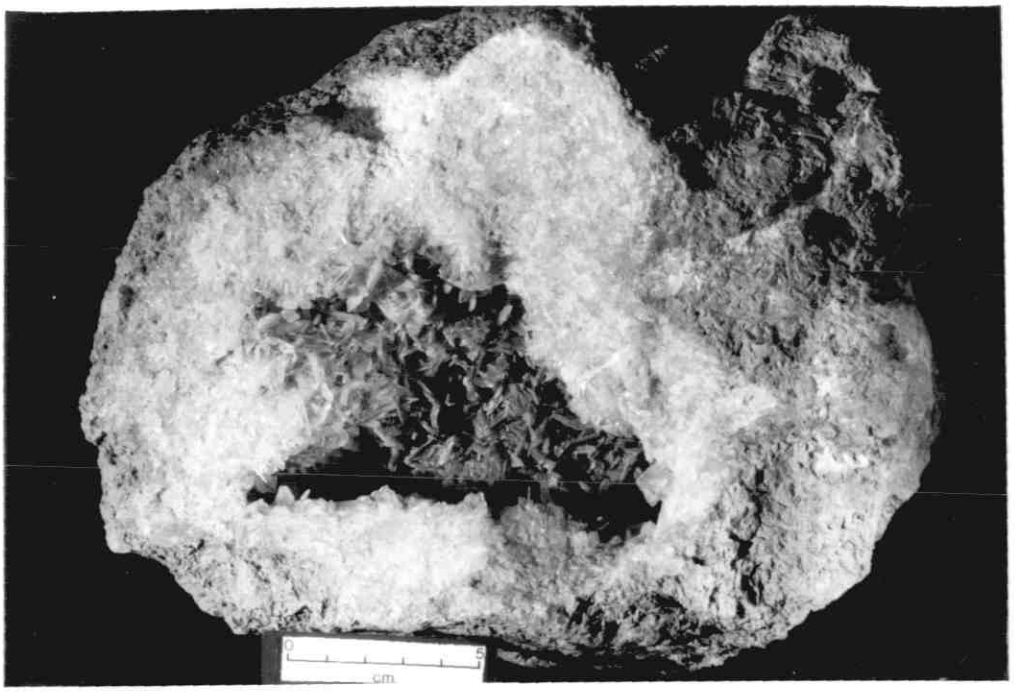

Plate 31: A large spheroidal celestite, with drusey cavity. Specimen YCO3.

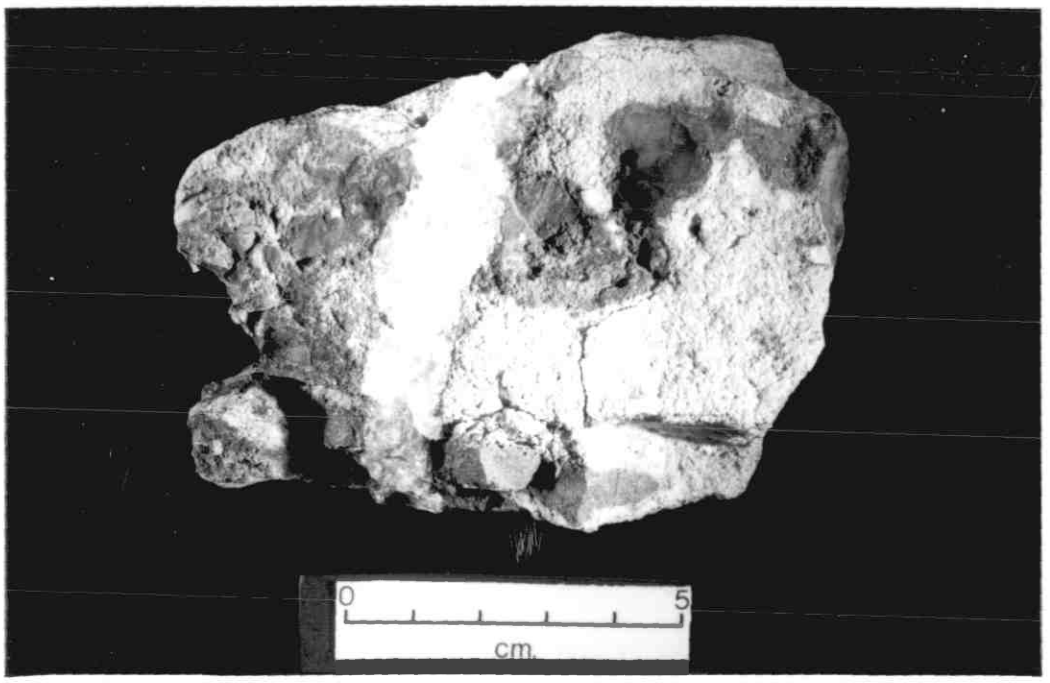

Plate 32: A mineralized quartzite from the Yate area, clearly displaying the cross-cutting relationship of the celestite to the earlier iron metasomatism (intermediate shades).

Fig 2.23 (overleaf): Geological sections at The Rectory.

1) Generalized E-W section across the east of the site, showing relationship of mineralization to Paleozoic rocks ,celestite sands and mudstone and effects of periglacial weathering.

2) Field sketch of sewer trench wall (71498314). Inset shows detail of mineralized marginal deposits and quartzite.

3) Fissure in quartzite with vein celestite infil, now weathered to a gravel.(71528312)

4) Field sketch of a sewer trench wall from (71518313) (L.H.) to (71548310) (R.H) showing celestite nuggets and celestite in paleo-cavity in quartzite.

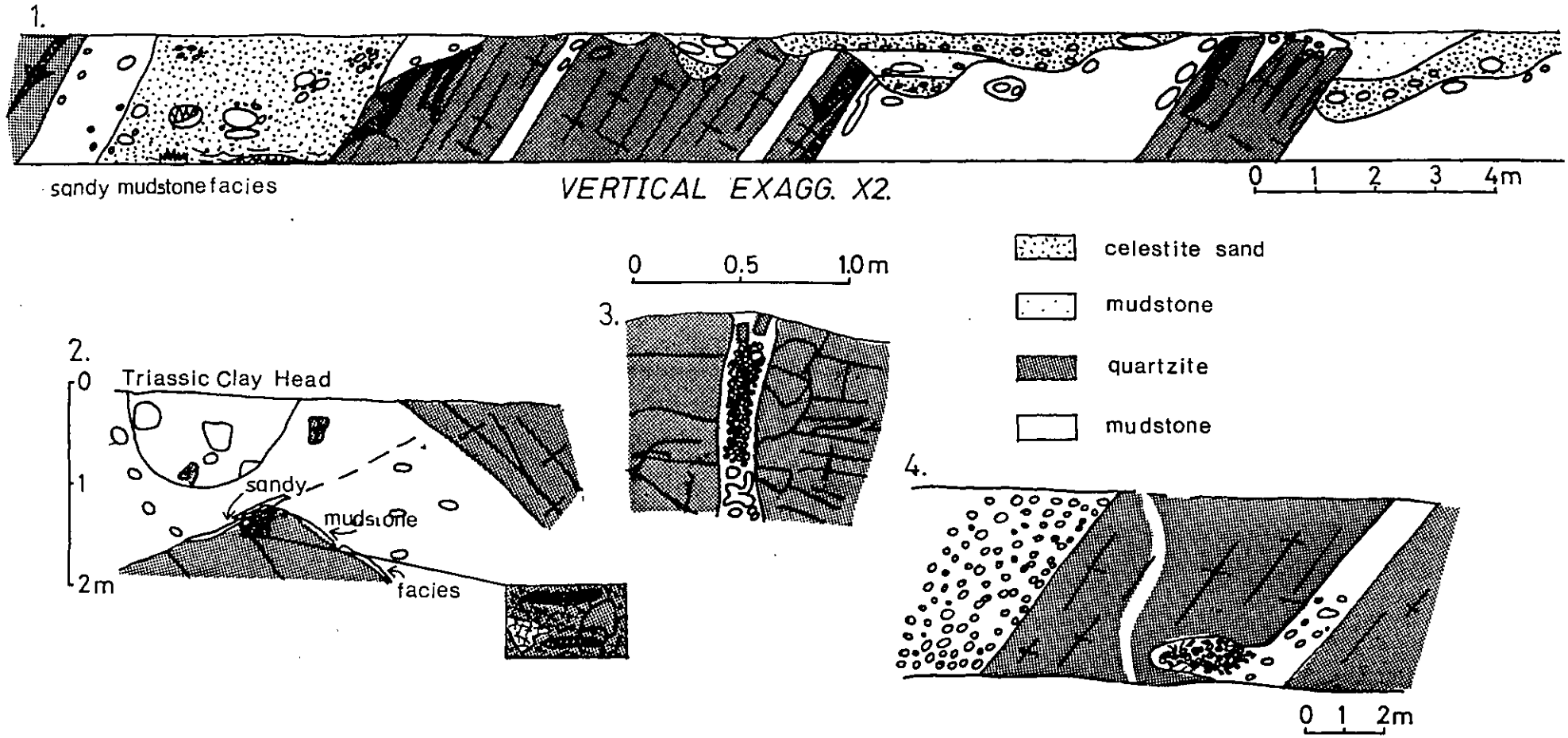
1.
sandy mudstone facies
VERTICAL EXAGG. X2.
0 1 2 3 4m
celestite sand
mudstone
quartzite
mudstone
0 0.5 1.0m
3.
2.
0
Triassic Clay Head
1
sandy
mudstone
2m
facies
4.
0 1 2m

The morphology and strati graphic positioning of the celestite nodules indicate that they may have formed by similar mechanisms to Type A celestite, that is, by growth in a soft sediment, possibly by replacement of macrocellular calcium sulphate. Permo-Triassic weathering may have altered the mudstones and sandstones in the basement, producing a regolith of fractured quartzite and a pedogenically reworked clay, in which the nodules could have formed. It is also possible that the green colour of the clays may have resulted from reduction of the free iron by mineralising solutions of an earlier calcium sulphate mineralisation; but evidence for an anhydrite or gypsum precursor can be established by petrographic examination only.

Alternatively, a deposit of nodular rather than tabular vein-like celestite may have resulted from the nucleation of celestite at restricted scattered sites in the dipping mudstones rather than along a plane. Such inhomogeneities in the concentration gradient of the depositional fluids may have arisen from the lack of fissures or bedding surfaces, along which a more continuous orebody would have developed.

2.5.2.2 Celestites replacing Carboniferous sandstones

Although Nickless et al (1976) stated that "celestite has not been observed in close association with sandstones" celestite was observed in Carboniferous sandstone at The Rectory, Yate Bypass and Winter's Field sites.

The celestite forms linings up to 10cm across along mudstone partings, bedding planes, fractures and joints and may also replace the sandstone either side of the fissures along small stringers less than 2cm wide or as a cement (Plate 32). It consists of fine to medium grained white or blue tabular or granular crystals. An effect analogous to lustre mottling is produced on some fracture surfaces. The quartzites are locally brecciated, presumably by the force of crystallization of the celestite, resulting in vugs.

Fig. 2.23 shows textures produced by the mineralisation of quartzitic sandstone as observed at The Rectory.

Here giant (up to 5cm diameter) orange or white comb-structured celestite crystals line joints and bedding plans, buckling the strata, to depths of 3m below the present day surface. Caverns are also filled with vein celestite, now weathered to a sand.

2.5.2.3. Celestites replacing Permo-Trias ironstones

Where replacive celestite comes into contact with ironstone concretions it selectively replaces the hematized mudstone in preference to goethite, which is left as relics in the mineralised area (Plate 33). The celestite usually is blue, grey or white, of varying texture.

In sandstones containing ironstone celestite selectively replaces hematite along mineralised fractures, leaving a rim of goethite on the walls of the celestite vein. The fracture is expanded as a result and in places brecciation of the wallrock may result. Where ironstone pervades the sandstone, the celestite veins transect the ironstone/sandstone contact. Areas that have been extensively hematized may however host much of the celestite.

2.5.2.4 Celestite replacing Triassic marginal deposits

The wadi fan deposits at The Rectory and at Yate Bypass are cemented by epigenetic celestite. Large deposits of Type B celestite have also been recorded at Goose Green West.

At Yate Bypass, sands and gravelly sands of the 'breccia facies' are cemented by two nodular layers of fine white and purple lathlike celestite impregnations up to 10cm thick (Fig. 2.2, 2,17). An association with red rather than yellow marginal deposits suggests that the celestite mineralisation preceded the dolomitization. The celestite can be traced onto the deflation debris of the pediment (Units 4 and 5), which it encrusts with nodules with characteristic spherical protuberances, 15cm across, containing hematized sandstone fragments and quartz pebbles (Plate 34).

Sediments of the 'sandy mudstone facies' are cemented by microcrystalline celestite and closely resemble

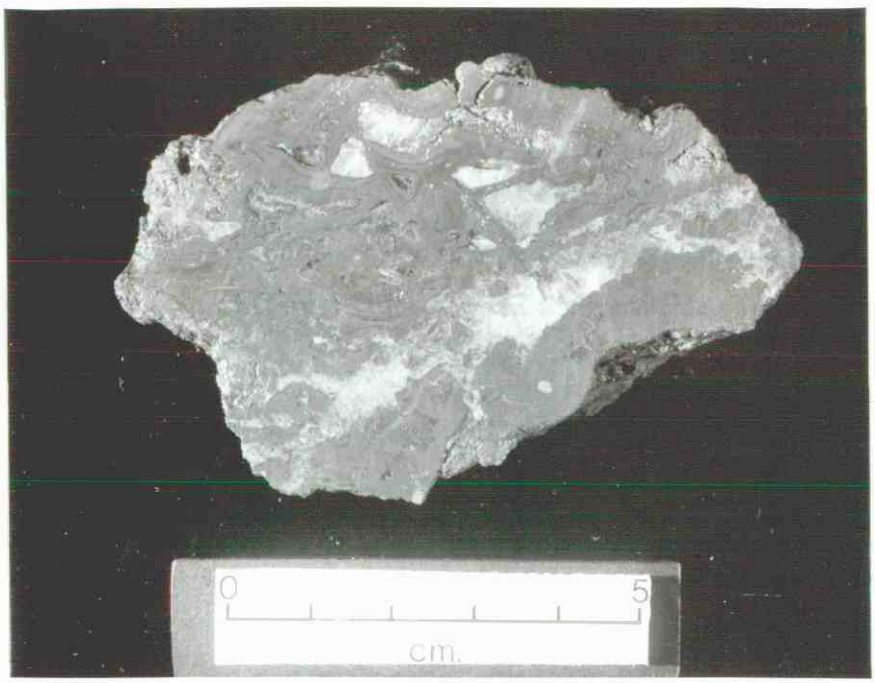

Plate 33: Celestite replacing ironstone concretion with selective replacement of hematized mudstone leaving geothite relics. Specimen BL01

Plate 34: Re-exhumed desert reg with quartzitic sandstone and ironstone debris mineralized with epigenetic nodular celestite. Yate Bypass Causeway, western sector.

vein selvedges as described in 2.5.1.1 (Fig. 2.24). Other rocks from The Rectory show druses and lenticular pockets, probably hollows left by the dissolution of calcium sulphate macrocells and coarse celestite cementing the matrix between the pockets (Figs 2.23,2.24).

The mudstone breccia facies at Goose Green contains a sinuous pipe-shaped orebody of Type B celestite up to 5m across and at least 200m long (Fig. 2.18). Viewed along the strike, the orebody consists of nodular masses of celestite, up to 1m in diameter haphazardly pervading the rock. However a pit at (71448370) also showed a remarkable terrace structure, with benches of celestite replacing higher levels from west to east (Fig. 2.18, Plate 35). This step-wise feathering out is well known from Type A deposits (Anon, 1960, see also 2.4.1). It implies that the source of the strontium lay immediately west, as viewed in section, from which the mineralisation filtered down to successively lower levels of crossing lithological boundaries. The smoothness and regularity of the benches indicates that after crystallization of the celestite it was planated by the stream that excavated the cut-and-fill channel. This structure obviously formed an extremely favourable environment for the deposition of the mineral.

In hand specimen much of the celestite resembles the compound vein fabric described above (2.5.2.1) (Plate 29) and may be of similar origin. It contains compacted areas of fine white granular, or deep red or transparent microcrystalline celestite up to 3cm in diameter separated by zones of mudstone breccia containing fine to coarse grained blue tabular celestite. The deposit also contains spherical impregnations of medium to coarse grained grey celestite of noticeably prismatic habit (Plates 3 and 25) replacing the mudstone hostrock.

2.5.2.5 Celestites replacing ?Triassic rocks at Summer Bridge, Tytherington

The three beds of nodular 'Type T' celestite at this locality occur as stratiform 'seams' but have certain unusual characteristics and cannot be assigned

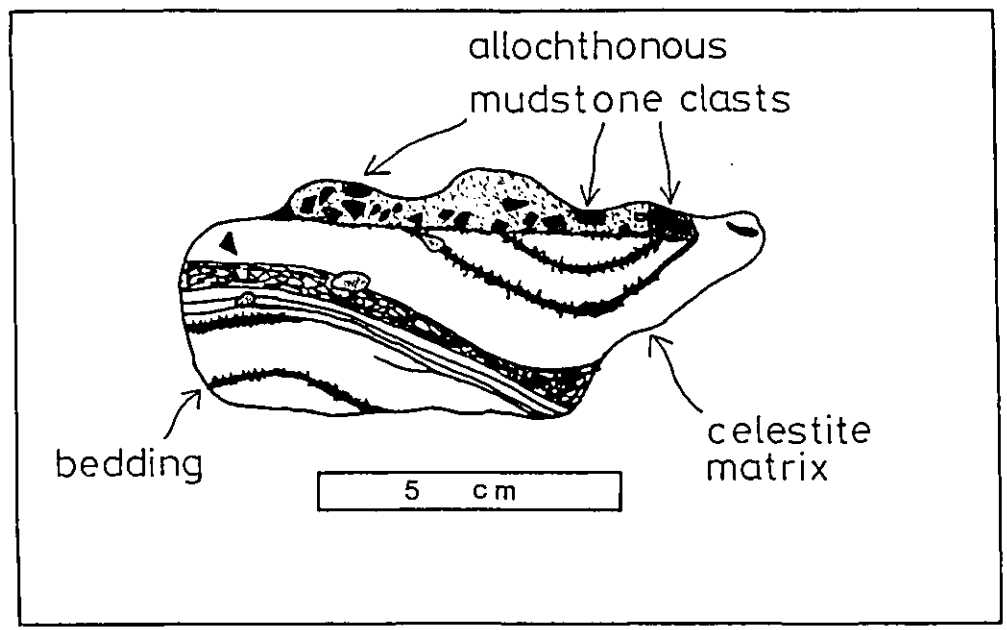

Fig 2.24: A 'celestite' of mineralized sandy mudstone. Specimen RY22

Plate 35: The Type B celestite orebody at Goose Green East, looking north. Celestite orebody is in mudstone breccia facies of marginal deposits. Note steps in orebody from left to right, producing 'terrace' structure. See also Fig. 2.18.

Plate 36: Epigenetic celestite vein at the contact of Units 12 and 14, on the north bank of the Yate Bypass cutting, north of Yate. Note chert pebbles (white) and celestite(pink) in the pebbley mud (Unit 14).

to any of the previous celestite types.

An epigenetic origin is ascribed to these celestites for three reasons: -

1) The nodules consist of medium to coarse grained impregnations of blue, grey, white and pink celestite (seams A and C) or pink tabular celestite (seam B). This form of celestite is not found at other localities of Type A celestite but is similar to other epigenetic celestites.

2) Sparry calcite has not been recorded.

3) The mudrock host of seam A, in particular, is not of an identifiable Triassic lithology.

Although there is obviously a temporal relationship between the mineralization and the faulting, a genetic link is more difficult to establish (see discussion in Chapter 5).

2.5.2.6 Celestite replacing terrace gravels of possible Quaternary age

A bed of fine to medium grained pink, white and blue celestite can be traced for 10m along the north bank of the Yate Bypass cutting at the junction of the chert pebble gravel and the gravelly mud (Fig. 2.17, Plate 36). The celestite impregnates the sandy matrix and includes chert pebbles and is clearly epigenetic. Immediately over the bed and elsewhere along the section, occur concretions of corroded celestite nodules but because of the weathered nature of the gravelly mud it is difficult to determine whether these have been transported or are weathered in situ.

The celestite is indistinguishable from the epigenetic celestite exposed veining marginal deposits on the south bank of the cutting (see 2.5.2.4) and may even be the equivalent of the upper celestite horizon in that exposure (Fig. 2.17).

2.5.3 Other epigenetic minerals of the Carboniferous mudstones

2.5.3.1 Baryte

Botryoidal masses of baryte were recorded in Millstone Grit mudstones at one locality along the causeway of the Yate Bypass (Fig. 2.2). Although baryte is a common gangue mineral of the Mendip Pb-Zn mineralization (Green and Welch, 1965) and occurs in the Carboniferous Limestone in the study area (Curtis, 1981) only trace amounts are found in the Bristol Coalfield (Kellaway, 1967). There is no apparent field relationship of the baryte to the celestites.

2.5.3.2 Gypsum

Gypsum occurrences have not previously been well documented in the Paleozoic rocks of the Yate Platform. From observations recorded by Sherlock (1918, 1938), independent enquiries and exposures in the Yate Bypass cutting (Fig. 2.2) it would appear that a 60m zone of pink alabastrine gypsum is present near to the centre of the Type C celestite belt (Fig. 2.12). The gypsum zone or belt consists of large nodular gypsum masses, up to 25cm across, either arranged in veins dipping with the Millstone Grit shales or as loose blocks in the overlying Clay Head. The enclosing rock is always bleached a green colour around the gypsum. In many hand specimens the gypsum contains red platey porphyroblasts up to 1.0cm in diameter scattered through the rock or concentrated at the nodule margins, where a 2.0cm border of red satin spar may also be present (see Plate 37). Red acicular porphyroblasts up to 0.2cm in length are also observed in one specimen.

The outer porphyroblasts in places preserve a relic texture of fine laths, showing foliation parallel to the edge of the nodule. Traces of celestite may also be present in inter-nodular areas of green mudstone or clay.

Field observations confirm Sherlock's (1918) statement that " ...occasionally gypsum replaces celestine locally in the Yate district and occurs in lenticular masses in

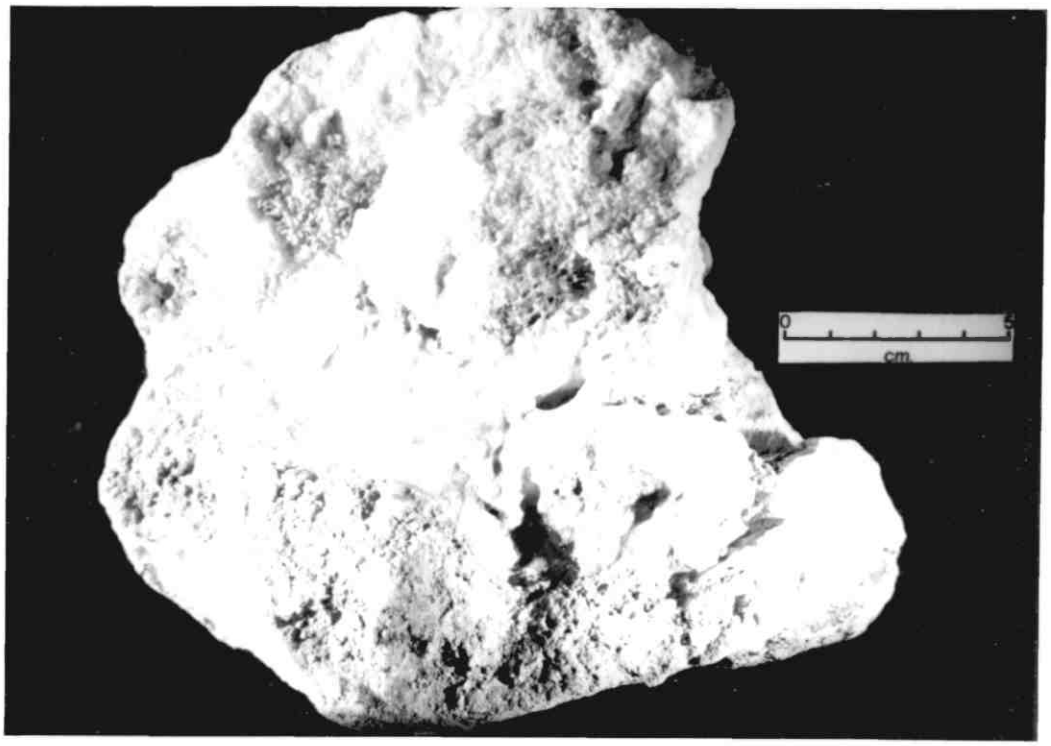

Plate 37: A typical alabastrine gypsum nodule from the gypsum zone of the Type C celestite belt at the Yate Bypass site. Gypsum appears white. Red platey porphyroblasts shown by P. Note smooth, water-worn outline of the nodule edge. Specimen BL34

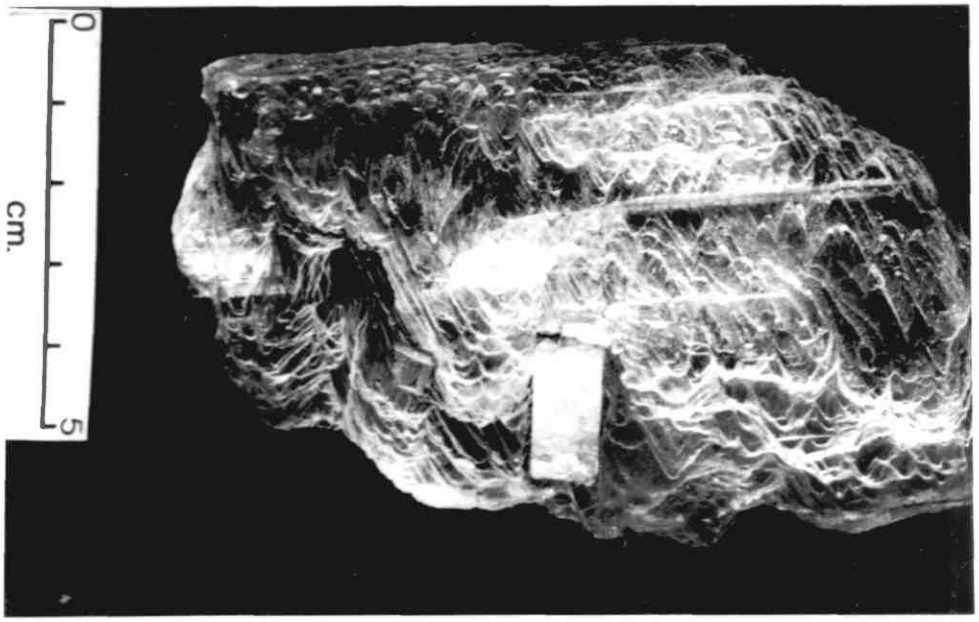

Plate 38: Selenite from near Hall End. It is suggested that the selenite crystallized in free space, surrounding the celestite lath (see text).

the middle of an area of celestine. The two minerals have sometimes been found in adjacent pits in the same field, yet were not intermixed."

A specimen of selenitic gypsum from near Hall End (712872) shows coarse transparent crystals with parallel growth surrounding a lath of white celestite (Plate 38). The relationship of the two minerals is not immediately obvious. A magnificent specimen on display in the Geology Museum at Bristol University, presumably from the Yate area, shows coarse clear selenite enclosed in a druse of Type C celestite, revealing that the selenite has grown in the void after the crystallization of the celestite. There is an aural tradition of large quantities of lime (=selenite?) infilling and surrounding giant druses in the Type C celestites of the West End district but until fresh exposures are opened up the field relationship of the two minerals will remain obscure.

The alabastrine gypsum is discussed in further depth in Chapter 3 where petrographic evidence is supplied to explain the megascopic textures described above.

2.6 MUMBLER DEPOSITS, CELESTITE SANDS AND CELESTITE GRAVELS

2.6.1 Introduction

During the Quaternary glaciations the rocks of the study area were subjected to intensive physical weathering in a periglacial climate. A full account of the processes acting in periglacial conditions is beyond the scope of this thesis ; the interested reader is referred to one of the standard texts (e.g. French, 1976; Pewe, 1969) dealing with this subject. The most important aspect for our purposes is that above a layer of permafrost an upper active layer of seasonally frozen ground was formed in the bedrock in which the rock was cryoturbated during alternate cycles of freezing and thawing.

The degree of deformation is a function of the porosity, permeability and composition of the bedrock. Argillaceous rock such as the Millstone Grit mudstones and Triassic marls were pulverised to a rock flour or Clay Head deposit, whereas more competent strata such as

limestones and quartzitic sandstones were broken up into a stoney Head containing rubble in a sandy matrix. This frost-shattering took place down to depths of at least 2m. Where beds of differing texture, porosity or permeability but of a similar degree of induration are present in the active zone, the differential action of the cryostatic forces in each bed combine to produce involutions such as pocket and plug, structures and festoons (Fig. 2.22, 2.23).

A Carboniferous Clay Head, consisting of a structureless light brown (2.5YR 6/4) lay, variegated green (10GY, 5G) and yellowish orange (10YR 8/8) clay containing angular pebbles and boulders of quartzitic sandstone, ironstone and celestite occurs at the Winter's Field, Yate Court, Leechpool, The Rectory and Yate Bypass sites and possibly also at other localities along the Yate Platform (Plate 39). An 'upper Head' without lithorelics was differentiated from a 'lower Head' at Winter's Field (Fig. 2.22). These 'in-situ' Head deposits have not been previously recognized in the Yate-Cromhall area and may have been overlooked as mudflow conglomerates of the 'Dolomitic Conglomerate' or the Permo-Triassic regolith produced by the reworking of the Paleozoic rocks during the Norian transgression. Briefly, the evidence for a periglacially reworked Quaternary deposit is:

1) A shore-line deposit of the Norian sea would be a moderately well sorted gravel and not a clay deposit with scattered pebbles (Pettijohn, 1975).

2) Thin sections (Plate 40) show a non-Triassic assemblage of bent laths of white mica up to 50 μm in an aphanitic non-calcareous groundmass of hematite and kaolinite.

3) In places the clay contains small powdery masses up to 4mm in diameter of pulverized celestite, presumably produced by the granulation of cleavage fragments.

Triassic Clay Head was reported by Hawkins and Kellaway (1971) near Bristol but has not previously been described from the study area because unless it contains a heterogeneous fabric it cannot be distinguished

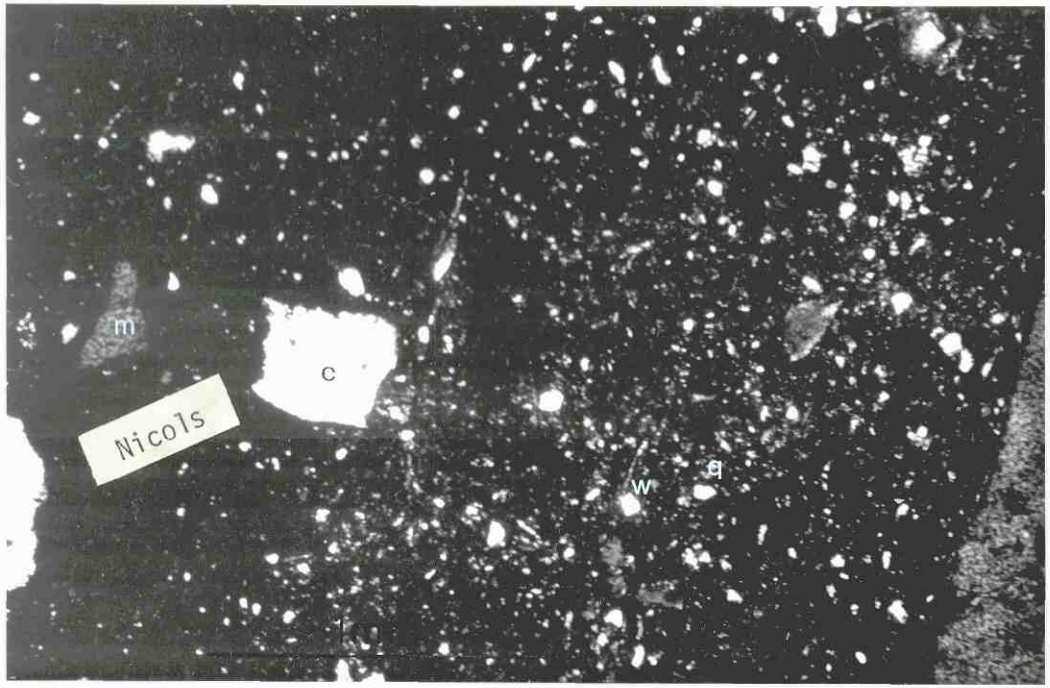

Plate 40: Photomicrograph of Carboniferous Clay Head, showing angular celestite fragments (c) and mudstone clasts (m) in a hematite (black) white mica (w) and quartz silt (q) matrix. Crossed Nichols

Plate 39: Detail of south face, Winter's Field, showing celestite sand (c) in Clay Head (Ç), overlain by terrace gravels deposits (t). White smears are fractured celestite mumblers.

from weathered marl or mudstone (see Sherwood and Hollis, 1966) without using geotechnical analysis. Nevertheless pockets of Triassic Clay Head consisting of structureless clays of 5YR hue with quartzitic sandstone and celestite pebbles occur in the central sector of the Goose Green site and possibly also in the eastern sector where gelifluxion; the slow seasonal movement downslope of the waterlogged active layer under gravity has also affected the strata causing slumping at the base of the incline producing outcrop pattern observed today (Fig. 2.2) and has also deflected the flame-structures down-slope (Plate 2). There is no evidence of gravity faulting or back-sliding associated with possible land-slips at this locality.

As the rocks described in this section are unconsolidated particle size analysis and heavy liquid separation has also been used in their study. As this quantitative work is basically an economic assessment of each of these lithologies these results are considered separately in the Economic Geology Chapter (6).

2.6.2 Periglacial weathering of the celestites

The reaction of the celestites to periglacial reworking varied according to the composition and attitude of the orebody. Veins of Type C celestite formed well cemented competent horizons in poorly indurated Carboniferous mudstones, which were broken up into prismatic blocks or 'mumblers' in the active zone and dispersed through the clay matrix. Frost heaving, upfreezing and stone tilting processes (French, 1976) orientated some mumblers with their long axes vertical and also displaced the mumblers towards the ground surface thus forming a trail over the present vein (Fig. 2.25, Plate 26).

The Type A celestites, unlike the epigenetic celestites grew in an unconsolidated host; consequently cryostatic pressures induced by the freezing of groundwater along crystal faces and sedimentary structures disaggregated the nodules rather than breaking them up into blocks. Most near-surface Type A celestites display to some extent the effects of cryogenesis, ranging from completely shattered seams or gravels to scattered

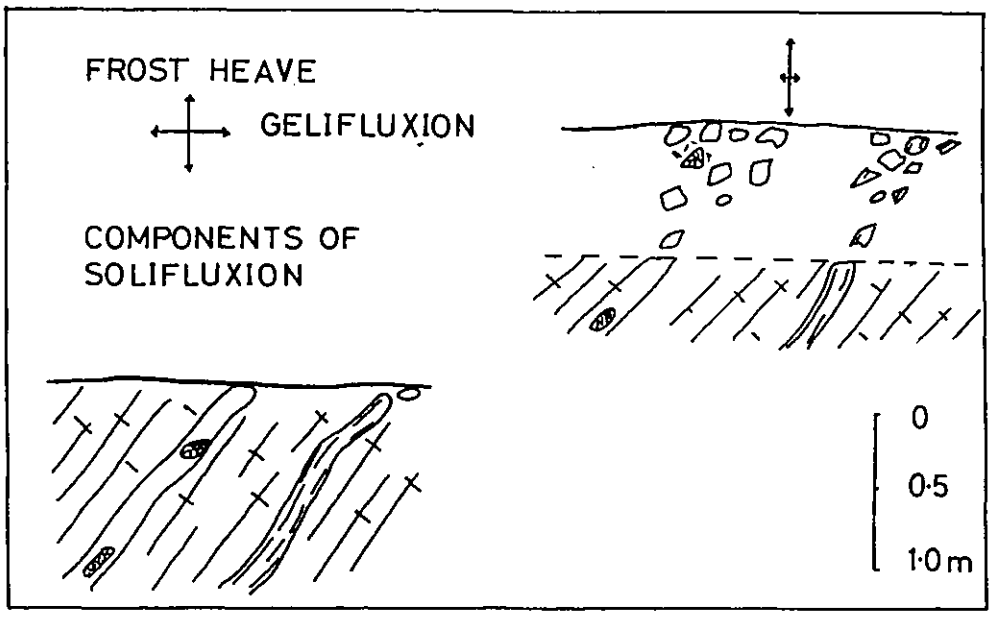

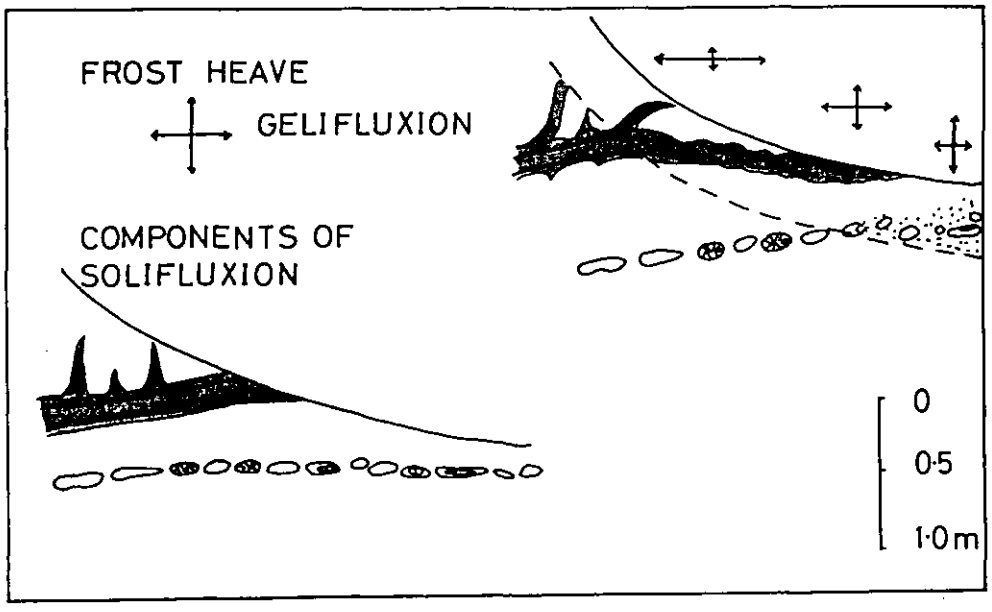

Fig 2.25: The effects of cryogenesis on Type C (upper) and Type A (lower) celestites

cleavage fragments representing broken-down nodules in Triassic Clay Head. Where celestite outcrops on a hillside, as at Goose Green, the seams are affected by gelifluxion and show dispersion of the nodule train in the direction of movement, and cambering of the orebody parallel to the slope (Fig. 2.25).

2.6.2.1 Mumbler deposits

The mumbler deposits or Type D celestites are found in the belt of land from Yate to Cromhall containing Type C celestite. The distribution of the known occurrences is shown on Fig. 1.9. An equal incidence of mumblers on the flats and in the depression of the 60m surface implies that remobilization of the celestite took place after 60m platform times.

The mumbler surfaces are smooth and planar and appear 'frosted', probably as a result of cryogenesis. In section the mumblers display the textures of Type C celestite they have been derived from. The most frequently observed types are of celestite replacing mudstone in particular the massive vein celestite. Sections of mumblers with an orientated fabric, for example compound vein celestite (Plate 29) show that the upper and lower surfaces of the mumbler are defined by the extent of the celestite bed, whereas the sides of the block transect the fabric. In mumblers of vein celestite the central zone/selvedge contact is truncated by the edges of the mumbler, thus proving that these specimens were not formed in situ. This does not however exclude the possibility that some mumblers of celestite formed in situ in mudstone that was later reworked, particularly where large specimens now occur regularly spaced in the Clay Head, as for example in the western part of The Rectory where nodular mumblers are found. Also it seems likely that 'beds' of mumblers up to 35cm thick as seen at Yate Court may have crystallized at their present positions. Other evidence for an in situ origin may be provided by relict textures such as stratification and mudstone inclusions (see Fig. 2.22, 2b). In some of these cases however the colour of the mudstone in the

mumbler does not correspond with that of the enclosing Clay Head, and here a comminuted origin can be confidently applied.

Celestite nodules that formed in mudstone near the Triassic surface, that is now represented by Clay Head, may be recognized from mumblers by the form of the celestite, and to a lesser extent, by nodular morphology (see 2.5.2.4). In places, of course, the nodules may themselves be broken up to form 'mumblers'. A similar process of dispersion may have resulted in the groups of nodules in the celestite sands at The Rectory (see below). The Rectory site also includes mumblers of celestite of mineralized wadi fan deposits. In places seams of Type A celestite may contain accumulations of celestite nodules, some of which may have smooth outer surfaces, apparently worn by external agencies. As these accumulations occur on a smaller scale than the mumbler deposits of Type C celestite and are found underlying moderately sloping land at Poundhouse Farm where there is no evidence for landslipping or solifluxion lobes they are not thought to have formed by periglacial action (see 5.3.1).

Part of the face at Winter's Field shows mumblers of celestite in Upper Head separated from barren Lower Head by a cryogenic contact (Fig. 2.22, 1d). Together with other evidence of epigenetic replacement celestite in overlying formations, where present, (Fig. 2.23), this suggests that the mumblers were formed before the main phase of cryoturbation.

The size of individual mumblers is a function of the diameter of the parent celestite. Vein celestite breaks down into boulders 8-15cm across. Small 'nuggets' of celestite, 5cm across probably represent fragmented thin celestite veins. These 'nuggets' are locally abundant (Fig. 2.23) and form dish-shaped orebodies extending over an area of about 5m and for depths at up to 1m in the Clay Head at the Yate Bypass site (Fig. 2.2). A quantitative investigation of the size distribution of the mumblers has been carried out by Altounyan (1979). The Clay Head also contains small quantities of scattered

crystals or cleavage fragments of celestite or epigenetic celestite, produced from the disintegration of drusey vein celestite.

2.6.2.2 Type A celestite gravels

A well-exposed example of a celestite gravel at Goose Green (Fig. 2.2, Plate 41) shows a 50cm seam of impregnations and macrocells of white tabular celestite now disaggregated into a coarse sand and gravel over a 'lag' of undisturbed celestite representing the base of the active zone. Similar gravels have been recorded at other localities by Nickless et al. (1976). The Goose Green gravel also shows additional evidence of fluvial reworking.

2.6.3 Other celestite sands and gravels

Superficial celestite sands and gravels of possible Quaternary age, produced from the reworking of underlying celestites, occur at The Rectory and Winter's Field sites.

2.6.3.1 The Rectory

Reddish brown (10R 5/3) medium-grained lithic and celestite sands, or sandy mudstones occur in the erosional remnants of small basins, seldom extending for more than 2m below present day ground surface, between, and also covering the Millstone Grit sandstones in the northern part of The Rectory site (Fig. 2.26). Where the sand overlies quartzitic sandstone it can be observed to grade down into what is presumably the source material of coarse celestite crystals lining bedding planes and joints in the rock. The contact of the sands with the underlying mudstones is distinct, and has been (?) cryogenically altered, so that steep dips occur, which may be reversed in some cases (Fig. 2.23).

Blocks of quartzitic sandstone, celestite mumblers and epigenetic celestite nodules also occur in the sand. Because of the weathered nature of the exposures it is difficult to establish whether the epigenetic celestite is in a position of growth or has been reworked from the Paleozoic rocks. Some of these celestite nodules are

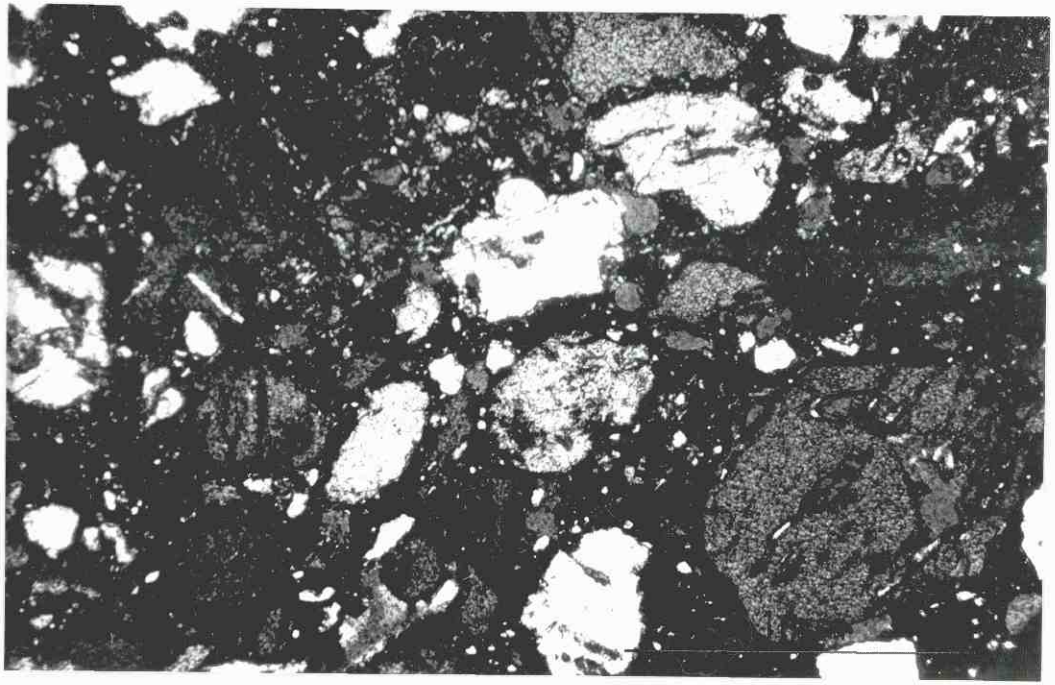

Plate 42: Photomicrograph of celestite sand from Winter's Field. All large crystals are of celestite, in a matrix of silt, white mica and hematite (black). Crossed Nicols s

Plate 41: Western pit face at Goose Green West, showing the effects of cryogenic weathering. Seam B (top of photo) has been shattered to an unconsolidated gravel, with at the base, a 'lag' of unweathered celestite representing the base of the active zone (head of hammer).

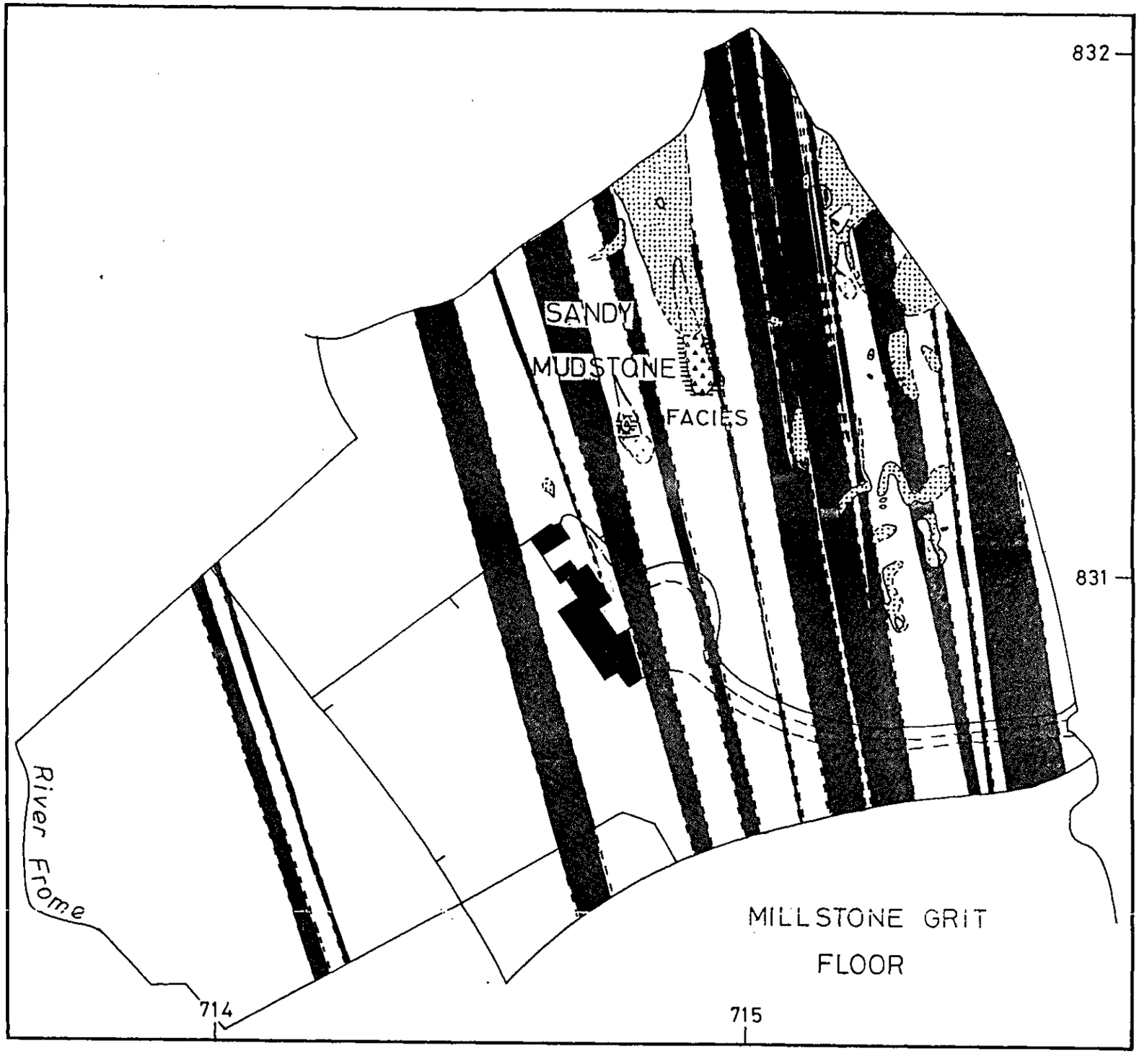

geological contact-observed

geological contact-indicated

celestite sands, and mudstones

0 100m

Fig 2.26: Geological sketch-map of the Rectory site

clustered into small zones 50cm across, suggesting that one large nodule was broken up by cryostatic forces.

2.6.3.2 Winter's Field

Pockets of celestite-rich sands and gravels, in the order of 50cm across, occur in Clay Head in the southern half of Winter's Field as the rifted cryoturbated remnants of a larger deposit that extended for at least $50m^2$ (Figs 2.22, 2.27, Plate 40).

The Clay Head forms injection plugs between the sand pockets which although in some cases may be enveloped by carbonaceous shales, still retain a planar stratification showing units approximately 1cm thick.

The commonest type of deposit is a reddish brown weakly consolidated gritty celestite sand containing quartzitic pebbles. The petrographic description of the sand is included here for clarity. In thin section, subangular cleavage fragments of celestite, 0.1-1.0mm in diameter occur with minor rounded quartz grains, quartzite fragments, sandy hematitic clay intraclasts and ribbon-like strips of mamillary ironstone in a matrix of 0.02mm diameter quartz silt, silt-grade flakes of white mica and aphanitic hematite (Plate 42).

At least 3 of the pockets observed contained a celestite gravel component, forming a border around the edge of the sand with crystals orientated sub-parallel to the walls or differentiated as the top of the pocket (Fig. 2.22). In one case a 1cm layer of purple-brown clay separated an inner zone of sand from the gravel (Fig. 2.22, 1c). The celestite crystals are of tabular habit, and are smeared with orange-brown goethite, producing a characteristic vivid colour in the field.

The sand may contain blocks of Type C celestite, usually of the 'nugget' mumbler variety or isolated coarse laths of celestite, similar to those in the gravel.

2.6.3.3 Interpretation of the celestite sands and gravels

An origin by the subaqueous reworking of exposed celestite veins is suggested by the sorting of the celestite

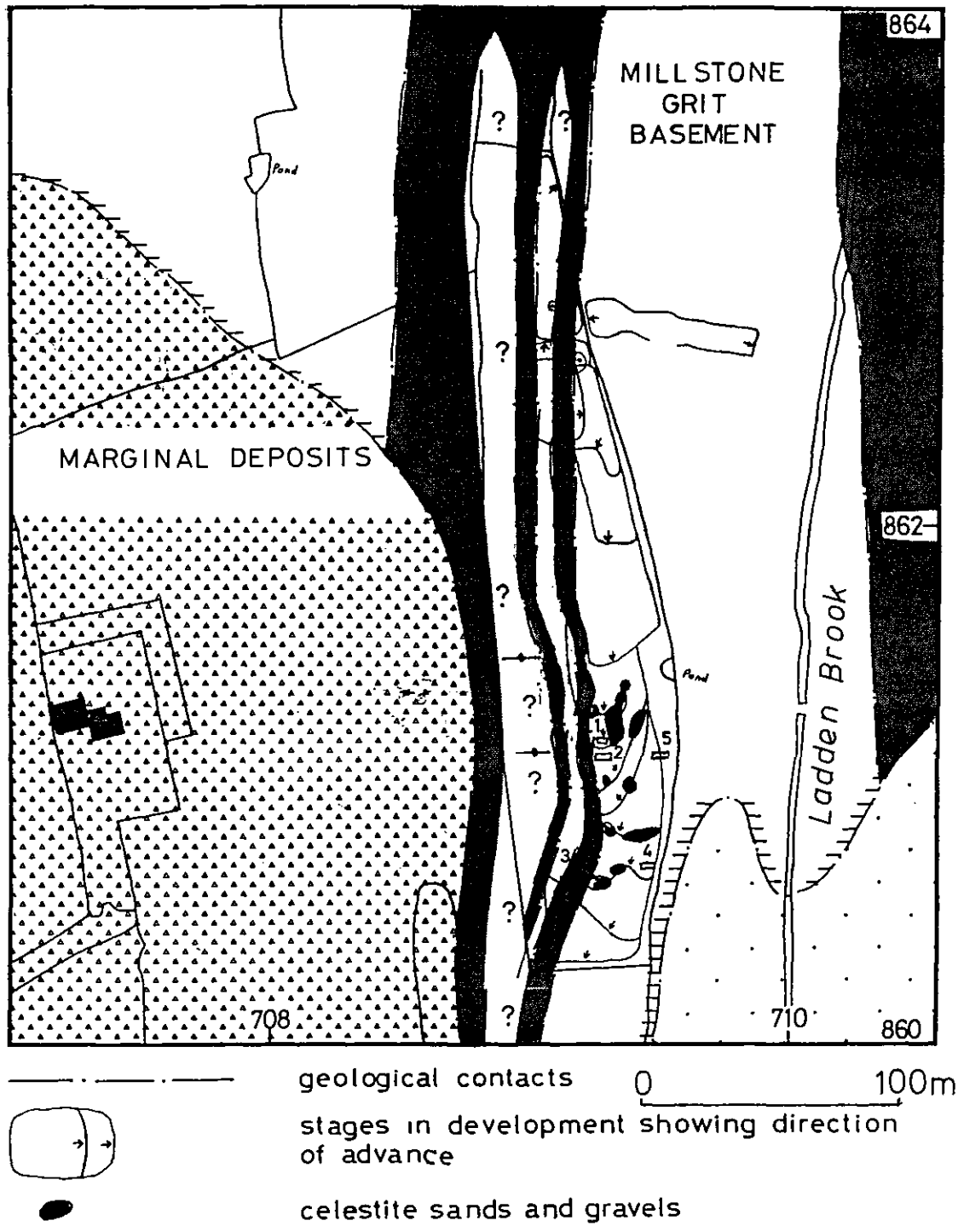

Fig 2.27: Geological sketch-map of the Winter's Field and Yate Court sites, showing location of B.M.C. test holes. Geological legend as in Fig 1.5. NB terrace gravels omitted

grains from most of the siliclastic detritus, well rounded quartzite clasts and the absence of a fine celestite silt fraction.

Without paleontological evidence the age of these small spreads of sediment is very difficult to establish. Intuitively one might suppose a Triassic but post-celestite age if the deposits were formed by the pene-contemporaneous reworking of the Type C sediments during the Norian advance; or a Quaternary age if the sediments were formed during the unroofing of the celestite-bearing strata and redeposited as beach or river-sands during the erosion of the 60m platform. It should be noted that both of these explanations assume that only one, ?Triassic, mineralization has taken place. No conclusions can be drawn on the possible distribution of the celestite sands except that similar occurrences may be expected at other locations within the Yate-Cromhall area.

The Rectory sands are in places overlain by or contain partings up to 40cm thick of reddish brown mudstone with celestite (Fig. 2.23). Although this stratum superficially resembles mudstone of the Yate Formation the underlying sands cannot be Triassic for they are clearly unconformable to the mineralized Millstone Grit mudstones and are in places derived from the celestite veins in the quartzites. If, as seems most likely, the epigenetic nodules are comminuted and not in-situ a post-Triassic date, most probably Quaternary, can be applied to the celestite sands.

The evidence for each of the alternatives at the Winter's Field site is as follows: -

a) Triassic, post-celestite age

1) Some of the sand pockets are veined by seams containing 'giant' celestite laths (Fig. 2.22, 2b).

2) The sand pockets may be outliers of the stratum mapped as Dolomitic Conglomerate by the Geological Survey immediately to the west.*

* At a late stage in the project the writer was able to investigate the 'Dolomitic Conglomerate' exposed at the Yate Lower Common site (Fig. 2.28). These sediments showed similar field relationships as the celestite sands but consisted mainly of sandstone and ironstone clasts.

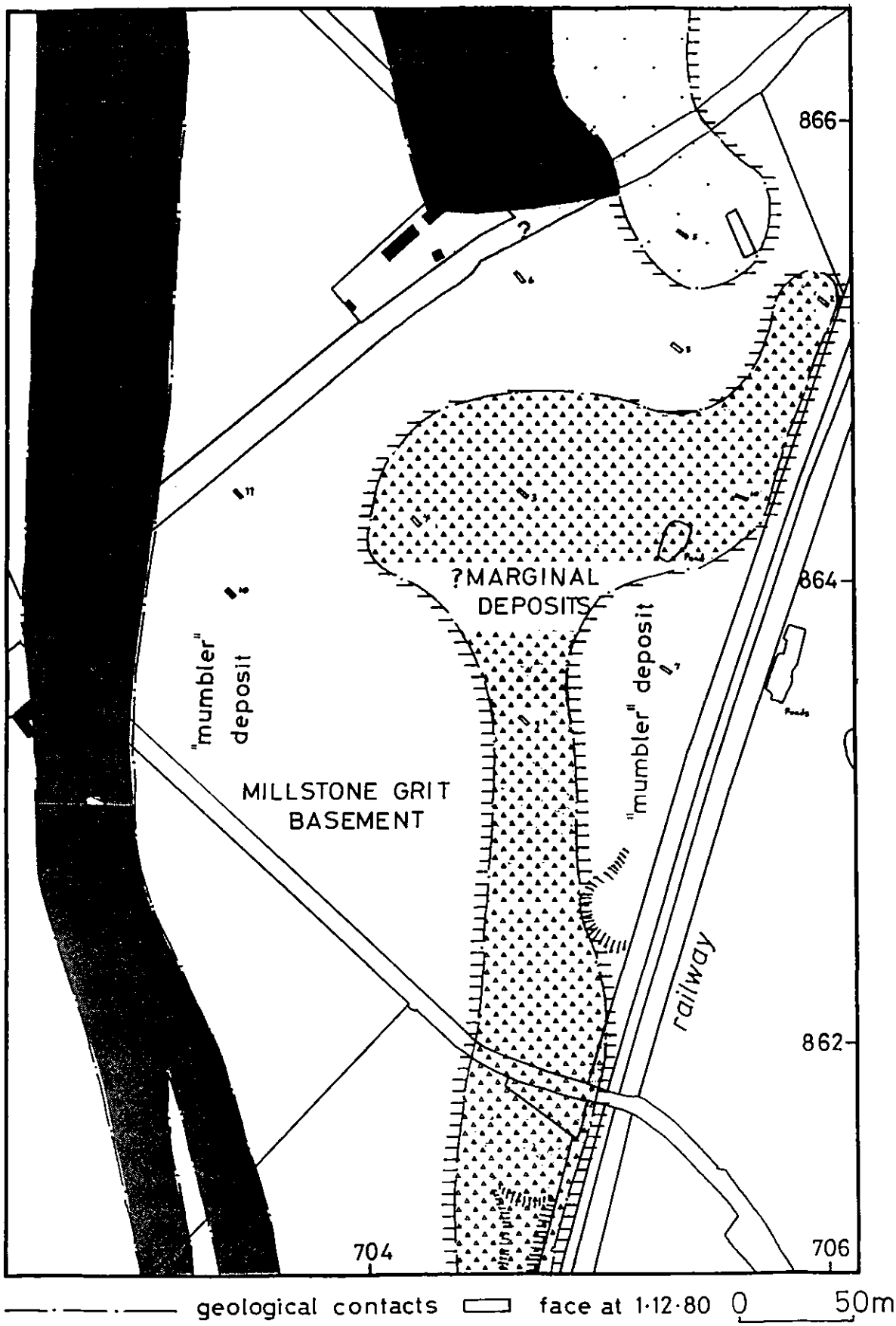

Fig 2.28: Geological sketch-map of the Yate Lower Common site, showing location of B.M.C. test holes.
Geological legend as in Fig 1.5. NB terrace gravels omitted

b) Quaternary age

1) Some of the pockets show a cross-cutting relationship to the fabric of the Clay Head (Fig. 2.22, 2a) suggesting that prior to cryoturbation the sand was deposited unconformably over the Clay Head and the celestite mumblers. (As both the celestite sands and the overlying terrace gravels are cryoturbated (1.4.4.1, Fig. 2.22) this implies two and possibly three periods of periglacial weathering, including a temperate stage when the gravels and sands were deposited).

2) The field relationship between the carbonaceous shale bed and the sand pockets indicates the periglacial reworking of the former was closely linked to the deposition of the sand (Fig. 2.22, 2c and 4).

CHAPTER 3 - PETROGRAPHY OF THE CELESTITES

This chapter includes the results of, and discussions on the thin section studies carried out on the Type A celestites, epigenetic celestites and gypsum rocks.

3.1 PETROGRAPHY OF THE TYPE A CELESTITES

3.1.1 Introduction

The petrographic studies were made of 64 celestites selected to cover as wide a range of macroscopic fabrics, textures, mineral associations and localities as possible.

To complement the microscopic examination an additional 20 sections were prepared for analysis using standard electron microprobe techniques. The microprobe analyses were used to detect small amounts of gypsum, high Mg-calcite and dolomite, where the presence of these minerals was suspected, and also to analyse all the celestite subtypes (see below) for barian celestite or barite. The instrument was calibrated and programmed for the quantitative analysis of Sr, Ba, Ca, Mg, Mn, and Fe at a detection limit of approximately 0.1 weight %. The microprobe analyses of selected crystals on which these analyses were performed are recorded in Tables 3.1 and 3.2.

Where necessary, whole-rock XRD analyses were also performed.

3.1.2 Celestite

3.1.2.1 Classification

In order not to prejudice the results of the petrographic investigations, the celestites were classified by a purely objective technique into thirteen fabric subtypes using the following four petrographic criteria:-

1. Presence or absence of anhydrite inclusions.
2. Granular fabric or lathlike (tabular) fabric.
3. Degree of clustering of crystals: ranging from 'scattered' to 'mosaic'.
4. Grain size.

By this method an independent check could be carried out on the significance of the varieties described in Chapter 2. Most celestites contain more than one subtype and several subtypes may resemble one another in many of their properties.

Table 3.1a: Quantitative Electron Microprobe Analysis of carbonate minerals

Mineral	Description	Sample	Ca%	Mg%[1]	Mn%[1]	Fe%[1]	Sr%
Calcite	Calcite rock	BY45	39.2	0.10	0.21	0.10	-
Dolomite	opaque rhomb-core	BY39	21.3	11.74	0.10	0.53	-
"	limpid rhomb-rim	BY39	22.6	11.54	0.10	0.10	-
"	opaque rhomb	BY39	23.0	10.81	0.10	1.46	-
High-Sr	inclusions/cel-1	WP25	34.1	4.33	0.10	0.10	1.30
carbon-	inclusions/cel-2	WP25	34.1	1.19	0.10	0.10	1.40
ate	inclusions/cel-3	WP25	33.7	1.42	0.10	0.10	1.81
"	inclusions/quartz	WP10	39.5	2.05	0.10	0.10	0.89

1.Values of 0.10% are below the detection limit

Table 3.1b: Quantitative Electron Microprobe Analysis of anhydrite

Mineral	Description	Sample	Ca%	Sr%	MSr[1]
Anhydrite	10μm inclusion-1	GG46	28.5	0.44	0.7
"	10μm inclusion-2	GG46	28.7	0.35	0.6
"	10μm inclusion-3	GG46	28.4	0.45	0.7
"	10μm inclusion-4	GG46	28.0	0.55	0.9

1.Mole fraction Sr in $(M.Sr,(100-M)Ca)SO_4$

Sample	Size (Fig. 3.3, 3.4)	Subtype	Core Sr	Core Ba	Core Ca	Core MBa[1]	Rim Sr	Rim Ba	Rim Ca	Rim MBa[1]
PF35	2a	P1	47.24	2.23	0.20	2.9	41.63	7.98	0.10	10.8
PF35	2b	P1	44.11	5.17	0.24	6.9	39.62	8.29	0.41	11.4
PF35	3a	P1	45.61	4.28	0.16	5.6	47.27	2.64	0.10	3.4
PF35	3b	P1	49.62	0.68	0.10	0.8	-	-	-	-
PF35	4	P1	47.01	3.26	0.10	4.2	44.85	5.41	0.10	7.1
PF35	5	P1	41.09	8.96	0.10	12.1	40.28	10.04	0.10	13.6
PF35	6	P2	-	-	-	-	48.91	1.38	0.10	1.8
PF32	1a	P1	-	-	-	-	[2]49.54	0.28	0.13	0.4
PF32	1b	P1	49.65	0.55	0.10	0.7	[2]40.35	5.89	0.10	8.5
PF32	1b	P1	49.65	0.55	0.10	0.7	[3]48.86	0.70	0.17	0.9
PF32	2a	P1	38.79	6.50	0.10	9.6	37.88	7.23	0.10	10.8
PF32	2b	P1	42.07	4.13	0.10	5.9	47.48	1.42	0.10	1.9
PF32	3	P1	36.10	6.90	0.10	10.7	-	-	-	-
SB07	1a	S6	49.04	0.72	0.10	0.9	49.06	0.82	0.10	1.0
SB07	1b	P1	37.18	7.65	0.10	11.6	36.42	7.91	0.10	12.1
SB07	2a	P1	48.81	0.91	0.10	1.2	37.89	7.24	0.10	10.8
SB07	2b	S6	49.56	0.59	0.10	0.7	50.31	0.37	0.10	0.5
SB07	3	S6	-	-	-	-	50.38	0.32	0.10	0.4
SB07	4a	P1	47.67	1.54	0.10	2.0	47.24	1.79	0.10	2.3
SB07	4b	S6	42.56	5.02	0.10	6.9	38.39	7.03	0.10	10.4

1. mole fraction Ba in (M.Ba, (100-M)Sr, Ca)SO_4
2. stratigraphically higher surface
3. stratigraphically lower surface

Table 3.2: Qualitative Electron Microprobe Analysis of Barian Celestite

In applying this classification, the effects of orientation and positioning of the celestite specimens in the thin sections must be considered and also the possibility of complete replacement of anhydrite by celestite, leaving no evidence of its precursor. Taking these factors into consideration, the subtypes are considered to be diagnostic of an individual paragenesis and each subtype can be interrelated to establish a diagenetic history for the celestites as a whole.

Throughout this account the terms anhydrite-free-celestite and celestite-with anhydrite are used to refer to celestite without, or containing anhydrite inclusions respectively. Because the anhydrite relics only testify to the distribution of the anhydrite precursor rather than to a set stage in evaporite diagenesis, these are descriptive rather than genetic terms; also the two celestites may, of course, form synchronously. In addition, because the former presence of gypsum is much harder to establish than that of anhydrite, any of the anhydrite-free celestites could, in fact, be replacements of that mineral (see below).

Thin sections of tabular or 'rhombohedral' celestite crystals show domed, rectangular, euhedral to subhedral outlines. Lozenge-shaped outlines result from the growth of two opposing prism faces. The 'spindle' celestite habit is due to the predominance of the {102} over the {001} form. Equidimensional cross-sections of granular celestite are carefully distinguished from the granular <u>mosaic</u> celestite fabric, which contains subhedral compromise boundaries that bear no relation to crystallographic axes or the trace of the {001} cleavage.

A summary of the main features of the thirteen subtypes is given in Table 3.3. These are now discussed, as follows.

3.1.2.2 Description and interpretation of celestite subtypes

a. Celestite-with-anhydrite

The S1* celestite fabric is present in many examples of

* The prefix 'S' indicates 'secondary' celestite after anhydrite

SUBTYPE	MAIN MICROSCOPIC FEATURES	SIZE(MINOR AXIS)	MICROPROBE ANALYSTS.%Ba	INTERPRETATION
S1	Tabular, an relics, individual to clustered euhedra	.2-1.0 mm	Average .5 (Bypass, Wapley)	Forming in and pervading anhydrite macrocells
S2	Tabular, an relics, scattered to coalesced euhedra	.05-.10 mm	Not detected (Wapley)	Forming on the rims of anhydrite macrocells
S3	Tabular, an relics, mosaic, subhedra	.05-.10 mm	Not detected (Wapley)	Completely replacing anhydrite
S4	'Rhombs', an relics, scattered, euhedra	.1-.5 mm	Not detected (Bypass)	Partially replacing anhydrite
S5	Tabular and granular, an relics, mosaic, subhedra and anhedra	.05-.30 mm	Not detected (Wapley)	Forming in anhydrite macrocells by rapid nucleation
S6	Tabular, an relics, coalesced to mosaic, euhedra and subhedra	+.5 mm	Not analysed	As for S1 celestite, also probably recrystallized cel.
P1	Tabular, an-free, scattered to coalesced euhedra	.2-1.0 mm	Average .5 (P. Farm) Barian cel. up to 10.0	Primary chemical sediment
P2	Tabular, an free, mosaic, subhedra	.05-.50 mm	Not detected (P. Farm)	Recrystallized celestite
P3	An-free, scattered to coalesced subhedra, cementing marl	up to 5 mm	Not detected (Wapley)	Cement
G1	Granular, an relics, coalesced, subhedra	approx 1 mm	Not detected (Bypass)	Replacing primary anhydrite, gyp.
G2	Granular, an relics, mosaic, euhedra and subhedra	.3-1.0 mm	Not detected (Wapley)	Replacing pseudomorphous anhydrite after gypsum
G3	Granular, an-free, mosaic, subhedra	approx. 1 mm	.1-.5 (Bypass)	Poikilotopic after subtype G4
G4	Granular, an-free, mosaic, euhedra and anhedra	.2-1.0 mm	Not detected (Bypass)	Pseudomorphing and replacing gypsum, ? forming in marl

TABLE 3.3: Summary of the main features of the 13 Type A Celestite subtypes

impregnations of tabular celestite, in particular the medium grained orange or grey laths in limestone, and the 'framework celestite' of quartz-rich celestites and the overgrowths on the pink celestite granules. showing right-angled re-entrants (Plate 43). Lozenge or spindle-shaped individuals may show strained extinction and deformation caused by the growth of sparry calcite (Plate 44). Crystal boundaries are straight and contacts enfacial. Inclusions of anhydrite and aphanitic aragonite (3.1.6.3) together with the 'framework celestite' texture suggests that the S1 celestite formed at the sediment surface from the piece-meal replacement of anhydrite in an aragonite mud. Anhydrite inclusions in adjacent late megaquartz (see 3.1.6.2) show that anhydrite co-existed with the celestite which apparently grew through the anhydrite crystals rather than within them. These 'framework celestites' are directly analogous to oth -er subaerially-formed evaporites, eg Lark's-foot gypsums (Truc, 1981) and baryte rosettes (Pettijohn, 1976, p 477).

Subtypes S2, S3, S4 and S5 are all fabrics of drusey macrocellular celestite. The S2 celestite crystals have prismatic terminations and are either arranged at right angles to the void or lie at a low angle to each other, forming a herringbone pattern (Plate 45) and mapping out ovoid areas now generally filled with sparry calcite or megaquartz; apparently relic fabrics of anhydrite macrocells. In S3 celestite, the crystals form a mosaic, with their long axes orientated perpendicular to bedding. Anhydrite inclusions are very common in the completely infilled white macrocellular variety (Plate 46). S4 celestite, the microscopic representation of pancake celestite of the 'rhombohedral' habit, consists of crystals aligned both parallel and perpendicular to the sides of the druse. A great many anhydrite inclusions, 10 µm in length and each showing parallel extinction are distributed evenly across the celestite crystals with their long axes parallel to the major axis of the celestite crystals (Plate 47). Subtype S5 occurs on the borders of, and in the centre of completely filled macrocells and appears microcrystalline to fine grained in hand specimen. Elements of the S5 mosaic fabric

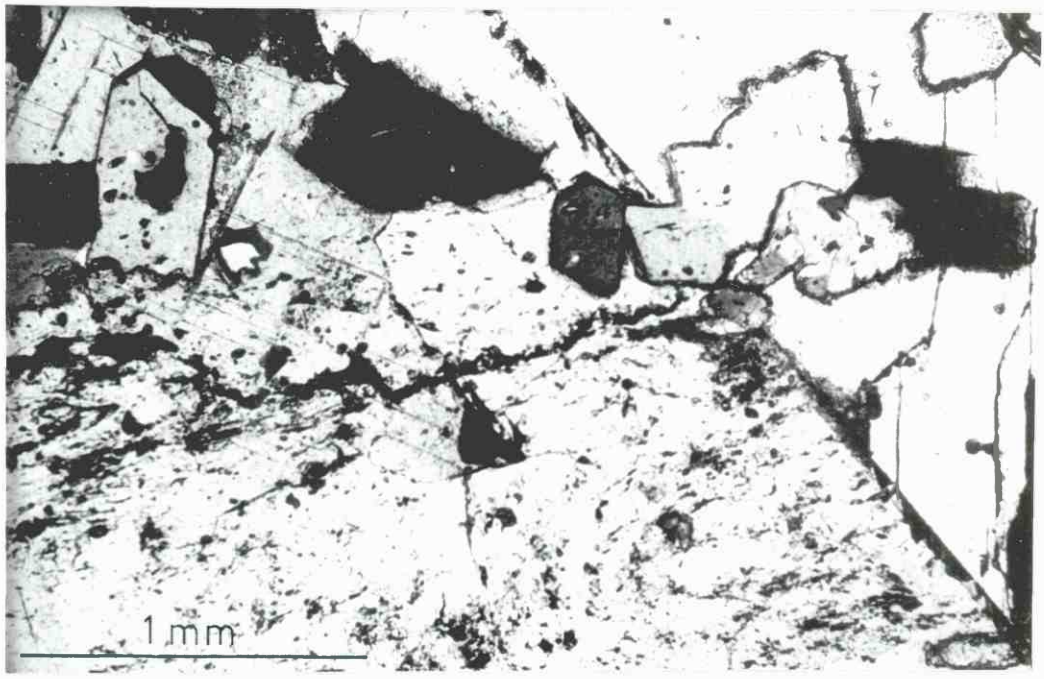

Plate 43: Photomicrograph of evaporite block showing lozenge quartz crystals with rhombic, hexagonal and rectangular outlines, P3 celestite with mudstone inclusions and overgrowth of S1 celestite. Specimen WP09. Crossed Nichols.

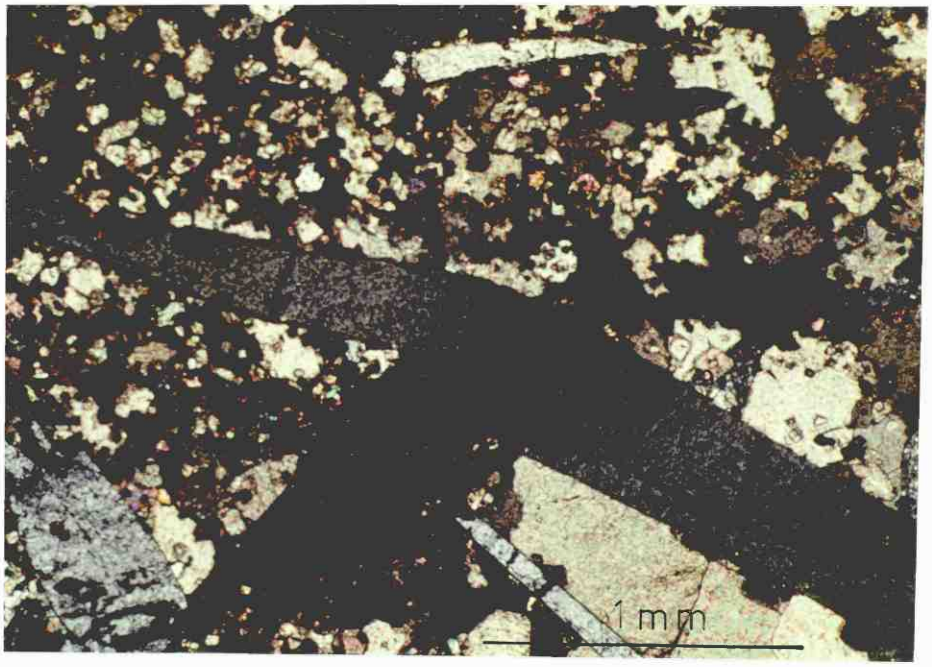

Plate 44: Photomicrograph of bent S1 celestite of "spindle" habit (low colours) and sparry calcite (high colours). Mosaic calcite occurs below celestite; subhedral calcite above, with tiny opaque dolomite rhombs. Specimen BY39. Crossed Nichols.

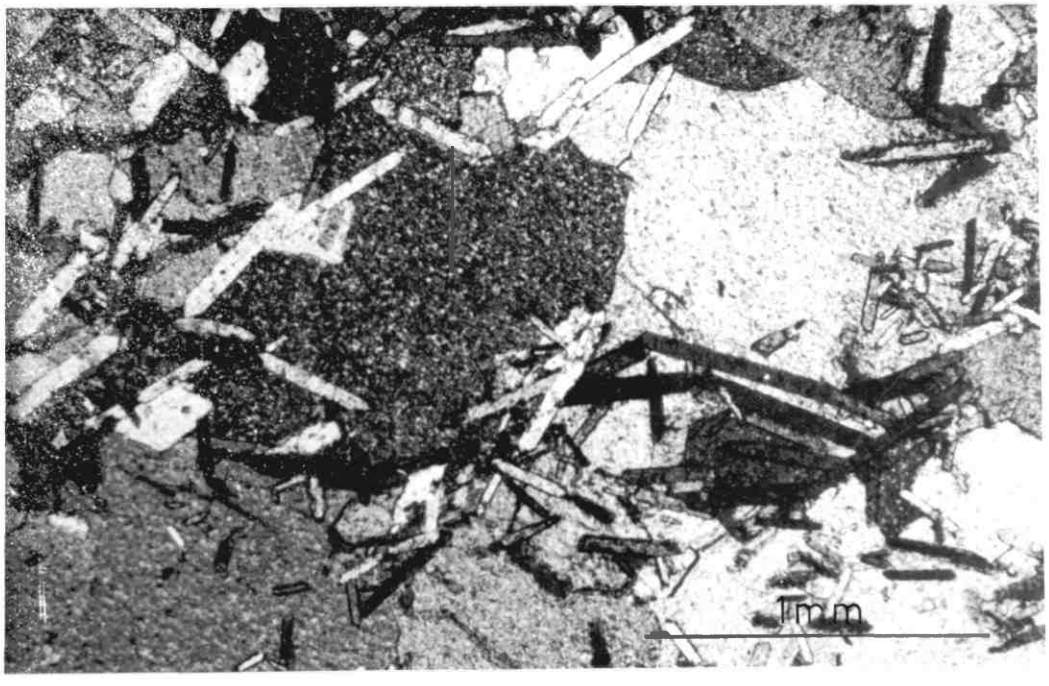

Plate 45: Photomicrograph of drusey macrocellular celestite showing herringbone texture of S3 celestite in sparry calcite. Specimen WP16. Crossed Nichols.

Plate 46: Photomicrograph of fine tabular celestite macrocell, showing mosaic of S3 celestite. Granular mineral is calcite.with small quantities of megaquartz (q). Specimen WP03. Crossed Nicols .

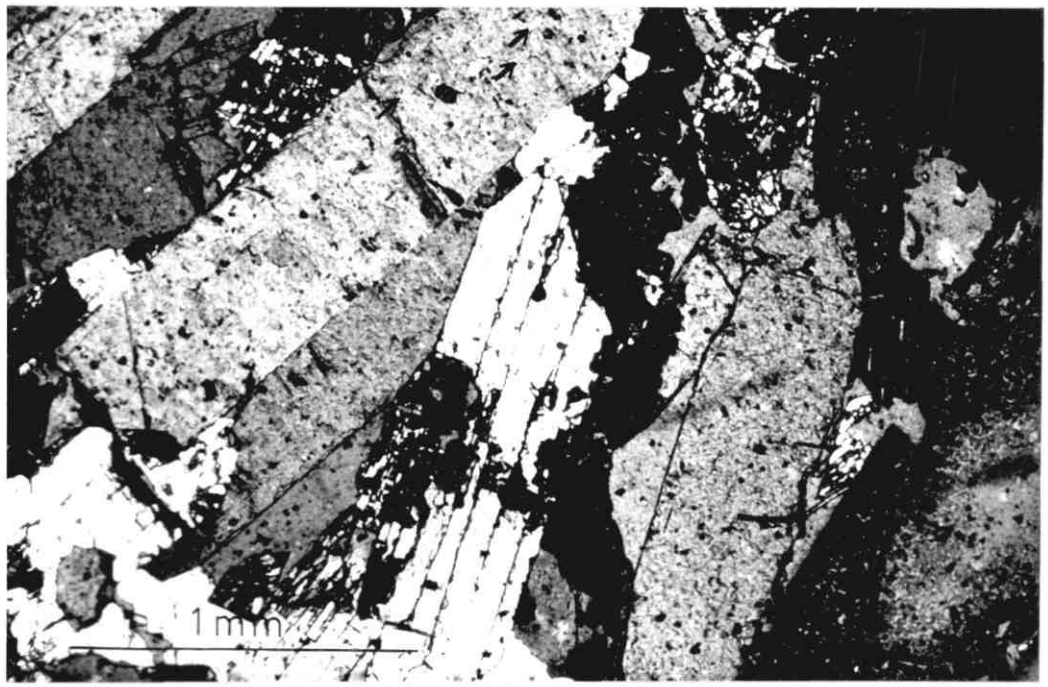

Plate 47: Photomicrograph of celestite of "flattened rhombohedron" habit. Note many small anhydrite relics, aligned parallel to the side of the celestite crystal (arrowed), subtype S4. Specimen GG46. Crossed Nichols.

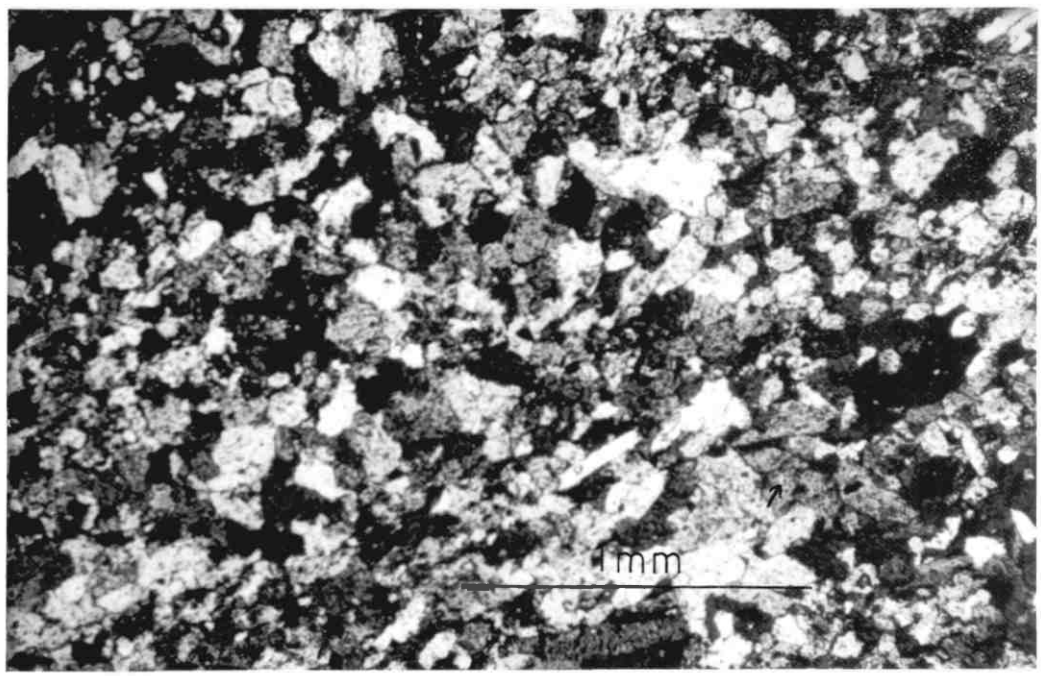

Plate 48: Photomicrograph of microcrystalline macro-cellular celestite showing inequigranular mosaic of S5 celestite. Anhydrite relics arrowed. Specimen WPO3. Crossed Nichols.

meet at triple junctions and contain only a few anhydrite relics (Plate 48).

Celestite of subtypes S2, S3, S4 and S5 has replaced macrocellular anhydrite. The characteristic herringbone fabric shows that nucleation of the S2 celestite took place along the edge of the macrocell and that growth occurred with the C axis at right angles to the macrocell. In many cases, dissolution of the anhydrite macrocell accompanied the crystallization of the celestite. Replacement by celestite was either partial or complete depending upon the concentration of Sr^{2+} ions near to the macrocell. Where the rate of dissolution exceeded the rate of celestite crystallization, voids were produced in which some S2 type celestite and the delicate drusey fabric of S4 celestite was formed. Replacement at the peripheries of the voids again produced orientated celestite laths, with rectangular anhydrite inclusions. The alignment of the anhydrite is a relic of an earlier texture.

Where crystallization was faster than the dissolution of the anhydrite, celestite crystals nucleated en mass within the anhydrite, producing the S3 type celestite mosaic fabric. Very rapid nucleation would have produced a finer grained fabric with few anhydrite inclusions preserved and this is found in the S5 type of celestite.

Subtype S6, the microscopic fabric of the common blue and red celestite impregnations consists of equigranular laths with planar contacts. The relic anhydrite content is variable, either absent completely, sparingly present as 50 - 100 um prisms, or arranged in belts, with gypsum, as a finer (10 um) grained variety (Plate 49). Much of the S6 celestite may be a coarser crystalline variant of the S1 subtype and probably has a similar origin. However, in crystals showing isolated or zones of minute anhydrite inclusions, some degree of recrystallization is suspected. The massive blue celestite included under this subtype only rarely contains relic anhydrite.

b. Anhydrite-free celestite

P1* celestite is an umbrella term for laths of anhydrite-

* The prefix 'P' indicates 'primary' celestite

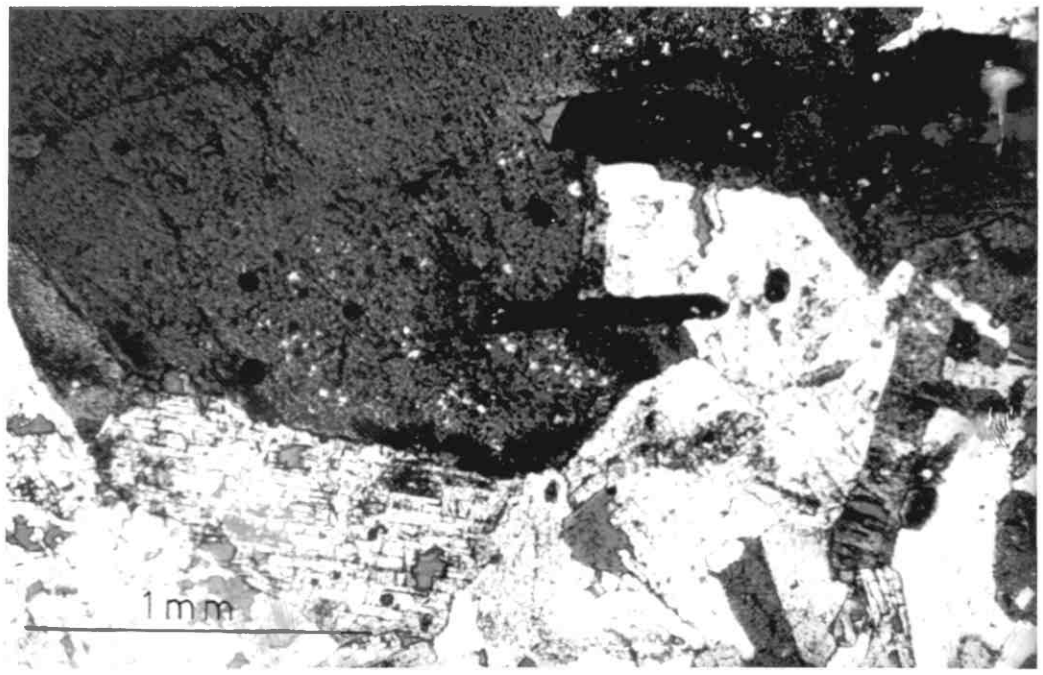

Plate 49: Photomicrograph of massive tabular celestite showing S6 celestite (large crystals) with belts of anhydrite and gypsum inclusions (centre and top right). Smaller crystals (bottom right) are of subtype G2. Specimen GG15. Crossed Nichols.

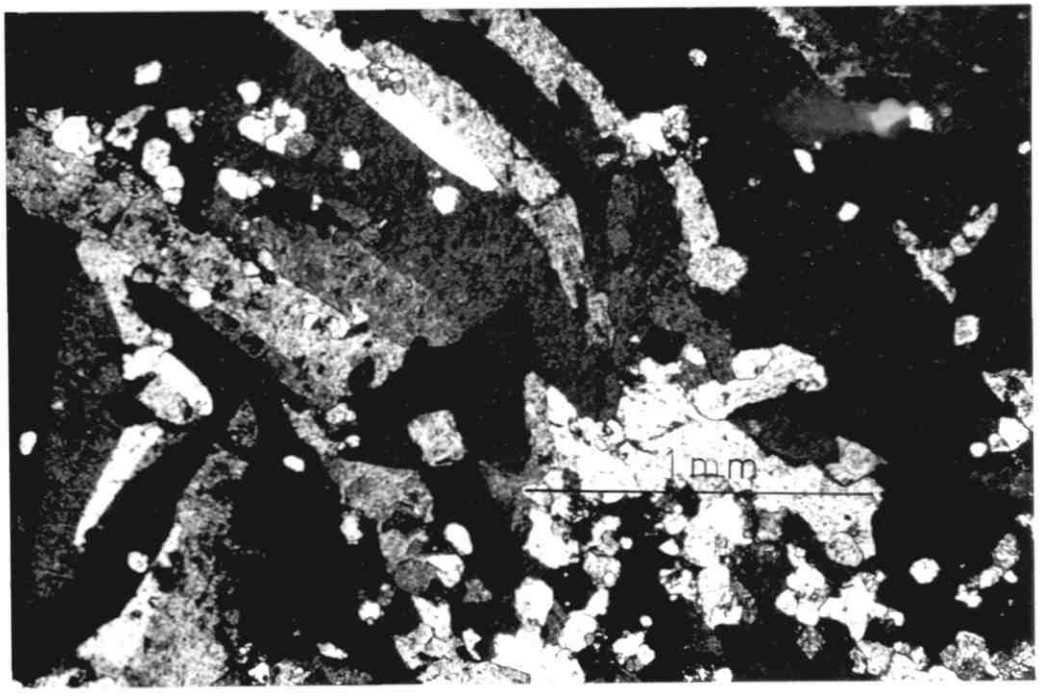

Plate 50: Photomicrograph of massive tabular celestite showing stacking of P1 celestite in "pile-of-brick" texture. Equant grains of sparry calcite show transition from mosaic (bottom R.H. corner) to scattered subhedra. Specimen GY45. Crossed Nichols.

free celestite and is represented in hand specimen by massive, or more rarely, macrocellular blue, white and red celestite. The colour of some red P1 celestite is due to small (50 μm) hematite dust stringers included near the crystal rims. Massive P1 celestite may show a 'pile-of-brick' texture interpreted in nodular anhydrite, (eg Carrozi, 1960; Shearman and Fuller, 1969) as indicating subsurface growth in an unconsolidated sediment (Plate 50). However, nucleation of the celestite crystals may have occurred either in the sediment or subaqueously, followed by sinking of the crystals and further growth at the sediment/ water interface. Barian P1 celestite (Table 3.3) is discussed separately in 3.1.2.3.

Subtype P2 consists of an equigranular mosaic fabric with lath-shaped crystals with gently crenulated contacts, meeting at triple boundaries. The fabric may be randomly orientated or foliated subparallel to the border of the specimen (Plate 51). In hand specimen P2 celestite is present as the light red macrocellular variety or as a transitional fabric in massive P1 celestite.

The mosaic fabric of P2 celestite suggests rapid nucleation at a large number of sites. Where P2 celestite coexists with P1 or barian P1 celestite, it is enclosed or veined by these other subtypes, suggesting that the P2 celestite formed earlier. Hand specimens of light red macrocellular celestite show displacive fabrics indicating a diagenetic origin (Plate 5). Furthermore, the observations listed below can be submitted as evidence for recrystallization of an earlier celestite fabric:

1) Where present, the P2 celestite always occurs at the centres of rosettes of P1 celestite.

2) The contrast in Ba content between P2 celestite (Ba not detected), and barian celestite (up to 10% Ba) (see Table 3.2).

3) Crenulate margins and triple boundaries: textures used by Bathurst (1971) as evidence for recrystallization of calcite in limestones.

4) Foliated fabric (Plate 51) possibly caused by swelling accompanying recrystallization, or compaction adjustment (Holliday and Shephard-Thorn, 1974)

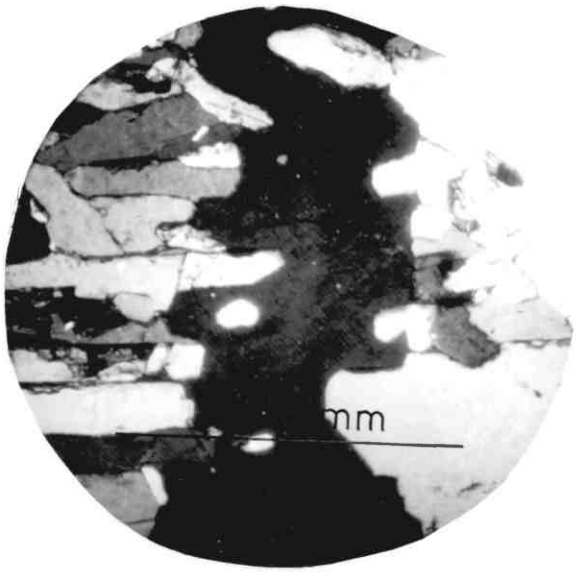

Plate 51: Photomicrograph of light red macrocellular celestite; subtype P2. Note foliation of subhedral celestite laths growing in earlier coarser crystal. Specimen PF35. Crossed Nicols.

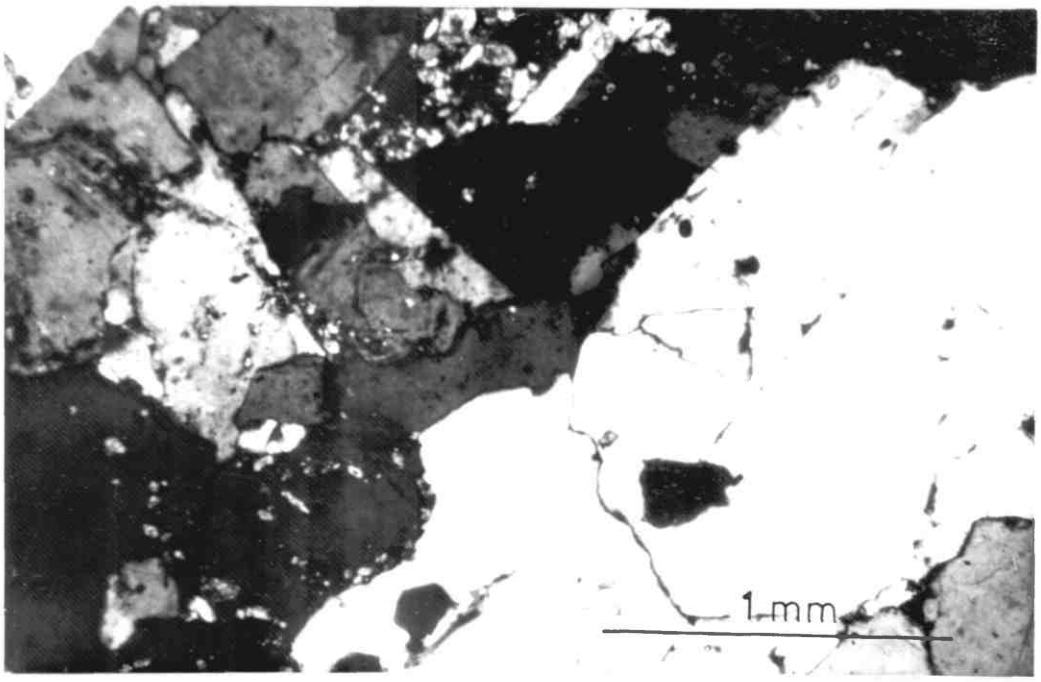

Plate 52: Photomicrograph of compact microcrystalline celestite (Plate 14) showing celestite of subtype G1 enclosing smaller crystals of subtype G4 (bottom centre) and S3 celestite (top centre). Specimen GGO6. Crossed Nichols.

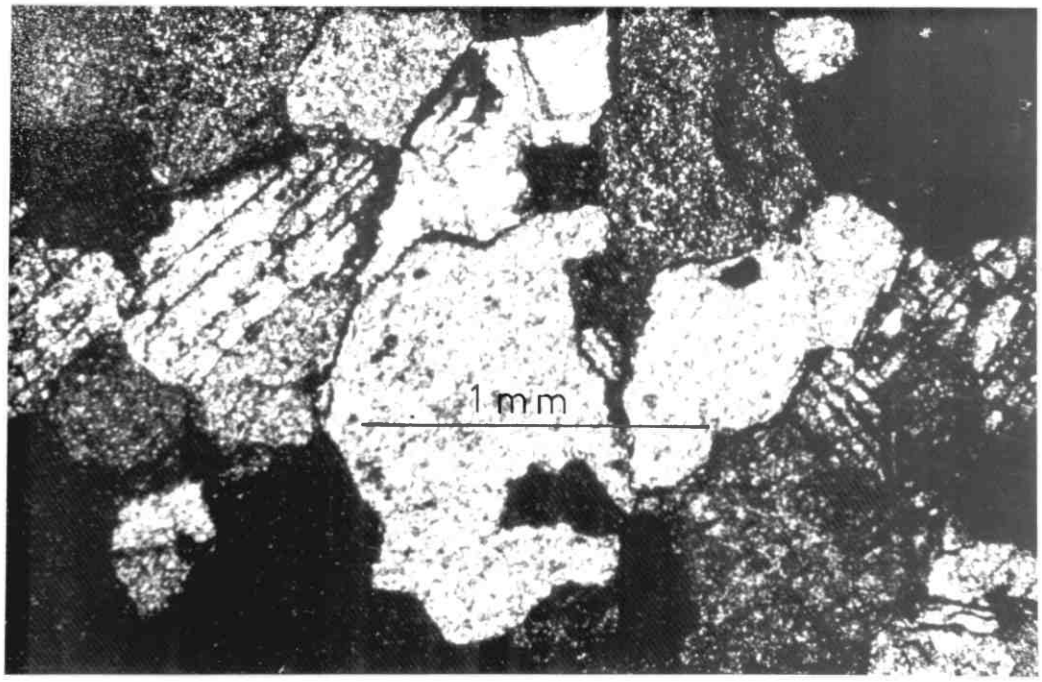

Plate 53: Photomicrograph of medium-grained red and white granular celestite, showing G3 fabric. Note aversion of grain contacts to triple boundaries, Specimen GG23. Crossed Nichols.

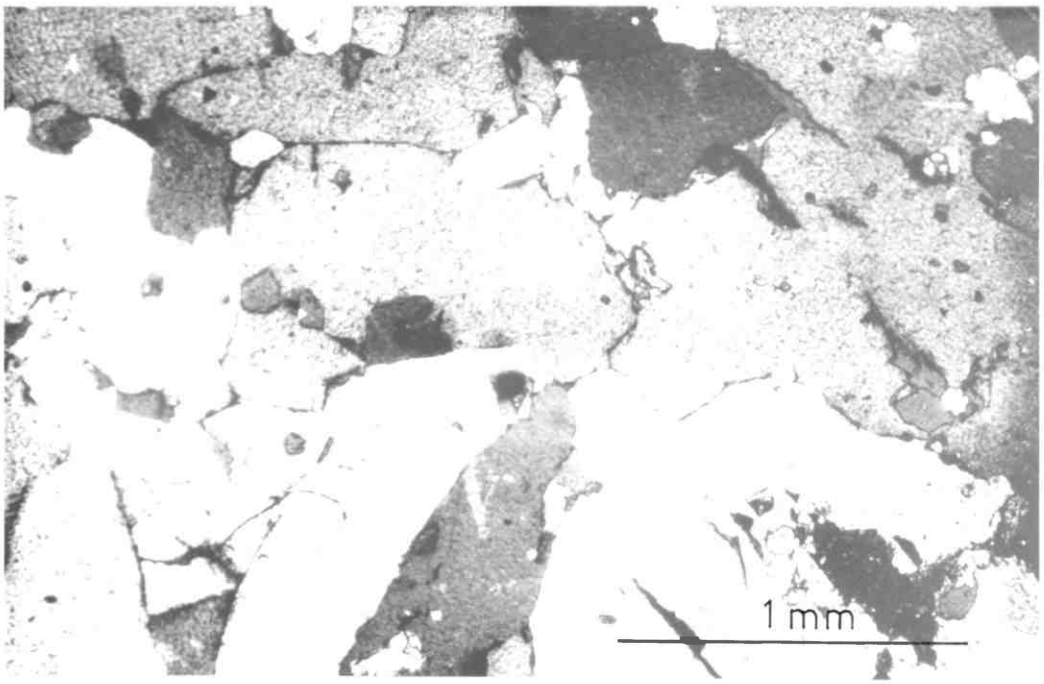

Plate 54: Photomicrograph of fine-grained granular celestite, showing G3 (large crystals) and G4 (small crystals) subtypes. Small calcite crystals along grain boundaries replace fine dolomite. Specimen GY61. Crossed Nichols.

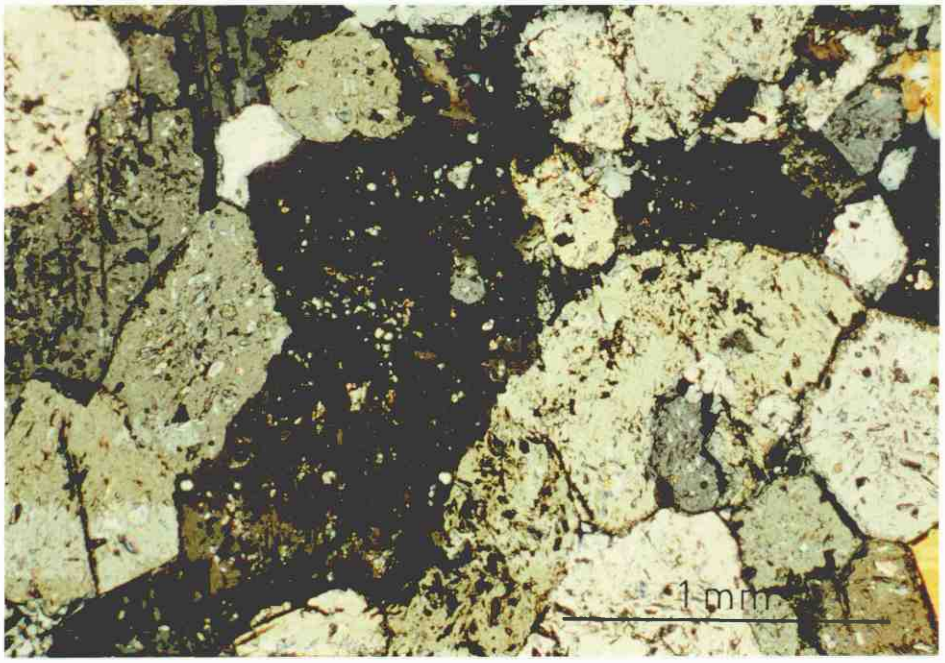

Plate 55: Photomicrograph of granular celestite showing mosaic G2 celestite with many inclusions of anhydrite (blue and orange interference colours), calcium carbonate (gold) and ?gypsum (grey). The calcium carbonate shows a consistent Sr content of 0.8 - 1.9% Sr (See Table 3.1) Specimen WP25 (lower half of Fig. 10a). Crossed Nichols.

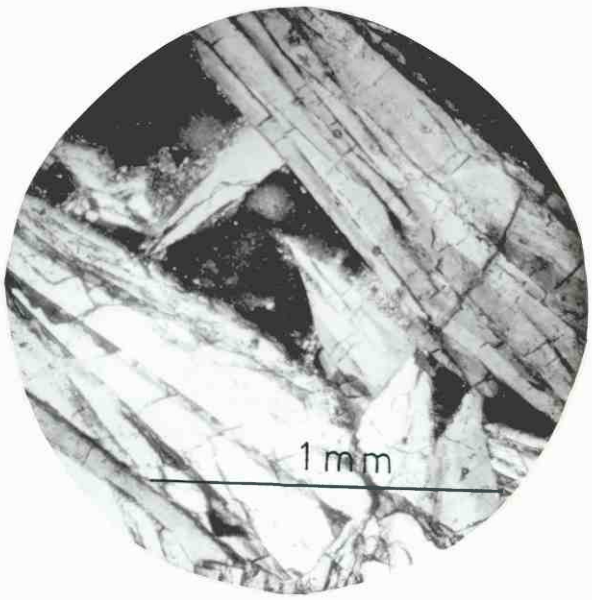

Plate 56: Photomicrograph of barian P1 celestite showing deformed nature of individual celestite laths. Specimen PF32. Crossed Nichols.

5) Absence of anhydrite relics.

To summarise, it is proposed that the P2 celestite evolved as follows:-

1) Replacement and pseudomorphing of anhydrite or gypsum macrocell by celestite.

2) Recrystallization of the celestite from the centre of the nodule outwards, resulting in the expulsion of Ba^{2+} ions, destruction of relics, growth of a mosaic fabric, and modification of the previous morphology by swelling, produced by the alignment of crystals in the new fabric.

3) Crystallization of primary P1 celestite at the margins of the P2 celetite. Barian celestite occurs where the advancing recrystallization front concentrated Ba^{2+} ions.

There is little evidence to suggest whether stages 2 and 3 occurred at the surface, or at depth. However, both took place before the crystallization of sparry calcite and are therefore early-diagenetic (see 3.1.3). In thin section the P3 fabric of the pink granule celestite shows laminae and strands of marl, with sutured contacts meeting at triple boundaries, indicating cementation of the marl (Fig. 43). The overgrowths are of a later, more rapid phase of celestite growth.

c. Granular celestite

Impregnations of, and macrocellular blue,white and red granular celestite show up to four fabrics in thin section. The coarser fabrics (G1 and G3) contain equant grains with slightly cuspate contacts, meeting at enfacial junctions (Plates 52, 53, 54). Subtypes G2 and G4 consist of inequigranular mosaics with triple junctions and highly suturered grain contacts. Subtype G2 is differentiated only by the presence of anhydrite relics (Plate 55). However, euhedra with pseudohexagonal, rhombic and twinned, rectangular outlines, often showing re-entrants, also occur scattered throughout the mosaic fabric (Plate 52, 53, 55). 'Net-textured' (West, 1964, 1965) celestite contains fabrics G2, G3, and G4 . It must be remembered that the mosaic fabrics may not necessarily contain crystals of a

true granular, or prismatic habit (see 3.1.2.1). In particular, grains showing sutured contacts (G2 and G4 celestite) may be tabular crystals blunted by solution phenomena during compaction (Carozzi, 1960). But because the G2 and G4 subtypes also include euhedral crystals with well formed faces, at least some of the units in the mosaic are of granular or prismatic habit.

Some of the granular euhedra of subtype G4 are enveloped by marl. For unknown reasons, nucleation presumably proceeded at each face at an approximately equal rate instead of rapidly perpendicular to the C axis and slowly along it, to give S1 or P1 celestite. Where the granular crystals occur in a mosaic, the following evidence can be used to propose an alternative origin for the granular subtypes:

1) Subtype G2 includes anhydrite and gypsum relics.

2) Larger crystals of G1 and G3 celestite may poikilotopically enclose those of subtypes G2 and G4.

3) Rectangular, rhombic and pseudohexagonal euhedra of G2 and G4 celestite are similar to, and may pseudomorph, primary gypsum crystals.

These primary gypsum crystals are the 'gypsarenites' of Carozzi (1960) or lozenge gypsum of Holliday and Shephard-Thorn (1974) , which are usually replaced soon after formation by secondary anhydrite (pseudomorphed if the replacement process is volume-for-volume) as diagenesis proceeds. The anhydrite inclusions in G2 celestite may probably be relics of this secondary anhydrite (see 3.1.6.1 and 3.1.6.2 for a fuller discussion on the relic calcium sulphates).

A four-stage paragenetical sequence for the granular celestite may now be considered, each stage corresponding to one subtype, as shown in Fig. 3.1. The proposed sequence of events is as follows:-

Stage 1: Subtype G4 formed by pseudomorphing of crystals of primary gypsum. After partial replacement, the celestite continued to crystallise from each pseudomorphed crystal, modifying the crystal shape and producing sutured embayments at the crystal boundaries.

Stage 2: Anhydrite-free G3 celestite precipitated between

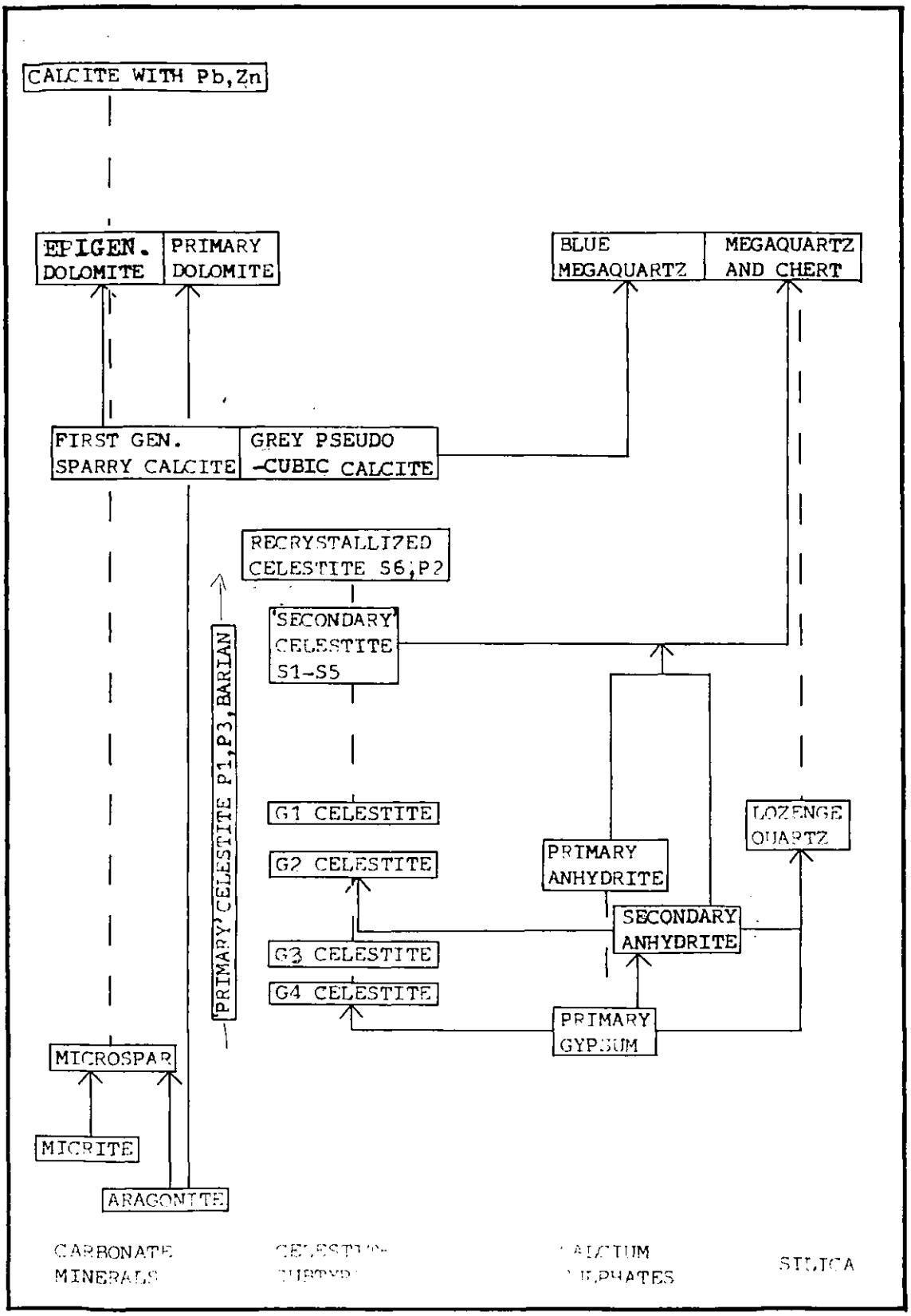

Fig 3.1: Temporal relationships between the authigenic minerals of the celestites of the study area. Key: arrowed lines indicate replacement, dashed lines substitution

pseudomorphs where overgrowth had not occurred and poikilotopically surrounded them

Stage 3: G2 celestite formed in other areas of the sediment where anhydrite was present, or, alternatively, nucleated later, after unreplaced gypsum in Stage 1 was dehydrated.. Celestite specimens with G2 celestite also show S1 celestite on erosion surfaces implying that the processes in Stage 3 occurred directly beneath the land surface at that time.

Stage 4: In areas where the dehydration of gypsum was only partial, so that both calcium sulphates coexisted, replacement by celestite produced two different fabrics. The first resulted from the replacement of anhydrite and consisted of granular and lathlike celestite (Subtype G2, from Stage 3 with a secondary celestite Subtype, eg S3). The second celestite fabric G1 celestite then grew in any remaining sulphates cementing the rock (Plate 52). Like Stage 3, this also occurred at shallow depths in the subsurface.

A gradation in fabrics can therefore be recognised from celestites of subtype G4 and G1 through subtypes G1, G2 and S3 to macrocells of subtypes S3, reflecting the relative amounts of gypsum and anhydrite in the original evaporite.

3.1.2.3 Barian Celestites

a. Introduction

Barian celestites may be defined as those containing at least 0.96% Ba by weight substituting for Sr. This figure represents the maximum Ba content of 'normal' celestites, as recognised in Chapter 4.

A celestite that assayed 2.88% Ba in the anlysis of the Main Analytical Series, specimen SB07 was reexamined by the electron microprobe in order to investigate further the distribution of Ba within the celestite crystals. Also a further two celestites from seams A and B at the Poundhouse Farm site, when analysed by the electron microprobe were found to contain barian celestite, and on one of these, specimen CH35, a detailed step traverse was performed.

b. Distribution of Ba in specimen SBO7

Two generations of celestite have been identified in sections but from Summer Bridge celestite, both impregnating illite-rich sandy mudstone (Seam B).

The first, forming the core of specimen SBO7 (Fig. 3.2; locations 1a, 2b, 3 and 4b) contains scattered small anhydrite relics and in texture resembles S6 celestite. The second later celestite occurs as slender elongate laths, typically .05 - .20 mm in diameter either as individuals, in interstitial mudstone or as splintery sheaf-like masses, nucleating on and cutting S6 celestite. The individual crystals, which seem to be a variety of P1 celestite occur oriented or randomly dispersed, and are fractured or bent (Fig. 3.2; Locations 1b, 2a and 4a). High Ba analyses predominate in the later celestite (Table 3.2), values of 7 - 8 % Ba being the most common. The coarser S6 celestite contains .32 - .90 % Ba, except for at site 4b where overgrowths of S1 celestite are suspected. Apart from the obvious distribution between the two forms of celestite, variations in Ba across the section appears to be random.

c. Distribution of Ba in Poundhouse Farm Celestite

Each section of Poundhouse Farm celestite was taken from a specimen showing white laths of P1 celestite bordering macrocells of light red primary celestite, in sparrudite. In specimen PF32, the white P1 celestite is present as a sheaf-like cluster near to the edge of a mass of red P1 celestite (Fig 3.2, Plate 56); in specimen PF35 it is more evenly distributed over both sides of a kidney-shaped mass of P2 celestite, giving the appearance of a desert rose from the outside of the specimen (Plate 57) with the laths radiating either side of the finer celestite core. Quantitative analyses were carried out on prismatic cross-sections of crystals showing a similar stage of development 0.2 - 0.5 mm in diameter. Only the white P1 celestite is barian in composition. Ba was semi- quantitatively detected in amounts less than 0.5% in the red celestite in specimen PF32 whereas in specimen PF35 (Point 'A' in Fig. 3.3), it could not be detected at all. Table 3.2 also shows that the Ba-content of the P1 celestite

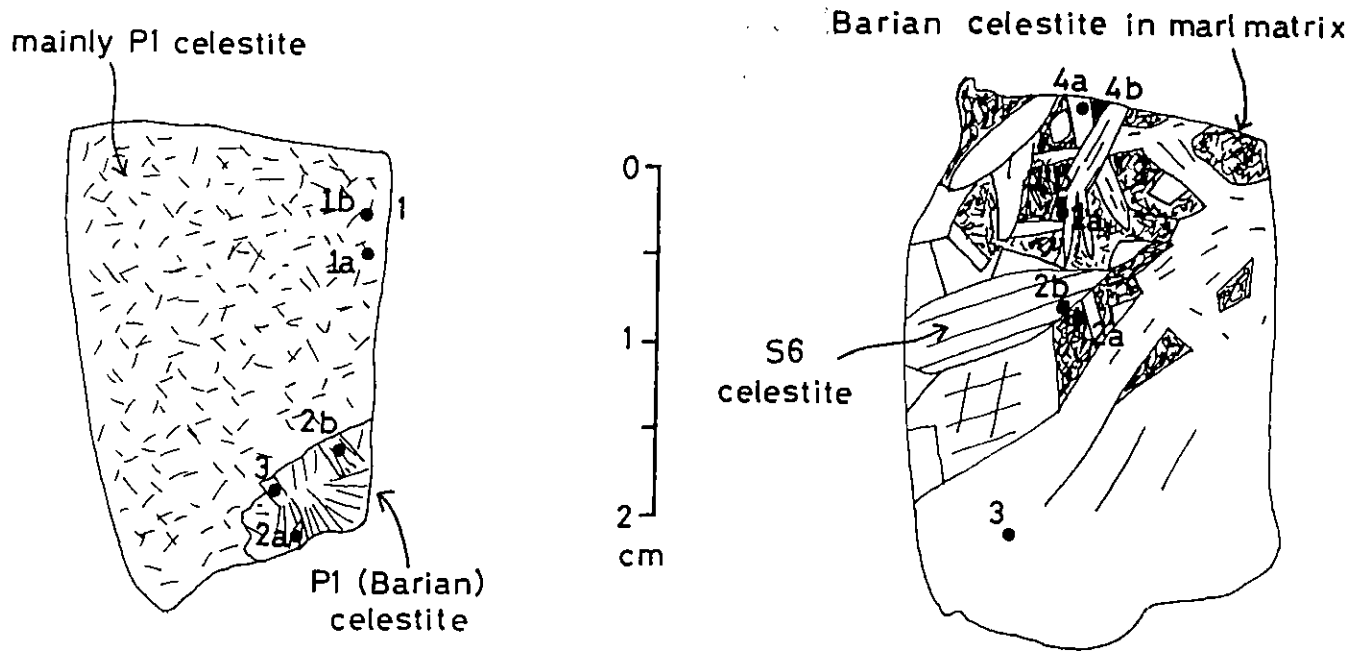

Fig 3.2: Sections of celestite specimens PF32 (left) and SB07 (right) showing location of microprobe analyses

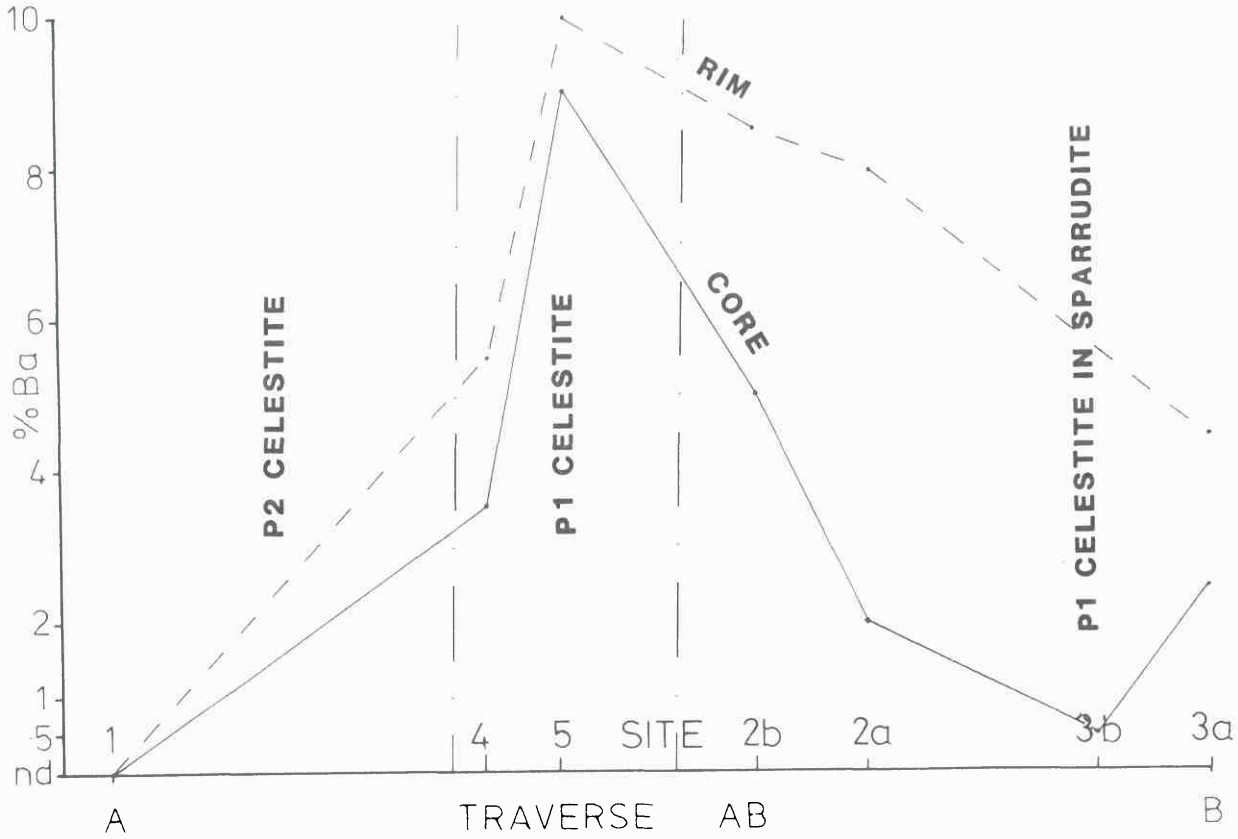

Fig 3.3: Microprobe point traverse across specimen PF35

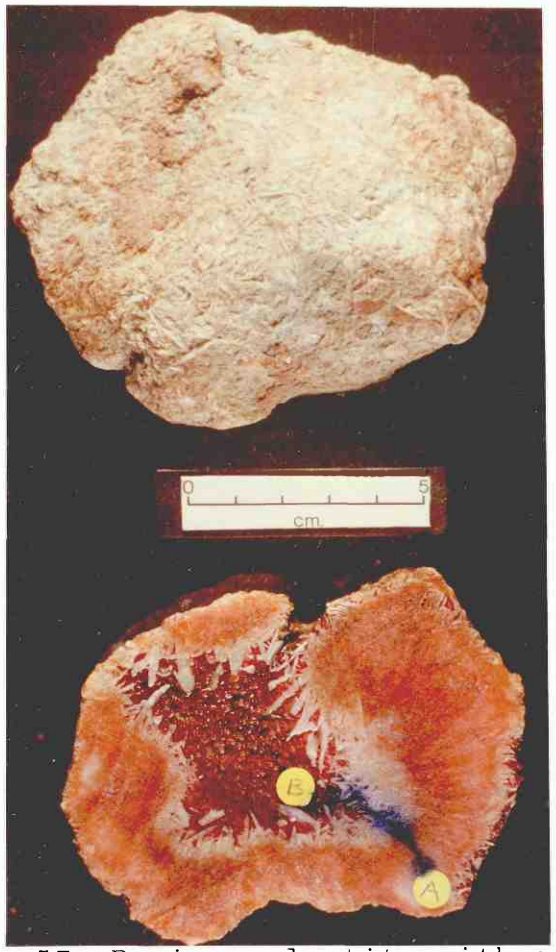

Plate 57: Barian celestite with sparrudite (stained with Alizarin Red S). A-B is microprobe traverse. Note deformed fabric.

varies greatly, both between locations in the same section and at each location across the celestite crystal itself. At 5 locations this latter variation occurs as an increase in Ba from the core of the crystal outwards, at 2 the variation is of the opposite sense and at one (specimen PF32, location 1b), where both rims were analysed, there is a large jump in the Ba content towards one side of the crystal only. The variation across the specimen is illustrated in Fig 3.3; here core assays of 1 - 2% Ba increase steadily from the centre of the specimen outwards towards the P2 celestite, peaking at a value of 8.96% Ba and then fall away. A less obvious pattern is seen in PF32; here there is a general decrease in Ba from the centre of the efforescence (location 2a, see Fig. 3.2) out into the "average" P1 celestite. The high Ba assay at location 1b (Fig 3.2) is produced from one of many white crystals of barian P1 celestite in the red P1 celestite matrix.

d. Interpretation

The observations recorded above show that barian celestite always occurs associated with celestites whose barian contents are of average or below average values. As the barian celestite is the later variety to form, it is suggested that this later celestite scavenged into physically deformed crystals (Plate 56) strained by the incoporation of the larger-ionic radius Ba^{2+} ion into the lattice, all the Ba remaining in the milieu after the maximum level of Ba (about 1%) had been taken up into the earlier celestite.

3.1.2.4 Conclusions

The subdivision of the Type A celestites into 13 subtypes on the basis of microscopic differences in fabric type, together with the identification of barian celestite has resulted in the recognition of different genetical processes (Fig. 3.1). These are:-

1) Replacement of gypsum by granular celestite (subtypes G3 and G4).

2) Replacement of anhydrite by granular and tabular celestite (subtypes S1 - S6, G1, G2).

3) Crystallization of anhydrite-free celestite (subtypes P1, P3, ,G3).

4) Recrystallization of celestite (subtype P2)

5) Crystallization of barian celestite (subtype P1).

3.1.3 Calcite

Calcite is an ubiquitous associate of Type A celestite both as an aphanitic cement in the marl host rock, and as a sparry calcite accessory mineral.

3.1.3.1 Aphanitic Calcite

In thin section, marl samples from Goose Green and Poundhouse Farm show a groundmass of micritic calcite that embays the sand and silt grade quartz grains. In some specimens, the micrite is coalesced into subhedra 0.05 - 0.50 mm in diameter, producing a clotted fabric which is syntaxially replaced by later sparry calcite (Plate 58). Microspar may also be present.

As the aphanitic calcite occurs both in marls containing no celestite as well as those containing celestite, anteceding sparry calcite, it may be interpreted as an early formed phase. This calcite may be chemically precipitated in an evaporitic sequence; replace aragonite thus formed, or be a mechanical accumulation of, for example, reworked desiccation crusts or weathered limestone country rocks, the depositional fabric having been obliterated by recrystallization to microspar and by the development of the clotted texture (Carozzi, 1960, p. 261).

3.1.3.2 Sparry Calcite

a. Description

The following variants of sparry calcite are recognised in thin section:

1) Coarse grained calcite

The calcite grains in the spararenites and sparrudites consist of subhedra of sparry calcite, 0.5 - 3.0 mm in diameter.

2) Mosaic calcite

Thin sections of limestone and yellow scalenehedral calcite show an equigranular mosaic of equant subhedra,

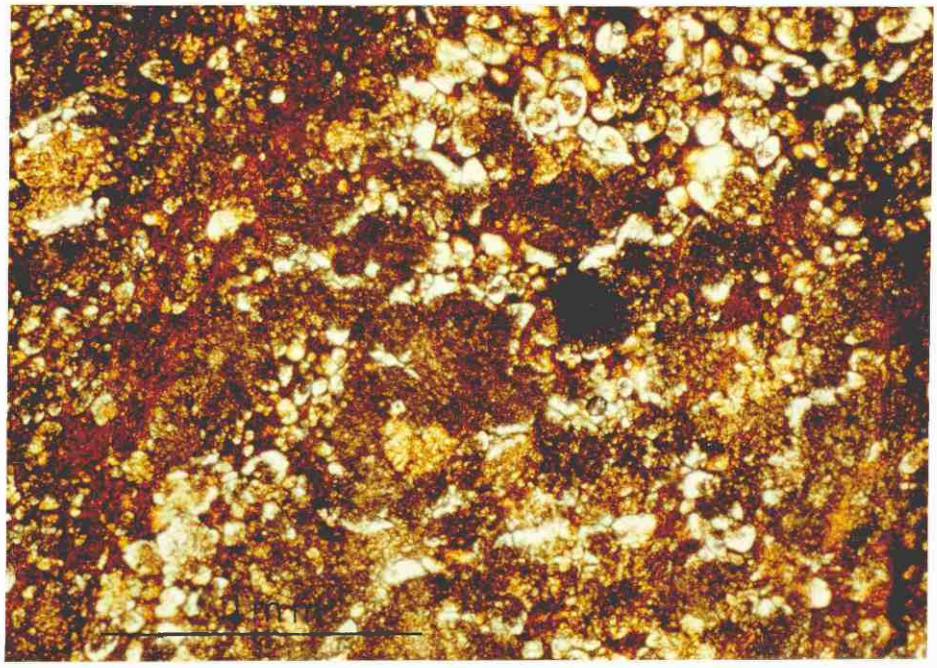

Plate 58: Photomicrograph of indurated marl rim of massive celestite module showing syntaxial replacement of micrite clots,(green) by sparry calcite (white). In an illite and aphanitic hematite (red) matrix. Specimen GG22 (see Plate 7). Plane polarized light.

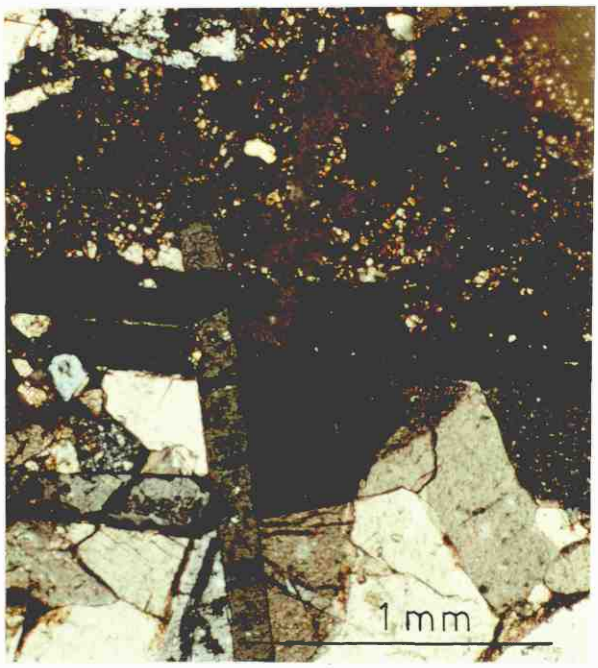

Plate 59: Photomicrograph of the erosion surface depicted in Plate 10a, Restriction of mosaic calcite to the area beneath the discontinuity (marked by flat-lying celestite laths) implies that the calcite nucleated before the deposition of the overlying marl. Note erosion of celestite crystals above the erosion surface. Fine, sparry calcite was last phase of diagenesis. Specimen WP25. C. Nichols.

averaging 0.5 mm in diameter with cuspate margins. The characteristic appearance of scalenohedral calcite is infilling interstitial space between 3 laths of S1 celestite (Plate 44), bending and fracturing the celestite laths, and rarely, replacing celestite. This calcite replaces lozenge quartz (see below) and is itself replaced by megaquartz (Plate 46). Close inspection of an erosion surface in this celestite revealed that the calcite probably grew before deposition of the overlapping sediment (Plate 59). Sections of grey pseudocubic calcite show a mosaic fabric enclosing herringbone celestite texture (Plate 45).

Mosaic calcite, consisting of subhedra 0.1 - 0.5 mm in diameter, borders many examples of P1, P2 or G3 celestite, and also occurs replacing S1 celestite in calcite rock. When tested for cathodoluminescence, this calcite gave a faint orange glow; the lilac calcite contained 0.21% Mn when analysed by microprobe (Table 3.1), the manganese presumably being reponsible for the colour of the calcite.

3) Calcite subhedra

Some specimens of limestone do not show a calcite fabric but consist of single calcite subhedra 0.1 - 0.5 mm across, growing in a marl matrix (Plate 44) or mud (Plate 60, 61). These grains may be transected by fine grained calcite or graded into the above 2 types.

4) Fine Sparry calcite

Most of the Type A celestites contain a fine equant sparry calcite subhedra or euhedra 0.02 to 0.05 - 0.10 mm in diameter, scattered randomly across the celestite, grading into a limestone mosaic (Plates 50, 52, 59) or pervading both celestite and limestone.

This calcite may nucleate on small inclusions in celestite, particularly P3 celestite and also in S1 celestite, possibly replacing relic anhydrite. In addition, interstitial marl in celestites usually hosts fine calcite crystals. Fine spary calcite is the last phase to form in the paragenetical sequence: it is synchronous with chert and may even replace dolomite (Plate 54). In a section cut across an erosion surface fine calcite is present above but

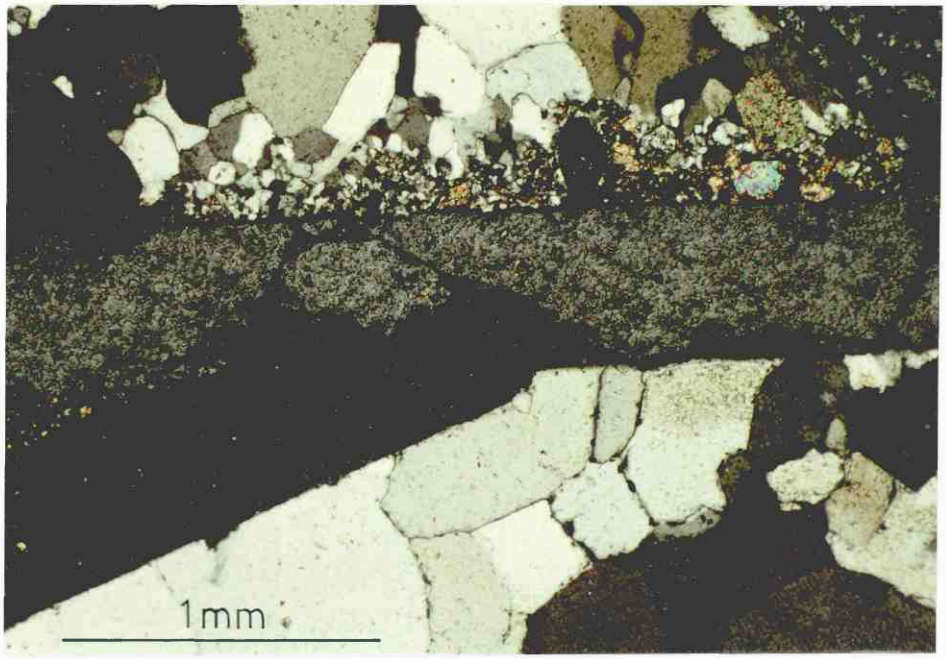

Plate 60: Photomicrograph of geopetal fabric in quartz-rich celestite, showing veneer of chert (low interference colours) and calcite scalenohedral (golden) on upper surface of S1 celestite lath (grey) in megaquartz mosaic (low colours). Specimen WP01. Crossed.Nichols.

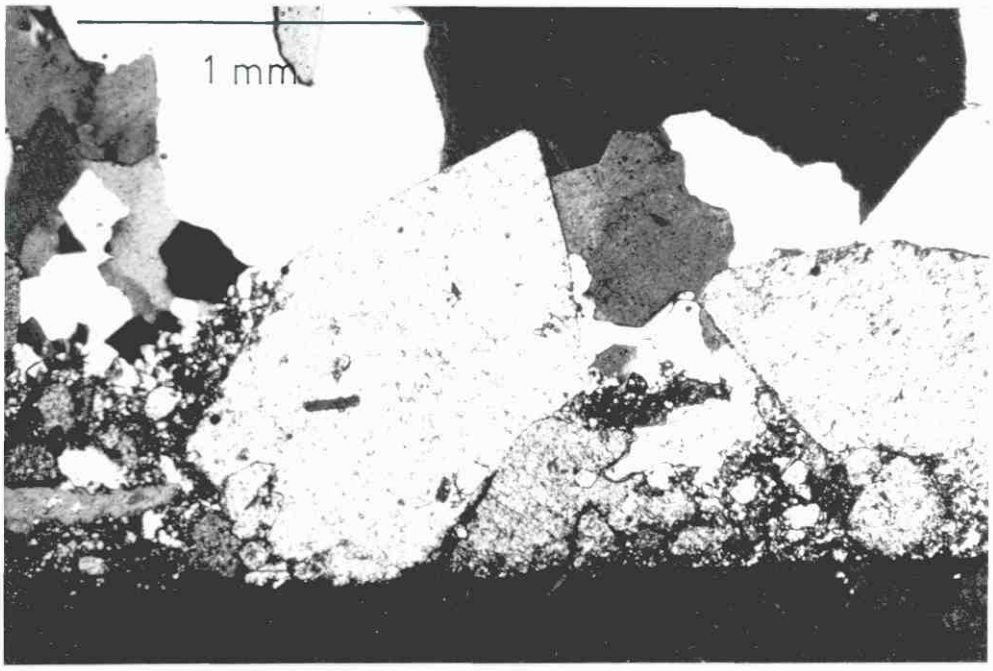

Plate 61: Photomicrograph showing detail of veneer in geopetal fabric, showing in-situ (centre) and comminuted (right) coarse calcite subhedra; fine calcite subhedra (light grey); early rounded quartz (grey) with anhydrite inclusions (extreme left) and megaquartz (light grey, centre right) in chert-calcite matrix. Specimen WP01. C. Nichols

not below the unconformity and grades into coarse spar, implying that its formation was the last event in early diagenesis. The preservation of slumped and foliated celestite, at Wapley, also suggests that lithification by fine calcite cement was restricted to upper beds in sequence of evaporites, for the cemented slumped horizon is distinct from the soft marl beneath.

b. General Discussion

As calcite is the principal dilutant of the celestite, its origin is of great interest. It is noted that, in most cases, crystallization of sparry calcite was preceded by the formation of celestite. Using this information, three alternative hypotheses may be postulated for the origin of the sparry calcite fabric:

1) The sparry calcite is a cement, the result of infiltration by groundwater rich in calcium and bicarbonate ions. A source of these ions can be found in the Carboniferous Limestone. Calcitization may have taken place at any subsequent time since the crystallization of celestite up to the present day.

2) The sparry calcite is a cement and is the manifestation of the Ca^{2+} released by the replacement of anhydrite, and in some cases aragonite, by celestite in a carbonate-rich environment. Alternatively sparry calcite and celestite resulted from the decomposition of strontianite ($SrCO_3$) with a calcium sulphate precursor.

3) The calcite is redistributed carbonate that was formed by the neomorphism (recrystallization) of an earlier carbonate phase.

Taken by itself, the petrographic evidence favours hypothesis 3. This conclusion is based upon the following considerations:-

1) Absence of strontianite.

2) Unlike most cements, the calcite fabric is not pervasive. Usually only the fine calcite <u>replaces</u> celestite and much of this is centred on inclusions of marl, or even aragonite in the celestite. The uniformity in grade of the sparrudites is also very striking, even near to celestite macrocells or vugs in marl (Plate 13).

3) There is an equal incidence of enfacial junctions and triple boundaries implying that more than one fabric-type may be present; however much of the calcite mosaic may be a cavity-filling and so the use of these criteria, used by Bathurst (1970) to distinguish cement from neomorphic calcite may not be possible in this case.

4) Sparry calcite occurs as abundantly with anhydrite-free celestites as with celestites-with anhydrite and so is unlikely to be a product of sulphate diagenesis.

5) Disparity in grain size between the calcite and the celestites.

6) Medium-grained subhedral calcite occurs syntaxically replacing clotted micrite.

7) Apart from certain examples of calcite-rock, the sparry calcite contains less then 0.1% Mn. No specimen of sparry calcite was found to contain detectable Fe or Mg and ankerite or siderite have also never been recorded. Such pure calcites are more favoured by the recrystallization of earlier carbonate, with consequent expulsion of impurities, than by the precipitation of an authigenic phase.

c. Epigenetic Calcite Rock

The above generalizations do not all apply in the case of the calcite rock. The mauve colouration, macrocellular megascopic texture, high Mn content (0.21 - 0.29%; Table 3.1), and association with non-ferrous sulphides and lath-shaped moulds (2.4.4.) suggest that the sparry calcite formed in this case is either a later neomorphic spar (Hypothesis 3) or an epigenetic cement (Hypothesis 1).

It is proposed that the second generation sparry calcite crystallized out from metal-rich brines, which percolating through the porous evaporite seams or sandy marl host, and recrystallized earlier limestone, expelling clay impurities towards the margins of a developing drusey quasi-macrocellular network. Brines ponded at the contact with the country rock were concentrated in metal sulphides and here non-ferrous sulphides were deposited.

d. Grey Pseudocubic Calcite

There is no petrographic evidence to indicate why this habit of calcite should occur in place of the usual scalenohedra. The poikilotopic relationship of the calcite

to the 'herringbone' celestite may indicate replacement of the anhydrite macrocell mapped out by this fabric; however well-formed drusey crystals suggest that some growth took place in free space. A clue to the origin of this calcite is that it never occurs in association with megaquartz (see below). As the calcite was apparently influenced by the distribution of the authigenic silica, it must have formed later.

3.1.3.3 Conclusions

The origin of each of the main varieties of calcite and their relationship to celestite is as follows:-

1 Aphanitic calcite constituted the cementing agent for the marls, in which celestite crystals later nucelated.

2 The crystallization of the celestite crystals induced the neomorphism of the aphanitic calcite, forming the sparry calcite of some limestones, yellow scalenohedral calcite, sparrudites and spararenites.

3 Later in the diagenesis, anhydrite in celestite at Wapley Common, that was not replaced by megaquartz (see below) was replaced by grey pseudocubic calcite.

4 At a later stage a separate calcite-sulphide mineralization produced epigenetic calcite rock. These stages are shown diagrammatically in Fig. 3.1.

3.1.4 Dolomite

3.1.4.1 Introduction

Celestites containing dolomite in this section include: celestites from the marginal deposits, Type B celestites replacing mudstone breccias and Type A celestites in yellow or greenish yellow marl and limestones.

3.1.4.2 Description

Two different varieties of dolomite are present. The first consists of tiny limpid subhedra, approximately 5 µm in diameter; these form the matrix of the yellow dolomite concretions at Poundhouse Farm.

The second occurs as rhombic euhedra, 10 - 50 µm in diameter, isolated or compacted replacing marl, sparry calcite or celestite; apparently as the last stage in the

stratiform celestite paragenesis (Fig. 3.1, Plate 44). These rhombs are either limpid or opaque and also zoned with hollow centres or cores of an opaque pigement, in places showing euhedral outlines. The dolomite in the fanglomerates (see 2.5.1.2) is comprised of the coarse, zoned variant. These crystals are compositionally Fe-rich dolomites (Table 3.1, Fig. 3.4) and an iron mineral, presumably goethite, constitutes the core.

3.1.4.3 Interpretation

The two dolomite varieties fall conveniently into the two dolomite classes, separated by a grain size of approximately 10 - 20 µm, summarised by Pettijohn (1975, pp. 361 - 364) from the results of earlier researchers as thinly bedded "primary" dolomite usually found with evaporites, and epigenetic dolomite after limestone, respectively.

The dolomite may be facies-controlled and so cut across stratigraphic planes so that the epigenetic dolomite is probably a time-stratigraphic equivalent of the "primary" (as shown in Fig. 3.1). For this reason the genetic terms "primary" and epigenetic cannot be accura tely applied to describe the dolomite and it is proposed that they be supplemented by terms: early diagenetic dolomite and late diagenetic dolomite respectively.

The early diagenetic dolomite could be an analogue of the fine chemical sediment known to be forming, from aragonite, at the present day in a hypersaline environment in the intertidal zones of sabkha flats or mudflats in the arid or semi-arid regions of the world, such as the Persian Gulf (Illing, Wells and Taylor, 1965) or the Bahamas (Shinn, Ginsburg and Lloyd, 1965). This interpretation is substantiated by the association of this dolomite with green beds indicating supposedly marine conditions (2.4.1.2.b.)

The late diagenetic dolomite replaced a sparry calcite precursor in one of the final stages in the diagenesis of the celestites. Therefore it may have formed at any time subsequent to the depostion of the celestites

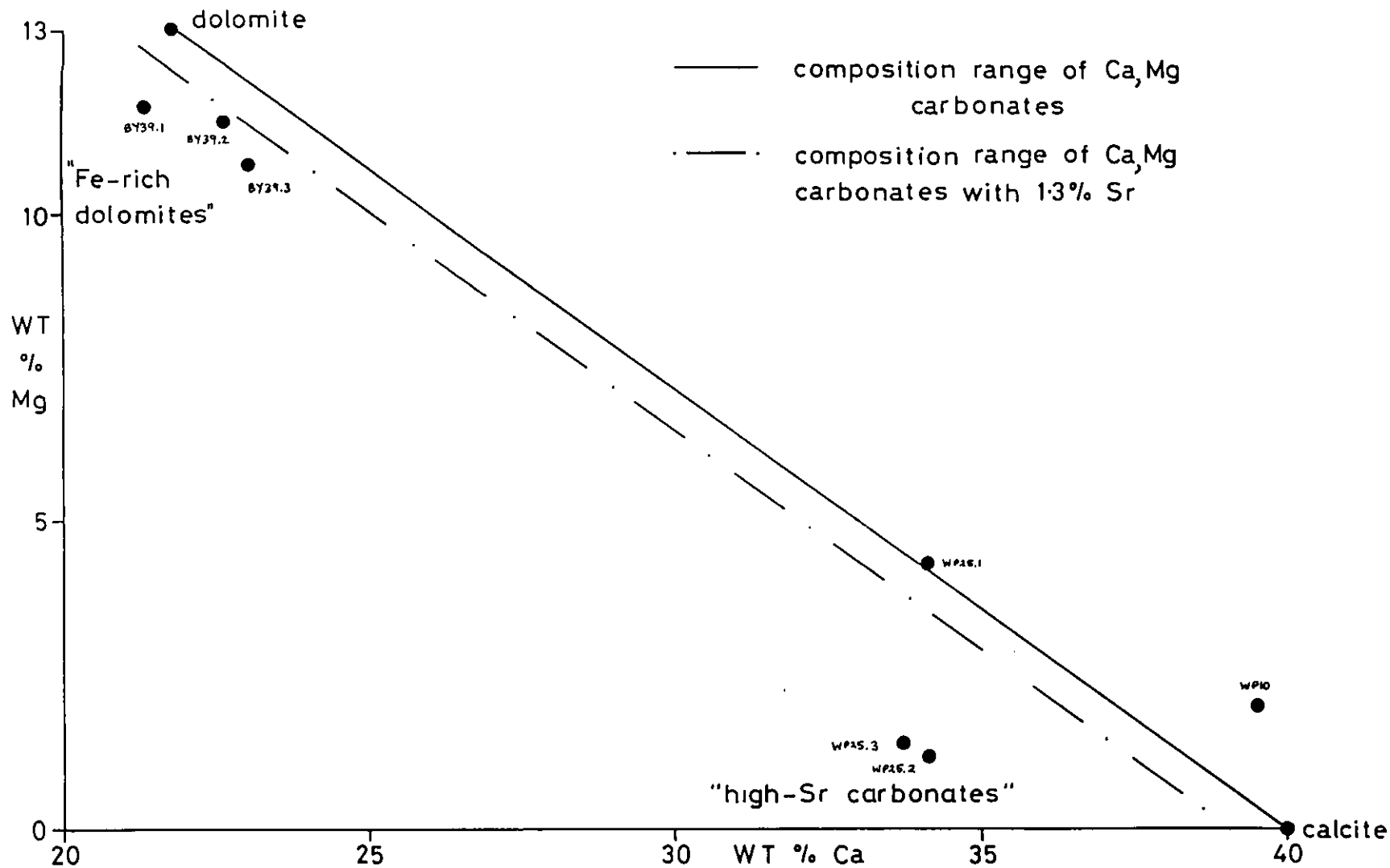

Fig 3.4: Graph showing the compositional range of the microprobe carbonate data

up to the present day. This dolomite occurs in continental flood facies marls and breccias (2.4.1.2b).

However, late diagenetic dolomite is a common constituent of many ancient carbonate rocks and its formation does not appear to be restricted to any one type of sedimentary or diagenetic environment. Nevertheless the interpretation of Folk and Land (1972) of limpid idiomorphic dolomite as the product of slow crystallization from very dilute solutions, is of direct relevance here especially as the idea was later developed by Folk and Siedlecka (1974) as evidence for "hyposaline" conditions which together with hyp--ersaline indicators such as evaporite nodules, length-slow chalcedony and penecontemporaneous dolomite (i.e. early diagenetic dolomite, as described above) were used to characterise "schizohaline environments". Furthermore Folk and Siedlecka (1974) proposed at least four situations in which schizohaline environments may arise of which one was a supratidal flat flooded by periodic rains; the model proposed for the Yate Formation in 2.4.1.2. It is also worthy of note that Folk and Siedlecka (1974) considered zoned dolomite as a particularly sensitive indicator of schizohaline conditions.

3.1.4.4 Conclusions

The early diagenetic dolomite of the dolomite rock was formed under hyper saline conditions, probably in the intertidal zone of the sabkha flat. The late diagenetic dolomite grew in the sediment, replacing sparry calcite and was formed after the crystallization of celestite; it is proposed that growth occurred under conditions of lower salinity, probably as a result of continental flooding. Both dolomite types formed penecontemporaneously, but from different processes, in a "schizohaline environment".

3.1.5 Authigenic Silica

The 3 varieties of authigenic silica identified in the Type A celestites from Wapley Common are: 1 lozenge quartz and lenticular aggregates, 2 : pervasive megaquartz, and 3 chert. The last two varieties usually occur together.

3.1.5.1 Lozenge quartz and lenticular aggregates

a Description

In thin section the lensoid quartz crystals described in 2.4.2.4 appear as lozenges of approximate size .5mm, showing enhedral lozenge-shaped, hexagonal, square and rectangular outlines, as shown in Plate 43. Many of these crystals show simple contact twinning, and are orientated with their long axes parallel to the bedding. These are habits that are not seen in crystals of quartz. In many cases, the opposing faces perpendicular to the bedding are serrated by saw-like embayments, appearing "ragged". Some sections show unorientated laths of anhydrite up to 50mm across, others, larger prismatic inclusions of a biaxial mineral, ?gypsum, or, more commonly, moulds where this mineral was dissolved out in the preparation of the slide (see 3.1.6.1, 3.1.6.2). Grains that are compounded, parallel to the bedding, retain all the features of the individual crystals and produce lenticular aggregates usually 2mm in length.

This form of silica is commonly observed poikilotopically enclosed by G2 or G3 celestite, which may corrode the quartz, which it therefore post-dates. It may also be replaced by sparry mosaic calcite. Thin sections show that the quartz crystallized before the slumping observed in the evaporite blocks.

b Interpretation (see also 3.1.2.2 and 3.1.6.1)

The crystal shapes of the individual grains, and, in some, the presence of gypsum inclusions indicate that quartz is pseudomorphing gypsum. But, the macrocellular shape of the lenticular aggregates and widespread anhydrite relics also strongly suggest that the silica has replaced anhydrite. This apparently contradictory evidence can be satisfactorily explained by proposing the following diagenetic history for the calcium sulphates. If secondary anhydrite was formed from the dehydration of gypsum by a mechanism of volume-for-volume replacement then, as the fine lathlike anhydrite crystals are much finer than the single large gypsum lenses, the shape of the host would be roughly preserved, particularly if the anhydrite laths were orientated parallel to opposing faces. The outlines of the gypsum

crystal perpendicular to the alignment of the anhydrite would then appear serrated, thus producing the ragged fabric described above. At the time of silicitization the quartz would then pseudomorph both dehydrated and unaltered gypsum.

The lenticular aggregates would be similarly formed by the replacement of gypsum, or anhydrite, crystals that coalesced at an early stage of diagenesis (West, 1964). There would now be less of a tendency for orientated anhydrite to preserve gypsum faces as more would now lie obliquely to the trend of the anhydrite.

The scheme outlined above is similar to others proposed by West (1964) and Holliday and Shephard-Thorn and is summarized in Fig 3.1.

3.1.5.2 Pervasive Megaquartz

a Description

In thin section the megaquartz appears as an anhedral mosaic of equant grains 0.5-1.0mm in diameter with curved, compromise boundaries, meeting at triple boundaries. The celestite laths are euhedral to the quartz, forming frameworks to the quartz mosaic (Plate 60), truncating individual grains and giving rise to mortar structure. A "veneer" of chert, with hematite, fine sparry calcite and coarse calcite scalenohedra usually occurs at the intersection of the celestite framework with the megaquartz, especially on the top surface of the celestite (Plate 61); this is the geopetal fabric of the handspecimen (2.4.2.4). Thin sections of the voids described in 2.4.2.4 show linings of megaquartz grading radially outward into thin stringers of chert. An identical fabric was recorded, as 'drusey quartz' by Adams (1920, plate XXIV F, p638) in superficial quartz veins; minute (5μm) anhydrite inclusions are present in megaquartz., immediately adjacent to celestite and also where the cellular structure is well developed.

Because of mutual incompatibility the relationship of megaquartz to calcite is difficult to determine. In certain areas in the mosaic calcite crystals substitute for megaquartz. Calcite crystals also frequently occur on the upper side of the geopetal structures, although not in positions of growth (Plate 61). In some cases the mega-

quartz fabric includes grains showing scalenohedral outlines, suggesting that the silica has pseudomorphed the calcite.

It can be reasonably assumed that the megaquartz post-dates the sparry calcite. Supplementary evidence, provided by ghost fabrics and other textures in 'blue' quartz indicate direct replacement in this particular variant.

b Interpretation

The megaquartz clearly crystallized after the celestite and therefore formed under different conditions to the lozenge quartz.

Anhedral mosaic megaquartz is, unfortunately, a non-diagnostic fabric (Adams, 1920; Arbey, 1980). It can form from the inversion (Siedlecka, 1972) or recrystallization of earlier silica, as a cavity-filling cement or as a replacement texture. The Wapley Common celestites, in particular, contain quartz that has characteristics of all 3 modes of emplacement. Features observed in these rocks that are indicative of each mode of origin are

1) Inversion/Recrystallization:
Mortar structure along planar intramosaic contacts (recrystallization fabric described by Adams 1920; equigranular texture; possible evidence of transformation of quartz silt to microspar; transition from megaquartz to microquartz without trace of fibrous intermediary (see Fig. 14 in Folk and Pittman, 1971, p1056); large number of 120° triple boundaries (criterion for neomorphic calcite, (Bathurst, 1971)); curved boundaries.
2) Cavity-fill:
Increase of grain size inward in cells of mosaic quartz, enhedral contact, and parallel configuration of quartz prisms adjacent to celestite framework; point extinction; geopetal fabric.
3) Replacement:
Anhydrite inclusions on borders of mosaic; geopetal fabric; sutured boundaries (Young, 1979).

This evidence suggests that the solutions that introduced the silica encountered pre-existing quartz, anhydrite and scalenohedral calcite inalattice of celestite laths, indicating exposure of the evaporite during the silification.

3.1.5.3 Chert

a Description

Chert is present in two forms. The first, the microquartz of Folk and Pittman (1971) consists of equigranular

anhedra 5-20 μm or 50 μm across and replaces the marl or mudstone fabric in interstitual areas and along stringers of marl in P3 celestite crystals (Plate 62), forms the matrix of the geopetal veneers, and borders voids in megaquartz. The second variant is cryptocrystalline chalcedony, showing strained extinction replacing celestite (Plate 63) or grading into a megaquartz mosaic. This may be fibrous forming spherulites centred on lozenge quartz (Plate 62) and producing a selvedge along the edges of S1 celestite laths (salt-and-pepper structure). By using a sensitive tint plate, the fibrous chalcedony was identified as the length-slow variety.

Chert corrodes some calcite; it may also appear to envelop scalenohedral calcite crystals that are not in positions of growth. It replaces lozenge quartz and celestite but is earlier than the late fine celestite with which it is commonly associated. The chert also transects lithological boundaries in specimens displaying slumping and so probably post-dates the deformation. The position of chert in the paragenetical sequence is shown in Fig.3.1. Because it is present in the geopetal veneer and also forms the borders of megaquartz it is believed to have crystallized slightly earlier than the megaquartz (see below).

b Interpretation

The chert has a similar origin to the megaquartz, and was formed soon after deposition in order to preserve the depositional fabrics of the sediments. Microquartz rather than megaquartz is the variant formed by the rapid precipitation of silica from supersaturated solutions (Folk and Pittman, 1971). These conditions were apparently satisfied in the Wapley Common celestites, at the interfaces between lozenge quartz and the depositing solutions, close to quartz silt in the marl matrix and along stringers in celestite (Plate 62). In addition, much of the microquartz in the veneers may also be a recrystallization product of quartz silt. Length-slow chaledony is the variety of silica formed by intermediate nucleation rates in a sulphate-rich environment (Folk and Pittman, 1971);in our

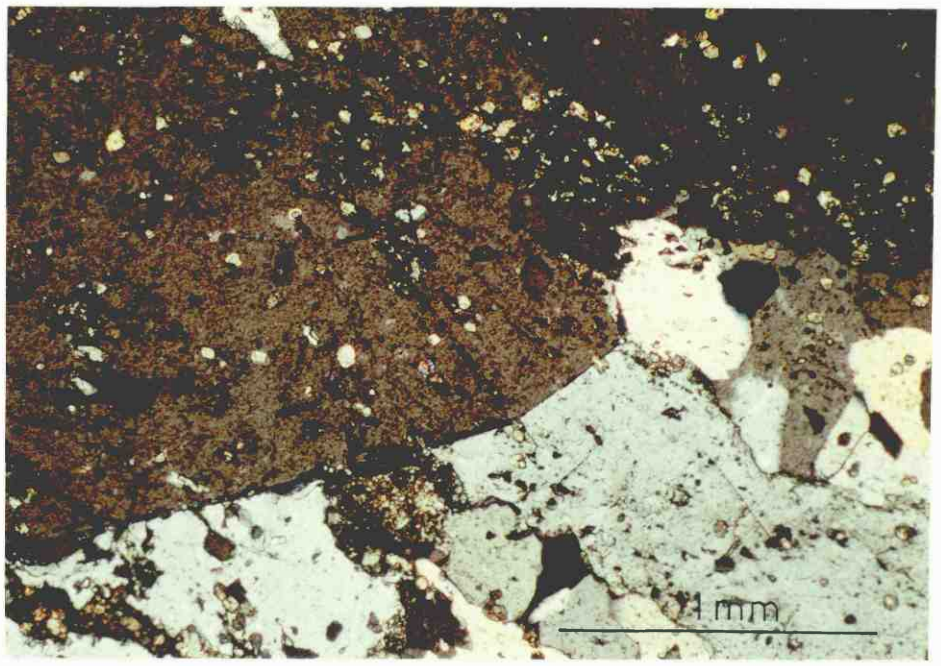

Plate 62: Photomicrograph of evaporite block showing 1, microquartz, with fine sparry calcite in marl trails in P3 celestite (top) and 2, spherulites of chalcedony surrounding earlier lozenge quartz (lower centre). Specimen WP09. Crossed Nichols.

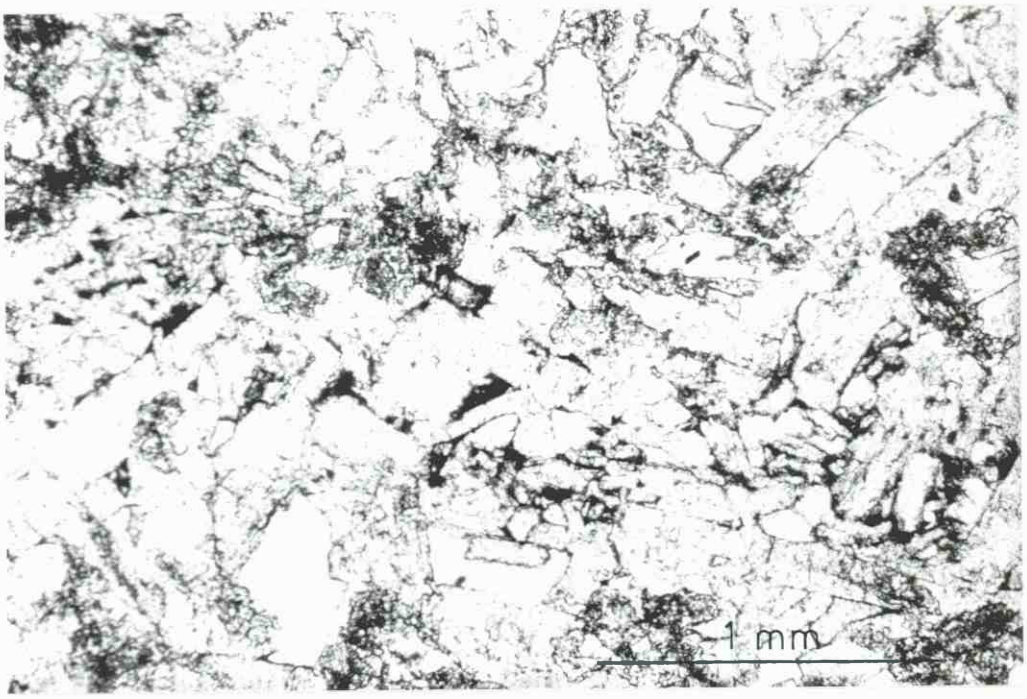

Plate 63: Photomicrograph of quartz-rich celestite showing pervasive chalcedony (high relief) in S2 and S3 celestite. Low relief crystals are authigenic quartz. Specimen WP16. Plane polarised light.

case it directly replaces celestite.

The source of the silica is considered in detail in Chapter 5.

3.1.5.4 Origin of the geopetal fabric

Plates 20, 60 and 61 show most of the features of this structure. Briefly, a veneer of microquartz, scalenohedral calcite and fine hematite, containing large crystals of calcite, some not in positions of growth, and grains of lozenge quartz,is trapped between the megaquartz mosaic, and, usually, the top surface of a coarse lath of S1 celestite.

The veneer may be interpreted differently for each of 4 different situations:

1) The veneer is a sedimentary trap in which fine aeolian or water-lain debris accumulated. Similar "mud partings" in crystal accumulates have been described by Kendall (1978).

2) The veneers represent the stringers between subsurface macrocells of anhydrite, in which coarse celestite laths grew. These formed at the upper surfaces of the anhydrite macrocells, possibly under the influence of favourable crystallization pressures at these positions, so that the laths appear to lie "underneath" the stringers. In finer celestite analogous growth of celestite at the margins of anhydrite macrocells resulted in herringbone texture.

3) The veneer is a solution breccia of the matrix surrounding an anhydrite macrocell that was replaced by megaquartz, the dissolution of anhydrite occured at a faster rate than the precipitation of silica.

4) The veneer is a collapse breccia of a pre-existing vug, lined with scalenohedral calcite that was later infilled with megaquartz. Note that in any of the first 3 situations recrystallization of the veneer from quartz silt to microquartz may have occurred before or after it came to rest at its present situation.

Because the evidence offered by the megaquartz fabric is ambiguous (see above) it is necessary to consider an origin that considers all 4 of the arguments expressed above.

A genetical model for the geopetal fabric using all the lines of evidence noted above, is shown in Fig. 3.5. Without the megaquartz cement, neither the framework celestite nor the geopetal fabric would have been preserved, as the soft sediment would have been reworked during the accumulation of the overlying stratum (Plate 59).

3.1.5.5 Conclusions

Two separate phases of silicification are proposed for the quartz-rich celestites from Wapley Common. First, quartz replaced primary gypsum and macrocellular anhydrite in early diagenesis. Then, after celestite crystallization a further mineralisation occurred at the surface of the sabkha. This resulted in a second stage of anhydrite replacement, corrosion of the celestite, chertification of the sediment and the destruction of the remaining porosity. The geopetal fabric was produced and preserved at this time.

A paragenetic scheme for the siliceous celestites is included in Fig. 3.1. The entire sequence may be interpreted within the context of one cycle of evaporite formation.

The silicification is therefore interpreted as syn-sedimentary rather than post-depositional. This is an important consideration to bear in mind when discussing the spatial distribution and origin of the silica (see Chapter 5).

3.1.6 Other minerals present in Type A celestite

Other minerals identified in trace amounts in thin section are briefly discussed below. No other minerals such as halite or strontianite were detected.

3.1.6.1 Gypsum

Although this mineral is not found in hand specimens of celestites textural evidence for the presence of primary (non-selenitic, non-alabastine) gypsum is plentiful. Stubby, rectangular, lozenge-shaped and pseudohexagonal anhedral grains, of approximate diameter .5mm occur at Goose Green as units in a mosaic of G2 or G4 celestite (3.1.2.2c) Plate 54) and at Poundhouse Farm and Wapley Common as lozenge quartz replaced by silica either individually or compounded into macrocells (3.1.5.1). Small 100 μm prismatic inclusions of gypsum may also occur in

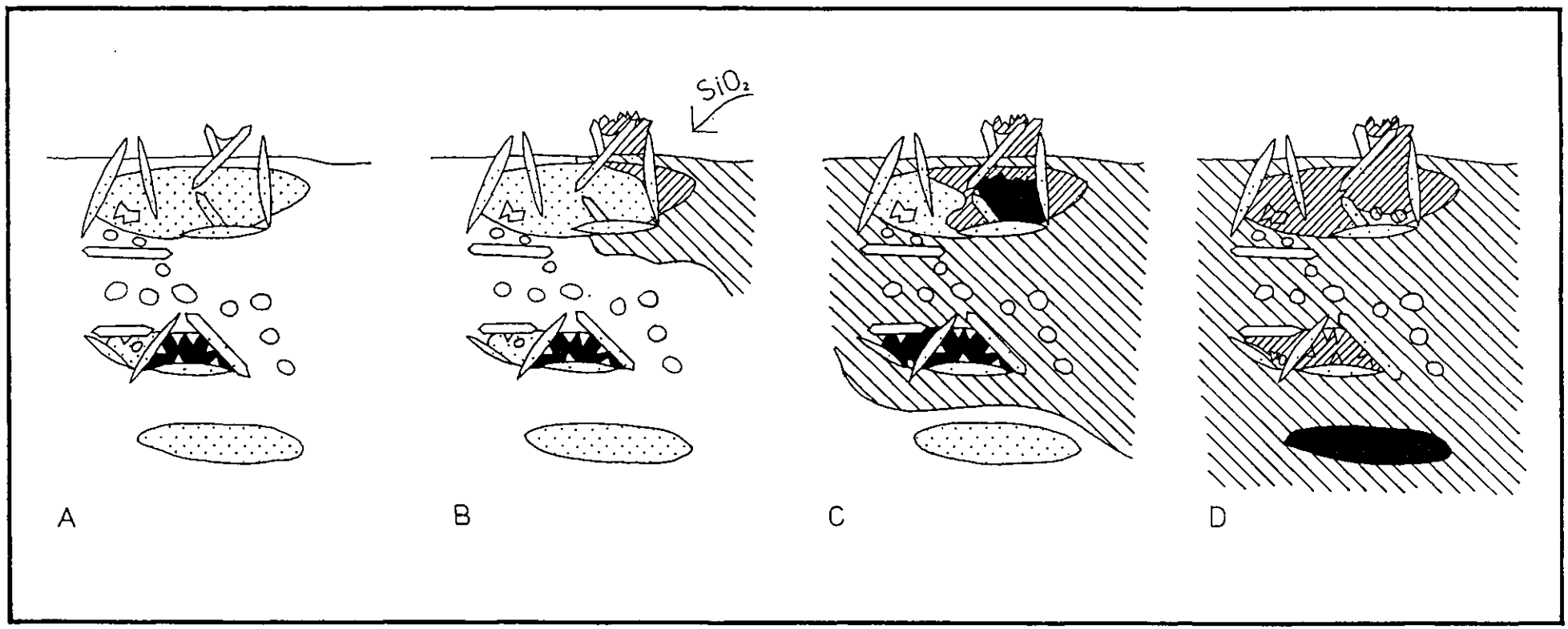

Fig 3.5 : Formation of the geopetal fabric in Wapley Common celestites (schematic)
Key: lath-shaped crystals: celestite; ovoid and triangular crystals: sparry calcite; stipple: anhydrite; closely-spaced ruling: megaquartz; widely-spaced ruling: chert; dark areas: cavities.

Explanation

Stage A, pre-silicification. Anhydrite macrocells intergrown with subtype S1 celestite. Sparry calcite present in central and upper macrocell only. Note pseudomorph of lozenge quartz crystals in upper macrocell.

Stage B, early silicification. Chert replaces marl from surface downwards. Anhydrite in upper macrocell partially replaced by megaquartz. Megaquartz at surface preserves eolian trap as geopetal fabric (Situation 1 in text)

Stage C, late silicification. Chert replaces entire sediment. Dissolution of anhydrite in upper and central macrocells produces voids. Chertified marl on left-hand side of upper macrocell produces geopetal fabric (Situation 2 in text).

Stage D, post-silicification. Megaquartz completely replaces anhydrite in upper macrocell and pseudomorphs calcite in central macrocell. Geopetal fabric formed by solution breccia (upper macrocell, Situation 3) and by collapse breccia (central macrocell, Situation 4).

other specimens of Wapley Common celestite and lozenge quartz.

These relic textures closely resemble descriptions of 'gypsarenite' by Carozzi (1960), 'lozenge and lense gypsum West (1964), Holliday and Shephard-Thorn (1974); all of which refer to primary gypsum, usually replaced soon after formation by secondary anhydrite (pseudomorphed if the replacement process is volume-for-volume) as diagemesis proceeds. Such anhydrite pseudomorphs have been recognised in celestites (3.1.2.2c); together with the ready replacement of gypsum by lozenge quartz, these explain why primary gypsum is so rarely seen in the celestites.

The relationship of the celestite subtypes to primary gypsum is illustrated in Fig. 3.1. The orientated simple contact (100) twinning in lozenge quartz when present in gypsum, is diagnostic of a subsurface growth by syngenetic-very early diagenetic processes in the top few centimetres of the host sediment (West 1964; Truc 1979, p176 and p236). Large expanses of mushy lozenge gypsum are forming at the present day in the intertidal zones of coastal sabkhas, for example in the Persian Gulf (Shearman 1966) and at Baja, California (Kinsman, 1969a).

3.1.6.2 Anhydrite

Small rectangular inclusions of anhydrite occur in all varieties of 'secondary' celestite, G1 and G2 celestite and megaquartz (Plates 47, 59). The size of the inclusions varies from 10 µm to 100 µm along the long axis; crystals of sizes 10 µm X 50 µm being most common. Some of the first inclusions have individual extinction, suggesting that each inclusion is a separate crystal. Apart from examples in S4 celestite (Plate 47), there is no relationship between the distribution or orientation of the inclusions and the crystallographic outline of the celestite; it is usual for the relic anhydrite to randomly pervade the host.

The fine texture suggests that the inclusions are mainly lamellae of the variety of secondary (replacing gypsum) anhydrite described as felty epigenetic (Carozzi, 1960, p426) or aphanitic anhydrite (e.g. Holliday and Shephard-Thorn (1974) . This fine grained anhydrite

was produced by dehydration and preserved as pseudomorphs. the habit of the primary gypsum crystals which were, later still, themselves replaced by quartz (see 3.1.5.1) or G2 celestite (Plate 49), proving that there was no loss of volume on alteration. Varieties of anhydrite are discussed in Chapter 5. Electron microprobe analyses of 4 anhydrite inclusions in specimen WT01 (Table 3.1) show a consistently detectable Sr content averaging 0.45%, corresponding to a composition of $(Ca_{.993}Sr_{.007})SO_4$.

3.1.6.3 High-Sr Carbonate

50 μm inclusions of an aphanitic carbonate in some specimens of S1 and G2 celestite from Wapley Common have been tentatively identified as aragonite on the evidence of a consistent detectable Sr microprobe analysis of 0.8-1.9% (see Table 3.1), and, in one case, fibro-radiate texture with concentric banding; a fabric characteristic of aragonite (Plate 55). The inclusions are the disorientated relics of larger areas of carbonate between anhydrite crystals, now present as inclusions in celestite.

These fine inclusions are very difficult to identify and aragonite has almost certainly been overlooked in other thin sections which were not analysed by microprobe. Scattered inclusions of sparry calcite subhedra may be used as indirect evidence of former aragonite crystals or aragonite mud; these are known to be the neomorphic products of an earlier carbonate phase (3.1.3.2).

The high Sr "carbonate" in the Wapley Common celestites is interpreted as a chemical precipitate. Aragonite muds containing a high Sr content are forming at the present day in many sedimentary environments but particularly in arid-zone mudflats (Illing, Wells and Taylor, 1965) and lagoons (e.g. Bathurst 1971). However the presence of metastable aragonite, like high-Mg calcite, in Triassic sediments is difficult to account for. It may be that the inclusions were protected by the enclosing celestite from changes in the physico-chemical environment that would induce inversion to calcite. However, if the analyses are plotted on a Ca-Mg diagram (Fig. 3.4) they show scatter about the Ca, Mg carbonate trend. Two analyses are also

deficient in Ca or Mg suggesting that the 'mineral' investigated might be an aphanitic mixture of (?high magnesium) calcite and strontianite. More work is required however before definite conclusions are drawn.

3.1.6.4 Non-ferrous sulphides

Galena and sphalerite occur associated with calcite rock at Goose Green and Cooper's Field. Sphalerite is also present, in trace amounts, in dolomitic limestones at Poundhouse Farm (seam H) and at Goose Green East (seam C); dispersed throughout the host rock.

In thin section both sulphides occur as small discrete grains, approximately 0.2mm in diameter, at intercrystalline contacts in the sparry calcite mosaic. The galena forms anhedra, usually with a reaction rim of translusent grey cerussite whereas sphalerite occurs as rectangular and cubic crystals, characteristically greyish-brown in plane polarized light; intergrowths of both minerals also occur.

Electron microprobe analysis did not detect other metals in either galena or sphalerite, indicating, from geothermometrical considerations, a very low temperature for the crystallization of sphalerite. It is assumed that the Keuper Marl provided an iron-rich depositional environment. However, Page (1980) examined polished sections of the Goose Green non-ferrous mineralisation and found as well as a low temperature sphalerite, a second, "mottled" sphalerite containing blebs of chalcopyrite, that are usually attributed to exsolution on cooling from a high temperature $ZnS-CuFeS_2$ solid solution (e.g. Edwards, 1965). A high temperature origin is also indicated by minor amounts of Ag, Sb, and Bi in galenas reported from the Bristol area by Carlton (1959) and Hamilton (1966); the relationship of the metallic ores to the evaporite deposits is discussed further in Chapter 5.

3.1.6.5 Microcrystalline goethite

Coatings of black earthy goethite appear at an 'alteration front' over crystals of drusey celestite or, especially in celestites near to the present-day surface. The goethite, which is identified by its XRD pattern,

probably results from the weathering out of hematite inclusions in the celestite.

3.2 PETROGRAPHY OF THE EPIGENETIC CELESTITES

3.2.1 Introduction

Eighteen thin sections were examined from a representative collection of Type B, Type C and Type Q celestites from the Winter's Field, Rectory and Yate Bypass sites. Using a similar classification procedure as outlined in 3.1.2.1, ten subtypes of 'E' (epigenetic) celestite were identified. Except for the Type B celestites which occur with calcite and dolomite the celestites are mainly monomineralic; as there is no doubt over the replacement origin of the celestites these are only briefly discussed below; a summary of the main features is given in Table 3.4.

About half of the Type C celestites are of granular or prismatic habit. Prismatic celestite sections parallel to the rhombic prism faces l {102} and d {101} (Fig. 2.10) show hexagonal outlines with only faint cleavage traces and may be mistaken for quartz. Tabular celestite only rarely exhibits lozenge-shaped or spindle outlines, which are therefore regarded as a sign of growth in an unconsolidated sediment only. However wasp-waisted crystals showing constriction and undulose extinction are common, especially in sections of comb-textured celestite (subtype E1) Plate 64).

3.2.2 Description and Interpretation

Features of a pervasive, replacement fabric such as re-entrants and enfacial junctions are shown in the first five subtypes (E1-E5) (Plates 65 and 66). Subtypes E1,E2,E3,E4 represent the central-zone and fine 'rab' celestite, compound and massive celestite, microcrystalline 'rab' celestite and thick tabular celestite variants, respectively, of the vein celestite described in 2.5.1. The fine purple celestite of the marginal deposits and other rocks in the Yate Bypass cutting (Type Q celestite) is classified as subtype E2. Subtype E6, replacing sandstone is depicted in Plate 67. Thin sections of replacement fabrics in mudstones and marginal deposits mudstones commonly show granular

SUBTYPE	MAIN MICROSCOPIC FEATURES	SIZE(MINOR AXIS)	INTERPRETATION	NEAREST TYPE A EQUIVALENT
E1	Tabular, an-free, scattered to mosaic subhedra	+1.0 mm	Replacing mudstone and fissure filling	S6, also S1,P1
E2	Tabular, an-free, mosaic, subhedra	approx .2 mm	Replacing mudstone and mudstone breccia	S3
E3	Tabular, an-free, scattered to coalesced subhedra	.1-.2 mm	Replacing mudstone	S1,S2
E4	Tabular, an-free, scattered to coalesced subhedra	approx 1.0 mm	Replacing mudstone	None
E5	Tabular, an-free, coalesced to mosaic euhedra	up to 1.0 mm	Replacing sandstone and ironstone	None
E6	?Tabular, an-free, scattered to coalesced subhedra and anhedra	up to 5.0 mm	Cementing sandstone, also poikilotopic after subtype E8	G3
E7	Granular, an-free, scattered to mosaic subhedra and anhedra	.1-1.0 mm	Replacing mudstone and fissure filling	G4
E8	Granular, an-free, scattered to mosaic euhedra, subhedra and anhedra	.05-.20 mm	Pseudomorphing and replacing gypsum	G4
E9	Granular, an relics, coalesced to mosaic euhedra, subhedra and anhedra	.1-1.0 mm	Replacing pseudomorphous anhydrite after gypsum	G2
E10	Prismatic, an-free, coalesced to mosaic euhedra	.5-1.0 mm	Replacing mudstone breccia	None

TABLE 3.4: Summary of the main features of the 10 Type B and Type C Celestite subtypes, and a comparison with those of Type A Celestite

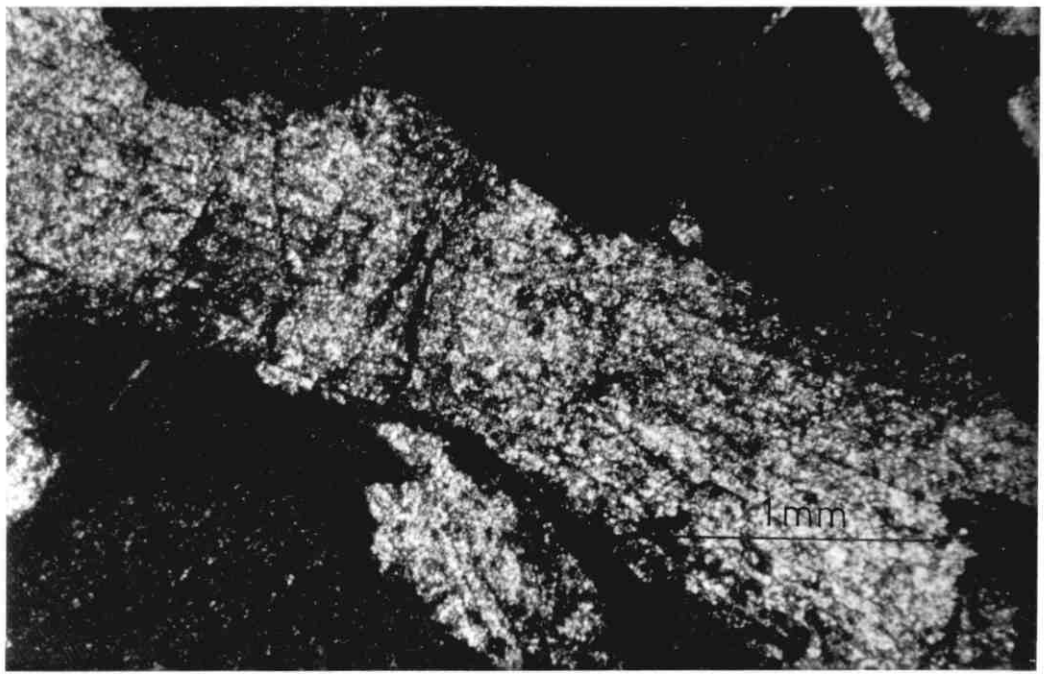

Plate 64: Photomicrograph of "wasp-waisted" thick tabular celestite, subtype E4. Specimen WF32. Crossed Nichols.

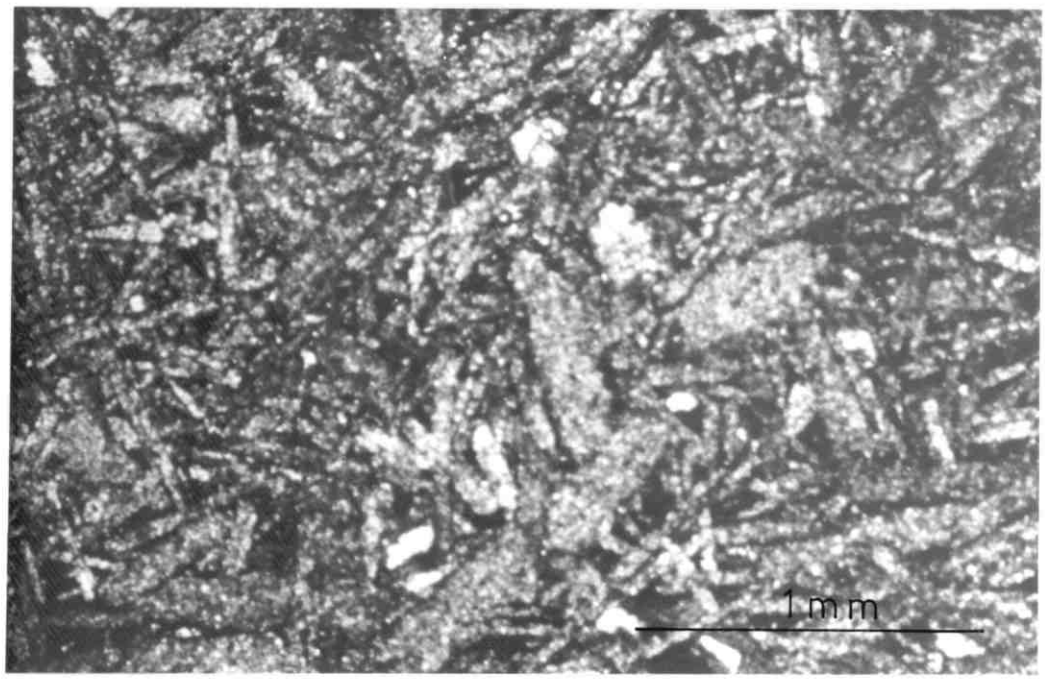

Plate 65: Photomicrograph of microcrystalline vein selvage, subtype E3 showing characteristic badly-formed laths in hematitic mudstone (dark) and quartz silt (low relief). matrix. The E3 crystals are corroded by the later El celestite (larger celestite crystals). The crystals grew by replacement rather than displacement (compare with Plate 50). Specimen WF36. Crossed Nichols.

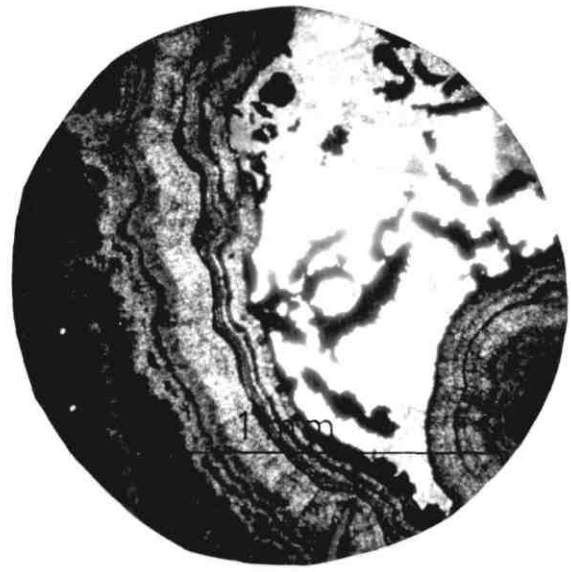

Plate 66: Photomicrograph of vein celestite replacing colloform, banded hematite-goethite ironstone (subtype E5). The goethite (dark grey) is left as relics in the celestite. Specimen BL01. Crossed Nichols.

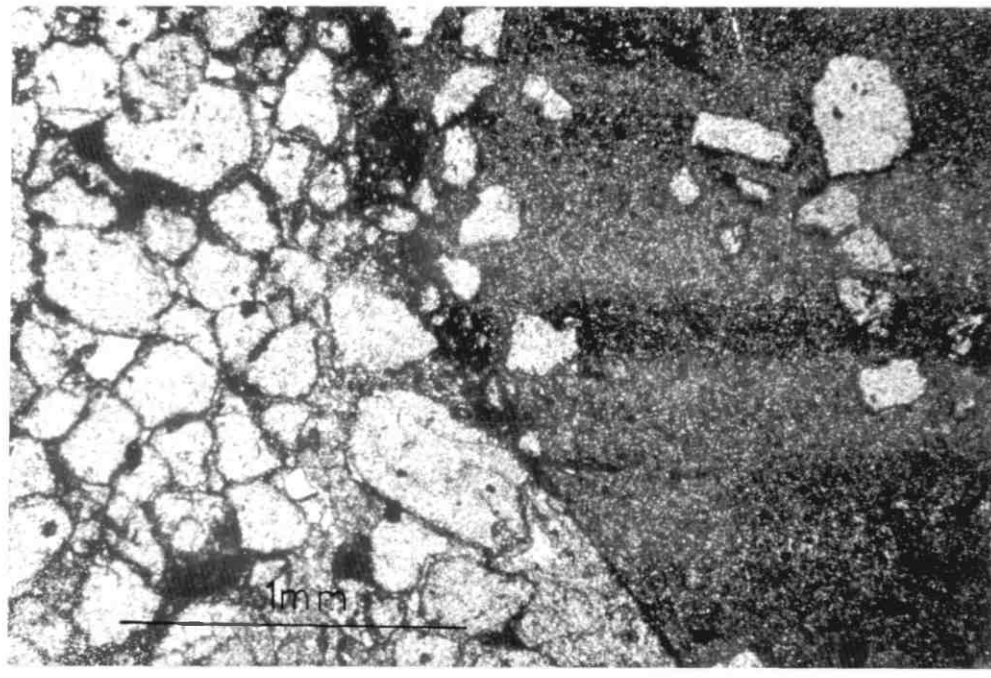

Plate 67: Photomicrograph of E6 celestite replacing quartzitic sandstone, showing corroded quartz relics. Specimen RY17. Crossed Nichols.

epigenetic celestite of subtype E7 substituting for the more usual lathlike form (Plate 68). This is probably celestite of a true granular or prismatic habit (see 2.3.2).

Subtype E8 occurs with E3 celestite in the microcrystalline celestite 'rab' particularly in the vicinity of the 'saddle-reef' textures or is present segregated in the yellow coloured layers described in 2.5.1.1 (Plate 30). Where the crystals are bordered by marl, the outer edges of the grains are not celestite crystal faces. In other cases the crystals are poikilotopically enclosed by E6 celestite. These observations suggest that the E8 celestite is a relic gypsum fabric, directly analogous to the G4 celestite in the Type A deposits. This earlier mineralisation may have produced the green colours in the mudstone, by the reduction of the Fe^{3+} in the illite (see 1.4.3.2). When the mudstone was subjected to the Sr-bearing solutions, laths of E3 celestite grew in the mudstone, and the gypsum was pseudomorphed by E8 celestite. Celestite mineralisation was most intense in the areas containing the gypsum and large crystals of E6 celestite also nucleated, poikilotopically enclosing the previous phase, and corroding crystals that had been pseudomorphed by celestite.

The growth of the E6 celestite produced swelling and the 'saddle-reef' texture was probably now developed (Plate 30). One explanation of the saddle-reef texture is that the crystal growth of the E6 celestite crystals was largely directed perpendicular to the bedding, causing buckling of overlying layers of previously cemented mudstone and producing, by a mechanism similar to flexural slip, small arcuate fissures in which coarse-void filling celestite (subtype E1) could later crystallize. Alternatively, the subtype E1 celestite may have formed in cavities resulting from the dissolution of an earlier calcium sulphate macrocell. In fact, anhydrite relics have been recorded in lenticular pockets of celestite in two mumblers of near-surface epigenetic celestite from The Rectory and Winter's Field sites. The E9 celestite subtype that is defined in these situations consists of an inequigranular mosaic in which highly sutured contacts and triple and quadruple boundaries are common and is similar in appearance to the G2 Type A

Plate 68: Photomicrograph of granular epigenetic celestite, subtype E7, in mudstone host. Specimen WF36. Crossed Nichols.

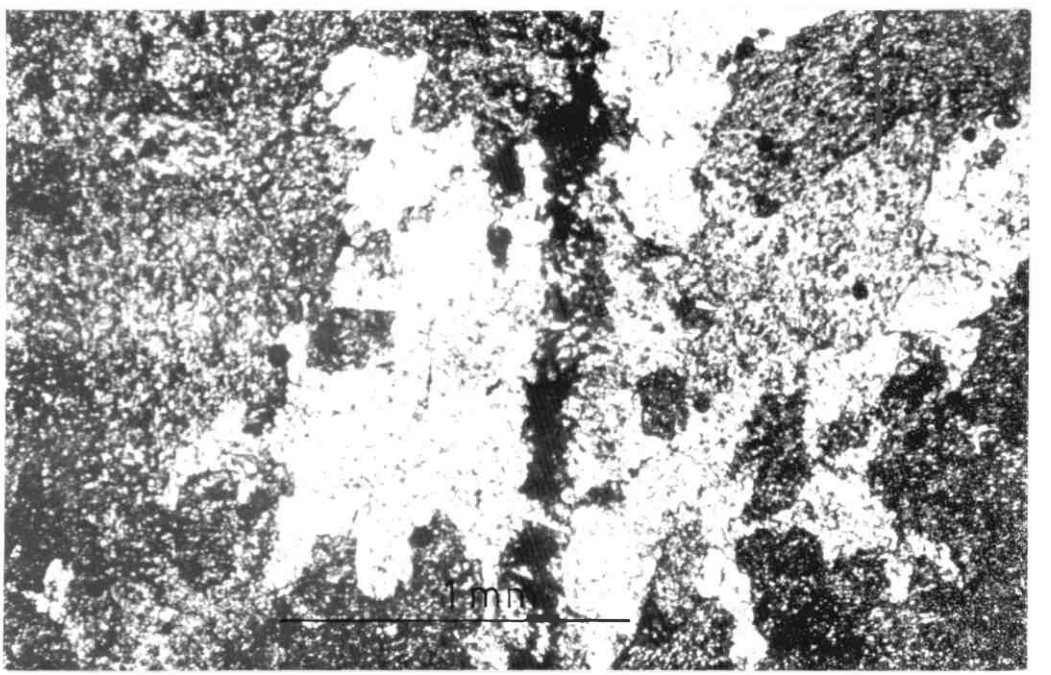

Plate 69: Photomicrograph of granular macrocellular gypsum showing anhedral porphyroblasts with castellated margins poikiltopically enclosing earlier prismatic gypsum. Specimen MIO3. Crossed Nichols.

celestite fabric. It is therefore suggested that macrocellular anhydrite was previously present in these samples, however as anhydrite relics also occur in E9 crystals enclosed by mudstone anhydrite masses or crystals smaller than macrocells must also have been present. It seems highly likely that, as in G2 celestite diagenesis (3.1.2.2c) the anhydrite replaced earlier granular gypsum crystals which were then pseudomorphed by the E9 celestite.

3.2.3 Conclusions

Epigenetic celestite crystallizes with tabular, granular and prismatic habit. Ten subtypes of epigenetic celestite, classified objectively using microscopic fabric criteria indicate that the Type B and Type C celestite orebodies grew by replacement of the Paleozoic and Triassic marginal deposits in a similar manner as the Type A celestites replaced gypsum and anhydrite (Table 3.4). Fabrics indicative of direct replacement of gypsum and anhydrite are also found in the epigenetic celestites but these are restricted to 'saddle-reef' textures in vein celestites and to drusey celestite cavities in epigenetic nodular celestites of near-surface origin.

3.3 PETROGRAPHY OF THE GYPSUM ROCKS

Thin section studies were performed on a selection of gypsums. These observations were complemented by qualitative whole rock XRD analysis.

3.3.1 Description of Gypsum Types

3.3.1.1 Granular macrocellular gypsum

In this variety coarse, mm-sized anhedral porphyroblasts form the bulk of the rock. A granoblastic fabric of an interlocking network of anhedra, 0.1mm across is also present; these show curved re-entrant boundaries. Where prismatic crystals occur, these are usually found intruding into the porphyroblasts, or, together with lozenge-shaped individuals, up to 1.0mm in diameter, poikilotopically enclosed by them. The prismatic crystals may show foliation and, like the porphyroblasts contain fine (< 0.05mm) anhydrite inclusions (Plate 69).

In some parts of the section the intercrystalline boundaries of the granoblastic fabric are not clearly defined. Under crossed polars the crystals in these areas act collectively to give strained extinction.

As in the celestites, the granular macrocellular gypsums are commonly "dusted" with anhedra of fine sparry calcite. XRD analyses of the Michaelwood gypsum show traces of anhydrite, pyrite and quartz.

3.3.1.2 Alabastrine gypsum

In thin section the alabastrine epigenetic gypsums differ from the granular, macrocellular gypsums in that the granoblastic fabric is foliated and consists of stubby prismatic straight-edged subhedra 0.05-0.10mm in diameter. Platey porphyroblasts, up to 5mm across, referred to in 2.3.3.3, show castellated contacts where they meet. At the contact with the granoblastic fabric, however, they are poorly defined and may include inclusions of prismatic gypsum.

Under the microscope the white, crystalline gypsum from Michaelwood also displays a porphyroblastic texture, but here the 1mm anhedral prismatic porphyroblasts cross-cut an inequigranular mosaic of prismatic anhedra, 0.2-1.0mm in diameter, some of which are bent and foliated. Areas of the specimen again also show diffuse grain boundaries, with strained extinction.

Relic anhydrite has not been detected in the thin sections of the alabastrine gypsum. XRD analyses of alabastrine gypsums show traces of pyrite and quartz, or celestite (Tortworth Copse gypsum only). Only Michaelwood gypsum contains detectable anhydrite.

3.3.1.3 Selenite

In thin section the Hall End selenite consists of macrocrystalline gypsum only. Anhydrite relics are not recorded.

3.3.2 Interpretation

The interpretation of porphyroblastic and granoblastic fabrics as indicators of secondary, mainly post-diagenetic, gypsum is now well established in the literature (West,1965;

Holliday 1970; Holliday 1978). Using Holliday's (1970) review the textures described above may be interpreted as follows:-

3.3.2.1 Granular macrocellular gypsum

a anhedral porphyroblasts

These are taken to be an early product of anhydrite hydration and may even date from early diagenesis of the gypsum precursor (Shearman, 1966). Where anhydrite relics are absent, recrystallization is implied. The prismatic gypsum crystals associated with the porphyroblasts may represent relics of an earlier gypsum, but not necessarily primary gypsum.

b granoblastic fabric

Fine anhedra showing a) curved re-entrant boundaries and anhydrite and b) diffuse boundaries and undulose extinction are ascribed to the direct replacement of anhydrite by the action of recent ground waters, or surface weathering (Holliday's (1970) Type 2 and Type 1 Hydration texture respectively.

3.3.2.2 Alabastrine gypsum - platey porphyroblasts and granoblastic fabric

This is a recrystallization product of the above textures, the disparity in grain size between the crystals and the straightness of the crystal faces reflecting the degree of diagenetic change (this interpretation is confirmed in this case by the absence of anhydrite). The platey porphyroblasts may however be relics of the initial hydration.

3.3.2.3 Selenite

The monomineralic texture and field relationships shown by the selenite indicate that it is a 'primary' deposit that crystallized out in the celestite druses. The time of formation of the selenite is unknown.

3.3.3 Conclusions

The above evidence suggests that the bulk of the Michaelwood and Aust Cliff gypsum is secondary. The granular macrocellular gypsum, the earliest product of hydration, preserves the structure of the anhydrite macrocells; this is progressively lost as later hydration and recrystallization produce first fine alabastrine gypsum, with porphyroblasts and later on, a crystalline gypsum.

The pink alabastrine gypsum of the Yate Platform resembles that of the Triassic deposits, both megascopically (compare earlier descriptions in 2.4.4 and 2.5.7.2, see also Fig. 4 in Holliday (1970, p736)) and in thin section, and a similar origin is suggested.

CHAPTER 4 - GEOCHEMISTRY OF THE CELESTITES

4.1 INTRODUCTION

The aims of the geochemical analyses of the celestites were threefold:-

1) To compare different analytical techniques and establish which are most suitable for the assaying of celestite.

2) To investigate and assess the composition of as wide a range of celestite varieties as possible from different localities and to determine if compositional charges, if present, are reflected in the celestite fabric.

3) To determine the composition of the celestite sands and gravels and of a few representative gypsums.

4.2 THE ANALYTICAL METHODS

4.2.1. Selection of Samples

The complete range of celestites analysed consisted of:

a) Fifteen Type A celestites from Goose Green, and three Type C celestites from Winter's Field.

b) Nine Type A celestites (quartz-rich celestites) from Wapley Common.

c) The main analytical series: 171 celestites and gypsums selected in order to investigate variations in composition both at the field and at the regional level. For the first objective, celestite quarries and roadway excavation at the Yate Bypass - Goose Green site were subjected to intensive sampling (Fig 4.1). In the eastern sector Type A celestites were sampled, where present, at an interval of 15m from seams A,B,B^1, and C in drainage ditches along the roadway, and from seams F and G in nearby pits. Type B,C and Q celestites were sampled, as exposed, across the site. Other celestites were collected from sites shown in Fig 4.2, each selected to be as representative as possible of the celestite varieties at each locality.

d) Thirty-two celestite sands, gravels, concentrates, and other rock types from the study area.

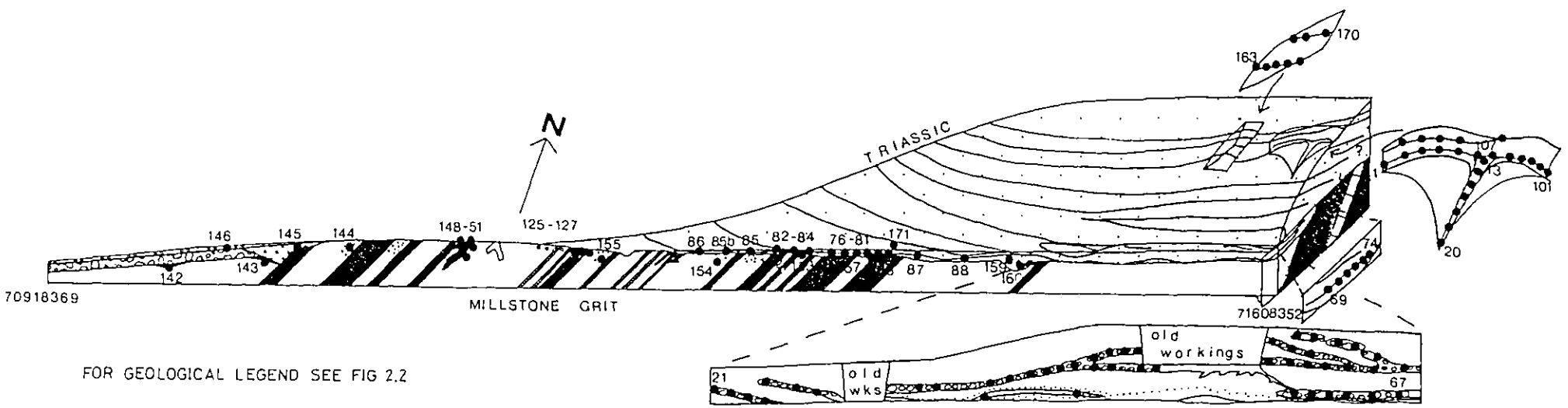

Fig 4.1: Location of celestite specimens along the Yate Bypass cutting

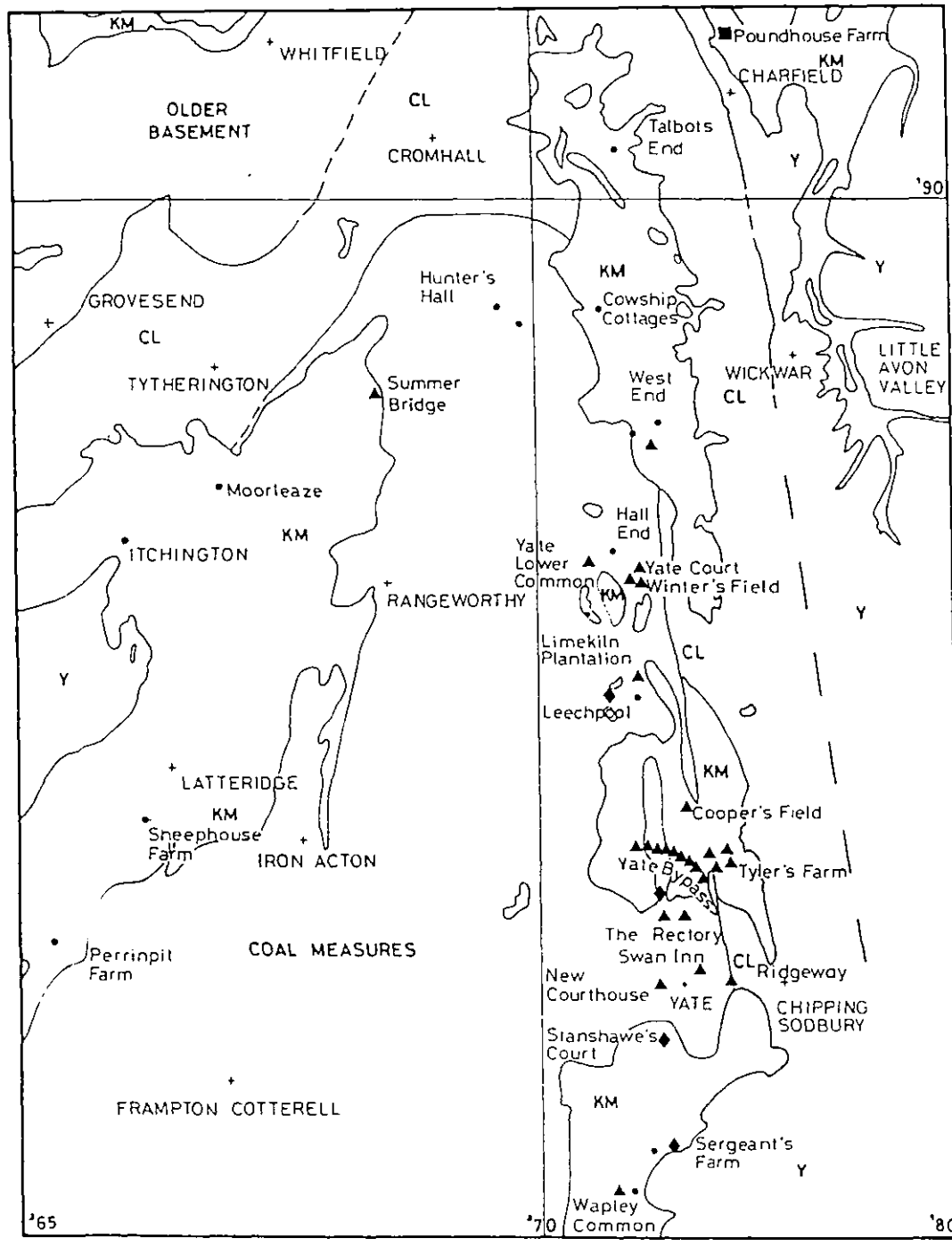

Fig 4.2: The study area, showing location of analysed celestites referred to in text. Source of data: triangles- this account; circles- Nickless et al. (1976); diamonds- Wood and Shaw (1976); square symbol; old records of the B.M.C. Ltd

Eleven replicate celestites and one replicate gypsum were collected to evaluate sampling error. Eight of the celestites were taken from one seam, F. The prefix nomenclature system used to describe the celestite samples is explained in Appendix I.

4.2.2. Description of Analysis

Three geochemical techniques were used in the analysis of the celestites; wet chemical analysis, spectrometric analysis and quantitative XRD analysis.* Details of each technique are included in Appendix II.

Wet chemical methods were used to analyse celestites throughout the project. The technique was continually assessed and refined during this time so that in all four different methods were applied:-

1. Sodium carbonate fusion. (SCF)
2. Hydrofluoric acid leach.
3. Mixed carbonate fusion. (MCF)
4. Lithium metaborate - lithium borate fusion. (LMF)

In each case determination of the metal ions was by atomic absorption spectrometry. (AAS)

Three kinds of spectrometric analysis were considered for inclusion in the analytical programme: portable isotope fluorescence (PIF), X-Ray fluorescence (XRF) and direct electron-excitation X-Ray spectrometry (XRS).

The Portable Isotope Fluorescence spectrometer was used by Nickless et. al. (1976) to analyse soil samples for strontium. Initially it was considered that this instrument might also be applied to determine the Sr content of run-of-mine ore and of celestite concentrate but as satisfactory guarantees could not be arrived at concerning the radiological safety of the instrument, this aspect of the project was abandoned. The feasibility of analysing the celestites using an XRF method was then investigated.

* It is recognised that XRD analysis is not strictly speaking, a geochemical technique. It is included in this chapter because the celestites are of simple mineralogy, and estimates of celestite and calcite content can be directly linked to the geochemistry.

Wood and Shaw (1976) used X-Ray fluorescence to determine Ba and Ca in an earlier study of celestites from the Yate area. However an XRF method was not thought to be applicable in this case for the following reasons:-

1. Separate preparing techniques are required for major and for minor elements, thus prolonging the analytical programme.

2. As the method of homogenising the sample is the same as the lithium metaborate fusion, there is no advantage in using XRF rather than AAS to determine the composition.

3. The Imperial College XRF spectrometer was not calibrated for carbonate and evaporite minerals.

Because of these difficulties, electron-excitation X-Ray spectrometry was used to analyse the celestites. However, the instrument used, the Telsec B300 Betaprobe, could not be used to determine Ba. The results of the analyses are given in Tables 4.1 to 4.8.

4.2.3. Comparison of the Analytical Methods

A number of specimens were analysed by both wet chemical and spectrometric methods, thus enabling a comparison of the two techniques to be made. The SrO and CaO data are contrasted on scatter diagrams in Fig. 4.3. Fig. 4.3a shows that there is poor correlation between the SrO values of the two analyses and that the wet chemical methods all give lower SrO values than the spectrometric. The enhancement of the LMF assays over the MCF, is also observed in the four specimens that were analysed by all three methods (MR01, MR02, MR04 and MR06). In these cases, the intermediate Sr assay (the L.M.F. assay) may be intuitively assumed to be nearest in true value (see Appendix II). There is unfortunately, no international celestite standard by which the accuracy of any method may be assessed.

The CaO data of the wet chemical and Betaprobe analyses show excellent agreement and lie close to a line at 45° to the origin (Fig. 4.3b). This is not so for the XRD analyses, however, where the equivalent Ca in the calcite and dolomite determinations is overestimated by a factor of two (Fig. 4.3c) although there is still good agreement between the two sets of data.

Table 4.1: Sodium carbonate fusions and HF acid leach analyses, in %, of twenty celestites and concentrates

Id'ty	Type	Sr	Sr*	Ba	Ca	Si	Mg	Al	Fe	K	Ba/Sr.10^{-2}*
CB01	celestite	32.2	47.0	0.50	0.00	0.04	0.00	0.05	0.050	0.030	1.06
CB02	celestite	33.7	46.4	0.40	0.50	0.04	0.00	0.05	0.050	0.120	0.86
CB03	celestite	32.5	44.7	0.48	1.00	0.92	0.12	0.05	0.137	0.240	1.07
CB04	celestite	29.2	46.6	0.25	0.00	0.44	0.10	0.05	0.137	0.150	0.54
CB05	celestite	33.0	47.2	0.30	0.00	0.06	0.00	0.05	0.095	0.030	0.64
CB06	celestite	40.6	47.1	0.30	0.00	0.16	0.10	0.05	0.050	0.030	0.64
CB07	celestite	32.2	46.9	0.40	0.00	0.17	0.00	0.05	0.050	0.060	0.85
CB08	celestite	29.2	45.9	0.35	0.75	0.30	0.00	0.05	0.095	0.120	0.76
CB09	celestite	33.2	47.3	0.15	0.00	nd	0.00	0.05	0.050	0.020	0.32
CB10	celestite	30.5	47.2	0.50	0.00	0.01	0.00	0.05	0.049	0.050	1.06
CB11	celestite	36.0	47.1	0.48	0.00	0.06	0.00	0.05	0.050	0.020	1.02
CB12	celestite	31.5	46.6	0.70	0.00	0.18	0.00	0.05	0.095	0.120	1.50
CB13	celestite	35.8	45.2	0.65	1.25	0.18	0.02	0.05	0.095	0.120	1.39
CB14	celestite	29.2	47.1	0.40	0.00	0.04	0.00	0.05	0.050	0.060	0.85
CB15	celestite	37.4	46.3	0.90	0.25	0.10	0.00	0.05	0.050	0.060	1.94
WF14	'rab'	41.7	-	0.30	0.00	-	0.02	0.42	0.054	-	0.72
WF15	'rab'	38.6	-	0.20	0.00	-	0.14	0.42	0.594	-	0.52
WF16	celestite	45.3	-	0.30	0.00	-	0.00	0.00	0.036	-	0.66
YCGG	concentrate	44.0	-	0.60	1.25	0.38	0.00	0.05	0.137	0.070	1.36
COOP	concentrate	-	-	0.60	2.00	0.18	0.00	0.05	0.125	0.040	-

* calculated by difference

Table 4.2: Sodium Carbonate - Potassium Carbonate fusion analyses in % of nine representative quartz-rich celestites from Wapley Common

Identity	Sr	Ba	Ca	$Ba/Sr.10^{-2}$
MR01	32.6	0.38	3.50	1.17
MR02	40.6	0.50	0.68	1.23
MR03	35.5	0.30	0.20	0.85
MR04	35.2	0.70	3.70	1.99
MR05	40.5	0.32	0.22	0.79
MR06	39.0	0.64	2.30	1.64
MR07	38.4	0.82	0.54	2.14
MR08	40.3	0.44	0.46	1.09
MR09	39.2	0.66	0.12	1.68

Table 4.3: Lithium metaborate fusion analyses in %* of four quartz-rich celestites from Wapley Common

Identity	Sr	Ba	Ca	Zn	$Ba/Sr.10^{-2}$
MR01	33.1	0.44	3.60	28	1.33
MR02	40.9	0.59	0.74	44	1.44
MR04	36.4	0.82	4.16	28	2.25
MR06	39.8	0.86	2.72	6	2.16

* Zn analyses in ppm

Table 4.4: Lithium Metaborate Fusion analyses, in %*

of the Main Analytical Series

Identity	No.	Sr	Ba	Ca	Zn	Na	K	Ba/Sr[1]	Na/K[2]
YB01	1	26.9	0.75	11.0	0.098	140	1.99	2.79	7
YB02	2	39.6	0.66	2.6	0.004	140	0.24	1.67	58
YB03	3	33.8	0.64	6.0	0.030	120	0.68	1.89	18
YB04	4	34.4	0.58	4.2	0.006	160	0.67	1.69	24
YB05	5	33.0	0.73	4.0	0.006	140	0.65	2.21	22
YB06	6	3.0	0.14	27.6	nd	80	1.43	4.67	6
YB07	7	28.1	0.57	13.4	0.048	100	1.38	2.03	7
YB08	8	35.4	0.72	4.6	0.004	180	0.76	2.03	24
YB09	9	39.7	0.85	1.2	0.023	100	0.42	2.14	24
YB10	10	40.5	0.64	3.0	0.006	180	0.38	1.58	47
YB11	11	34.4	0.63	2.2	0.027	140	0.90	1.83	16
YB12	12	29.1	0.64	8.0	0.061	120	0.90	2.20	13
YB13	13	39.1	0.65	1.2	0.004	200	0.53	1.66	38
YB14	14	38.0	0.54	3.0	0.027	120	0.50	1.42	24
YB15	15	41.3	0.55	0.8	0.258	140	0.60	1.33	23
YB16	16	39.1	0.61	2.6	0.034	80	0.67	1.56	12
YB17	17	41.4	0.71	1.4	nd	80	0.30	1.71	27
YB18	18	43.2	0.75	0.2	0.002	100	0.67	1.74	15
YB19	19	45.3	0.70	0.2	0.012	100	0.57	1.55	18
YB20	20	44.5	0.80	0.2	0.002	80	0.42	1.80	19
YB21	21	-	0.61	0.2	0.005	100	0.56	-	18
YB22	22	42.2	0.58	0.1	0.052	100	0.55	1.37	18
YB23	23	-	0.61	0.2	0.001	100	0.33	-	30
YB24	24	-	0.58	0.2	0.001	140	0.26	-	54
YB25	25	-	0.46	0.2	0.003	80	0.32	-	25
YB26	26	41.0	0.55	0.2	0.001	100	0.11	1.34	91
YB27	27	-	0.74	0.2	0.004	80	0.24	-	33
YB28	28	-	0.59	0.2	0.002	120	0.18	-	67
YB29	29	44.4	0.63	0.2	0.003	160	0.29	1.42	55
YB30	30	41.9	0.51	0.4	0.007	80	0.25	1.22	32
YB31	31	31.1	1.05	6.2	0.016	120	1.00	3.38	12
YB32	32	43.8	0.98	0.8	0.035	120	0.73	2.24	16
YB33	33	43.5	0.09	0.8	0.052	180	0.61	0.21	30
YB34	34	43.9	0.29	1.2	0.013	340	0.63	0.66	54
YB35	35	45.4	0.46	1.6	0.002	100	0.47	1.01	21
YB36	36	40.4	0.17	2.0	nd	80	0.60	0.42	13
YB37	37	16.2	0.46	15.4	0.081	160	2.16	2.84	7
YB38	38	9.3	0.30	18.2	0.013	140	1.99	3.23	7
YB39	39	7.7	0.51	15.6	0.141	80	0.92	6.62	9
YB40	40	42.9	0.51	1.4	0.009	120	0.43	1.19	28
YB41D	41D	44.3	0.60	1.8	0.065	100	0.78	1.35	13
YB42	42	42.3	0.22	2.0	0.011	120	0.28	0.52	43
YB43	43	13.6	0.46	3.4	0.003	140	0.61	3.38	23
YB44	44	3.4	0.12	29.2	0.044	120	1.87	3.53	6
YB45	45	34.9	0.78	9.4	0.008	80	0.65	2.23	12
YB46	46	14.9	0.61	19.8	0.008	120	1.19	4.09	10
YB47	47	30.4	0.60	10.4	0.004	100	1.48	1.97	7
YB48	48	42.8	0.37	1.8	0.013	80	0.24	0.86	33
YB49	49	43.3	0.30	0.5	0.022	80	0.37	0.69	21
YB50	50	43.5	0.36	0.4	0.018	60	0.52	0.83	12
YB51	51	44.5	0.58	0.2	0.013	140	0.26	1.30	54
YB52	52	43.0	0.54	1.4	0.003	160	0.57	1.26	28
YB53	53	48.0	0.37	0.4	nd	100	0.14	0.77	71
YB54	54	44.4	0.71	0.4	0.011	40	0.57	1.60	7

Table 4.4 (continued)

Identity	No.	Sr	Ba	Ca	Zn	Na	K	Ba/Sr[1]	Na/K[2]
YB55	55	45.5	0.56	0.4	0.024	20	0.60	1.23	3
YB56	56	44.0	0.65	0.2	0.003	40	0.42	1.48	10
YB57	57	18.2	0.58	16.4	0.002	40	0.36	3.19	11
YB58	58	40.5	0.45	3.8	0.016	20	1.99	1.11	1
YB59	59	42.6	0.64	1.2	nd	40	1.08	1.50	4
YB60	60	46.6	0.23	0.8	nd	40	0.58	0.49	7
YB61	61	45.4	0.23	1.2	nd	20	0.53	0.51	4
YB62	62	45.8	0.43	0.6	nd	140	1.00	0.94	14
YB63	63	44.1	0.64	0.2	nd	60	0.41	1.45	15
YB64	64	46.9	0.27	0.2	nd	60	0.47	0.58	13
YB65	65	45.2	0.77	0.2	nd	20	0.11	1.70	18
YB66	66	49.0	0.17	0.2	0.004	100	0.75	0.35	13
YB67	67	41.1	0.63	0.2	0.001	100	0.35	1.53	29
YB68	68	-	-	nd	nd	nd	0.16	-	0
YB69	69	-	0.70	0.2	nd	20	0.32	-	6
YB70	70	-	0.69	0.2	.007	20	0.16	-	13
YB71	71	44.3	0.81	0.2	0.008	40	0.47	1.83	9
YB72	72	-	0.68	0.2	0.011	20	0.71	-	3
YB73	73	-	0.56	0.2	0.005	60	0.41	-	15
YB74	74	44.2	0.80	nd	nd	60	0.37	1.81	16
YB76	76	-	0.64	nd	0.004	20	0.40	-	5
YB77	77	-	0.31	nd	0.014	20	2.61	-	1
YB78	78	-	0.61	nd	nd	60	0.65	-	9
YB79	79	-	0.40	1.0	0.025	40	0.36	-	11
YB80	80	-	0.79	0.2	nd	20	0.35	-	6
YB81	81	41.2	0.69	0.2	nd	20	0.37	1.67	5
YB82	82	41.6	1.15	0.4	nd	80	0.17	2.76	47
YB83	83	43.1	0.33	0.4	nd	40	0.74	0.77	5
YB84	84	38.7	1.77	0.2	0.002	40	0.37	4.57	11
YB85	85	38.9	1.91	0.2	nd	20	0.57	4.91	4
YB85B	85B	-	0.87	nd	nd	-	-	-	-
YB86	86	-	0.62	0.1	0.006	40	0.22	-	18
YB87	87	41.5	1.47	2.2	0.006	20	0.90	3.54	2
YB88	88	41.0	0.76	0.6	nd	60	0.23	1.85	26
CF06	89	43.3	0.64	0.2	0.027	20	0.17	1.48	12
CF07	90	40.5	0.57	0.4	0.008	60	0.62	1.41	10
CF08	91	41.4	0.19	2.2	0.002	40	0.17	0.46	24
CF09	92	45.0	0.40	0.4	0.007	60	0.51	0.89	12
RI01	93	43.9	0.31	0.4	nd	60	0.46	0.71	13
RI02	94	47.3	0.21	0.2	0.001	20	0.17	0.44	12
RI03	95	42.7	0.26	1.8	0.002	40	0.13	0.61	31
NC01	96	40.2	0.73	2.6	nd	60	0.82	1.82	7
NC02	97	42.7	0.33	0.4	0.017	20	0.33	0.77	6
NC03	98	44.7	0.61	0.4	0.130	40	0.28	1.36	14
NC04	99	39.6	1.00	nd	0.011	60	0.51	2.53	12
YB89	101	41.6	0.53	1.2	nd	120	0.37	1.27	32
YB90	102	34.6	0.67	10.2	0.077	80	0.34	1.94	24
YB91	103	41.4	0.63	0.6	nd	100	0.44	1.52	23
YB92	104	35.5	0.88	5.0	nd	100	0.25	2.48	40
YB93	105	41.0	0.72	3.0	0.032	60	0.46	1.76	13
YB94	106	42.2	0.65	0.6	nd	80	0.32	1.54	25
YB95	107	32.9	0.79	8.0	0.010	80	0.88	1.79	9
YC02	110	42.7	0.78	2.8	0.020	160	0.45	1.83	36
YC05	111	45.1	1.11	1.2	0.002	120	0.98	2.46	12
LP03	112	45.0	0.40	0.4	0.001	100	0.41	0.89	24

Table 4.4 (continued)

Identity	No.	Sr	Ba	Ca	Zn	Na	K	Ba/Sr[1]	Na/K[2]
RY05	120	42.6	0.59	0.4	nd	100	0.27	1.38	37
RY15	121	43.6	0.40	0.8	nd	80	0.41	0.92	20
RY13	122	43.1	0.51	nd	0.006	80	0.63	1.18	13
RY16	123	42.0	0.43	0.4	0.003	80	0.66	1.02	12
RY12	124	44.0	0.20	1.2	nd	80	0.43	0.45	19
BL01	125	10.4	0.13	nd	0.088	60	1.26	1.25	5
BL04	126	46.3	0.52	nd	nd	40	0.93	1.12	4
BL05	127	33.0	0.56	nd	0.039	80	0.43	1.70	19
WF23	128	45.5	0.99	0.2	nd	200	4.90	2.18	4
WF24	129	41.3	0.30	0.2	nd	100	0.74	0.73	14
LC01	130	-	0.80	nd	nd	120	0.26	-	46
WE01	131	-	0.32	0.4	nd	180	0.89	-	20
SB01	132	44.1	0.72	0.2	nd	100	0.98	1.63	10
SB02	133	43.6	0.60	0.2	nd	160	0.79	1.38	20
SB03	134	41.7	0.29	nd	nd	80	0.60	0.70	13
SB04	135	41.8	0.62	0.2	0.040	60	0.49	1.48	12
SB05	136	42.5	0.60	0.2	0.031	120	0.35	1.41	34
SB06	137	40.0	0.39	0.3	nd	120	0.33	0.98	36
SB07	138	40.9	2.88	0.2	nd	100	0.36	7.04	27
SB08	139	41.4	0.72	nd	nd	60	0.84	1.74	7
SB09	140	45.0	0.48	0.2	0.175	120	0.55	1.07	22
SB10	141	43.7	0.49	0.1	nd	100	0.26	1.12	38
BL09	142	43.8	1.23	0.4	nd	100	0.24	2.81	42
BL10	143	37.1	1.45	0.1	nd	120	0.56	3.91	21
BL14	144	-	0.59	0.4	nd	140	0.58	-	24
BL13	145	26.0	1.02	0.2	nd	140	0.43	3.92	33
BL18	146	45.4	1.07	nd	nd	180	0.35	2.36	51
BL20	148	-	0.65	0.2	nd	180	0.96	-	19
BL21	149	-	0.86	0.2	0.003	260	1.41	-	63
BL22	150	-	0.76	0.2	0.028	840	0.67	-	125
BL23	151	-	0.80	nd	0.005	220	1.18	-	19
BL24	152	43.5	0.76	0.1	0.002	120	0.41	1.75	29
BL25	153	34.5	0.18	0.1	0.003	nd	0.74	0.52	14
BL26	154	10.4	0.96	nd	0.001	120	1.09	9.23	11
BL27	155	44.1	0.68	2.0	nd	120	0.71	1.54	17
BL29	157	44.9	0.46	0.1	nd	120	0.88	1.02	14
BL30	158	43.2	0.39	nd	nd	180	0.35	0.90	51
GG37	159	45.3	1.36	0.4	nd	100	0.99	3.01	10
GG38	160	43.9	0.62	0.8	0.003	100	0.69	1.41	14
SI01	161	46.7	0.47	0.1	0.002	160	0.47	1.01	30
SI02	162	-	0.44	0.1	nd	140	0.43	-	33
TF15	163	35.1	0.53	6.4	nd	120	0.61	1.51	20
TF16	164	28.6	0.44	12.4	0.002	120	1.31	1.54	9
TF17	165	33.1	0.60	7.4	nd	100	0.73	1.81	14
TF18	166	42.7	0.45	7.4	0.005	120	0.55	1.05	22
TF19	167	30.9	0.49	10.4	0.029	100	0.93	1.59	11
TF20	168	43.2	0.56	2.2	nd	100	0.66	1.30	15
TF21	169	39.3	0.45	2.2	nd	140	0.99	1.14	14
TF22	170	35.0	0.54	5.4	0.001	180	1.04	1.54	18
GG39	171	42.5	0.25	0.6	nd	160	0.62	0.59	26

* Na values in ppm

1 Ba/Sr . 10^{-2}

2 Na/K . 10^{-6}

Table 4.5: Composition of twenty-one celestites and celestite concentrates

Id'ty	Type	SiO_2	Al_2O_3	Fe_2O_3	MgO	CaO	SrO	SO_3	TOTAL	CaO	Na_2O*	K_2O	SrO	BaO	Zn
		Betaprobe(%)								LMF/AAS(%)					
COOP	con.	0.57	0.06	0.04	0.05	5.25	49.8	39.2	95.1	5.32	430	1.03	39.4	0.67	0.003
WAPL	con.	18.76	0.43	0.17	0.08	2.45	43.5	34.6	100.0	2.80	320	1.85	39.4	0.66	0.003
POWA	con.	1.00	0.13	0.60	0.00	0.43	54.6	42.8	99.6	0.70	490	0.56	45.9	1.07	nd
POWB	con.	0.72	0.07	0.08	0.03	2.41	53.3	41.6	98.1	2.52	430	0.56	-	0.56	nd
TYTH	con.	1.78	0.11	0.21	0.04	0.91	53.7	42.3	99.0	1.12	430	0.75	-	10.05	0.001
9680	con.	3.53	0.38	0.55	0.05	2.38	51.0	40.1	98.0	-	-	-	-	-	-
										SCF/AAS(%)					
CB01	cel.	0.00	0.00	0.00	0.00	0.82	55.2	42.8	98.8	[1]0.00	-	0.04	-	0.56	-
CB03	cel.	2.59	0.72	0.32	0.56	2.65	50.3	39.6	96.7	[2]1.40	-	0.29	-	0.50	-
CB06	cel.	0.00	0.00	0.00	0.00	0.23	56.2	42.9	99.3	[3]0.00	-	0.04	-	0.34	-
WF25	'rab'	5.65	2.26	1.25	0.24	0.25	49.7	39.5	98.8	0.28	380	3.45	-	0.71	nd
D12	cel.	5.93	1.85	0.99	0.23	0.23	50.4	39.6	99.3	0.28	160	2.85	-	0.48	0.010
										MCF/AAS(%) (LMF/AAS%)					
MR01	qrc	16.09	0.82	0.64	0.19	5.13	41.0	32.6	96.5	4.90	-	-	38.6	0.42	-
										(5.04)			(39.1)	(0.49)	(0.003)
MR02	qrc	5.61	0.51	0.46	0.12	1.04	51.5	40.1	99.4	0.95	-	-	48.0	0.56	-
										(1.04)			(48.3)	(0.66)	(0.004)
MR03	qrc	4.81	0.80	0.45	0.21	0.39	52.2	40.3	99.1	0.28	-	-	42.0	0.33	-
MR04	qrc	5.68	0.75	0.41	0.23	5.65	45.8	35.8	93.7	5.18	-	-	41.6	0.78	-
										(5.82)			(43.0)	(0.92)	(0.003)

Table 4.5 (continued)

Id'ty	Type	SiO_2	Al_2O_3	Fe_2O_3	MgO	CaO	SrO	SO_3	TOTAL	CaO	Na_2O*	K_2O	SrO	BaO	Zn
		Betaprobe(%)								MCF/AAS(%) (LMF/AAS%)					
MR05	qrc	1.99	0.33	0.10	0.08	0.37	54.3	40.0	97.8	0.31	-	-	47.9	0.36	-
MR06	qrc	3.43	0.32	0.10	0.11	3.31	49.1	35.9	92.2	3.22	-	-	46.1	0.71	-
										(3.73)			(47.1)	(0.95)	(0.002)
MR07	qrc	12.23	0.17	0.09	0.03	0.79	49.0	38.8	101.1	0.76	-	-	45.4	0.92	-
MR08	qrc	3.91	0.50	0.30	0.11	0.77	52.7	41.6	99.9	0.64	-	-	47.7	0.49	-
MR09	qrc	13.77	0.54	0.48	0.10	0.16	48.1	37.9	101.0	0.17	-	-	46.4	0.74	-
MR10	qrc	79.47	0.11	0.00	0.00	0.10	16.1	12.3	108.1	-	-	-	-	-	-

* Na_2O values in ppm

1 also contains 0.09% SiO_2, 1.00% Al_2O_3, 0.08% Fe_2O_3, 0.00% MgO

2 also contains 1.97% SiO_2, 1.00% Al_2O_3, 0.20% Fe_2O_3, 0.20% MgO

3 also contains 0.17% SiO_2, 1.00% Al_2O_3, 0.08% Fe_2O_3, 0.00% MgO

con. = concentrate, cel. = celestite, qrc = quartz rich celestite

Table 4.6: Composition of nine celestite sands and gravels

Id'ty	A86	RY02	RY03	WF06	WF09	WF10	WF15	WF21	WF23
Type	gravel	sand	sand	solum	sand	gravel	sand	sand	sand
Betaprobe (%)									
SiO_2	6.57	12.03	24.06	22.84	13.35	-	18.40	18.02	13.89
Al_2O_3	2.36	4.15	9.54	6.86	4.48	-	6.03	5.62	4.67
Fe_2O_3	0.86	2.70	5.42	2.15	2.58	-	3.64	2.63	2.16
MgO	0.34	0.57	1.15	0.61	0.33	-	0.78	0.24	0.24
CaO	0.23	0.21	0.30	0.19	0.17	-	0.15	0.18	0.18
SrO	49.37	43.77	30.90	36.02	43.44	-	38.66	40.18	43.88
SO_3	38.80	35.10	24.72	29.32	34.62	-	30.93	32.22	34.79
TOTAL	98.53	98.53	96.10	97.99	98.96	-	98.58	99.09	99.31
LMF/AAS (%)									
CaO	0.14	0.14	0.14	0.04	0.14	0.07	-	-	-
Na_2O*	220	590	540	320	490	110	-	-	-
K_2O	3.90	6.89	-	9.09	5.38	1.51	-	-	-
SrO	-	-	31.03	35.52	-	-	-	-	-
BaO	0.39	0.30	0.16	0.50	0.23	0.67	-	-	-
Zn	0.007	0.001	0.024	0.052	0.001	0.002	-	-	-

* Na_2O values in ppm

Table 4.7: Lithium metaborate fusion analyses in %*, of seven gypsum specimens

Id'ty	No.	Type	Ca	Sr	Ba	Zn	Na	K
TC01	108	alabastrine	21.4	0.32	0.04	70	100	0.08
ME02	109	alabastrine	21.8	0.32	0.01	20	120	0.30
MI02	116	white crystalline	22.0	0.48	0.04	20	80	0.02
MI04	117	gran. macrocell.	21.6	0.40	0.04	nd	160	0.83
MI05	118	alabastrine	21.6	0.37	0.05	nd	80	0.25
BL19	119	alabastrine	21.2	0.18	nd	2110	80	0.43
BL19	147	(replicate)	23.8	0.67	0.04	510	120	0.23
BL28	156	alabastrine	19.8	0.32	0.04	8850	160	0.56

* Zn, Na values in ppm

Table 4.8: Calcite and dolomite content of the evaporite mineral fraction of selected celestites as determined by X-ray Diffraction analysis

Identity	No.	Calcite %	Dolomite %
YB01	1	80	1.6
YB02	2	18	nd
YB03	3	52	nd
YB04	4	28	nd
YB05	5	19	nd
YB06	6	~100	~0.5
YB07	7	58	1.2
YB08	8	25	nd
YB09	9	12	nd
YB10	10	15	nd
YB11	11	9	0.4
YB12	12	43	0.9
YB14	14	14	nd
YB16	16	12	0.6
YB18	18	nd	nd
YB20	20	nd	nd
YB31	31	57	nd
YB32	32	2	nd
YB33	33	4	nd
YB37	37	57	2.4
YB38	38	86	4.3
YB39	39	82	5.7
YB41D	41D	~100	~1.0
YB43	43	17	nd
YB44	44	57	0.6
YB45	45	25	nd
YB45D	45D	12	nd
YB46	46	65	nd
YB47	47	52	2.1
YB48	48	nd	nd
YB57	57	53	nd
YB58	58	37	1.5
YB59	59	3	nd
Nos 63,64,65,71,74) 82,84,85a,87,88)		nd	nd
CF06	89	nd	nd
CF07	90	0.5	nd
CF08	91	7	nd
CF09	92	nd	nd
RI03	95	29	nd
RI03	95D	33	nd
NC01	96	8	nd
NC04	99	nd	nd
YB89	101	12	nd
YB90	102	36	nd
YB99	103	27	nd
YB92	104	13	nd
YB93	105	42	nd
YB94	106	nd	nd
YB95	107	33	nd
YC02,YC05	110,111	nd	nd
LP03	112	nd	nd

Table 4.8 (continued)

Identity	No.	Calcite %	Dolomite %
RY05,15,13,16	120-124	nd	nd
BL01,04,05	125-127	nd	nd
WF23,24	128,129	nd	nd
SB01-SB10	132-141	nd	nd (0.8 in SB04)
BL09	142	nd	3.2-5.0
BL10	143	nd	nd
BL14	144	2	nd
BL18,20,23	146,148,151)		
24,25,26	152,153,154)	nd	nd
27,29,30	155,157,158)		
GG37	159	6	0.5
GG38	160	5	nd
SI01	161	nd	nd
GG39	171	nd	nd
PF13	-	16	3.5
PF21	-	8	nd
PF31	-	6	0.8
PF32	-	47	0.9
PF51	-	7	nd
PF71	-	52	nd
PF72	-	nd	nd
PF81	-	6	nd
PF82	-	2	0.3
PF84	-	16	nd
PF99	-	1	nd
WE01	-	nd	nd
WE02	-	1	nd
WE04a	-	23	nd
WE04b	-	1	nd

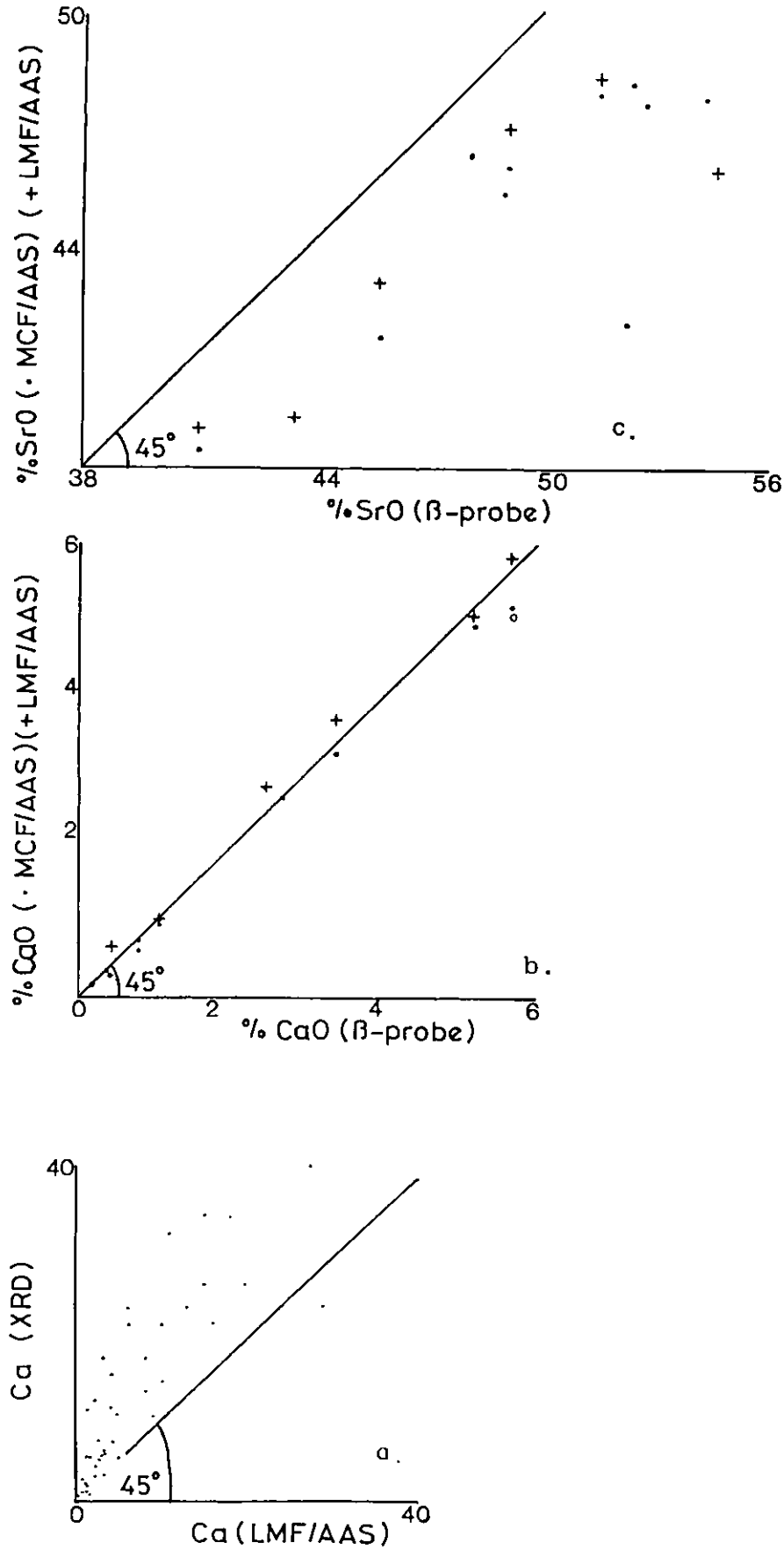

Fig 4.3: Comparison of wet chemical and spectrometric methods: a) Ca data (Tables 4.4,4.9); b) CaO data (Table 4.8); c) SrO data (Table 4.8)

This implies that there is an overestimate in the calcite content by a factor of five. This is probably produced by enhanced reflection from the {104} plane.

4.2.4. Conclusions on the applicability of the techniques

From Appendix II, it may be concluded that of the wet chemical methods, only the LMF/AAS technique provides both a precise and accurate determination of Sr. Furthermore, as the samples analysed formed part of a batch analysis, a further refinement of the method could decrease the precision even further. The Betaprobe technique is quicker and easier to use, although precision is poorer than the MCF and LMF methods. It may possibly overestimate Sr, although this cannot be fully determined.

For the minor elements; Ba can only be determined by wet chemical methods for which the LMF technique gives the best precision, whereas Ca may be accurately determined by either a Betaprobe or a fusion technique, with a lower precision. A calibrated quantitative XRD method also provides a rapid, non-destructive method for the determination of calcite and dolomite, but unfortunately, overestimates the mineral contents by a factor of two.

Regarding the other minor elements (Fe,Al,Si,Mg,K) the simultaneous determination of all except potassium by the Betaprobe is an overriding factor in its application. However, as these elements are mostly derived from the clastic fraction of the celestites, an estimate of the percentage sum of their oxides could be easily made by subtraction of the quantities, strontia, barium oxide and lime, and equivalent SO_3 and CO_2 from 100 per cent.

The hybrid technique employed by the Bristol analysts, Waterfall and O'Brien Ltd. uses a EDTA titre following a sodium carbonate fusion to provide a total alkali earth content whence Sr is found by difference. It may be possible that this method too is of poor precision.

To conclude, the method selected is dependant upon the end purpose and the analytes required. If Ba is not required, then the Betaprobe provides a fast and relatively precise technique. However, since the Ba content is needed for most commercial purposes, the LMF/AAS method is recommended.

4.3 STATISTICAL INTERPRETATION OF THE ANALYTICAL DATA

4.3.1. Introduction

The assays of the Main Analytical Series (Table 4.4), the calcite and dolomite determinations (Table 4.8) and the presence/absence data compiled from a listing of the physical properties of 174 celestites (Appendix III) were analysed using the CDC Cyber 174 Computer at Imperial College Computer Centre using a range of standard statistical techniques.

First, the frequency distribution of each elemental assay/mineral content population were determined using program BGIRAF (S.A.M. Earle). Next, the TAXON2 program (R.J. Howarth) was used to apply cluster analysis to all three sets of data. By first computing a similarity matrix and then methodically pairing off values with an equal measure of resemblance, this program constructs a dendrogram from which a hierarchy of relationships can be established.

TAXON2 supplied options to perform the following operations, among others:

1) Analysis in the R- or Q- mode (i.e. the relationship between the properties of the samples, or between the samples themselves).

2) Construction of similarity matrix using the Pearson correlation coefficient r or the Euclidian space distance coefficient d (Davis, 1973) for the assays and the Jaccard-Sneath coefficient of association J (Sneath, 1957) for the presence/absence data. This is defined as:

$$J_{ij} = A_1 / (A_1 + A_2)$$

where A_1 is the sum of the mutual "like" matches of the variables i and j.

A_2 is the sum of the mutual "unlike" matches of the variable i and j.

(The Sokal-Michener coefficient (Sokal and Michener, 1958) which includes mutual absences, was not used as it linked at high levels, properties known to be mutually exclusive).

3) Graphical dendrogram output, by the weighted pair-group method.

This procedure was applied to the chemical data using the following permutation of variables and samples: 159 samples and the 6 variables Sr, Ba, Ca, Zn, Na and K; 159 samples and the 4 variables Ba/Sr,Na/K, Ca and Zn and 95 samples and the 7 variables Sr, Ba, Zn, Na, K, CC and DOL. TAXON2 initially, was also applied to all 174 samples and 75 variables in the binary data matrix.

The presence/absence observations had previously been coded by the symbols 0 and 1 so that subsequent data listings were readily given to interpretation by eye. Because of this, program RSORT (Howarth R.J. and Brown C.J.) was written to simultaneously present results of the R- and Q-mode analyses of the presence/absence data. The listing of the restructured binary data, produced by positioning each sample and variable number according to their positions in the R- and Q- mode hierarchies, was found to facilitate the interpretation. In addition, by plotting the Q- mode hierarchy of the assays/mineral content against the R- mode listing obtained from the binary data RSORT was also used to determine the interrelationship of both types of data.
In short, it was hoped that the most successful application of cluster analysis coupled with a manipulation of the hierarchical listings would fulfil the following objectives:

1) R- mode Analysis.
To determine the relationship, if any, between each assay/mineral content estimate, and thereby establish more fully the nature of the (main) mineralisation.

2) Q- mode Analysis.
To empirically classify the celestites according to their compositions, and to compare these results with those from earlier attempts (e.g. Nickless et. al., 1975).

3) Simultaneous RQ Analysis.
To quantify the relationship, if any such existed, between certain properties of celestites, and to assess their significance.

4) Simultaneous RQ Analysis.
To determine the relationship between the assay/mineral content and the physical properties of the celestites;

and to comment upon the effect of compositional changes on the morphology and petrology of these rocks.

An alternative cluster analysis method known as non-linear mapping (NLM), originally developed at the Rome Air Development Center, New York, and modified for use at ICCC by Dr R.J. Howarth, was applied to the 7- variable, 95 sample assay data set in order to evaluate this method of classification. Details of the technique are given by Sammon (1969) and Howarth (1973). The scatter plot produced is readily interpreted by eye and can be compared with the clustering in the dendrograms. The major advantage of this method of classification over the hierarchical dendrogram analysis, is that original relationships are preserved more clearly (once an object is linked to a dendrogram cluster, its influence over the rest of the data set is severely diminished).

4.3.2. Results

4.3.2.1. Population types and significance test.

Table 4.9 includes the main features of the histograms of the LMF assays and the calcite and dolomite determinations shown in Fig. 4.4. Visual inspection was used to classify the histograms into normal or lognormal distributions. The frequency distributions of Ba/Sr, Zn, K and Na/K, and to a lesser extent those of Ca, CC (calcite) and DOL (dolomite), are strongly skewed and are approximately lognormal. In the last three examples the class on the extreme left of the histogram is an artifact produced by the coding of 'not-detected' - type data. The Ba data can either be described as normal or lognormal. Although the Sr histrogram shows a slight negative skew, it is not sufficient to classify the Sr data as lognormal. It is possible that the Sr distribution represents a (random) selection of high - Sr assays drawn from a larger population of celestites, with the spread of values representing the analytical errors in estimating the population mean. The high Sr assays would then have little geographical significance. The Na data, are normally distributed.

Table 4.9: Frequency Distributions of Assays and Mineral Contents

Population	Total celestite $n_T=159$			Type C celestites $n_C=26$			Type A celestites $n_A=117$			H: $\bar{X}_A=\bar{X}_C$	
Parameters	Form	$\bar{X}_T$	s_T	Form	$\bar{X}_C$	s_C	Form	$\bar{X}_A$	s_A	$\bar{X}_A-\bar{X}_C$	CI
Sr	N	38.8	9.3	N	38.6	11.1	~N	38.2	9.6	0.4	4.0
Ba	L	0.55	1.68	L	0.58	1.68	L	0.52	1.65	0.06	0.71
	(N	0.62	0.34)	(N	0.64	0.26)	(N	0.58	0.27)	0.06	0.14
Ca	~L	0.5	7.3	~L	0.2	6.8	L	0.7	6.8	0.5	3.1
Zn	L	0.009	2.944	L	0.010	3.133	L	0.009	2.972	0.001	1.251
Na	N	100	80	N	140	150	N	90	50	50	30
				(L	110	20)	(L	70	30)		
K	L	0.52	1.89	~L	0.63	1.91	L	0.74	1.93	0.11	0.80
Ba/Sr	L	1.48	1.86	L	1.51	1.96	L	1.45	1.84	0.06	0.79
Na/K	L	150	30	L	180	20	L	140	30	40	12.7.
CC	~L	0.3	46.9	~L	0.0	5.9	L	1.3	48.0	1.3	20.0
DOL	~L	0.02	6.6	-	0.0	-	L	0.03	8.3	0.0	2.8

Explanation of symbols: n= number of samples
N= normal population
~N= approximately normal population
L= lognormal population
( )= an equally accurate description of the distribution

$\bar{X}$= population mean
s= population standard deviation
CI= $z_{.025} \cdot s_T \cdot (\frac{1}{n_A} + \frac{1}{n_C})^{\frac{1}{2}}$, the 95% confidence interval for the hypothesis $H:\bar{X}_A=\bar{X}_C$

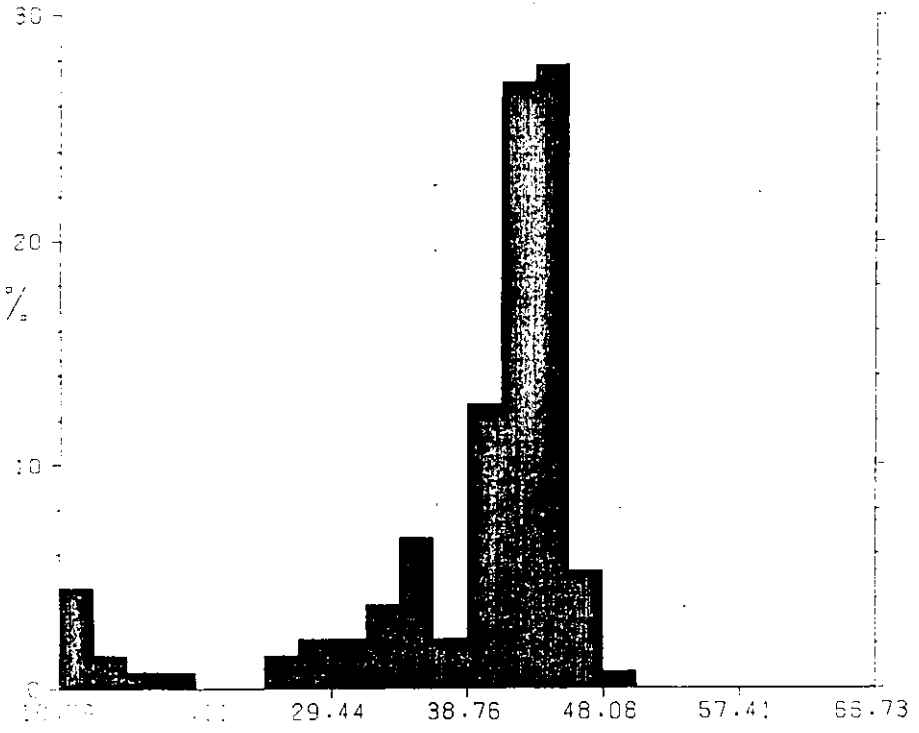

NO. OF OBSERVATIONS = 133
MEAN = 38.76 STD DEV = 9.323

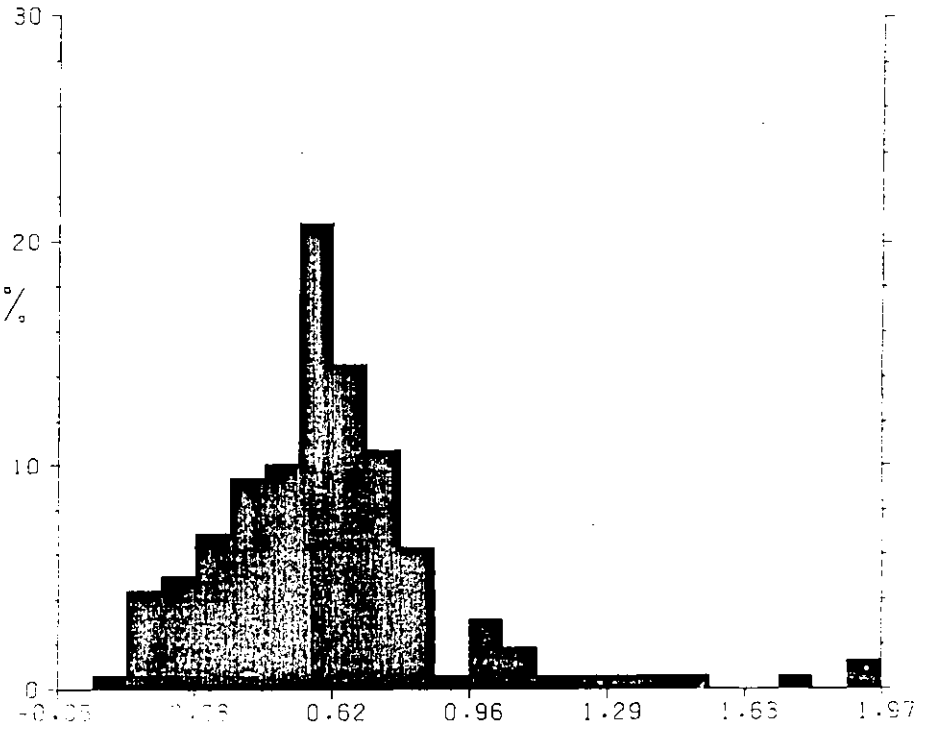

NO. OF OBSERVATIONS = 158
MEAN = 0.62 STD DEV = 0.337

Fig 4.4: Histograms of assay and mineral content data

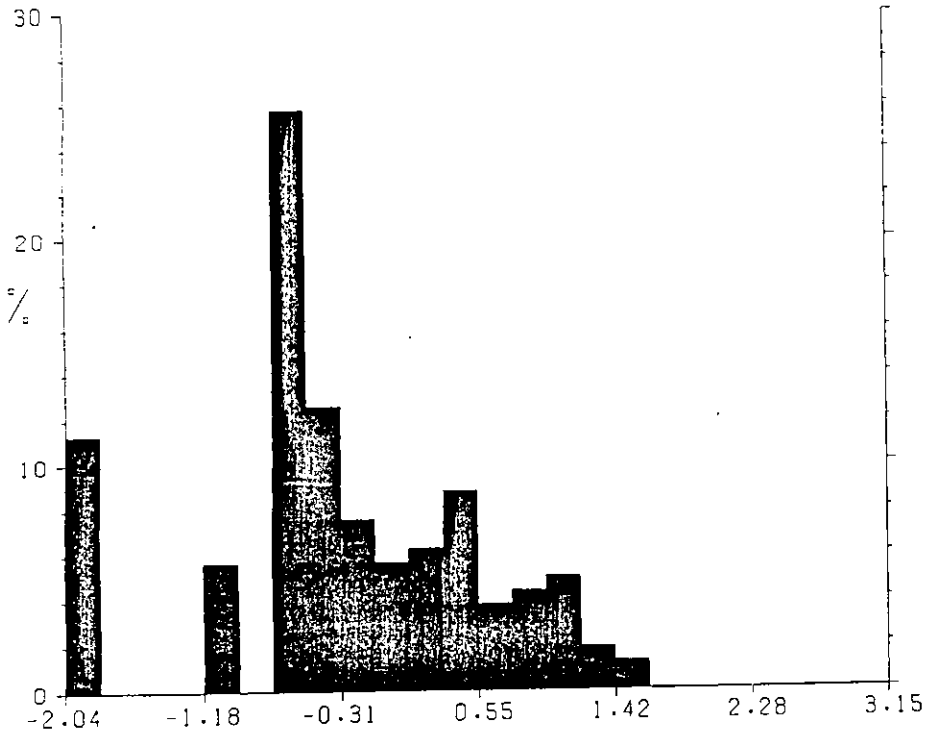

CD
NO. OF OBSERVATIONS = 159
MEAN = -0.31 STD DEV = 0.866
NO. OF LOG10 TRANSFORMS = 1

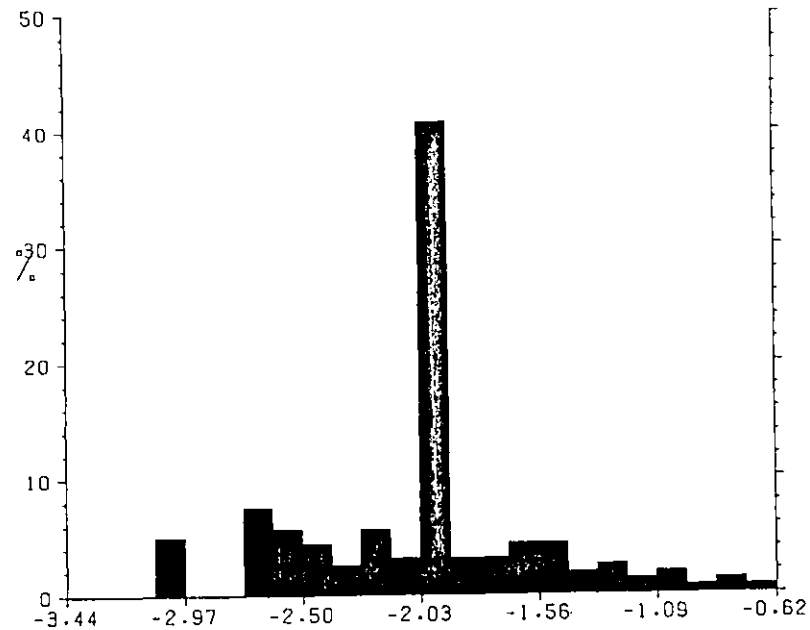

ZN
NO. OF OBSERVATIONS = 159
MEAN = -2.03 STD DEV = 0.469
NO. OF LOG10 TRANSFORMS = 1

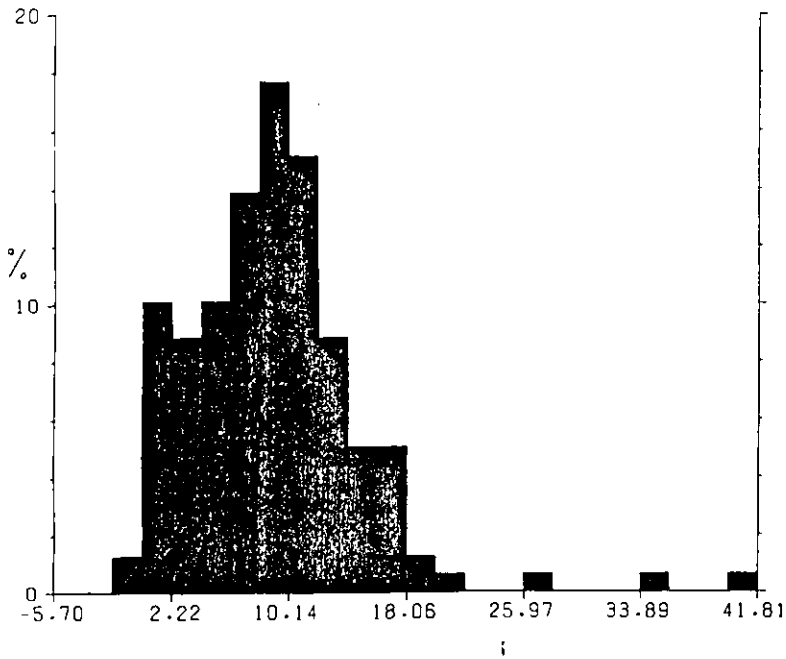

NA
NO. OF OBSERVATIONS = 158
MEAN = 10.14 STD DEV = 7.917

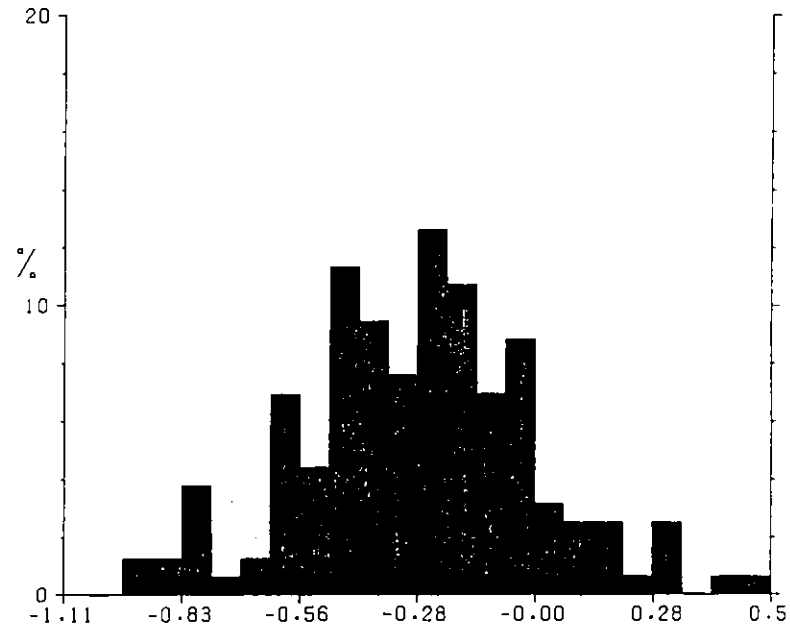

K
NO. OF OBSERVATIONS = 158
MEAN = -0.28 STD DEV = 0.277
NO. OF LOG10 TRANSFORMS = 1

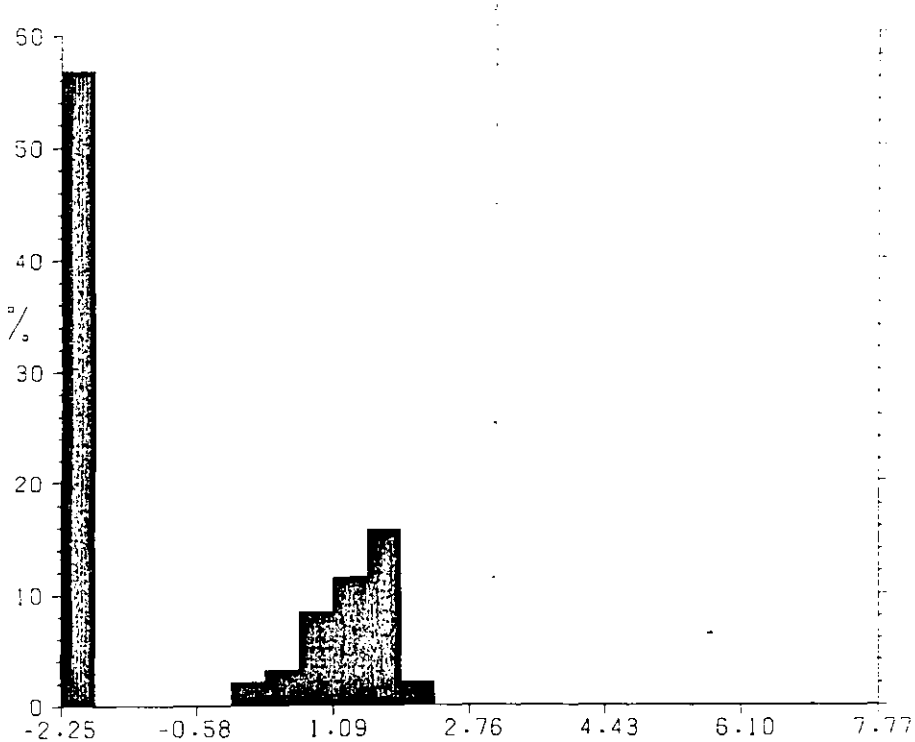

CALCITE
NO. OF OBSERVATIONS = 95
MEAN = -0.58 STD DEV = 1.671
NO. OF LOG10 TRANSFORMS = 1

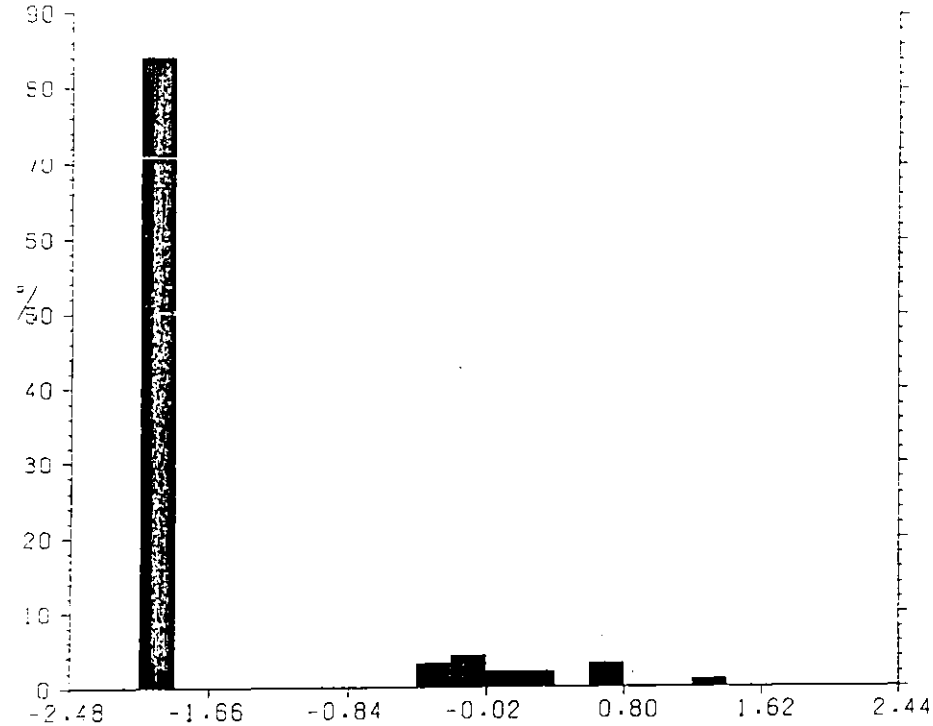

DOLOMITE
NO. OF OBSERVATIONS = 95
MEAN = -1.66 STD DEV = 0.819
NO. OF LOG10 TRANSFORMS = 1

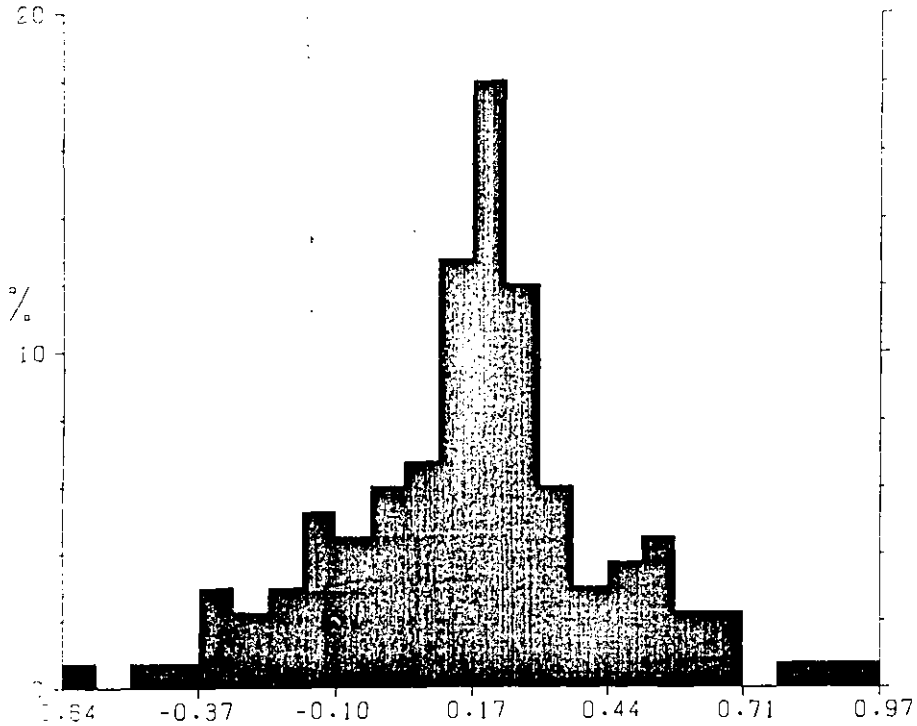

FA/SR
NO. OF OBSERVATIONS = 133
MEAN = 0.17 STD DEV = 0.269
NO. OF LOG10 TRANSFORMS = 1

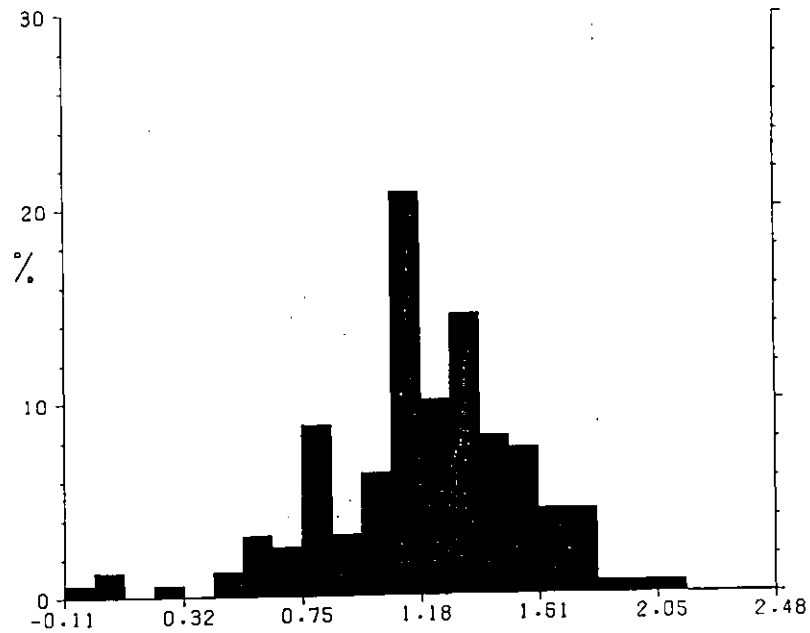

NA/K
NO. OF OBSERVATIONS = 158
MEAN = 1.18 STD DEV = 0.431
NO. OF LOG10 TRANSFORMS = 1

Program BGIRAF was also applied to two sample splits corresponding to 'sub-populations' of Type A and Type C celestite. Because the variance of the combined population was known, the means of the two 'sub-populations' were compared using the z statistic (Table 4.9). Na and Na/K are the only two variables for which the means are significantly different at the 95% confidence level, the Type C Na content being greater.

4.3.2.2. R- mode Analysis

a. Similarity matrices (assays data)

Table 4.10 shows that, excluding the cases where correlations arise where one variable forms part of another, the r similarity matrices contain 16 different significant correlations at the 99.9% level. The relationship between the variables is also demonstrated by the value of the distance coefficients listed in Table 4.11. Unlike the Pearson coefficient, d is not bounded and cannot be interpreted by standard statistical analysis. It can be used, however, as a check on the value of r, especially where errors due to the summation of constant - sum data are introduced into the computations in the comparison of two or more major components. In this case, for example, the Sr and Ca assays are not independent because they must always total to a constant cation percentage, and a change in the content of one, automatically affects the value of the other, giving an induced negative correlation.

Such a comparison can be made by plotting values of r against values of d (Fig. 4.5a). As there is no simple relationship between the two similarity measures, each point has to be empirically allocated to one of four fields:

a) F1 $r < /r_{99.9}/$ (the range of insignificant r values, 27 points.)

b) F2 $r < -r_{99.9}$ $d < .300$* (Sr with Ca,CC,DOL, K and Zn).

c) F3 $r < -r_{99.9}$ $d > .700$* (CC with Na/K).

d) F4 $r > +r_{99.9}$ $d > .700$* (CC with Ca, Zn, K, Ba/Sr, DOL; Ca with K, Ba/Sr and DOL; DOL with K, Zn).

A graphical explanation of the significance of each sector may be found in Fig. 4.5b. High correlations only occur in F2, F3 and F4.

Table 4.10: Pearson Coefficient Correlation Matrices

a. 10 variables, 159 samples

	Sr	Ba	Ca	Zn	Na	K	Ba/Sr	Na/K	CC	DOL
Sr	1.000									
Ba	0.070	1.000								
Ca	-0.796	-0.154	1.000							
Zn	-0.216	-0.094	0.198	1.000						
Na	-0.107	0.018	0.039	0.056	1.000					
K	-0.388	-0.027	0.390	0.118	0.160	1.000				
Ba/Sr	-0.608	0.646	0.372	0.069	0.038	0.217	1.000			
Na/K	0.237	0.031	-0.214	-0.084	0.656	-0.345	-0.148	1.000		
CC	-0.726	-0.192	0.887	0.372	0.075	0.384	0.330	-0.292	1.000	
DOL	-0.334	-0.069	0.346	0.341	0.129	0.312	0.157	-0.147	0.357	1.000

b. 7 variables, 95 samples

	Sr	Ba	Zn	Na	K	CC	DOL
Sr	1.000						
Ba	0.174	1.000					
Zn	-0.341	-0.171	1.000				
Na	-0.104	-0.047	0.059	1.000			
K	-0.354	-0.055	0.173	0.275	1.000		
CC	-0.726	-0.192	0.372	0.075	0.384	1.000	
DOL	-0.334	-0.069	0.341	0.129	0.312	0.357	1.000

Values underlined are significant at the 99.9% level ($r_{.001,159}=.267$; $r_{.001,95}=.338$)

Table 4.11: Distance Coefficient Correlation Matrices

a. 10 variables, 159 samples

	Sr	Ba	Ca	Zn	Na	K	Ba/Sr	Na/K	CC	DOL
Sr	1.000									
Ba	0.368	1.000								
Ca	0.231	0.757	1.000							
Zn	0.237	0.773	0.813	1.000						
Na	0.305	0.834	0.810	0.834	1.000					
K	0.287	0.817	0.839	0.831	0.866	1.000				
Ba/Sr	0.322	0.884	0.804	0.780	0.838	0.829	1.000			
Na/K	0.350	0.818	0.748	0.774	0.884	0.786	0.802	1.000		
CC	0.260	0.695	0.889	0.768	0.764	0.782	0.755	0.723	1.000	
DOL	0.224	0.734	0.792	0.867	0.850	0.825	0.745	0.797	0.753	1.000

b. 7 variables, 95 samples

	Sr	Ba	Zn	Na	K	CC	DOL
Sr	1.000						
Ba	0.378	1.000					
Zn	0.231	0.730	1.000				
Na	0.532	0.647	0.550	1.000			
K	0.278	0.787	0.803	0.612	1.000		
CC	0.225	0.695	0.763	0.563	0.781	1.000	
DOL	0.188	0.734	0.821	0.514	0.825	0.752	1.000

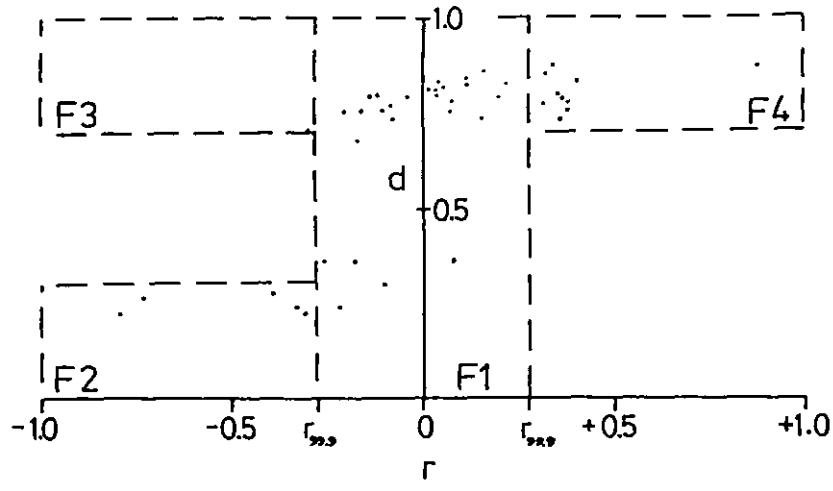

a.

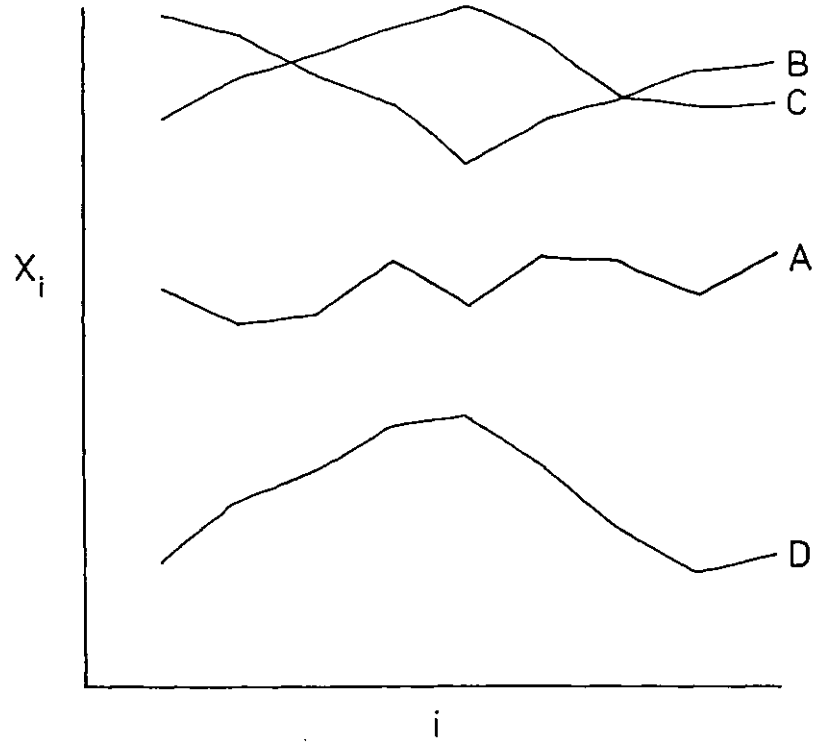

b.

Fig 4.5: Interpretation of the distance coefficent, d

(Fig 4.5b after Davis, 1973)

Variable A is not correlated to B,C,D and is separated by a large distance (Field F1)
Variable B is negatively correlated to C; both are close together (F2)
Variables B and D are negatively correlated and far apart (F3)

Variables C and D are positively correlated and far apart (F4)

Large negative values of r coupled with small d spacings characterise the data in F2 implying that each variable is present, on average, in constant concentrations but in proportionally differing amounts. As already suggested above, each negative correlation in this field therefore is artificially induced by constant sum data. The remaining 11 points in F3 and F4 represent correlations that are both significant and high.

b. Dendograms (assay data)

Two important deductions may be drawn from the additional information contained in the r variable-dendograms in Fig. 4.6 and 4.7.

1. Ca (or CC), DOL, Zn and K are always clustered together and are well separated from Sr.
2. Ba (or Ba/Sr) and Na (or Na/K) may be grouped to either the multielement or the Sr branch at low levels in the hierarchy.

The dichotomous nature of the clustering is emphasised even more strongly in Fig. 4.6 where the incorporation of Ba, Ba/Sr, Na and Na/K in the multielement branch adds to the antipathy. Note that the lack of any <u>positive</u> correlation of Sr with one other element is as important a factor in the mechanics of clustering as the strong induced negative correlations.

c. Similarity matrices and dendograms (presence and absence data)

The similarity matrix of the binary data is not included because of its size (covering 75 variables) and the absence of a satisfactory theoretical background to the Jaccard-Sneath coefficient.

Prior to analysis by program RSORT the dendogram contained 24 clusters (Table 4.12). At a later stage in the analysis nineteen variables were eliminated or amalgamated for reasons given in 4.3.2.4. The revised structure produced by reanalysis by TAXON2 now contained 12 major clusters (Fig. 4.8).

Fig. 4.8 indicates that the plethora of celestite varieties may be successfully and objectively classified by this technique. Type C celestites can be separated from Type A celestites by the grouping of the properties

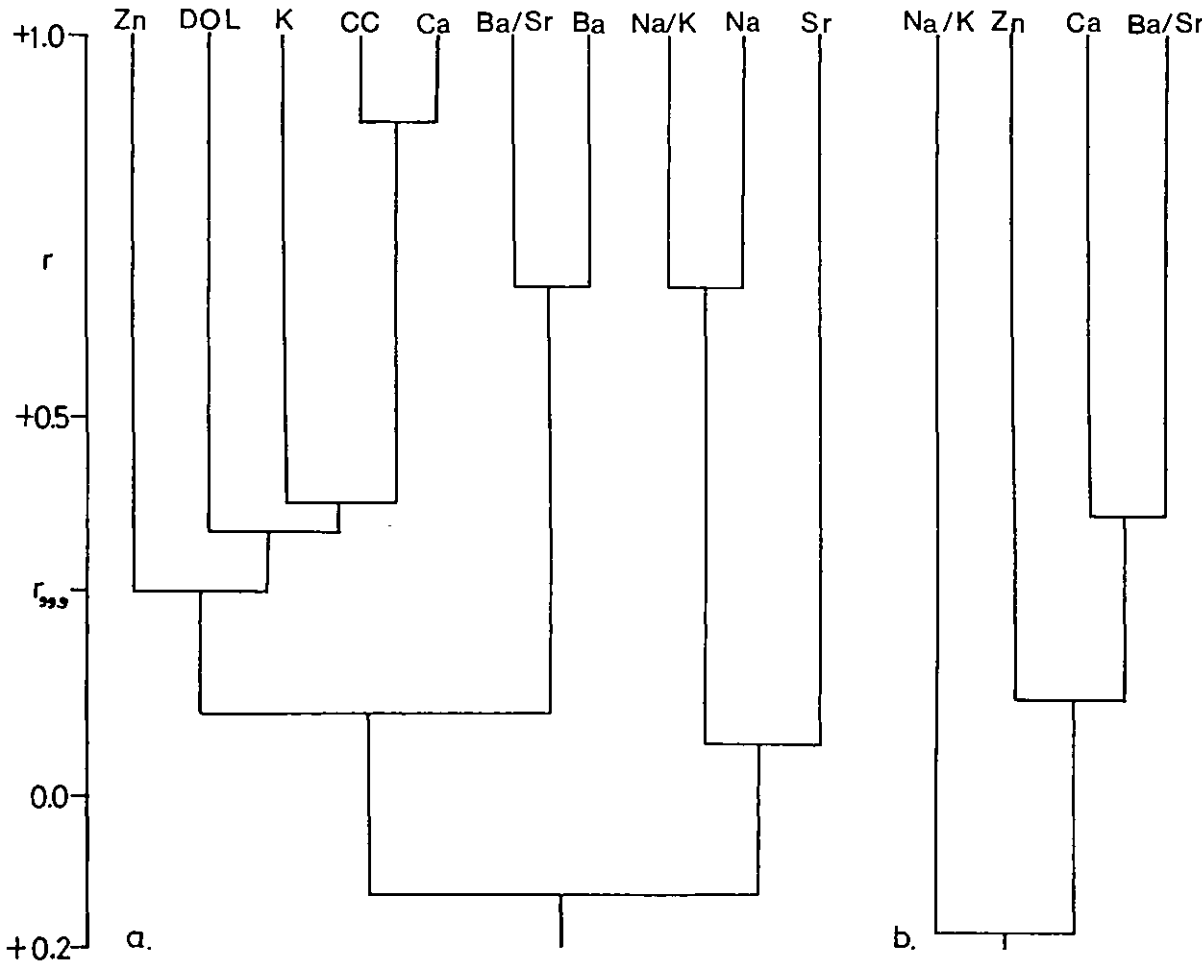

Fig 4.6: Dendrograms of variables (Pearson coefficent)
a: 10 variables; b: 4 variables; c: 6 variables; d: 7 variables

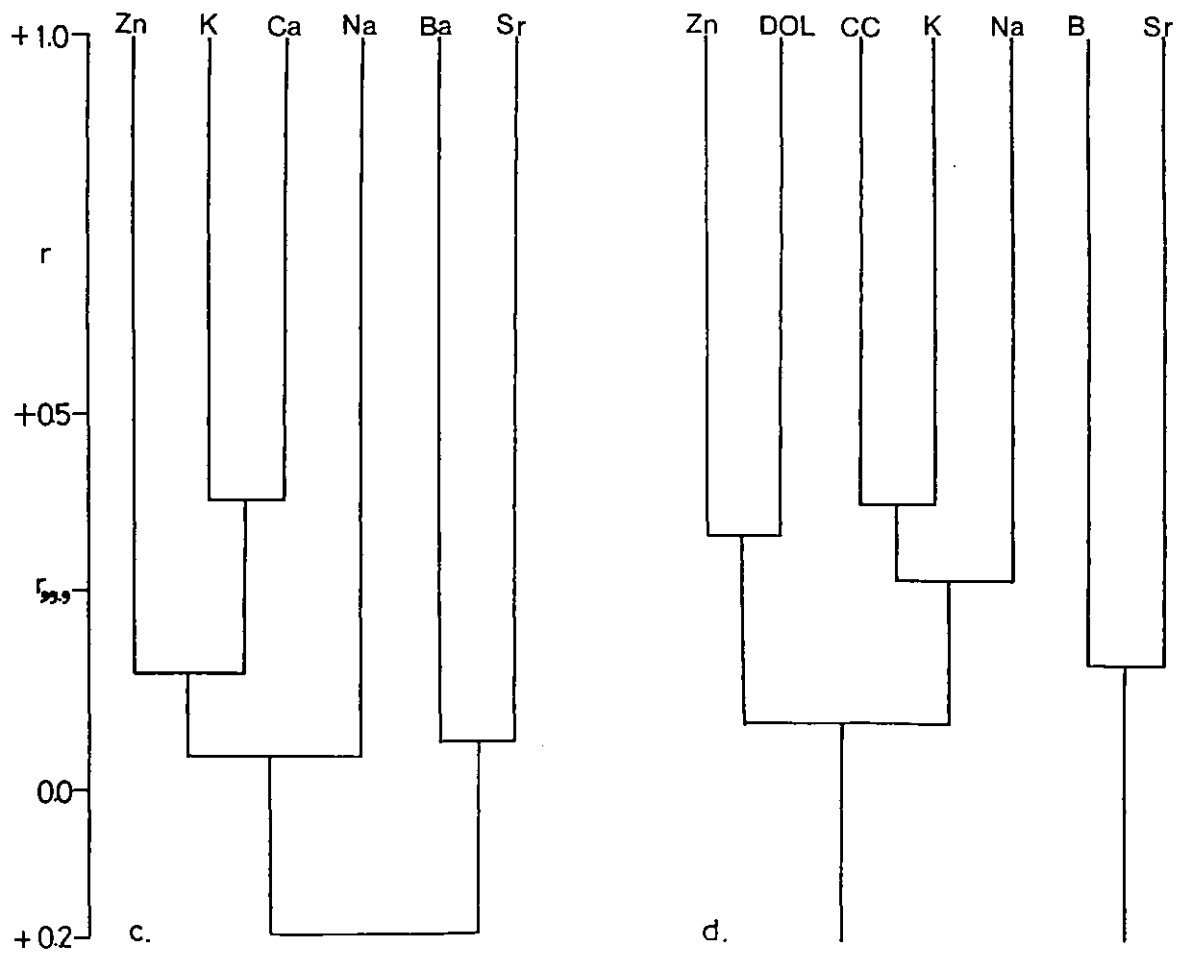

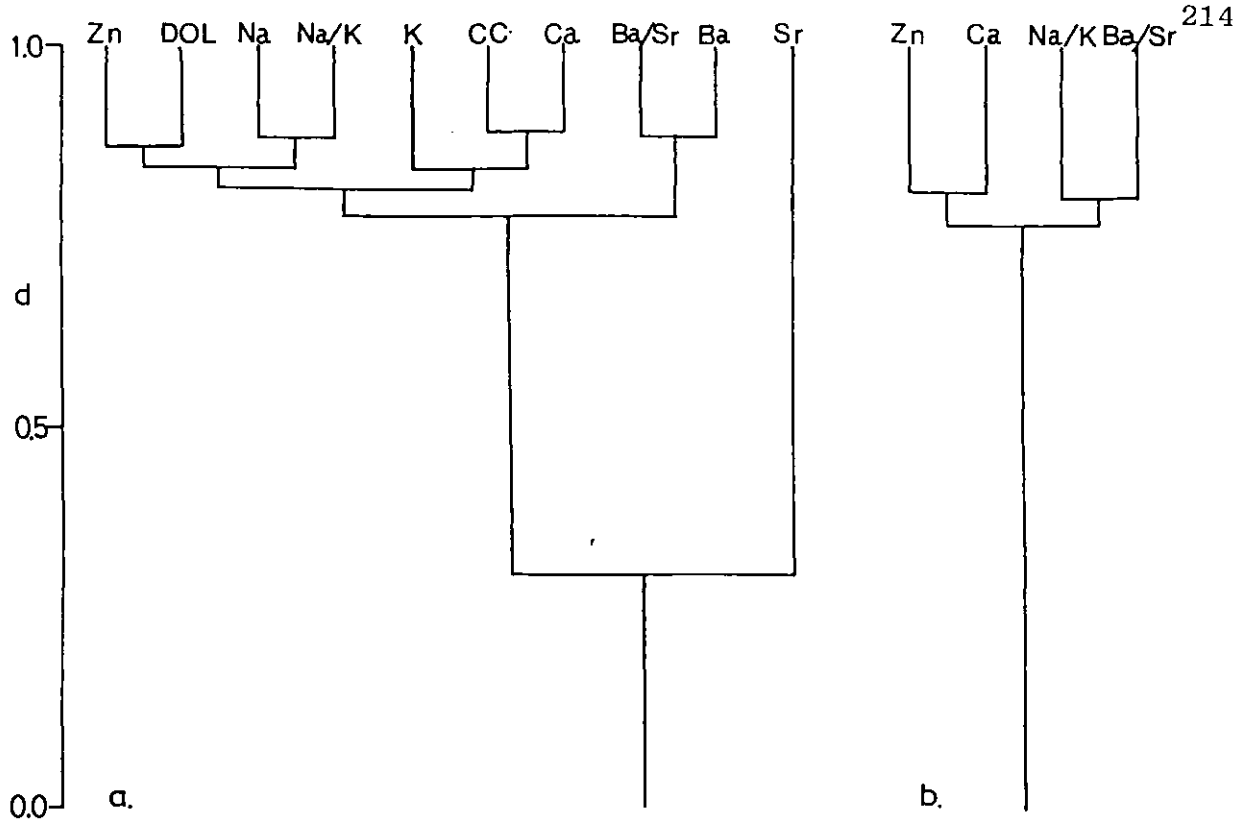

Fig 4.7: Dendrograms of variables (distance coefficent)
a: 10 variables; b: 4 variables; c: 6 variables; d: 7 variables

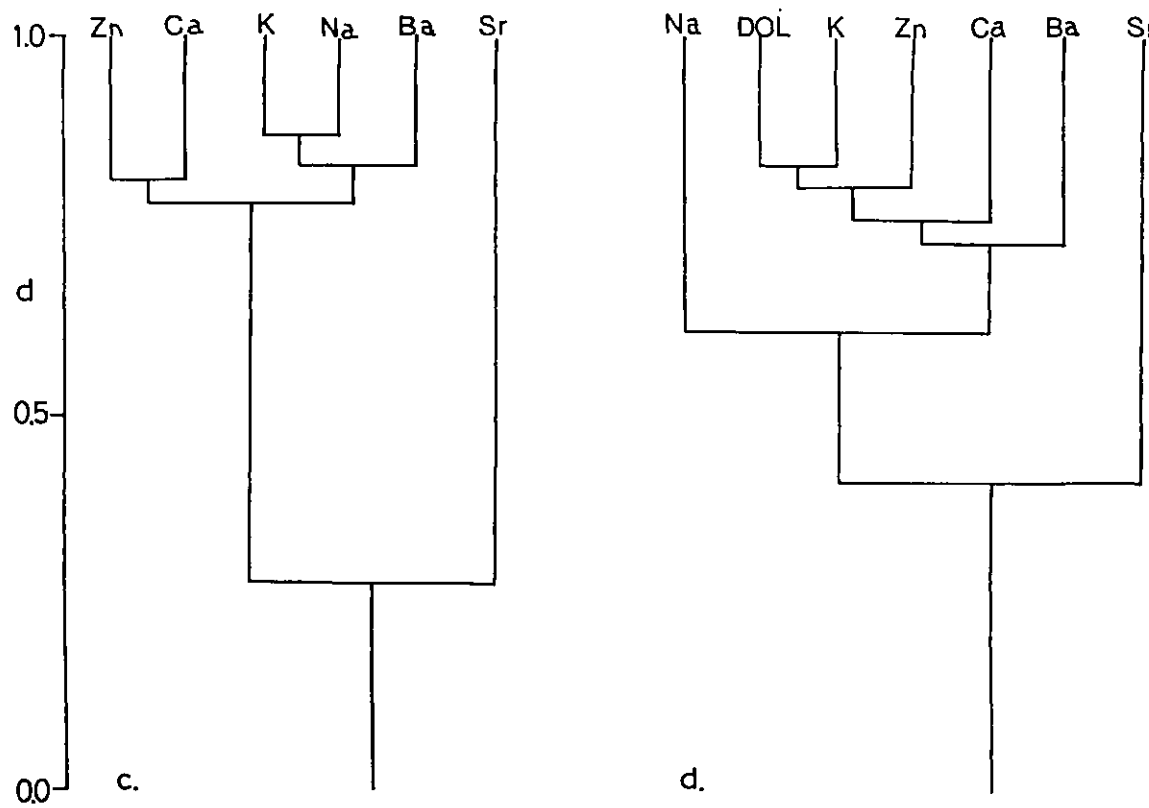

Table 4.12: The principal R-mode clusters of the presence/absence data

1	ANGULR,+1UNIT
2	RED
3	BREAK
4	FWHITE,FGRAN,MLATH,MGRAN,MWHITE
5	MBLUE
6	ROUND,MASSIV,SMOOTH,MACMAS
7	FPINK,MPINK,MRED
8	MORANG
9	CCRIM
10	BG,SILTY,CALC,INDURD,CFINE,MACIMP,COMMAC,MUDMAC, SPECK,FRED
11	LMST
12	STRAT,XLII
13	VUGMAC,CELMAC,BICVUG,FINOUT,NETVUG,NOCHGE,MUDINV, FORANG,RNDVUG
14	REDNAM,GLEYED,CLUIMP,FPURPL,MPURPL
15	FLATH,FBLUE
16	CGREY,CPURPL
17	FGREY,MGREY
18	CPINK,CRED,CORANG,CLATH,VWHITE,CGRAN,CBLUE
19	XLRTLE
20	MOULDS
21	OCHRE,BLASTS
22	AG,SCAIMP,MOTTLE,CINCEL,C+CEL,CINMUD
23	SANDY,MESH,X-CUT,MUDVUG
24	CCUBIC

Fig 4.8: Dendrogram of variables of the presence/absence data (Jaccard-Sneath coefficent)

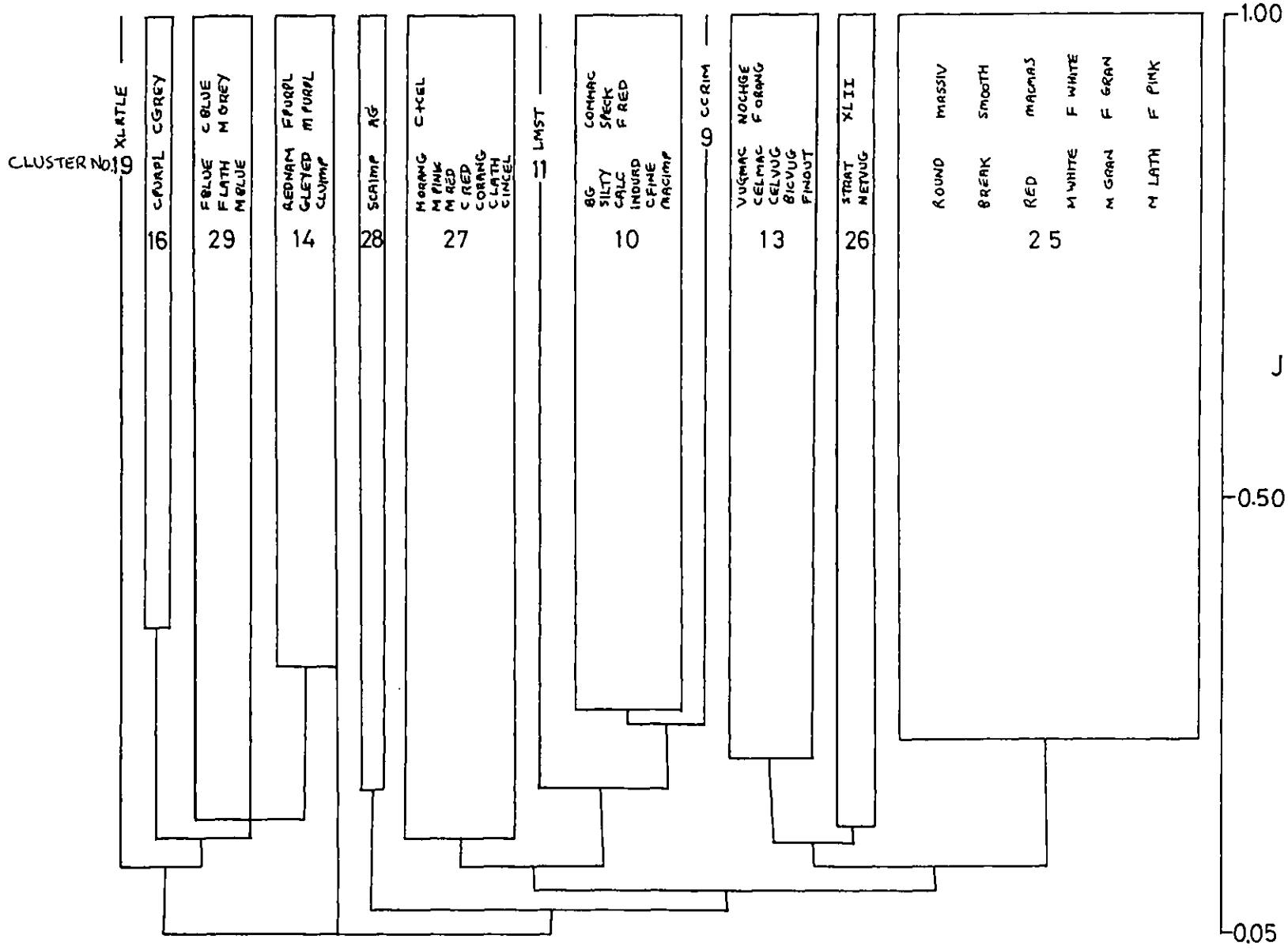

in clusters 14,16,19 and 29. For example, the two commonest forms of Type C celestite, containing a central zone of blue tabular crystals or a massive impregnating fabric are differentiated by clusters 14 and 29. Coarse purple and grey celestite (group 16) and comb-structured vein celestite (group 19) are also clustered with these two types.

The varieties of Type A celestite characterised by the variables in each of the other groupings are:

cluster 28: impregnations of fine tabular celestite

cluster 27: impregnations of medium and coarse grained celestite

clusters 9,10 and 11: light red macrocellular celestite host rocks

cluster 13: drusey macrocellular celestite

cluster 26: schistose fabric in massive celestite

cluster 25: mostly massive celestite

Most of the principal Type A celestite varieties are therefore recognised. The absence of white celestite variables (e.g. MWHITE) in cluster 27 in particular is probably due to the deficiency of cluster analysis referred to in 4.3.1.

4.3.2.3 Q-mode Analysis

a. Dendograms (assay data and mineral content data)

Fig. 4.9 shows dendograms for two of the permutations of sample no./variables submitted for cluster analysis. It should be noted that as the R-mode analysis highlighted the lack of positive Sr correlations, each classification scheme is based upon the presence of accessory minerals in the celestite. In consequence it is important to assume that the accessory mineral content mirrors the abundance in the sampled environment.

A feature of each dendogram is the marked separation of 2 broad celestite groups, one of which is characterised by calcitic celestites and the other by specimens of more usual composition, including a large number of "normal celestites". There is little, if any, significant discrimination between samples of Type A,B and C celestite in the

Fig. 4.9: Q-mode analysis dendograms for the celestites of the main analytical series

a. 6 variables, 159 samples

b. 7 variables, 95 samples

At least seventeen prominent clustering patterns can be recognized in the dendograms. Note that, because of differences between the dendograms, subdivisions will not always contain a full complement of samples.

Calcitic celestites (> 10% Ca; > 57% calcite)

Classes

1. High Zn and K content (> 0.048% Zn, > 1.38% K)

In Fig. 4.9 one sample is classified separately due to a high dolomite content.

2. High K content (> 0.93% K)
3. High Zn content (0.141%Zn), deficiency in Sr
4. Deficiency in Sr
5. Others

Certain other high Zn celestites may join these clusters at a lower level of d (Fig. 4.9a) but do not contain sufficiently high calcium to be classified with them.

Ordinary celestites

Classes

6. Intermediate Ca content (approx. 4.10% Ca)
7. High Na content (8.40 ppm Na) Not present in 4.9b
8. Deficiency in Sr(10.4%)/high Zn content(.088%)
9. High K content, intermediate Ba content (> 0.80%Ba) (> 1.09% K)
10. Very high K content (4.90% K)
11. High K / intermediate Ca content (1.99% K, 3.8% Ca)
12. Very high Ba content (2.88% Ba)
13. High Ba content (> 1.47% Ba)
14. ?Low Na /high Ba content (100-140 ppm Na, > 1.02% Ba)
15. Deficiency in Sr
16. High Zn content (> 0.130% Zn)
17. Very high Zn content (0.258% Zn)
18. "Normal" celestites composition

The symbols in Fig. 4.9b correspond to the classes on the NLM plot (Fig. 4.12)

Key: ▲ Dolomite rich ■ Sr deficient △ V. high Zn □ High Ba

● Calcite rich ◆ High alkali ○ V. high Ba ◇ Normal

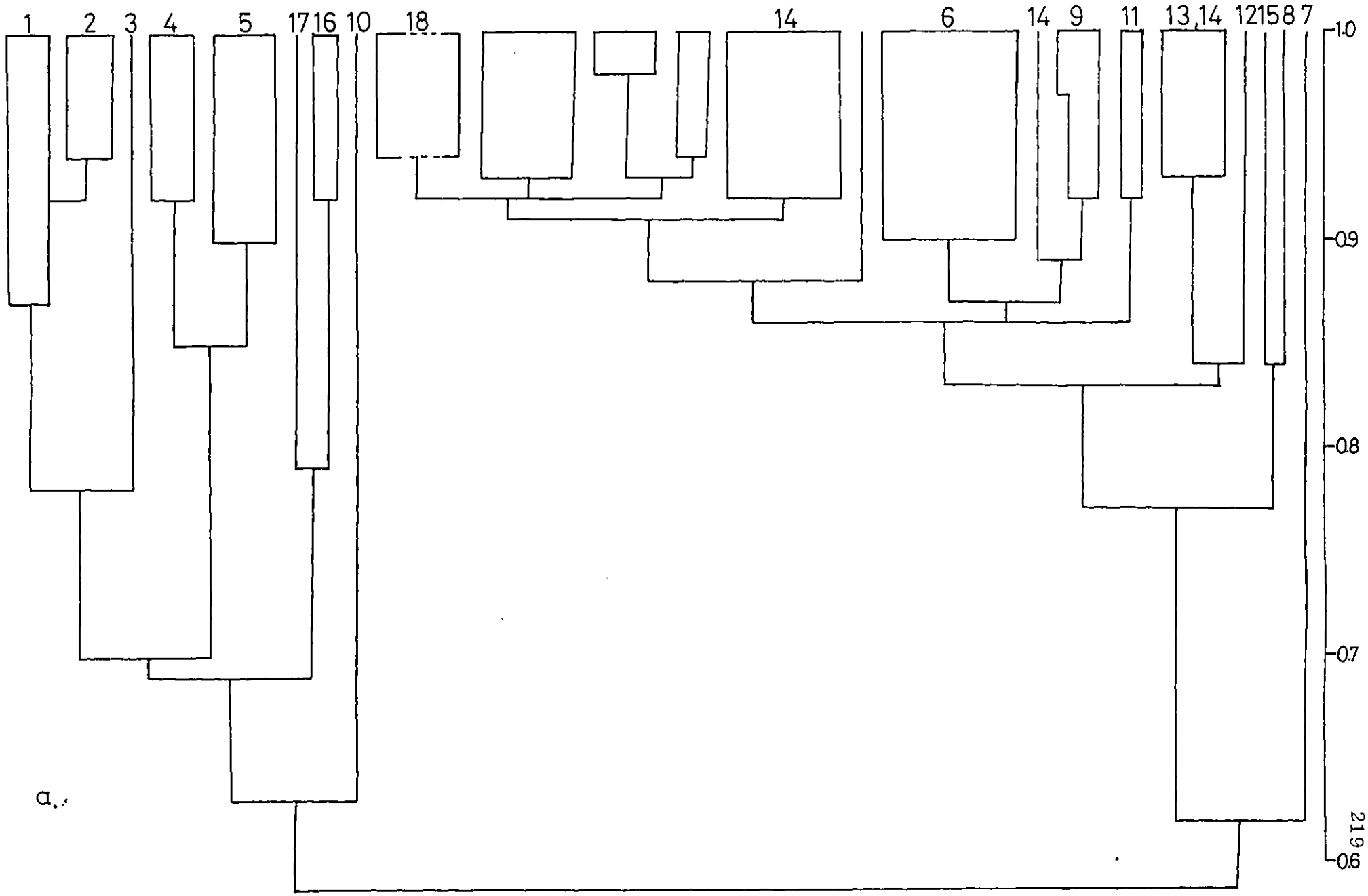

a.

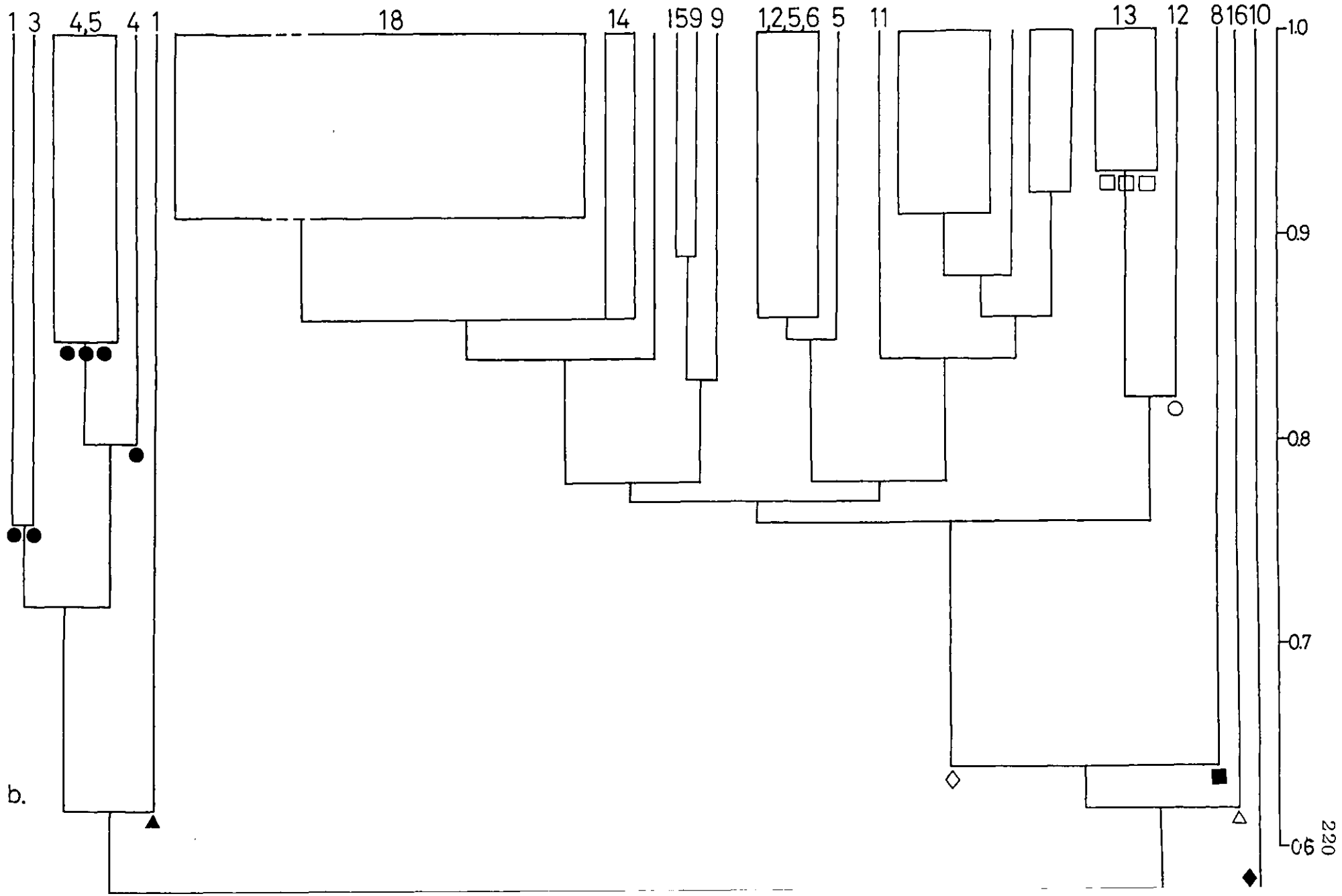
1 3 4,5 4 1 18 14 15 9 9 1,2,5,6 5 11 13 12 8 16 10
1.0
0.9
0.8
0.7
0.6
b.

latter group emphasising the objective nature of the procedure. These celestites are clustered differently in each variable/ sample permutation (Fig. 4.9a and b) according to which variables are acting as the main components. The power of each variable in decreasing magnitude of influence in each dendogram is approximately:

1. 6 variable dendogram Ca-Na-Ba-K-Sr-Zn
2. 7 variable dendogram CC-Na-Ba-Zn-Sr-K-DOL

b. Interpretation

The compositional groups as identified by the Q-mode clustering are plotted for the Yate Bypass - Goose Green celestites in Fig. 4.10. The most significant features of Fig. 4.10 are

1. The separation of the barian celestites (classes 13 and 14) from the calcitic celestites and the spatial separation of these two classes from each other.
2. The restriction of the calcitic celestites and those of intermediate composition (class 6 and 11) to the eastern sector.
3. The restriction of celestites high in Zn in the eastern sector of the Bypass (with the exception of celestite 125 which belongs to class 16).
4. The random distribution of the potassic class, with an apparent association with class 7 celestite in the western sector.

A regional synthesis of the Q-mode clustering cannot be attempted here because of the small number of celestites from other localities in the Q-mode class. Only three celestites, from New Courthouse (NCO3), Winters' Field (WF23) and Summer Bridge (SB07), are classified apart from the average celestites.

4.3.2.4 Simultaneous RQ-mode analysis of presence /absence data

TAXON2 initially added 46 major Q-mode groupings to the 24 principal R-mode clusters outlined earlier, giving a product of 1004 combinations, or cells, to be sorted by RSORT. As the RSORT analysis produced a very complex pattern it was decided to omit 19 variables and repeat the TAXON2, RSORT procedure. This resulted in a corresponding

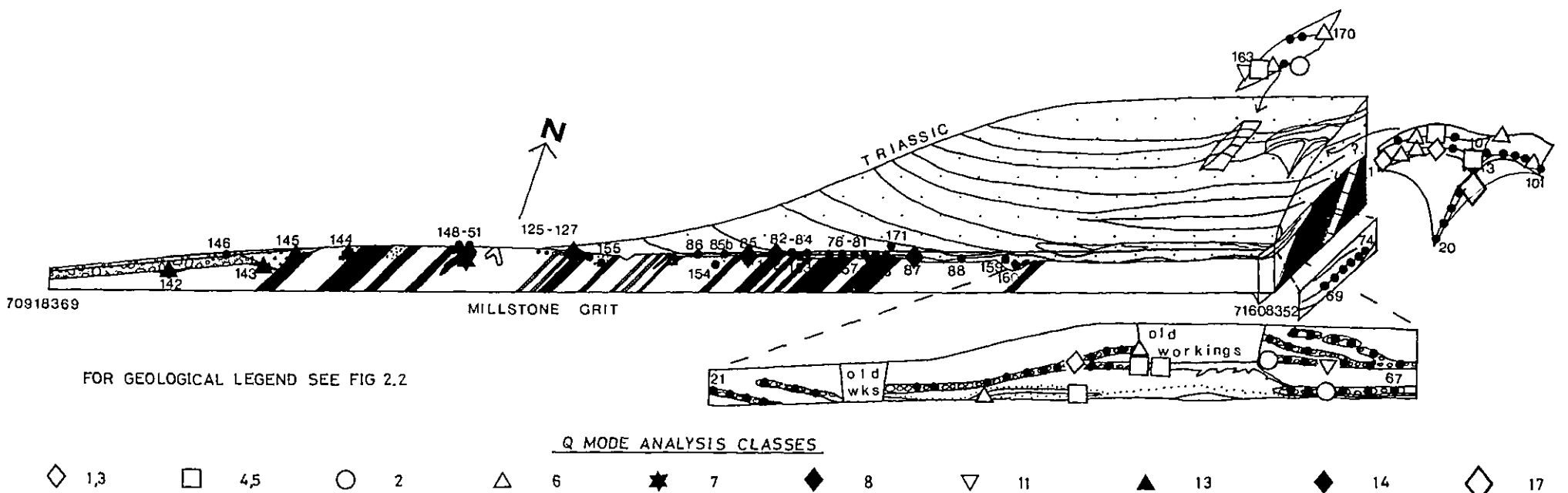

Fig 4.10: Interpretation of the Yate Bypass celestites by Q-Mode Cluster Analysis of assay and mineral content data

reduction in the number of Q-mode groupings from 46 to 33, so that the RSORT analysis was then applied to 33x12=396 cells. These data are shown schematically in Table 4.13. Variables were rejected if they contained few positive observations, occurred in most of the object groups or were largely subordinate to other variables.

The most interesting features of the RQ-mode pattern are:

1) The 'Quaternary' celestites are linked with Type A celestites.

2) Type B celestites contain characteristics of both Type A and Type C celestites.

3) The 'Tytherington' celestites are grouped with Type C celestites.

4) Massive Type A celestite is the most abundant variety.

5) Drusey macrocellular celestite often occurs with the massive, solid macrocellular variety.

By plotting the distribution of the R-groupings in the samples over the Yate Bypass - Goose Green site it is possible to attach a geological as well as a mineralogical interpretation to the data. Fig. 4.11 shows the distribution of the specimens belonging to R-mode clusters 13 (representing drusey macrocellular celestite), 10 (light red macrocellular celestite) and 28 (representing impregnation in dolomitic marl). This clearly shows that the macrocellular celestite and dolomitic marl are the dominant varieties in the eastern sector, but that further west this type is not as common, and drusey macrocellular and massive and solid macrocellular celestites predominate. There are insufficient specimens in the MAS to apply this analysis on a regional scale.

4.3.2.5 Simultaneous RQ-mode analyses of presence /absence data and assays/mineral contents

Using the computer to plot the principal Q-mode clusters of the assays (6 variable case) against the 24 original R-mode clusters of the presence/absence data it was possible to establish relationships between the composition of the celestites and their appearance in hand specimen. From the listing produced, the following conclusions were drawn: (a simplified version of the listing is given in Table 4.14).

Table 4.13: Relationship of the R-mode clustering structure to the Q-mode clustering structure for the presence/absence data

	R-MODE CLUSTER NO.											
Q-MODE CLUSTER NO.	25	26	13	9	10	11	27	28	14	29	16	19
1	X		/		X		/			/		
2	X		X		X		/					
3	X	X		X	X		/			/		/
4	X		X	/	/	X			X	/		
5	X	X	X	X	/	X		X		/		
6	X		/		/							
7	X				X		X	X				
8	X	/	X	/	X		/					
9	X	/	X		X		/	/				
10	X				X		/		X	/		
11	X		/		/		/		/	X		
12	/								X	X		
13	X		X		X		X					
14	X		/		/	/			/	/		
15	X				X		X		/	/		
16	X				X		X		/		/	
17	/				X	X	/	/				
18	X		/		/		X				/	
19	/								X	X	/	
20	X				X		/	X				
21	X				X		/			/		
22	X			/	X					/		
23	X		/							/		
24	X					/	/			/		
25	X		/									
26	X	/					X			/		
27	X									/		
28	X				/				/			
29	/				X	X	/		/	/		
30	X							/		/		
31	X											/
32	X				X		X	X				
33	X								X	X		

KEY: X strong degree of association, / weak degree of assoc'n

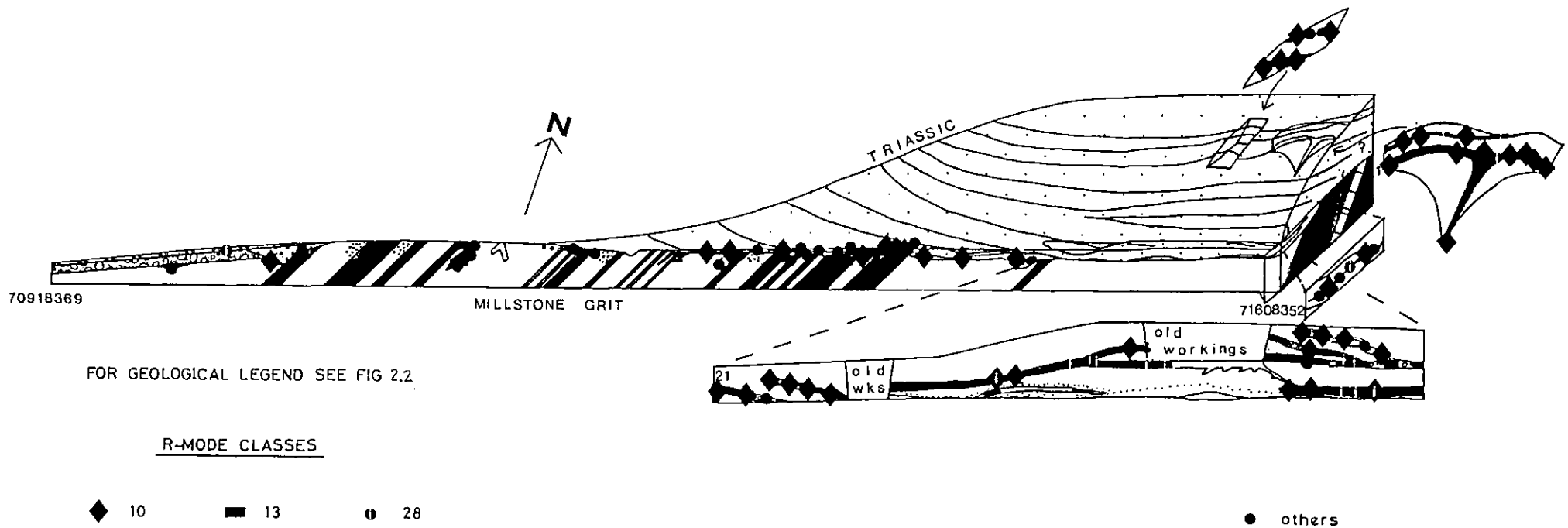

Fig 4.11: Interpretation of the Yate Bypass celestites by simultaneous RQ-Mode Analysis of presence/absence data

Table 4.14: Relationship of the R-mode clustering structure of the presence/absence data to the Q-mode clustering structure for the assay data (6 variable, 159 sample case)

	Q-MODE CLUSTER		R-MODE CLUSTER NO. (see Fig. 4.8 for key)																							
	No. (see Fig. 4.9)	Summary	1	2	3	4	5	6	7	8	9	10	11	12	13	14	15	16	17	18	19	20	21	22	23	24
calcitic celestites	1	10%Ca High K,Zn Low Sr	/		/	/			/		X	X								/				/		
	2	10%Ca High K	X	X	X	/			/		/	X								/				/	/	
	3	10%Ca High Zn Low Sr	X									X	X						X			X				
	4,5	15%Ca	X	X		X			X	X	/	X	/									/		X	/	
"ordinary" celestites	16,17	High Zn, v. high Zn	/		X			/				X				X				/						
	10	Very high K			X			/							/	X		X	X							
	18	Normal compositions (1)	X	X	X	X	X	X	/	/	/	X	/	/	/		/			/				/	/	
	Unspecified	Low Ba	X	/	X	X	/	X	X			/								/						
	Unspecified	Normal compositions (2)	X	X	X	X		X	/											/	/					
	Unspec,inc 14	Moderate Zn	/			/			/	/		/				X				X				/		
	Unspecified	Moderate Ca, Na	X		X	X	X			X		/		X			X							/	/	
	6	4-10% Ca	X	/	/	X	/	X	/	/	/	X								X				X	/	
	9, incl. 14	High K, intermed. Ba			X	/										X					/					
	11	High K, intermed. Ca	/	X		X	/	X				/												/		
	12,13,incl 14	High Ba, v. high Ba	X	X		/		/	/			/				/				/						
	8,15	Low Sr, high Zn	X	/	/	/	/													/						
	7	High Na	X		X											/			/					/		

Key: X strong degree of association / weak degree of association

1) Massive celestite is included in all of the compositional types.

2) Schistose massive and drusey macrocellular celestite are principally correlated with the normal celestites. This indicates that the Ca in the relic anhydrite in these celestites is not responsible for the calcitic celestites.

3) Light red macrocellular celestite and marl is correlated with all the calcitic and intermediate Q-mode clusters implying that this is a calcite-rich variety.

4) The Type C celestites cover a wide range of the Q-mode clusters in the "ordinary" celestites, possibly reflecting variations in the geochemistry of the Millstone Grit wallrock.

5) Lath-shaped moulds are found only with some calcitic celestites.

6) The high-Ba celestites are fine-to-coarse grained predominantly white celestites common to Type C occurrences and, with a calcareous rim in red marl, Type A occurrences.

7) Most of the high-Zn assays are taken from light red macrocellular celestite in marl; some however, are also found in Type C celestites.

8) The one high Na sample discovered contains no unusual physical properties.

9) A high K content is a feature of all celestites with a marl or mudstone component.

10) The Ca in the calcitic celestites and "intermediate calcium" celestites can be traced to a marl, sparry calcite or dolomitic marl component.

4.3.2.6 Non-linear mapping

a. Method

The 95 samples were first allocated to classes corresponding to Type A (A), Type B (B), Type C (C),? Quaternary (Q) and Summer Bridge, Tytherington (T), celestites on the basis of the 7 variables, normalized to equal weight.

The NLM plot shows the principle structure is a closely-packed cloud reflecting the 'normal' celestite compositions with little, if any, separation between the A,B,C,Q and T classes (Fig. 4.12). The outlying samples were differentiated from the central cluster by drawing in an outer limit to the 'normal' celestites and applying the usual criterion of within-group variance (Howarth, 1973), labelling where

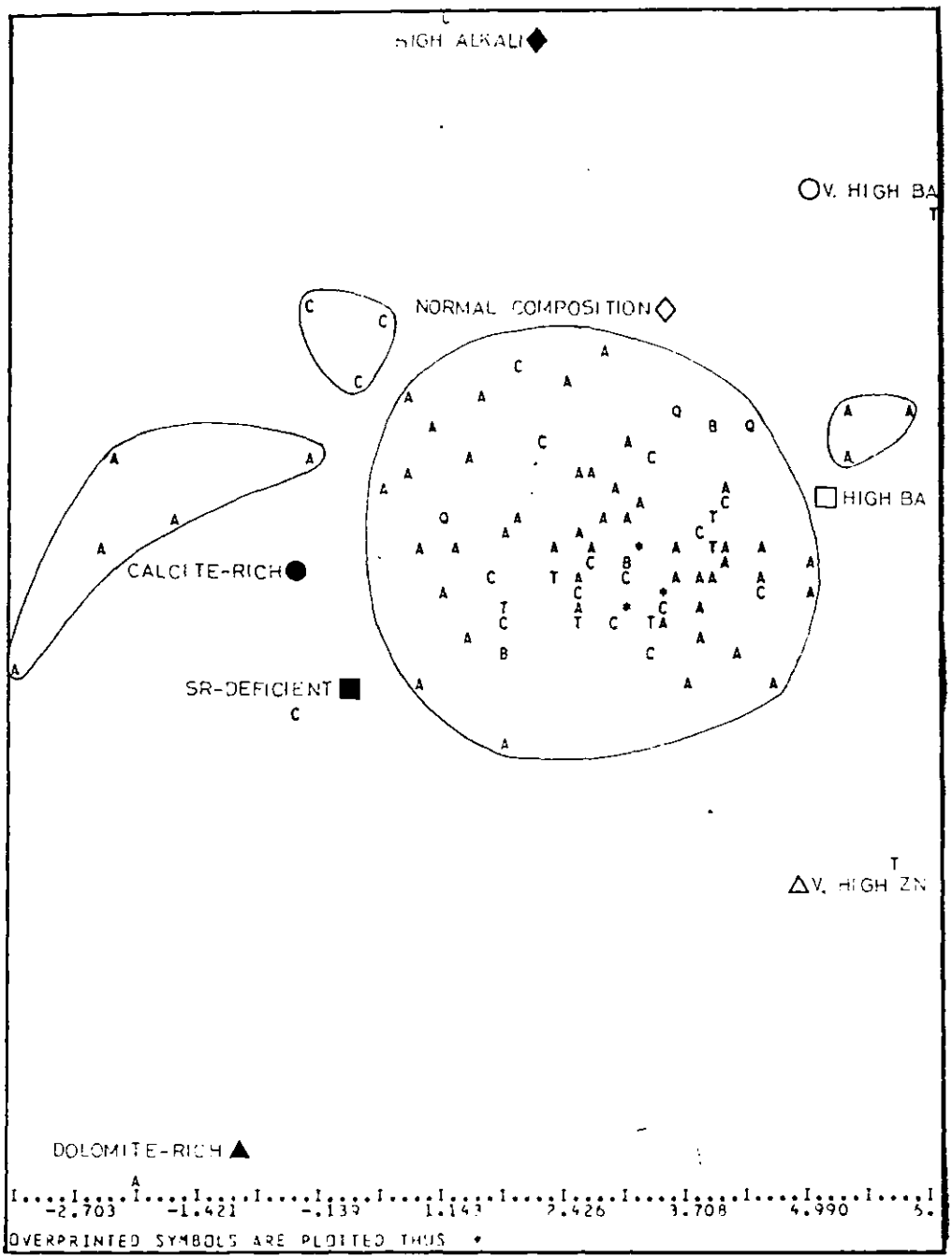

Fig 4.12: Classification of 95 celestites by non-linear mapping
Key: A- Type A celestites; B- Type B celestites; C- Type C celestites; Q- Type Q ('Quaternary') celestites; T- Type T ('Tytherington') celestites

appropriate. The following groups were thus recognized:

a) Calcite-rich celestites (> 57% Calcite)*
b) High-Ba celestites (> 1.47%Ba)
c) Dolomite-rich celestites (23,9% dolomite)*
d) High alkali celestites (20ppm Na, 4.90%K)
e) Sr-deficient (10.4%Sr)
f) Very high-Ba celestites (2.88%Ba)
g) Very high-Zn celestites (0.175%Zn)

The clustering of the three Type C celestites to the left hand side of the central cloud is due to missing Sr values and is completely artificial.

Repeating the NLM analysis on unnormalized data resulted in what was basically a scatter plot for Sr and Ca. Only five samples fell outside a long continuum.

b. Comparison of Non-Linear Mapping with Cluster Analysis.

Synbols used to distinguish between the NLM groupings are plotted on the 7 variable, 95 sample dendrogram in Fig. 4.9b. The excellent agreement between the two types of classification attests to the significance of the groupings found.

4.4 INTERPRETATION OF OTHER DATA

4.4.1. Comparison of the MAS analysis with those of other celestites

The observations above may be compared with other celestite data (Tables 4.1, 4.2, 4.3 and 4.5), on which statistical studies have not been performed. It is difficult to make straight comparisons between the data sets of the Sr analyses because of varying degrees of effectiveness of the different analytical methods (Fig. 4.3a). However, whereas the SCF data (Table 4.1) are deficient in Sr in comparison with those of the M.A.S., the Wapley Common celestites (Table 4.2 and 4.3) appear to contain similar levels of Sr, so the Sr levels can be directly compared. Ignoring the effect of the high SiO_2 assays of the Wapley Common celestites, with the exception of specimens MR01, MR04, MR06 and MR07 which contain Ba and Ca in quantities approaching the threshold values of Fig. 4.9, all of the

* This is probably an overestimate (See 4.2.3).

celestites considered here would be classified as "normal" celestites by NLM or cluster analysis. White medium-grained granular impregnations and tabular impregnations of celestite produce assays of 0.82 and 0.86% Ba in samples MR04 and MR06 respectively. The lithologies responsible for the high Ca values are either fine sparry calcite cement (MR01), grey pseudocubic calcite (MR06) or both calcite forms (MR04).

The Wapley Common celestites all contain at least 2% SiO_2 signifying detrital quartz and chert (difficult to recognise with the naked eye). High values of SiO_2 in specimens MR07, MR09 and MR10 are apparently due to mega-quartz in hand specimen ("blue" quartz in MR07) whereas the high assay in MR01 is probably derived from lozenge quartz.

4.4.2. Celestite sands and gravels (Table 4.6)

There is a good agreement between the SrO analysis of samples RY03 and WF06, as analysed by the Betaprobe and LMF/AAS methods. The SrO content of the nine sediments ranges from 30.90% in specimen RY03 to 49.37% in A86. Each is accompanied by a BaO assay of similar magnitude as in a consolidated celestite, the maximum value of CaO recorded is 0.30% suggesting leaching of much of the carbonate in the sediment and emphasising the reworked origin of these rock types. The slightly higher CaO Betaprobe analyses may be due to poor calibration (the lowest celestite standard contained 0.5% CaO).

The SiO_2, Al_2O_3, Fe_2O_3 and K_2O values are probably all derived from the clastic fraction of the celestites whose mineralogy is dominated by illite, quartz and hematite.

4.4.3 Gypsum (Table 4.7)

The LMF/AAS analyses are briefly discussed below. Minor amounts of Sr and traces of Al and Si were detected in two specimens (BL19 and BL28) analysed by Betaprobe. Fe or Mg was not recorded.

Calcium

The calcium analyses are all rather low (pure gypsum contains 23.3% Ca) probably because the analytical method was 'stretched' to accommodate Ca analyses of this magnitude.

Strontium

The strontium analyses for the LMF fusions fall in the range 0.18-0.67%. These figures are higher than the range of 0.02-0.28% Sr reported by Butler (1973) in primary gypsum at Baja, California and are also greater than the values for secondary gypsum reported by Holliday (1967) (mean of 601ppm) and West (1973) (mean of 1159 ppm Sr). The figures therefore, suggest that trace amounts of celestite are present in all of the gypsums, in quantities below the XRD detection limit. As there is no apparent significant difference between the Sr content of gypsums from within the celestite-producing area (Hall End and Broad Lane specimens) from those on the margins (Tortworth Copse), and the Newark Gypsum at Michaelwood it is suggested that this celestite is late diagenetic, probably derived from the inversion of relatively high-Sr anhydrite rather than a product of the main celestite mineralization. Holliday (1967) recognised similar celestite in secondary gypsum from Spitzbergen.

Barium

The ratio of barium to strontium, ranging up to 20×10^{-2}, is appreciably higher than would be expected if the barium was only present in the trace celestite in the gypsum, indicating that small amounts of Ba^{2+} may be substituting for Ca^{2+} in the gypsum lattice or that baryte may be present. However, as the analyses in Table 4.9 are at the detection limit for the Ba techniques, these results should be interpreted with caution.

Sodium

The sodium content of the gypsum is relatively constant at 80-160ppm and is at a similar level to the trace sodium in the celestites (see above).

Potassium

Potassium is present in amounts up to 0.828%. If this is present as minor amounts of illite, as seem likely, then it would also help to lower the gypsum content and therefore depress the Ca analyses.

Zinc

The zinc analyses are of great interest in that two compositional groups can be recognised:

(1) High (510 - 8,850 ppm) values in the Broad Lane (Yate Bypass) samples.

(2) Trace amounts in gypsum from other localities ($<$70 ppm). Although no zinc minerals were detected in X-ray analysis, the two Broad Lane specimens may contain sphalerite as part of the epigenetic Pb-Zn mineralization at that locality (Fig. 4.10 shows that the Broad Lane gypsum is situated near to high Zn celestite of class 8.)

4.5 DISCUSSION - THE DISTRIBUTION OF Sr, Ba, Ca, Zn, Na AND K

4.5.1. Introduction

The results in 4.3 and 4.4 are now summarised and discussed in detail with regard to the distribution of the six elements in the celestites of the Yate Bypass area and more generally, over the study area.

The regional geochemical maps are a synthesis of the information available on the composition of the celestites in the study area, the source of which is given in Fig. 4.2. The values plotted are averages of the data at each site. Because anomalous values are reduced during the averaging, the data have been plotted at half-standard deviation intervals, as in Fig. 4.4. It has been assumed that the different sets of data are all equivalent.

4.5.2. Strontium

The absence of a high positive correlation between strontium and any other variable (4.3.2.2.) suggests that no other element accompanied the strontium mineralization. Sr data have little geochemical significance as they merely reflect the proportion of celestite to sparry calcite, or marl or Millstone Grit bedrock in the specimen (see 4.3.2.1.). The Sr deficient celestite recognised by non-linear mapping is a Type C celestite, specimen BL01 replacing an ironstone concretion.

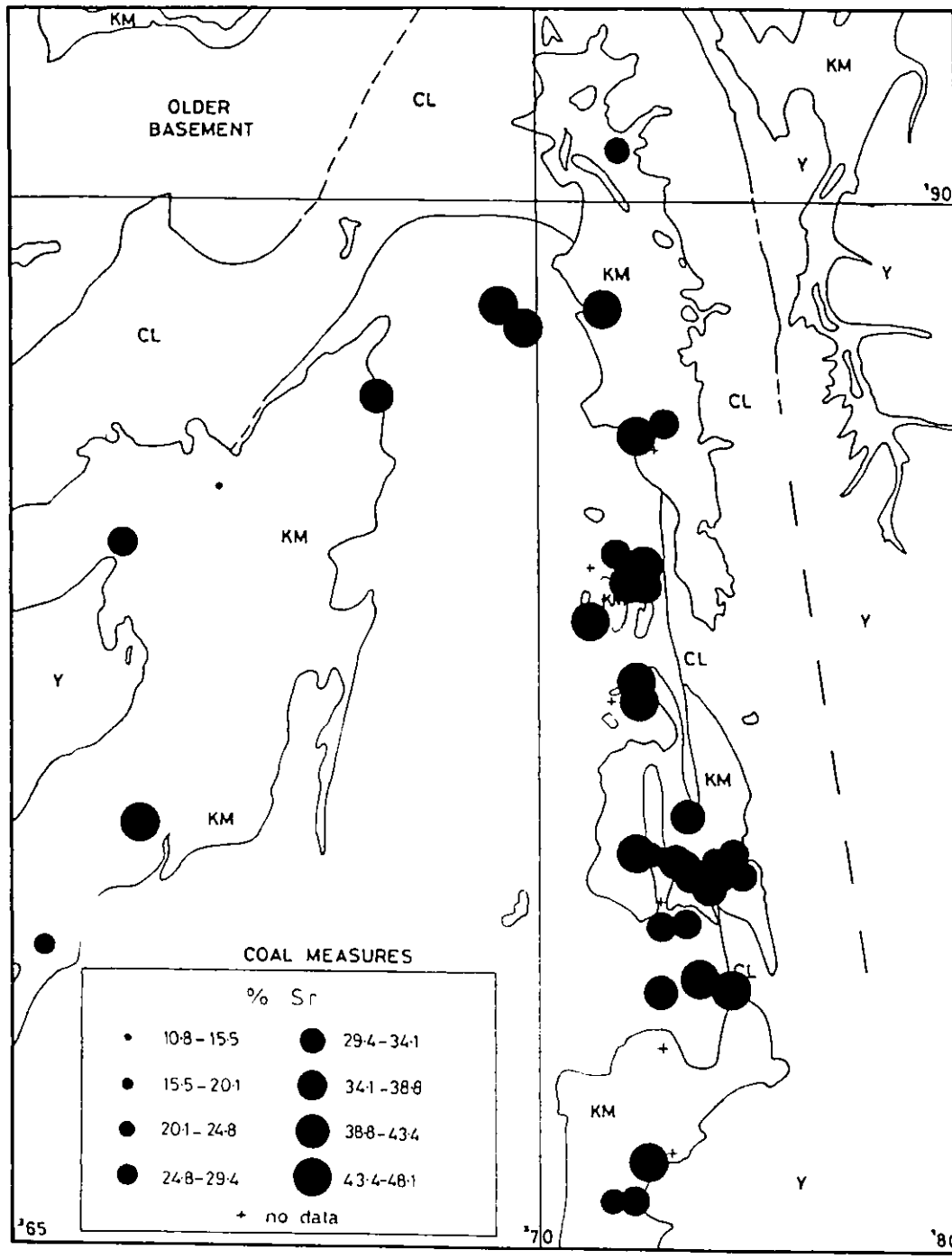

Fig 4.13: Distribution of Sr in the celestites of the study area

The regional plot of the Sr analyses therefore, shows a uniform distribution of values, with only quartz-rich celestites at Moorlease and Perrinpit Farm standing out from the general pattern (Fig. 4.13).

The economic significance of the Sr assays of the celestite sands and gravels is discussed in Chapter Six.

4.5.3. Barium and Ba/Sr

Although the Ba/Sr and calcite variables are significantly correlated at the 99.9% level (Fig. 4.2 and 4.3), Ba, like Sr does not appear to be related to any of the other elements determined above. Q-mode (4.3.2.3.) and RQ-mode (4.3.2.5.) analysis differentiated four classes of high-Ba celestites, two of which were also recognised by non-linear mapping (4.3.2.6.), of fine to coarse grained white celestite.

Although baryte and celestite are isostructural and a complete solid solution series probably exists, most natural occurrences are of compositions near the two end members (Berry and Mason, 1959). The ten celestites analysed by Bernstein (1979) from various world localities, for example, only contain up to 1.37% Ba. For this reason, it is suggested that the term: barytocelestite be restricted to celestites containing approximately 50 mole percent Ba and a new term Barian celestite be introduced to describe celestites with significantly high content of Ba set at a value of 0.96% Ba, corresponding to a subsidiary peak at a value of the mean plus one standard deviation of the Ba frequency distribution (Fig. 4.4). This corresponds to a composition of $(Sr_{98.6}\ Ba_{1.4})SO_4$.

Collie, (1879) described two varieties of "barytocelestine" from Keuper Marl at Clifton, Bristol. The first type wasof blue celestite, showing serrated edges and rosette-texture in thin section and assaying at an average of 46.3% Ba and 12.3% Sr and was compared to other "baryto-celestines" of composition $2BaS_4.SrSO_4$ from various other world localities. Collie also analysed specimens of a second type of "baryto-celestine" as follows: "reddish, opaque, agglomerated" containing 0.71% Ba, fibrous mineral containing 4.33% Ba and "blue to reddish" coarse celestite with 2.47

and 6.42% Ba.
The close similarity of the first specimen to light red macrocellular celestite of average Ba content and of the second specimen to efflorescences of barian celestite (Fig. 3.3) is worthy of note.

A barian white fibrous celestite from Filton, Bristol of Lilstock Formation age analysed by Wood and Shaw (1976), contained 3.12% Ba, and vein celestite from Oaklands, near Almondsbury, which they also analysed, contained 6.50% Ba. A white fibro-radiate 'barytocelestite' from Redland, Bristol on display at the I.G.S. Museum is very similar in appearance to the sheaf-like efflorescences seen in hand specimens of Poundhouse Farm celestite (Fig. 3.3).

The minimal positive correlation of Ba with Sr (4.3.2.2.) indicates that the barium is present, substituting for Sr in varying minor amounts in the barian-celestite, for if the barium occurred separately in a 'barytocelestine' - type mineral, a low negative correlation would be expected and if baryte were to occur, a high negative correlation would result.

If the Sr and Ba values are plotted on a scatter diagram, they fall below the curve representing the 'ideal' celestites of the celestite-baryte compositional series, so that these celestites may be regarded as undersaturated in respect to Ba. Even the so-called barian celestites do not contain sufficient barium for the 'ideal' celestite composition to be attained. This may be due to other elements e.g. Ca substituting for strontium in celestite. Table 3.2 for example, illustrates barian celestite containing up to 0.24% Ca in Poundhouse Farm celestites.

The concept of an 'ideal' celestite, containing an equivalent amount of Ba substituting for Sr, may be applied to specimens containing relatively smaller amounts of celestite, in which barian celestite is indicated only by Ba/Sr ratio values greater than that of an 'ideal' celestite. The minimum Ba/Sr ratio of an ideal celestite is given by 100 x 0.96/46.9 = 2.05 (where 46.9 is the weight % Sr of the ideal celestite). Using this factor, sixteen additional <u>barian celestites</u> may be detected in the samples of the M.A.S. Fig. 4.14 summarises the distribution of the barian celestite in the Yate Bypass - Goose Green profile as recognised by the

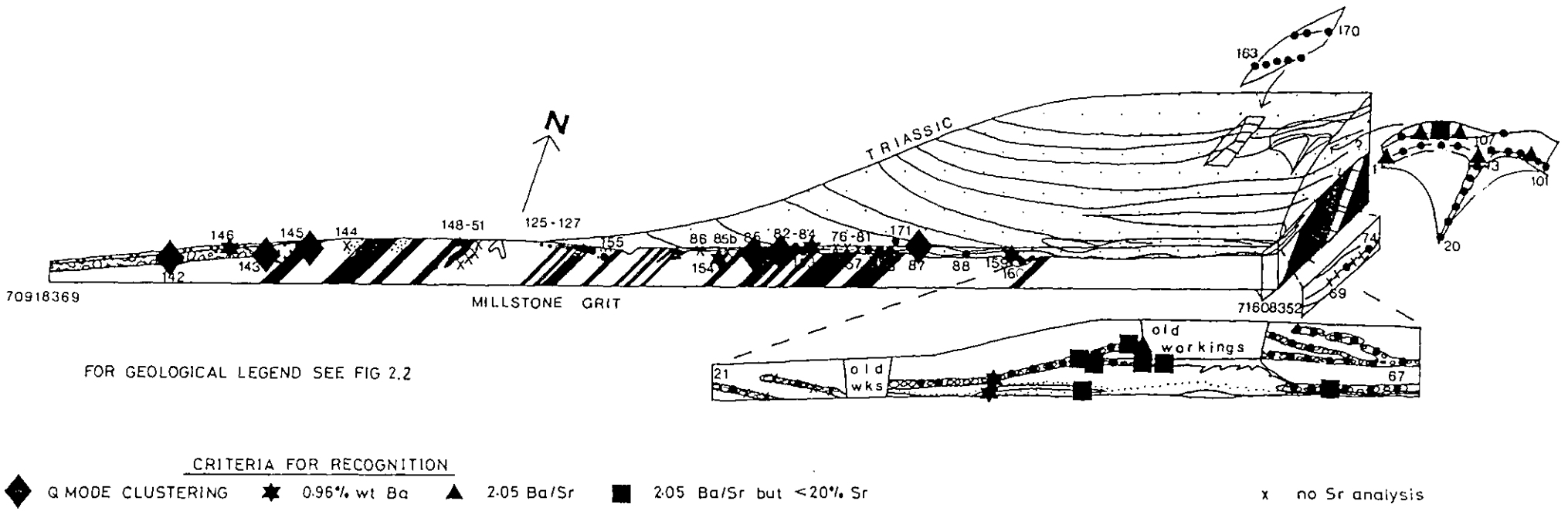

Fig 4.14 : Distribution of barian celestites along the Yate Bypass cutting

Q-mode clustering, 0.96% Ba and Ba/Sr criteria. Celestites of the two Q-mode classes are well grouped along the sampling traverse and also occur close to the other barian celestites not differentiated by cluster analysis. This close grouping of the barian celestites at certain locations suggests either that 1. at these positions the celestites more efficiently scavenged the available Ba in the immediate environment, or 2. the environment was locally enriched in barium. The Ba/Sr criterion recognises other barian celestites in the marl in the eastern sector, but many of these are calitic celestites (see 4.3.2.3.) with a low Sr content ($<$ 19%) so that the ratio is less reliable. The barian celestites that are thought to be significantly different are mostly present in the Tylers Farm cutting, and like the other Type A barian celestites of the central sector, show negative correlation with the light red macrocellular celestites (Fig. 4.11).

The regional distribution of Ba and Ba/Sr (Figs. 4.15, 4.16) shows no obvious geologic or regional control and occurrences of barian celestite at each of the sites, may be attributed to local factors rather than a large scale trend. Celestites of 'barian celestite' composition were recorded by Nickless et. al. (1976) at many localities, indicating that they are a common form of celestite. Suspected barian celestites at the Wapley Common site, previously mentioned in 4.4.1., may be corroborated here by the values of their Ba/Sr ratio (see Table 4.3). In addition, old records of the Poundhouse Farm site show a mean Ba content of 0.99% for celestites from twenty-six test holes. The highest concentrations of Ba were reported from nodule trains of seams A,B, and to a lesser extent, C and F (Fig. 2.9). Note also that the mean of the Summer Bridge celestites falls within the 0.62-0.79% Ba class, even though specimen SBo7 was separated by both NLM and cluster analysis.

4.5.4. Calcium, calcite and dolomite contents

The induced high negative correlation of the variables Ca and CC (calcite), together with DOL (dolomite), K and Zn, against strontium, is expressed in the Q-mode dendrograms (Fig. 4.9) and N.L.M. plot as (Fig. 4.12) separate clusters of calcitic celestites containing +4.0% Ca*.

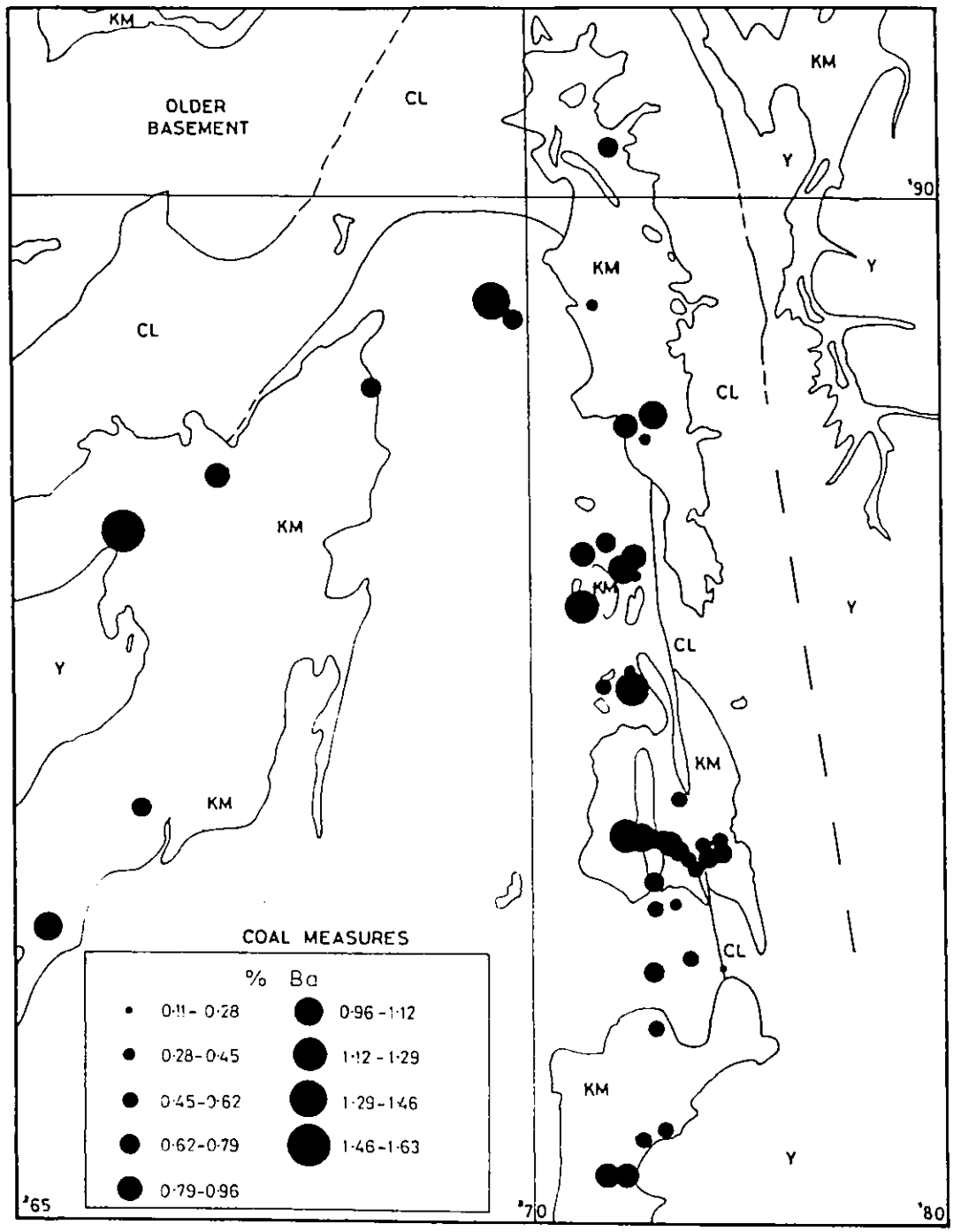

Fig 4.15: Distribution of Ba in the celestites of the study area

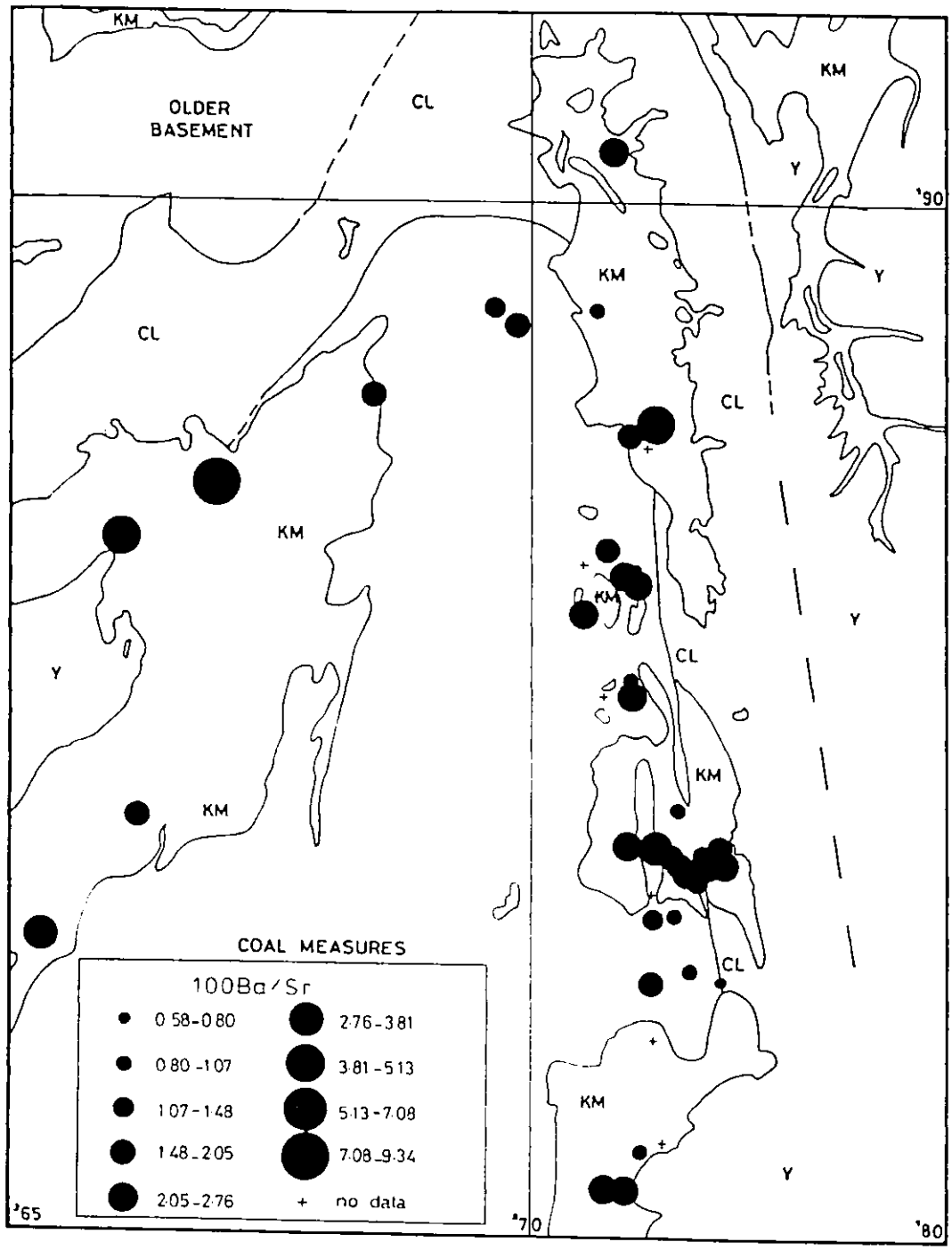

Fig 4.16: Variation of the ratio: 100Ba/Sr in the celestites of the study area

Sparry calcite either present as scalenohedral calcite, limestone, cement in the host marl or, to a lesser extent, dolomite is responsible for the calcitic celestites (4.3.2.5). The histogram for Ca shows that there are a large number of celestites with a Ca content of between 0.18 and 0.49% which do not contain calcite (Fig. 4.4). As these included epigenetic as well as Type A celestites with Triassic marl, it is possible that some of the calcium at this level is substituting for strontium in the celestite lattice. Crystals of the Poundhouse Farm celestites for example, contain up to 0.24% Ca; also Bernstein (1979) reported 0.03-0.70% Ca in ten global celestites. The Ca may also be derived from anhydrite relics in some of the celestites.

Figs. 4.10, 4.11 and 4.17 show that the sparry calcite and dolomite is mainly restricted to two zones in the eastern sector of the Yate Bypass. These cut across stratigraphical contacts and quite clearly represent different facies of the Yate Formation. Minor quantities of calcite are present in two Type B celestites (Nos 159 and 160) and one Type C celestite (No 144). Dolomite without calcite as recorded in the epigenetic celestite of the cobble gravel bed (No 142) is due to complete replacement of the calcite cement.

The regional distribution of Ca (Fig. 4.18) shows that with the exception of the Hall End, Yate Court Rectory and New Courthouse sites, celestites containing more than 0.49% Ca are restricted to Type A occurrences only. Only at New Courthouse is the Ca present as calcite. Calcitic celestites occur at Perrinpit Farm, Itchington, West End, and Wapley Common; at the last locality the calcite is also present as the grey pseudocubic variety (4.4.1.) Like Ba, there is no obvious regional or distributional trend for the Ca analyses.

4.5.5. Zinc

Zinc shows a strong association with the variables Ca, CC (calcite), DOL (dolomite), (Fig. 4.6, 4.7) and K, and apparently belongs to the sparry calcite/marl component of the celestites.

* See discussion in 4.2.3.

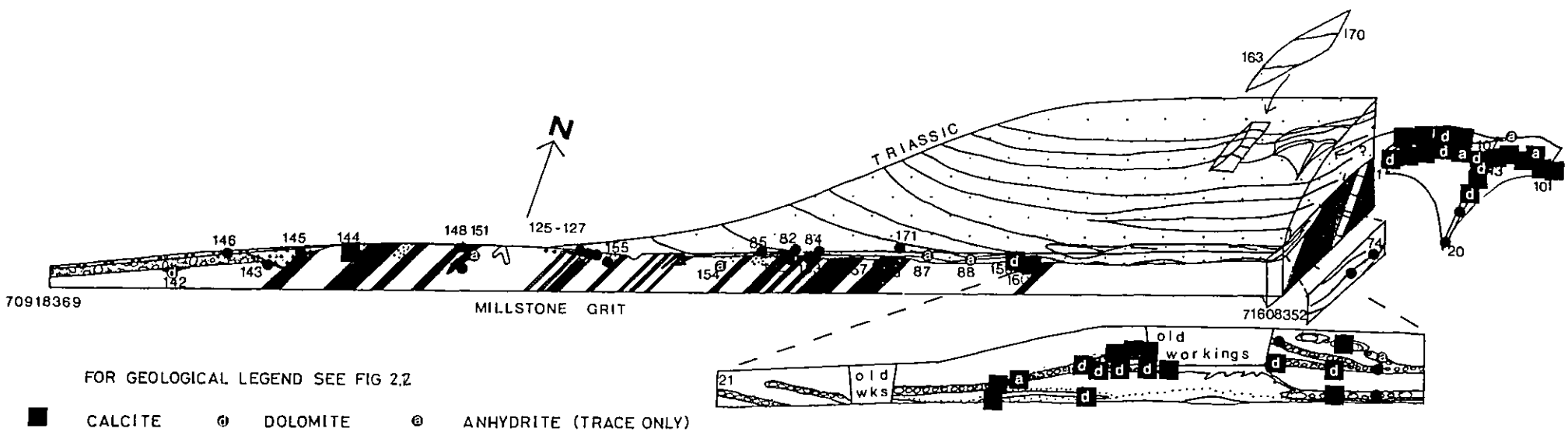

Fig 4.17: Distribution of calcite and dolomite along the Yate Bypass cutting

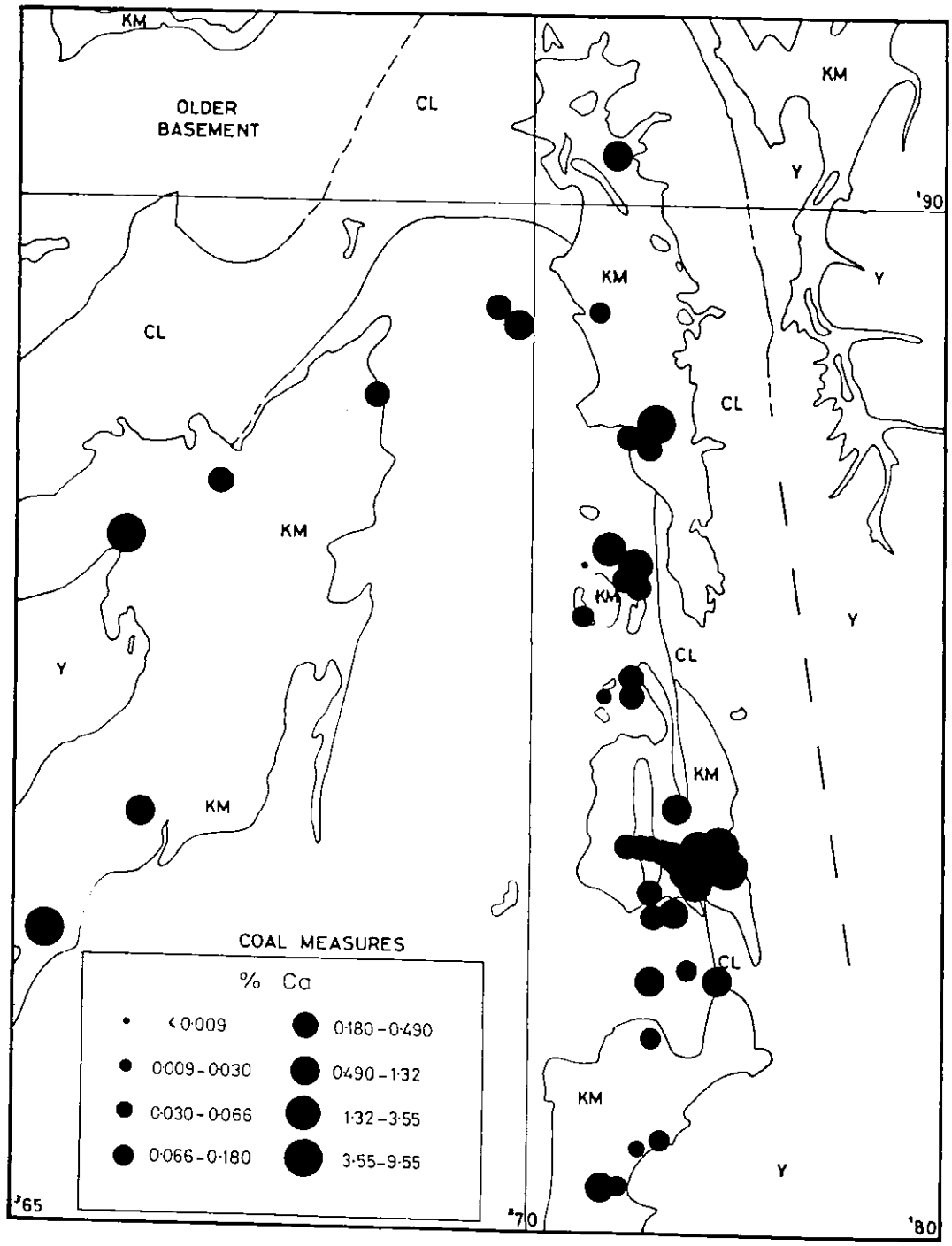

Fig 4.18: Distribution of Ca in the celestites of the study area

However, one of the high - Zn classes differentiated by Q-mode clustering, class 8 (Fig. 4.9) also contains marl-free Type C celestites and a Tytherington (Summer Bridge) celestite. The Tytherington celestite is of sufficiently anomalous composition to be clustered separately by NLM analysis (Fig. 4.12).

Bernstein (1979) could not detect Zn in the celestites that he analysed and it seems reasonable to ascribe the Zn assays to the analysis of small amounts of sphalerite.

High-Zn celestites occur mainly sporadically distributed along seams B and F in the marl of the eastern sector of the Yate Bypass (Fig. 4.10), usually in association with light red macrocellular celestite (4.3.2.5.). The restriction to two horizons suggests the epigenetic mineralization was restricted to the more permeable strata at these levels (Fig. 2.3). The most extensive mineralisation occurs in seam F above the crop of the Tanhouse Limestone, suggesting that this unit may have acted as a reservoir for the Zn-bearing fluids. High-Zn celestites were only recognised from the Goose Green/Yate Bypass, Summer Bridge and New Courthouse sites. Celestites from other locations generally contain between .009 and .012%Zn (the modal class of the distribution is Fig. 4.4). In addition, old company records show up to 0.60% Zn in celestite and limestones from Poundhouse Farm.

4.5.6. Sodium, Potassium, Na/K

The range of sodium values observed (Table 4.1)is of similar magnitude to that of 60-510 ppm reported by Bernstein (1979) in ten celestites from various world localities. Like barium, sodium does not show a preference for the celestite nor the calcite/marl component of the specimens (4.3.2.2.). The uncalibrated Betaprobe data show two trends for Na, reflecting celestites of high and low Na content (Appendix II.2). However, there are no striking lithological or genetic differences between the two groups. The specimen, M.A.S. number 150, differentiated in the cluster analysis is only one of two samples with an Na content (840 ppm) above two standard deviations of the total mean of 100 ppm (Table 4.1).

As this sample is of Type C celestite veining Millstone Grit mudstone, it is thought unlikely to contain sodium minerals (e.g. halite) and is probably an analytical flyer produced by a faulty analysis. Elimination of this one value would depress the Type C celestite mean in Table 4.1 to a value near that of the Type A celestites, removing any significance in the difference between the two types.

All the evidence presented in this chapter indicates that K is largely derived from the clastic component of the celestites. In particular, the Tytherington celestite differentiated by NLM analysis (4.3.2.6.) contains unusually high quantities of illite claystone. However, Bernstein (1979) recorded 17-81 ppm K in ten global celestites. Although these values are below the detection limits of the fusion methods similar low quantities of K were recorded by Betaprobe analysis (Appendix II.2).

The Na/K ratios are included in the study for comparative purposes only. A high negative correlation with the calcite variable (4.3.2.) reflects the independence of the Na distribution.

4.5.7. Other elements

Bernstein (1979) recorded 3-30 ppm Mg, 5-64 ppm Fe and minor quantities of Al and Si in ten celestites at concentrations below the detection limits of the methods employed here. The analyses recorded in Tables 4.1, 4.5 and 4.6 are entirely due to separate mineral species, namely quartz (authigenic and detrital), clay minerals, hematite, hematite/goethite ironstone and dolomite. Si and Fe are the major contaminants, with values of up to 79.5% SiO_2 in quartz rich celestites and 5.42 Fe_2O_3 in the celestite sands.

4.6 SUMMARY

The geochemical evidence presented above indicates that the celestites crystallised in response to a strontium metasomatism in the study area. Where the geochemical environment was enriched in Ba, barian celestites were formed.

The celestites also contain an average content of 100 ppm Na, and up to approximately 0.5% non-carbonate Ca, substituting for Sr. Values of calcium above this amount are due entirely to the assay of sparry calcite, or more rarely, dolomite. Celestites containing more than 4% Ca with similarly high levels of K, indicating admixed mudstone of marl or Zn (sphalerite), are here termed calcitic celestites.

Although the main elements do not show regional trends in their distribution, a detailed traverse at a larger scale indicates that both barian and calcitic celestites may be the result of local effects due to variations in facies. Associated with the compositional variations are differences in celestite varieties along the celestite seams.

CHAPTER FIVE - THE ORIGIN OF THE CELESTITES

5.1 INTRODUCTION

The aim of this chapter is to describe the sedimentary history for the celestites of the study area and discuss the source of the strontium. Additional evidence from the Wapley-Bitton area (Nickless et al. 1976) (Fig. 5.1) is included where required.

Before this can be attempted it is first necessary to clarify the relationship of the celestite paragenesis (Fig. 3.1) to that of the gypsum rock. The origin of the red celestites is central to this discussion.

5.2 DIAGENETIC HISTORY OF THE CELESTITES AND THE GYPSUM ROCK

5.2.1 Diagenetic Framework

Fig. 5.2 is a paragenetical scheme for the evaporites, constructed from hand specimen observations (2.4.2) and petrographic analysis (3.1, 3.3).

5.2.1.1 Stratigraphic Relationships

Each celestite seam of the Poundhouse Farm and Tortworth Copse successions has a secondary gypsum equivalent in the Aust sequence (Fig. 1.8) indicating that the stratigraphic distribution of both types of evaporite is controlled by that of a common anhydrite precursor. Although 'primary' celestites or anhydrite-free celestite may also be found at these horizons the 'secondary' celestite fabrics (3.1.2) are generally the commonest types observed. The areal extent of the celestite over the interval of the Severnside Evaporite Bed or Newark Gypsum (Fig. 5.3) is a direct reflection, then, of differences in the early diagenetic environment. Detailed examination of the Wapley-Bitton area (Fig. 5.4) shows that macrocellular granular and pink alabastrine gypsum form the principal evaporite in two districts or zones where celestite formation did not significantly occur.

The division of the evaporite into gypsum and celestite is as well defined stratigraphically as it is spatially. The Tortworth succession (Fig. 1.8, 2.3) contains an alabastrine gypsum seam sandwiched between celestite horizons. A similar distribution is also shown

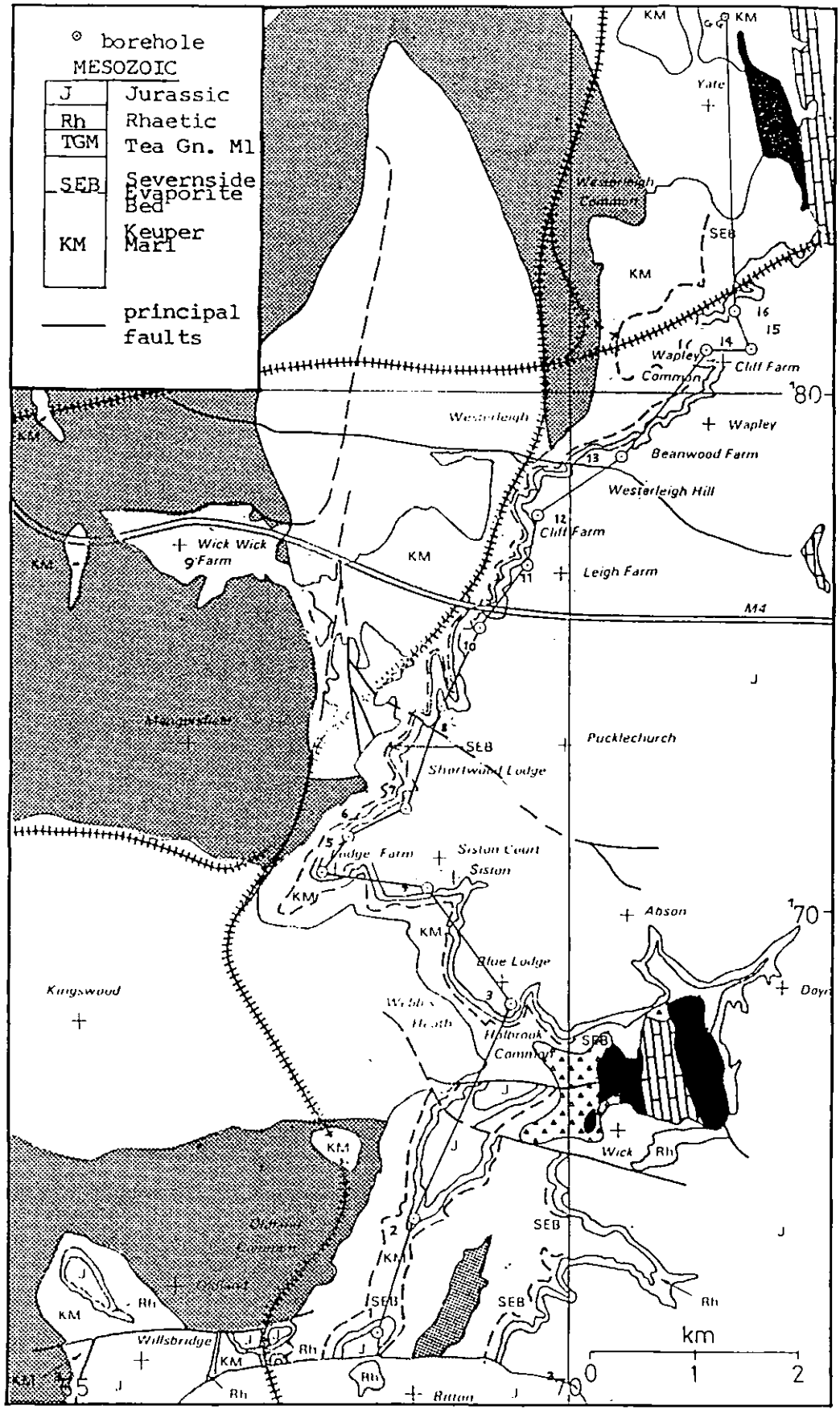

Fig 5. 1 : The Wapley-Bitton Area, as defined by Nickless et.al. (1976). Basement geology simplified from fig 1.5 Mesozoic geology as in key (note use of older terminology).

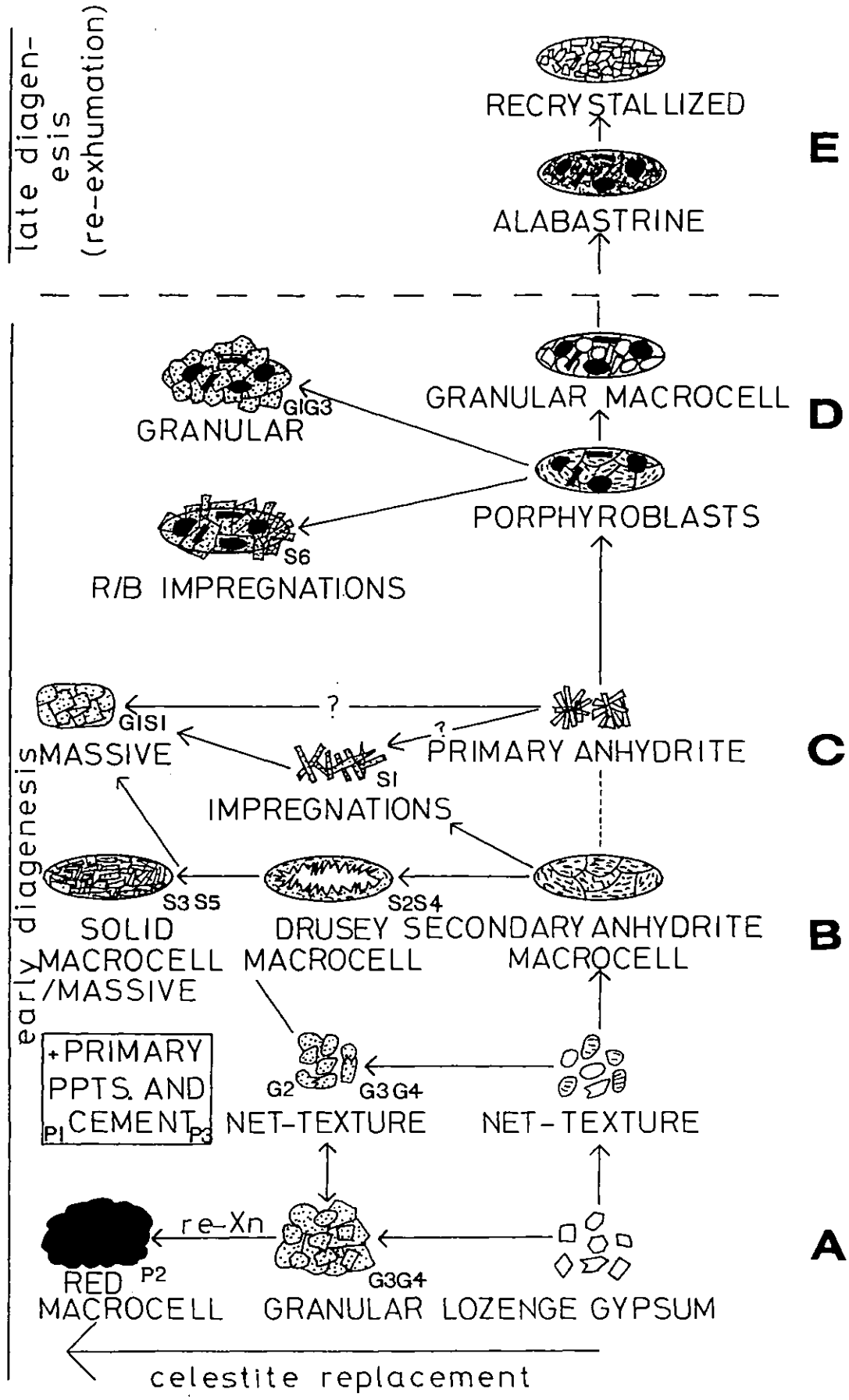

Fig 5.2: Flow diagram showing relationship of gypsum and celestite parageneses. Lettered stages on R.H. side correspond to scheme of Holliday and Shephard-Thorn (1974)

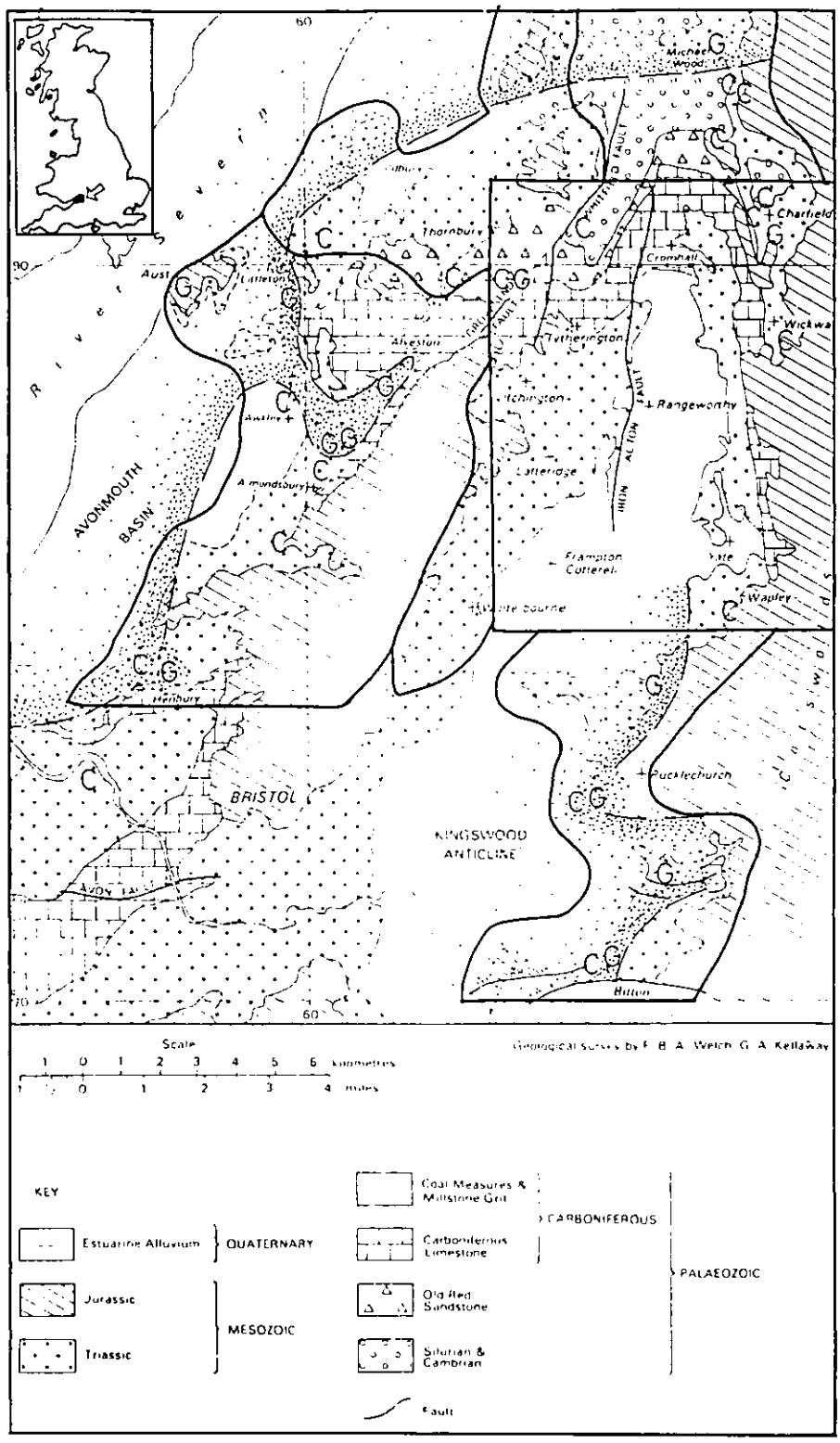

Fig 5.3: Regional extent of the celestite (C) and the gypsum rock (G) (after Nickless et al., 1976)

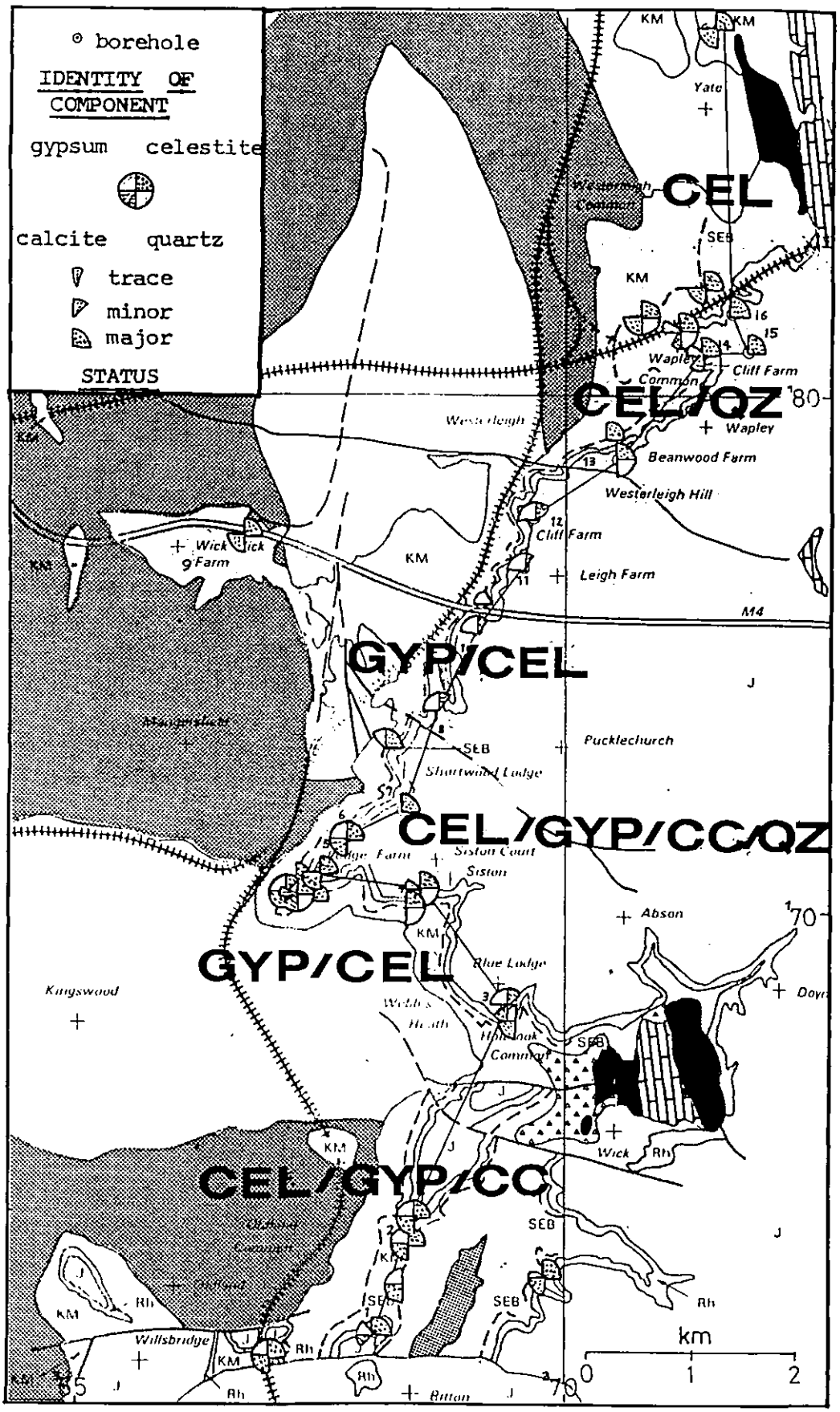

Fig 5.4 : Semi-quantitative estimates of the gypsum, celestite, sparry calcite and megaquartz content of the evaporites of the Wapley-Bitton Area (Compiled from data in Curtis, 1974; Nickless et al 1976; Wood and Shaw, 1976 and current investigation).
For explanation of geology see Fig 5.1

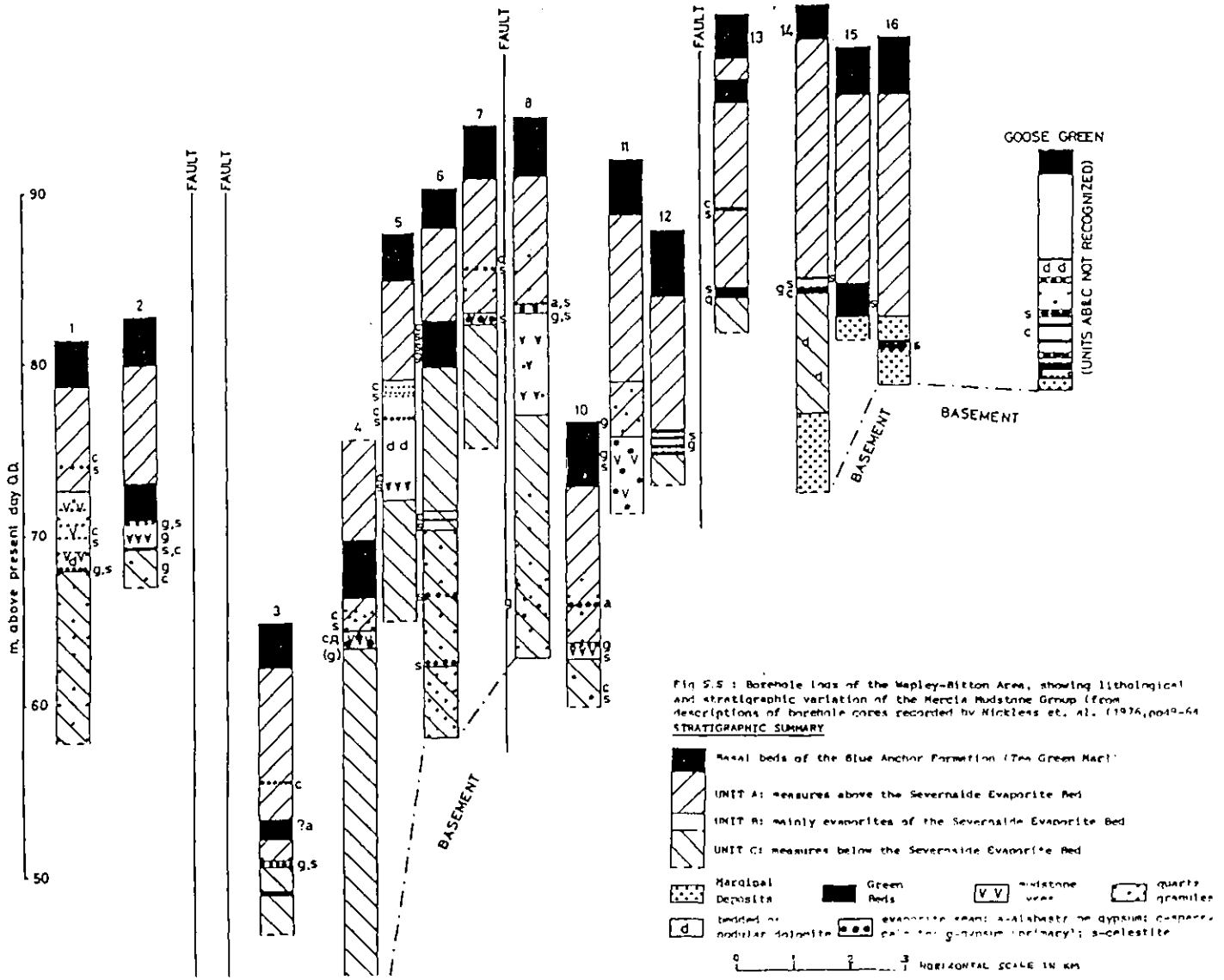

Fig 5.5 : Borehole logs of the Wapley-Bitton Area, showing lithological and stratigraphic variation of the Mercia Mudstone Group (from descriptions of borehole cores recorded by Nickless et. al. (1976,p049-64

in the logs of the Wapley-Bitton area (Fig. 5.5) although the situation is here complicated by the presence of primary lozenge gypsum and difficulties were encountered in interpreting Nickless et al.'s (1976) core descriptions.

The presence of alternate secondary gypsum and celestite beds in the stratigraphic column is unequivocal evidence for a syngenetic-early diagenetic origin for the celestite, ruling out any possibility of a major post-burial mineralization.

5.2.1.2 Early Diagenesis

Stages A, B and C (Fig 5.2) represent early diagenetic processes taking place in the sabkha sediment. The different textures in the celestites resulted from the replacement of each calcium sulphate type. Lozenge gypsum, indicating a low supratidal-intertidal environment (eg. Shearman, 1966) was replaced by G4 celestite or lozenge quartz. The gypsum was dehydrated as it passed into the supratidal zone through the accretion of the sabkha (Kirsman, 1969a) and irregular nodular masses or macrocells of secondary anhydrite began to form (West, 1965, Holliday and Shephard-Thorn, 1974). The macrocell fabric was pseudomorphed by the celestite. 'Replacement' was by a dissolution/precipitation mechanism (3.1.2.2). 'Net-texture' resulted where the shapes of individual gypsum grains was preserved. Evidence for 'primary' anhydrite is scarce (3.1.6.2), and criteria for primary anhydrite (Shearman, 1966) such as chickenwire-texture can have other interpretations (Holliday and Shephard-Thorn, 1974). Enterolithic folds, also indicative of primary anhydrite (Shearman, 1966), are absent in the Avon celestites but occur in anhydrite in green mudstone in the Stowell Park borehole (Fig. 1.8) where they are contrasted with bands and patches of possible secondary anhydrite in red marl (Green and Melville, 1956). It is therefore possible that some of the celestite in the green beds may be after primary anhydrite.

5.2.1.3 Origin of the Red Celestite

The two red celestite fabrics; light red macrocellular and reddish brown impregnations, are statistically significant varieties (4.3.2.2.c). The colour distribution

suggests a relict texture (2.4.3.5), in the case of the red macrocells, a recrystallization fabric (3.1.2.2).

a Light red macrocellular celestite.

The following observations indicate that the light red macrocellular celestite resulted from the recrystallization of celestite that had replaced gypsum (Fig. 5.2).

1) Unlike anhydrite and celestite, gypsum is monoclinic and replacement of gypsum by celestite may favour recrystallization.

2) Although most of the light red macrocellular celestite is tabular (subtype P2), some is of the granular G4 subtype (Table 3.3).

3) Similar celestites from Tortwood Copse, examined by Nickless et al. (1976), contained gypsum relics.

4) The zonal distribution of this variety (Fig. 4.11) suggests a primary mineralogical control as there is no other reason why only some of the celestite in the seam should recrystallize.

The light red macrocellular celestite may be a recrystallization product of more than one stage of the diagenesis and so must be interpreted cautiously. In addition, many workers (eg. Shearman, 1966; Kinsman, 1969; Glennie and Evans, 1976) record a second type of primary gypsum forming nodules, masses or sand crystals in the supratidal environment of modern sabkhas. The allocation of the red macrocellular celestite to Stage A (Fig. 5.2) is based upon the observation that this is the predominant type in 'extra' celestite seams at the Poundhouse Farm site and in other horizons in the Wapley-Bitton logs (Fig. 5.5, boreholes 4 and 6), and that it usually occurs with sparry calcite (2.4.3.2), the recrystallization product of limestones which formed (2.4.1.2) in green mudstone below wave-base (see below).

b Reddish brown impregnations of celestite.

Although it is difficult to match thin-section observations with hand specimens of the impregnations of red celestite, it can be asserted that celestite-with-anhydrite is generally white whereas anhydrite-free celestite may be either red or white. Hence it may be reasoned that the red impregnations also reflect a gypsum

precursor (Fig. 5.2) and the white impregnations, celestite in which anhydrite has been completely replaced. Supplementary evidence is provided by the S6 celestite microfabric of this variety, which shows evidence for recrystallization (Plate 49).

It is suggested that the reddish brown impregnations formed by the replacement of granular macrocellular gypsum at Stage D (Fig. 5.2). The gypsum porphyroblasts now appear as reddish brown coloured centres in the impregnating fabric, the myriad shapes and forms of the porphyroblasts (Holliday, 1970) and local recrystallization producing a plethora of textures (2.4.5). An early diagenetic origin for this gypsum was proposed by Holliday (1970) and it is suggested that this gypsum represents the selenite crystals forming at the present day from the hydration of anhydrite by continental flooding in the landward side of the Persian Gulf sabkhas (Shearman, 1966).

c Cause of the pigmentation.

It may be argued that the red colour of these celestites is due to differences in composition. Microprobe analyses of the principal minor elements, Ba and Ca, show no correlation with the colour of the celestites (Table 3.3) but it is possible that the red colour is produced by variations in magnitude of an unidentified trace component below 0.1%weight. Friend and Allchin (1944) detected 85ppm Au in reddish brown Yate celestite and 30-55ppm Au in other blue English celestites and attributed both colours to differential scattering of light by colloidal gold. Only traces of iron were recorded. Berstein (1979) later showed that the blue colour of celestite was due to absorption by orbital transition within monovalent radicals, stabilized by traces of K^+ substituting for Sr^{2+}, but ignored the English celestites. Berstein (op. cit.) also argued that the colour of certain 'orange' celestites was produced by up to 50ppm of copper (as Cu^+). As a high K content is a feature of all celestites with a marl or mudstone component (4.3.2.5), much of which is blue (Fig. 4.8), Berstein's conclusions can be affirmed for blue celestite. This also indicates that red (and white)

celestite did not grow directly in marl but in an earlier authigenic phase; ie. anhydrite or gypsum. Furthermore, because Friend and Allchin (1944) did not detect transition elements such as Cu, Mn or Zn in the Yate celestites it seems logical to ascribe the red colour to a deficiency of potassium caused by textural effects rather than as a direct compositional effect.

5.2.1.4 Late Diagenesis

The predominance of the granular macrocellular fabric in the Aust and Michaelwood gypsum indicates that most of the anhydrite was hydrated at Stage D. The remainder of the gypsum was converted to alabastrine gypsum at Stage E. West (1964, 1965) and Holliday (1970) consider this to be a late diagenetic event (Fig. 5.2).

5.2.2 Problems in the Diagenetic Framework, and 'Quaternary' Celestites

There are two main difficulties with the diagenetic history outlined above. First, Nickless et al. (1976) reported celestite replacing alabastrine gypsum in the Wapley-Bitton area. Now it is possible that this celestite represents the minor quantity formed during the hydration of anhydrite, as observed in the Yate Bypass gypsum (4.4.3). Alternatively Nickless et al. (1976) may have misinterpreted a drusey macrocellular celestite fabric, surrounding, but not replacing, a gypsum core. However, if the observations are correctly reported, the gypsum must be early diagenetic, as is the celestite. The G4 celestite fabric would then be re-interpreted as a relict fabric of a recrystallized alabastrine gypsum rather than a primary gypsum; the interpretation of the P2 subtype would also fall under suspicion.

The second difficulty lies in the interpretation of the satin spar gypsum (2.4.5). Although there is much debate over the origin of satin spar veins (Shearman et al., 1973) most workers favour a post-consolidation origin during deep burial (Shearman et al., 1972; Holliday, 1978). However, fibrous Type A celestite pseudomorphs satin spar gypsum at Awkley (Fig. 5.3) (Nickless et al., 1976). Fibrous anhydrite is also known to occur (Green and Melville,

1956) and Nickless et al.'s (1976) interpretation may be in error. Alternatively, the celestite may be a primary vein deposit.

Both anomalies may be explained in two ways:-

1) The two varieties of secondary gypsum described are early-diagenetic forms. Current understanding of secondary gypsum formation would then require drastic revision.

2) Some celestite crystallized between Stages D and E. The possibility of a late diagenetic, Quaternary mineralization has been noted earlier, in regard to the Yate Bypass gravels (2.5.1.4). However, these 'Type Q' celestites resemble other examples of epigenetic celestite both in hand specimen (2.5.2.6) and in thin section (3.2.2) and are classified with Type A celestites using factor analysis (4.3.2.4) and so must belong to the main mineralization. If this is the case, then the 'terrace gravels' of the Yate Bypass cutting must be marginal deposits of Triassic age (2.5.1.4), and not Quaternary deposits.

5.2.3 Conclusions

The evidence presented here suggests that, on the whole, both the celestite and gypsum parageneses are consistent with an early diagenetic origin for the celestite, contemporary with the initial stages of secondary gypsum formation. Difficulties remain in the interpretation of late diagenetic events because of a lack of information on the calcium sulphates and the Quaternary geology of the area under review.

5.3 DEPOSITIONAL ENVIRONMENT OF THE CELESTITES

5.3.1 Introduction

Textures such as arcuate druses, funnel-shaped celestites showing slumping (2.4.3), giant flat-lying crystals dusted with dolomite (2.4.4) and geopetal fabric in framework celestite (3.1.5.4) have been mentioned earlier as evidence for near-surface growth of the celestite in a soft unconsolidated matrix. However, as fabrics indicating a subaerial environment such as chickenwire texture,

evaporite 'crusts' and erosion surfaces (2.4.3) may be relic fabrics of the earlier calcium sulphate phases a subaerial origin cannot be applied with certainty to the celestites. Evidence for calcretes is also lacking (2.4.1.2).

Most of the celestites occur in green or mottled beds (Fig. 2.3) indicating a saline a queous environment (2.4.1.2.a). It may therefore be argued that celestite crystallization followed marine inundation. This would be either directly at the water-sediment interface or in the phraetic zone of a recently flooded sabkha. The supporting evidence for this argument is:-

a) The exposure textures listed above mainly occur in more poorly developed celestites in red marls of the blocky mudstone facies, for which a possible subaerial origin is implied (2.4.1.2.a).

b) Celestite crystals pre-date the slumping in the funnel-shaped celestites (2.4.3.4) for which a possible subtidal origin may be reasonably applied.

c) A suba queous origin may be implied for the primary celestite precipitate (subtype P1) (3.1.2.2.b).

High evaporation rates leading to vadose precipitation would not be necessary if the milieu contained a sufficiently high concentration of Sr^{2+} ions. Processes which may have enhanced the Sr content are considered in detail in 5.4.

It is emphasized that continental flooding, although linked with transgressive events, was not directly responsible for the crystallization of the celestite for the epigenetic celestites would then be distributed over all of the pediment and this is not the case (see 2.2.1).

Therefore on this evidence alone, a two-stage origin may be proposed for the Type A celestites:-

1) Subaerial growth of calcium sulphate minerals in the sabkha sediment.

2) Marine inundation, and crystallization of celestite. Most of the celestite in the sabkha sediment grew below the water-table level; some however grew upwards in the red sediment immediately below the surface. 'Primary' celestite (subtypes P1 and P3) formed where calcium sulphate minerals were locally not present.

A two-stage origin is also favoured from geochemical

considerations, for if high concentrations of Sr and Ca were to be simultaneously present in sea water containing sulphate ions, the common ion effect would favour the precipitation of celestite and inhibit the crystallization of gypsum/anhydrite. However, removal of the Ca at the gypsum stage of halokinesis would result in a remainder of sulphate ions which would react with a later influx of Sr to precipitate celestite.

The origin of the accumulations of celestite nodules (2.4.2) may now be considered. As similar gradations are observed in the subsurface Wapley-Bitton evaporites (Fig. 5.5, boreholes 10, 11 and 12) as described at outcrop at Poundhouse Farm, surface effects (eg. cryoturbation) cannot be responsible, and penecontemporaneous reworking by wave-action may be the agency producing the accumulations and variegation (Anon, 1960; Curtis, 1974). The sedimentary environment of the Norian celestites is summarized in Fig. 5.6.

5.3.2 Facies Analysis

The statistical analysis of the petrology, geochemistry and XRD determinations is summarized in Fig. 5.7. Several diachronous facies of distinctive mineralogy are recognized as follows:-

1) Sparry calcite/dolomite facies.

2) A possible lozenge gypsum-celestite facies now represented by light red macrocellular celestite (see 5.2.3).

3) An anhydrite-celestite facies represented by drusey macrocells.

The last two facies may be immediately recognised as diagnostic of intertidal-low supratidal and supratidal environments respectively (5.2.3).

The sparry calcite/dolomite facies includes nodular limestones and represents an intertidal-subtidal environment (2.4.1.2.b). Fig. 5.7 suggests that although the aphanitic calcite precursor (3.1.3) is common to many lithologies of the Yate Formation it was primarily concentrated in the neretic sediments. This relationship is lost on a regional scale where the distribution of the precursor of the sparry calcite can be related to specific events in the erosion of the Carboniferous Limestone floor

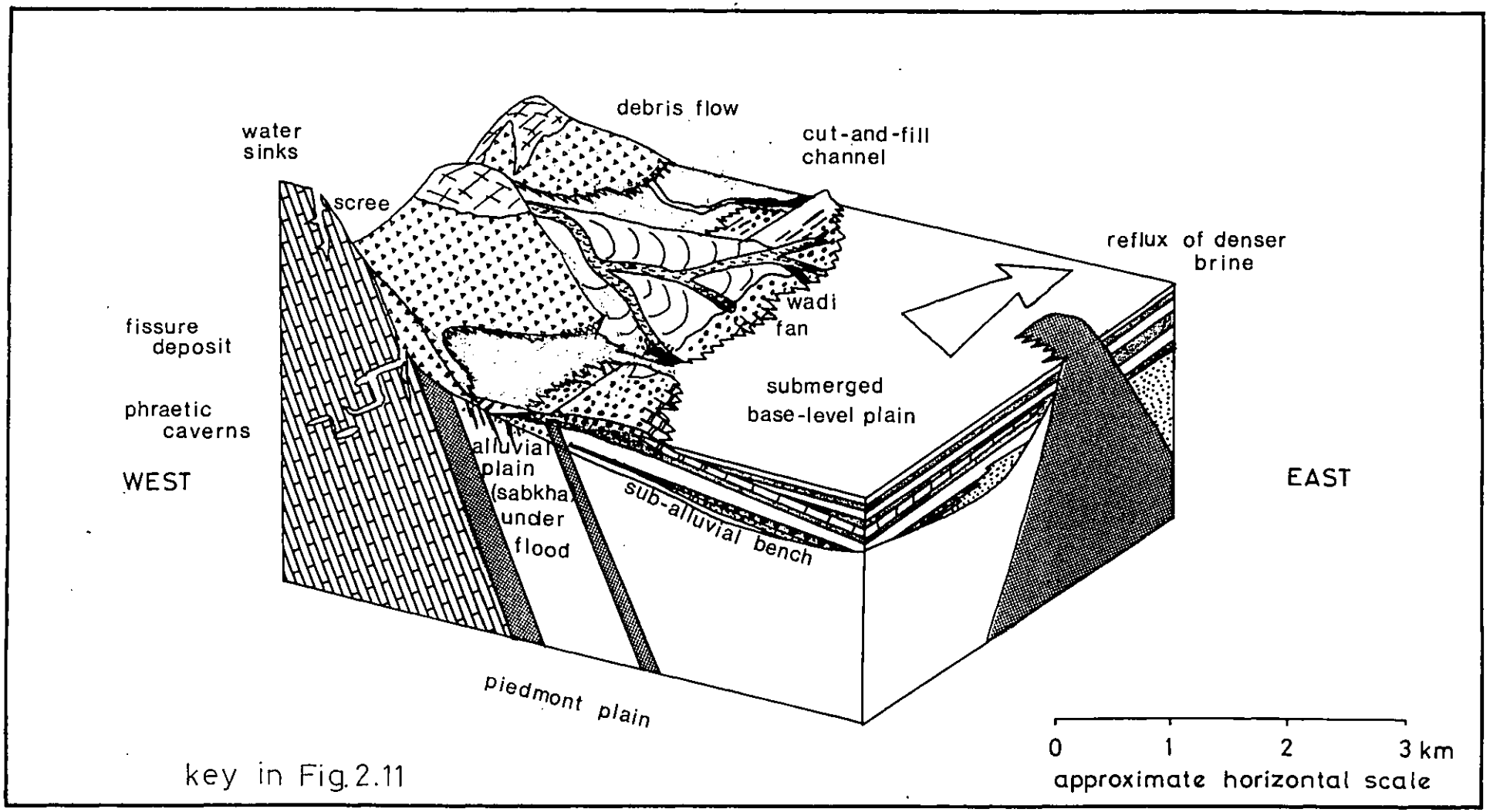

Fig 5.6: Sedimentary environments of the Norian celestites

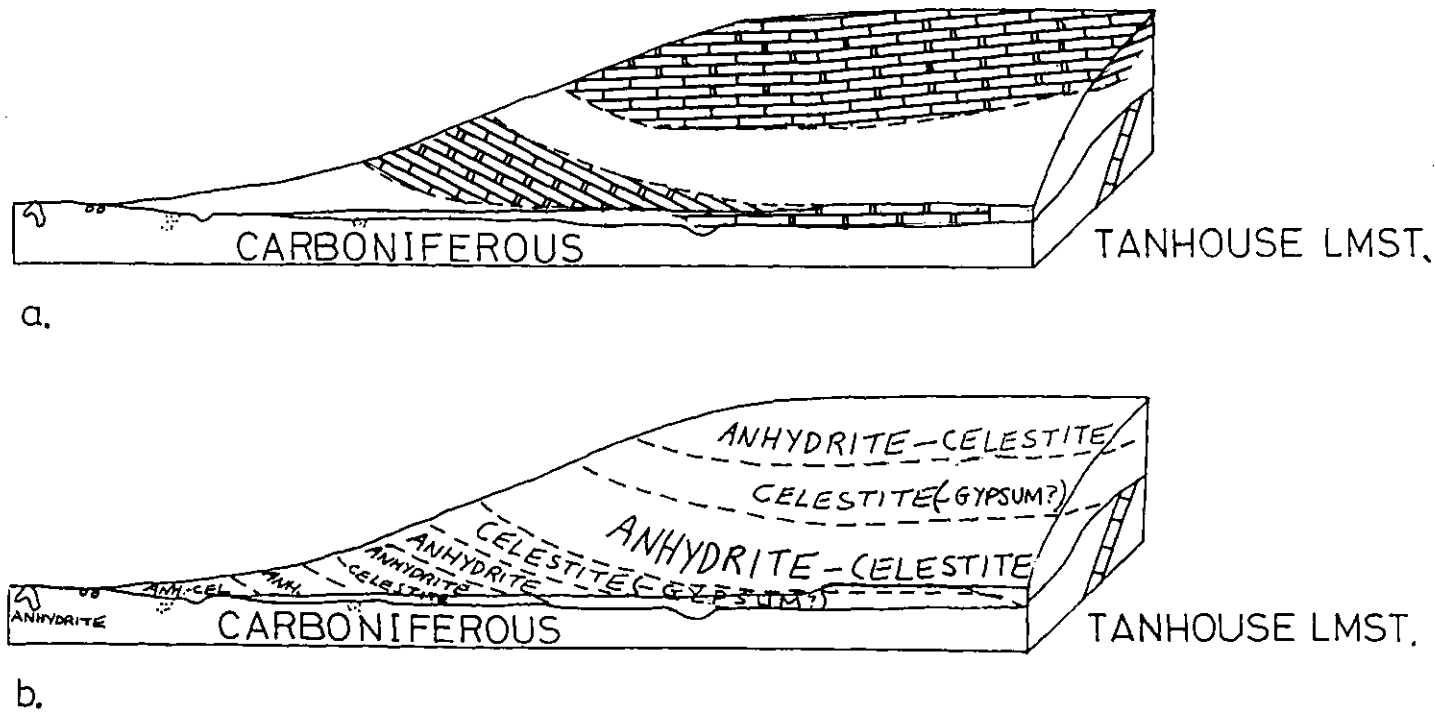

Fig 5.7: Facies of the Yate Formation at Goose Green.
Generalized from Figs 4.10,4.11,4.17. a- sparry calcite/dolomite facies; b-sulphate minerals (including other suggested phases in parentheses)

(Table 5.1). Only the aphanitic calcite of the Perrinpit Farm celestites appear to have been a pure chemical precipitate, as the nearest limestone hills are over 3.5km to the west (Fig. 2.12). Another factor aiding deposition may have been the Pennant Sandstones of the Paleozoic floor, near which high pH silicic groundwaters precipitated calcium carbonate at enhanced rates (Fig. 5.4).

5.3.3 Sedimentary History of the Yate Bypass Celestites

The Yate Bypass - Goose Green area may be thought of as a microcosm of the Yate platform. A paleographical reconstruction (Cave, 1977) (Fig. 5.8) indicates that the area consisted of two narrow cuvettes separated by a ridge of Paleozoic rocks, now containing Type C celestites (Fig. 2.2). The western depression contains Triassic marginal deposits and gravels of uncertain age (Fig. 2.2). The marginal deposits are interpreted as the sediments of a northward-flowing Triassic river (the 'proto-Frome'). Evidence for such a river is provided by the present-day course of the Frome Near Nibley (Fig. 1.9) where the river leaves the course of its Triassic predecessor (Fig. 5.8) and swings round through 90 degrees cutting a gorge through Pennant Sandstones, which formed a central area of high ground in Triassic times (Nickless et al., 1976, Fig. 13). The eastern depression contains over 8m of Yate Formation sediments and celestites, overlying a buried 'cut-and-fill' channel. The Goose Green succession (Fig. 2.3) is complex, and records an uneasy equilibrium between sedimentation and flooding in the eastern enclave. Dolomites possibly provide evidence for rapidly changing salinities in a schizohaline environment (3.1.4). Each green bed records a marine incursion, followed in eight cases by the crystallization of celestite. Each event was quickly followed by a resumption of continental deposition, so that desiccation cracks were not formed (2.4.1.2.a, 2.4.2.5).

The celestite seams may be grouped into two cyclic units or cyclothems; seams A to D and E to H, each consisting of thicker evaporite beds in 'laminated mudstone facies' type marls passing up through flame structures into thinner seams in 'blocky mudstone facies' sediments

Locality or district	Event
Southern part of the Wapley-Bitton area (Fig 5.4)	Erosion of the Clifton Down Limestone of the Wick inlier
Wapley Common/ Sergeant's Farm	Erosion of the Tanhouse Limestone at Yate
Yate Bypass/ Tyler's Farm	Erosion of Hotwells Limestone 200m east
Talbot's End	Erosion of Hotwells Limestone and Clifton Down Limestone at Talbot's End
Itchington	Erosion of Hotwells Limestone north of Itchington
Poundhouse Farm/ Tortworth Copse	? Erosion of the Wenlock Limestone of the Little Avon Platform

Table 5.1: Correlation of the calcitic celestites of the study area and Wapley-Bitton area with contemporary shore-line events

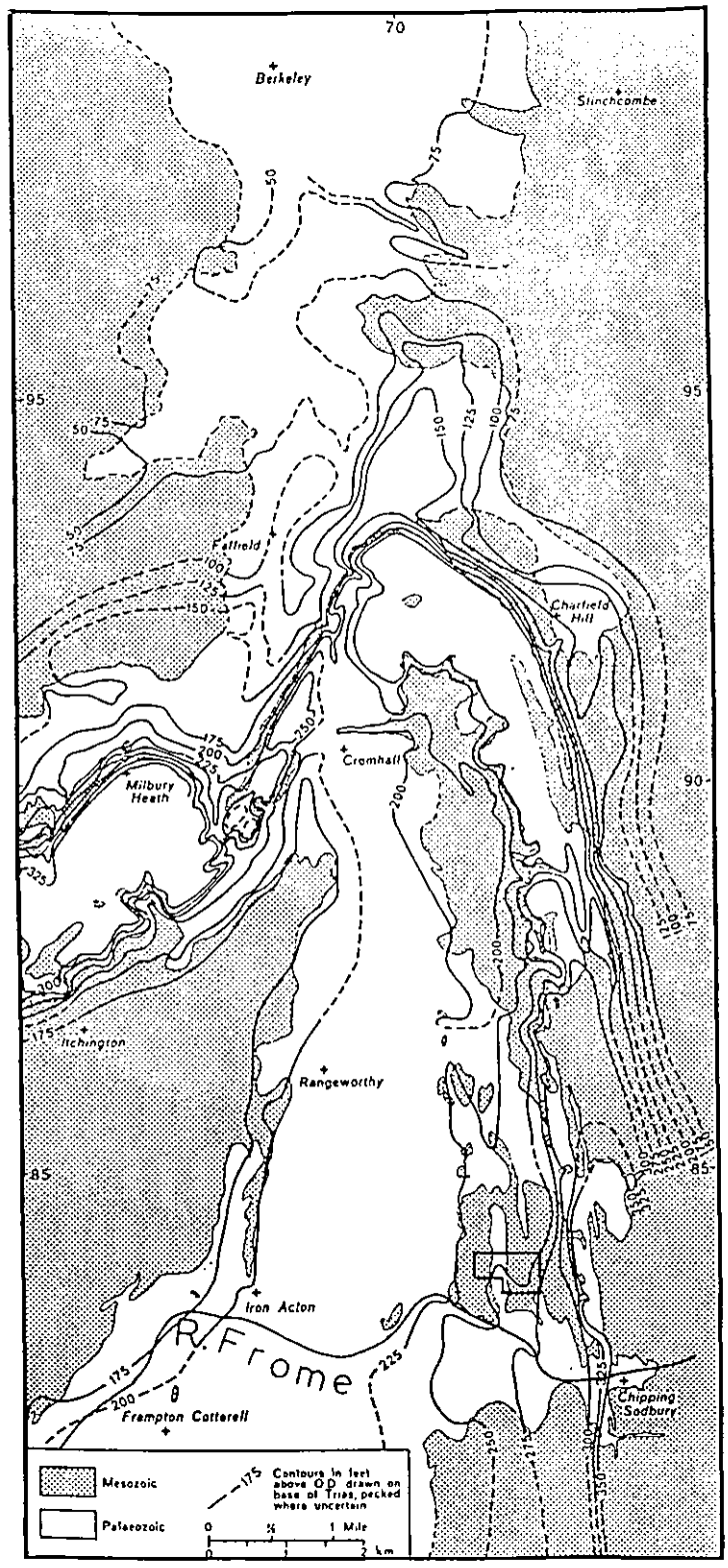

Fig 5.8: Map showing contours drawn on the sub-Triassic surface (from Cave,1977). The Yate Bypass-Goose Green area is boxed. Present-day course of the Frome super--imposed.

(2.4.1.2.a). These cyclothems, however, differ from other published examples (eg. Wills, 1976; Arthupton, 1980) in that the thickest evaporite concentrations occur near the base of the cycle. Using the two cyclothems as a framework, the sedimentary history of the area can be broadly outlined in six stages, as follows (Fig. 5.9):-

a) Deposition of coastal sabkha deposits in eastern cuvette. The proto-Frome flows in a wadi fan and channel. In the southern depression anhydrite deposits form close to the intervening ridge (2.4.1).

b) Marine incursion. Quartz grains, siltstones and sandy marls indicate that continental flooding may have been influential (2.4.1.2). Some anhydrite hydrated to granular macrocellular gypsum. Celestite crystallizes in seams A and B, and as epigenetic deposits in the western enclave (NB. in this case 'down-pediment' of the Type A celestite). The eastern channel is mineralized also.

c) Regression, formation of minor seams (C and D) and dolomitization of earlier seams and marginal deposits.

d) Return of continental conditions. ? Cobble gravel deposited.

e) Marine incursion as in (b). Celestite forms in seams E and F in green sediments. Mudstones laid down in western cuvette.

f) Regression, formation of thin celestite horizons (G and H) and predominance of early diagenetic dolomite in intertidal mudflat up to Blue Anchor Formation times. ? Deposition of chert gravel in response to erosion of Tanhouse Cherts up-pediment (Fig. 2.2).

5.3.4 Sedimentary History of the Wapley Common Celestites

The quartz-rich Wapley Common celestites serve as a useful basis to discuss the diagenetic formation of the accessory minerals megaquartz and chert. The silicification of evaporites is not an uncommon phenomenon (see for example, West, 1964; Mukhergin, 1969; Folk and Pittman, 1971; Siedlecka, 1972; Chowns and Elkins, 1974; Young, 1979). In the study area silica is restricted to the Itchington-Moorleaze and Wapley Common districts (Fig. 2.12) and also occurs in the south of the Wapley-Bitton area

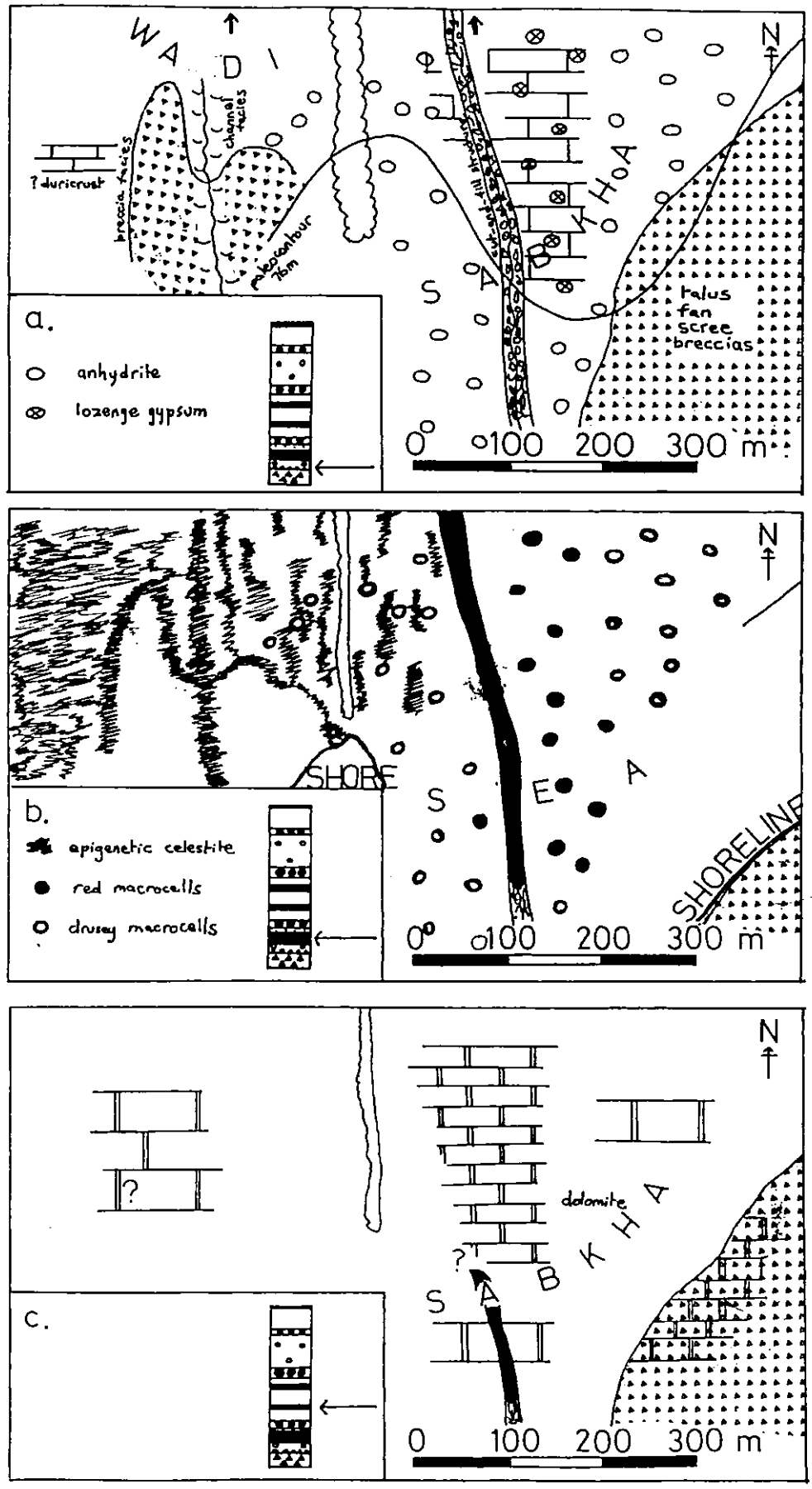

Fig 5.9: Reconstruction of the sedimentary history of the Yate Bypass area.

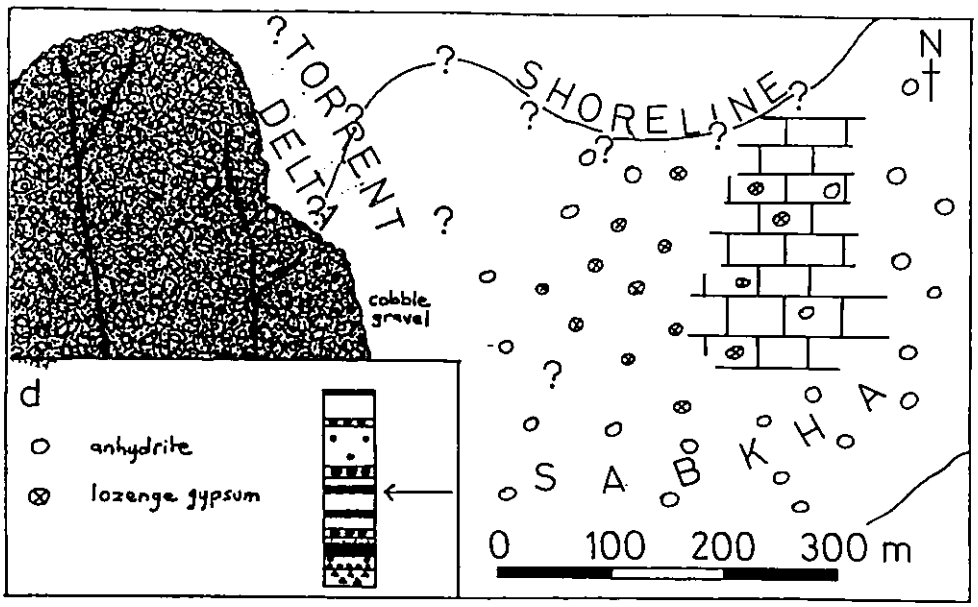
TORRENT DELTA
SHORELINE
N
cobble gravel
d
anhydrite
lozenge gypsum
SABKHA
0 100 200 300 m

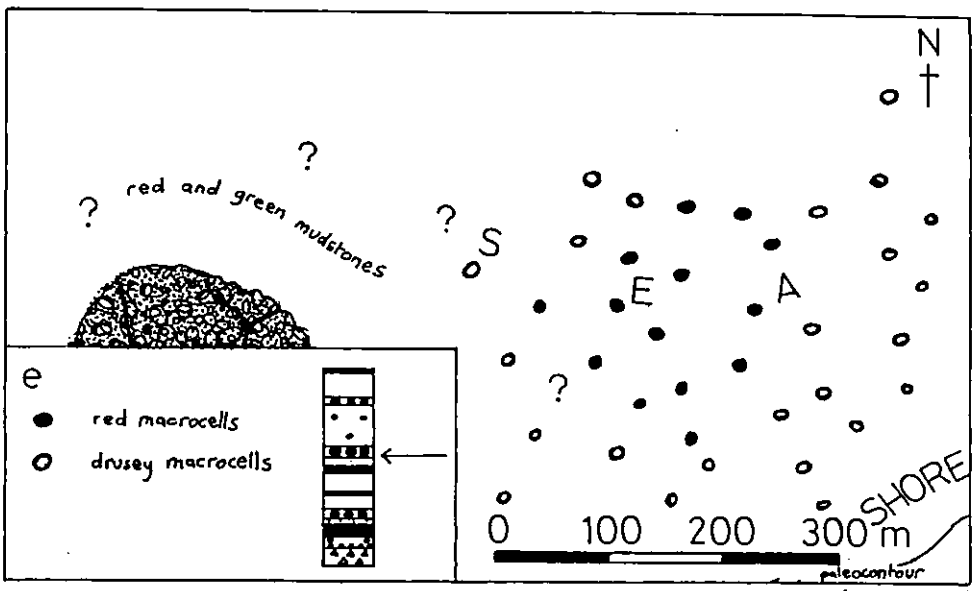
N
red and green mudstones
SEA
e
red macrocells
drusey macrocells
SHORE
0 100 200 300 m
paleocontour

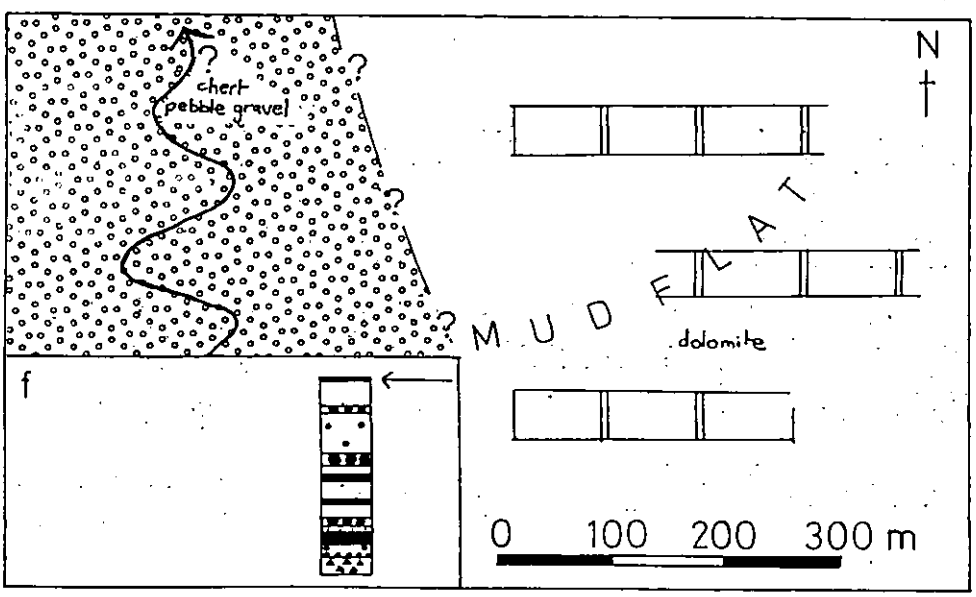
N
chert pebble gravel
MUD FLAT
dolomite
f
0 100 200 300 m

(Fig. 5.4), however at each locality it can form the major component of the evaporite, due in part to a low level of Sr mineralization, and an input of silica is required to explain the quantities present.

5.3.4.1 Source of the Silica

A syndepositional origin is indicated by the fabrics described in 2.4.2.4 and 3.1.5.

The quartz-rich celestites differ from modern silcretes in that they formed at the sabkha surface rather than at depth below a calcrete; differences also occur in mineralogy and texture (eg. Watts, 1980). There is no evidence for a hydrothermal origin as proposed by Curtis (1974).

The quartz-rich celestites all formed in Triassic sabkha sediments at the same stratigraphic height as major Carboniferous mudrock/quartzite contacts on the pediment slope (Figs. 1.5, 5.4), and it seems logical to attribute the source of the silica to Si-rich brines produced from the chemical weathering of the quartzites and concentrated at these localities. Small lagoons of high pH brines may also have probably developed over the Carboniferous rocks. As the Norian transgression reached these higher levels the pH of the brines was lowered by mixing with the less alkaline groundwaters and possibly even sulphuric acid in the immediate vicinity of the sulphate minerals. A gelatinous silica precursor was precipitated, similar to that forming today in modern carbonate lake sediments (Peterson and Von der Borch, 1965). Alternatively, continental flooding may have flushed the Si-rich brines down on to the sabkha, dissolving anhydrite leaving ovate voids (Plate 21) and precipitating silica.

5.3.4.2 The Wapley Common Celestites

The diagenetic history of the Wapley Common celestites is summarized in Fig. 5.10. This shows the mineralogy of the sabkha sediment in the emergent phase between the two celestite/flood episodes. Interaction of three dynamic processes; accretion, submergence (and celestite mineralization) and silicification produced two silica

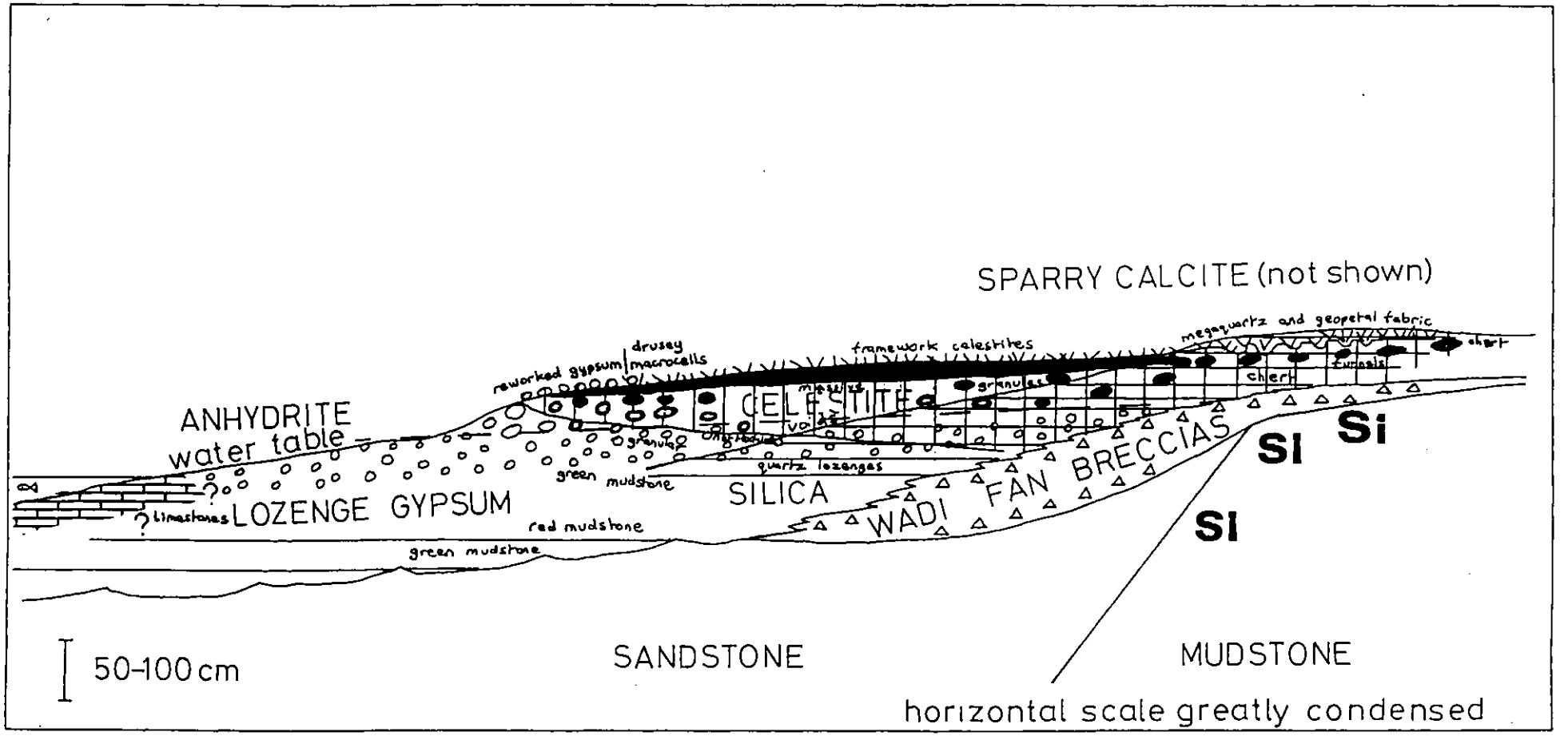

Fig 5.10: Reconstruction of the early diagenetic history of the Wapley Common quartz-rich celestites

stages in the paragenesis (Fig. 3.1). Silicification was preserved as the Carboniferous contact was overstepped and more usual Yate Formation sediments were deposited.

5.3.5 The Sedimentary History of the Celestites of the Study Area and Wapley-Bitton Area

The geology of the region during an acme of celestite formation in Severnside Evaporite Bed times is summarized in Figs. 5.6 and 5.11. At this stage most of the land had sunk beneath the Norian Sea. Eustatic changes and climatic effects of regional scale (Fig. 1.8) produced fluctuating episodes of extreme aridity and slow sedimentation, and flooding, resulting in microcyclothems of colour, textural and compositional layering in the Yate Formation. Nodular celestites (Type A celestites) crystallized out in the water-laden sabkha sediment during or following marine incursion, often replacing nodular anhydrite. In certain areas, on the outlying platforms and in topographic lows in the Wapley-Bitton area (Figs. 5.4, 5.5) celestite formed in lesser amounts and the anhydrite persisted, to be later replaced by secondary gypsum. Epigenetic celestites crystallized out in the marginal deposits and in fractures in the Paleozoic bedrock. Accessory minerals, mainly sparry calcite and authigenic silica also grew locally in the sabkha sediment.

5.4 SOURCE OF THE STRONTIUM

Possible models for the origin of the strontium in the celestites can be divided into those involving sedimentological processes taking place in the Triassic sedimentary environment and others involving an input of strontium from older rocks or mineralizing fluids. Many of the theories in the second group emphasize the difference in Sr content between aragonite (8,000ppm Sr), dolomite (200-600ppm Sr) and calcite (400ppm Sr) (Kinsman, 1969b). All must account for the fact that the mineralization is only a Sr-metasomatism (4.5.2).

5.4.1 Triassic Origin

Minor amounts of the celestite are undoubtedly

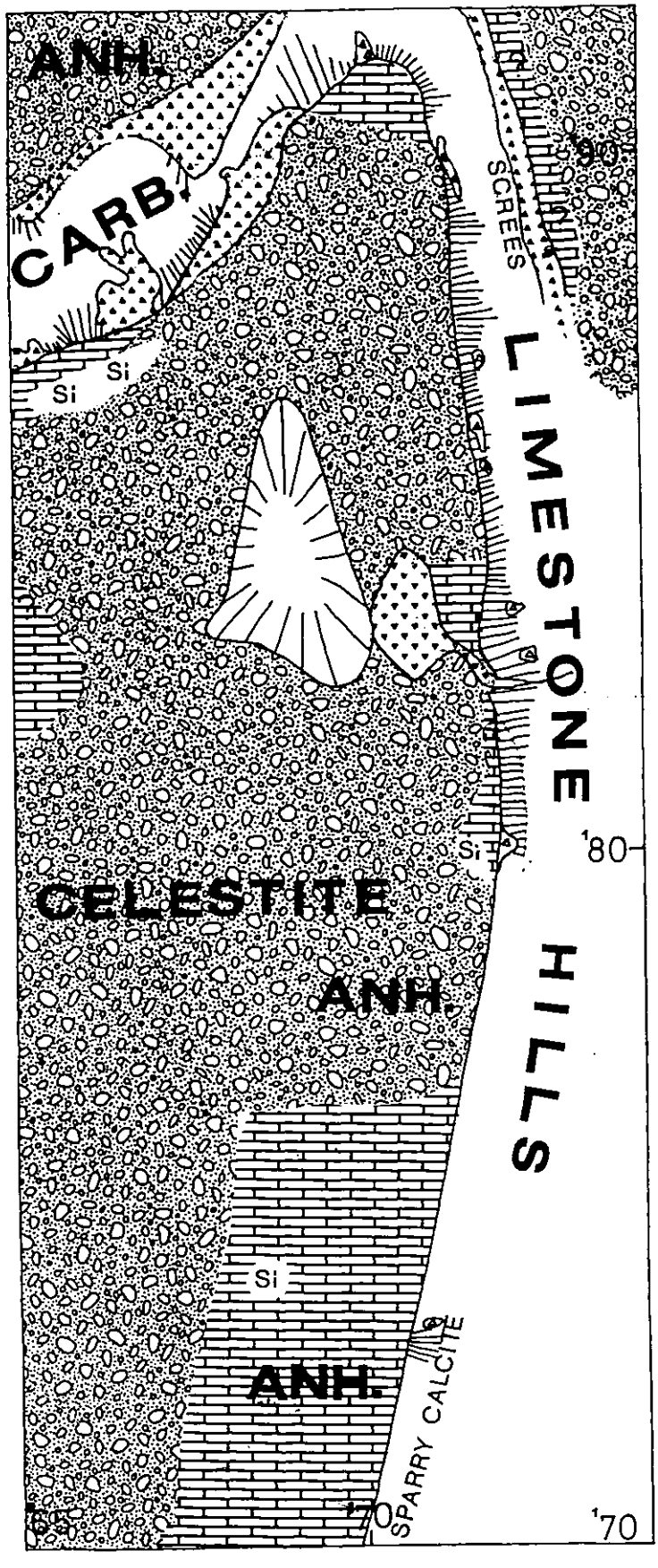

Fig 5.11: The study area and Wapley-Bitton area in Severnside Evaporite times

authigenic precipitates. Such celestite is forming today in the Persian Gulf and Californian coastal sabkhas from dolomitization reactions in the carbonate substrate (Evans and Shearman, 1964; Kinsman, 1969a).

Trace amounts of authigenic celestite are ubiquitous components of ancient sulphate-carbonate associations such as the Zechstein (Burkov, 1977) and the 'baryto-celestine' recorded throughout England in the calcareous members of the Blue Anchor and Lilstock Formations (Thomas, 1973) is probably of similar origin. In the case of the Lilstock Formation celestites a syngenetic origin involving simple fractionation by precipitation from sea-water would result in a celestite/baryte mixture (see Renault and Brower, 1971) rather than the barian celestite, as observed (4.5.3). In addition, at least some of the barian celestite of the Yate Formation is a second generation phase produced by the scavenging of Ba^{2+} ions (3.1.2.3). The evidence for an authigenic origin is:-

1) Lack of correlation of Ba with Zn, calcite or dolomite precludes an epigenetic origin (4.5.3, 4.5.5).

2) Some barian celestite was formed from a recrystallizing purer celestite of the P2 subtype (see 3.1.2.2). In other cases the barian composition is a reflection of the enriched Ba content of the sedimentary environment, for example nearby baryte deposits at Yate Bypass (Figs. 2.2, 4.14) and sanidine-rich detritus at Summer Bridge (2.5.1.3) (Wedepohl (1978) quotes up to 1.8% Ba in K feldspars.)

As the reaction:-

$$SrCO_3 + CaSO_4 \longrightarrow SrSO_4 + CaCO_3$$

has a negative Gibb's free energy value it is unlikely that the celestite/calcite assemblage of the Type A celestites had formed by the diagenetic reaction of strontianite with anhydrite. Furthermore, strontianite is not recorded in the celestites and the sparry calcite is of neomorphic origin (3.1.3.2).

Minor amounts of aphanitic celestite occur in modern carbonate sediments in South Australian lagoons (Skinner, 1963). Baker (1902) proposed that the Avon celestites

had directly precipitated from seawater. Many workers (eg. Collins, 1975; Burkov, 1977) state that celestite precipitates at the gypsum stage of halokinesis. However, as the Type A celestites clearly crystallized after the calcium sulphates a primary chemical precipitate from seawater cannot explain the quantities of celestite observed. Furthermore, isotope work by Wood and Shaw (1976) does not favour a marine source for the Sr. Wood and Shaw's (1976) isotope data also clearly differentiated Norian celestites from Lilstock Formation barian celestites for which an authigenic origin, possibly involving connate brines, has been proposed earlier.

Recent results of Sr and O isotope work carried out at the Scottish Universities' Research and Reactor Centre on quartz-celestite nodules from Dulcote Quarry, Somerset (Jocelyn and Harman, unpublished results) indicate that non-marine Sr may have combined with marine sulphate ions to precipitate celestite. Furthermore, a single $\delta^{34}S$ value of +16.7‰ for Yate celestite is consistent with a marine sulphate of Permo-Triassic age (H.F. Shaw, personal communication).

5.4.2 Carboniferous Limestone Source

Sherlock and Hollingworth (1938) proposed that a river containing strontium ions flowing into an inland sea near Yate caused the precipitation of celestite by interaction with the calcium sulphate-saturated seawater. Although Sherlock and Hollingworth (op. cit.) did not mention the source of the Sr it is implied that this was considered to be the Carboniferous Limestone hinterland.

Thomas (1973) and Nickless et al. (1975) suggested that the Sr was derived from the inversion of aragonite in the limestone. The Clifton Down Limestone and Mudstone, the Gully Oolite and the Hotwells Limestone of the Chipping Sodbury area are lagoonal-type limestones (Murray and Wright, 1971), particularly rich in what were once aragonitic sediments and faunas (see for example, Bathurst, 1971, p.262).

Wood and Shaw (1976) suggested that the dolomitization of the Carboniferous Limestone may have supplied the large quantities of Sr in the celestites. Although Wood

and Shaw (op.cit.) provided isotope data to show that the Sr was modified by percolation through the Triassic and Coal Measures sediments an early diagenetic origin was still implied. However, only two formations of the Carboniferous Limestone in Avon contain dolomite; the Clifton Down Mudstone and Black Rock Dolomite. Furthermore, the dolomitization must have been early diagenetic, for aragonite could not have persisted in the sediments up to Triassic times. Also, the Triassic dolomitization in the Mendip Valleys was "patchy in occurrence and of limited lateral extent" (Green and Welch, 1965). A similar phenomenon in the study area is unlikely to have released Sr^{2+} in the quantities required.

Paleogeographical evidence suggests a genetic link between the Type A celestites and the Carboniferous Limestone floor (Fig. 2.2). At the time that the Type A celestites were being deposited the Norian waters came into contact with Hotwells Limestone Wallrock. Also, most of the secondary gypsum deposits can be correlated with a non-limestone Paleozoic shore. Additional evidence is provided by the course of the proto-Frome (Fig. 5.8) which would have drained a Carboniferous Limestone hinterland at this time, thus confirming Sherlock and Hollingworth's (1938) hypothesis.

5.4.3 Magmatic or Hydrothermal Source

There are no known igneous massifs in the area north-east of Bristol and a magmatogenic, hypothermal or volcanogenic source for the Sr (Burkov, 1977) may be dismissed. There is no evidence whatsoever for a hot springs origin for the Sr (Baker, 1902) and the present hydrothermal activity in the Bristol area involves meteoric waters (Edmonds, 1981).

Sr is a minor component of some epithermal-mesothermal deposits (Burkov, 1977) and occurs as strontianite in the U.K. with Pb-Zn-Ba deposits at Strontian, Scotland and in the North Pennine orefield (Thomas, 1973). Various workers (eg. Kellaway, 1967; Thomas, 1973; Campain, 1981) have tried to relate the celestite deposits with the Mendip Pb-Zn-Ba-Ca-Fe mineralization north of Bristol on the basis of stratigraphic agreement of the two mineral

occurrences and on 'Triassic' Pb-isotope dates for galenas from both Carboniferous and Jurassic host-rocks (Moorbath, 1962). Although some connection is possible, a hydrothermal source for the Sr can be dismissed for the following reasons:-

1. The nearest mineralized occurrence to the celestites is the fissure-filling in Carboniferous Limestone at Chipping Sodbury (724832) regarded by Curtis (1981) as post-middle Jurassic in age.

2. The epigenetic calcite rock-sulphide mineralization post-dates the celestite (Fig. 3.1) and unlike the celestite is localized in occurrence.

There is no evidence to substantiate Thomas' (1973) claim that a zoning of celestite with decreasing amounts of baryte occurs away from hydrothermal 'emanating centres'. The Ba distribution is randomly distributed across the study area (Figs. 4.15, 4.16); also Ba is not strongly correlated with either Sr or Zn (4.5.3).

3. At least some of the sulphide mineralization is a high temperature phase (3.1.6.4) indicating subsurface deposition in an impervious Mesozoic 'blanket' (Green, 1956) rather than in a phraetic environment.

Although the East Midland epithermal-telethermal base metal mineralization is in a similar sedimentary setting to that of the Bristol area (Ford and King, 1968), baryte and not celestite occurs in the Triassic sediments. Workers investigating these deposits have no justification for genetically relating the authigenic celestites of the region with the base metal mineralization (eg. Ford and King, 1968).

5.4.4 Discussion

It can be concluded, that although a marine origin for the celestites is almost certain, an input of Sr was necessary to precipitate the celestite. The available evidence suggests that the Carboniferous Limestone was the source of the strontium. However, the aragonite/calcite inversion occurs in early diagenesis (eg. Bathurst, 1971) and the model of Nickless et al. (1975) does not satisfactorily explain how the Sr was retained in the limestone up to the Norian celestite event. Similarly, regarding

the dolomites, the Clifton Down Mudstone is probably a penecontemporaneous replacement of an aragonite mud, such as described by Illing, Wells and Taylor (1965) and the Black Rock Dolomite, if epigenetic, is pre-Hercynian (Green and Welch, 1965).

Thomas' (1973) model overcame the problem of the residence time of the strontium by incorporating the exsolved Sr^{2+} ions in strontianite and pore fluids. This was released, together with that from locally-recrystallized calcite as hydrothermal solutions passed through fissures in the Carboniferous Limestone. Objections to the leaching mechanism are:-

1) Strontianite is not recorded in the Carboniferous Limestone in the study area.

2) Celestite is not found in the Triassic cap-rocks in the North Pennine orefield, where the leaching mechanism was first demonstrated by Ineson (1969).

3) The celestite mineralization and Mendip hydrothermal mineralization were two separate events.

However, it is quite possible that pore fluids may have acted as reservoirs for the Sr^{2+} ions, for the limestones were conformably overlain by sediments of the Millstone Grit Series and were not subjected to episodes of emergence which would have flushed out the saline fluids. Sealed by silicified impervious cap-rocks, the connate brines were prevented from migrating and the Sr content of the fluids increased by further leaching of the limestone wallrock and minor epigenetic dolomitization (Collins, 1975) during deep burial. Modern formation waters are greatly enriched in strontium (Collins, 1975).

Some of the strontium-rich brines were undoubtedly lost as the limestones underwent orogenesis during the Hercynian earth movements. It may be argued that the Sr released during this time became trapped in deep basement structures and was subsequently introduced into the phraetic circulation at a later stage. However, apart from the localizing influence of the deeper fractures in the Carboniferous mudrocks in the north of the study area, there is no evidence for a structural control on the distribution of the celestites. The Iron Acton Fault is

the only major structural lineament of the area which may have acted as a conduit for the strontium. However, as the celestites at this locality are epigenetic with regard to the reconstituted Fault gouge-like sediments (2.5.1.3, 2.5.2.5, 4.3.2.4) such an explanation seems unlikely.

The desert weathering conditions which prevailed into late Triassic times (Kellaway and Welch, 1948) had little effect on the Carboniferous Limestones and the brines were not released into the hydrosphere. Chemical weathering was accelerated as the climate ameliorated in the Norian (Robinson, 1957), and a karst topography developed. Rivers such as the proto-Frome became established and an underground drainage network was developed (Fig. 2.11). Phraetic caverns with swirl holes and bedded waterlain sediments may be observed at Slickstones Quarry (704915) near Talbot's End (Robinson, 1957) and at Tytherington Quarry (660887). Additional evidence is provided by the Tortworth Gorge (Fig. 1.9), possibly the collapsed remnant of a Triassic cavern underlying the col in the paleographical map (Fig. 5.8).

Previous to the Norian advance the liberated strontium was dissipated and celestite was not formed. As the Norian seawaters encroached over the limestone wallrock, groundwaters and springs at the toes of the talusfans and ephemeral streams containing Sr^{2+} and HCO_3^- ions issued directly into the sea. During episodes of submergence the seawaters entered the sabkha hydrology, precipitating celestite by reaction with the SO_4^{2-}-rich brines (5.3.1) and replacing earlier evaporite minerals in the substrate. Meanwhile epigenetic celestites crystallized out where the Norian sea came into direct contact with Triassic marginal deposits and Millstone Grit sediments of the pediment floor. As the sea retreated again small brine pools accumulated near to quartzitic sandstone ridges, and Type C celestites were formed.

There is little present-day evidence for ancient groundwaters in the British Isles, most having been presumably recharged during the Pleistocene Ice Age.

However one possible analogue of the Avon Sr-bearing fluids may be the deep brines of the Wessex Basin, which are of Tertiary age and which were partially flushed out during the Alpine Orogeny (A. H. Bath, personal communication, 1982). Also Downing (1967) has postulated that the saline groundwaters of the Carboniferous Limestone of the East Midlands may be derived from connate brines.

Even allowing for a sequence of events as outlined above it is still difficult to envisage how Sr-rich brines would have remained in what is now the Avon district in quantities sufficient to form the celestites over a period as long as the 130 m.a. that radiometric dating techniques indicate as the time interval between the Lower Carboniferous and the Triassic.

5.5.5 Conclusions

The celestites were deposited in a marine environment as the influx of Sr^{2+} ions from the Carboniferous Limestone reacted with the sulphate in the Norian milieau. The Sr was released during the early diagenesis of the limestones. The problem of the residence time of the Sr in the limestone has not been satisfactorily explained.

CHAPTER SIX - MINING AND EXPLORATION GEOLOGY

The applied geology content of the project was restricted to four main areas of interest, as follows: -

1) Laboratory grain size distribution studies of the Clay Head matrix of the mumbler deposits and of the celestite sands and gravels.

2) Geochemical prospecting for celestite.

3) Geophysical prospecting for celestite.

4) A critique of the current methods of exploration and assessment.

6.1 THE GRAIN SIZE DISTRIBUTION OF CELESTITE

6.1.1 Introduction

The size distribution of celestite in the Clay Head, Type A celestite gravel and celestite sands was determined to provide information on the physical fractionation of the celestite within each type of deposit.

Samples chosen for analysis included: soils and Type A celestite gravels from Goose Green West (Fig. 6.1); Clay Head and soil from Winter's Field; celestite sands and gravels from Winter's Field and The Rectory; Stoney Head from The Rectory.

6.1.2 Method

Grain size analyses were carried out on the sand and gravel fractions of the samples using standard sieving techniques. A decantation method was used to split, and obtain samples of, the silt and clay fractions. Later in the analysis the Warman Cyclosizer (Kensall and McAdam, 1963) was applied to classify the silt-grade material of some of the samples.

The celestite content of the gravel and sand fractions was determined by point counting. Immersion media were employed in the petrographic examination of the fine sand fractions. Even so, celestite and quartz could not always be distinguised, due to heavy iron staining of the particles.

A standard heavy liquid centrifuging and freezing technique using tetrabromoethane (TBE, specific gravity $2.96cm^{-3}$) was used to separate the heavy mineral fraction (mainly celestite and opaque iron oxides) in the silt- and clay-grade material. The celestite content of each size class could then be determined by estimating, by point

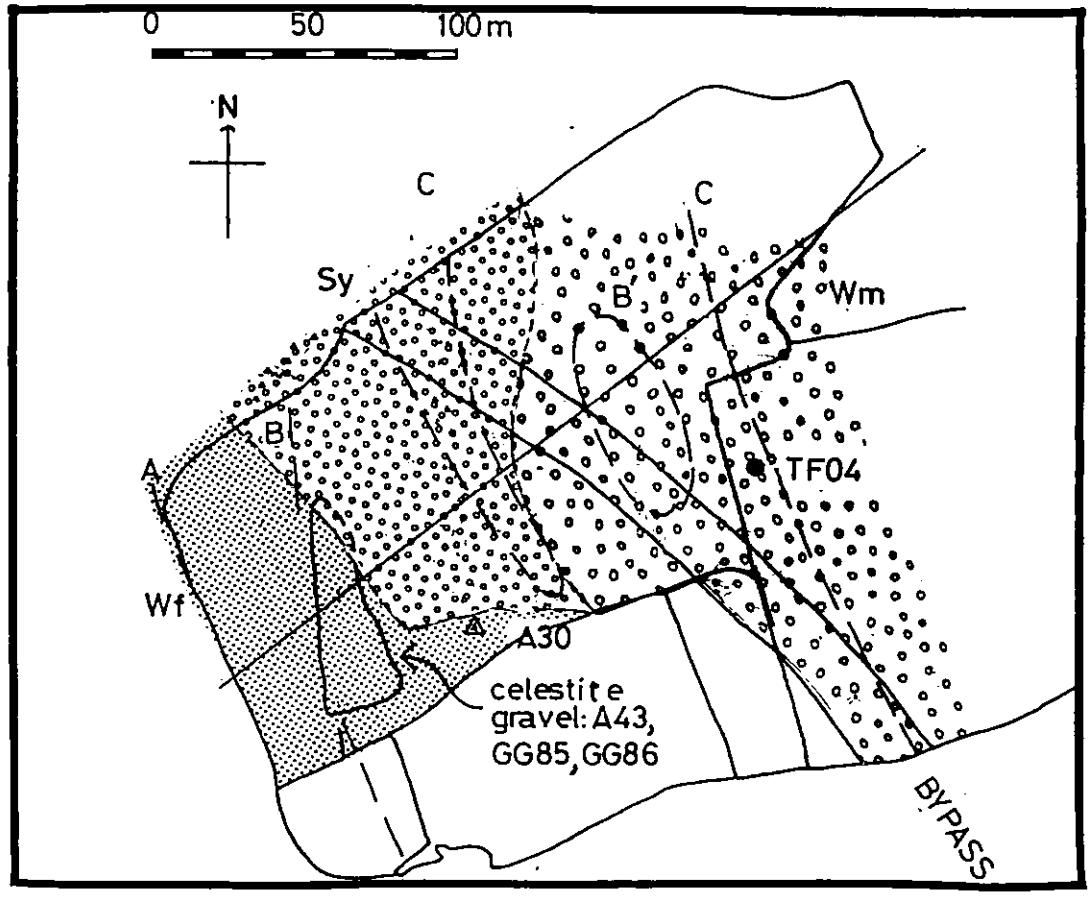

Fig 6.1: The Goose Green area, showing distribution of the soil series (modified from Soil Survey sheet 251) and sample locations

Key: Sy- Spetchley series; Wf- Whimple series; Wm- Worcester series

counting, the celestite percentage in the heavy mineral fraction. The following values were calculated for each sample:-

1) The quantity of celestite in each size class.

2) The quantity of celestite in each class expressed as a percentage of the total (excluding the gravel fraction). Cumulate frequency curves, and the statistical parameters of the celestite distributions are shown in Fig. 6.2 and Table 6.1.

Table 6.1: Grain-size parameters† of the celestite component of the Clay Head, celestite sands and celestite gravels

†(from Inman, in Blatt, Middleton and Murray, 1980)

Specimen	Type	Mdϕ median	Mϕ mean	6ϕ sorting
WF02	Clay Head	+1.8	+2.0	1.6
WF04	Clay Head subsoil	+1.4	+1.4	1.6
RY01	Stoney Head	-*	-*	-*
GG85	Peripheral gravel sample	-*	-*	-*
GG86	Type A celestite gravel	+1.1	+1.0	1.2
RY02	Celestite sand	-*	-*	-*
RY03	Clayey celestite sand	+0.2	+0.3	0.8
WF06	Subsoil on celestite sand	+0.3	+0.5	1.1
WF09	Celestite sand	+1.2	+1.1	1.3
WF10	Nodule gravel segregation	+1.4	+1.8	2.1
WF14	Celestite sand	+0.9	+0.8	1.1

3) The amount of celestite in each class. This is graphically illustrated in the histogram plots (Fig. 6.3).

4) The amount of celestite in the whole sample, expressed as a percentage of the total weight (Table 6.2).

Table 6.2: Comparison of Sr estimates: Clay Head, celestite sands and celestite gravels

Specimen	$SrSO_4$ content (6.1.2)**	Sr estimate (6.1.2)**	%Sr (LMF/AAS)	%Sr (β)
WF02	13.5	6.44	6.60	11.2
WF04	18.9	8.99	8.60	-
RY01	60.3	28.7	-	14.2
GG85	13.0	6.20	7.80	9.6
GG86	97.2	46.4	-	41.8
RY03	52.3	25.0	26.3	26.2
WF06	52.9	25.2	-	30.5
WF09	78.3	37.4	-	36.8
WF14	70.4	33.6	-	32.8

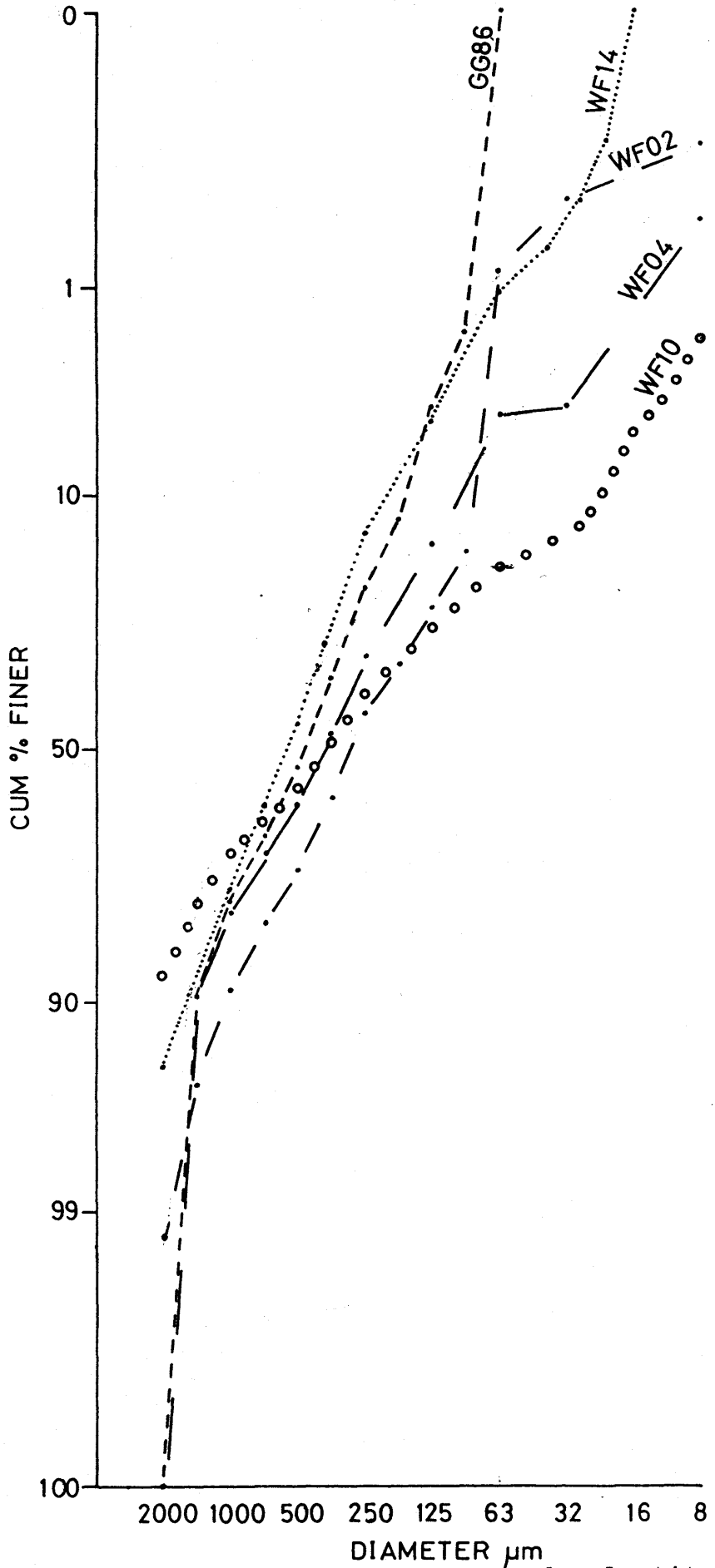

Fig 6.2: Cumulate frequency curves of celestite populations

Fig 6.3: Histograms of grain size distribution data

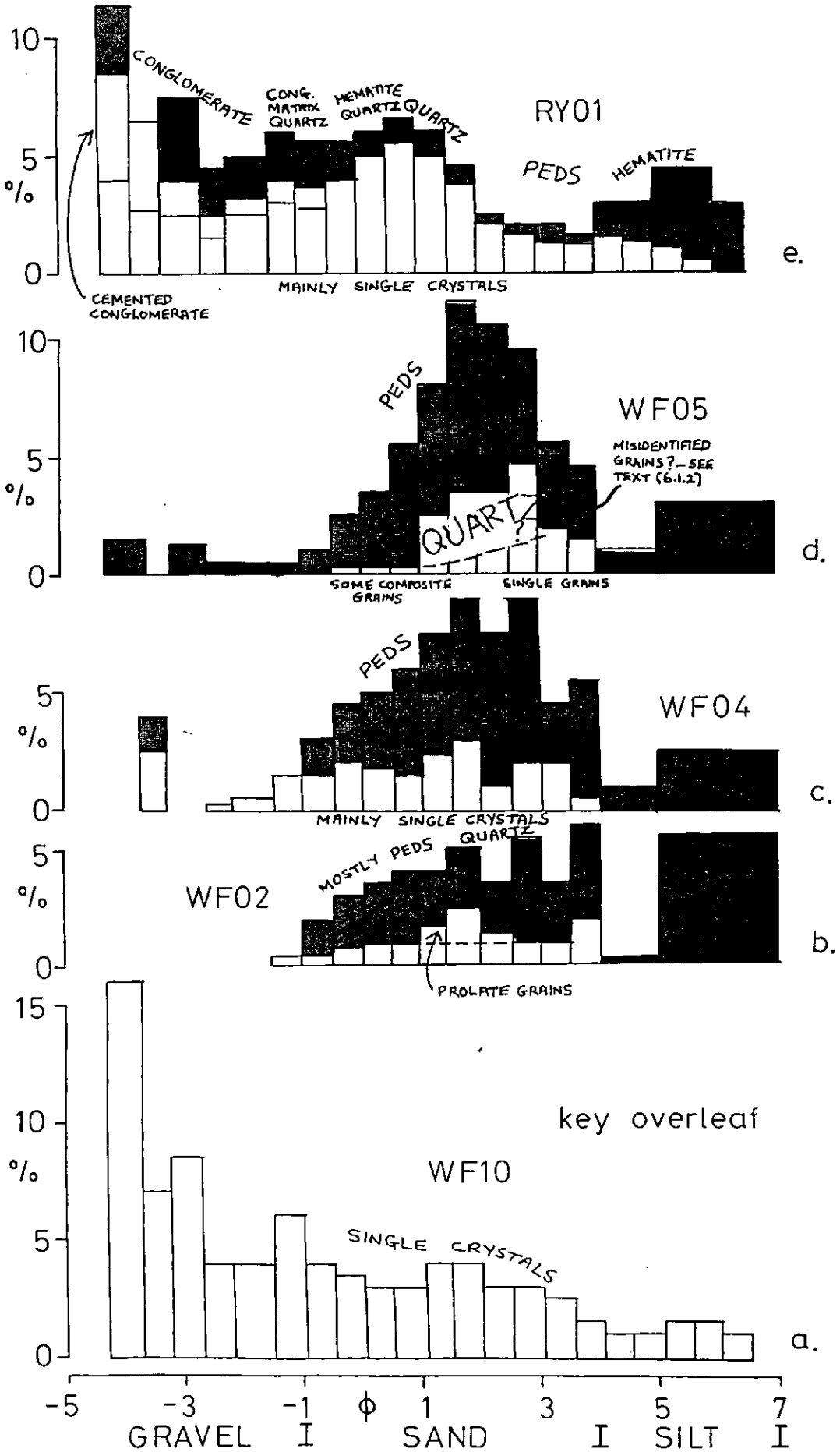

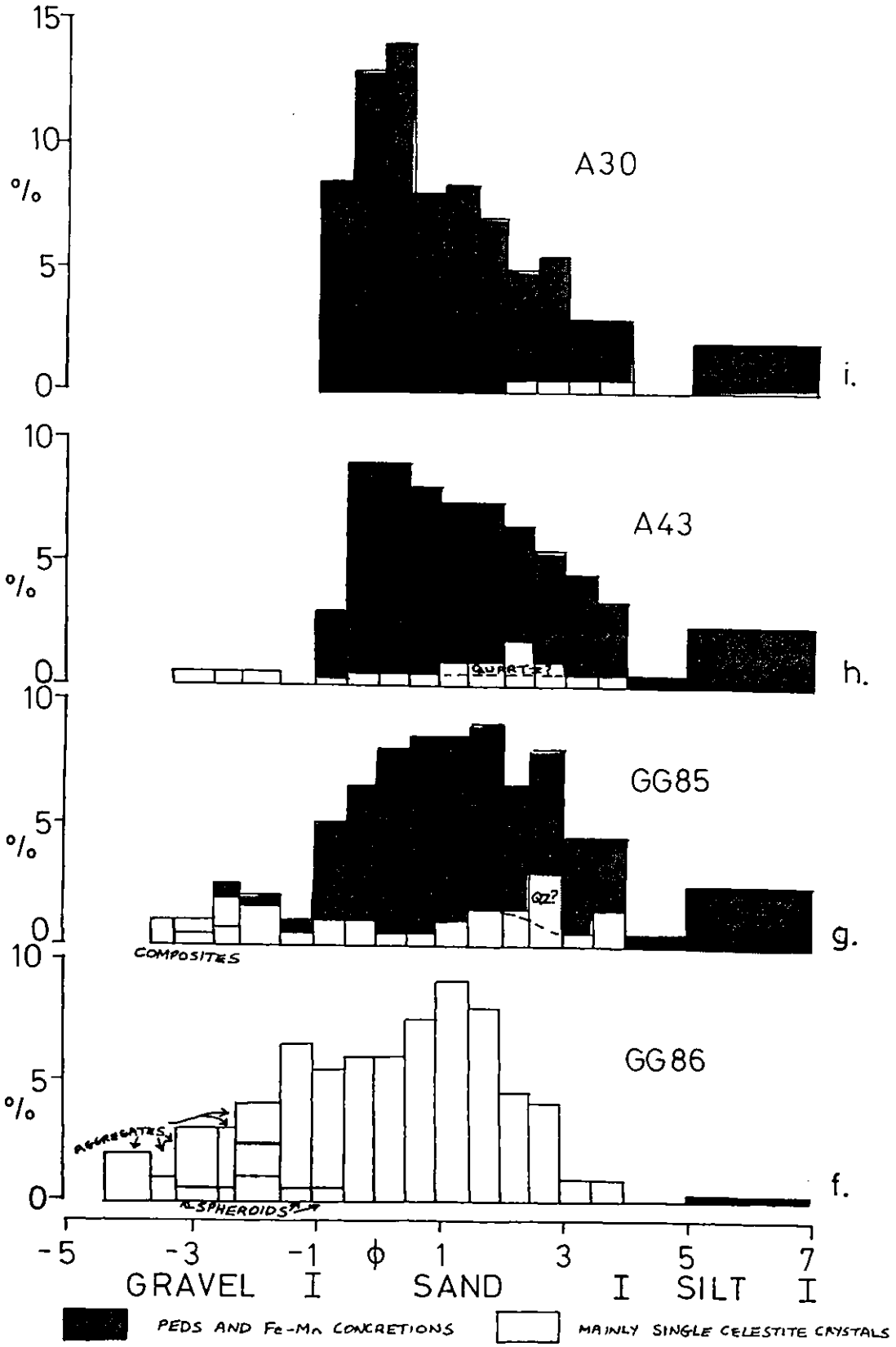
15
10
%
5
0
A30
i.
10
5
%
0
A43
QUARTZ?
h.
10
5
%
0
GG85
QZ?
COMPOSITES
g.
10
5
%
0
GG86
AGGREGATES
SPHEROIDS
f.
-5
-3
-1
ϕ
1
3
5
7
GRAVEL
SAND
SILT
PEDS AND Fe-Mn CONCRETIONS
MAINLY SINGLE CELESTITE CRYSTALS

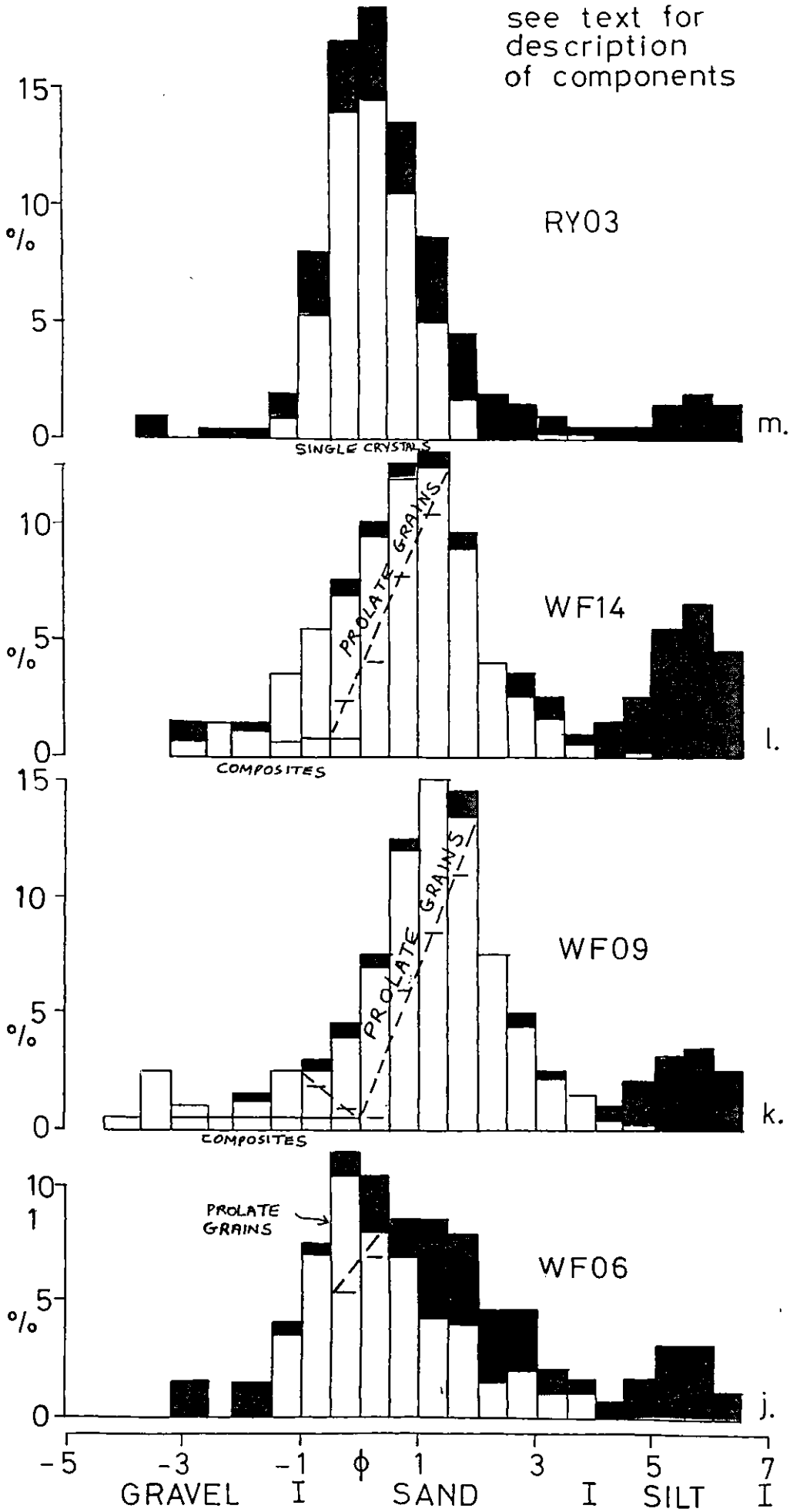
see text for
description
of components
RY03
m.
SINGLE CRYSTALS
WF14
l.
PROLATE GRAINS
COMPOSITES
WF09
k.
PROLATE GRAINS
COMPOSITES
WF06
j.
PROLATE
GRAINS
%
15
10
5
0
-5
-3
-1
ϕ
1
3
5
7
GRAVEL
SAND
SILT

* Statistical measures have no significance where multiple populations are present
** Excluding gravel fraction

6.1.3 Distribution of Celestite within the Clay Head

A detailed investigation of the size distribution of the mumblers has been separately undertaken by Altounyan (1979), using bulk mineral handling techniques. The data discussed here are only concerned with the quantities of fragmented epigenetic celestite found dispersed throughout the Clay Head (2.6.2.1).

The grain size histograms of the Clay Head and subsoil (Figs. 6.3b, c) show an even distribution of celestite across the gravel and sand fraction indicating fragmentation of larger celestite crystals controlled to some extent by the initial size distribution. Additional evidence is provided by the cumulative frequency curves, which follow Rosin's law for crushed crystalline aggregates (see Blatt, Middleton and Murray, 1980, P.69). In Specimen WF04 4.0% of the celestite is silt-grade. Altounyan (1979) determined that only 3-4% of the celestite in bulk samples of Clay Head from which larger (+7.5mm) mumblers had been hand sorted was finer than coarse silt grade (0.053mm); but that 20% of the celestite was finer than medium sand grade (0.60mm). These figures reflect the tendency of the cemented vein celestite to fracture rather than shatter, producing a minimal mechanical dispersion into the fine sand to mud-grade fractions.

The celestite grains are mostly transparent cleavage fragments although prolate forms of the 'thick tabular' habit have also been found (subtype E4; see 3.2). Quartz grains and Carboniferous sandstone, siltstone and mudstone clasts also occur in the Clay Head. The subsiduary peaks in the 3.5-4.0ϕ histogram classes and the discontinuity in the cumulative frequency curves are probably artifacts (Pettijohn, 1975).

The physical and compositional inhomogeneity of the Clay Head material is reflected in the wide variation in the Sr analyses (Table 6.2). As well as the two specimens in Table 6.1, other examples of Clay Head from Winter's

Field assayed at 0.28, 0.80, 1.20 and 17.3% Sr (Betaprobe and LMF/AAS analysis).

The Stoney Head specimen, RYO1, which is from a rubbly lens in the Clay Head and assays at 14.2% Sr, contains many fragments of celestite-cemented Millstone Grit conglomerate and a breakdown component, including a fine celestite sand (Fig. 6.3e). The discrepancy between the point-count estimate and the assay (Table 6.2) is caused by the inadvertent inclusion of iron-stained quartz with the celestite count.

Grain size analysis of a typical soil from over mumbler deposits at the Winter's Field site (Fig. 6.3d) shows a large quartz medium sand compoment, derived from the terrace gravels, with traces of sand-grade celestite. The geochemical contrast (Hawkes and Webb, 1962) between the celestite and the soil is at a maximum in the $-\frac{1}{2}$ to $\frac{1}{2}\phi$ (coarse sand) and $3-4\phi$ (very fine sand) fractions.

6.1.4 Distribution of Celestite within the Type A Celestite Gravel

The histogram of the size distribution of the Type A celestite gravel (Fig. 6.3f) shows that three components are present. These are:-

1) A silt and a clay fraction consisting of mudstone peds only.

2) A coarse celestite sand with a low sorting parameter (Table 6.1) containing three habits of celestite:-

a) Tabular or bladed, transparent, white, orange or yellow cleavage fragments or crystals.

b) As above, but prolate.

c) Equant grains of indeterminate habit, including granular celestite.

3) A gravel component of composite grains consisting of aggregates of the above types and of rounded spheroids of finer granular celestite. The gravel is evidently derived from celestite of the coarse white tabular-fine white granular variety (2.4.2.3).

Both types of composite grain are subrounded to subangular implying possible rounding by water currents.

The absence of celestite of silt-grade or finer may be explained by winnowing away of the fines by current

action or because cryogenesis tended to shatter the celestite nodules rather than fracture them and silt-grade celestite was not produced. Also, because the Goose Green gravel is an in-situ deposit (Plate 41) the frequency distribution in Figs. 6.2 and 6.3f probably reflects the original size distribution of the celestite crystals within the seam rather than as a result of weathering.

Possible fracturing mechanisms are better displayed in samples taken from the periphery of the gravel (GG85) and the topsoil over the gravel (A43). In both cases the celestite grains show a more even distribution across the sand classes, suggesting a progressive diminution of the larger crystals or aggregates. Furthermore a topsoil situated further away from the gravel subcrop (A30, Fig. 6.1) only contains celestite in the 2-4ϕ fraction, suggesting that the fracturing only reduces the celestite down to that size range.

A subsiduary peak at 2.5-3ϕ on the histograms is caused by the quartz sand component of the marl (Figs. 6.3g, i). As in the Winter's Field soil (see above), maximum contrast is shown in the very coarse and very fine size fractions of the soil.

The Sr assays of the two gravels correspond reasonably well with those determined by the point counting technique. The high Sr values may indicate that any calcite originally present in the seam has been leached out by surface weathering.

6.1.5 Distribution of Celestite within the Other Celestite Sands and Gravels

The celestite sands at The Rectory and Winter's Field sites (2.6.3) form a well defined compositional and textural group of sediments containing a medium-to-coarse-grained sand of epigenetic celestite with low ($\sim$ 1.0) parameters of sorting (Table 6.1; Figs. 6.2, 6.3j-m). Three types of sand-grade celestite were observed:-

1) Tabular or equant cleavage fragments, subrounded and heavily iron-stained pink or vermilion. Some of the coarse silt celestite is well rounded.

2) Prolate crystals of prismatic habit, the breakdown product of crystalline aggregates, including wasp-waisted

grains from comb-textured celestite (3.2).

3) Coarse compound grains of granular celestite 0.5-1.0mm across (subtypes E7 and E9) (see Table 3.4).

The celestite accounts for 52-79% of the sand-, silt- and clay-grade of the sample giving Sr analyses of 25-38% (Table 6.1). Other components include:- fine sand and silt-grade quartz, Carboniferous sandstone pebbles (containing well rounded quartzitic sandstones), fine sand to silt-grade goethite, clay to sand-grade clasts of Millstone Grit and possible Triassic mudstones, red hematite and, in some cases, silt-grade pyrite.

The sorting is further proof for a subaqueous reworking of the celestites (2.6.3) as an in-situ disintegration would smooth out the initial distribution of crystal sizes (Fig. 6.3b, c). Such an even, perhaps polymodal distribution is shown in the size distribution of a gravel segregation within the celestite sands, Specimen WP10, (Fig. 6.2, 6.3a) in which a higher measure of sorting is recorded (Table 6.1). The celestite particles are cleavage fragments rather than discrete crystals and suggest a later stage of cryogenic fracturing acting upon a nodule that was comminuted with the celestite sand detritus. The high proportion of silt- and clay-grade celestite in Specimen WP10 (18% less than 0.066mm; Fig. 6.2) is in accordance with the observations of Merefield (1975), who found two particle size populations of abraded sand-grade crystals and silt-grade chippings in baryte sands of cryogenic origin in North Devon. Similar effects are also well known from the weathering of quartz (eg. Rogers et al., 1963). However, the figure of 18% is substantially reduced (to 8.0%) if the gravel fraction is also included in the calculations.

On the whole, the symmetric shape of the grain size distribution of the celestite sands, and the presence of a fine tail, argue more for a river sand rather than a beach sand origin (Blatt, Middleton and Murray, 1980, PP.72-73) (see discussion in 2.6.3.3).

6.1.6 General Conclusions

Different breakdown mechanisms have been identified in each of the sediment types discussed. In the Clay Head,

fragmentation of the drusey celestite has resulted in a celestite sand component. On the other hand there is less evidence for fragmentation or fracturing in the Type A celestite gravels, and shattering and disaggregation of the celestite seam is responsible for the wide distribution of grain sizes in this rock. The Winter's Field and Rectory sands are sorted, waterlain deposits of local origin and consist of more than 50% celestite by weight.

6.2 GEOCHEMICAL EXPLORATION

6.2.1 Introduction

Geochemical sampling of soils by Nickless et al. (1976) proved to be a useful tool in the regional assessment of the resource. The samples were taken at depths of 0.5-1.0m from the surface at intervals of 10, 20 or 50m. From their data they were able to trace the outcrops of the Severnside Evaporite Bed across southern Gloucestershire but they attached no quantitative significance to their results.

It was decided that a more detailed programme of soil sampling might be of use in the recognition of celestite within individual fields and with this aim, the Goose Green West, Goose Green East and Winter's Field sites were sampled before the start of mining operations (Figs 6.4, 6.5, 6.6). In addition, the distribution of Sr and Ba was determined in the host rocks of the celestites.(Table 6.1).

6.2.2 Sampling Technique

The spacings of the soil samples varied according to the site. A separation of 15.3m (50ft) was selected for the Goose Green site after consideration of the procedures of Nickless et al. (1976). At Goose Green East this was reduced, for purposes of experiment, to 7.7m (25ft). The sampling grid at Winter's Field accommodated 23 traverse lines 7.7m (25ft) apart in anticipation of many narrow steeply dipping celestite veins less than a metre thick.

2.2kg (five pound) samples were taken at depths of 13cm (Goose Green East), 17cm (Goose Green West, Winter's

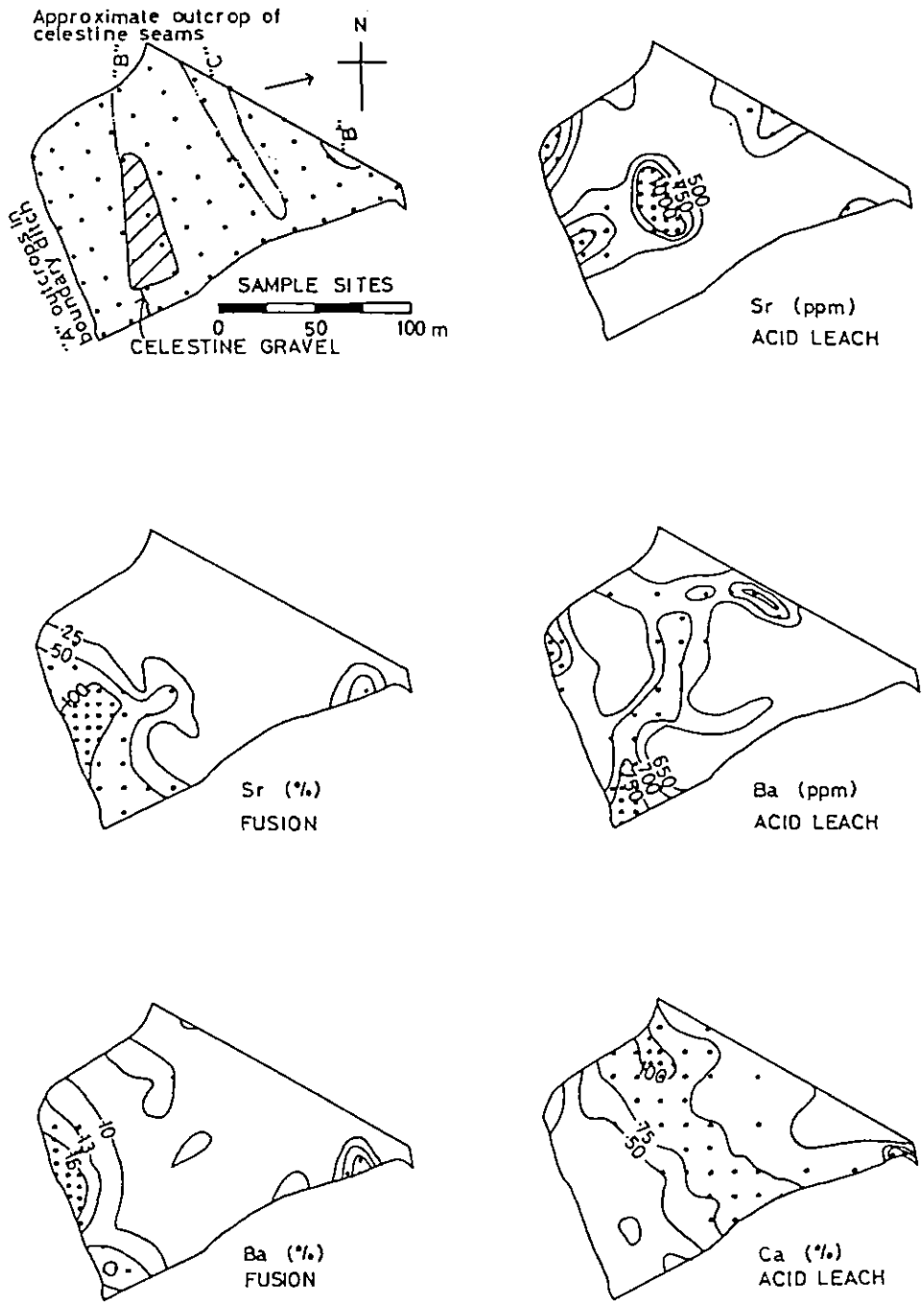

Fig 6.4: Geochemical plots for the elements at Goose Green West.

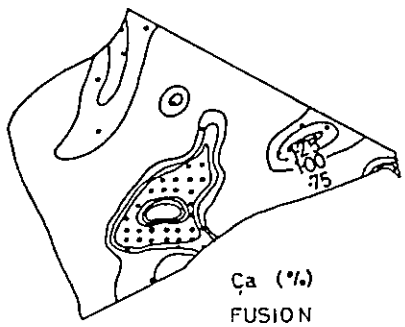

Ca (%)
FUSION

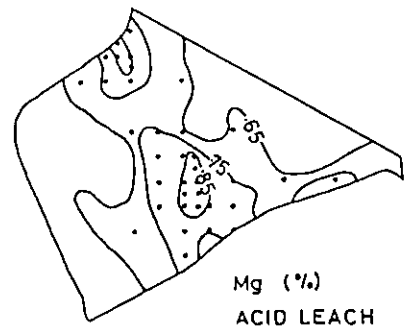

Mg (%)
ACID LEACH

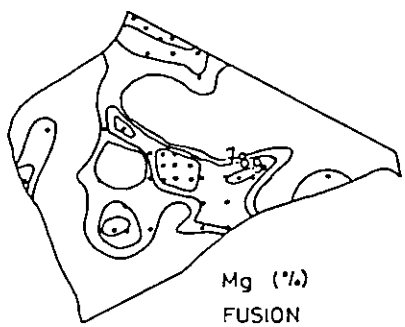

Mg (%)
FUSION

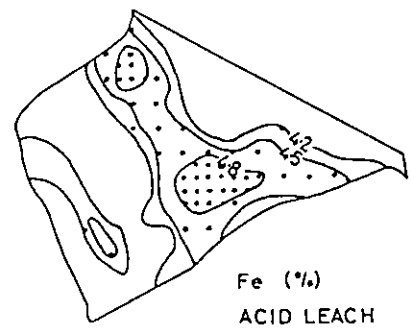

Fe (%)
ACID LEACH

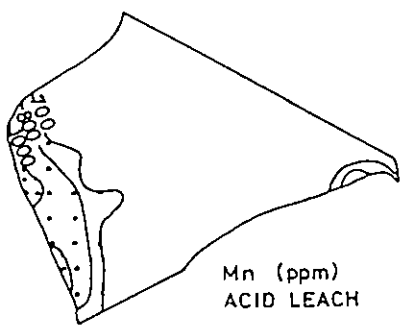

Mn (ppm)
ACID LEACH

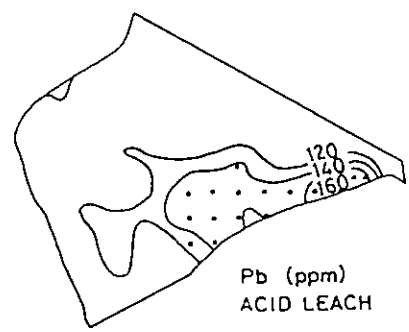

Pb (ppm)
ACID LEACH

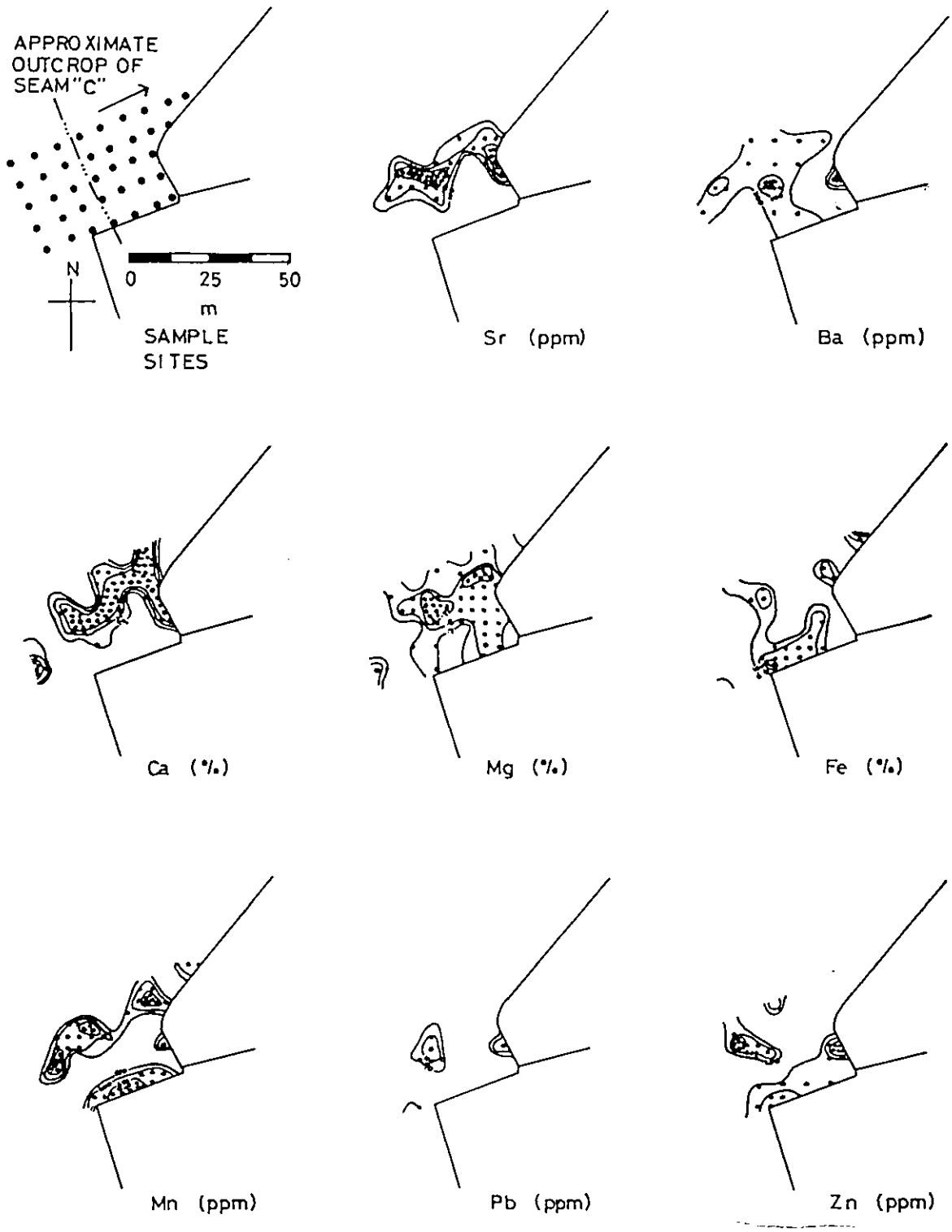

Fig 6.5: Geochemical plots for the elements at Goose Green East

a. Samples taken at 25cm depth

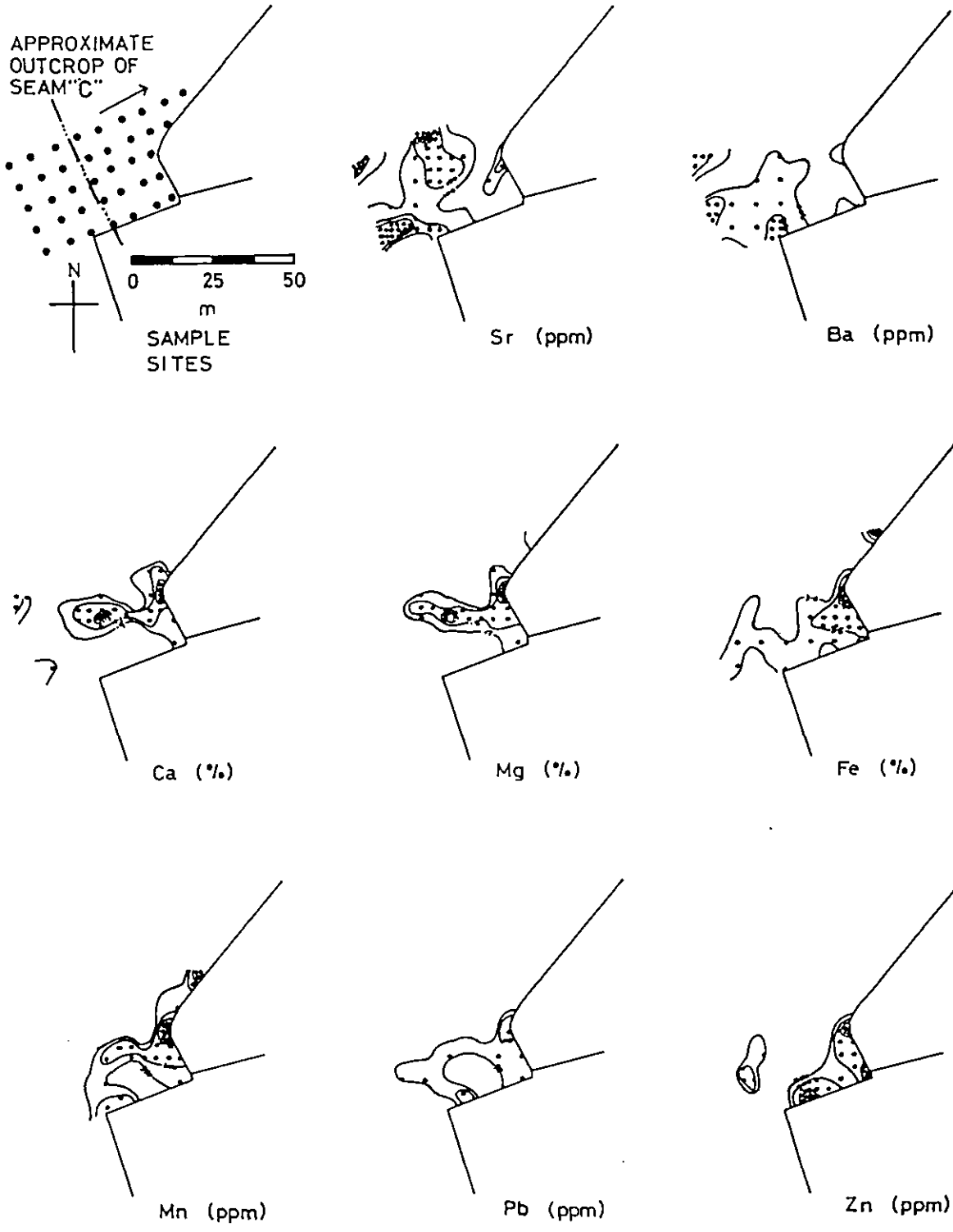

b. Samples taken at 13cm depth

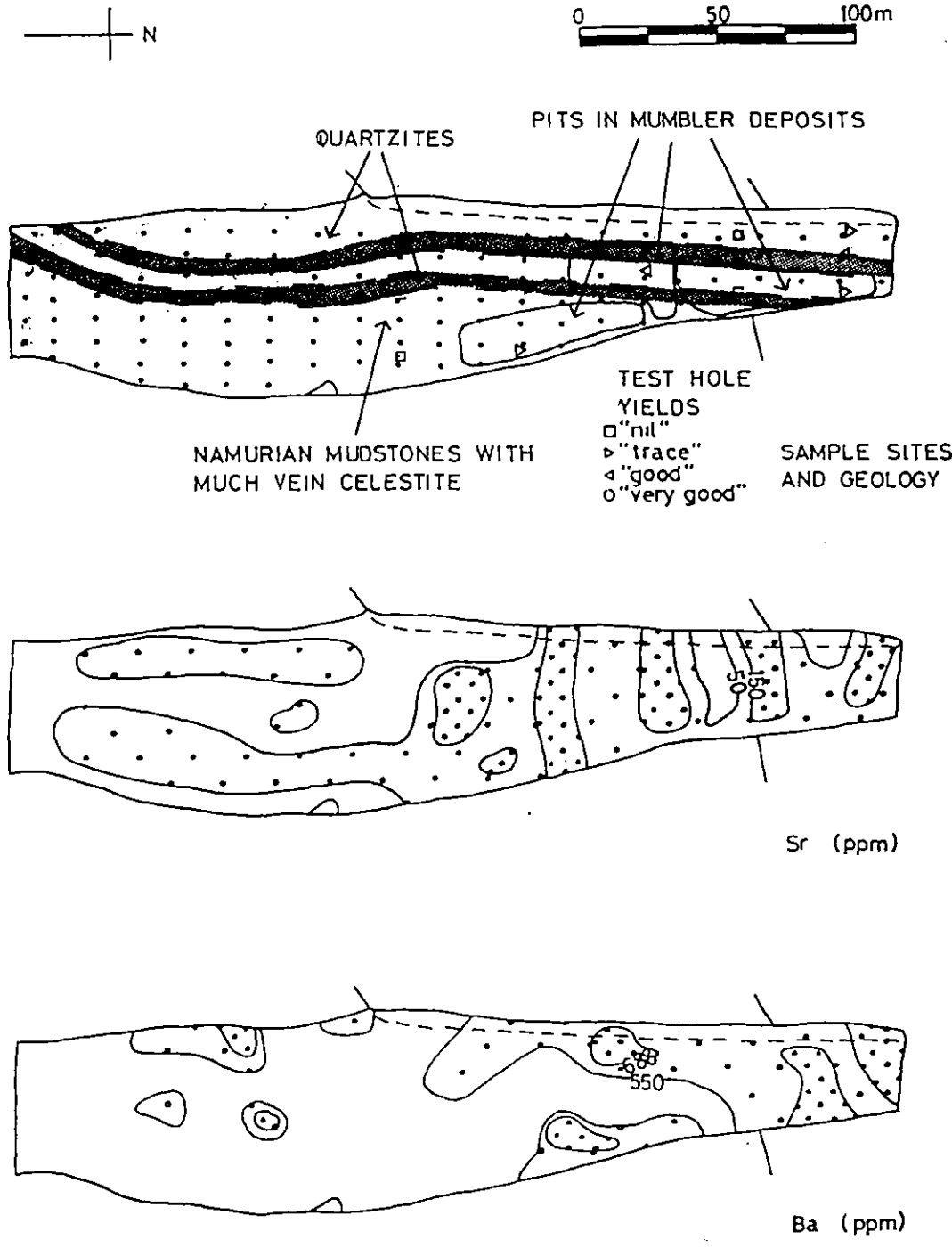

Fig 6.6: Geochemical plots for the elements at Winter's Field

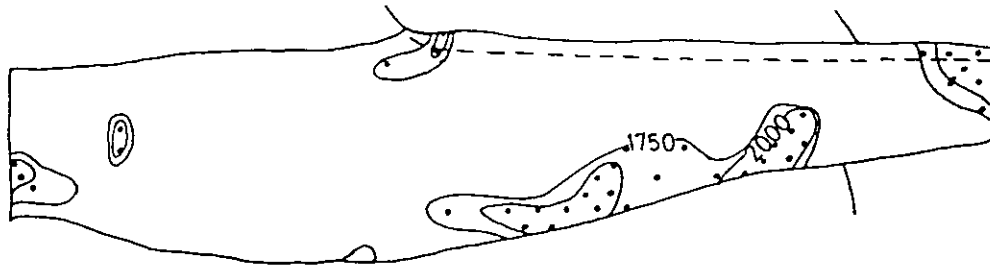

Ca (ppm)

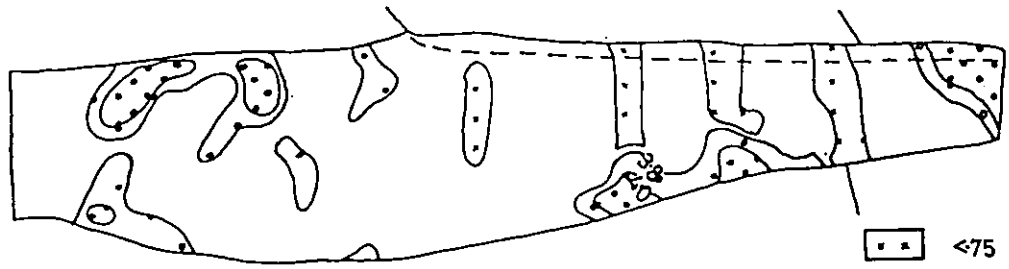

Fe (%)

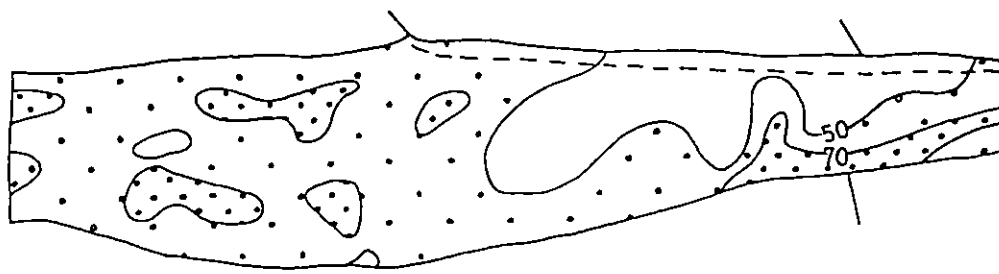

Pb (ppm)

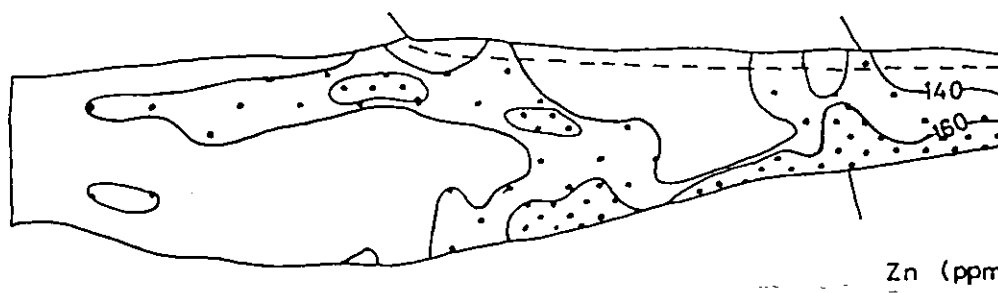

Zn (ppm)

Field) and 25cm (Goose Green East) to investigate the possible effects of sampling at different levels in the same soil horizon (A2-E-B1). The figures 13, 17 and 25 correspond to the depth in centimetres at which a sample was recovered from two, two-and-a-half and three full turns of the auger. The soil depths sampled by Nickless et al. (1976) are considered to have been taken in weathered bedrock (BC horizon) rather than in a representative soil of the underlying beds. It was felt that there was too great a risk in the deeper samples of inadvertently including isolated celestite nodules or of sampling the marl between the nodules in the seam. Background levels for unmineralised areas away from the celestite-producing districts (Nickless et al., 1976) were established by sampling soils at 17cm depths from similar host-rocks (Table 6.3).

Table 6.3: Details of Background Soils

Spec.	GR(ST)	Parent Material	Horizon	Soil Series
H2	701841	Coal Measures sandstone	A2	Swindon Bank
H3	696856	Coal Measures shale	A2	Dale
H4	698856	Coal Measures shale	A2	Dale
H5	719837	Yate Formation	A2/B1	Worcester
H6	722818	Yate Formation	A2	Unknown
H7	692791	Yate Formation	A2	Worcester
H8	680854	Yate Formation	A2/B1	Worcester

6.2.3 Analysis

The analytical methods employed were hot nitric acid digestion and sodium carbonate fusion (see Appendix II.4). The former is a standard method for the determination of metal ions in soils. Rock samples from Goose Green, Wellstead Nursery and Winter's Field were also analysed by this technique. Only the Goose Green West soils were analysed by sodium carbonate fusion.

At a later stage certain of the soils and rocks were analysed using the lithium metaborate fusion described in Appendix II.1.7.

The results of the analyses are given in Figs 6.4-6.7 and are summarised in Table 6.4. The contouring of the geochemical maps was by visual examination only.

6.2.4 Interpretation of the soil assays

The results clearly show that the sampling grids, which were aligned with the strike of the celestite outcrop pattern, do not always accord with the trends of the geochemical distributions. The geochemical maps (Figs 6.4, 6.5, 6.6) are now discussed for each locality.

Table 6.4: Means of the soil assay distributions

	Locality and method of extraction					
	Goose Green (West)	Goose Green (West)	Goose Green (West)	Goose Green (East)	Goose Green (East)	Winter's Field
Element	Acid leach	Fusion	Acid / Fusion	Acid leach[1]	Acid leach[2]	Acid leach
Sr ppm	485	3357	14.4%	100	100	50
Ba ppm	616	930	66.2%	300	300	550
Ca ppm	6433	7246	88.8%	9000	9000	1500
Mg ppm	6689	6780	98.7%	8000	8000	-
Fe %	4.1	-	-	3.0	3.0	3.5
Mn ppm	612	-	-	500	550	-
Pb ppm	113	-	-	85	70	-
Zn ppm	-	-	-	220	220	140

1 Samples taken at 13cm depth

2 Samples taken at 25cm depth

6.2.4.1 Goose Green West (Fig. 6.4)

The Sr, Ba and to a lesser extent, Mn plots conform to the subcrop pattern of the celestite seams. The subcrop of seam A is indicated to be near the extreme SW boundary of the field. The surface expression of B is limited to certain highs in the centre of the plots and is well masked by the Spetchley soils containing a thin layer of alluvium (Findlay, 1975) (Fig. 6.1). The position of seam C can only be inferred from some rather isolated features. Seam D is marked by a small anomaly in the Whimple series soils in the eastern corner of the field, of smaller magnitude than those of the soils of the Worcester series. This is a reflection of the influence of the thin loamy drift present in the superficial layer of the Whimple profile (Findlay, 1975).

The Ba (acid leach) pattern is more complex than the Ba (fusion) or Sr maps, and extends over the Spetchley soils, suggesting that part of the Ba plot may be a false anomaly (see below). The Mn map traces the distribution of pedogenic Fe, Mn oxides or amorphous goethite.

The Fe, Mg and Ca (fusion) plots can be correlated with the distribution of the Spetchley series soils, and probably result from the weathering of the thin spread of alluvium over the centre of the field. Anomalous values in the Pb and Ca (acid attack) plots represent a dispersion halo of the epigenetic sphalerite-galena-calcite rock mineralisation, previously noted along seam C in the Yate Bypass cutting (Fig. 4.11). Whereas the Pb anomaly has been smothered by the alluvial blanket, the more mobile Ca has been incorporated into the topsoil over the seam.

6.2.4.2 Goose Green East (Fig. 6.5)

The assays of the samples taken here are also elaborate in pattern. The whole area is in Whimple series soils overlying at 50-70cm, seam C. Zn analyses were included following the discovery of reports of zinc mineralisation in old company records.

Because Goose Green East was sampled on a larger scale than Goose Green West it is difficult to compare the geochemical patterns of the two sites. Goose Green

East is underlain by gently sloping ground and the subcrop of seam C is much more complicated than the stylized representation in Fig. 6.5. However, comparing the magnitudes of the analyses of the two localities it is apparent that there is a depletion in the value of Sr and Ba, which is unexpected when it is considered that the Goose Green East site contains a higher density sampling pattern directly over a celestite seam. The Pb and Mn values are also slightly lower than at Goose Green West (Table 6.4). If a background was established from the Sr and Ba data of Goose Green West it would include the assays of the soils of the Goose Green East site, and seam C would not be suspected.

The lower elemental values reported for Sr, Ba, Pb and Mn are almost certainly due to two effects:

1 a subsurface layer of comminuted mudstone, as described in 1.4.4.2 and 2.6.1.

2 dilution of the A and B horizons of the Whimple series by fine loamy Head (Findlay, 1975).

The mean Zn value of 220 ppm is higher than the averages of 44,50 and 70ppm quoted by Wedepohl (1978) for worldwide and North American soils and is probably due to weathering of the sphalerite along seam C.

The 13cm and 25cm samples do not differ significantly in value or pattern. Hence the depth at which the samples were taken in the B horizon is not of significance. In this case it is also concluded that no advantage is gained from doubling the number of samples taken (halving the sampling interval to 7.7m (25').

6.2.4.3 Winter's Field (Fig. 6.6)

Winter's Field was sampled after the Bristol Mineral Company Ltd. had excavated 15 test holes, at the localities shown. The symbols give a rough qualitative estimate of yield. The samples were mainly taken from the A2 horizon of Swindon Bank and Stanley series soils.

The Sr map reveals that the soil samples trace patches of disturbed and replaced land resulting from the introduction of the test holes. Apart from several distinct anomalies which result from the selection of

celestite blocks disturbed by the above activity, dispersion of Sr through the soil is very low. In the south of the field, two strips of land containing 50-150 ppm Sr correspond to the outcrop of the Millstone Grit mudstones. The low value of Sr reported over the rich Type C and D celestite deposits at this site confirm the conclusions of an earlier regional soil survey (Nickless et al., 1976) (see below).

The poor dispersion of Sr and Ba is partly due to the blanketing effect of the loamy Head layer in the upper part of the Stanley profile. This thin layer of drift is characteristically derived from interbedded quartzites (Findlay, 1975).

It is interesting to note that, apart from iron, the superposition of the test holes on the sampling grid does not coincide with enhanced concentrations of the other elements. The Zn pattern is to a small degree correlated with the underlying geology, and the Ca plot almost certainly reflects the small pockets of Yate Formation marls observed in the NE quadrant of the site. Anomalous fringes on the eastern side of the field may also be due to enrichment of these elements in river alluvium, mapped by the Geological Survey up to the border on this side.

6.2.5 Dispersion of Sr and Ba

In the previous section it was demonstrated that only the Sr and Ba analyses reflected the celestite distribution at Goose Green West. However, because of surface effects, the degree of correlation was poor and at the other two sites celestite could not be detected at all.

The dispersion of Sr and Ba throughout the soils and host rocks of the celestite is depicted schematically in Fig. 6.7. This illustrates the greater extracting power of the fusions over the acid leach, a reflection of the different ways in which Sr and Ba occur in the specimen. The lithium metaborate fusion (LMF/AAS method) is a total analysis whereas the acid leach cannot break down silicates and can only sparingly dissolve celestite. The sodium carbonate fusion (SCF/AAS method) if completely effective

Fig 6.7: Chemical dispersion of Sr and Ba in the host rocks of the celestites and their soils

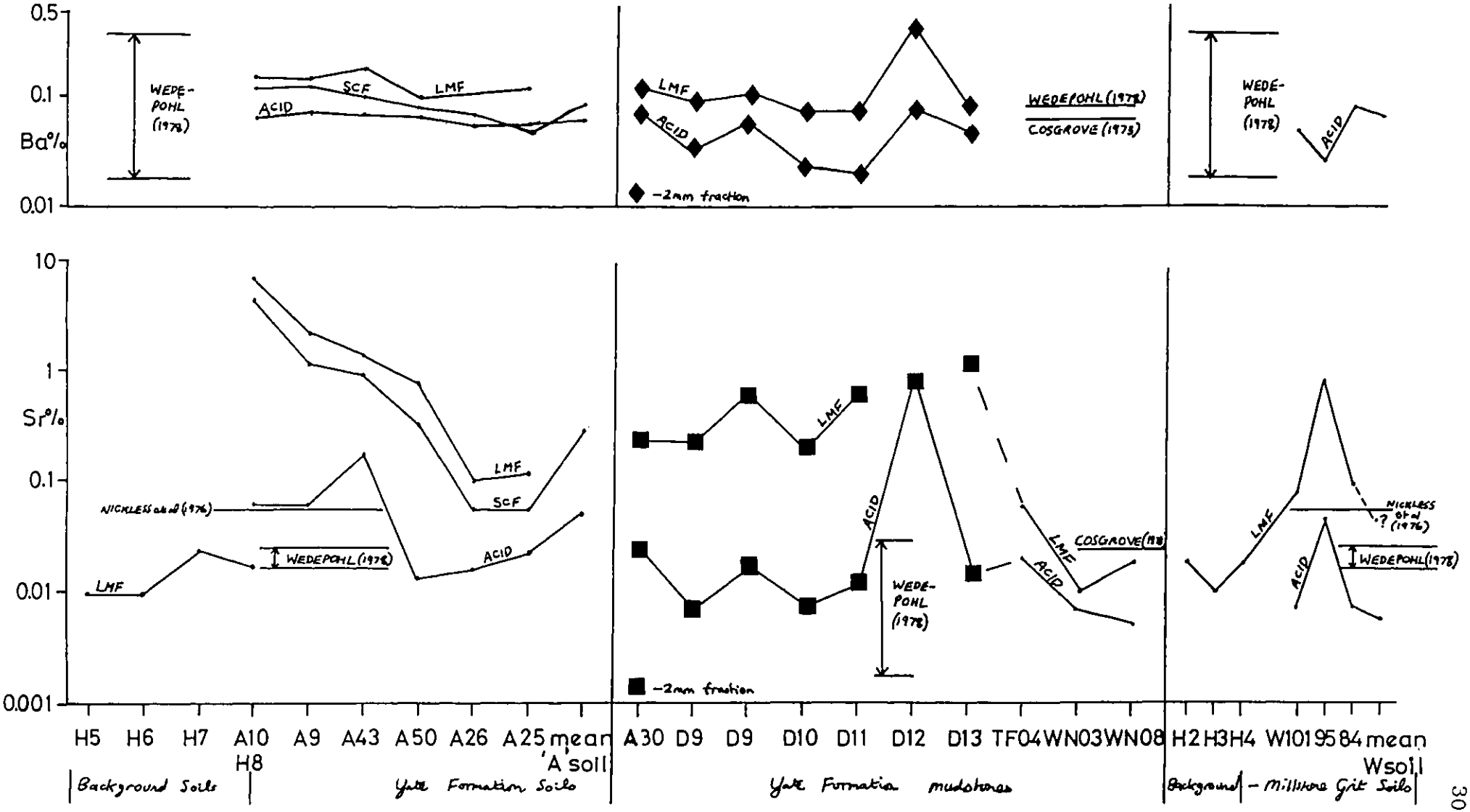

would also give a total analysis.

The acid leach of the soils determines Sr and Ba adsorbed on colloids, clay minerals and organic matter and bonded on to clays, pedogenic hydrous oxides and metallo-organic compounds (Hawkes and Webb, 1962; Perel'man, 1977), and can be used to provide an estimate of the non-silicate, non-sulphate Sr or Ba in topsoil thereby indicating the amount of secondary dispersion that has occurred. In the rock samples, the acid-extractable Sr or Ba is absorbed on to clays and may be also present in carbonate minerals (Wedepohl, 1978).

6.2.5.1 Strontium

Fig. 6.7a indicates that the Sr is mostly present in an acid-resistant form, presumably as discrete crystals.

a Yate Formation

The five Yate Formation mudstones show a range of values from 0.21-1.11% Sr, with a mean of 0.55%. Petrographic analysis showed that traces of celestite were present.

As there is unfortunately no published geochemical data on the Mercia Mudstone Group with which these values may be compared, the Yate Formation sediments have been equated with the Permian Red Bed mudstones of south-west England. This is a similar lithofacies but not associated with celestite mineralization, for which Cosgrave (1973) reported an average Sr content of 307ppm (0.03%). Wedepohl (1978) quoted an average Sr value in Phanerozoic argillaceous rocks of 20-360ppm. The effect of the celestite in the Yate Formation sediments is therefore to apparently raise the Sr level an order of magnitude higher than the values that would be otherwise expected.

As the acid leach assays are contained within these 'background' values it can be assumed that, at this level, Sr occurs within the mudstones in an acid-extractable form rather than as for example a minor fixed element in clastic silicates. This Sr cannot have been derived from the weathering of celestite and must be endogenic, as Specimens WN03 and WN08, taken from the Wellstead Nursery site where celestite has not been reported, gave acid-leach and total analyses in this range (Fig. 6.7a).

b Millstone Grit

A LMF/AAS analysis of 400ppm Sr for a Millstone Grit mudstone from Goose Green (not shown in Fig. 6.7) falls in the range of 10-520ppm for British Carboniferous mudrocks (Ramsbottom et al., 1981) and is only slightly greater than Wedepohl's (1978) average shale (20-360ppm Sr). Nickless et al. (1976) attributed similar low values of Sr in Carboniferous mudstones and soils to a "minimal dispersion .... due to leaching through the highly fractured Coal Measures" but did not state what type of mechanism (endogenic or exogenic) was involved. It is possible that a low primary dispersion of Sr through the Carboniferous mudstones has resulted in an even poorer secondary dispersion.

Two specimens of 'unmineralised' quartzite from sandstone intercalations in the central and eastern sectors of the Yate Bypass contained 0.05% and 0.08% Sr (LMF/AAS analysis), a considerable enhancement in Sr over the <10ppm figure reported by Sabrine et al. (1965) in a geochemical survey of British Carboniferous quartzites and quartzitic sandstones. These enrichments are to be expected if the quartzites formed reservoirs for the Sr-rich fluids, as postulated by Nickless et al. (1976).

c Soils

The distribution of Sr in the soils (Fig. 6.7a) shows that:

1 The threshold value of 500ppm (Nickless et al., 1976) is greater than the Sr analyses of the background soils and Wedepohl's (1978) average soil data, indicating a slight regional Sr enhancement of the soils of the celestite resource.

2 Over half of the SCF/AAS Sr determinations at Goose Green together with a similar number at Winter's Field have analyses in the order of 500-1000 ppm Sr. These values of soils sampled near to subcropping celestite are only slightly greater than the threshold. Together with the low Sr acid leach/fusion ratios of the soils (Table 6.4) this indicates a poor secondary dispersion of the Sr.

There are two components of the secondary dispersion,

involving chemical breakdown and mechanical redistribution of the celestite. Because celestite is almost insoluble in the pedogenic environment chemical dispersion is minimal; also free Sr produced may migrate as the bicarbonate and be leached out of the lower part of the solum (Perel'man, 1977). In addition to this, mechanical dispersion is also retarded so that few fragments of celestite are included in the topsoil. At Goose Green possible anomalies are masked by alluvium and loamy drift and over Winter's Field by an inhomogeneous clay Head mantle and superficial layer of Terrace Gravel and loamy drift, so that celestite was only detected where the surface cover had been disturbed by trenching (Fig. 6.6, 6.7a (sample WA95)).

6.2.5.2 Barium

a Rocks

The Yate Formation mudstones show values ranging from 600-1000ppm Ba, indicating a slight enrichment in Ba over the average of 533ppm recorded by Cosgrave (1973) and the 628ppm Ba of the average shale (Wedepohl, 1978). Similar values were also reported by Wood and Shaw (1976) in 'celestite-free' marls from Sergeants' Farm and Charfield. Also, the value of 700ppm Ba recorded by Wood and Shaw (op. cit.) for a grey Leechpool shale is higher than the 10-430ppm range for Carboniferous mudrocks (Ramsbottom et al., 1981). 50-75% of the Ba in the Yate Formation mudstones is produced by an acid-resistant phase (Fig. 6.7b), suggesting that trace amounts of barian celestite, baryte or possibly even sanidine (2.5.5) are responsible for the enhanced Ba content of these rocks.

b Soils

Fig. 6.7b shows that the different Ba determinations of the soils are proportionally nearer in value than the Sr analyses; an average of 66.2% of the Ba is present in an acid extractable form (Table 6.4) indicating a greater degree of secondary dispersion. As with Sr, the major factor in the dispersion of Ba is the activity of the sulphate, however the effect of adsorption and bonding

is much stronger, producing the wide range of soil values reported by Wedepohl (1978), and more specifically, false anomalies in the alluvial Spetchley soils (6.2.4.1).

6.2.5.3 Summary

The primary (endogenic) dispersion of Sr throughout the host rocks largely restricts Sr to the mineral celestite. This minimises the secondary chemical dispersion of Sr. Furthermore, the secondary mechanical distribution of Sr as celestite is also limited.

The host rocks are enriched in Ba, some of which is present in celestite. Adsorption and bonding effects
is present in celestite. Adsorption and bonding effects
combine to produce a false soil anomaly for Ba.

6.2.6 Geostatistical analysis of the soil data

6.2.6.1 Introduction - basic principles

Geostatistics is the application of techniques of estimation to sample values that are affected by their relationships with their neighbours and their positions (Clark, 1979). The Sr and Ba (fusion) soil assays were geostatistically evaluated to determine the configuration and the optimum number of samples required for the soil sampling program. The analysis is carried out as usual by plotting on a 'semi-variogram' the spacings of the samples against the variances of the assay differences between sample pairs. The expression plotted is

$$\gamma(h) = \frac{\Sigma(f(x+h) - f(x))^2}{2n} \qquad \text{----- (1)}$$

where f(x) and f(x+h) are two sample assays a distance h apart, n is the number of 'paired samples' to be found at that distance, and $\gamma(h)$ is the value of the semi variogram function.

An'ideal' semi-variogram model is given by the Matheron scheme (Clark, 1979). In this case, $\gamma(h)$, which is a measure of the reliability of each sample assay, increases steadily with distance as the samples pass outside each others' 'zone of influence'. At a certain distance ('the range' of the mineralisation or phenomenum

being studied) $\gamma(h)$ reaches a maximum value (the 'sill') and becomes constant. Samples taken at intervals greater than the range are no longer interrelated and have assays which are totally uncorrelated; the maximum sampling interval is therefore given by the range. The optimum sampling interval is determined as the value of h for which some condition of precision, usually in the form of a confidence level, can be met.

By extending these ideas into two dimensions it is then possible to calculate the standard error introduced in assigning the assay value of a sample to the area (usually a grid rectangle) in which it lies. This 'estimation variance' is obtained from geostatistical functions derived from the semi-variogram. (For a more detailed exposition see Royle (1975) or Clarke (1979)).

6.2.6.2 Application

Semi-variograms were computed for each element/ analysis combination of the Goose Green West soil assay data (Fig. 6.4). The operation was performed in four directions: along the E-W grid axis ('across the strike'), the N-S grid axis ('along the strike') and the two long diagonals to test for the possible effects of geometrical anisotropy (Royle, 1975). The semi-variogram plots are shown in Fig. 6.8.

6.2.6.3 Discussion

Fig. 6.8 shows that two different semi-variogram plots are present. The Type 1 semi-variogram resembles a half-wavelength of a sine function, with $\gamma(h)$ values oscillating around the value of the statistical variance s^2. Such highly irregular semi-variograms indicate random behaviour with no spatial correlation between any of the assays used in their construction (Royle, 1975; Clark, 1979). All of the Sr-acid plots are of this type; the random behaviour reflecting the low acid leach values and the poor secondary dispersion.

By way of contrast, the Type 2 semi-variogram shows a steady increase in the value of $\gamma(h)$, indicating that the assays are all well correlated within the sampling intervals considered (Royle, op. cit., Clark, op. cit.).

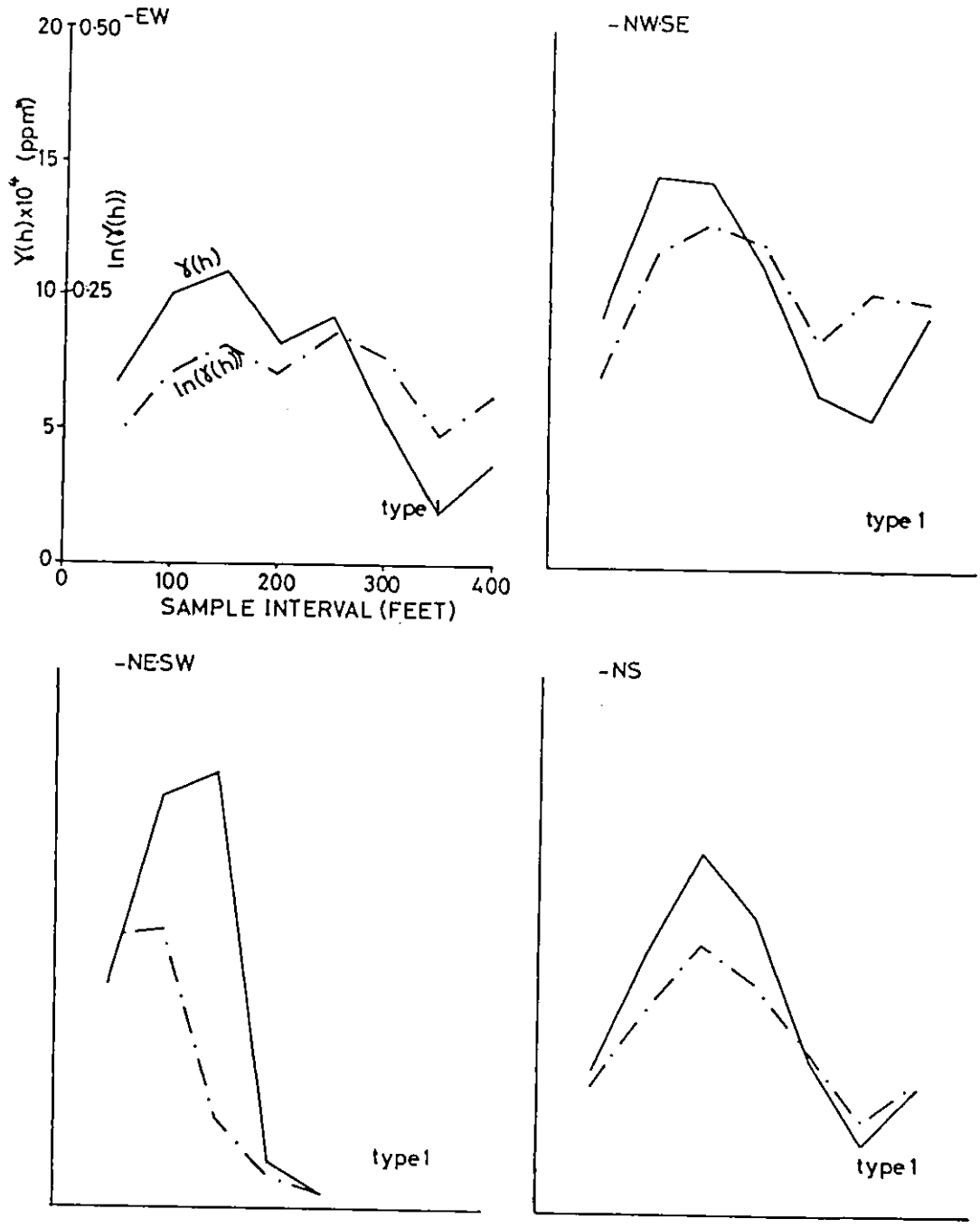

Fig 6.8: Semi-variograms of the Sr and Ba data of Goose Green West.

a. Sr, acid leach

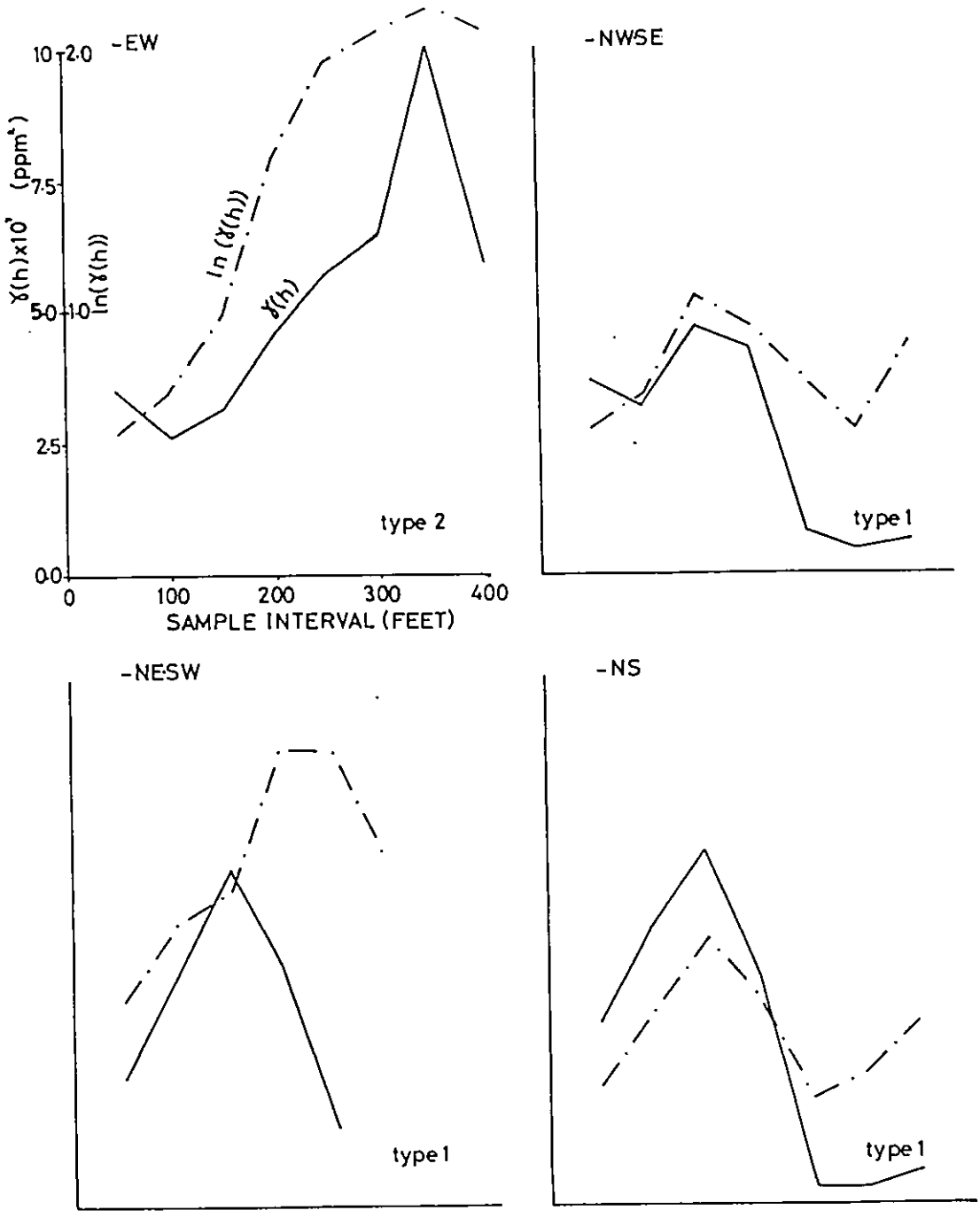
-EW
-NWSE
-NESW
-NS
γ(h)x10⁴ (ppm²)
ln(γ(h))
ln (γ(h))
γ(h)
10
2.0
7.5
5.0
1.0
2.5
0.0
0
100
200
300
400
SAMPLE INTERVAL (FEET)
type 2
type 1
type 1
type 1

b. Sr, fusion

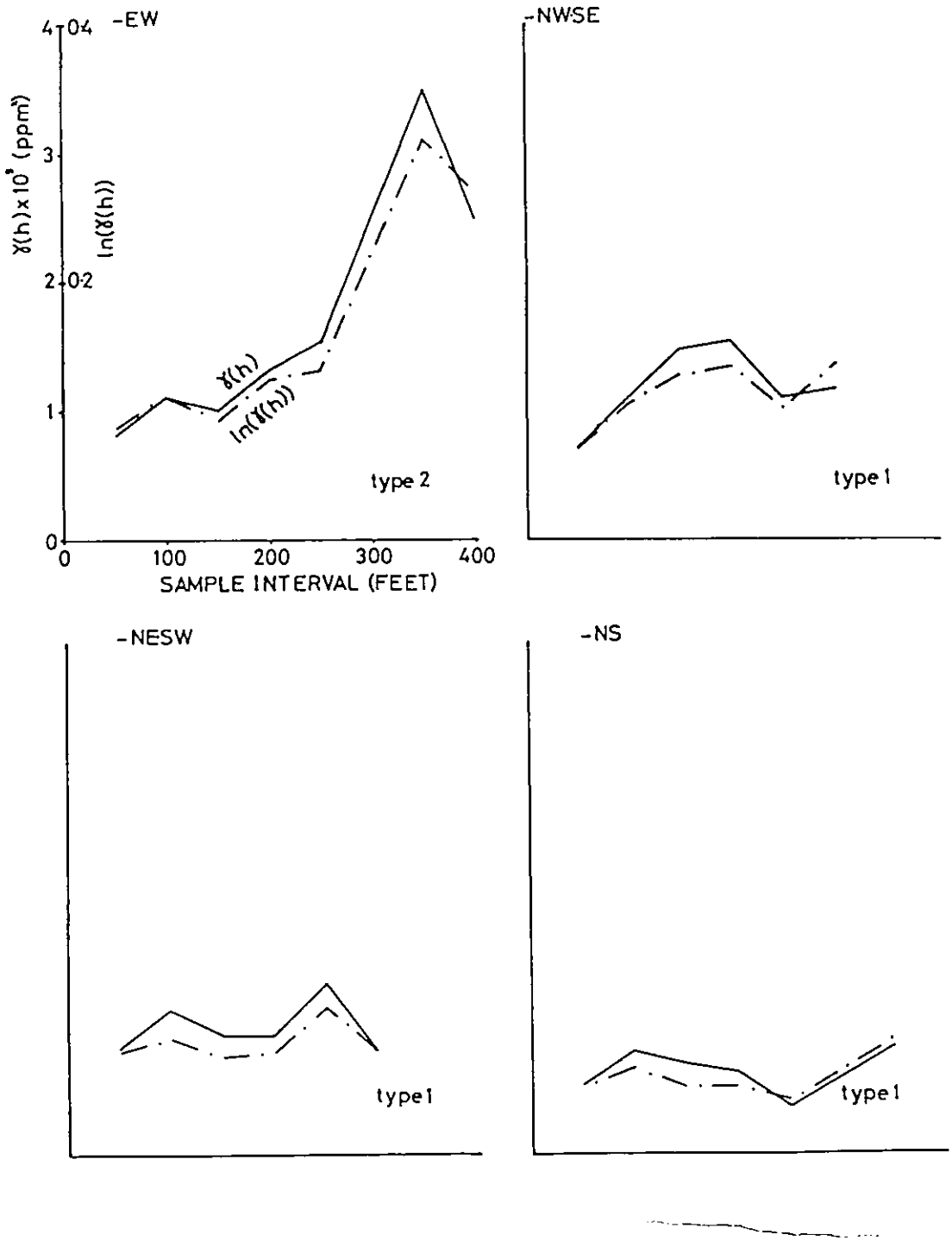
-EW
-NWSE
-NESW
-NS
γ(h)x10⁶ (ppm²)
ln(γ(h))
4
3
2
1
0
0·4
0·2
γ(h)
ln(γ(h))
type 2
type 1
type 1
type 1
type 1
0
100
200
300
400
SAMPLE INTERVAL (FEET)

c. Ba, fusion

Type 2 semi-variograms are only shown in the 'EW' plots indicating that continuity of the data only exists at right angles to the strike. Because there is no sill, it is not known whether the Type 2 semi-variograms belong to an 'ideal' model such as the Matheron scheme. However the EW plot of the Sr (fusion) data (Fig. 6.8b) resembles and may be a near-origin form of the Matheron model determined by S.A.M. Earle (AGRG, unpublished results, 1975), from the Sr soil assays of traverses taken across the strike of mineralisation in the regional survey of Nickless et al. (1976). Estimation variances calculated from Earle's (op. cit.) model semi-variogram indicate an optimum sampling interval at the 99% confidence level of:

a one sample every 1320ft (400m) or

b one sample taken at random in an 800ft (245m) segment in a series of such segments.

This spacing is applicable to a regional survey; in a field survey samples could be taken at any interval up to 1320ft (400m) across the strike. However along the strike the Sr (fusion) semi-variogram indicates random behaviour. It may be argued that the first two or three points may represent the steady rise in the value of $\gamma(h)$ expected if the semi-variogram is of the 'ideal' type (Fig. 6.8b,c). Beyond the range of 100-150ft (30-45m) the value of $\gamma(h)$ would then fall off, as the variance becomes constant. The sampling interval along a grid line oblique to the dip of the mineralisation can, therefore, with a certain degree of assurance be fixed at 30m (100') i.e. before the crest of the half-wave is reached.

6.2.6.4 Summary

The geostatistical analysis showed that only the Sr (fusion) and Ba (fusion) assays when considered across the strike can be used to indicate the underlying mineralisation. Samples may be taken at intervals of up to 400m in this direction. Along the strike the situation is complexed and an optimum sampling interval of 30m is suggested, with reservations.

6.2.7 The Applicability of a Stream Sediment Survey

As the soil sampling program proved that Sr, and possibly Ba, Pb and Zn analyses may be used as indicators of celestite, the distribution of these elements was investigated in the stream sediments of the region reviewed by Nickless et al. (1976) together with those of the Mendip district. The data assessed was that previously collated by Webb et al. (1978) as part of a national stream sediment sampling program.

A preliminary evaluation of the Sr, Ba, Pb and Zn analyses reveals that the geochemical background of the Sr, Ba and Zn distributions are elevated with respect to the national 'average' or median. This is not so for the Pb analyses which are therefore of no interest.

Anomalous Sr values are recorded from sediments of streams which drain the area of celestite-bearing land as recognised by Nickless et al. (1976) but also from other stream sediments, possibly near to where previously unrecorded outcrops of celestite may occur.

The frequency distribution of the Sr assays is lognormal (Fig. 6.9). Because of the anomalous nature of the Sr values in the study area the method of interpretation adopted was as good as any, and possibly more instructuve than the standard techniques based on the standard deviation of the frequency distribution (eg. Hawkes and Webb, 1962). Values of 0-500ppm were taken to represent the elevated background of the area above which three grades of anomaly, represented by data in the 500-1000, 1000-2000 and >2000ppm Sr classes were arbitrarily selected. All may be held to be significantly greater than the 99.9th percentile value of the national distribution (477ppm Sr; Webb et al., 1978).

Fig. 6.9 shows the excellent correlation between the anomalous Sr values and the extent of celestite-bearing land (Fig. 1.4), particularly on the east of the study area. However the 'elevated background' Sr values of the stream sediments in the vicinity of Itchington may indicate that the resource sheet of Nickless et al. (1976) is oversimplified in this area.

Anomalies at Chipping Sodbury and Cromhall (Fig. 6.9)

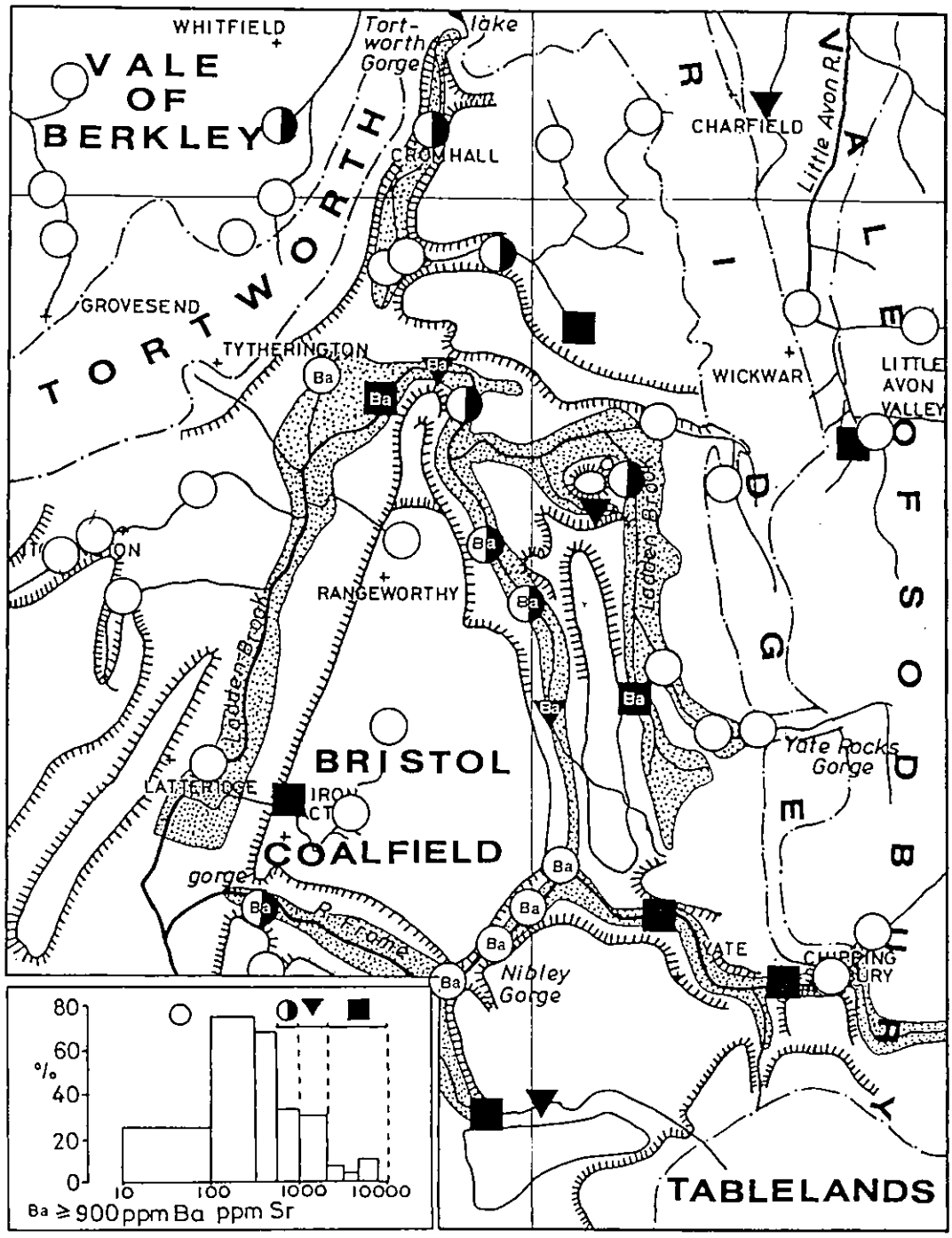

Fig 6.9: Sr and Ba in the stream sediments of the study area. Inset: Histogram of Sr data for the area north-east of Bristol. (after Webb et al., 1978).
For legend to geomorphology see Fig 1.9.

are probably due to small amounts of Sr in limestone stream sediment. However, other Sr anomalies at (677842) and (677831) near Iron Acton and at (697812) and (702811) near Rodford, north-west of Wapley Common, may be produced by previously undetected Type C celestite deposits in mudstone intercalations of the Pennant Sandstone (Fig. 1.5). The amount of celestite present may only be small, as both occurrences lie stratigraphically beneath the nearest Type A deposits.

South of the study area, anomalies situated near (699728), (682731), (679729) and (675743) in the Webb's Heath district (Fig. 6.10) may testify to similar deposits in Lower Coal Measures mudstones bedrock. Two further anomalies at (665797) and (672783) in the Folly Brook drainage basin may indicate small areas of Type A and Type C celes tite peripheral to the Wick Wick outlier.

An anomaly at (606916) in the Thornbury-Oldbury district occurs immediately north of, and is probably an extension of, the Littleton outcrop (see Nickless et al., 1976). Similar, less pronounced Sr anomalies are found at several sites in the Aust-Henbury area, mostly drainage ditches in estuarine alluvium or peat. The Michaelwood-Wickwar area contains a single anomaly at (713940).

Strontium anomalies in the stream sediments of the south Bristol-Mendip district can be used to extend the occurrences listed by Nickless et al. (1976) (Fig. 6.11). In the Barrow Gurney-Regilbury area anomalies in stream bed samples east of Weston-super-Mare and in streams near to Chew Valley Lake indicate further occurrences at the same stratigraphic level as in the area in between. South of Mendip large anomalies at Westbury occur with others of lesser magnitude along the Rivers Axe and Whitelake. Further south the Somerset levels contain many other low magnitude Sr anomalies in alluvium and peat at the stratigraphic level of the 'Keuper Marl' or Blue Anchor Formation.

The Sr anomalies are situated directly over the known occurrences and have a relatively short decay pattern and are therefore excellent indicators for the celestite ore.

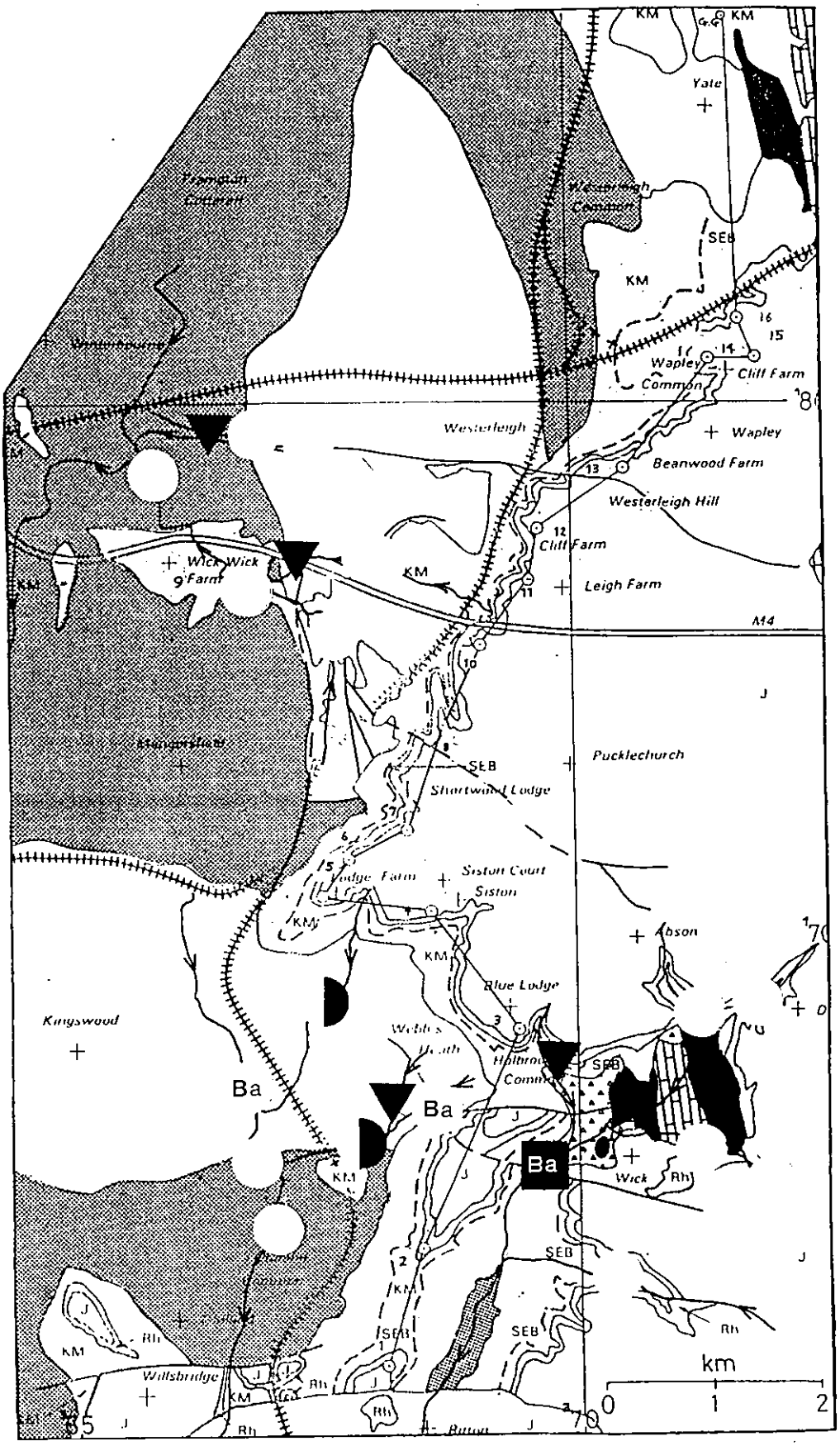

Fig 6.10: Sr and Ba in some stream sediments of the Wapley-Bitton area. See Fig 5.1 for geological legend, Fig 6.9 for key to geochemical symbols (after Nickless et al., 1976; Webb et al., 1978)

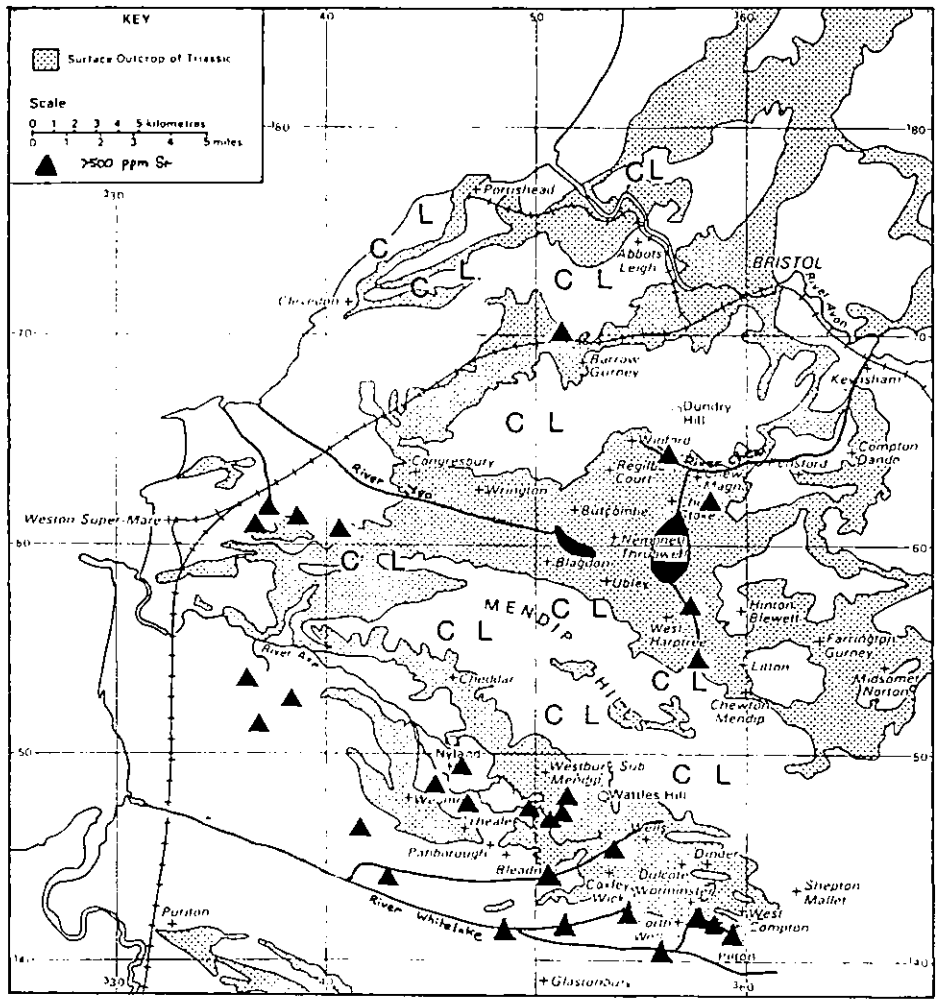

Fig 6.11: Sr anomalies in the stream sediments of the south Bristol-Mendip district (after Nickless et al., 1976; Webb et al., 1978)

Although the mineralogy and the size distribution of the stream sediment is unknown it is anticipated that the Sr is present as a celestite sand produced by the weathering of seams or veins in the thalweg. However it is thought that the anomalies taken from estuarine alluvium and peat may be of syngenetic hydromorphic origin, produced by the sequesting of Sr on to iron and manganese oxides in areas of sluggish drainage and low pH, Eh conditions (Hawkes and Webb, 1962).

As most of the Ba values fall within the 99.9th percentile of the national population the anomalous Ba values cannot be the product of lithological or geochemical factors unique to the region under review.

Anomalous Ba samples, containing values above the threshold of the elevated background (900ppm) are shown in Figs. 6.9 and 6.10. Many of the Ba anomalies either correlate with the distribution of the Type C celestites (Fig. 5.1) or the Carboniferous mudstones in which they occur (Fig. 1.5). The five anomalies along the Frome are all downstream of, and may be derived from baryte deposits such as that described from the Yate Bypass in 2.5.7.1.

High Ba values are especially common in the south Bristol-Mendip district where they are correlated with baryte veins in Carboniferous Limestone.

Zn values cannot be correlated with celestite deposits but can be traced to areas of Zn mineralization.

6.2.8 Summary and Discussion

The soil sampling program has shown that the primary dispersion of the elements considered was such that only Sr, and to a lesser extent Ba, were concentrated along beds of celestite. The secondary chemical dispersion of Sr^{2+} from the celestite is minimal and anomalous Sr values are only found in soil samples containing celestite fragments. However, celestite fragments are not always present even in the topsoils over the orebodies. This effect was especially noticed in prospecting for Type C celestite (Nickless et al., 1976) because of the tendency of the Type C celestite to weather into blocks, producing few smaller celestite fragments (6.1.3). In addition,

most of the terrace gravels in the Yate-Cromhall area are celestite free and would therefore dilute any celestite detritus produced by the weathering of underlying celestite.

Much of the Ba in the soils is dispersed in false anomalies and Ba can only therefore be used with limited success in prospecting for celestite.

Geostatistical analysis has shown that although the Sr assays of the regional survey samples can be inter-related in an 'ideal' Matheron type model at distances of up to 400m along traverses perpendicular to the strike, along the strike this distance is drastically reduced to distances of about 30m. This is probably caused by irregularities in the morphology of the celestite seams, as described in 2.4.1.

The problems of poor chemical and mechanical dispersion of the celestites could be overcome by a total Sr analysis of only those particle sizes which show maximum geochemical contrast (ie. the coarse sand and very fine sand fractions, see 6.1) in soils sampled along the strike at 30m intervals. In the coarse fractions the fragmented celestite is clearly visible to the eye and sieving of the topsoil down to 0.7mm would allow the coarser celestite to be used in prospecting for celestite without the need for chemical analysis.

The stream sediments of the area to the north-east of Bristol are all enriched in Sr, Ba and Zn, However, only Sr can be used as an indicator of celestite at the regional level. The form in which the strontium is present in the stream sediments is not known in detail but in most cases it is anticipated that fine detrital celestite is present overlying celestite in the thalweg. The regional stream sediment survey is a useful complement to the regional soil survey (Nickless et al., 1976) and unlike the latter it can be used to detect deposits of Type C celestite.

6.3 GEOPHYSICAL EXPLORATION

6.3.1 Resistivity Survey

Various geophysical exploration methods to detect the celestite ore were considered and tried.

It was initially thought that there may be a contrast in electrical conductivity between the beds or veins of celestite (which may act as an electrolyte) and the enclosing clay or marl. As resistivity surveys are relatively cheap, do not require the calibration of sophisticated equipment and can be operated by semi-skilled personnel, an application of this kind was tested in the summer of 1979.

Exhaustive trials were carried out at Goose Green and Tylers' Farm, The Rectory and Winter's Field to investigate:-

1) Seams of Type A celestite in Yate Formation mudstones.

2) ? Celestite of Type B which according to old company records floors shallow Yate Formation basins between quartzite ridges.

3) Celestite of Ty pe C in periglacially disturbed Millstone Grit mudstones.

6.3.1.1 Method

A 'Megga' resistivity meter was used to measure the apparent resistivities of points 2m, 5m or 10m along traverses favourably placed with respect to the strike of lithological boundaries (Fig. 6.12). The electrodes were spaced according to the Wenner configuration. All observations were taken in dry weather to eliminate errors arising from changes in humidity.

Two sounding operations with an expanding Schlumberger Array were also carried out 5m in, above the face at Tylers' Farm North.

6.3.1.2 Results and Interpretation

The results of the field investigations are illustrated in Fig. 6.13 and are discussed for each locality.

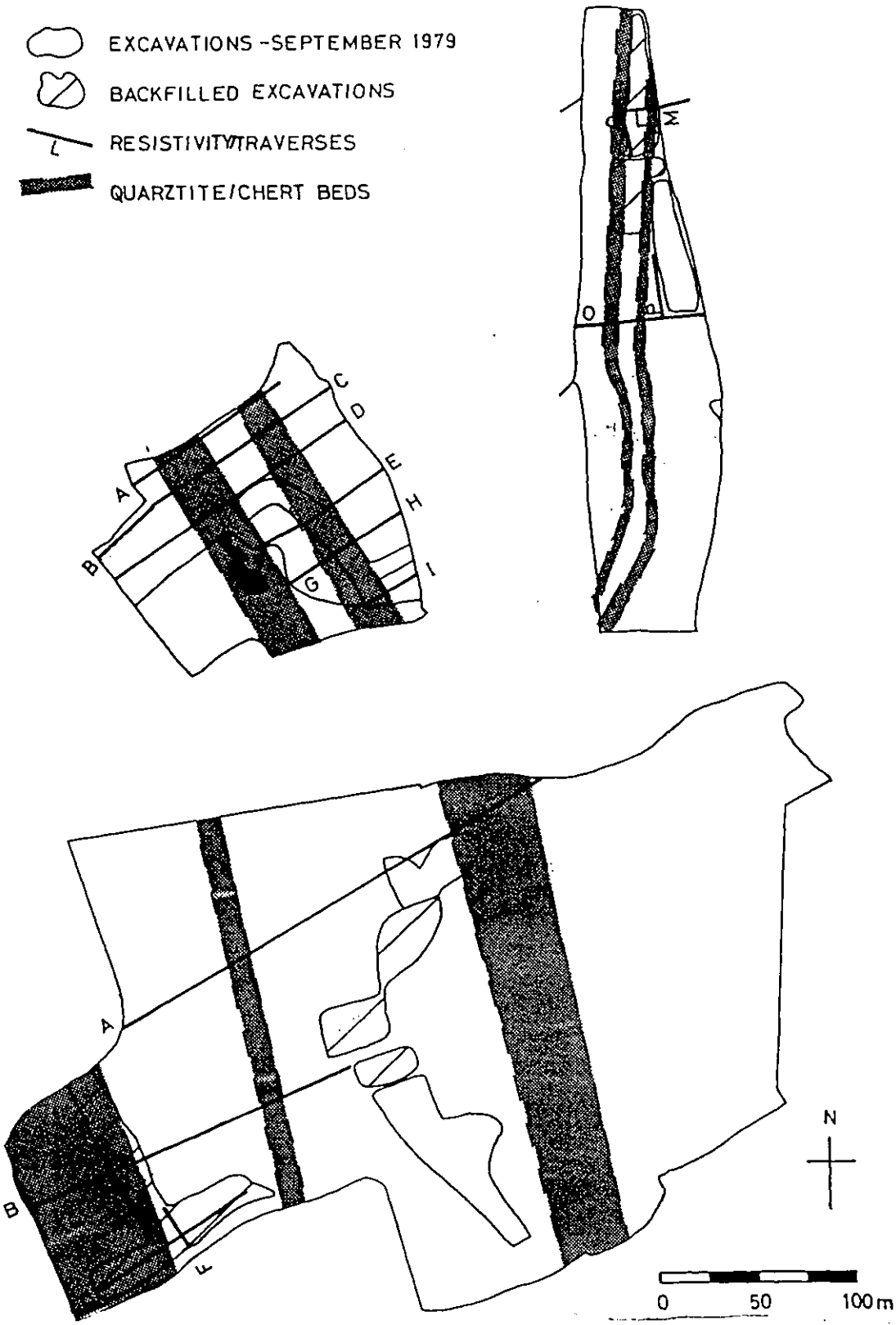

Fig 6.12: The resistivity traverses at the Rectory, Winter's Field and Goose Green/ Tyler's Farm sites

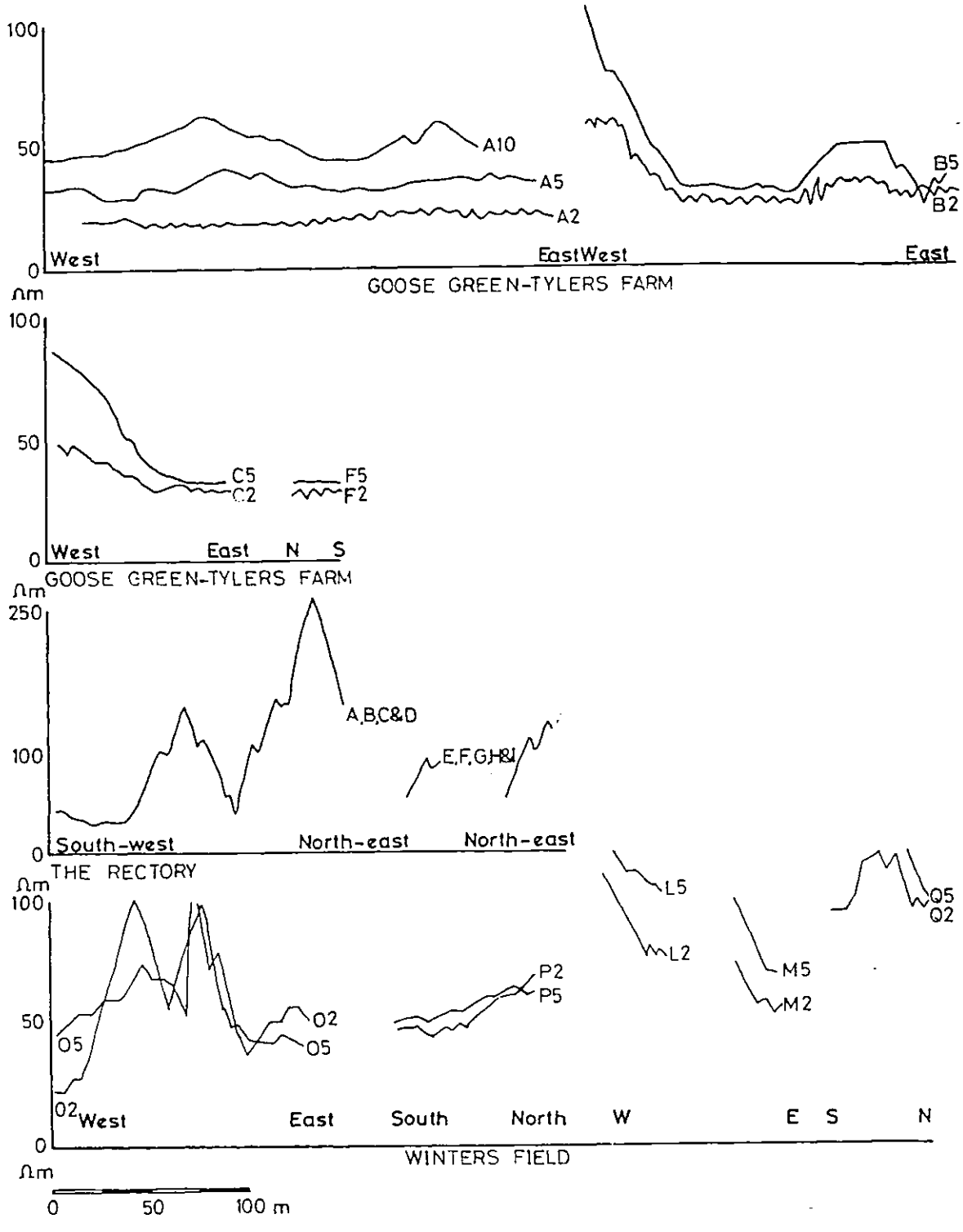

Fig 6.13: Apparent resistivities at the field sites

a. Goose Green and Tylers' Farm

Traverses A2, A5 and A10 were taken along a line at right angles to the projected outcrop at spacings of 2m, 5m, 10m respectively. B2 and B5 were similar traverses parallel to the A traverses and staggered to the SE. Profile C was a similar shorter traverse across backfilled ground whereas profile F was set out across backfilled ground at right angles to C.

In all of the plots the overriding influence was the presence beneath the Yate Formation cover of Millstone Grit quartzitic sandstone and chert. Small irregularities in the A2, B2 and F2 traverses cannot be attributed with certainty to any subsurface feature and occur in both virgin and backfilled ground. Because the C2 plot is more smoothed in comparison it is thought that they may be due to climatic or instrumental causes.

Neither the celestite seams nor the massive body of Type B celestite were detected in any of the traverses (Fig. 2.2). The resistivity curves from the electric sounding showed a two-layer earth, in this case Yate Formation overlying Millstone Grit beds (not shown in Fig. 6.13). The two thick seams of celestite seen in the face (E and F) did not make any impression on the resistivity trace.

b. The Rectory

Although Kellaway and Welch (1961) mapped only one quartzitic sandstone band the several parallel traverses at The Rectory showed quite clearly the presence of two wide anomalies corresponding to two thick quartzitic layers.

Fig. 6.12 shows the outcrop of the quartzitic sandstones as evaluated at the level of the 5m hemisphere of resistance and transposed to surface datum. This shows close agreement with the geology revealed during the opening up of the site later (Fig. 2.26). 'Shoulders' on the side of the peaks are now known to be caused by many subsidiary quartzitic beds. Although celestite was not detected in the resistivity plot a prediction that the two lows under the site of the road and to the west of

the mapped quartzite would contain celestite was later confirmed during excavations when Type B, C and D celestite was found (Fig. 2.23).

c. Winter's Field (Fig. 2.27)

Traverses 02 and 05 were taken across the strike of the Namurian strata. The resistivity plots of these lines are text-book examples of traverses across a less conductive layer dipping steeply in conductive measures. The 05 trace is slightly offset from the 02 trace and to the left of the profile yields resistivities greater than 02 whereas to the right this relationship is reversed. The 0 traverses proved that the quartzitic sandstones mapped by the Geological Survey did not extend up to the western limit of the field and that they also contained a median parting of mudstone.

Traverses P2 and P5 are almost identical in magnitude, stressing the similar electrical properties of the deeper mudstones and the superficial clay Head which here is rich in celestite mumblers. Traverses L, M and Q all demonstrate the powerful effect of the subsurface resistor (the quartzitic sandstone) beneath a conducting layer (Head or backfill), which is of such magnitude as to render identification of the near surface lithologies very difficult.

6.3.1.3. General Discussion

The resistivity survey was not able to prove seams of celestite and only recorded changes in lithology below the unconformity. The differences that have been observed were those between Yate Formation/Millstone Grit mudstones and Millstone Grit quartzites and cherts. Contrary to initial expectations, there is insufficient resistivity contrast between the celestite and the host rocks.

Land that has been back-filled should be better drained and therefore have a lower resistivity. As contrasts have not been found, either in intensity or in variation in resistivity between backfilled and virgin land the technique cannot be applied to detect areas of old workings. The Yate Formation has been weathered and reworked to such

an extent that the apparent resistivity has been depressed to the range of values found in backfilled land.

6.3.2. Other Methods

The adoption of other geophysical surveying methods were also considered. Magnetic methods are clearly not applicable and, considering the rather limited success of the resistivity survey, Induced Polarization or Electromagnetic techniques were not tried as they were unlikely to be successful.

Because the only significant physical characteristic of celestite is its high specific gravity,gravity methods may come under consideration. It is thought, however, that the thin celestite seams would not constitute a distinguishable gravity entity. In addition, gravity surveys involve the levelling of ground, calibration of instruments and are relatively expensive.

The application of seismic techniques by other workers in the past has not been a success because the celestite beds are not regular enough or thick enough to give strong reflections.

No signals of any magnitude were detected from celestite crystals submitted to 'Harwell' and 'Canberra' multichannel gamma ray spectrometers, so that radioactive methods cannot be applied.

6.3.3. Summary

The measurement of apparent resistivities can be used to show the presence or absence of beds of quartzite or chert in the Millstone Grit. As the quartzite/ mudstone contact is a preferred site for the deposition of Type C celestite a resistivity survey may indirectly help in prospecting for celestite.

Magnetic, Induced Polarization, Electromagnetic, Seismic and Radioactive techniques cannot be used in the detection of celestite deposits. The writer feels that the application of a gravity survey would not be successful, for reasons given above.

6.4 A REVIEW OF CURRENT METHODS OF EXPLORATION AND ASSESSMENT

6.4.1 Current Exploration Practice

The major prospecting technique applied by the Bristol Mineral Company Ltd. is the excavation of 'test holes' by JCB back-hole excavator. These are V-shaped trenches, approximately 3m x 1m, excavated to depths of up to 6m. On occasions the method of probe bar boring may also be applied. These are small-diameter hand bores, used where the overburden is relatively soft and the celestite can be detected by impact.

The number of trenches dug depends on the quality and quantity of celestite encountered in the first trenches, the size of the field and the willingness of the landowner to have his land disturbed should the trials be unsuccessful.

6.4.2 Current Assessment Practice

The celestite sorted from the spoil at each test hole is weighed and multiplied by the area of the trench to give a yield, expressed in tonnes/acre. The average of the yields is then computed and multiplied by the acreage to give a total yield at that site. Typical average yields for working sites range from 500-800 tonnes/acre, with individual test hole yields ranging up to about 1700 tonnes/acre for Type A celestite and 3800 tonnes/acre for Type C celestite.

This method was first used by E.C.C. Ltd. in 1969 in a systematic evaluation of several celestite-producing areas using trenching on a 100m grid (Fig. 6.14a). Yields of less than 150 tonnes/acre were considered sub-economic and were omitted from the subsequent calculations when surrounded by land containing higher values. As exploitation of the celestite proceeded, it was found that the rather optimistic tonnage estimates produced did not correspond to the quantity of celestite quarried.

Nickless et al. (1976) used trenching or augering at the level of the field site to estimate tonnages which, with reservations, were then extended over each of the six

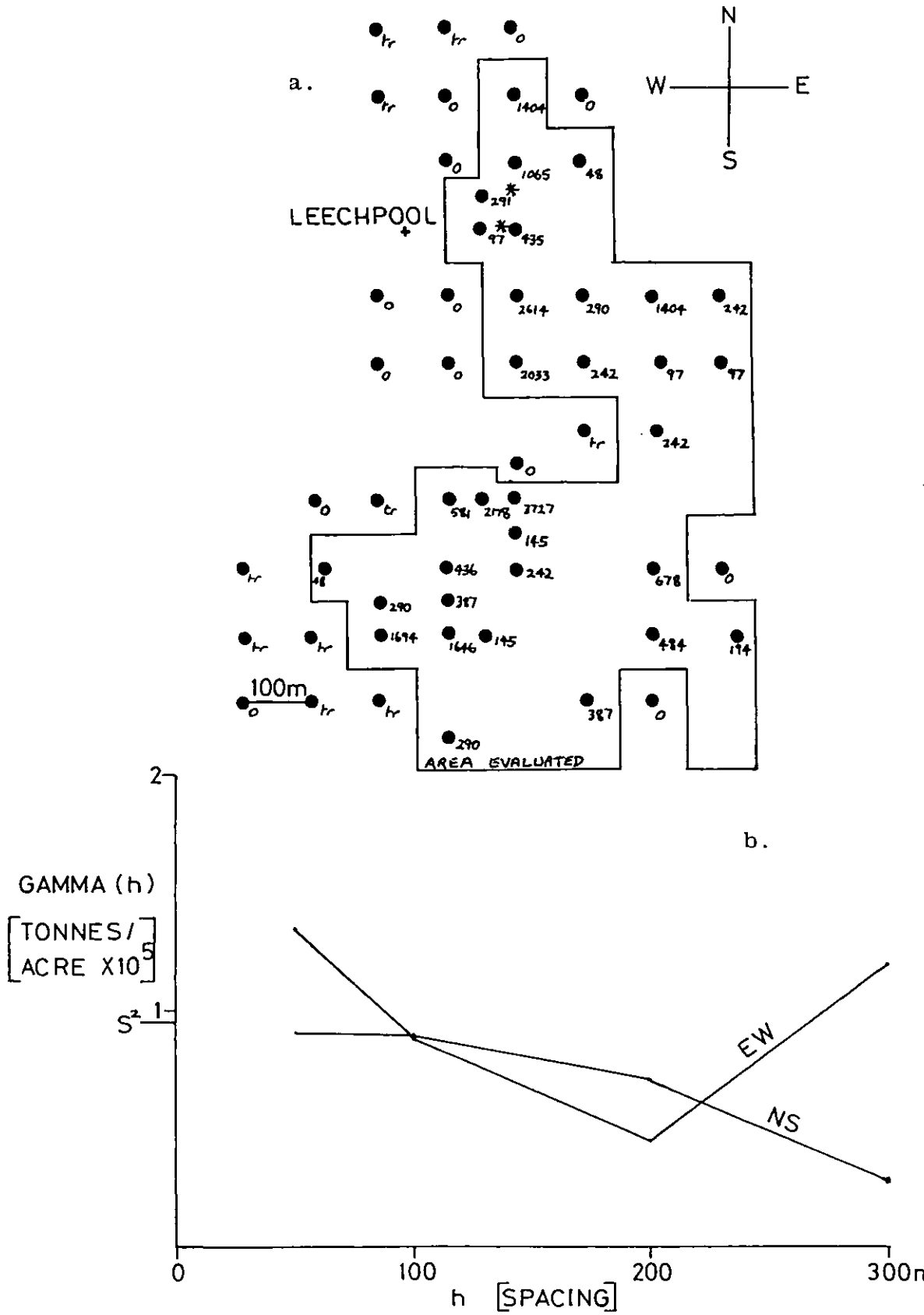

Fig 6.14 : The Leechpool Area; location of test holes and semi-variograms of yields (*= later assessment)

celestite-producing areas. These workers did not include confidence limits in their assessments and fully acknowledged the unsatisfactory nature of the procedures adopted.

6.4.3 Critical appraisal of the exploration and assessment methods

The nature of the celestite deposits is such that any estimate of tonnage from exploration trenches has to be regarded with caution. This is because of the wide variation in yields from adjacent test holes, or even from 'replicate' test holes at the field level of assessment (see Table 6.5). Identifiable geological factors influencing the yields include: -

1) proximity to quartzite/mudstone contact (Type C celestites only)
2) extent of clay Head (this tends to evenly disperse the celestite blocks)
3) number and aerial extent of celestite seams (Type A celestites)
4) continuity and thickness of celestite seams (Type A celestites)

Furthermore, combining the yields of each test hole to assess the tonnage of the site leads to further inaccuracies for the following reasons: -

a) the yields may show a lognormal distribution and no allowance is made for this in the tonnage estimate
b) meaningful confidence limits cannot usually be applied to the tonnage estimate from the small number of trenches
c) reserve underestimation results from mechanical limitations of the back-hoe used in the excavations, as this cannot dig deeper than about 6m - in most cases beds of indurated marl or even thick seams of celestite may substantially reduce this figure

Because of a paucity of data the relationship between yield estimates and tonnages extracted cannot always be determined. Where figures are available difficulties in interpretation arise because the limits

Table 6.5: Variation in test hole yields as shown by replicate test holes at the Poundhouse Farm site

No:	1973 program tonnes/acre	No:	1980 program tonnes/acre
A2	1296	X4	867
A10	768	X3	668
A12	240	X2	60
A13	1728	X1	359
B3	1392	X5	347

For location of test holes see Figs 2.9, 6.15.

Table 6.6: Comparison of expected and actual yields for the West End and Yate Lower Common sites

	West End	Yate Lower Common
Expected yield from all test hole data, and the average of the entire site	585 t/ac[1] 19.5 ac	771 t/ac 18.5 ac
Expected yield for a 'potential extraction area' independently assessed by consultants and the acreage of that area	1210 t/ac 6.7 ac	1212 t/ac 6.6 ac
Expected yield (Nickless et al., 1976)	561 t/ac	-
Actual yield and the acreage quarried up to 31.12.81 (source of data: B.M.C. Ltd.)	969 t/ac 7 ac	680 t/ac 12 ac

1 using data from 10 of the 17 test holes at this site

of economic ground evaluated do not correspond with that dug in practice; some areas of some fields (e.g. hedgerow borders, the ground under the top-soil heaps) are inadvertently sterilized and ore is not recovered. There are also philosophical differences over whether to include barren testholes, or the entire site in the reserve estimate, leading to over or under estimation of tonnage. Examples of these practical difficulties are given in Table 6.6. These are usually overcome in mining practice by dividing the orebody up into smaller panels of ore but here the lower value of the celestite and the small area of the sites preclude this practice.

6.4.4 Geostatistical assessment of the test hole data

The test hole yields of the Poundhouse Farm, Wapley Common and Leechpool areas were geostatistically evaluated in order to clarify the points raised above, and to establish whether there was any structure to the data. The first two sites provided detailed information at the field level; Poundhouse Farm was trenched on a grid system by E.C.C. Ltd. in 1973 and Wapley Common randomly, by Nickless et al. (1976) and by B.M.C. Ltd. in 1980-81 (Figs 2.2, 2.5). The Leechpool area is part of the 1969 100m grid network and provides information on Type A, Type C and mumbler deposits in a typical weathered Millstone Grit terrain.

Semi-variograms of the yields at Poundhouse Farm and Leechpool sites are shown in Figs 6.14 and 6.15. Each show random behaviour (see 6.2.6.3) with more systematic irregularities indicating underlying trends (Clark, 1979). As there is no correlation between any of the yields this implies that for purposes of tonnage estimation, test holes may be randomly positioned at these sites. However, a Matheron scheme of the type:

$$\text{Sill} = 191506 \quad \text{range} = 125\text{m}$$

$$\gamma(h) = 191506 \text{ for } h > 125$$

$$\gamma(h) = 2298h - 0.05h^3 \text{ for } h \leqslant 125 \qquad \text{---(2)}$$

may be fitted, with reservations, to the Wapley Common data (Fig. 6.16) (see Royle 1975; Clark 1979 for discussion of the Matheron scheme). The yields are correlated up to 125m, indicating an optimum spacing of 100m

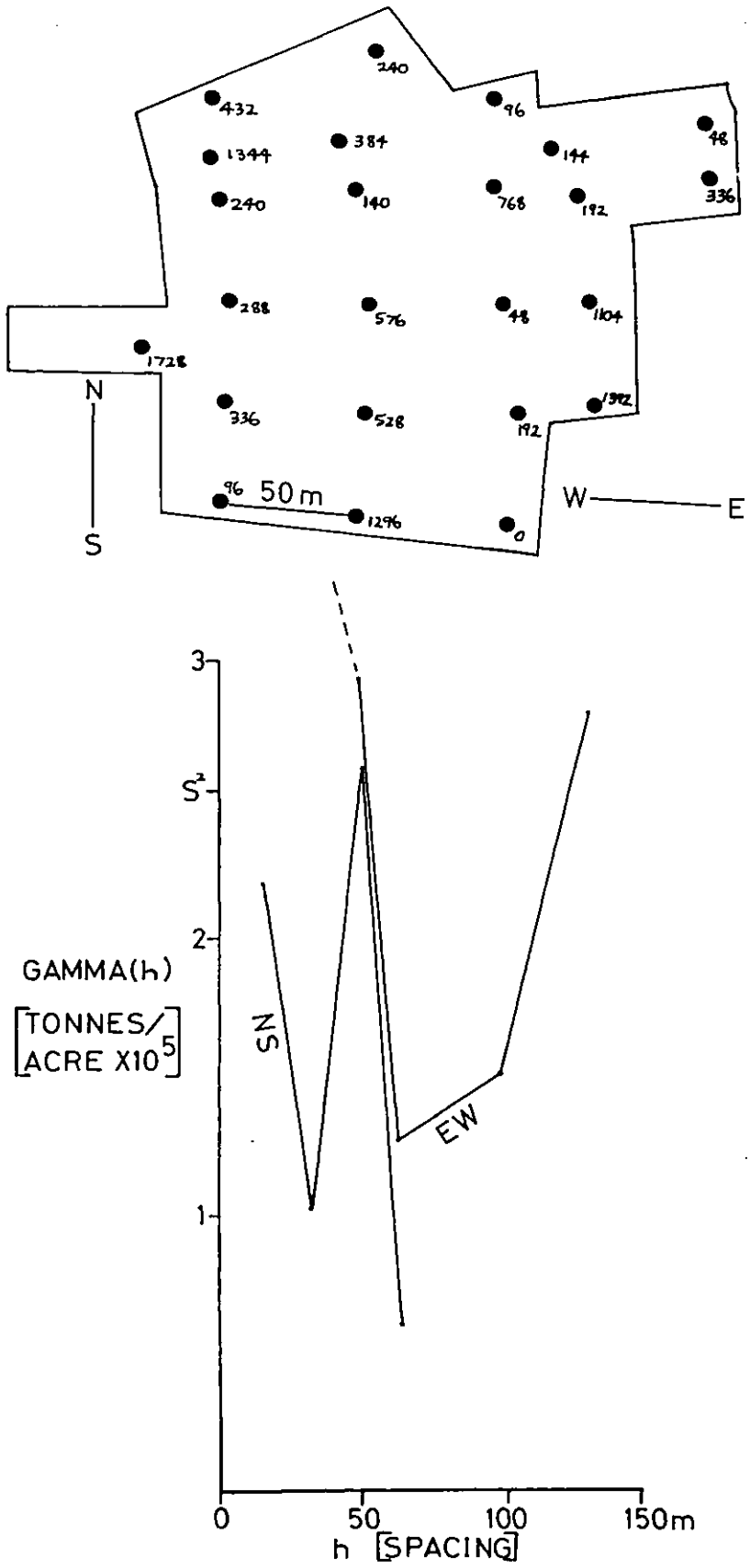

Fig 6.15: Semi-variograms of the test hole yields of the Poundhouse Farm site

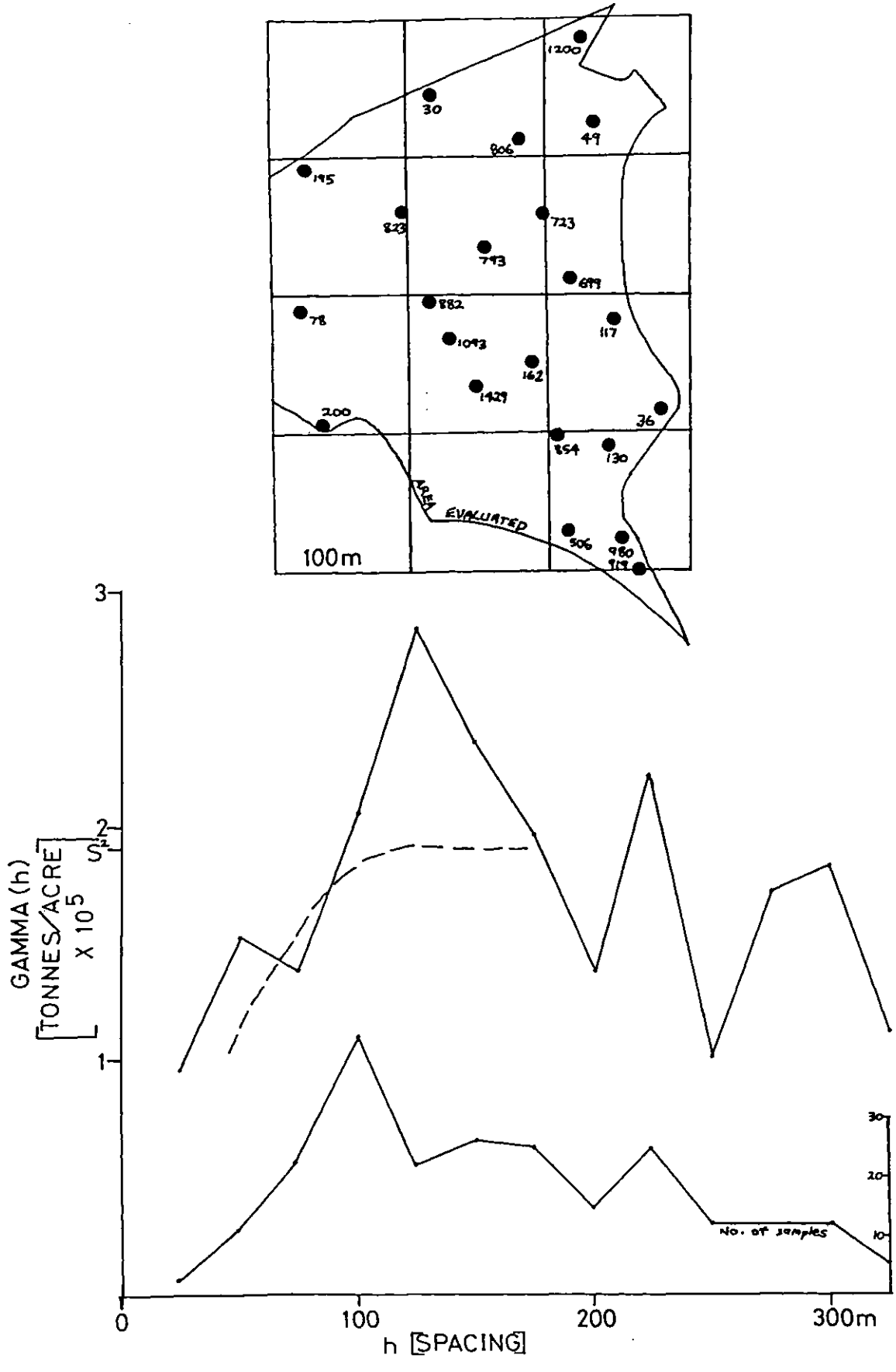

Fig 6.16: Semi-variogram of the test hole yields of the Wapley Common site

for the test holes. The Wapley Common site is underlain by gently dipping celestite seams subparallel to the ground and the trenches are randomly arranged, so that geometrical isotropy is assumed (see Royle, 1975).

The Wapley Common site is now briefly evaluated, as an example of the improved estimation techniques possible when the geostatistical model is known: -

1) The site is first divided up into panels by placing a grid over the test holes as shown in Fig. 6.16.

2) The yield of each panel is given by the mean of the values contained therein. A standard error for each estimate of 330 tonnes/acre may be determined from equation (2) and the expression for the estimation variance given by Royle (1975, p36). This rather large figure would be reduced by the operation known as kriging (e.g. Royle 1975, David 1977, Clark 1979) if the test holes were systematically positioned.

3) Because the test holes are randomly arranged, the mean and statistical variance of the data cannot be improved upon as estimators of the <u>total</u> tonnage. In this case, the test holes in Fig. 6.16 give an estimate of 11429 tonnes. The tonnage variance is given by:

$$\frac{s_T^2}{T^2} = \frac{s_Y^2}{Y^2} + \frac{s_A^2}{A^2} \qquad \text{-------- (3)}$$

where T is the tonnage estimate, Y the mean yield and A the area. As A is accurately known in advance, and T/Y = A, this reduces to:

$$s_T^2 = s_Y^2 \,.\, A^2 \qquad \text{-------- (4)}$$

As the area outlined in Fig 6.16 contains 19.79 acres;

$$s_T^2 = 191506 \,.\, (19.79)^2$$

whence $s_T = \pm\ 8660$ tonnes.

Assuming normality, this gives a 95% confidence interval of 0-28750 tonnes, clearly emphasizing the uncertainty associated with the estimate. Again, estimation of yields systematically arranged on a grid network would substantially reduce this figure.

6.4.5 Conclusions

The application of exploration techniques that do not disturb the ground surface has not been a success (sections 6.2 and 6.3). Lightweight portable drills have proven to be unsatisfactory (Nickless et al., 1976). A 1m auger used sparingly by these workers was only possibly effective in excavating Yate Formation mudstone as its application was thus limited. Auger holes also cannot be successfully back-filled. The excavation of test holes would therefore seem to be the best method of any of the options considered.

At present the number, and the positioning of the test holes at each site is governed by commercial, environmental and geographical constraints. The geostatistical assessment has shown that in general the local geological conditions and the distribution of celestite are so unpredictable that trenching on a grid pattern would not offer any improvement over the present practice. However, it is also obvious that a widely spaced test hole pattern will provide more geological information on the celestite over the entire site. For assessment purposes, the mean and variance of the test hole data cannot be usually improved upon as estimators of the total tonnage, and the mineral recovered from one test hole for the tonnage over an arbitrary range of influence.

In areas where stratiform Type A celestite underlies gently sloping land (e.g. Wapley Common, West End) the following procedure is suggested: -

1) Trench along a square grid at 50 or 100m intervals, depending upon the acreage of the site. Where field boundaries intersect the grid offset the test hole locations accordingly.

2) Compute the semi-variogram and hence determine whether a geostatistical model can be used to describe the deposit. If so, it should then be possible using estimation variances as described by Royle (1975) to calculate a narrower confidence interval for the total tonnage estimate and also to krige the individual panels in order to determine more precisely the tonnage distribution over the site.

It need also be added that careful supervision and a knowledge of the stratigraphy are necessary requirements for all the applications suggested above, and that all test holes should be logged for future reference.

CHAPTER SEVEN - CONCLUSIONS AND RECOMMENDATIONS

7.1. ECONOMIC SIGNIFICANCE OF THE CELESTITE DEPOSITS

1) Five economically significant celestite types have been recognized. The first three types, Type A, B and C, constitute the original evaporite deposit which crystallized from the Sr^{2+}- enriched waters of the Norian sea. Figs 7.1 and 7.2 are estimates of the extent of celestite-bearing land in the study area and Wapley-Bitton area, constructed using constraints of present-day relief, paleogeography, lithology and sedimentological analysis. Only Type A celestite under an overburden depth of less than 3m is shown. The Type A celestites formed in the Yate Formation mudstones and marls principally as an early diagenetic replacement of supratidal calcium sulphate , mainly anhydrite. Type B and Type C celestites (the 'epigenetic celestites') were deposited in marginal deposits and Paleozoic rocks, respectively, as the sea overstepped the sub-Triassic surface. Reworking of the evaporite deposits produced the two other significant types; Type D celestites and celestite sands. Type D celestites or mumbler deposits were derived by the periglacial weathering of Type C celestites during the Quaternary Ice Age. Celestite sands may have been deposited following sub-aqueous reworking of the epigenetic celestites either during the Norian transgression or by fluvio-glacial activity as the celestites were re-exhumed during a Pleistocene ice-retreat. Little is known of the distribution of the re-worked celestites; although mumbler deposits have been described from various localities of Type C celestite celestite sands have not hitherto been systematically recorded. It is thought that both types of deposit may be present locally, throughout the Yate-Cromhall belt of epi-genetic celestites (Fig 7.1).

2) Type A celestites are found at up to eight horizons below the base of the Blue Anchor Formation with calcite, dolomite and in some cases, authigenic silica. Celestites with a high component of sparry calcite (calcitic celestites) occur throughout the study area. The calcite is a recrystallization product of the fine grained Carboniferous Limestone detritus or cement and forms crystals 0.02 - 3.00mm in diameter intergrown with the celestite although

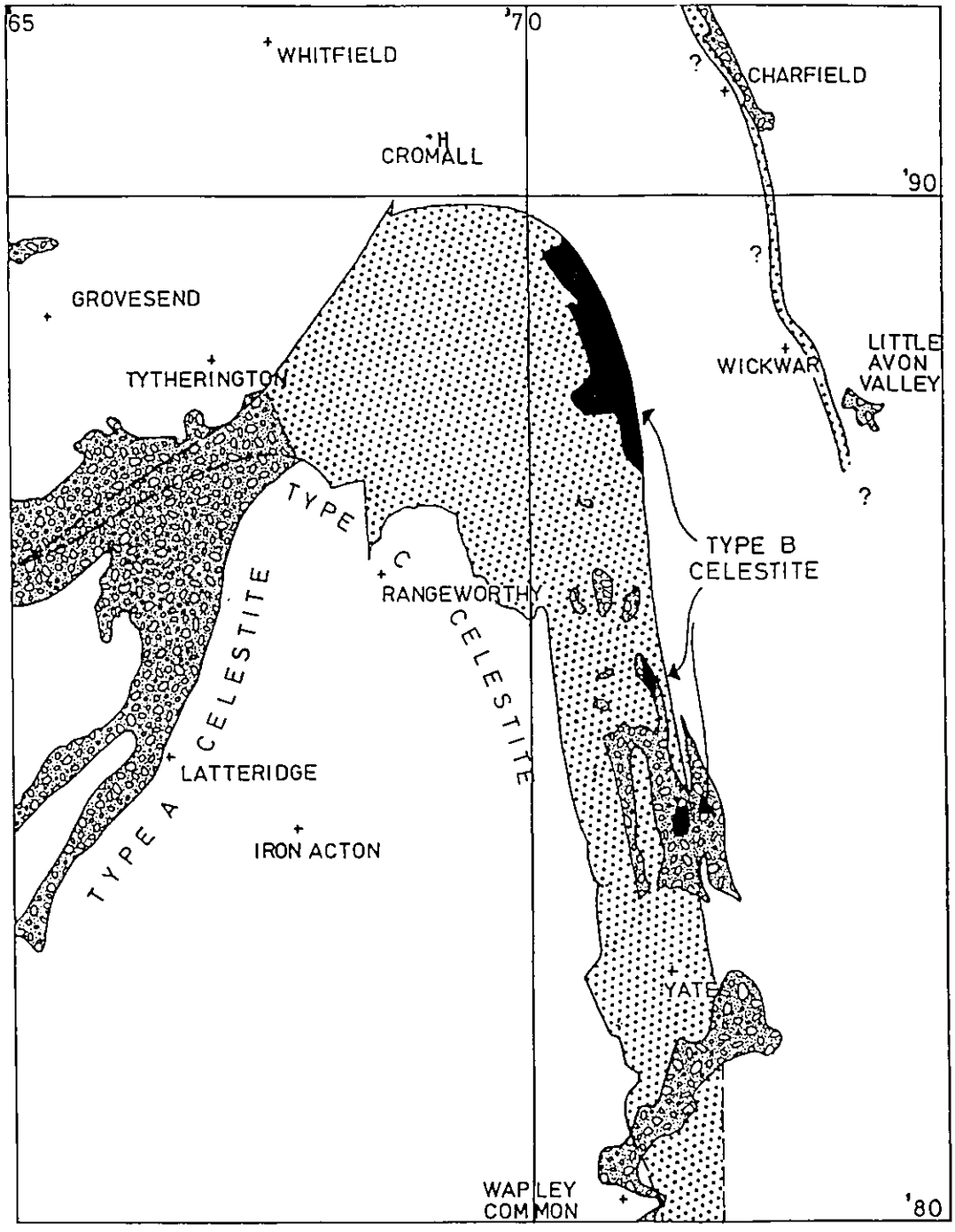

Fig 7.1: Extent of celestite-bearing land in the study area (after Nickless et al., 1976)

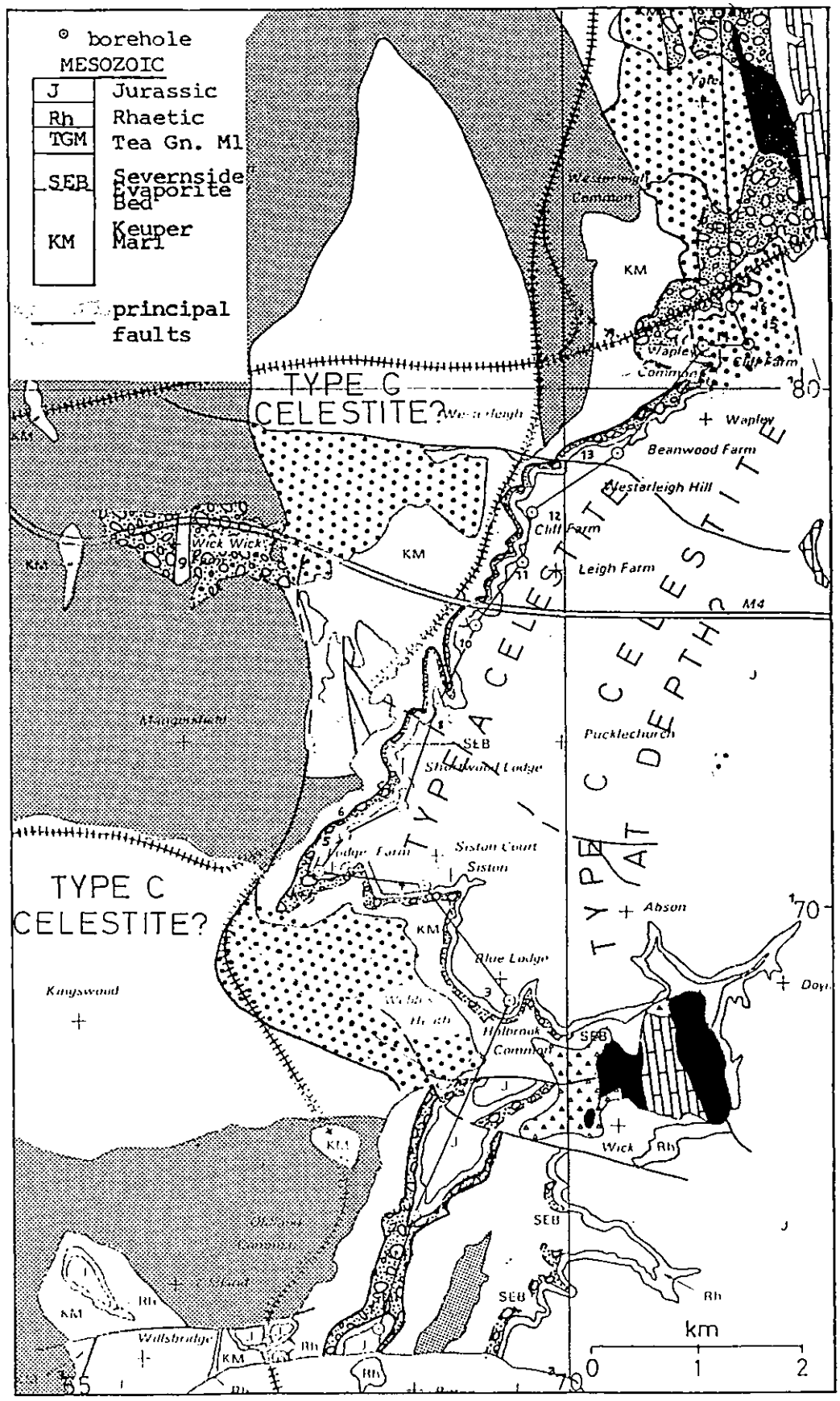

Fig 7.2: Extent of celestite-bearing land in the Wapley-Bitton area (after Nickless et al., 1976)

calcite below 0.5mm across can also replace celestite. Dilution by calcite is a serious cause for concern and has been investigated by Alanby (1979) and also by Page (1980) who has submitted a process design study to overcome the problem.

Dolomite is less commonly associated with the Type A celestites and is usually late diagenetic, replacing calcite.

Authigenic silica (megaquartz and chert) is more restricted in occurrence but where it occurs it can completely replace the celestite. The quartz-rich celestites of Wapley Common for example contain on average 37.9% Sr (Table 4.2). These sub-economic celestites could be upgraded by blending with a purer celestite concentrate. Further work is required to ascertain whether the processing scheme proposed by Page (1980) would also beneficiate the quartz-rich celestites.

The celestite itself only contains two elements, Ca and Ba, in amounts greater than 0.1%. The red celestites are as pure as the blue or transparent varieties. The calcium is present at levels of about 0.2-0.5% i.e. slightly above the minimum specifications stated by Thomas (1973). Ca occurs in the celestite lattice and in anhydrite inclusions. Barium is present in greater abundance than calcium, averaging 0.6%, well below the critical specification of 1.2% Ba (Thomas, 1973). However barian celestites containing 0.96% Ba have also been recognised. Some of the barian celestite is characteristically white and sheaf-like and could be separated from the ore before washing. The removal of all the barian celestite would be impractical and it is thought that these high Ba values would be averaged out by mixing with celestites of more usual composition during the washing of the ore.

The distribution of Type A celestite shown in Fig. 7.1 is basically that outlined by Nickless et al. (1976). To the west of the Bristol Coalfield, yields are sub-economic and the celestite has a generally high calcite or quartz content. Exploration work in this area should be concentrated on the outcrop, where celestite is known to occur, rather than the dip-slope, where its existence is less certain. A tonnage of over 100,000 tonnes has been calculated by Nickless et al. (1976) for the indicated, Type A resource

of the Yate-Cromhall area, to which can be added at least 1,650 tonnes from the Charfield district which Nickless et al. (op cit) regarded as sub-economic.

The remaining parts of the Michaelwood-Wickwar area and the Thornbury-Oldbury and Aust-Henbury areas do not contain Type A celestite in the quantities or of the quality required for economic extraction. Only the indicated Type A resource of the Wapley-Bitton area is thought capable of providing an economic yield of celestite. However calcite, gypsum and quartz are common accessory minerals throughout this area and celestite only occurs in minor amounts in two of the six mineralogical zones shown in Fig. 5.4 . The tonnage of over 200,000 tonnes calculated by Nickless et al. (1976) should therefore be reduced by about a third to account for this.

The total resource of Type A celestite is therefore in the order of 230,000 tonnes. This celestite Type represents the main resource for future exploitation.

3) The most economically significant Type B celestite deposits are the mineralized river channels or 'cut-and-fill' features seen at Goose Green West. The possible locations of other such deposits are shown in Fig. 7.1. Large tonnages are to be expected from these rather localized deposits; 3 ft. seams have been recorded in the Hall End-Cowship district (Anon, 1960).

4) The Type C celestites mainly consist of fissure filling and concretions of various types although some may replace calcium sulphate minerals. Free of Triassic sediment, the Type C celestites are only very rarely contaminated by calcite although barian celestites may occur as in Type A celestites.

Most of the Type C celestite occurs in Millstone Grit mudstones, from which it is easily extracted. Many of the occurrences show development of a 'rab' or microcrystalline celestite border to the celestite veins which is rejected as spoil. This material consists of celestite laths up to 0.2mm across cementing the mudstone, and assays at 39-42% Sr (Table 4.1, 4.5). Unfortunately interstitial mudstone is not liberated from the microcrystalline celestite by the Hall End crushing plant and inclusion of the rab with the

run-of-mine celestite ore would affect the quality of the celestite product. Improved processing techniques, or blending of the concentrates would be required to recover this material.

By contrast, most celestite veins in the Carboniferous sandstones and Permian ironstones cannot be mined at present because of dilution by the host rock. Contrary to the observations of Nickless et al. (1976), veins of celestite up to 10cm across also occur in Carboniferous sandstone. These thicker celestite masses were once exploited by breaking up the sandstone using a tractor/ripper combination (Anon, 1960) and could also be economically worked at the present.

The deposits on the east of the Coalfield consist of the inferred and part of the hypotheoretical (see 1.1) resource of Nickless et al. (1976) (Fig. 7.1). The estimate of over 60,000 tonnes for the inferred resource (Nickless et al., op. cit.) seems reasonable. In addition the hypotheoretical resource contains an unknown tonnage in land where celestite yields have not been well documented, for example the Bagstone (690872) deposit (Sherlock and Hollingsworth, 1938). Fig 7.1 also includes a narrow strip of land to the south of Tytherington which may contain a 'mirror image' of the Yate Platform deposits. It is recommended that any future test holes excavated in this region be dug down to the Paleozoic rocks otherwise the deposit may not be detected.

Apart from the Type C celestite recorded at Whitfield and Charfield (2.5.1.1.) little is known of possible celestite in Paleozoic rocks outside the Tortworth Ridge.(Nickless et al., 1976). Epigenetic celestite may occur along a narrow strip of land bordering the Little Avon Platform but the host rock is mainly Old Red Sandstone and economic deposits are not thought to be present.(Fig 7.1). There is an unconfirmed report of epigenetic celestite at Wickwar (Baker, 1902).

Analysis of the Wapley-Bitton area indicates that Type C celestite may outcrop in the Webb's Heath and Wick Wick districts, as well as along a buried strip of Paleozoic floor further east (Fig 7.2) (see also 7.2 below).

5) The Type D celestites form an in-situ Head

deposit containing blocks of Type C celestite, broken up by cryostatic forces in a weathered clay mantle. The mumblers usually overlie a vein of Type C celestite and by following the trend of the mumblers downwards the Type C bed can be located. The corollary also applies, that where celestite is absent in the clay Head Type C celestite is unlikely to occur in the Carboniferous strata beneath.

The significance of the mumbler deposits is that the celestite is pre-concentrated into blocks down to 3-4cm diameter thus facilitating exploitation. The Clay Head also contains disseminated cleavage fragments produced by the ice-shattering of crystals of drusey vein celestite. Both the disseminated celestite and the smaller mumblers are overlooked by the sorters; Altounyan (1979) has estimated that up to 70% of the total celestite may be rejected in this manner. However 80% of the -2.5mm celestite spoil is coarser than 0.6mm in diameter (Altounyan, op. cit.).

These are serious practical difficulties to be overcome if the clay Head, as well as the hand-picked mumblers are to be exploited as a celestite ore (Altounyan, op. cit.). A considerable rise in the value of the mineral would be required for the operation to be economically feasible. However, were this possible all of the land between Cromhall and Yate underlain by Millstone Grit mudstones could be reworked for the mineral.

6) Celestite sands, locally reworked water-lain derivatives of the epigenetic celestite are coarse poorly sorted deposits containing on average 33.4% Sr. These sediments occur as rafts within the clay Head and could be selectively quarried. Although the sands could be upgraded by removal of the clay component in the washing plant Fe contamination from sand-grade ironstone clasts would still constitute a problem. Further work is needed on the feasibility of the recovery of this material.

7.2 Exploration for and assessment of celestite deposits

1) Geochemical prospecting using soil sampling techniques has been successfully applied at a regional level to map out the Type A celestites (Nickless et al., 1976). Similarly, the extent of celestite bearing

land is also reflected in the Sr content of the stream sediments of the area to the north-east of Bristol. These indicate prospects with anomolous Sr values where celestite has not been hitherto recorded, particularly near Iron Acton, Rodford, Wick Wick and Webbs' Heath, where Type C celestite may be present. Celestite is also indicated in the stream sediments of the Barrow Gurney-Regilbury area south of Bristol where a celestite horizon, with some calcite (Nickless et al. 1976), 3-10m below the Blue Anchor Formation, probably extends along the foot of the Westbury Formation scarp from Chew Valley Lake to Weston-super-Mare.

2) Soil sampling methods have met with limited success in the assessment of individual deposits. The technique fails at the field level because the two elements, Sr and Ba, used to indicate celestite mineralisation are only present in celestite itself. Because celestite is relatively insoluble, secondary dispersion of Sr and Ba has been minimal and anomalous Sr and to a lesser extent Ba values are only detected where celestite fragments are present in the soil. Therefore celestite may only be found where seams or veins of celestite, or their derivatives are sampled at outcrop. Whereas this technique is sufficient to approximate the regional extent of celestite, difficulties are met at a larger scale where the effects of irregularities in the nature of the celestite horizons, topography, and superficial deposits all combine to prevent inclusion of celestite in the top soil, or complicate the interpretation of the geochemical map. In some extreme cases, the B.M.C. Ltd., in follow-up work to the regional survey (Nickless et al. 1976), could not find any celestite at all.

In addition it need hardly be added that geochemical prospecting supplies no information on the tenor or tonnage of an ore deposit such as the celestites. For example, although seam B at Goose Green West was proven by soil sampling (Fig. 6.4) the bed was not thick enough to be exploited.

The above considerations did not commend the further use of stream-sediment sampling at the field level.

3) . The nature of the celestite deposits is such that they do not constitute a distinguishable geophysical

entity. Resistivity, radioactive and seismic techniques have all failed; other methods are either too sophisticated or are not applicable for this type of mineral commodity.

4) A pilot study involving a geobotanical sampling technique could if successful be applied in the prospecting for celestite. A qualitative study of the Sr content of eight plant genera was made as early as 1876 (Stoddard, 1876), however, a biogeochemical study of part of the Study Area using oak leaves yielded extraordinary results (Nickless et al. 1976).

5) The only successful prospecting technique at the field level is trenching, provided the work is carefully supervised and the test holes are positioned at locations of maximum geological interest. Geostatistical analysis of the test hole yields has demonstrated that such an arrangement is as good as any in the estimate of the total tonnage of the site and the variance connected with that estimate. An improved estimation of both the total tonnage and the tonnage for smaller panels of ore may however be possible where stratiform Type A celestite underlies the land surface and a grid network of test holes, at spacings of 50 or 100m is recommended in this situation.

6) The above conclusions may have wider implications on prospecting for celestites or similar orebodies of medium economic value (e.g. baryte) elsewhere. In these cases a regional stream sediment or soil sampling survey could be used equally well to delineate the extent of the ore-field, but beyond this level the techniques are no longer effective and trenching techniques must be used.

REFERENCES

Adams, S.F. 1920. A microscopic study of vein quartz. Econ. Geol. 15, 623-664.

Alanby, J.C.C. 1979. The UK celestite extraction industry, reserves and the environment. Unpubl. MSc. Dissertation Imperial College, London.

Allen, J.R.L. 1970. Physical processes of sedimentation. George, Allen and Unwin, London. 248pp.

——————— 1974. Studies in fluviatile sedimentation: implications of pedogenic carbonate units, Lower Old Red Sandstone, Anglo-Welsh outcrop. Geol J. 9, 181-205.

Altounyan, M.E. 1979. Technical, economic and environmental implications for improved celestite recovery at Yate, Bristol. Unpubl. MSc. Dissertation Imperial College, London.

Arbey, F. 1980. Les formes de la silice et l'identification des evaporites dans les formations silicifees (Silica forms and evaporite identification in cherts). Bull. Cent. Rech. Explor-Prod. Elf-Aquitaine. 4, 309-365.

Arthurton, R.S. 1980. Rhythmic sedimentary sequences in the Triassic Keuper Marl (Mercia Mudstone Group) of Cheshire, northwest England. Geol J. 15, 43-58.

Audley-Charles M.G. 1970. Triassic paleography of the British Isles. Q. J. Geol. Soc. London 126, 49-90.

Anon, 1960. Celestite production in Gloucestershire. Mine and Quarry Eng. 26, 363-373.

Baker, B.A. 1902. Celestine deposits of the Bristol District. Proc. Bristol Nat. Soc. 9, 161-165.

Bathurst, R. 1971. Carbonate sediments and their diagenesis. Developments in Sedimentology, 12. Elsevier. 620pp.

Bernstein, L.R. 1979. Colouring mechanisms in celestite. Am. Mineral. 64, 160-169

Berry, L.G. and Mason, B. 1959. Mineralogy. Freeman, S.Francisco. 360pp.

Blatt, H., Middleton, G. and Murray, R. 1980. Origin of Sedimentary rocks. Prentice-Hall, New Jersey. 782pp.

Buckland, W. and Conybeare, W.D. 1824. Observations on the south-western coal district of England. Trans. Geol. Soc. 2nd Series 1, 210-316.

Burkov, V.V. 1977. Deposits of Strontium. In: Smirnov, V.I. Ore deposits of the USSR Volume III Pitman, 463-477.

Butler, G.P. 1973. Strontium geochemistry of modern and ancient calcium sulphate minerals. In: Purser, B. (Ed) The Persian Gulf, Springer, Berlin. 423-453.

Campain, R.P. 1981. Lithogeochemistry in relation to the lead-zinc deposits of Mendip, Somerset. Unpubl. D.I.C. Dissertation Imperial College, London.

Carlton, Linda 1959. An occurrence of galena at Flax Bourton. Proc. Bristol Nat. Soc. 29, 491-492.

Carozzi, A.V. 1960. Microscopic Sedimentary Petrography. John Willey, N.Y. 485pp.

Cave, R. 1977. Geology of the Malmesbury District, Mem. Geol. Surv. G.B. 343pp

Chowns, T.M. and Elkins, J.E. 1974. The origin of quartz geodes and cauliflower cherts through the silicification of anhydrite nodules. J. Sediment. Petrol. 44, 885-903.

Clark, Isobell 1979. Practical Geostatistics..Applied Sci. Publishers, London.

Collie, N. 1879. On the celestite and baryto-celestite of Clifton. Proc. Bristol Nat. Soc. 2, 292-300.

Collins, A.G. 1975. Geochemistry of oilfield waters. Developments in Petroleum Science, 1, Elsevier. 496pp.

Cooke, R.U. and Warren, A. 1973. Geomorphology in deserts. Batsford, London. 374pp.

Cosgrove, M.E. 1973. The geochemistry and mineralogy of the Permian Red Beds of southwest England. Chem. Geol. 11, 31-47.

Cuff, C. 1973. The crystallography and geochemistry of authigenic calcium sulphate and carbonate minerals of the recent sediments of the Trucial Coast. Unpubl. PhD. Thesis University of London.

Curtis, M.T. 1974. Minerals from the Upper Evaporite Horizon of the Keuper Marl at Yate. Proc. Bristol Nat. Soc. 33, 73-78

Curtis, M.T. 1981. The mineralization of Southfields Quarry, Chipping Sodbury, Avon. Proc. Bristol Nat. Soc. 40, 36-44.

David, M. 1977. Geostatistical ore reserve estimation. Elsevier, 364pp.

Davis, J.C. 1973. Statistics and Data Analysis in Geology. John Willey, N.Y. 550pp.

Downing, R.A. 1967. The Geochemistry of ground waters in the Carboniferous Limestone in Derbyshire and the East Midlands. Bull. Geol. Surv. G.B. 27, 289-307.

Edmunds, W.M. 1981. Contribution in: Scott, P.W. and Senior J.R. Geothermal Energy: Report of a Symposium. Proc. Yorkshire Geol. Soc. 43, 347-356.

Edwards, A. B. 1965. Textures of the ore minerals and their significance. Aust. Inst. Min. Metall. Melbourne.

Elliot, R.E. 1961. The stratigraphy of the Keuper Series in southern Nottinghamshire. Proc. Yorkshire Geol Soc. 33, 197 -234.

Erdosh, G. 1967. Density-Fraction X-Ray Analysis: A new technique of modal analysis of rocks. Can. J. Earth. Sci. 4, 1093-1117.

Evans, G. and Shearman, D.J. 1964. Recent celestite from the sediments of the Trucial Coast of the Persian Gulf. Nature 202, 385-386.

Findlay, D.C. 1975. Soils of the southern Cotswolds and surrounding country. Rothamsted Experimental Station, Harpenden, Herts. 252pp.

Folk, R.L. 1959. Practical petrographic classification of limestones. Bull. Am. Assoc. Petrol. Geol. 43, 1-38.

———— and Land, L.S. 1972. Mg/Ca vs. salinity: a frame of reference for crystallization of calcite, aragonite and dolomite (abs). Geol Soc. Am. Ann. Meet. Prog. p508.

———— and Pittman, J.S. 1971. Length-slow chalcedony: a new testament for vanished evaporites. J. Sediment. Petrol. 41, 1045-1058.

———— and Siedlecka, A. 1974. The "schizohaline" environment: its sedimentary and diagenetic fabrics as exemplified

by Late Paleozoic rocks of Bear Island,Svalbard. Sediment. Geol. 11, 1-15.

Ford, T.D. and King, R.J. 1968. Mineralization in the Triassic rocks of south Derbyshire. Trans. Inst. Min. Metall. 77, B42-43.

Friend, J.N. and Allchin. J.P. 1940. Colloidal gold as a colouring principle in minerals. Mineralog. Mag. 25, 584-596.

French, H.M. 1976. The Periglacial Environment. Longman, London. 309pp.

Freytet, P. 1973. Petrography and paleo-environment of continental carbonate deposits with special reference to the Upper Cretaceous and Lower Eocene of Languedoc (Southern France) Sediment. Geol. 10. 25-60.

Gardner, H.F. 1974. The Origin of Landscapes. Oxford. 734pp.

Glennie, K.W. and Evans, G. 1976. A reconnaissance of the Recent sediments of the Ranns of Kutch, India. Sedimentology. 23, 625-647.

Green, G.W. 1956. The Central Mendip Lead-Zinc Orefield. Bull. Geol. Surv. G.B. 14, 70-90.

———— and Welch F.B.A. 1965. The geology of the country around Wells and Cheddar. Mem. Geol. Surv. G.B. 225pp.

———— and Melville R.V. 1956. The stratigraphy of the Stowell Park Borehole. Bull. Geol. Surv. G.B. 11, 1-33.

Hamilton, D. 1966. Disseminated galena in Rhaetic shales at Almondsbury, near Bristol. Proc. Bristol Nat. Soc. 31, 221-224.

Hawkes, H.E. and Webb, J.S. 1962. Geochemistry in mineral exploration. Harper and Row. N.Y. 415pp.

Hawkins, A.B. and Kellaway, G.A. 1971. Field meeting at Bristol and Bath with special reference to new evidence of glaciation. Proc. Geol. Assoc. London 82, 267-292.

Holliday, D.W. 1967. Secondary gypsum in Middle Carboniferous rocks of Spitsbergen. Geol. Mag. 104, 171-177.

———— 1970. The petrography of secondary gypsum rocks : a review. J. Sediment. Petrol. 40, 734-744.

Holliday, D.W. 1978. Petrology of Basal Purbeck (Upper Jurassic) gypsum rocks of the Broadoak Borehole, Sussex. Rep. Inst. Geol. Sci. 78/3 31-38.

——————— and Shephard-Thorn, E.R. 1974. Basal Purbeck evaporites of the Fairlight Borehole,Sussex. Rep. Inst. Geol. Sci. 74/4. 14pp.

Howarth, R.J. 1973. Preliminary assessment of a Nonlinear Mapping Algorithm in a geological context. Math. Geol. 5, 39 -57.

Hsu, K.J. and Schneider, J. 1973. Progress report on dolomitization- hydrology of the Abu Dhabi sabkha. In: Purser, B. (Ed), The Persian Gulf Springer, Berlin.409-423.

Illing, L.V., Wells A.J. and Taylor, J.C.M. 1965. Penecontemporary dolomite in the Persian Gulf. In: Pray, L.C. and Murray , R.C. (Eds), Dolomitization and limestone diagenesis Soc. Econ. Paleont. Mineralog. Spec. Publ. 13, 89-111.

Ineson, P.R. 1969. Trace-element aureoles in limestone wallrocks adjacent to lead-zinc-barite-fluorite mineralization in the northern Pennine and Derbyshire ore fields. Trans. Inst. Min. Metall. 78, B29-40.

Kellaway, G.A. 1961. The Bristol storm water tunnel. Unpubl. Rep. Inst. Geol. Sci.

——————— 1967. The Geological Survey Ashton Park Bore-Hole and its bearing on the geology of the Bristol District. Bull. Geol. Surv. G.B. 27, 49-164.

——————— and Welch, F.B.A. 1948. Bristol and Gloucester District. British Regional Geology, Inst. Geol. Sci.

Kendall, A.C. 1978. Facies models 11: Continental and supratidal (sabkha) evaporites. Geoscience Can. 5, 66-78.

Kensall, D.F. and McAdam, J.C. 1963. Design and operating characteristics of a hydraulic cyclone elutriator. Trans. Inst. Chem. Eng. 41, 84-95.

Kent, P.E. 1949. A structure contour map of the surface of the buried pre-Permian rocks of England and Wales. Proc. Geol. Assoc. London 60, 7-104.

Kinsman, D.J.J. 1969a. Modes of formation, sedimentary associations and diagenetic features of shallow-water and

supratidal evaporites. Bull. Am. Assoc. Petrol. Geol. 53, 830-840.

Kinsman, D.J.J. 1969b. Interpretation of strontium concentrations in carbonate minerals and rocks. J. Sediment Petrol. 39, 486-508.

Klein, G. de V. 1962. Sedimentary structures in the Keuper Marl (Upper Triassic). Geol. Mag. 99, 137-144.

Klug, H.P. and Alexander, L.E. 1954. X-Ray Diffraction procedures for polycrystalline and amorphous materials. John Willey, N.Y. 716pp.

McPherson, J.G. 1979. Calcrete (caliche) paleosols in fluvial redbeds of the Aztec Siltstone (Upper Devonian), South Victoria Land, Antartica. Sediment. Geol. 267-285.

Merefield, J.R. 1975. Incorporation in soil of barytes derived from mineral veins in south-west England. Sediment. Geol. 14, 135-148.

Moorbath, S. 1962. Lead isotope abundance studies on mineral occurrences in the British Isles and their geological significance. Phil. Trans. R Soc. 254A, 295-360.

Mukherji, K.K. 1969. Supratidal carbonate rocks in the Black River (Middle Ordovician) Group of south-west Ontario, Canada. J. Sediment. Petrol. 39, 1530-1545.

Murray, J.W. and Wright, C.A. 1971. The Carboniferous Limestone of Chipping Sodbury and Wick, Gloucestershire. Geol. J. 7, 255-270.

Nickless, E.F.P., Booth S.J. and Mosley P.N. 1975. The celestite deposits of the Bristol area. Trans. Inst. Min. Metall. 84, B62-64.

_____ 1976. The celestite resources of the area to the north-east of Bristol with notes on occurrences north and south of the Mendip Hills and in the Vale of Glamorgan: Description of 1:25 000 resource sheet ST68 and parts of ST59,69,79,58,78,67 and 77. Miner. Assess. Rep. Inst. Geol. Sci. 25, 83pp.

Ollier, C.D. 1955. The Triassic sandstones of the Bristol region. Proc. Bristol Nat. Soc. 29, 57-71.

Page, P.W. 1980. A process design study for an English

celestite ore deposit. Unpubl. MSc. Dissertation Imperial College, London.

Perel'man, A.I. 1977. Geochemistry of elements in the supergene zone. Translated from Russian, Jerusalem, Israel program for scientific translations.

Peterson, M.N.A. and von der Borch, C. C.1965. Chert: modern inorganic deposition in a carbonate-precipitating locality. Science. 149,1501-1503.

Pettijohn, F.J. 1975. Sedimentary Rocks. Harper. 628pp.

Pewe, T.L. 1969. (Ed). The Periglacial Environment. McGill-Queens, Montreal. 487pp.

Potter, P.E., Maynard, J.B. and Pryor W.A. 1980. Sedimentology of shale. Springer-Verlag, N.Y. 306pp.

Ramsbottom, W.H.C., Sabine, P.A. Dangerfield, J. and Sabine, P.W. 1981. Mudrocks in the Carboniferous of Britain. Q. J. Eng. Geol. London.14, 257-262.

Reed, F.R.C. and Reynolds, S.H. 1908. On the fossiliferous Silurian rocks of the southern half of the Tortworth inlier. Q. J. Geol. Soc. London 64, 512-545.

Reynolds, S.H. 1947. The Aust Section. Proc. Cotteswold. Nat. Field Club 29, 29-39.

Renault, M. and Brower, E. 1971. Solubility and enthalpy of Ba-$SrSO_4$ solid solution series. US Bur. Mines. Circ. 116, 28pp.

Robinson, P.L. 1957. The Mesozoic fissures of the Bristol channel area and their vertebrate faunas. J. Linn. Soc. (Zool) 43, 260-282.

Rogers, J.J.W., Krueger, W.C. and Krog, M. 1963. Sizes of naturally abraded materials. J. Sediment. Petrol. 33, 628-632.

Royle, A.G. 1975. A Practical Introduction to Geostatistics. University of Leeds. 103pp.

Sabine, P.A., Guppy, E.M. and Sergeant, G.A. 1969. Geochemistry of Sedimentary Rocks. I. Petrography and chemistry of arenaceous rocks. Rep. Inst. Geol. Sci. 69/1 66pp.

Sammon, J.W. 1969. A nonlinear mapping for data structure analysis. IEEE Trans. Computers C-18 5, 401-409.

Siedlecka, A. 1972. Length-slow chalcedony and relics of sulphates- evidence of evaporitic environments in the Upper Carboniferous and Permian beds of Bear Island, Svalbard. J. Sediment. Petrol. 42, 812-816.

Shearman, D.J. 1966. Origin of marine evaporites by diagenesis. Trans. Inst. Min. Metall. 75,B208-215.

——————— and Fuller, J.G.C.M. 1969. Phenomena associated with calcitization of anhydrite rocks, Winnipegosis Formation, Middle Devonian, Saskatchewan, Canada. Proc. Geol. Soc. London 1658, 235-239.

_____, Mossop, G.D., Dunsmore, H. and Martin, M. 1972. Origin of gypsum veins by hydraulic fracture. Trans. Inst. Min. Metall. 81, B149-155.

_____

1973. Origin of gypsum veins by hydraulic fracture. Discussions and contributions. Trans. Inst. Min. Metall. 82, B66-67.

Sherlock, R.L. and Smith, B. 1918. Gypsum, anhydrite, celestite and strontianite. Mem. Geol. Surv. G.B. 64pp.

——————— and Hollingsworth, S.E. 1938. Gypsum and anhydrite, and celestite and strontianite. Mem. Geol. Surv. G.B. 98pp.

Sherwood, P.T. and Hollis, B.G. 1966. Studies of the Keuper Marl: chemical properties and classification tests, Ministry of Transport RRL Rep. 41, Crowthorne.(Road Research Lab.).

Shinn, E.A., Ginsburg, R.N. and Lloyd, R.M. 1965. Recent supratidal dolomite from Andros Island, Bahamas. In: Pray, L.C. and Murray, R.C. (Eds), Dolomitization and limestone diagenesis Soc. Econ. Paleont. Min. Spec. Publ. 13, 112-123.

Skinner, H.C.W. 1963. Precipitation of calcian dolomites and magnesian calcites in the southeast of South Australia. Am. J. Sci. 261, 449-472.

Smithe, F. 1892. The minerals of Gloucestershire: observations on celestite. Proc. Cotteswold. Nat. Field Club 10. 71-81.

Smith, R.A. 1963. The Geomorphology of south Gloucestershire: a study of part of the Bristol.Avon drainage basin. Unpubl. PhD. Thesis Bristol University, England.

Smoot, J.P. 1978. Origin of the carbonate sediments in the Wilkins Peak Member of the lacustrine Green River Formation (Eocene), Wyoming, U.S.A. In: Matter, A. and Tucker, M.E.(Eds) Modern and ancient lake sediments. Int. Assoc. Sediment. Spec. Pubn. 2, Blackwell. 109-127.

Sneath, P.H.A. Some thoughts on bacterial classification. J. Gen. Microbiol. 17, 184-200.

Sokal, R.R. and Michener, C.D. 1958. A statistical method for evaluating systematic relationships. Univ. Kansas Sci. Bull. 38, 1409-1438.

Stoddard, W.W. 1876. On the occurrence of Celestite in the Keuper marls, and its influence on the composition of plants. Mineralog. Mag. 1, 4-7.

Sutcliffe, J.A.M. 1822. The Geology of the Avon. 8vo. Bristol.

Tatlock, D.B. 1966. Rapi. modal analysis of some felsic rocks from calibrated X-Ray Diffraction patterns. Bull. US Geol. Surv. 1209, 1-41.

Thomas, I.A. 1973. Celestite including references to strontian -ite. Miner. Resour. Consult. Comm. Miner. Dossier 6.

Thompson, M. and Howarth, R.J. 1978. A new approach to the estimation of analytical precision. J. Geochem. Explor. 9, 23-30.

Tomlinson, C.W. 1916. The origin of red beds. J. Geol. 24, 153-179.

Truc, G. 1979. Evaporites d'un bassin continental subsident (Ludien et Stampien de Mormoiron-Pernes, sud-est de la France) In: Depots Evaporitiques Chambre Synd. Recherche Prod. Petrole Gaz Naturel, Editions Technip, Paris.

Trueman, A.E. 1938. Erosion levels in the Bristol district. Proc. Bristol Nat. Soc. 8, 402-428.

Tucker, M.E. 1977. The Marginal Triassic deposits of South Wales: continental facies and paleography. Geol. J. 12, 169-188.

_____ 1978. Triassic lacustrine sediments from South Wales: shore-zone clastics, evaporites and carbonates. In: Matter A. and Tucker, M.E. (Eds), Modern and ancient lake

Threlfall, R.E. 1951. 100 years of Phosphorus making. Albright and Wilson Ltd., Oldbury. 341-345.

sediments. Int. Assoc. Sediment. Spec. Pubn. 2, Blackwell. 205-224.

Tunbridge, I.P. 1981. Sandy high-energy flood sedimentation-some criteria for recognition, with an example from the Devon-ian of SW England. Sediment. Geol. 28, 79-95.

Van Houten, F.B. 1962. Cyclic sedimentation and the origin of analcime-rich Upper Triassic Lockatong Formation, West-Central New Jersey and adjacent Pa. Am. J. Sci. 260, 561-576.

Warrington, G., Audley-Charles, M.G., Elliot, R.E., Evans,W.B., Ivimey-Cook, H.C., Kent, P.E., Robinson, Pamela L., Shotton, F.W. and Taylor F.M. 1980. A correlation of Triassic rocks in the British Isles. Spec. Rep. Geol. Soc. London 13, 78pp.

Watts, N.L. 1980. Quaternary pedogenic calcretes from the Kalahari (South Africa): mineralogy, genesis and diagenesis. Sedimentology 27, 661-686.

Weaver, T. 1824. Geological observations on part of Gloucestershire and Somerset. Trans. Geol. Soc. 2nd Series 1, 317-368.

Webb, J.S., Thornton, I., Thompson, M., Howarth, R.J. and Lowenstein, P.L. 1978. The Wolfson Geochemical Atlas of England and Wales. Oxford. 74pp.

Wedepohl, K.H. 1978. Handbook of Geochemistry, Vol.II Springer-Verlag, Berlin.

Welch, F.B.A. and Kellaway, G.A. 1961. ST78SW. Inst. Geol. Sci. 1: 10 560 Geological Sheet.

West, I.M. 1964. Evaporite diagenesis in the Lower Purbeck Beds of Dorset. Proc. Yorkshire Geol. Soc. 34, 315-330.

——— 1965. Macrocell structure and enterolithic veins in British Purbeck gypsum and anhydrite. Proc. Yorkshire Geol Soc. 35, 47-58.

——— 1973. Contribution to discussion in: Shearman D.J., Mossop, G.D., Dunsmore, H., and Martin, M. 1973. Origin of gypsum veins by hydraulic fracture. Trans. Inst. Min. Metall. 82, B66-67.

Wills, L.J. 1976. The Trias of Worcestershire and Warwickshire. Rep. Inst. Geol. Sci. 76/2.

Wood, M.W. and Shaw, H.F. 1976. The geochemistry of celestites from the Yate Area near Bristol. (U.K.) Chem. Geol. 17, 179-193.

Worssam, B.C. 1963. The stratigraphy of the Geological Survey Upton Borehole, Oxfordshire. Bull. Geol. Surv. G.B. 20, 107-156.

Young, H.R. 1979. Evidence of former evaporites in the Cambo-Ordovician Durness Group, Northwest Scotland. Sediment. Geol. 22, 287-303.

APPENDIX I - LOCATION INDEX FOR SPECIMENS MENTIONED IN THE THE TEXT

Prefix	Location of site	Grid Reference (Square ST)
Concentrates		
9680	Mixed concentrate of that date	-
COOP	Mr. Cooper's Field	714842
POWA	West End	710876
POWB	Yate Lower Common	704864
TYTH	Summer Bridge	686878
WAPL	Wapley Common	707803
YCGG	Yate Court/Goose Green	713860/714836
Celestites, Gypsum, Calcitic rocks		
BL	Broad Lane (Yate Bypass)	713837
CB	Goose Green W & E) (Goose Green)	714836/715837
	Tylers' Farm S)	716836
CF	Cooper's Field	714842
GG	Goose Green West and East	714836/715837
HE	Hall End	708870
LC	Yate Lower Common	704864
LP	Leechpool	709853
MR	Wapley Common	707803
MI	Michaelwood	704954
NC	New Courthouse (Yate)	712825
PF	Poundhouse Farm	722923
RI	Ridgeway	720825
RY	The Rectory	715831
SB	Summer Bridge	686878
SI	Swan Inn	716826
TC	Tortworth Copse	716926
TY	Tylers' Farm N & S (Goose Green)	716837/716836
WE	West End	710876
WF	Winter's Field	707861
WP	Wapley Common	707803
YB	Yate Bypass	709837/716835
YC	Yate Court	713860
Additional host rocks and soils		
A	Goose Green West	714836
D	Goose Green West	714836
H	Various localities	-

APPENDIX II: DETAILS OF ANALYTICAL METHODS: WET CHEMICAL ANALYSIS, BETAPROBE ANALYSIS, QUANTITATIVE XRD ANALYSIS, ANALYSIS OF SOILS

II.1 WET CHEMICAL ANALYSIS

.1.1. Sampling error

The discontinuous nature of the celestite/calcite seams was clearly shown in large differences in value between many of the replicate samples. The Ba, Ca, and Zn analyses showed a precision of 20-50%, +50% respectively. For the three celestites analysed for Sr, the precision was in the order of 50%.

II.1.2. Sample Preparation

The celestites were powdered by crushing, using a tungsten carbide mortar followed by grinding for ten minutes in an agate Tema mill. For the large number of samples in the M.A.S. a slightly more sophisticated technique using a jaw crusher, tungsten carbide disc mill and agate Tema mill was employed.

The celestite powders were then coned and quartered before chemical analysis.

II.1.3. Analytical errors

As is current Applied Geochemistry Research Group (A.G.R.G.) practice, samples were randomised and included with duplicates and reagent blanks before determination to cancel out errors caused by operator bias and instrumental defects and to estimate precision. The precision of the various techniques is shown in terms of values of the relative standard deviation in Table II.1. As a larger number of duplicates were used in the fourth method, precision was also evaluated using control charts as described by Thompson and Howarth (1978). (Table II.2).

Table II.1: Values of the relative standard deviation in % for four elements

METHOD	Sr	Ba	Ca	Zn
SCF/AAS*	4.7	0.20	4.0	-
MCF/AAS	0.5	3.3	5.3	-
LMF/AAS*	0.3	1.2	2.3	72.7

* Other elements were not present in sufficiently high amounts for error determination.

Table II.2: Precision of the LMF/AAS method (%)

ELEMENT	Sr	Ba	Ca	Zn	Na	K
PRECISION	10.20	10.20	2.50	20.50	50	50

II.1.4 Sodium carbonate fusion

The first analytical method applied was essentially an adaptation of the sodium carbonate fusion as used by Messrs. Waterfall and O'Brien Ltd., analysts to the Bristol Mineral Company Ltd., whose assistance in the early stages of the analytical program is gratefully acknowledged.

The attack obtains an acidic solution of Sr and other minor and trace element ions by dissolving strontium carbonate, formed by the double decomposition of celestite with molten sodium carbonate. 0.25g of the powdered subsample was fused with 1.0g of anhydrous sodium carbonate for 10-15 minutes in a nickel crucible over a Meka burner flame. The crucible was periodically shaken to ensure homogeneous mixing of the molten salts. The fused mixture was removed from the crucible by immersion in a beaker containing hot deionized water and by the addition of 40ml of 6M HCl. The liquor was then transferred to a 250ml volumetric flask and made up to volume as a 1M HCl solution. Finally, following vigorous agitation, the solution containing the dissolved salts was transferred to a 150ml bottle to await analysis. This final solution represents a 1000x dilution of the concentration of the salts in the celestite.

The solutions were determined for Sr, Ba, Ca, Fe, Mn, Mg, Al, Zn and K, using an air/C_2H_2 fuel mix and for Ba, using N_2O as the oxidant, on atomic absorption photospectrometers.

For the determination of Mg, Ca and in some instances Sr, the solutions were further diluted in 0.5% or 1% lanthanum chlorite. This is necessary to eliminate interference effects caused by molecular absorption in the flame. The master solutions were diluted a further 40 or 50 times in deionized water to bring the Sr concentration into the range of the AA.

For each metal determination the instrument was calibrated using standard solutions made up in a matrix of similar composition to the test solutions.

II.1.5 Hydrofluoric acid leach

Seventeen celestites were analysed for Si using a HF/HCl digestion in special polypropylene bottles in a low temperature oven. Si was determined as the borate, using AAS. The method involves a separate attack to the other analytes and so was not repeated.

II.1.6 Mixed carbonate fusion

A modified carbonate fusion, incorporating several improvements on the SCF/AAS method, was used by Mr. M. Ramsey of the A.G.R.G. to analyse nine celestites from Wapley Common.

0.25g of powdered celestite was dried to remove possible traces of water, mixed with 1.5g of sodium and potassium carbonate fusion mixture in a nickel crucible and ignited in a muffle furnace for 80 minutes at 500-850°C and 30 minutes at 850°C. The fused sets were leached with deionized water onto a filter paper then leached with 6M HCl into a 250ml volumetric flask and made up to volume.

The solutions were analysed by AAS using a N_2O/C_2H_2 flame for Sr and Ba and an air/C_2H_2 flame for Ca and Zn. The solutions were diluted, where necessary, as in I.1.4.

II.1.7 Lithium metaborate-lithium borate fusion

A technique similar to the sodium carbonate fusion, but instead employing a flux of one part of lithium borate ($LiBO_2$) to two parts of lithium metaborate ($Li_2B_4O_7$) was used in a trial batch of Wapley Common celestites and later in the analysis of the Main Analytical Series, together with other celestite sands, gravels and concentrates.

This is a standard technique for the analysis of silicate rocks currently in use at the Geology Department, Imperial College.

For each sample 0.1000g of powdered celestite and 0.6000g of flux were weighed and mixed in a silica crucible, then transferred to a graphite crucible and heated for 30 minutes in a muffle furnace at 1000°C. The fused bead was then dissolved in a nitric acid solution, later made up to volume in a 100ml volumetric flask. The solution was finally transferred to a 150ml bottle.

The solutions were determined for Ba, Ca, Zn, Na and K using AAS as before. Aliquots diluted a further 50X for Sr were prepared, as an economy measure, only for certain important samples and to check on celestites showing high Ba or Ca contents.

II.1.8 Assessment of the wet chemical methods

The precision of the SCF/AAS method was quite acceptable (Table II.2) but because the Sr assays are of celestites containing up to 47.5% Sr this means that the standard deviation at that level is no better than (4.7 /100)X47.5 = 2.2% Sr. Also, a serious underestimate in the Sr assay, and a smaller though equally significant shortfall in the Ca content was suspected (Table 4.1). An extensive series of tests carried out in order to optimise the technique indicated that increasing the fusion time to 30 minutes and filtering of the fusion melt enhanced the Sr assays into the range expected. However precision still remained poor because of errors in the weighing of the powder and reading of the spectrometer dial, loss of test solution during the transferring and diluting operations and loss of sample due to corrosion of the Ni crucibles.

The precision of the improved mixed carbonate fusion is a marked improvement over the earlier method (Table II.1). However because of the amount of time required for each analysis this could not be used for the batch analysis of large numbers of celestites.

A comparison of the Sr assays of the Wapley Common celestites MR01, MR02, MR04 and MR06 in Tables 4.2 and 4.3 showed good correlation but a significant enhancement of the LMF over the MCF analysis. An independent check using Betaprobe analysis (see below) suggested that the higher LMF analysis corresponded most closely to the true Sr content, and that the underestimation mentioned above had been overcome by this technique.

II.2 BETAPROBE ANALYSIS

Celestites, celestite sands and gravels and other sediments, gypsums and soils were analysed by the Telsec 8300 Betaprobe based at the Institute of Geological Sciences, Grays' Inn Road, London. The Betaprobe is a 12 channel

simultaneous direct electron excitation X-Ray Fluorescence spectrometer calibrated for the determination of Sr, Ca, Mg, Fe, Al, Si and S. Uncalibrated spectrometer count output is also available for Na, K, F, P and Ti in the other five channels. The assistance of Mr. A.R. Davis in the analysis of the celestites is gratefully acknowledged.

Powdered homogenized samples were ground for thirty minutes in a tungsten carbide Tema mill, mixed with 20% by weight of graphite powder and pressed onto lead discs. These were analysed in the instrument for a pre-set time interval (twenty seconds for the celestites and celestite sands; fifty seconds for the other types). Output of the analytical data was effected by means of a microcomputer system.

Prior to the analysis the instrument was calibrated by running six standards of artificially prepared "celestites" of known composition, ranging from 17.68% SrO, 13.65% SO_3 and 10.00% MgO, Al_2O_3, Fe_2O_3, CaO and SiO_2 to 54.50% SrO, 42.10% SO_3 and 0.50% MgO, Al_2O_3, Fe_2O_3, CaO and SiO_2. Precision and drift were monitored by the repeated analysis of a control sample at certain stages in the analytical program. Values of the relative standard deviation for the seven analytes are shown in Table II.3. The effects of drift were found to be negligible.

Table II.3: Relative standard deviation values for seven oxides, in %, as determined by Betaprobe analysis

SrO	SO_3	MgO	Al_2O_3	Fe_2O_3	CaO	SiO_2
2.08	0.76	151.00	0.00	9.00	1.23	2.07

Table II.3 shows that the precision of the technique is excellent except for MgO and Fe_2O_3 for which very low values were analysed near the detection limits. Table 4.6 contains some samples of compositions outside the range annotated above. These should be interpreted with caution.

By plotting the raw uncalibrated spectrometer count data for K, Na, F, P and Ti on scatter diagrams against SrO, representing celestite and Al_2O_3 representing the

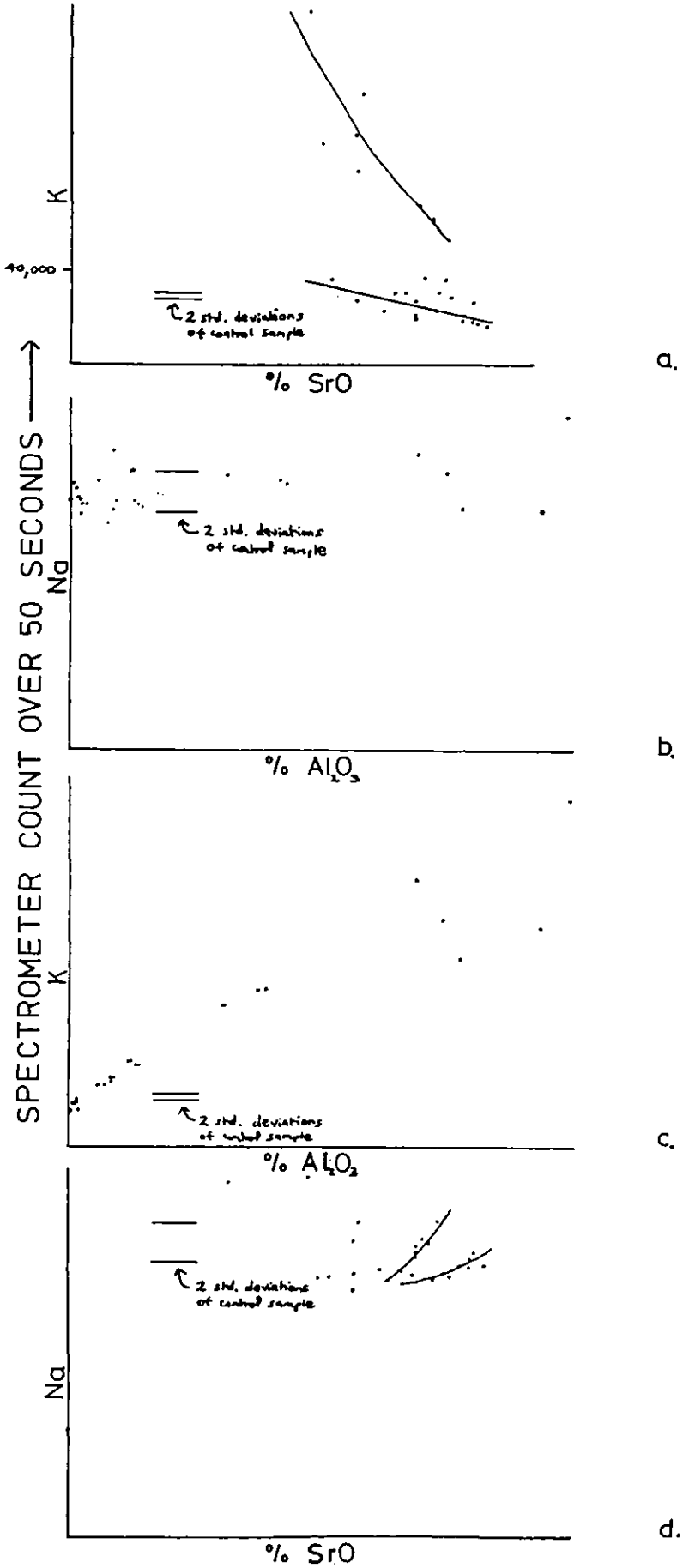

Fig II.1: Interpretation of the uncalibrated data

clastic component it was possible to detect broad compositional trends for the celestites and the celestite sands and gravels. Control samples were also plotted to provide an estimate of the random variation of these data. (Fig. II.1). High positive correlation of K with Al_2O_3 and negative correlation with SrO confirmed that K was mostly present as a component of the clay minerals. However a second regression line of nearly zero gradient also indicates that K is present in celestite up to a value of 40,000 counts. (Fig II.1a).

The data in the Na/SrO diagram falls into three fields: a cloud containing the celestite sands and two regression lines for the celestites. (Fig. II.1d). The Na/Al_2O_3 plot (Fig. II.1b) shows a low positive correlation with the celestite sands and gravels in very similar positions to those in Fig. II.1c. The values of the steeper regression line plot above those of the gentler gradient on Fig. II.1b indicating that the variation in Na is independent of the alumina content. The Na content of the celestite sands and gravels is therefore a function of the clay content, the Na^+ substituting for K^+ in the clay mineral lattice (Berry and Mason, 1959). Traces of F were detected in the celestites in variable amounts; P however was not detected. A high positive correlation of Ti with Al_2O_3 and a negative correlation with SrO indicated concentration in the clastic fraction. Particularly high values were recorded in celestite sands containing detrital ironstone from Winters' Field and The Rectory.

II.3 QUANTITATIVE XRD ANALYSIS

II.3.1 Introduction

As qualitative work showed that the strongest reflections of celestite, calcite and dolomite were contained within the 30-37° 2θ interval of the CoKα diffractogram, and that the intensities varied in proportion to the amount of the mineral present, a quantitative method was developed to provide a rapid analytical technique for the determination of calcite and dolomite in the celestites.

In an earlier study, Cuff (1973) compared the intensities of the calcite (10$\bar{1}$4) reflection with those of

ten other common sabkha minerals and was able to determine the minerology of evaporite samples to a 10 per cent precision. He prepared a series of artificial standards by adding proportionate weights of calcite to pure specimens of the ten other minerals and, after XRD analysis, by plotting the calcite content of each standard against a factor derived from the reflection heights, constructed calibration curves from which the composition of the evaporite samples could be directly obtained.

Other workers have developed techniques using interval standards such as fluorite to calibrate the diffractogram reflections (e.g. Erdosh, 1967). These were not considered for this investigation because of the additional analytical time involved in accurately weighing and admixing the standard and also because the effects due to absorption of X-Rays caused by inhomogenuities in the sample matrices were not too serious.

The technique developed was loosely based on Cuff's (1973) method and was applied to 127 carefully selected celestites, including 6 duplicates. The range was extended to 29-39° 2θ in order to search for the main reflections of any other mineral likely to be present (e.g. strontionite, anhydrite, baryte, aragonite, quartz, sphalerite, gypsum, halite, magnesite, feldspar or goethite).

II.3.2 Method

Prior to analysis, each celestite powder was hand ground in an agate mortar to pass a 300 mesh sieve, in order to minimise effects due to microabsorption, extinction and preferred orientation (and therefore packing differences), maximise intensities and increase the reproductivity of the peaks (refer to Klug and Alexander, 1954; Tatlock 1966).

The samples were firmly packed, using a glass slide into an aluminium cavity mount and scanned on a Phillips X-Ray powder diffractometer using CoK radiation. Standards of calcite/celestite powders containing 5,10,30, 50, 70 and 90% calcite were prepared by mixing proportional amounts of powdered coarse yellow scalenohedra with pure celestite of sample CB05. The dolomite/calcite/celestite

standards were prepared by spiking two previously made up calcite/celestite powders with small amounts of a pure powdered dolomite. Dolomite/celestite standards were not used because dolomite, where present, almost always occurred with high concentrations of calcite, and it was easy to alter previously prepared calcite standards to match the matrix of these celestites.

Where necessary, a silicon disc standard was used on each new day of analysis to check that the generator and circuitry had stabilized at normal operational levels.

II.3.3 Determination of calcite and dolomite content

As experimental trials showed that the $(\bar{2}11)$ celestite peak was least susceptible to enhanced intensities caused by preferred orientation effects this was selected for the analysis. Values of the parameters

$$\frac{100\ I'}{I + I'} \quad \text{and} \quad \frac{100\ I''}{I' + I''}$$

where I is the peak height of celestite (211) - background
I' " calcite (104) - background
I'' " dolomite (211) - background

for the standards were plotted against the calcite content as shown in Fig. II.2. The working curves produced could then be used to estimate the calcite content of the celestites. Because the dolomite content in Fig. II.2b only refers to a calcite/dolomite mixture each value was then multiplied by a conversion factor to give the dolomite percentage of the total sample. This resulted in an overestimation of the calcite component of about 2% absolute in calcite/celestite/dolomite standards containing 27-30% calcite.

Scatter diagrams of I'' versus dolomite percentage were plotted to estimate the approximate dolomite percentage of calcite-free samples (Nos 135 and 142).

II.3.4 Errors

Errors due to instrumental drift, packing of the powder into the mount, sampling, and misreading of the chart recorder were identified and evaluated by duplicate analyses and a series of monitoring and precision tests. Typical

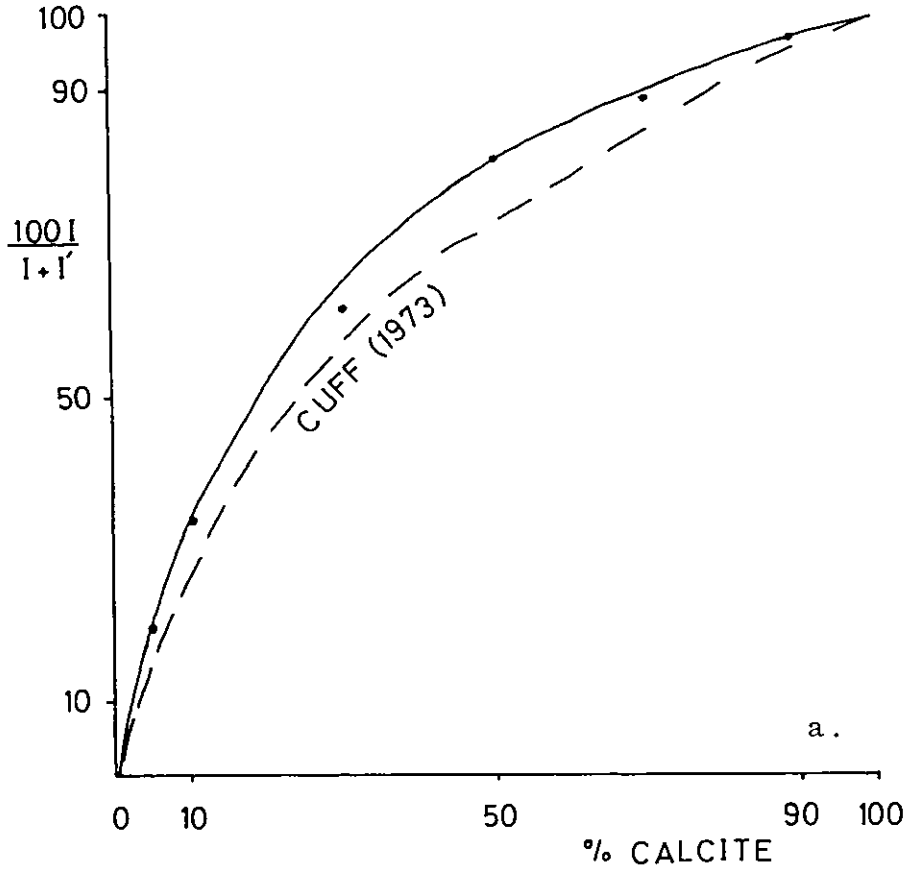

Fig II.2: Calibration curves for a. celestite-calcite b. celestite-calcite-dolomite standards (after Cuff, 1973)

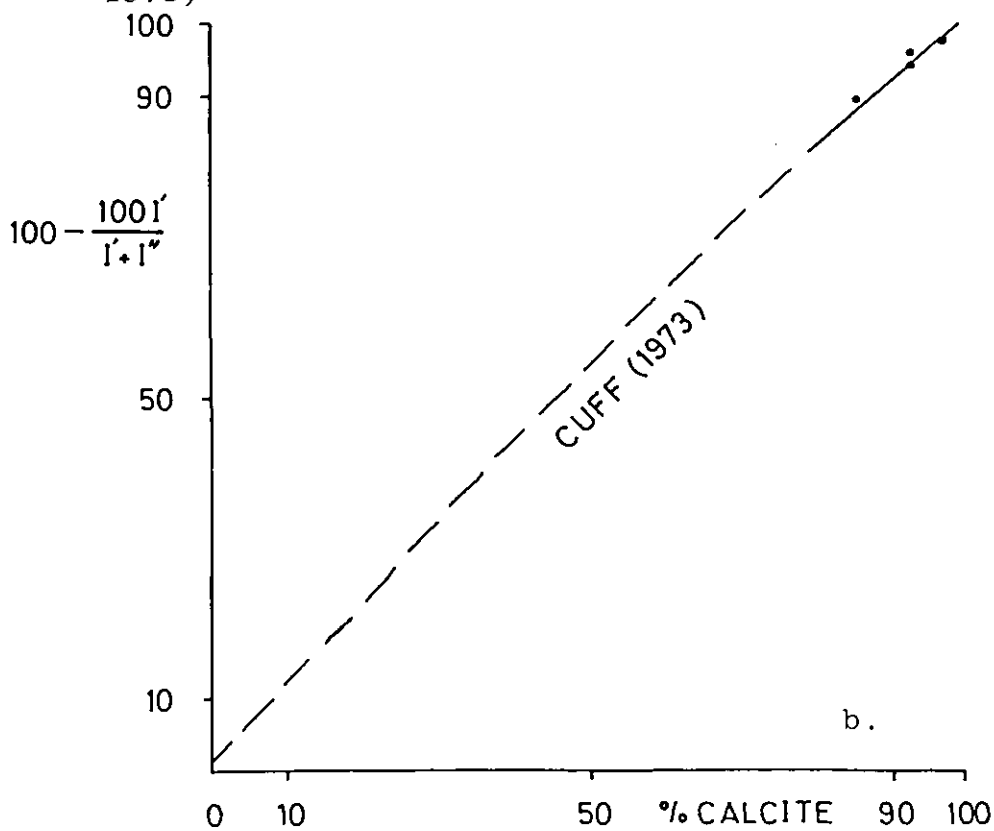

values of the first two errors were found to be 13.8 and 5.8% (relative to mean). The recording error is banded between 1.4 and 16.4%. The sampling error, which of course is confounded with the other three, was determined by precision chart to be between 20 and 50% for calcite and about 50% for dolomite.

II.3.5 Effect of absorption

As mass-absorption effects can raise or depress the heights of the celestite, calcite and dolomite peaks, the mass absorption coefficients were calculated of all the likely components present in the celestites. (Table II.4).

Table II.4: Mass absorption coefficients of 10 minerals and oxides, calculated from the data of Klug and Alexander (1954) (CoK radiation)

Compound	$SrSO_4$	$BaSO_4$	$CaSO_4$	$CaCO_3$	$CaMg(CO_3)_2$	Fe_2O_3
MAC	120.55	297.02	111.48	106.59	71.37	42.30

Compound	SiO_2	Al_2O_3	MgO	$KAl_3Si_3O_{10}OH_2$
MAC	53.29	48.01	42.82	57.74

Table II.4 suggests that the Ba-rich celestite and clay minerals, in particular, could affect the mass absorption of the bulk sample. Although in fact Ba-rich celestite was not present in sufficient quantities to significantly alter the MAC of celestite (120.55) the presence of iron and clay minerals in the sample substituting for calcite would lower the MAC of the whole sample. However calculations of the range of MAC values expected in the data of Nickless et al (1976) showed that on average the MAC of a clay-celestite matrix approached that of calcite so that corrections for absorption differences were not necessary.

II.4 CHEMICAL ANALYSIS OF SOILS

II.4.1 Sample Preparation

The -2mm fractions of the soils were crushed to pass an 80 mesh sieve by hand grinding in a porcelain pestle. After coning and quartering, the samples were ignited for four hours at 450°C to drive off volatile matter.

The soils were then randomized as in II.1.3.

II.4.2 Nitric acid leach

0.2g samples were digested in hot HNO_3, diluted and determined for Sr, Ba, Ca, Zn, Pb, Fe, Mg, and Mn by AAS.

II.4.3 Sodium carbonate fusion

The sodium carbonate fusion employed was basically the same as that described in II.1.4. 0.2g of sample was fused with 1g of sodium carbonate for one hour in a nickel crucible in a muffle furnace. The melt was extracted in hot deionized water, made up in an acid solution and analysed for Sr, Ba, Ca, Zn, Pb, Fe, Mg and Mn by AAS.

The method was later abandoned because of corrosion in the nickel crucible.

II.4.4 Precision

Precision, determined from control charts, varied with each analytical run, but was generally of an acceptable standard. Values of precision of the Sr and Ba determinations were as follows: Sr (acid leach): 10-50%; Sr(fusion): 10-20%; Ba (acid leach): 10-50%; Ba (fusion) 20-50%.

APPENDIX III - EXPLANATION OF BINARY CODED VARIABLES USED TO DESCRIBE CELESTITES OF THE MAIN ANALYTICAL SERIES

Variable	Feature
+1UNIT	part of a larger specimen
ROUND	rounded outline
ANGULR	angular outline
SMOOTH	smoothed exterior
CCRIM	marl rim
BREAK	celestite breaks away from marl
RED	red marl
AG	green marl (10Y, 5GY)
BG	green marl (10GY, 5G)
OCHRE	goethite deposit
REDNAM	red Namurian mudstone
GLEYED	gleyed Namurian mudstone
MOTTLE	mottled red marl
CALC	marl effervesces in 10% HCl
INDURD	indurated marl
SILTY	silty marl
SANDY	spararenite
MOULDS	lath-shaped moulds
MASSIV	massive
STRAT	stratified, banded macrocells
MACMAS	massive to macrocellular
COMMAC	compact macrocellular
VUGMAC	drusey macrocellular
CELMAC	light red macrocellular
MUDMAC	separate macrocells in marl
SPECK	'speckled' structure
MESH	chicken-wire texture
MACIMP	macrocellular to impregnated
CLUIMP	clustered impregnations
SCAIMP	scattered impregnations
LMST	limestone
X-CUT	more than one celestite generation
XLRTLE	crystals at right angle to border
XL11	crystals parallel to border
BLASTS	porphyroblasts
F BLUE	fine blue
FWHITE	" white

Variable	Feature
FORANG	fine orange
F PINK	" pink
F RED	" red
FPURPL	" purple
F GREY	" grey
F GRAN	" granular
F LATH	" lathlike
M BLUE	medium blue
MWHITE	" white
MORANG	" orange
M PINK	" pink
M RED	" red
MPURPL	" purple
M GREY	" grey
M GRAN	" granular
M LATH	" lathlike
C BLUE	coarse blue
CWHITE	" white
CORANG	" orange
C PINK	" pink
C RED	" red
CPURPL	" purple
C GREY	" grey
C GRAN	" granular
C LATH	" lathlike
RNDVUG	round druses
BICVUG	biconvex druses
MUDVUG	vugs in marl
NETVUG	inter-macrocellular druses
CELVUG	druses in celestite
MUDINV	mudstone centre to vugs
FINOUT	texture of celestite decreases outwards
NOCHGE	no change in celestite texture
CINCEL	scalenohedral calcite in celestite
CINMUD	scalenohedral calcite in marl
C+CEL	scalenohedral calcite
CCUBIC	pseudocubic calcite
C FINE	celestite effervesces in 10% HCl